Universidade do Minho
Escola de Engenharia

Silvia Maria Mihaila

Routes to Advance Vascularized Bone Tissue Engineering Constructs

novembro de 2014

Universidade do Minho
Escola de Engenharia

Silvia Maria Mihaila

Routes to Advance Vascularized Bone Tissue Engineering Constructs

Tese de Doutoramento em Bioengenharia

Trabalho realizado sob a orientação da
Professora Maria Manuela Estima Gomes
e da
Doutora Alexandra Margarida Pinto Marques

novembro de 2014

DECLARAÇÃO

Nome: Silvia Maria Mihaila

Endereço electrónico: silvia.mihaila@dep.uminho.pt

Titulo da Tese: Routes to Advance Vascularized Bone Tissue Engineering Constructs

Orientadores: Professora Maria Manuela Estima Gomes

e Doutora Alexandra Margarida Pinto Marques

Ano de conclusão: 2014

Designação do Doutoramento: Bioengenharia

Universidade do Minho,5-11-2014_____

Assinatura:_____

STATEMENT OF INTEGRITY

I hereby declare having conducted my thesis with integrity. I confirm that I have not used plagiarism or any form of falsification of results in the process of the thesis elaboration. I further declare that I have fully acknowledged the Code of Ethical Conduct of the University of Minho.

University of Minho, 5th of November 2014

Full name: **SILVIA MARIA MIHAILA**

Signature: _____

Do not be afraid to step into the unknown,

The only thing you will lose is fear*.*

(unknown)

ACKNOWLEDGEMENTS

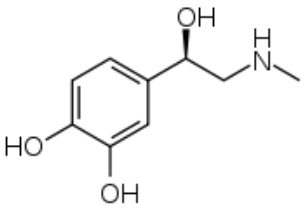

Chemical Name: (*R*)-4-(1-Hydroxy-2-(methylamino)ethyl)benzene-1,2-diol
Synonyms: adrenaline
Formula: $C_9H_{13}NO_3$
CAS Nr: 51-43-4
Molecular weight: 183.204g/mol

6 years ago the chemist within me could only read the intriguing assemble of atoms and their interactions. Only until I have decided to take a leap of faith and change gears, I have come to understand the power of this molecule. If we think of a doctoral thesis as a marathon, the rush of adrenaline keeps us running. In many ways, this marathon might appear to be a solitary and isolating process, as I, myself, had to do the running. At the same time, I would have never been able to run and reach the finish line without the assistance and support of so many wonderful people, that have put their trust in me and believed that the day when I will write these words will come. As I stumbled on my track and my legs got weak, many arms have lifted me and gave me the strength and courage to continue and press forward, getting more eager to break that ribbon.

And what is an athlete without a coach? I have been fortunate to have two extraordinary coaches: Professor Manuela Gomes and Dr. Alexandra Marques. From the beginning of this adventure, they have equipped me with the necessary tools to bring this race to the end. When my thoughts were scattered in all directions, they were the ones that brought focus in my sight, by challenging me with focused questions, reflecting back and anticipating the potential obstacles that I might face. Therefore, I deeply appreciate their guidance in the scientific matters and stimulating discussions, which allowed me to see different aspects of my research in a broader perspective, and offering me the freedom to pursue my ideas and become a more independent researcher.

I am inspired by your dedication, strength and determination, especially under pressure, time limit and when I most needed to move forward. I am grateful to Manuela for always being there when I needed and strongly guarding my interests. She showed me that the way we deliver our message sometimes can be more important that the message itself. To Xana I would like to bring my appreciation for encouraging me to not to be afraid of getting lost in the maze of science and how to be critical with myself and my research. Though sometimes science might have been difficult, she showed me that this is exactly what makes it so enjoyable. Embrace it and have fun.

I would also like to thank Professor Rui L. Reis for not only giving me the opportunity to join the 3B's Research Group, but also providing everything that was necessary to pursue my research. During my PhD, I was honored and proud to witness several outstanding

achievements of Prof Rui, which are the testimony of a man that believed in his dream, and did not give up until he made it happen. And he is not afraid to dream big. His dedication, enthusiasm, and vision are his legacy for my career.

I would also like to acknowledge Professor Ali Khademhosseini for accepting to be my co- supervisor and for allowing me to work at his prestigious lab. I have learned a great deal from his unique perspective on research, his sharp insight on almost any issue and constant support, which extends until today.

Doctor Akhilesh Gaharwar, who has not only been my lab mentor, but also my friend, also deserves a special acknowledgment. You condiment your research with passion and dedication, and had been a rewarding experience, both professionally and personally. The work on this thesis would have never been possible if it wasn't for our long, but fruitful discussions. Thank you for the constant help and useful scientific inputs. But most importantly, I will always treasure our friendship and your unconditional support.

I would also like to acknowledge the Foundation for Science and Technology (FTC) and MIT- Portugal Program for my personal doctoral grant (SFRH/BD/42968/2008). It has been an honor to be part of this renamed program and to learn from the best professors from different areas of Bioengineering, both in Portugal and at MIT.

I have I've also been fortunate to have a great group of colleagues in 3B's, thank you for all the support and for sharing so many experiences. I have learned so much from all of you, from figuring out what research is, to improving my organization skills, to learning how to present my work. Your constructive criticism and collaboration have been tremendous assets throughout my PhD.

With many of you, we started as colleagues, running this race alongside, and we ended up as friends. Not only are you the people I can discuss my research with and goof off with, but also you are confidants who I can discuss my troubles with and who stand by me through thick and thin. This, I believe, is the key to getting through a PhD– having good friends to have fun with and complain to.

I would like to start with a joyful group of special ladies, my "misses": Diana, Alessandra, Ana Catarina, Margarida and Ana. We've laughed together and you have been kind when I needed to cry. When others doubted, you remained a fan. When I became too serious, your humor and friendly sarcasm allowed me to laugh and lightened my perspective. You were/are my confidant, conscience, rear end kicker, phone comrade, ride to the lab and back, etc. I just cannot thank you enough for all of your support, empathy and encouragement. I can only say that I am blessed to have you as friends.

Along with them, I would like to take the ones that have survived my "fine" cuisine attempts (the legendary beringela!!!) and my pessimistic sermons and embarked with me in this journey. My "partners in crime": Pedro (Che) C, Joao R, Mariana, Ester, Pedro B,

Nelson, Pedro C, (Mr.) Praveen, Wojciech, Nuno, Alvaro, Alexander and Kara, you have been my a constant support and I am privileged of having your friendship. As each ones paths are going in a different direction, I hope that they will meet at some point and rewind those late evenings when we could enjoy life to its fullest and cherish every moment we spend together. These memories will always bring a smile on my face.

Next I would like to thank Dr. Elena Popa, or as I call her, my dear friend Elena. I cannot begin to express my gratitude and feelings for this woman. We've laughed, cried and among other things, we survived. She's been as tough on me as she's been supportive and caring. Thank you Elena for being persistent and encouraging, for believing in me, and for the many precious memories along the way.

I would also like to mention by dear friends from Boston: Doga and Nafis. Though we are living on different continents, our friendship has proven to be strong enough to withstand distance. I thank you for being always there for me, crying and laughing, and never judge me, but accept me just as I am, with my flaws. I am looking forward for that warm hug of yours. I extend this gratitude to the "Landsdowne folks": Faramarz, Sam, Alpesh, Nasim, Gulden, Nesli (next stop Basel?), Lina (you were a beautiful bride), Davide and Giorgio (I miei ragazzi), Maria (You rock, girl!) and Deborah. You guys are great! I carry each one of you in my heart and I am looking forward to meet you again and, who knows, go to a Bob Sinclair concert…again.

I am deeply appreciative of the many individuals who have supported my work and continually encouraged me through the writing of this dissertation: Ana Rita, Clara, Ana G. Viviana, Ana Regina, Diana P, Isa, Daniela F, Claudia, Liliana, Simone, Luis, Albino, Daniela C, Rogerio, Mariana C, Ana F. Without their time, attention, encouragement, thoughtful feedback, and patience, I would not have been able to see it through.

And most of all for my loving, encouraging, and patient husband Dennis whose faithful support during the final stages of this PhD is so appreciated. He has been central to my completion of this thesis, as he has given me confidence I lost along the way and motivated me in so many ways. Through his eyes I've seen myself as a capable, intelligent woman who could do anything once I made up my mind. As I ramble, I still have not found the words that describe or express how I feel for this man and what his presence in my life has meant. He loves me like no one else has and has changed me for the better (as did Miss ☺). Thank you with all my heart and soul. I love you and am forever indebted to you for giving me your life, your love, and your heart. Your complete and unconditional love carries me through always.

I thank my God, my good Father, for letting me go through all the difficulties. I have experienced Your guidance day by day. I will keep on trusting You for my future.

I finish with Romania, where the most basic source of my life energy resides: my family. I have an amazing family, unique in many ways. Their support has been unconditional all these years, they've given up many things for me to be at where I am today, they have cherished with me every great moment and supported me whenever I needed it, even at distance. "Wherever you are and whatever you do, do not forget the nest you left out from and you will always have a home here" my father kept saying. These words helped me survive the difficulties of being abroad. This thesis is dedicated to you, Mom and Dad.

(**RO**) ***Sunt ceea ce sunt azi datorita voua.***
Aceasta teza e pentru voi

ABSTRACT

One of tissue engineering (TE) challenges concerns the vascularization of engineered constructs upon implantation into the defect. In fact, for the survival of the engineered tissue beyond the oxygen diffusion limit, the formation of new blood vessels is mandatory. Therefore, this thesis aimed at designing routes towards advanced vascularized bone analogs, based on the combination of cells, biomaterials and inorganic components. The major objectives of this thesis were **1)** to identify a single cell source to obtain both endothelial (ECs) and osteoblast-like cells (OBs); **2)** to identify the optimal conditions in which these cells synergistically communicate; **3)** to trigger the osteogenic differentiation of stem/stromal cells by inorganic osteoinducers and **4)** to design 3D hydrogel systems for the controlled spatial distribution of cells.

The use of adipose tissue (AT) as a cell pool for TE purposes is highly appealing, since its stromal vascular fraction (SVF) contains stem/stromal-like cells (hASCs) that can be differentiated into specific lineages, enhancing their potential use in a clinical setting. Under this context, the SSEA-4$^+$ cellular subset of SVF (SSEA-4$^+$hASCs) was proven to hold enhanced differentiation potential into ECs- and OBs-like cells, the most relevant cell types for bone vascularization TE routes. Using immunomagnetic selection tools, SSEA-4$^+$hASCs were successfully separated and differentiated towards both endothelial and osteogenic lineages. Furthermore, it was found that culturing these obtained ECs and pre-OBs at an initial ratio of 75:25 in a mixture of standard endothelial and osteogenic media, cells synergistically communicate to encourage the full differentiation of pre-OBs and the maintenance of ECs phenotype. Culturing SSEA-4$^+$hASCs in presence of sNPs in basal condition lead to the deposition of a collagen-enriched matrix relevant for bone TE. When in combination with standard osteogenic factors, sNPs were able to significantly increase the osteogenic commitment of both hMSCs and SSEA-4$^+$hASCs.

Finally, to address the tri-dimensionality of the bone, hydrogels templates, based on kappa-carrageenan (*κ*-CA) and chitosan (CHT), were designed to accommodate SSEA-4$^+$hASCs-derived ECs and OBs. The CHT coated *κ*-CA hydrogel microfibers, arranged in such a fashion to mimic the blood vessel network, were able to support the endothelial signature of entrapped ECs. These, upon assembly within a pre-OBs loaded matrix, are appealing to be templates to attain a 3D microvascular network. By decorating κ-CA with photocrosslinkable units, hydrogels with tunable mechanical properties and high recovery rates after deformation we obtained. The controlled spatial distribution of cells was achieved by patterning the hydrogels in well-defined geometries.

In summary, the research work described in this thesis addressed new strategies within the TE field that might inspire the development of improved vascularized bone-engineered constructs. The use of SSEA-4$^+$hASCs was proven to be an endearing choice of undifferentiated cells, while their combination with sNPs and κ-CA hydrogels displayed numerous advantages. Nonetheless, the unraveling of the real potential of these cells, alone or in combination with sNPs and/or κ-CA hydrogels, towards promoting vascularized bone formation yet requires *in vivo* confirmation.

RESUMO

Um dos desafios da engenharia de tecidos consiste na vascularização após a implantação do implante no defeito. De facto, para a sobrevivência do substituto do tecido é essencial a difusão de oxigénio assim como a formação de novos vasos sanguíneos. Portanto, esta tese explora novas estratégias para o desenvolvimento de análogos de osso vascularizado, com base na combinação de células, biomateriais e componentes inorgânicos. Os objetivos principais desta tese foram: **1)** identificar uma única fonte celular para obter tanto as células endoteliais (ECs), como as osteoblastos (OBs); **2)** identificar as condições ideais em que estas células comunicam de uma forma sinérgica; **3)** desencadear a diferenciação osteogénica das células estaminais através dos osteoindutores inorgânicos e **4)** projetar sistemas de hidrogéis em 3D para controlar a distribuição espacial das células.

O uso do tecido adiposo como uma fonte de células é altamente atraente para engenharia de tecidos. As células estaminais derivadas do tecido adiposo (*hASCs*) podem ser diferenciadas em linhagens específicas, melhorando assim o seu potencial para aplicações clínicas. Neste contexto, a população SSEA-4$^+$, identificada na fração vascular do tecido adiposo (SSEA-4$^+$hASCs), foi a que demonstrou melhor potencial de diferenciação em células endoteliais (ECs) e osteoblastos (OBs), as células mais envolvidas na vascularização óssea. Usando ferramentas de seleção imunomagnéticas, as SSEA-4$^+$hASCs foram separadas e diferenciadas em ambas linhagens: endotelial e osteogénica. Além disso, verificou-se que a cultura de ECs e pré-OBs numa razão inicial de 75:25, num meio de cultura misto, levou a uma comunicação celular sinérgica, incentivando a diferenciação completa das pré-OBs e a manutenção do fenótipo endotelial das ECs.

A cultura das SSEA-4$^+$hASCs na presença de nanopartículas de silica (*SNPs*) num meio basal, levou à deposição de uma matriz enriquecida em colagénio, essencial na regeneração óssea. Em combinação com fatores osteogénicos, as *SNPs* foram capazes de significativamente aumentar o compromisso osteogénico de ambas as células mesenquimais humanas e SSEA-4$^+$hASCs.

Finalmente, para resolver a tridimensionalidade do osso, modelos 3D com base em hidrogéis de kappa-carragenina (*κ-CA*) e quitosano (*CHT*), foram desenvolvidos para acomodar as ECs e OBs. Microfibras de κ-CA revestidas com CHT, dispostas de tal forma que mimetizam a rede vascular, foram capazes de manter a assinatura endotelial das ECs. Após o arranjo dentro de uma matriz enriquecida em pré-OBs, espera-se que agissem como padrões para gerir uma rede microvascular funcional. Seguinte, a decoração da κ- CA com unidades foto-reticulaveis rendeu hidrogéis com propriedades mecânicas ajustáveis e altas taxas de recuperação após a deformação. Uma distribuição controlada de células foi obtido por *patterning* em geometrias bem definidas.

Em resumo, o trabalho de investigação descrito nesta tese propõe novas estratégias dentro da engenharia de tecidos que podem inspirar o desenvolvimento de construções de osso vascularizado. O uso das SSEA-4$^+$hASCs provou ser uma escolha cativante de células não diferenciadas, enquanto a combinação com *SNPs* e hidrogéis de κ-CA exibiu várias vantagens. No entanto, o desenrolar do verdadeiro potencial destas células, individualmente ou em combinação com *SNPs* e/ou hidrogéis de *κ-CA*, no sentido de promover a formação de tecido ósseo vascularizado, ainda requer confirmação *in vivo*.

TABLE OF CONTENTS

LIST OF ABBREVIATIONS AND ACRONYMS

#

ΔΔCt – delta delta critical threshold

2D – bi-dimensional

3D – tri-dimensional

% – percentage

κ – *kappa*

ι – *iota*

λ – *lambda*

δ – tao

ζ – zeta

A

A – amper

Å – Angstrom = 1.0 x 10^{-10} m

α-MEM – minimum essential medium eagle-alpha modification

A-W – Apatite-Wollastonite

ac-LDL – acetylated low-density lipoprotein

AG – anhydro-D-galactose

ALP – alkaline phosphatase

ANOVA – analysis of variance

APC – allophycocyanin

ARS – Alizarin Red S

AT – adipose tissue

ATR – attenuated total reflection

B

BCIP – 5-bromo-4-chloro-3-indolyl phosphate

βGP – beta-glycerophosphate

BET – Brunauer–Emmett–Teller theory

BMP – bone morphogenetic protein

BMSCs – bone marrow-derived mesenchymal cells

BSA – bovine serum albumin

BSPs – bone sialoproteins

β-TCP – β-tricalcium phosphate

C

°C – Celsius

CA – carrageenans

Ca^{2+} – calcium ion

$CaCl_2$ – calcium chloride

Ca-GP – calcium glycerophosphate

Calcein AM – calcein acetoxymethyl ester

CaPs – calcium phosphates

CAS N° – Chemical Abstract Service Number

Cat N° – catalog number

CCD – charge-coupled device

cDNA – complementary deoxyribonucleic acid

CHT – chitosan

Cl^- – chloride ion

CLSM – confocal laser scanning microscopy

CNTs – carbon nanotubes

Col I – collagen type I

Col II – collagen type II

CO_2 – carbon dioxide

–COOH – carboxyl group

Ct – critical threshold

D

DA – N-acetylation degree

Da – Dalton

DAF-2DA – 4,5-diaminofluorescein diacetate

DAPI – 4,6-diamidino-2-phenyindole dilactate

DBM – demineralized bone matrix

DD –N-deacetylation degree

DEX – dexamethasone

DHE – dihydroethidium
DI – deionized water
diH_2O – distilled water
DIL – 1,1´-dioctadecyl-3,3,3´,3´ tetramethylindocarbocyanine
DLS – dynamic light scattering
DM – degree of methacrylation
DMEM – medium
DMSO – dimethyl sulfoxide
DNA – deoxyribonucleic acid
D_2O – deuterated water (deuterium oxide)
DPBS – Dulbecco's phosphate buffered saline
DNA – deoxyribonucleic acid
dsDNA – double-stranded DNA

E

EBM – endothelial basal medium
ECGS – endothelial cell growth supplement
ECM – extracellular matrix
ECs – endothelial cells
EDS – energy dispersive spectroscopy
EDTA – ethylenediaminetetraacetic acid
EDX/EDS – energy-dispersive X-ray spectroscopy
EGM-2 MV – microvascular endothelial growth medium
EGMP – ethylene glycol methacrylate phosphate
ELISA – enzyme-linked immunosorbent assay
eNOs – endothelial nitric oxide synthase
EPCs – endothelial progenitor cells

F

F-actin – actin filaments
FBS – fetal bovine serum
FGF – fibroblast growth factor
FITC – fluorescein isothiocyanate
FTIR-ATR – Fourier transform infrared spectroscopy with attenuated total reflection
Fwd – forward

G

g – gram
G – β-D-galactose
G'' – storage modulus
G' – loss modulus
GAGs – glycosaminoglycans
GAPDH – glyceraldehyde 3-phosphate dehydrogenase
GelMA – methacrylated gelatin
GFP – green fluorescent protein
GFs – growth factors
xg – centrifugal force

H

h – hour(s)
^{1}H NMR – proton nuclear magnetic resonance
^{1}H – protium
^{2}H – deuterium
HA – hydroxyapatite
hASCs – human adipose tissue-derived stem cells
HiFBS – heat-inactivated fetal bovine serum
hMSCs – human mesenchymal stem cells
HUVECs – human umbilical vascular endothelial cells
Hz – hertz

I

IC_{50} – half maximal inhibitory concentration

IG – ionotropic gelation
IGF – insulin–like growth factor
IL-1 – interleukin–1
IL-6 – interleukin–6
IPN – interpenetrating network
Irgacure 2959 – 2-hydroxy-1-(4-(hydroxyethoxy)phenyl)-2-methyl-1-propanone

J

J – joule

K

K^+ – potassium ion
κ-CA – *kappa*-carrageenan
KCl – potassium chloride
K_2HPO_4 – dipotassium phosphate

L

L – liter
LDH – lactate dehydrogenase
LDL – low density lipoprotein

M

m – meter
min – minute(s)
Mg^{2+} – magnesium
M-CSF – macrophage colony-stimulating factor
MA – methacrylic anhydride
MA-κ-CA – methacrylated κ-CA
MAlg – methacrylated alginate
MMPs – matrix metalloproteinases
mRNA – messenger ribonucleic acid
MSDS – Material Safety Data Sheet
MSCs – mesenchymal/stromal stem cells
MTS – (3-(4,5-dimethylthiazol-2-yl)-5-(3carboxy-methoxyphenyl)-2-(4-sulfophenyl)-2H-tetrazolium)
MTT – 3-(4,5-dimethylthiazol-2-yl)-2,5-diphenyltetrazolium bromide
MW – molecular weight
M_W – wet weight
M_{DF} – final dry weight
M_{DI} – initial dry weight

N

N – normal growth medium
NaCl – sodium chloride
NBT – nitro blue tetrazolium
NCBI – National Center for Biotechnology Information
$NaHCO_3$ – sodium bicarbonate
NaOH – sodium hydroxide
NCPs – non-collageneous proteins
$–NH_2$ – amine
NH_4Cl – ammonium chloride
nm – nanometer
NOx –nitric oxide

O

OC – osteoconductive medium
OCN – osteocalcin
OD – optical density
–OH – hydroxyl groups
OI – osteoinductive medium
ONC – osteonectin
OPF – oligo(poly(ethylene glycol) fumarate
OPN – osteopontin
$–OSO_3^-$ – sulphate
OST – complete osteogenic medium (or OI)

P

Pa – pascal
PAA – polyacrylamide
PBS – phosphate buffer saline
PCR – polymerase chain reaction
PDMS – polydimethylsiloxane
PDGF – platelet-derived growth factor
PE – phycoerythrin
PEC – polyelectrolyte complex
PEG – polyethylene glycol
PEGDA – PEG diacrylate
PEI – poly (ethylene imine)
Pen/Strep – penicillin/streptomycin
pFA – paraformaldehyde
PHEMA – poly(2-hydroxyethyl methacrylate)
PI – photoinitiator
PLGA – poly(actic-co-glycolic) acid
PLEOF – poly(lactide-co-ethylene oxide fumarate)
PLs – platelet lysates
PMMA – poly(methyl methacrylate)
PNIPAAm – poly(N-isopropylacrylamide)
p*NP** – ***p-nitrophenol
p*NPP** – ***p-nitrophenol phosphate
PO_4^{3-} – phosphate
PPF – poly(propylene fumarate)
PPGmM – poly(propylene glycol)monomethacrylate
PPO – poly(propylene oxide)
PRP – platelet-rich plasma
PVA – poly(vinyl alcohol)

R

Rev – reverse
RGD – arginine-glycine-aspartate
rhBMP–2 – recombinant BMP–2
rhIGF–1 – human recombinant insulin growth factor–1
RNA – ribonucleic acid
RNS – reactive nitrogen species
ROS – reactive oxygen species
rpm – rotation *per* minute
RUNX2 – Runt-related transcription factor-2
RT-PCR – reverse transcriptase polymerase chain reaction

S

sec – second(s)
SBF – simulated body fluid
SD – standard deviation
SDS – sodium dodecyl sulphate
SEM – scanning electronic microscopy
Si-OH_4 – silanol group
Si$(OH)_4$ – **(**ortho)silicic acid
sNPs – silicate nanoplatelets
SO_4^{2-} – sulphate
SOx – superoxide
SSEA-4 – stage specific embryonic antigen-4
SVF – stromal vascular fraction

T

δ – loss angle
TCPS – tissue culture polystyrene
TE – tissue engineering
TEM – transmission electron microscopy
TGF-β1 – transforming growth factor beta-1
TMSPMA – 3-(trimethoxysilyl)propyl methacrylate
TNF-α – tumor necrosis factor-α
TNF-β – tumor necrosis factor-β

U

U – unit(s)

UEA-1 – *Ulex Europaeus-1*

UV – ultraviolet

V

V – volt

vs – versus

v/v – volume per volume

vWF – von Willebrand factor

W

w/ – with

w/o – without

wt/v – weight per volume

LIST OF FIGURES

LIST OF TABLES

SHORT CURRICULUM VITAE

Silvia Maria Mihaila was born on the 15th of August 1984 in Brasov, Romania. She is currently a Marie Curie Postdoctoral fellow at the Department of Urology (Radboud University Medical Center, Netherlands).

Regarding previous education, she received her BSc degree in 2008 in Physics and Chemistry from the Faculty of Science and Materials' Engineering, Transilvania University, Brasov, Romania, with a final grade of 9/10. In 2007 she spent 6 months at Department of Chemistry of the Science and Technology Faculty, Coimbra University, Portugal, developing hydrogel membranes for the controlled delivery of porphyrinic agents used in the photodynamic therapy of cancer, under the supervision of Profs Artur J.M. Valente and Abílio J.F.N. Sobral.

In April 2008 she started to work as a junior researcher at the Faculty of Science and Technology, New University of Lisbon, Portugal in the development of biomaterials with on/off controlled release features, under the supervision of Prof. Ana Aguiar Ricardo.

In October 2008, she started pursuing her PhD in Bioengineering Systems under the scope of the MIT-Portugal Program. The first year of the Doctoral Program was focused on providing strong knowledge in Innovation and Leadership, as other areas of bioengineering from biomaterials and nanotechnology to stem cell research.

In this first year she was involved in the Bio-teams project (innovation project), in which students engaged in establishing go-to-market strategies for technologies developed within the main Portuguese research centers.

In September 2009, she started her PhD research at the 3B's Research Group, at University of Minho, Portugal, under the supervision of Prof. Manuela Gomes and Dr. Alexandra Marques. Her worked was focused in identifying and exploring the potential of cellular subsets of adipose tissue together with the use of new biomaterials, in the development of novel approaches in addressing the vascularization of bone tissue constructs.

Between 2011 and 2012 she was a visiting student at the Khademhosseini Lab, at Harvard-MIT Division of Health Sciences and Technology (HST), MA, USA, developing photocrosslinkable hydrogels and exploring the potential of inorganic nanoplatelets as osteoinducers for the osteogenic differentiation of stem cells.

As a result of her research work, Silvia Mihaila is the author refereed journals (5 published and 1 submitted), 1 book chapter and 3 communications in international conferences.

LIST OF PUBLICATIONS

The present thesis is based on the following publications:

International refereed journals

1. Mihaila SM, Gaharwar AK, Reis RL, Khademhosseini A, Marques AP, Gomes ME, "Silicate nanoplatelets enhance the osteogenic differentiation of SSEA-4 positive selection of human adipose derived stem cells", Biomaterials 2014, 35(33): 9087-99, doi: 10.1016/j.biomaterials.2014.07.052 (***IF: 8.31***).

2. Mihaila SM, Popa EG, Reis RL, Marques AP, Gomes ME, "Fabrication of endothelial cell-laden carrageenan microfibers for microvascularized bone tissue engineering applications", Biomacromolecules 2014, 15(8): 2849-60, doi: 10.1021/bm500036a (***IF: 5.37***).

3. Mihaila SM, Resende MF, Reis RL, Gomes ME, Marques AP, "Co-culture of single source derived endothelial and pre-osteoblasts cells: optimization of culture medium and cell ratio", submitted 2014

4. Gaharwar AK*, **Mihaila SM***, Swami A, Patel A, Sant S, Reis RL, Marques AP, Gomes ME, Khademhosseini A, "Bioactive silicate nanoplatelets for osteogenic differentiation of human mesenchymal stem cells", Advanced Materials 2013, 25(24): 3329–36, doi: 10.1002/adma.20130058 ***(IF=15.41.)***

This paper was highlighted in science media (Harvard Gazette and Science Daily: http://ht.ly/l1E35) as a current hot topic in tissue engineering

5. Mihaila SM, Gaharwar AK, Reis RL, Marques AP, Gomes ME, Khademhosseini A, "Photocrosslinkable kappa-carrageenan for tissue engineering applications", Advanced Healthcare Materials 2013, 2(6): 895-907 doi: 10.1002/adhm.201200317 (***IF=4.88***).

This paper has been given coverage in the online MaterialView platform for emerging research (http://www.materialsviews.com/tissue-engineering-scaffolds-from-natural-polymers/) and was ranked as the 2nd most downloaded paper from Advanced Healthcare Materials Journal for the month of June 2013.

6. Mihaila SM, Frias AM, Pirraco RP, Rada T, Reis RL, Gomes ME, Marques AP, "Human Adipose tissue-derived SSEA-4 sub-population multi-differentiation potential towards the endothelial and osteogenic lineages", Tissue Engineering part A, 19(1-2): 235-46, doi: 10.1089/ten.TEA.2012.0092 (***IF=4.25***).

Book chapters:

1. Mihaila SM, Reis RL, Marques AP, Gomes ME, “Hydrogels in bone tissue engineering: a multi-parametral approach” in “Application of Hydrogels in Regenerative Medicine”, 2013

COMMUNICATIONS IN INTERNATIONAL CONFERENCES:

Oral Presentations:

1. Mihaila SM, Popa EG, Reis RL, Marques AP, Gomes ME, “3D fiber based platform to control cell-cell interactions for bone vascularization approaches”, Society for Biomaterials (SFB), Boston, USA, 2013

2. Mihaila SM, Gaharwar A, Reis RL, Marques AP, Gomes ME, Khademhosseini A, “Methacrylated kappa-carrageenan as a photocrosslinkable biopolymer for tissue engineering applications”, Biomedical Engineering Society (BMES), Atlanta, USA, 2012

3. Mihaila SM, Frias AM, Pirraco RP, Rada T, Reis RL, Gomes ME, Marques AP, “Adipose tissue-derived SSEA-4 sub-population differentiation towards the endothelial lineage”, Sociedade Portuguesa de Células Estaminais e Terapia Celular (SPCE-TC), Caldas das Taipas, Guimarães, Portugal, 2010

Poster Presentations:

1. Mihaila SM, Gaharwar A, Reis RL, Marques AP, Gomes ME, Khademhosseini A, “Tailoring kappa-carrageenan properties for tissue engineering applications”, MIT Engineering System Division-Polymer Day, Boston, USA, 2011

Mihaila SM, Coutinho DF, Reis RL, Marques AP, Gomes ME, “Methacrylated kappa-carrageenan as a photocrosslinkable polymer”, Frontiers in Biomedical Polymers (FBPS), Madeira, Portugal, 2011

2. Mihaila SM, Frias AM, Pirraco RP, Rada T, Reis RL, Gomes ME, Marques AP “Human Adipose tissue-derived SSEA-4 sub-population can be differentiated towards the Endothelial and osteogenic lineages”, International Society for Stem Cell Research (ISSCR), Toronto, Canada, 2011

3. Mihaila SM, Frias AM, Pirraco RP, Rada T, Reis RL, Gomes ME, Marques AP, “Adipose tissue-derived SSEA-4 sub-population demonstrates promising features for bone tissue engineering”, TERMIS-NA, Orlando, USA, 2010

4. Mihaila SM, Frias AM, Pirraco RP, Rada T, Reis RL, Gomes ME, Marques AP “Adipose tissue-derived SSEA-4 sub-population demonstrates promising features for bone tissue engineering”, 2nd Meeting of the Institute for Biotechnology and Bioengineering (IBB), Braga, Portugal, October, 2010

TRAINING

1. NSF Summer Institute Short Course on Materiomics, May 2011, Boston, USA.

2. 3rd Marie Curie Cutting Edge Practical Training Course, September 2009, 3B's Research Group, Braga, Portugal.

3. Certification in "Supercritical Fluids-Green Solvents in Chemical Engineering" Life Long Learning Intensive Course, June 2008, Thessaloniki, Greece.

SECTION I

REVIEW OF LITERATURE

Chapter I

Hydrogels in Bone Tissue Engineering: a Multi-Parametric Approach

ABSTRACT

Hydrogels have gained interest as templates in bone tissue engineering, essentially due to their resemblance to tissues extracellular matrix. In fact, due to their high hydration state, they provide a suitable environment for cell encapsulation, growth and differentiation, as well as active ingredients loading and release. However, they lack mechanical stability and ability to calcify. This chapter will review the multi-parametric aspects considered in the design of hydrogels as template for bone regeneration, by exploring current strategies aimed at improving hydrogels mineralization and consequently bone regeneration. Moreover, design tools for the introduction of micro-architectural features and generation of shape controlled tissue modules based on hydrogel matrices, will be also analyzed, with particular emphasis on targeting neovascularization, i.e., on the use of hydrogels as supportive templates for *in situ* development of vascular networks.

This chapter is based on the following publication:

Mihaila SM, Reis RL, Marques AP, Gomes ME, "Hydrogels in Bone Tissue Engineering: a Multi-Parametric Approach", book chapter in "Applications of Hydrogels in Regenerative Medicine", 2013, Editors: Mohammad Reza Abidian, Umut Atakan Gurkan and Faramarz Edalat

I.1. INTRODUCTION

Bone is a complex supporting tissue with functions in the movement and in the maintenance of postural stability in cooperation with muscles. Despite its hard structure, bone exists in a constant state of dynamic turnover, known as remodeling, even when growth and modeling of the skeleton have been complete[1,2]. It is estimated that approximately 6% of all human bones are remodeled in a year[3]. However, upon injury, the quality of life of patients dramatically changes. The burden of severe long-term pain and limitation in performing basic tasks, such as walking, frequently causes social and psychological distress. Even though bone has a notable regenerative ability, a considerable bone loss and a hostile microenvironment, as it happens in the case of severe trauma, tumors resection, surgical revisions or developmental deformities, can hinder this capacity[4].

Despite decades of intensive research, the grafting of autologous bone derived from the iliac crest remains the gold standard of bone replacement treatments. Unfortunately, the amount of available bone graft is limited and the surgical harvesting involves sever donor-site pain and morbidity, which can be as high as 25%[5]. Moreover, besides being an expensive procedure, some complications, such as bone non-unions and blood loss[6,7], may occur thus requiring additional medical procedures. Cadavers allogeneic bone grafts have been used as alternatives providing a structural host tissue to grow. Nonetheless, albeit avoiding donor-site morbidity, these grafts possess low osteoinductive properties[8] and their success is often jeopardized due to infections, transmitted diseases, delayed inosculation and immunogenicity issues[9].

The significant clinical shortcomings of auto/allografts have been a strong impetus for the development of alternative approaches for bone replacement and regeneration. Worldwide, approximately 2.2 million bone graft procedures (autologous or banked bone) take place annually[9], and these numbers are expected to grow due to aging population. The bone graft substitute market was evaluated at $1.9 billion in 2010 and is forecast to reach $3.3 billion in 2017. The main driving force of the market is the increase in orthopedic procedures, aging population and increased preference of emerging bone graft substitutes over auto/allografts. Demineralized bone matrix (DBM), produced by the extraction of the mineral content from allogeneic bone, contains growth factors and proteins relevant to the bone microenvironment[10]. Whilst the osteoinductive effect of DBM has been well documented in animal studies, there are merely few reports on human clinical studies[11], as its-heterogeneity has an impact on DBM properties and clinical performance[12]. The increased interest in providing robust solutions has nourished the expansion of the researchers vision towards understanding the complex and multi-parametric aspects of bone regeneration (mechanics, chemistry, biological components, integration) using bio-inspired parameters for designing new bone substitutes.

The avenue of tissue engineering (TE) explores these facets of bone repair/healing by the use of cells, scaffolds and in some instances biological factors combinations towards the replacement, repair or restoration of function of a damaged tissue[8,13,14]. The selection of the most suitable material to produce the scaffolds to be used in bone TE is a determinant step towards achieving appropriate mechanical support, biocompatibility, proper integration with the host tissue, osteoinductive, osteoconductivity, among others. Several materials, such as metals[15], ceramics[16], and polymeric systems[17], have been proposed for bone replacement, but in the context of TE, the poor degradability of ceramic scaffolds and the non-degradability of metallic compounds impairs new bone tissue ingrowth. Polymers, on the other hand, are known for enabling the design of their chemistry and architecture during synthesis and processing, thus allowing tailoring 3D scaffolds degradation rate to match the regeneration/repair rate of the tissue to be replaced.

Until recently, the majority of the polymeric bone substitutes were pre-fabricated constructs that require surgical implantation via invasive procedures. Clinically, there is an increased demand for materials that can be implanted under minimally invasive procedures, such as a simple injection[18,19]. Ideally, the viscosity of such materials should be low enough to allow its injection within the defect site and consequent hardening after injection taking advantage of mild crosslinking routines. This strategy would enable the incorporation of drugs, cells, and growth factors in the viscous solution before administration[20]. From a TE standpoint, and considering that within natural tissues cells are embedded in a tri-dimensional (3D) network combining a complex extracellular matrix (ECM), soluble bioactive factors products of homo- and hetero-typical cell-cell and cell-ECM interactions[21], microenvironments that closely mimic those features are prone to successfully lead tissue regeneration. Various 3D templates based on hydrogels, that provide biomimetic environments depicting motifs inspired by the role of ECM in regulating bone regeneration, have been proposed[22,23,24]. Such matrices are conceived to integrate bone tissue and facilitate regeneration by potentiating the bone's inherent capacity to heal, thus acting as *in situ* bioreactors.

In this chapter, the bone matrix deposition and mineralization requirements will be presented in the perspective of using hydrogels as 3D templates with tunable properties that may fulfill these specifications. First, a brief overview on the bone biology and the dynamic role of ECM in bone remodeling/regeneration will be provided. Subsequently, this chapter will focus on strategies to engineer ECM-mimicking hydrogels by using inorganic components, matrix chemistry, spatial cells distributions and growth factors as elements of multi-parametric approaches towards a successful bone TE outcome.

I.2. BONE REGENERATION FEATURES

I.2.1. A snapshot on bone biology and ECM role in regeneration

Bone is a specialized connective tissue that is exquisitely designed as the load-bearing structure of the body. Its configuration, consisting in a combination of a dense, compact structure (cortical bone) with a highly porous one (cancellous/trabecular bone), provides the main resources to accomplish this task. Cortical bone makes up to 80% of the total bone mass in adults and comprises an extremely dense mineral structure, mainly hydroxyapatite, (HA), derived from calcium phosphates (CaPs)[25], with low porosity (20%) and high mechanical compressive strength (190 MPa)[26] and an elastic modulus of around 20 GPa[27]. The functional unit of cortical bone structure is represented by the osteon that contains central haversian hollow canals that host nerves and blood vessels[28]. In contrast, cancellous bone, which accounts for the remaining 20% of the total bone mass[29], does not have osteons, due to the high porosity (50-90%) and surface area that encourages a superior penetration of blood microvessels. Due to its sponginess feature, the cancellous bone is characterized by low mechanical properties (~10MPa)[26] and an elastic modulus of around 15 GPa[27]. Cancellous bone is mainly constituted of type I collagen and small amounts of non-collagenous proteins (NCPs) such as osteocalcin (OCN), osteopontin (OPN), osteonectin (ONC), bone sialoproteins (BSPs), and bone morphogenetic proteins (BMPs)[30,31]. It has been demonstrated that collagen serves as an organic template or framework for bone mineralization and provides the bone tensile strength and flexibility[32], while the anionic NCPs act as nucleators or inhibitors of mineral deposition[31,33]. Recent studies have identified a polysaccharide-enriched matrix, such as glycosaminoglycans (GAGs), at the organic-mineral interface in bone[34], with important role in both bone formation and bone homeostasis, possibly guiding mineral size, morphology and crystallinity[35]. The carboxyl or sulfate groups of GAGs are thought to contribute to the interfacial interaction and balance between inorganic and organic phase (**Figure I.1**). On the other hand, the inorganic phase contributes to bone stiffness and is responsible for its compressive strength, due to its energy-storing capacity. Although collagen may have less effect on bones biomechanics than inorganic components, it may have a profound effect on bone brittleness[32]. There is evidence that reduction of collagen content can reduce the energy required to cause bone failure (toughness) and increase the fracture risk (osteoporosis)[36].

Bone mineralization is thought to start with the synthesis of the organic matrix that then acts as a template for the deposition of insoluble, dispersed, amorphous CaPs. The formation of CaPs depots is mediated by the presence of calcium-binding moieties and the enzyme-mediated production of free phosphates[37]. The anionic proteins attached to collagen are believed to mediate the stabilization of the amorphous CaPs in the early stage of mineralization and the subsequent formation of nano-sized particles[38]. These precursors

undergo several crystalline phase transitions before reaching a stable crystalline apatitic CaPs, or HA. These nanocrystals act as nucleation sites for further crystal growth until the inorganic, crystalline phase overtakes the template[39].

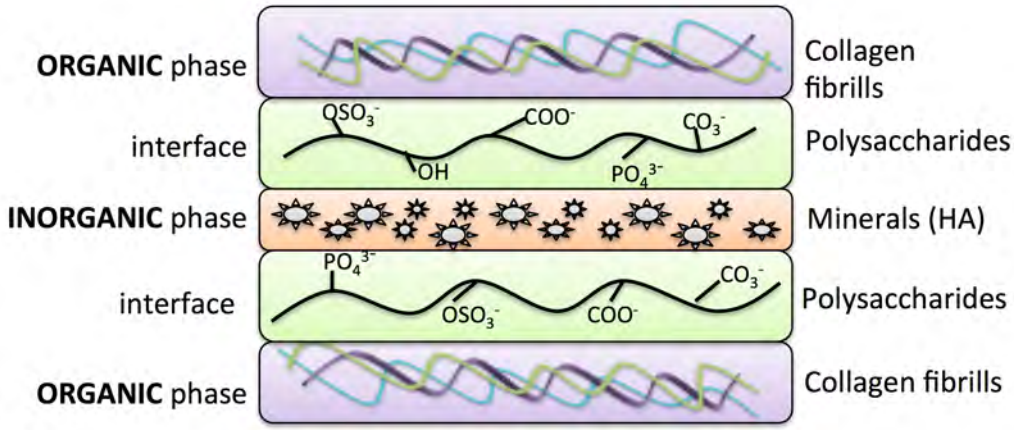

Figure I.1. Recapitulating the bone-matrix composition: representation of the inorganic and organic compartments, as well as the GAGs-enriched region at the organic–mineral interface.

Bone is constantly remodeling its mineralized matrix, which is a complex process that relies on the synchronization of bone resorption and bone deposition events coordinated by cells (osteoprogenitors and differentiated, mature cells) (**Figure I.2**). Within the bone structure relies the bone marrow that comprises of hematopoietic cells and supporting stroma. Until recently, stromal cells were thought to contribute solely to the hematopoietic microenvironment, however, they are now recognized as being progenitor cells of skeletal tissues[40,41] Osteoprogenitor cells (osteoblast precursor cells) found on the internal surface of bones, can be also found on the external side of the bone, in the periosteum[42] and may also reside in the microvasculature supplying bone. They are derived from mesenchymal/stromal stem cells (MSCs) in the bone marrow where they are found in a resting phase. Upon stimulation, these cells can be activated towards secreting and modeling bone matrix. As a consequence, many bone TE strategies rely on the ability of MSCs to commit towards osteogenic lineage and restore the mineralized matrix[43].

Osteoblasts, anchorage dependent cells, are highly responsive to the mechanical and chemical stimuli that are propagated through multiple cell-cell and cell-matrix interactions[44]. During collagen-enriched matrix deposition, osteoblasts secrete bone-related proteins and active factors that trigger the invasion of endothelial cells and the development of a vascular network within the matrix[45,46], concomitant with the matrix mineralization[30]. Osteocytes, terminally differentiated osteoblasts, are entrapped in the mineralized ECM and have an active role in the maintenance of ECM and homeostasis[46]. They are also responsible for sensing the mechanical stress and signaling for bone remodeling[47]. While osteoblasts deposit the organic matrix, osteoclasts that are easily recognized by their multinuclearity, are

responsible for bone breakdown and resorption[48]. Additionally, an unbalanced remodeling can lead to osteoporosis (bone resorption > bone formation) or osteopetrosis (bone resorption < bone formation)[49]. Despite its intrinsic ability to self-regenerate and remodel, inherent osseous processes are not able to repair a large defect. It is therefore mandatory to consider the structural features of ECM along with the biological principles that master the cell-cell and cell-matrix interactions while developing novel strategies towards bone regeneration.

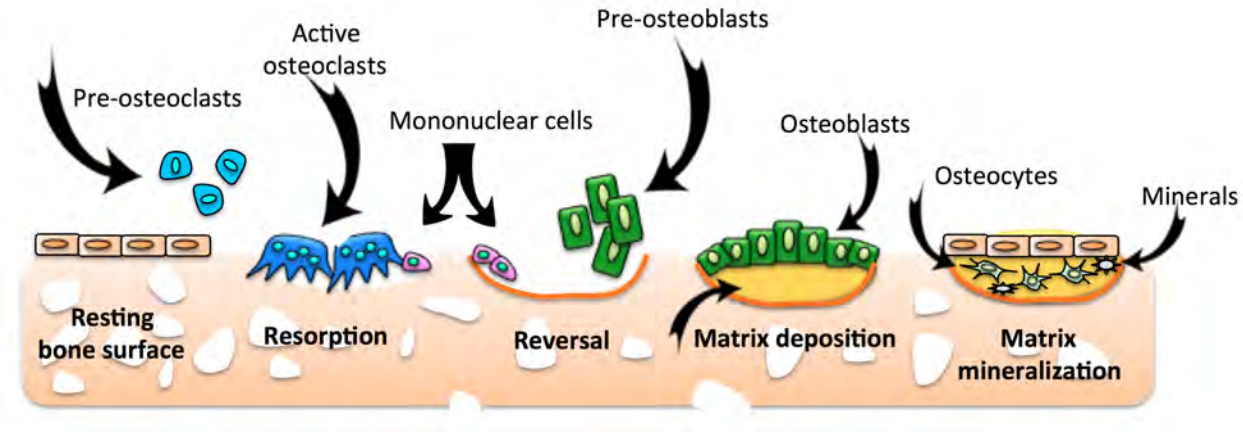

Figure I.2. Bone remodeling cycle orchestrated by the osteo-relevant cells: osteoprogenitors, osteoclasts, osteoblasts and osteocytes. Bone remodeling involves the removal of mineralized bone by osteoclasts followed by the formation of bone matrix through the osteoblasts that subsequently become mineralized. The remodeling cycle consists of three consecutive phases: resorption, during which osteoclasts digest old bone; reversal, when mononuclear cells appear on the bone surface; and formation, when osteoblasts lay down new bone over the area previously remodeled by osteoclasts, until the resorbed bone is completely replaced. The activity of osteoclasts and osteoblasts is controlled by the osteocytes.

I.2.2. Growth factors involved in bone regeneration

Bone regeneration is a multistep process that involves the interplay between several cells such as inflammatory cells, vascular cells, mesenchymal progenitor cells and osteocytes. *In vivo,* their behavior is orchestrated by a specific set of growth factors (GFs) and cytokines that dictate cellular proliferation, migration and differentiation during bone repair[50]. In the first step of bone healing, inflammatory GFs and cytokines, including fibroblast growth factor (FGF), interleukin-1 (IL-1) and -6 (IL-6), macrophage colony-stimulating factor (M-CSF) and tumor necrosis factor-α (TNF-α), are involved in the recruitment of inflammatory cells. As the formation of the fracture callus occurs, high concentrations of pro-osteogenic factors, such as platelet-derived growth factor (PDGF), TGF-β, FGF-1, insulin-like growth factor (IGF), and bone morphogenic proteins (BMPs), stimulate the engagement of mesenchymal progenitor cells and their subsequent proliferation and differentiation. Concomitantly, pro-angiogenic

factors, such as vascular endothelial growth factor (VEGF), FGF, BMPs and TGF-β, trigger the invasion of endothelial cells (ECs) into the newly formed soft callus re-establishing vascular network connection. Additionally, the intimate crosstalk between osteoblasts and ECs is mediated through the release of VEGF by osteoblasts that act on ECs to promote angiogenesis, and through the release of BMPs by ECs, which lead osteogenic differentiation[51]. The role of indirect cellular signaling, through the release of endogeneous GFs, is complemented by the direct cell-cell contact via gap junctions coupling, for example between ECs and osteoblasts[52].

I.3. HYDROGELS

Hydrogels are 3D crosslinked insoluble and hydrophilic polymeric networks that are formed by the reaction of one or more monomers through hydrogen bonds or van der Waals interactions between the constitutive chains[24,53]. The hydrogel network can be fabricated via physical or chemical crosslinking methods. While physical crosslinking is achieved by the formation of physical bonds, the chemical crosslinking consists in the formation of stable covalent bonds, mediated by crosslinking agents, between the polymer chains[54]. Hydrogels can be classified according to their origin (natural or synthetic), method of preparation (homopolymers, copolymers, interpenetrating networks), internal architecture (amorphous, semicrystalline or hydrogen bonded structures) or electric charge (anionic, cationic, neutral, amphiphilic)[24]. In addition, hydrogels exhibit a great versatility for the integration of biomacromolecules or sensitive drugs aimed at directing tissue regeneration. The mild encapsulation options enable the controlled load/release of these active ingredients without jeopardizing their activity (**Figure I.3**). From a practical point of view, there is a number of hydrogels can be implanted using minimally invasive surgical procedures, at the target (injury) site, since they can be applied as a liquid that further hardens *in situ*.

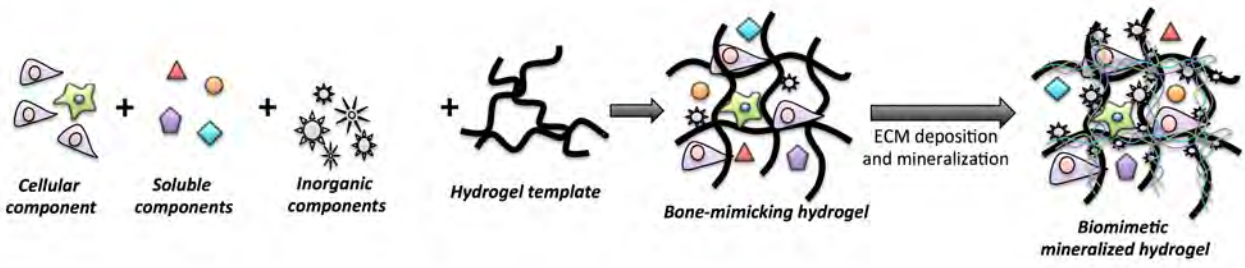

Figure I.3. Hydrogels bear the potential of incorporating cells, bioactive agents and inorganic ingredients, thus, enabling the formation of a 3D biomimetic mineralized bone-like template.

I.3.1. Synthetic vs natural hydrogels

Synthetic hydrogels provide chemically programmable and reproducible platforms as their architecture can be easily tailored, allowing a better control over their properties, such as

degradation, swelling, mechanical performance, bioactivity etc. Polyethylene glycol (PEG) is one of the most extensively used non-degradable polymer for hydrogels fabrication due to its hydrophobicity and facilitated chemical functionalization through available reactive end-chain moieties. Other non-degradable polymers used for bone tissue engineering applications include poly(2-hydroxyethyl methacrylate) (PHEMA)[55] and poly(methyl methacylate) (PMMA)[56]. Polymers such as poly(vinyl alcohol) (PVA)[57], poly(actic-co-glycolic) acid (PLGA)[58], poly(propylene oxide) (PPO)[59], poly(propylene fumarate) (PPF)[60] or oligo(poly(ethylene glycol) fumarate) (OPF)[61] have been also proposed for applications in TE. Worth mentioning are the thermoresponsive polymers, such as poly(N-isopropylacrylamide) (PNIPAAm)[62,63], that are able to form free-standing hydrogels at physiological temperature (37^{o}C), enabling their use as injectable delivery devices without the use of external crosslinkers, that might jeopardize the cellular viability or the activity of growth factors. Even though there is a wide range of synthetic polymers, with tailorable chemical backbone, their use is often limited by biocompatibility issues and poor degradability[64].

On the other hand, natural-origin polymers stand out as nature-inspired bio-entities with attractive biocompatibility and biodegradability features. In fact, these materials are more prone to undergo enzymatic degradation as many of the enzymes responsible for that process are found in the human body. The monomer chemistry, chain length and flexibility enable a unique control of hierarchical organization (macromolecular architecture) and functionality. This molecular print directly influences the crosslinking, gelation and processing/handling properties together with the degradation patterns and cellular response[65]. Hence, there is a wide range of natural-origin polymers (chitosan[66], hyaluronic acid[67], chondroitin sulphate[68], pullulan, dextran[69], alginate[70], xanthan[71], pluronic F127[72], carboxymethyl cellulose[73], carrageenan[74] or gellan gum[75]) that have been intensively investigated under the scope of TE. However, their use is associated with high degrees of variability, limited processing routes or lack of cellular responsive tags, respectively. For both synthetic and natural-origin polymers, the grafting of peptide sequences within their backbone, such as arginine-glycine-aspartate (RGD) or matrix metalloproteinases (MMPs)-sensitive domains, allows modulating the cells attachment, as well as their migration and proliferation within the hydrogel along with its controlled degradation[76].

For a more comprehensive review on natural and synthetic hydrogels used in TE field, please consult other exhisting literature[17,65]. The following section will focus on the current strategies towards the use of hydrogels as templates to sup ort mineralization, blood vessels formation and bone formation.

I.3.2. Hydrogels as ECM mimics

Hydrogels are characterized by their ability to retain large amounts of water or biological fluids (up to 99%), due to the presence of the insoluble 3D polymeric and interconnected microporous network. The aqueous environment enables the oxygen diffusion and fluid transport, such as nutrients and cell metabolic by-products, in and out of the hydrogels[24,77]. This 3D environment facilitates the mastering of biochemical and biomechanical interactions with encapsulated cells. Moreover, by grafting functional groups, specific cellular processes such as adhesion, spreading, proliferation, differentiation and consequent matrix deposition and organization can be triggered. These features resemble those of the native ECM, therefore, hydrogels have been increasingly considered as candidate materials for TE applications. For instance, protein-based scaffolds or hydrogels, such as collagen[78,79], gelatin[80,81] and fibrin[82] are very attractive due to their ability to mimic the ECM biodegradability and inherent biochemical properties.

Recently, it has been also proposed obtaining hydrogels incorporating DBM, as it contains GFs, NCPs and type I collagen, key elements of the bone ECM. In order to facilitate handling, formulation and reliable delivery in clinical applications, the DBM particles were incorporated into water-soluble gels, such as the hyaluronic acid[83] or carboxymethylcellulose[84]. Sawkins *et al.* proposed the processing of DBM as a soluble, hydrogel-like formulation, to avoid the use of liquid carriers. The DBM processing involved a mineral extraction in acid conditions, followed by lyophilization steps. Further, the DBM was dissolved in pepsin and the gelation of the DBM pre-gel solution occurred within at 37^{o}C, upon pepsin neutralization. The DBM hydrogels exhibited sigmoidal gelation kinetics (formation of collagen aggregates at higher concentration) consistent with the nucleation and growth mechanism found in bone[85]. However, further studies need are required to assess the osteoinductivity and osteoconductivity of these hydrogels, and where their *in vitro* potential can be translated into *in vivo* settings.

Meanwhile, bone TE strategies have extensively exploited the glycan components (GAGs) to address the formation and maintenance of bone tissue. The carboxyl or sulfate groups of GAGs are thought to contribute to the interfacial interaction and balance between inorganic and organic phase. The resemblance of some polysaccharides with GAGs chemistry has enabled their use as templates for bone mineralization[66]. Several GAGs-analogs were proposed for bone tissue engineering, such as chitosan[66], hyaluronic acid[67], chondroitin sulphate[68], pullulan and dextran[69], together with other biomaterials (alginate[70], xanthan[71], pluronic F127[72], carboxymethyl cellulose[73], carrageenan[74] or gellan gum[75]).

TE approach aims at replicating the interactions that naturally occur in the bone tissue by using ECM-like structures (scaffolds), cells and/or growth factors in a coordinated fashion to achieve a biomimetic construct. Moreover, these scaffolds should be finely tailored towards

mimicking the intricate and organized ECM meshwork into a dynamic native microenvironment (**Figure I.4**).

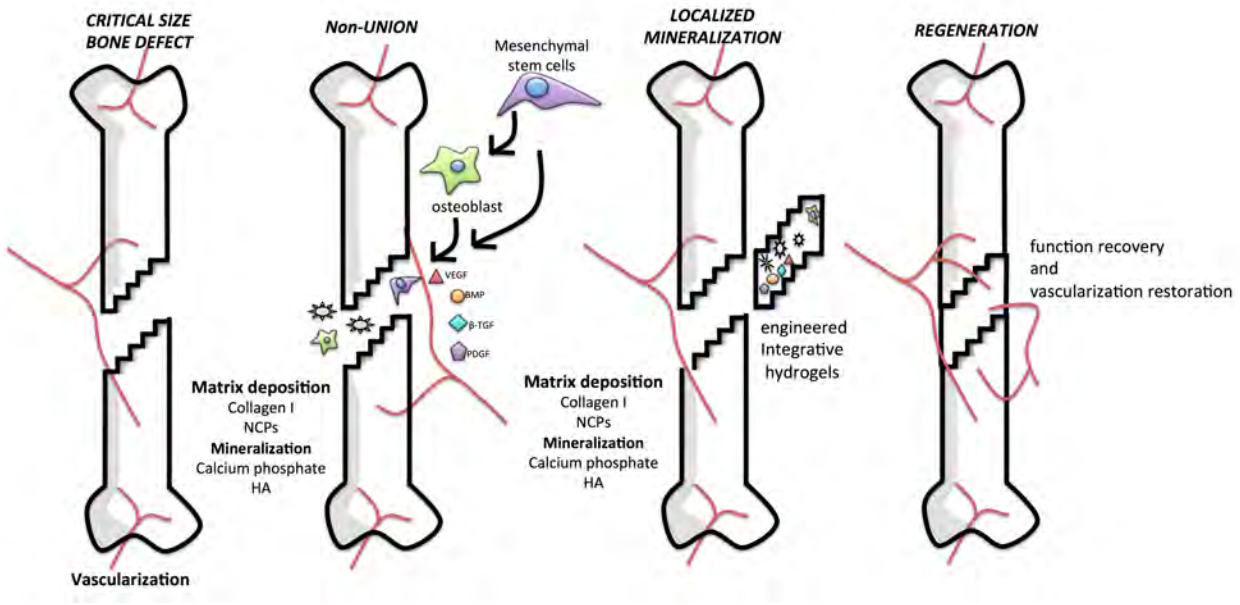

Figure I.4. TE approach for the bone regeneration and restoration of vascularization, including a multi-faceted strategy: cells, inorganic components, soluble factors and 3D matrix.

I.4. HDYROGELS MINERALIZATION

The development of bone-like composites with improved mechanical and biomineralization features calls for a biomimetic approach inspired in natural bone. The use of hydrogels as modular scaffolds has been mainly considered for soft TE (skin, cartilage, cardiovascular applications), however, their versatility has resulted in increased interest in assessing their potential to replicate the organic phase involved in bone healing together with acting as templates for mineralization. Still, hydrogels are associated with a number of limitations, such as their lack of mineralization capacity upon implantation[64], or the inherent poor mechanical properties that restrict their use to non-load-bearing applications[86]. However, the network biomimetic reinforcement can be achieved by the addition of other phases[64,87,88] or other approaches, such as chemically-, GFs- or cell- induced mineralization, which will be briefly discussed below.

I.4.1. Incorporation of inorganic components in hydrogels

The concept of combining hydrogels with inorganic components for bone tissue engineering is inspired by the composite nature of bone itself. As it happens during bone healing, inorganic elements act as seeds for HA formation, enabling and reinforcing the integration with host surrounding bone tissue[89]. The hydrated state of hydrogels permits the initiation of apatite deposition by the heterogeneous nucleation of apatite induced by the phosphate, silica and calcium ions dissolved from the ceramic components[38,90]. While hydrogels can

provide an excellent 3D template to foster cell growth and ECM deposition, the presence of inorganic minerals enables their osteoconductivity (i.e. supporting the bone formation) by acting as substrates with high affinity for proteins and GFs, which directly affects the adhesion, proliferation and differentiation of progenitor cells. Moreover, the addition of inorganic particles, by reinforcing the network strength, has been shown to increase hydrogels stiffness, in turn known to play a role in cell differentiation, including towards the osteogenic lineage[91]. Nonetheless, due to the elasticity of the hydrogel network and facilitated handling, brittle ceramic particles can be delivered in a moldable or injectable formulation. For instance, Oliveira *et al.*[73] evaluated the potential of carboxymethylcellulose, hydroxypropylmethylcellulose and alginate hydrogels as injectable HA microspheres carriers, using an orthopedic injectable device designed for minimal invasive bone surgeries.

There are many nano- and microstructured bioactive inorganic materials, such as bioglasses or apatitic CaPs (hydroxyapatite, HA) that can be used to render mineralized hydrogels. These materials form a strong bond with naturally occurring HA, present at the implantation site[92], enabling a smooth integration of the implant with the host bone tissue. Bioglasses are amorphous solids containing silica (SiO_2<60 w%) that are bioactive due to their high reactivity in aqueous environments. The most commonly used forms of CaPs are β-tricalcium phosphate (β-TCP), amorphous calcium phosphates and apatitic calcium phosphate (HA). These ceramic materials strongly resemble the nanostructured mineral phase of bone and are found in many normal and pathological calcified tissues in the human body[93]. In addition, carbonated apatites have a buffering effect on the acidic pH caused by the degradation by-products, thus minimizing excessive acid environment and inflammation at the implantation/injury site[94].

In fact their combination with varied biomaterials and 3D structures aiming at bone regeneration has been following different strategies with interesting outcomes, recently and thoroughly reviewed[95,96,97].

Recently, carbon nanotubes (CNTs) and graphene[98] were proposed as reinforcing agents of hydrogels, due to their outstanding mechanical properties. For instance, the rod-like shape and nanoscale dimensionality of CNTs allow the morphological mimicking of fibrillar (rod-like) proteins, such as collagen, present in bone ECM, thus, acting as guiding templates for mineral deposition[99,100]. Even more, the combination of nano-scaled single walled CNTs with biomimetic features and HA nanoparticles significantly enhanced the mechanical properties of a chitosan hydrogel and synergistically improved osteoblasts adhesion and proliferation[101]. Despite of being inert materials that cannot be mineralized, recent studies showed that graphene-based hydrogels promote cell adhesion, spreading and proliferation, and stimulate the osteogenic differentiation of stem cells, without additional inducers[97]. Graphene based hydrogels were shown to preserve the osteogenic differentiation of

encapsulated bone marrow MSCs, under hypoxic conditions[102]. When subcutaneously implanted in rats, the graphene films produced minimal capsule formation and mild host tissue response, with evidence of blood vessel formation and mineralization[97]. Thus, the nano-scale biomimetic features of these systems, together with the hydrogel 3D structure, created a favorable environment to support *in vitro* osteogenic differentiation of cells and *in vivo* mineralization.

I.4.2. Soaking / incubation treatments

Within the bone TE context, bioactive materials stand out as preferred candidates for development of bone-mimicking constructs, due to their ability to induce and sustain apatite deposition in physiological relevant conditions. If the organic polymer is provided with apatite-forming ability, it is expected to dynamically resemble the organic phase of bone.

In literature, several *in vitro* methods have been developed to induce the spontaneous mineralization of biomaterials or to assess whether a certain material composition undergoes biomimetic mineralization. Amongst these methods, the soaking/incubation of materials in mineralization baths has gained considerable interest. With the development of simulated body fluid (SBF), a polyionic mixture, that contains polyelectrolytes in concentrations nearly equal to those found in human plasma[103], biomimetic processes to deposit/coat apatite on organic polymers have been proposed. The biomineralization process is based on the consumption of Ca^{2+} and PO_4^{3-} ions, present in the SBF solution, thus, resulting in the spontaneous growth of bone-like apatite nuclei on the surface of biomaterials. Additionally, testing the apatite-forming abilities of biomaterials enables to predict their mineralization behavior *in vivo* after implantation. In fact, the bioactivity assessment, under SBF treatment, is a pre-requisite for screening material compositions as suitable for bone TE. Noteworthy, the outcome of an SBF treatment is highly depended on the composition of the formulation – either the chemical backbone possesses functional groups that sustain the biomimetic mineralization or the formulation contains CaPs precursors (already discussed in section I.4.1) that act as nucleation sites towards apatite deposition.

For instance, knowing that carboxyl groups (–COOH) have a catalytic effect for heterogeneous apatite nucleation in SBF, Ichibouji *et al.*[104] prepared hydrogels from various pectins containing –COOH groups. The authors report differences in the amount of bound calcium and mineral formation and suggest that the apatite-forming ability of the pectin gels is governed by not only the amount of carboxyl groups, but also changes in Ca^{2+} concentration and pH in surrounding solutions.

Similarly, Zainuddin *et al.* showed the formation of a 0.5µm apatitic layer on the surface of chemically defined PHEMA hydrogels upon immersion in SBF[105]. The calcification process

occurred predominantly through spontaneous precipitation of CaPs. Reducing the relative number of oxygen atoms in the copolymers had a direct effect of early calcification, however, there were no differences in the extent of mineralization for prolonged soaking times. In the case of poly(ethylene imine) (PEI), the crosslinked hydrogels were shown to be efficient templates for CaPs deposition in SBF. In contrast, the non-crosslinked PEI did not lead to the phosphate nucleation and its subsequent growth in SBF[106]. The authors suggested that the un-crosslinked PEI is more protonated, and thus can release more protons, leading to the decrease of the local pH and, in consequence, a higher solubility of CaPs, hindering its precipitation.

Despite the promising results, a limitation of using soaking treatments is the deposition of the apatitic layer only at the interface between SFB and the hydrogel substrate. The incorporation of CaPs precursors in the hydrogel during its formation allows a homogeneous distribution of bioactive aagents throughout the entire structure. Upon immersion in SBF, these precursors act as nucleation sites or inorganic “seeds” that lead to *in situ* formation of HA and further crystal growth. The addition of inorganic agents (detailed in section I.4.1.) is one of the most popular method to introduce nucleation sites within inert hydrogels. As an example, Couto *et al.*[107] developed thermo-responsive hydrogels with bioactive features based on the combination of chitosan (CHT) / beta-glycerophosphate (βGP) and bioactive glass nanoparticles. A CaPs-like layer was detected at the surface of the hybrid hydrogels, however, at a closer view, crystalline deposits were detected in the interior of the hydrogels, indication that the mineralization occurred beyond their surface.

Alternatives to the addition of inorganic agents during hydrogel formation, involve the diffusion of Ca^{2+} and PO_4^{3-} ions that triggers the *in situ* deposition of CaPs. For instance, Azami *et al.*[108] employed a double diffusion method whereby $CaCl_2$ and Na_2PO_4 diffused in a gelatin hydrogel to form amorphous CaP in the bulk interior of the gel. Subsequent incubation into SFB lead to the maturation of the mineral phase into nanocrystalline hydroxyapatite. Similarly, the development of nano-structured composites in alginate hydrogels was achieved by *in situ* crystallization of HA in the presence of $CaCl_2$ and Na_2HPO_4[109]. The nano-sized crystals were evenly distributed in the hydrogel network, while the crystal size and morphology could be controlled by the material properties.

Concluding, entrapping precursor phases inside a hydrogel that result in their biomimetic conversion to nano-crystalline HA, is an attractive strategy for *in vivo* applications, as the crystal maturation process with SBF can be reproduced within the body. It should be mentioned that mineralization by incubation in SBF can be significantly enhanced by either functionalizing the chemical backbone with negatively charged moieties (see section I.4.4) or by incorporating biomacromolecules with calcium-binding domains, such as casein, fibroin and alginate (see section I.4.5).

I.4.3. Alkaline phosphatase-mediated mineralization

The formation of *in situ* mineralization nucleation sites within hydrogels, catalyzed by enzymes that trigger its temporal and spatial development is becoming a route of great interest to generate matrices for bone regeneration [110].

Alkaline phosphatase (ALP) is an important player in bone remodeling that acts as a catalyst in initiating calcification. More specifically, the catalytic mechanism involves the cleavage of phosphates from organic phosphomonoesters, thereby increasing the local concentration of inorganic phosphates that act as mineralization promoters, resulting into an enzyme-mediated deposition of carbonated apatite[111,112]. At the same time, the catalytic nature of ALP extends to the role of decreasing the concentration of extracellular pyrophosphates that acts as inhibitors of apatite crystal growth. Consequently, ALP loaded hydrogels constitute not only an alternative to CaPs enriched matrices, in which the CaPs tend to aggregate[113,114], but also work as *in situ* self-promoter of mineralization[61,75,115]. Although the harsh processing conditions of ALP-surface coated implants might compromise its activity, the entrapment of ALP into hydrogels during gelation was proved to be mild enough to preserve ALP initial catalytic activity[61]. In a similar approach, ALP was immobilized on PHEMA using a copolymerization method that did not affect the enzyme catalytic activity. As a result, after immersion in SFB for 17 days, mineralized depots could be observed[116]. Moreover, due to its molecular weight, 185 kDa[117], and the reduced pore size of hydrogels, ALP release by diffusion[61] and loss of active component at the injury site where the hydrogel was applied is significantly hindered. After ALP incorporation, gels were incubated in a calcium glycerophosphate (Ca-GP) solution. Ca-GP diffused into the hydrogel, where under the action of ALP, phosphate was released which reacted with calcium ions to form CaPs. Incorporating ALP into gellan gum led to the formation of CaPs and increased in the stiffness of the matrix. The functionalization with polydopamine of ALP-loaded gellan gum hydrogels, not only improved the previous outcomes, but also enhanced cellular attachment and the cytocompatibility of the mineralized gels[75].

Xie *et al*.[118] incorporated osteinductive HA particles into an alginate hydrogel matrix with physically immobilized ALP and showed that ALP-mediated mineralization provided a homogeneous mineral distribution, smaller crystal size, enabling the increase of Young's moduli. Using a functionalized peptide amphiphile hydrogel matrix that resembles the scaffolding framework of natural collage, together with ALP, it is possible to drive the controlled spatial distribution of the enzyme-mediated nucleation sites and consecutively, templating the HA deposition. Even more, due to the role of ALP to control temporal variables in bone mineralization, Spoerke *et al.* proved that both spatial and temporal elements are essential to achieve *in vitro* mineralization[110].

Moreover, it was shown that ALP induced the mineralization with CaP of injectable thermosensitive CHT/ βGP hydrogels while accelerating their gelation, which is an attractive feature for clinical applications[115]. The mechanism in which ALP accelerated the gelation process can be explained by the potential of ALP to split β-GP into phosphate ions and glycerol, which can promote the ionic and hydrophobic interactions between the chitosan chains, in turn promoting gel formation, concomitantly with their reaction with Ca^{2+}, leading to *in situ* formation of CaPs[61].

In a similar manner, mineralization of collagen type I, PEG- or OPF-derived hydrogels was achieved by physically immobilizing ALP and, subsequently, soaking them in a Ca^{2+} and β-GP containing solutions, that acted as substrates for ALP. When OPF hydrogels were implanted in a rat subcutaneous model, only those containing immobilized ALP were able to induce mineralization[119]. Specifically, small mineral deposits were observed at the periphery of the hydrogels near the dermis/scaffold interface, as a consequence of the ALP release. However, the covalent bonding of ALP constitutes an advantage over the physical immobilization of ALP and incorporation of inorganic particles within the hydrogel that are easily diffused to the transplantation site, thus reducing the expected level of mineralization. Therefore, ALP was covalently linked to dentine-derived collagen sheets to induce their mineralization, which was confirmed upon subcutaneous implantation in rats[120]. Similarly, covalently bonded ALP-fibrin scaffolds were shown to promote a significant increase in the percentage of bone volume per total volume when compared with the empty defect *in vivo* bone formation in a mouse calvarial defect[121].

Finally, ALP has also been used as a screening agent for assessing the mineralizability of novel hydrogel systems. Gongormus *et al.* used ALP-mediated mineralization to evaluate the mineral formation in several formulations of a self-assembled peptide hydrogels[122].

I.4.4. Functionalization of hydrogels

Another approach that has been proposed to induce hydrogels mineralization is the functionalization of their side chains or backbone polymers with negatively charged moieties such as carboxyl ($COOH^-$), hydroxyl (OH^-) or phosphate (PO_4^{3-}) groups. The rationale relies on mimicking the biomineralization mechanism that naturally occurs during bone healing, when NCPs calcium-binding proteins, generally negatively charged (acidic or phosphorylated)[33], act as nucleation sites for apatitic nanocrystals growth. The anionic domains attract Ca^{2+} that, subsequently, leads to an ionic saturation that triggers the CaP precipitation. Similarly, by alternating sequences of PO_4^{3-}, $COOH^-$ or OH^- moieties along the polymeric chain of the hydrogels, it is possible to decorate the hydrogel with apatitic-nucleating properties. Thus, the chemical modification of hydrogels with anionic functional groups enables the development of hydrogel with the ability to nucleate mineralization.

The modification of a PEG diacrylate (PEGDA) hydrogel with photoreactive phosphate-containing molecule, ethylene glycol methacrylate phosphate (EGMP), lead to the formation of a mineral phase throughout the hydrogel, capable of sequestring osteopontin which then promoted MSCs adhesion and spreading[123]. Similarly, PEG hydrogels modified with phosphoesters groups were able to drive extensive and uniform mineralization upon immersion in osteogenic medium for 3 weeks[124], while PEG hydrogel having pendant side chains terminating in –COOH were shown to act as templates for mineralization. However, the ability of these hydrogels to undergo template mineralization was found to be strongly depended on the length of the side chain, which directly influenced the hydrophobicity of the material, a design parameter that needs to be taken into consideration for the development of bone-like materials[125].

The introduction of hydroxyl-containing silanol (Si-OH) in injectable PNIPAAm-PEG dimethacrylate copolymer initiated apatite formation[90]. The extent of Si-OH content enabled the system to be tuned in regard to the compressive moduli that can range from 50 to 700kPa without altering the thermo-responsiveness ability of the hydrogels. These hydrogels provided Ca^{2+} bonding sites and induced subsequent mineralization when soaked in SBF. The challenge of this material system is to balance the network-forming and modulus-enhancing copolymer, while maintaining an injectable hydrogel for potential tissue regeneration.

By manipulating the structure and density of mineral-nucleating ligands presented on the hydrogels, Song *et al.* prepared libraries of PHEMA-based copolymerized with functional groups[38]. This study showed that synthetic organic matrices could be integrated with biominerals with varied affinity, morphology and cristallinity. Strong adhesion between the organic and inorganic phases was achieved for hydrogels functionalized with either carboxylate of hydroxyl ligands. The mineral-nucleating potential of hydroxyl-conjugated matrices broadened the design parameters for the development of bone-like composites and control over the material performance.

I.4.5. Biomacromolecules-driven mineralization

The primary amino acids sequence of the NCPs found in bone, BSP, OPN, OCN, ONC, includes a high density of aspartic and glutamic acids residues, which have a high affinity towards Ca^{2+} ions[39]. A wide range of naturally occurring biomacromolecules, such as proteoglycans, GAGs[126], and casein[96] or fibroin[127], possess calcium-binding domains. Considering the hydrogel matrix as a bone ECM substitute, biomacromolecules can be immobilized within the matrix where they act as “ionic pumps” and encourage the formation of nucleation sites, thus enabling the initiation of apatitic mineral deposition and subsequent mineralization. For instance, casein, a calcium carrier phosphoprotein found in milk, lead to

the mineralization of PHEMA hydrogels to which was physically immobilized[128]. Interestingly, nucleation sites of CaPs deposits in the form of nano-scaled nodules (20-30nm) were observed exclusively in the casein-enriched domains.

The interpenetrating network (IPN) formed by embedding silk fibroin in 3D polyacrylamide (PAA) networks allowed the deposition of apatitic-like minerals, when the hydrogels were immersed in SFB. The hydrogels were uniformly covered with a mineral layer whose morphology depended on their composition. A higher content of silk fibroin within the hydrogel (30/70, 50/50) led to a more uniform coating of the surface with an apatite-like mineral phase. However, increasing the silk fibroin:PAA ratio led to a decrease in the compressive strength of the gels (from 151 kPa for pure PAA to 62kPa for 50/50 ratio) due to the increased swelling of the hydrogel matrix[129]. Recently, Lin *et al*.[130] proposed a ABA triblock copolymeric hydrogel with both thermoresponsive and mineralization properties. PNIPAAm was chosen as the stimuli-responsive outer blocks due to its phase transition temperature, while phosphorylated poly(acrylic acid) was designed as the B block of the copolymer, due to its high affinity towards calcium ions, that benefit the biomineralization process. These hydrogels were shown to have a self-mineralization capability after being incubated in SBF for 2 weeks, thus leading to *in situ* HA deposition.

Alginates are one example of glycans with great affinity to calcium ions. A series of systems have been developed by the addition of alginate to hydrogels to promote mineralization in which alginate acts as a permeable organic matrix that supports the deposition of the minerals, while arresting the Ca^{2+} and PO_4^{3-} ions inside the polymeric “cages”[131]. Gelatin, a denaturated form of collagen, was modified through intrinsic interactions with different concentrations of calcium-binding alginate, leading to the formation of porous IPN hydrogels[131]. The apatite-forming ability was favored by the increase of the alginate:gelatin ratio. In a similar manner, Cha et al. covalently incorporated negatively charged methacrylated alginate (MAlg) in poly(propylene glycol)monomethacrylate (PPGmM), so that charge density, hydrophobicity and pore size of the hydrogels could be separately controlled with mass fraction of MAlg and PPGmM. The authors highlighted that not only charge density (existence of Ca^{2+} binding sites), but also the hydrophobicity and pore size of the hydrogel are major variables to be considered in the integrative design of a 3D mineralized matrix that allow one to identify osteon variables, critical for bone development and repair. However, this should be preceded by studies that relate these hydrogel screening formulations to the incorporated amounts of apatite[132].

I.4.6. Peptide-mediated mineralization

In a similar fashion as presented in the section above, peptidic sequences, with calcium binding affinity, can be conjugated on the hydrogel backbone, however, there are also

hydrogel formulations that are based exclusively on polymerized polypeptides. The versatility of the peptide design allows the synthesis of hydrogels with specific chemistries and architectures that enable the tuning of the properties of the molecular matrix towards different behaviors[133], such as cell adhesion, proliferation and differentiation.

The incorporation of bioactive peptide motifs such as RGD is one of the most popular route to enhance functionality, while proteolytically degradable peptide motifs (such as those recognized by cell-secreted MMPs, is a common approach to address biodegradability to levels that are more in tune with tissue remodeling and regeneration[134]. For instance, when MSCs were cultured with MMPs domain containing hyaluronic acid hydrogels, the osteogenic differentiation occurred accompanied by an intense mineralization of the matrix. However, switching to a less permissive matrix (without MMPs-domains), the differentiation of MSCs was shifted towards adipogenesis[135].

The combination of RGDs with MMPs is mandatory to render the networks to be degraded, *via* cell-secreted MMPs, and easily invaded by cells. Bone regeneration was shown to depended on the proteolytic sensitivity of these matrices that assist the MMP-mediated invasion of cells, as it affects their spreading, migration and organization[136]. For example, MMP-sensitive hyaluronic acid hydrogels loaded with BMP-2 and MSCs demonstrated to promote the highest mature bone formation in a calvaria defect[137], when compared with hydrogel without MMPs-sensitive domain, with or without BMP-2.

More recently, the incorporation of other biological components of the ECM, such as GAGs, and, in particular, heparin is yielding interesting results[133]. On the other side, there are strategies that focus on peptidic hydrogels with sequences that allow the dissolution of inorganic particles or calcium sequestration and subsequent mineralization. For example, Amosi *et al.* designed β-sheet-forming amphiphilic peptides rich in aspartic acid residues and carboxyl groups (P_{FD}-5) to improve bone regeneration by β-TCP particles[138]. This peptide hydrogel formulation was found to accelerate the dissolution of β-TCP, while acting as efficient Ca^{2+} depots, and induce the osteoblast differentiation *in vitro*. The in vivo studies in a rat distal femoral model showed a stronger regeneration capacity obtained in those defects treated with β-TCP-loaded hydrogels, indicating that the peptidic hydrogels and the mineral synergistically act to enhance bone regeneration, in the same range as the performance of matrices presenting cell-binding motifs or loaded with GFs.

Nonoyama *et al.* synthesized two β-sheet peptides with one ($(LE)_8$) or two glutamic acid residues ($(VEVSVKVS)_2$) per molecule, respectively, that self-assembled into nanofibers and formed a hydrogel structure in the presence of calcium ions[139]. The viscoelastic properties of both formulations increased with the addition of Ca^{2+} ions, reaching values that were compatible to their use as bone fillers, which potentiate their application to a defined injectable scenario. Then phosphate ions were added to the calcium containing $(LE)_8$,

amorphous calcium phosphate was formed along the peptide fiber at neutral pH. On the other hand, $(VEVSVKVS)_2$ hydrogels enabled the deposition of HA, at basic pH. Besides providing a template for mineralization, calcium ions increased the mechanical performance of both formulations, which had a direct influence over the cristallinity of HA.

I.4.7. Growth factor-mediated mineralization

In order to assess bone regeneration both in vitro and in vivo, numerous studies have elaborated hydrogel-based systems that allow the release of BMP-2 in a controlled manner, by manipulating the network properties. Solorio *et al.* encapsulated recombinant BMP-2 (rhBMP-2) within gelatin hydrogel microspheres (2-6μm diameter) with different crosslinking degrees to induce bone formation using hMSCs. These authors showed that higher degrees of crosslinking of the gelatin resulted in higher loading efficiency and slower release rate. The release of rhBMP-2 from the microspheres caused a three- to eight-fold increase in the expression of BSP sialoprotein[140]. Even more, the release kinetics of GFs can be adjusted by the hydrogel diffusion properties. For instance, Ludmila *et al.* showed that rhBMP-2-loaded hyaluronic acid hydrogels produced a more osteoinductive response when compared to a chitosan one of similar design[141]. However, it should be noted that, although more bone formation was observed in the hyaluronic acid hydrogel, the bone formed in the chitosan formulation was described as being in a more mature state with significantly higher levels of calcification. This increase in maturation within the chitosan/rhBMP-2 hydrogels was attributed to the more rapid breakdown of the hydrogel leading to a faster release of the rhBMP-2. In a further study conducted by the same group, the rhBMP-2 CHT hydrogel was supplemented with -TCP, which improved the osteoinduction at the cost of slower mineralization with more overall bone growth observed, but less mineralization. They attributed this effect to the slower release of rhBMP-2 from the scaffold due to the affinity of rhBMP-2 to bind to β-TCP[142]. Furthermore, since the complex process of in vivo bone regeneration involved the interaction of multiple GFs and cytokines, the combined delivery of multiple factors has attracted researcher's interest. The association of the osteinductive activity of BMPs with the effect of other growth factors has been shown to enhance bone formation in vivo. Simmons *et al.* showed that the combination of BMP-2 and TGF-β3 in RGD-alginate hydrogels, results in a synergistic effect to enhance bone formation in a mice model[143], that was not observed when GFs were delivered separately. In another study, Raiche *et al.*[144] used a two-layered gelatin hydrogel to obtain combined and sequential delivery of the BMP-2 and IGF-I. The early delivery of BMP-2 followed by increase release of BMP-2 and IGF-I after 5 days, resulted in the largest mineralized content. Even more, simultaneous delivery of both GFs did not significantly change ALP activity or matrix calcium content.

Recently, platelet-rich plasma (PRP) has been studied as a promising alternative source of bioactive agents that can be release in physiological concentrations. Upon activation, when PRP is called platelet lysates (PLs), releases a wide range of biologically relevant proteins, including GFs, such as PDGF, TGF-β, bFGF and VEGF among others. In fact, in combination with thrombin, PRP forms gel-like that can be exogenously applied to tissues to promote wound healing, bone growth, and tissue sealing due to the cocktail of GFs. Moreover, PLs are becoming attractive for bone regeneration, as they promote cell growth, differentiation and recruitment[145]. Santo *et al.* proposed PLs loaded chondroitin sulphate-chitosan hydrogels for the enhancement of cellular viability, proliferation and calcium deposition, suggesting an increased osteogenic differentiation of MSCs[68]. Even more, PLs hold the potential of inducing the formation of a vascular network through the release of VEGF, simultaneously with that of BMP-2[146].

I.5. BOTTOM-UP /INTEGRATIVE APPROACHES

Bottom-up approaches comprise bio-inspired strategies to reproduce the hierarchical architecture of natural bone tissue by mimicking its microstructural features. Single units at micro- or nano-scale that serve as building blocks for further assembling have been used to construct spatially controlled structures. These modular units can be created by cell sheeting, cell-laden microfabrication or 3D direct cell-loaded hydrogel printing, and assembled in such a way to mimic the native microstructural repeating biofunctional unit of the bone tissue, which is the osteon[147]. The osteon is comprised of a dense collagen network impregnated with inorganic precursors and NCPs. During bone formation, the organization of collagen into osteon-like structures enables hydroxyapatite deposition. These multifaceted aspects, allow the integrative spatio-temporal relations between bone organic matrix and hydroxyapatite mineral deposition. Osteon organization has inspired for example, a strategy in which osteoblast-like cells were seeded on dense collagen/chitosan hydrogel matrices that replicate the 3D fibrillar collagen pattern, and that showed to enhance bone-like hydroxyapatite production[148,149]. Similarly, Xu *et al.*[150] developed a multi-functional substrate for bone formation based on a fiber-reinforced laminated hydrogel nanocomposite system aimed at mimicking the laminar structures (osteons) of bone. Layers of electrospun poly(L-lactide) fiber mesh were coated with poly(lactide-co-ethylene oxide fumarate) (PLEOF) hydrogel precursor solution, previously loaded with HA and grafted with RGD sequences to create local adhesion sites for MSCs. Subsequently, these layers were stacked, pressed together and crosslinked to produce a laminated fiber-reinforced composite with osteoinductive and cell adhesive properties. The lamination dramatically increased the Young modulus up to 570±130 MPa, within the range of wet human cancellous bone, when compared with the moduli of the hydrogel (0.5±0.07 MPa) or fiber

mesh (140±3 MPa), alone. However, these values are still below the elastic moduli of the native osteon lamellae (7-22.5GPa)[151]. The RGD-PLEOF hydrogel provided a bimodal degradation profile: a slow degradation rate for structural stability and a fast degradation rate of the hydrogel that was substituted by ECM deposited by the differentiating cells.

I.5.1. Patterning hydrogels

Micromolding and photolithography of hydrogels has been frequently used to generate 3D cell-laden microgel units. Micromolding of hydrogels uses poly(dimethyl siloxane) (PDMS) molds microfabricated with a variety of shapes and sizes. In the first step, the pre-polymer solution with encapsulated cells is casted over the PDMS mold, followed by the crosslinking by changing pH, temperature, ionic strength or UV light application to generate a hydrogel with the exact microstructural design of the PDMS molds[147]. As these platforms can provide spatial distribution of biochemical triggers, they may enable, for example, the study of guided tissue (bone) regeneration. For instance, PEG hydrogel micro-patterns (10μm) were deposited on the surface of silicon wafers, in order to create cell anti-adhesive templates, providing a spatial control over cell interactions with the substrate. When loaded with VEGF, the cells aggregated at the boundaries of the PEG pattern and proceeded towards the osteogenic differentiation[152].

Similarly, photolithography allows the transfer of a certain pattern into a hydrogel, by using photomasks with different patterns in specific-localized regions. Using this technology, a pre-polymer solution of a photocrosslinkable hydrogel containing a photoinitiator is placed under a mask and crosslinked under UV light exposure. The hydrogel crosslinks only in the areas under which the photomasks allow the penetration of the UV light, generating microstructural hydrogel modules with determined shape and size[147]. Recently, Jeon *et al.* engineered a novel micro-patterned alginate/PEG hydrogel system to spatially control hydrogel physical properties on the micro-scale by single or dual-crosslinking mechanisms that allowed stiffness patterning, as well. The micro-patterned checkerboard, with single and double crosslinks, allowed the examination of the effect of the size of these hydrogel patterns on the behavior of encapsulated adipose derived stem cells. By manipulating the micro-pattern size and the crosslinking mechanisms, the physical properties of alginate hydrogels were spatially tunable. Thus, as the micro-pattern properties dictated the behavior of encapsulated cells, in the stiffer patterns, cells formed clustered structures, larger for increased pattern size, and differentiated into the osteogenic lineage. Following this approach the local control over cell behavior was achieved ultimately, allowed the engineering of complex bone constructs with dual cell-type using a single stem cell source[153].

By applying photolithography principles it has been also possible to fabricate cell-laden microgels that can be assembled into 3D architectures[154]. So far, the bottom-up assembly of these units provides a powerful and highly scalable approach to form biomimetic 3D tissue constructs that replicate the microstructural organization of native tissue[155].

Another bottom-up approach that has been explored for bone TE is 3D cell, tissue and organ printing, based on rapid prototyping technologies, such as bioplotting, ink jet printing, laser deposition and dispensing tools[156]. The printing of cell-laden hydrogels allows the mimicking of anatomical organization of cells, matrix and bioactive molecules for obtaining functional engineered tissue. To replicate the bone tissue, osteogenic cell-laden alginate hydrogels were deposited using a 3D fiber deposition method, in 0/90 and 0/45:0/90 configurations [156]. By exchanging the printing syringe during deposition, it was possible to print hydrogels strands loaded with different cells (endothelial and MSCs) within a single scaffold, indicating that this 3D fiber deposition system can be suitable for the development of bone grafts containing multiple cell types[157]. The same authors performed an *in vivo* follow-up of printed thermosensitive gelatinous hydrogel loaded with MSCs and endothelial cells, and demonstrated the retention of spatially organized heterogeneous cell organization induced by the printing. The osteogenic differentiation of cells was localized in the parts corresponding to osteoprogenitor cells-loaded hydrogel units, while perfused blood vessels were formed in the endothelial progenitors cell-laden part of the constructs[158].

I.5.2. Gradients in hydrogels

During bone remodeling and regeneration, spatial and temporal gradients regulate various cell behaviors such as proliferation, organization and differentiation. These gradients are often derived from the cell-cell and cell-ECM interactions within the surrounding environment[159]. For instance, the engineering of bone-cartilage interface, referred as osteochondral TE, poses the challenge of addressing both bone and cartilage regeneration into an integrated approach. To date, the most commonly used strategy to engineer an osteochondral construct is the fabrication of a polymer scaffold consisting of two distinct regions, with different properties (porosity, mechanical strength, diffusion and biological performance) to mimic the natural bone and cartilage ECM environments.

Recently, Galperin *et al.*[160] developed an integrated bi-layered scaffold based on degradable poly(hydroxyethyl methacrylate) hydrogels. The first layer was designed with a monodispersed pore size of 38 µm and pore surfaces decorated with HA particles to promote osteogenic differentiation of MSCs, while the second layer had 200µm pores coated with hyaluronan to trigger the articular cartilage regeneration. The bi-layered construct supported the simultaneous matrix deposition and cell growth of two distinct cell populations. Similarly, Kim *et al.*[161] developed a bi-layered composite OPF hydrogel with modulating dual

growth factors release kinetics. IGF-1 and TGF-β3 were loaded in gelatin microparticles that were then embedded in the OPF hydrogel. At 12 weeks post-implantation in a rabbit model, the results showed that the delivery of IGF-1 alone positively affected osteochondral tissue formation, when compared with the dual delivery of GFs. However, this approach does not provide a continuous and smooth transition between the two layers, as it is found in the native osteochondral space. To overcome these drawbacks, Wang *et al.*[162], designed a gradient gel maker to control the continuous bi-directional distribution of growth factors in alginate and silk hydrogels. The gradient distributions of PLGA and silk microspheres loaded with rhBMP-2 and with human recombinant IGF-1 (rhIGF-1), in the silk scaffold, enabled the osteogenic and chondrogenic differentiation of MSCs along the concentration gradients of rhBMP-2 and cross-gradient rhBMP-2/rhIGF-1. However, the MSCs differentiation did not follow the growth factor gradients in alginate scaffold, most likely due to the range and slope of gradients or due to the rapid diffusion of the active ingredients. These findings suggest that besides creating the gradient, the substrate properties need to be tuned in such a way to enable the concentration range and diffusion kinetics most suitable for the desired outcome.

Beside the biochemical cues, matrix mechanics directly affect the cell differentiation. Chatterjee *et al.*[163] developed a combinatorial screening method to rapidly screen the effect of hydrogels stiffness on the osteogenic differentiation of MSCs. A stiffness gradient spanning a 30-fold range in compressive modulus (10 kPa to 300kPa) was created in a 6cm hydrogel slab, by increasing the concentration of photocrosslinkable PEG. The gradients enabled systematic screening of osteoblast differentiation and demonstrated that hydrogels of modulus ≈225 kPa (≈16% PEG by mass) or higher were required for inducing significant mineralization. These results demonstrate that variation of only a material property, stiffness, can be used to induce “graded” osteogenesis and generation of a mineralized tissue gradient that could be applied to integrate hard and soft tissues such as a tendon or a ligament.

I.6. THE VASCULARIZATION HURDLE IN ENGINEERING OF BONE TISSUE

Both cancellous and cortical bone, although presenting different organization, contain a highly vascularized network that is essential to supply nutrients and oxygen to the cells, and remove metabolic by-products. Despite the advances made in bone TE, the classical strategies have been restricted mainly due to the lack of vascularization within the engineered bone analog, resulting in a poor graft integration and failure of the construct upon implantation. In an effort towards clinical success of these constructs, new TE concepts have emerged to incorporate vascular cues and induce vascular network formation within engineered bone constructs in an attempt to recapitulate bone physiology. The need

for a vasculature network is even more demanding when engineering 3D large tissue constructs. Hydrogels have been proposed as delivery vehicles of vascular agents or as matrices that enable the invasion of the hosts own vasculature network into the construct. Among these are: (**1**) directing cellular responses by the release of growth factors and (**2**) microfabricating vascularized microscale structures using single or multiple-cell culturing approaches.

I.6.1. Growth factor delivery

As mentioned above, cells respond to chemical and physical inputs by the activation of a cascade of events that are mediated by growth factors signaling. A number of studies have been attempted to reproduce this signaling process *in vitro* and *in vivo* through the controlled delivery of exogenous growth factors to direct cell behavior and fate. The first clinical trials aimed at assessing strategies for promoting bone formation and neovascularization, included the delivery of VEGF and BMPs at the injury site. However, no significant effects or exhibited limited efficiency[164] were observed, highlight their inability to activate the signaling machinery. The poor outcome of the direct injection was attributed to their mode of delivery, which usually was performed by simultaneous injection of both growth factors, as a bolus. Such uncontrolled delivery of growth factors results in rapid distribution into the body, which translates in systemic and diffused, rather than localized responses. Moreover, the relatively short half time of GFs, might render initial excess levels, followed by a shortage of GFs. Noteworthy, a relatively narrow therapeutic window of GFs dose is expected to target tissue regeneration, whereas extreme doses will most likely lead to severe side effects, as already observed[165]. Moreover, maintenance of constant GFs levels is only potentially achieved with multiple injections or continuous administration; bio-inspired alternative routes have been explored.

In an ideal situation, the localized delivery of GFs should be compatible with physiologically relevant doses and allow preserving their activity for long periods of time. Moreover, the carrier materials should simultaneously foster the communication with host cells in order to play an active role in the regeneration process. The highly swollen 3D networks of hydrogels, have proved to be powerful candidates to fulfill these requirements[166], as they can enable diffusion of relevant GFs, with tunable release profiles, while providing the 3D support for the formation of bone and/or a vascular network. The GFs can be either freely embedded in the hydrogel or covalently bound to the polymer backbone, while the release kinetics can be tailored by alternating the material diffusion coefficient, crosslinking degree, degradation rate or the initial loading dose. For example, the release profile of PDGF from carrageenan hydrogel microbeads matched that of usually required for the development of a fully functional vascular network, that demonstrate the potential of these systems for bone

TE[167]. Even more, the dual delivery of PDGF and VEGF resulted in highly dense and well-established vessel network compared with the bolus injection of either of the growth factors alone[168]. Similarly, PEG diacrylate hydrogels functionalized with heparin were shown to be able to deliver VEGF in a sustained and controlled manner. When implanted in a chick chorioallantoic membrane, the heparin-PEG hydrogel showed superior angiogenic potential in stimulating new blood vessel formation compared with un-functionalized ones, which were characterized by a more rapid release of VEGF[169].

Furthermore, the application of a VEGF/alginate hydrogel in critical–sized defects of rat calvariae resulted in increased blood vessel density, when compare with the bolus delivery. Even though there was no difference in bone regeneration at 4 weeks of implantation, there was a significant increase in bone regeneration in the VEGF/alginate treated defects. This study provides evidence that blood vessel formation is tightly coupled with bone formation[170].

As vascularization underlies the success of guided bone regeneration, the ideal scenario would be to deliver a cascade of multiple GFs to simultaneously induce angiogenesis and mineralization, in order to produce a vascularized bone tissue substitute. The simultaneous delivery of VEGF and BMP-2 from gelatin hydrogels resulted in a synergistic effect, promoting both high osteogenic responses and blood vessel formation in a 8mm rat cranial defect[171]. The effect of sequential delivery of GFs on supportive vascular network formation, in parallel with bone formation was also investigated by Kempen *et al*., who proposed a sequential dual delivery system, inspired by the sequential release of GFs observed during normal bone healing[172]. BMP-2 was loaded in PLGA hydrogel microspheres that were further embedded into a PPF rod by photo-crosslinking. In parallel, a gelatin hydrogel was processed as a tubular implant and impregnated with VEGF before association with the PPF rod previously loaded with BMP-2 loaded microspheres. The system allowed an initial release of VEGF, followed by a sustained release of BMP-2 in later time points. Although VEGF alone did not induce bone formation, it did increase the formation of a supportive vascular network in ectopic implants. In combination with local sustained release of BMP-2, VEGF significantly enhanced ectopic bone formation, when compared to BMP-2 alone[173].

These results indicate that correct GFs types and combinations, and delivery approach (simultaneous or sequential) greatly affect osteogenic differentiation of cells, new bone and blood vessel formation.

I.6.2. Microfabricated hydrogels for vascularized bone TE

Angiogenesis, as a prerequisite for osteogenesis, implies an intimate crosstalk between osteoblast and ECs. The latter self-assemble into vascular tubes when surrounded by ECM and exposed to angiogenic factors, such as VEGF or BMPs. To stabilize the new blood vessels, endothelial cells must functionally interact with mural cells, such as pericytes or

smooth muscle cells that, in turn, provide support and stability. This particularity in terms of rearrangement as functional vascular networks, has been the inspiration model used in microfabrication techniques to design hydrogels structures to generate 3D-vascular–like networks. West *et al.*[174] have decorated PEG hydrogels with RGD sequences to support ECs adhesion and alignment, while the covalent immobilization of VEGF on PEG patterned surfaces, enhanced tubule formation[175]. Nikkhah *et al.* created highly organized endothelial cord structures using micro-patterned methacrylated gelatin (GelMA). The alignment of HUVECs was significantly enhanced within 50µm microchannels and by varying the geometrical micro-features of the GelMA patterns, it was possible to optimize the formation of stable lumen-like structures for more that 2 weeks.

The lumen configuration was reproduced by Lee *et al.*[176] by using a microfluidic device to generate hollow alginate microfibers with different diameters (50-250 µm). These microfibers were loaded with ECs and were further embedded in agar-gelatin-fibronectin hydrogels, to assess the cellular viability and organization. Similarly, Takei *et al.*[177] successfully fabricated artificial endothelized tubes with determined 3D configurations, as starting point for a self-developing capillary-like network in a collagen gel. Briefly, cell-enclosing hydrogel fibers of 250 and 500µm diameters were embedded in a collagen gel and used as templates. The enzymatic degradation of the hydrogels fibers resulted in the development of channels with the fibers 3D configurations. The degradation of the fibers allowed the release of endothelial cells and their adhesion to the collagen gel. Culturing the cells in FGF–enriched medium trigger the migration of ECs in the collagen gel and the self-assembly into capillary-like structures.

The integration of these systems with matrices containing osteoprogenitor cells, osteoblast-like cells, osteo-related GFs or bioactive agents is expected to address the development of a functional vasculature within the bone constructs, concomitant with mineralization and new bone formation. For example, Trkov *et a*l. investigated the functional interactions between hMSCs and endothelial cells, using a simple, yet controllable hydrogel system[178]. Cells were encapsulated in 3D micro-printed fibrin hydrogel channels, to enable precise control of the cellular spatial distribution distance between two cell populations (500-2000 µm). The endothelial cells-secreted factors established a distance-dependent chemotactic gradient in the hydrogel matrix that stimulated directional protrusion of hMSCs within the construct, accompanied by uniform osteogenic differentiation. However, due to the lack of consensus over the appropriate cell combinations and culturing conditions, the hydrogels matrices are merely used as model platforms for the cellular interactions to be tested, limiting their potential applications as heterotypic cells matrices for bone remodeling.

I.7. FINAL REMARKS

The complex organization of bone tissue requires the development of multi-faceted strategies that address its regeneration at all structural and functional levels. This chapter provides insights over the use of hydrogels as potential candidates for bone tissue engineering and regeneration. The highly hydrated state of the 3D network offers significant advantages over traditional ceramic and stiff polymers, in what concern biocompatibility, biodegradability, drug and cell delivery, and injectability. From a clinical standpoint, these features may prevail over hydrogels low mechanical properties and lack of bioactivity. Moreover, current tissue engineering strategies address these disadvantages rendering hydrogels with high controllable mechanical robustness and patterned mineralization features, by (**1**) addition of inorganic phases, (**2**) *in situ* crystallization of hydroxyapatite inside the hydrogels (**3**) enzymatically induced mineralization, (**4**) functionalization of hydrogel with negative moieties or (5) calcium-binding molecules. Moreover, bottom-up approaches have been stimulating scientists as they envisage reconstruction of bone physiology using cell-laden building blocks by spatially controlling cellular and mechanical distribution. Additionally, hydrogels can be engineering in such a way that they acquire the ability to guide the restoration of functional vasculature within the bone tissue-engineered construct, simultaneously promoting functional bone formation.

Ultimately, hydrogels are versatile tools that, through a multi-parametric design, allow the development of functionalized bone analogs that can be easily implanted at the defect/injury site, and further integrated within the host tissue.

REFERENCES

1. Crockett, J.; Rogers, M.; Coxon, F.; Hocking, L.; Helfrich, M., Bone remodelling at a glance. *J Cell Sci* **2011,** *124*, 991-998.
2. Hill, P.; Orth, M., Bone remodelling. *British Journal of Orthodontics* **1998,** *25*, 101-107.
3. Jimi, E.; Hirata, S.; Osawa, K.; Terashita, M.; Kitamura, C.; Fukushima, H., The current and future therapies of bone regeneration to repair bone defects. *International journal of dentistry* **2012,** *2012*, 148261.
4. Gugala, Z.; Gogolewski, S., Healing of critical-size segmental bone defects in the sheep tibiae using bioresorbable polylactide membranes. *Injury* **2002,** *33 Suppl 2*, B71-6.
5. Kim, D. H.; Rhim, R.; Li, L.; Martha, J.; Swaim, B. H.; Banco, R. J.; Jenis, L. G.; Tromanhauser, S. G., Prospective study of iliac crest bone graft harvest site pain and morbidity. *The spine journal : official journal of the North American Spine Society* **2009,** *9* (11), 886-92.
6. Arrington, E. D.; Smith, W. J.; Chambers, H. G.; Bucknell, A. L.; Davino, N. A., Complications of iliac crest bone graft harvesting. *Clinical orthopaedics and related research* **1996,** (329), 300-9.
7. Lohmann, C. H.; Andreacchio, D.; Koster, G.; Carnes, D. L., Jr.; Cochran, D. L.; Dean, D. D.; Boyan, B. D.; Schwartz, Z., Tissue response and osteoinduction of human bone grafts in vivo. *Archives of orthopaedic and trauma surgery* **2001,** *121* (10), 583-90.
8. Laurencin, C.; Khan, Y.; El-Amin, S. F., Bone graft substitutes. *Expert review of medical devices* **2006,** *3* (1), 49-57.
9. Giannoudis, P. V.; Dinopoulos, H.; Tsiridis, E., Bone substitutes: an update. *Injury* **2005,** *36 Suppl 3*, S20-7.
10. Greenwald, A. S.; Boden, S. D.; Goldberg, V. M.; Khan, Y.; Laurencin, C. T.; Rosier, R. N.; American Academy of Orthopaedic Surgeons. The Committee on Biological, I., Bone-graft substitutes:

facts, fictions, and applications. *The Journal of bone and joint surgery. American volume* **2001,** *83-A Suppl 2 Pt 2*, 98-103.
11. De Long, W. G., Jr.; Einhorn, T. A.; Koval, K.; McKee, M.; Smith, W.; Sanders, R.; Watson, T., Bone grafts and bone graft substitutes in orthopaedic trauma surgery. A critical analysis. *The Journal of bone and joint surgery. American volume* **2007,** *89* (3), 649-58.
12. Gruskin, E.; Doll, B. A.; Futrell, F. W.; Schmitz, J. P.; Hollinger, J. O., Demineralized bone matrix in bone repair: history and use. *Advanced drug delivery reviews* **2012,** *64* (12), 1063-77.
13. Langer, R.; Vacanti, J. P., Tissue engineering. *Science* **1993,** *260* (5110), 920-6.
14. Costa-Pinto, A. R.; Reis, R. L.; Neves, N. M., Scaffolds based bone tissue engineering: the role of chitosan. *Tissue engineering. Part B, Reviews* **2011,** *17* (5), 331-47.
15. Niinomi, M., Metallic biomaterials. *Journal of artificial organs : the official journal of the Japanese Society for Artificial Organs* **2008,** *11* (3), 105-10.
16. Samavedi, S.; Whittington, A. R.; Goldstein, A. S., Calcium phosphate ceramics in bone tissue engineering: A review of properties and their influence on cell behavior. *Acta biomaterialia* **2013**.
17. Kohane, D. S.; Langer, R., Polymeric biomaterials in tissue engineering. *Pediatric research* **2008,** *63* (5), 487-91.
18. Jayabalan, M.; Shalumon, K. T.; Mitha, M. K., Injectable biomaterials for minimally invasive orthopedic treatments. *Journal of materials science. Materials in medicine* **2009,** *20* (6), 1379-87.
19. Dreifke, M. B.; Ebraheim, N. A.; Jayasuriya, A. C., Investigation of potential injectable polymeric biomaterials for bone regeneration. *Journal of biomedical materials research. Part A* **2013,** *101* (8), 2436-47.
20. Nguyen, M. K.; Lee, D. S., Injectable biodegradable hydrogels. *Macromolecular bioscience* **2010,** *10* (6), 563-79.
21. Geckil, H.; Xu, F.; Zhang, X.; Moon, S.; Demirci, U., Engineering hydrogels as extracellular matrix mimics. *Nanomedicine (Lond)* **2010,** *5* (3), 469–484.
22. Lutolf, M. P.; Weber, F. E.; Schmoekel, H. G.; Schense, J. C.; Kohler, T.; Muller, R.; Hubbell, J. A., Repair of bone defects using synthetic mimetics of collagenous extracellular matrices. *Nature biotechnology* **2003,** *21* (5), 513-8.
23. Place, E. S.; Evans, N. D.; Stevens, M. M., Complexity in biomaterials for tissue engineering. *Nature materials* **2009,** *8* (6), 457-70.
24. Slaughter, B. V.; Khurshid, S. S.; Fisher, O. Z.; Khademhosseini, A.; Peppas, N. A., Hydrogels in regenerative medicine. *Advanced materials* **2009,** *21* (32-33), 3307-29.
25. Rodan, G. A., Introduction to bone biology. *Bone* **1992,** *13 Suppl 1*, S3-6.
26. Sikavitsas, V. I.; Temenoff, J. S.; Mikos, A. G., Biomaterials and bone mechanotransduction. *Biomaterials* **2001,** *22* (19), 2581-93.
27. Rho, J. Y.; Ashman, R. B.; Turner, C. H., Young's modulus of trabecular and cortical bone material: ultrasonic and microtensile measurements. *Journal of biomechanics* **1993,** *26* (2), 111-9.
28. Hillier, M. L.; Bell, L. S., Differentiating human bone from animal bone: a review of histological methods. *Journal of forensic sciences* **2007,** *52* (2), 249-63.
29. Salgado, A. J.; Coutinho, O. P.; Reis, R. L., Bone tissue engineering: state of the art and future trends. *Macromolecular bioscience* **2004,** *4* (8), 743-65.
30. Hidalgo-Bastida, L. A.; Cartmell, S. H., Mesenchymal stem cells, osteoblasts and extracellular matrix proteins: enhancing cell adhesion and differentiation for bone tissue engineering. *Tissue engineering. Part B, Reviews* **2010,** *16* (4), 405-12.
31. Young, M. F., Bone matrix proteins: more than markers. *Calcified tissue international* **2003,** *72* (1), 2-4.
32. Viguet-Carrin, S.; Garnero, P.; Delmas, P. D., The role of collagen in bone strength. *Osteoporosis international : a journal established as result of cooperation between the European Foundation for Osteoporosis and the National Osteoporosis Foundation of the USA* **2006,** *17* (3), 319-36.
33. Hunter, G. K.; Hauschka, P. V.; Poole, A. R.; Rosenberg, L. C.; Goldberg, H. A., Nucleation and inhibition of hydroxyapatite formation by mineralized tissue proteins. *The Biochemical journal* **1996,** *317 (Pt 1)*, 59-64.
34. Wise, E. R.; Maltsev, S.; Davies, M. E.; Duer, M. J.; Jaeger, C.; Loveridge, N.; Murray, R. C.; Reid, D. G., The organic-mineral interface in bone is predominantly polysaccharide. *Chem. Mater.* **2007,** *19* (21), 5055–5057.
35. Lamoureux, F.; Baud'huin, M.; Duplomb, L.; Heymann, D.; Redini, F., Proteoglycans: key partners in bone cell biology. *BioEssays : news and reviews in molecular, cellular and developmental biology* **2007,** *29* (8), 758-71.

36. Burr, D. B., The contribution of the organic matrix to bone's material properties. *Bone* **2002,** *31* (1), 8-11.
37. Parfitt, A. M., What is bone mineralization? *The Journal of clinical endocrinology and metabolism* **2003,** *88* (10), 5043.
38. Song, J.; Malathong, V.; Bertozzi, C. R., Mineralization of synthetic polymer scaffolds: a bottom-up approach for the development of artificial bone. *Journal of the American Chemical Society* **2005,** *127* (10), 3366-72.
39. Palmer, L. C.; Newcomb, C. J.; Kaltz, S. R.; Spoerke, E. D.; Stupp, S. I., Biomimetic systems for hydroxyapatite mineralization inspired by bone and enamel. *Chemical reviews* **2008,** *108* (11), 4754-83.
40. Shi, S.; Wang, C. Y., Bone marrow stromal stem cells for repairing the skeleton. *Biotechnology & genetic engineering reviews* **2004,** *21*, 133-43.
41. Haynesworth, S. E.; Goshima, J.; Goldberg, V. M.; Caplan, A. I., Characterization of cells with osteogenic potential from human marrow. *Bone* **1992,** *13* (1), 81-8.
42. Nakahara, H.; Goldberg, V. M.; Caplan, A. I., Culture-expanded human periosteal-derived cells exhibit osteochondral potential in vivo. *Journal of orthopaedic research : official publication of the Orthopaedic Research Society* **1991,** *9* (4), 465-76.
43. Owen, M., Marrow stromal stem cells. *Journal of cell science. Supplement* **1988,** *10*, 63-76.
44. Bennett, J. H.; Moffatt, S.; Horton, M., Cell adhesion molecules in human osteoblasts: structure and function. *Histology and histopathology* **2001,** *16* (2), 603-11.
45. Fuchs, S.; Hofmann, A.; Kirkpatrick, C., Microvessel-like structures from outgrowth endothelial cells from human peripheral blood in 2-dimensional and 3-dimensional co-cultures with osteoblastic lineage cells. *Tissue engineering* **2007,** *13* (10), 2577-88.
46. Pirraco, R. P.; Marques, A. P.; Reis, R. L., Cell interactions in bone tissue engineering. *Journal of cellular and molecular medicine* **2010,** *14* (1-2), 93-102.
47. Nomura, S.; Takano-Yamamoto, T., Molecular events caused by mechanical stress in bone. *Matrix biology : journal of the International Society for Matrix Biology* **2000,** *19* (2), 91-6.
48. Teitelbaum, S. L., Bone resorption by osteoclasts. *Science* **2000,** *289* (5484), 1504-8.
49. Lazner, F.; Gowen, M.; Pavasovic, D.; Kola, I., Osteopetrosis and osteoporosis: two sides of the same coin. *Human molecular genetics* **1999,** *8* (10), 1839-46.
50. Makhdom, A. M.; Hamdy, R. C., The Role of Growth Factors on Acceleration of Bone Regeneration During Distraction Osteogenesis. *Tissue engineering. Part B, Reviews* **2013**.
51. Malizos, K. N.; Papatheodorou, L. K., The healing potential of the periosteum molecular aspects. *Injury* **2005,** *36 Suppl 3*, S13-9.
52. Villars, F.; Bordenave, L.; Bareille, R.; Amedee, J., Effect of human endothelial cells on human bone marrow stromal cell phenotype: role of VEGF? *Journal of cellular biochemistry* **2000,** *79* (4), 672-85.
53. Khademhosseini, A.; Langer, R., Microengineered hydrogels for tissue engineering. *Biomaterials* **2007,** *28* (34), 5087-92.
54. Hennink, W. E.; van Nostrum, C. F., Novel crosslinking methods to design hydrogels. *Advanced drug delivery reviews* **2002,** *54* (1), 13-36.
55. De Giglio, E.; Cometa, S.; Ricci, M. A.; Zizzi, A.; Cafagna, D.; Manzotti, S.; Sabbatini, L.; Mattioli-Belmonte, M., Development and characterization of rhVEGF-loaded poly(HEMA-MOEP) coatings electrosynthesized on titanium to enhance bone mineralization and angiogenesis. *Acta biomaterialia* **2010,** *6* (1), 282-90.
56. Jefferiss, C. D.; Lee, A. J.; Ling, R. S., Thermal aspects of self-curing polymethylmethacrylate. *The Journal of bone and joint surgery. British volume* **1975,** *57* (4), 511-8.
57. Ma, Y.; Zheng, Y.; Huang, X.; Xi, T.; Lin, X.; Han, D.; Song, W., Mineralization behavior and interface properties of BG-PVA/bone composite implants in simulated body fluid. *Biomedical materials* **2010,** *5* (2), 25003.
58. Lin, Z. Y.; Duan, Z. X.; Guo, X. D.; Li, J. F.; Lu, H. W.; Zheng, Q. X.; Quan, D. P.; Yang, S. H., Bone induction by biomimetic PLGA-(PEG-ASP)n copolymer loaded with a novel synthetic BMP-2-related peptide in vitro and in vivo. *Journal of controlled release : official journal of the Controlled Release Society* **2010,** *144* (2), 190-5.
59. Rey-Rico, A.; Silva, M.; Couceiro, J.; Concheiro, A.; Alvarez-Lorenzo, C., Osteogenic efficiency of in situ gelling poloxamine systems with and without bone morphogenetic protein-2. *European cells & materials* **2011,** *21*, 317-40.
60. Wang, S.; Lu, L.; Yaszemski, M. J., Bone-tissue-engineering material poly(propylene fumarate): correlation between molecular weight, chain dimensions, and physical properties. *Biomacromolecules* **2006,** *7* (6), 1976-82.

61. Douglas, T. E.; Messersmith, P. B.; Chasan, S.; Mikos, A. G.; de Mulder, E. L.; Dickson, G.; Schaubroeck, D.; Balcaen, L.; Vanhaecke, F.; Dubruel, P.; Jansen, J. A.; Leeuwenburgh, S. C., Enzymatic mineralization of hydrogels for bone tissue engineering by incorporation of alkaline phosphatase. *Macromolecular bioscience* **2012,** *12* (8), 1077-89.
62. Fitzpatrick, S. D.; Jafar Mazumder, M. A.; Lasowski, F.; Fitzpatrick, L. E.; Sheardown, H., PNIPAAm-grafted-collagen as an injectable, in situ gelling, bioactive cell delivery scaffold. *Biomacromolecules* **2010,** *11* (9), 2261-7.
63. Liao, H. T.; Chen, C. T.; Chen, J. P., Osteogenic differentiation and ectopic bone formation of canine bone marrow-derived mesenchymal stem cells in injectable thermo-responsive polymer hydrogel. *Tissue engineering. Part C, Methods* **2011,** *17* (11), 1139-49.
64. Mano, J. F.; Sousa, R. A. B., L.F.; Neves, N. M.; Reis, R. L., Bioinert, biodegradable and injectable polymeric ma- trix composites for hard tissue replacement: state of the art and recent developments. *Composites Science and Technology* **2004,** *64* (6), 789–817.
65. Mano, J. F.; Silva, G. A.; Azevedo, H. S.; Malafaya, P. B.; Sousa, R. A.; Silva, S. S.; Boesel, L. F.; Oliveira, J. M.; Santos, T. C.; Marques, A. P.; Neves, N. M.; Reis, R. L., Natural origin biodegradable systems in tissue engineering and regenerative medicine: present status and some moving trends. *Journal of the Royal Society, Interface / the Royal Society* **2007,** *4* (17), 999-1030.
66. Zhong, C.; Chu, C. C., Biomimetic mineralization of acid polysaccharide-based hydrogels: towards porous 3-dimensional bone-like biocomposites. *Journal of Materials Chemistry* **2012,** *22* (13), 6080–6087.
67. Manferdini, C.; Guarino, V.; Zini, N.; Raucci, M. G.; Ferrari, A.; Grassi, F.; Gabusi, E.; Squarzoni, S.; Facchini, A.; Ambrosio, L.; Lisignoli, G., Mineralization behavior with mesenchymal stromal cells in a biomimetic hyaluronic acid-based scaffold. *Biomaterials* **2010,** *31* (14), 3986-96.
68. Santo, V. E.; Gomes, M. E.; Mano, J. F.; Reis, R. L., Chitosan-chondroitin sulphate nanoparticles for controlled delivery of platelet lysates in bone regenerative medicine. *Journal of tissue engineering and regenerative medicine* **2012,** *6 Suppl 3*, s47-59.
69. Fricain, J. C.; Schlaubitz, S.; Le Visage, C.; Arnault, I.; Derkaoui, S. M.; Siadous, R.; Catros, S.; Lalande, C.; Bareille, R.; Renard, M.; Fabre, T.; Cornet, S.; Durand, M.; Leonard, A.; Sahraoui, N.; Letourneur, D.; Amedee, J., A nano-hydroxyapatite--pullulan/dextran polysaccharide composite macroporous material for bone tissue engineering. *Biomaterials* **2013,** *34* (12), 2947-59.
70. Lima, A. C.; Batista, P.; Valente, T. A.; Silva, A. S.; Correia, I. J.; Mano, J. F., Novel methodology based on biomimetic superhydrophobic substrates to immobilize cells and proteins in hydrogel spheres for applications in bone regeneration. *Tissue engineering. Part A* **2013,** *19* (9-10), 1175-87.
71. Dyondi, D.; Webster, T. J.; Banerjee, R., A nanoparticulate injectable hydrogel as a tissue engineering scaffold for multiple growth factor delivery for bone regeneration. *International journal of nanomedicine* **2013,** *8*, 47-59.
72. Lippens, E.; Vertenten, G.; Girones, J.; Declercq, H.; Saunders, J.; Luyten, J.; Duchateau, L.; Schacht, E.; Vlaminck, L.; Gasthuys, F.; Cornelissen, M., Evaluation of bone regeneration with an injectable, in situ polymerizable Pluronic F127 hydrogel derivative combined with autologous mesenchymal stem cells in a goat tibia defect model. *Tissue engineering. Part A* **2010,** *16* (2), 617-27.
73. Oliveira, S. M.; Almeida, I. F.; Costa, P. C.; Barrias, C. C.; Ferreira, M. R.; Bahia, M. F.; Barbosa, M. A., Characterization of polymeric solutions as injectable vehicles for hydroxyapatite microspheres. *AAPS PharmSciTech* **2010,** *11* (2), 852-8.
74. Popa, E. G.; Caridade, S. G.; Mano, J. F.; Reis, R. L.; Gomes, M. E., Chondrogenic potential of injectable kappa-carrageenan hydrogel with encapsulated adipose stem cells for cartilage tissue-engineering applications. *Journal of tissue engineering and regenerative medicine* **2013**.
75. Douglas, T.; Wlodarczyk, M.; Pamula, E.; Declercq, H.; de Mulder, E.; Bucko, M.; Balcaen, L.; Vanhaecke, F.; Cornelissen, R.; Dubruel, P.; Jansen, J.; Leeuwenburgh, S., Enzymatic mineralization of gellan gum hydrogel for bone tissue-engineering applications and its enhancement by polydopamine. *Journal of tissue engineering and regenerative medicine* **2012**.
76. Zhu, J.; Marchant, R. E., Design properties of hydrogel tissue-engineering scaffolds. *Expert review of medical devices* **2011,** *8* (5), 607-26.
77. Drury, J. L.; Mooney, D. J., Hydrogels for tissue engineering: scaffold design variables and applications. *Biomaterials* **2003,** *24* (24), 4337-51.
78. Guenther, D.; Oks, A.; Ettinger, M.; Liodakis, E.; Petri, M.; Krettek, C.; Jagodzinski, M.; Haasper, C., Enhanced migration of human bone marrow stromal cells in modified collagen hydrogels. *International orthopaedics* **2013**.
79. Wang, L.; Stegemann, J. P., Thermogelling chitosan and collagen composite hydrogels initiated with beta-glycerophosphate for bone tissue engineering. *Biomaterials* **2010,** *31* (14), 3976-85.

80. Liu, X.; Smith, L. A.; Hu, J.; Ma, P. X., Biomimetic nanofibrous gelatin/apatite composite scaffolds for bone tissue engineering. *Biomaterials* **2009,** *30* (12), 2252-8.
81. Ben-David, D.; Kizhner, T. A.; Kohler, T.; Muller, R.; Livne, E.; Srouji, S., Cell-scaffold transplant of hydrogel seeded with rat bone marrow progenitors for bone regeneration. *Journal of cranio-maxillo-facial surgery : official publication of the European Association for Cranio-Maxillo-Facial Surgery* **2011,** *39* (5), 364-71.
82. Lohse, N.; Schulz, J.; Schliephake, H., Effect of fibrin on osteogenic differentiation and VEGF expression of bone marrow stromal cells in mineralised scaffolds: a three-dimensional analysis. *European cells & materials* **2012,** *23*, 413-23; discussion 424.
83. Schwartz Z; Goldstein M; Raviv E; Hirsch A; Ranly DM; BD, B., Clinical evaluation of demineralized bone allograft in a hyaluronic acid carrier for sinus lift augmentation in humans: a computed tomography and histomorphometric study. *Clin Oral Implants Res* **2007,** *18* (2), 204-211.
84. Reynolds MA; Aichelmann-Reidy ME; Kassolis JD; Prasad HS; MD., R., Calcium sulfate-carboxymethylcellulose bone graft binder: Histologic and morphometric evaluation in a critical size defect. *Journal of biomedical materials research. Part B, Applied biomaterials* **2007,** *83* (2), 451-458.
85. Sawkins, M. J.; Bowen, W.; Dhadda, P.; Markides, H.; Sidney, L. E.; Taylor, A. J.; Rose, F. R.; Badylak, S. F.; Shakesheff, K. M.; White, L. J., Hydrogels derived from demineralized and decellularized bone extracellular matrix. *Acta biomaterialia* **2013,** *9* (8), 7865-73.
86. Burdick, J. A., Bioengineering: Cellular control in two clicks. *Nature* **2009,** *460* (7254), 469-70.
87. Khan, Y.; Yaszemski, M. J.; Mikos, A. G.; Laurencin, C. T., Tissue engineering of bone: material and matrix considerations. *The Journal of bone and joint surgery. American volume* **2008,** *90 Suppl 1*, 36-42.
88. Rezwan, K.; Chen, Q. Z.; Blaker, J. J.; Boccaccini, A. R., Biodegradable and bioactive porous polymer/inorganic composite scaffolds for bone tissue engineering. *Biomaterials* **2006,** *27* (18), 3413-31.
89. Boccaccini, A. R.; Blaker, J. J., Bioactive composite materials for tissue engineering scaffolds. *Expert review of medical devices* **2005,** *2* (3), 303-17.
90. Ho, E.; Lowman, A.; Marcolongo, M., In situ apatite forming injectable hydrogel. *Journal of biomedical materials research. Part A* **2007,** *83* (1), 249-56.
91. Rowlands, A. S.; George, P. A.; Cooper-White, J. J., Directing osteogenic and myogenic differentiation of MSCs: interplay of stiffness and adhesive ligand presentation. *American journal of physiology. Cell physiology* **2008,** *295* (4), C1037-44.
92. Kamitakahara, M.; Ohtsuki, C.; Miyazaki, T., Review paper: behavior of ceramic biomaterials derived from tricalcium phosphate in physiological condition. *Journal of biomaterials applications* **2008,** *23* (3), 197-212.
93. Dorozhkin, S. V.; Epple, M., Biological and medical significance of calcium phosphates. *Angewandte Chemie* **2002,** *41* (17), 3130-46.
94. F.Bronner; Farach-Carson, M. C.; Roach, H. I., *Bone- metabolic functions and modulators*. Springer: New York, 2012.
95. Bleek, K.; Taubert, A., New developments in polymer-controlled, bioinspired calcium phosphate mineralization from aqueous solution. *Acta biomaterialia* **2013,** *9* (5), 6283-321.
96. Fan, Z.; Wang, J.; Wang, Z.; Li, Z.; Qiu, Y.; Wang, H.; Xu, Y.; Niu, L.; Gong, P.; Yang, S., Casein Phosphopeptide-Biofunctionalized Graphene Biocomposite for Hydroxyapatite Biomimetic Mineralization. *The Journal of Physical Chemistry* **2013,** *117* (20), 10375−10382.
97. Lu, J.; He, Y.-S.; Cheng, C.; Wang, Y.; Qiu, L.; Li, D.; Zou, D., Self-supporting graphene hydrogel film as an experimental platform to evaluate the potential of graphene for bone regeneration. *Advanced Functional Materials* **2013,** *23* (28), 3494–3502.
98. Shin, S. R.; Bae, H.; Cha, J. M.; Mun, J. Y.; Chen, Y. C.; Tekin, H.; Shin, H.; Farshchi, S.; Dokmeci, M. R.; Tang, S.; Khademhosseini, A., Carbon nanotube reinforced hybrid microgels as scaffold materials for cell encapsulation. *ACS nano* **2012,** *6* (1), 362-72.
99. Kuboki, Y.; Terada, M.; Kitagawa, Y.; Abe, S.; Uo, M.; Watari, F., Interaction of collagen triple-helix with carbon nanotubes: Geometric property of rod-like molecules. *Bio-medical materials and engineering* **2009,** *19* (1), 3-9.
100. Newman, P.; Minett, A.; Ellis-Behnke, R.; Zreiqat, H., Carbon nanotubes: Their potential and pitfalls for bone tissue regeneration and engineering. *Nanomedicine : nanotechnology, biology, and medicine* **2013,** *9* (8), 1139-58.
101. Im, O.; Li, J.; Wang, M.; Zhang, L. G.; Keidar, M., Biomimetic three-dimensional nanocrystalline hydroxyapatite and magnetically synthesized single-walled carbon nanotube chitosan nanocomposite for bone regeneration. *International journal of nanomedicine* **2012,** *7*, 2087-99.
102. S., M.; C., W., Graphene hydrogel and method for using the same. *patent application* **2013,** *US 20130230496 A1*.

103. Kokubo, T.; Takadama, H., How useful is SBF in predicting in vivo bone bioactivity? *Biomaterials* **2006,** *27* (15), 2907-2915.
104. Ichibouji, T.; Miyazakia, T.; Ishida, E.; Sugino, A.; Ohtsuki, C., Apatite mineralization abilities and mechanical properties of covalently cross-linked pectin hydrogels. *Materials Science and Engineering: C* **2009,** *29* (6), 1765–1769.
105. Zainuddin; Hill, D. J.; Whittaker, A. K.; Chirila, T. V., In-vitro study of the spontaneous calcification of PHEMA-based hydrogels in simulated body fluid. *Journal of materials science. Materials in medicine* **2006,** *17* (12), 1245-54.
106. Shkilnyy, A.; Graf, R.; Hiebl, B.; Neffe, A. T.; Friedrich, A.; Hartmann, J.; Taubert, A., Unprecedented, low cytotoxicity of spongelike calcium phosphate/poly(ethylene imine) hydrogel composites. *Macromolecular bioscience* **2009,** *9* (2), 179-86.
107. Couto, D. S.; Hong, Z.; Mano, J. F., Development of bioactive and biodegradable chitosan-based injectable systems containing bioactive glass nanoparticles. *Acta biomaterialia* **2009,** *5* (1), 115-23.
108. Azami, M.; Moosavifar, M. J.; Baheiraei, N.; Moztarzadeh, F.; Ai, J., Preparation of a biomimetic nanocomposite scaffold for bone tissue engineering via mineralization of gelatin hydrogel and study of mineral transformation in simulated body fluid. *Journal of biomedical materials research. Part A* **2012,** *100* (5), 1347-55.
109. Xie, M.; Olderoy, M. O.; Andreassen, J. P.; Selbach, S. M.; Strand, B. L.; Sikorski, P., Alginate-controlled formation of nanoscale calcium carbonate and hydroxyapatite mineral phase within hydrogel networks. *Acta biomaterialia* **2010,** *6* (9), 3665-75.
110. Spoerke, E. D.; Anthony, S. G.; Stupp, S. I., Enzyme Directed Templating of Artificial Bone Mineral. *Advanced materials* **2009,** *21* (4), 425-430.
111. Golub, E. E.; Boesze-Battaglia, K., The role of alkaline phosphatase in mineralization. *Curr. Opin. Orthop.* **2007,** *18*, 444-448.
112. Orimo, H., The mechanism of mineralization and the role of alkaline phosphatase in health and disease. *Journal of Nippon Medical School = Nippon Ika Daigaku zasshi* **2010,** *77* (1), 4-12.
113. Leeuwenburgh, S. C.; Jansen, J. A.; Mikos, A. G., Functionalization of oligo(poly(ethylene glycol)fumarate) hydrogels with finely dispersed calcium phosphate nanocrystals for bone-substituting purposes. *Journal of biomaterials science. Polymer edition* **2007,** *18* (12), 1547-64.
114. Lee, K.; Oh, M. H.; Lee, M. S.; Nam, Y. S.; Park, T. G.; Jeong, J. H., Stabilized calcium phosphate nano-aggregates using a dopa-chitosan conjugate for gene delivery. *International journal of pharmaceutics* **2013,** *445* (1-2), 196-202.
115. Douglas, T. E.; Skwarczynska, A.; Modrzejewska, Z.; Balcaen, L.; Schaubroeck, D.; Lycke, S.; Vanhaecke, F.; Vandenabeele, P.; Dubruel, P.; Jansen, J. A.; Leeuwenburgh, S. C., Acceleration of gelation and promotion of mineralization of chitosan hydrogels by alkaline phosphatase. *International journal of biological macromolecules* **2013,** *56*, 122-32.
116. Filmon, R.; Basle, M. F.; Barbier, A.; Chappard, D., Poly(2-hydroxy ethyl methacrylate)-alkaline phosphatase: a composite biomaterial allowing in vitro studies of bisphosphonates on the mineralization process. *Journal of biomaterials science. Polymer edition* **2000,** *11* (8), 849-68.
117. Bruder, S. P.; Caplan, A. I., A monoclonal antibody against the surface of osteoblasts recognizes alkaline phosphatase isoenzymes in bone, liver, kidney, and intestine. *Bone* **1990,** *11* (2), 133-9.
118. Xie, M.; Olderøy, Ø. M.; Zhang, Z.; Andreassen, J. P.; Strand, B. L.; Sikorski, P., Biocomposites prepared by alkaline phosphatase mediated mineralization of alginate microbeads. *RSC Advances* **2012,** *2*, 1457-1465.
119. Bongio, M.; Nejadnik, M. R.; Birgani, Z. T.; Habibovic, P.; Kinard, L. A.; Kasper, F. K.; Mikos, A. G.; Jansen, J. A.; Leeuwenburgh, S. C.; van den Beucken, J. J., In Vitro and In Vivo Enzyme-Mediated Biomineralization of Oligo(poly(ethylene glycol) Fumarate Hydrogels. *Macromolecular bioscience* **2013,** *13* (6), 777-88.
120. van den Bos, T.; Oosting, J.; Everts, V.; Beertsen, W., Mineralization of alkaline phosphatase-complexed collagen implants in the rat in relation to serum inorganic phosphate. *Journal of bone and mineral research : the official journal of the American Society for Bone and Mineral Research* **1995,** *10* (4), 616-24.
121. Osathanon, T.; Giachelli, C. M.; Somerman, M. J., Immobilization of alkaline phosphatase on microporous nanofibrous fibrin scaffolds for bone tissue engineering. *Biomaterials* **2009,** *30* (27), 4513-21.
122. Gungormus, M.; Branco, M.; Fong, H.; Schneider, J. P.; Tamerler, C.; Sarikaya, M., Self assembled bi-functional peptide hydrogels with biomineralization-directing peptides. *Biomaterials* **2010,** *31* (28), 7266-74.

123. Nuttelman, C. R.; Benoit, D. S.; Tripodi, M. C.; Anseth, K. S., The effect of ethylene glycol methacrylate phosphate in PEG hydrogels on mineralization and viability of encapsulated hMSCs. *Biomaterials* **2006,** *27* (8), 1377-86.
124. Wang, D. A.; Williams, C. G.; Yang, F.; Cher, N.; Lee, H.; Elisseeff, J. H., Bioresponsive phosphoester hydrogels for bone tissue engineering. *Tissue engineering* **2005,** *11* (1-2), 201-13.
125. Phadke, A.; Zhang, C.; Hwang, Y.; Vecchio, K.; Varghese, S., Templated mineralization of synthetic hydrogels for bone-like composite materials: role of matrix hydrophobicity. *Biomacromolecules* **2010,** *11* (8), 2060-8.
126. Embery, G.; Rees, S.; Hall, R.; Rose, K.; Waddington, R.; Shellis, P., Calcium- and hydroxyapatite-binding properties of glucuronic acid-rich and iduronic acid-rich glycosaminoglycans and proteoglycans. *European journal of oral sciences* **1998,** *106 Suppl 1*, 267-73.
127. Marelli, B.; Ghezzi, C. E.; Alessandrino, A.; Barralet, J. E.; Freddi, G.; Nazhat, S. N., Silk fibroin derived polypeptide-induced biomineralization of collagen. *Biomaterials* **2012,** *33* (1), 102-8.
128. Dragusin, D. M.; Giol, D. E.; Serafim, A.; Vasile, E.; Zecheru, T., Casein-PHEMA: in vitro formation of nanometric Ca-P nuclei. *Digest Journal of Nanomaterials and Biostructures* **2011,** *6* (4), 1909-1918.
129. Zaharia, C.; Tudora, M. R.; Stancu, I. C.; Galateanu, B.; Lungu, A.; Cincu, C., Characterization and deposition behavior of silk hydrogels soaked in simulated body fluid. *Materials Science and Engineering: C* **2012,** *32* (4), Pages 945–952.
130. Lin, Z.; Cao, S.; Chen, X.; Wu, W.; Li, J., Thermoresponsive Hydrogels from Phosphorylated ABA Triblock Copolymers: A Potential Scaffold for Bone Tissue Engineering. *Biomacromolecules* **2013,** *14* (7), 2206-14.
131. Stancu, I. C.; Dragusin, D. M.; Vasile, E.; Trusca, R.; Antoniac, I.; Vasilescu, D. S., Porous calcium alginate-gelatin interpenetrated matrix and its biomineralization potential. *Journal of materials science. Materials in medicine* **2011,** *22* (3), 451-60.
132. Cha, C.; Kim, E. S.; Kim, I. W.; Kong, H., Integrative design of a poly(ethylene glycol)-poly(propylene glycol)-alginate hydrogel to control three dimensional biomineralization. *Biomaterials* **2011,** *32* (11), 2695-703.
133. Liu, X.; Wang, X.; Wang, X.; Ren, H.; He, J.; Qiao, L.; Cui, F. Z., Functionalized self-assembling peptide nanofiber hydrogels mimic stem cell niche to control human adipose stem cell behavior in vitro. *Acta biomaterialia* **2013,** *9* (6), 6798-805.
134. Bokel, C.; Brown, N. H., Integrins in development: moving on, responding to, and sticking to the extracellular matrix. *Developmental cell* **2002,** *3* (3), 311-21.
135. Khetan, S.; Guvendiren, M.; Legant, W. R.; Cohen, D. M.; Chen, C. S.; Burdick, J. A., Degradation-mediated cellular traction directs stem cell fate in covalently crosslinked three-dimensional hydrogels. *Nature materials* **2013,** *12* (5), 458-65.
136. Lutolf, M. P.; Lauer-Fields, J. L.; Schmoekel, H. G.; Metters, A. T.; Weber, F. E.; Fields, G. B.; Hubbell, J. A., Synthetic matrix metalloproteinase-sensitive hydrogels for the conduction of tissue regeneration: engineering cell-invasion characteristics. *Proceedings of the National Academy of Sciences of the United States of America* **2003,** *100* (9), 5413-8.
137. Kim, J.; Kim, I. S.; Cho, T. H.; Kim, H. C.; Yoon, S. J.; Choi, J.; Park, Y.; Sun, K.; Hwang, S. J., In vivo evaluation of MMP sensitive high-molecular weight HA-based hydrogels for bone tissue engineering. *Journal of biomedical materials research. Part A* **2010,** *95* (3), 673-81.
138. Amosi, N.; Zarzhitsky, S.; Gilsohn, E.; Salnikov, O.; Monsonego-Ornan, E.; Shahar, R.; Rapaport, H., Acidic peptide hydrogel scaffolds enhance calcium phosphate mineral turnover into bone tissue. *Acta biomaterialia* **2012,** *8* (7), 2466-75.
139. Nonoyama, T.; Ogasawara, H.; Tanaka, M.; Higuchi, M.; Kinoshita, T., Calcium phosphate biomineralization in peptide hydrogels for injectable bone-filling materials. *Soft Matter* **2012,** *8*, 11531-11536.
140. Solorio, L.; Zwolinski, C.; Lund, A. W.; Farrell, M. J.; Stegemann, J. P., Gelatin microspheres crosslinked with genipin for local delivery of growth factors. *Journal of tissue engineering and regenerative medicine* **2010,** *4* (7), 514-23.
141. Luca, L.; Rougemont, A. L.; Walpoth, B. H.; Gurny, R.; Jordan, O., The effects of carrier nature and pH on rhBMP-2-induced ectopic bone formation. *Journal of controlled release : official journal of the Controlled Release Society* **2010,** *147* (1), 38-44.
142. Lewandrowski, K. U.; Hile, D. D.; Thompson, B. M.; Wise, D. L.; Tomford, W. W.; Trantolo, D. J., Quantitative measures of osteoinductivity of a porous poly(propylene fumarate) bone graft extender. *Tissue engineering* **2003,** *9* (1), 85-93.
143. Simmons, C. A.; Alsberg, E.; Hsiong, S.; Kim, W. J.; Mooney, D. J., Dual growth factor delivery and controlled scaffold degradation enhance in vivo bone formation by transplanted bone marrow stromal cells. *Bone* **2004,** *35* (2), 562-9.

144. Raiche, A. T.; Puleo, D. A., In vitro effects of combined and sequential delivery of two bone growth factors. *Biomaterials* **2004,** *25* (4), 677-85.
145. Visser, L. C.; Arnoczky, S. P.; Caballero, O.; Kern, A.; Ratcliffe, A.; Gardner, K. L., Growth factor-rich plasma increases tendon cell proliferation and matrix synthesis on a synthetic scaffold: an in vitro study. *Tissue engineering. Part A* **2010,** *16* (3), 1021-9.
146. Wahlstrom, O.; Linder, C.; Kalen, A.; Magnusson, P., Acidic preparations of platelet concentrates release bone morphogenetic protein-2. *Acta orthopaedica* **2008,** *79* (3), 433-7.
147. Nichol, J. W.; Khademhosseini, A., Modular Tissue Engineering: Engineering Biological Tissues from the Bottom Up. *Soft Matter* **2009,** *5* (7), 1312-1319.
148. Silvent, J.; Nassif, N.; Helary, C.; Azais, T.; Sire, J. Y.; Guille, M. M., Collagen osteoid-like model allows kinetic gene expression studies of non-collagenous proteins in relation with mineral development to understand bone biomineralization. *PloS one* **2013,** *8* (2), e57344.
149. Chicatun, F.; Pedraza, C. E.; Ghezzi, C. E.; Marelli, B.; Kaartinen, M. T.; McKee, M. D.; Nazhat, S. N., Osteoid-mimicking dense collagen/chitosan hybrid gels. *Biomacromolecules* **2011,** *12* (8), 2946-56.
150. Xu, W.; Ma, J.; Jabbari, E., Material properties and osteogenic differentiation of marrow stromal cells on fiber-reinforced laminated hydrogel nanocomposites. *Acta biomaterialia* **2010,** *6* (6), 1992-2002.
151. Bensamoun, S.; Fan, Z.; Brice, I.; Rho, J. Y.; Ho Ba Tho, M. C., Assessment of mechanical properties of human osteon lamellae exhibiting various degrees of mineralization by indentation. *Journal of Musculoskeletal Research* **2008,** *11* (3), 135-143.
152. Subramani, K.; Birch, M. A., Fabrication of poly(ethylene glycol) hydrogel micropatterns with osteoinductive growth factors and evaluation of the effects on osteoblast activity and function. *Biomedical materials* **2006,** *1* (3), 144-54.
153. Jeon, O.; Alsberg, E., Regulation of Stem Cell Fate in a Three-Dimensional Micropatterned Dual-Crosslinked Hydrogel System. *Adv. Funct. Mater.* **2013**.
154. Qi, H.; Ghodousi, M.; Du, Y.; Grun, C.; Bae, H.; Yin, P.; Khademhosseini, A., DNA-directed self-assembly of shape-controlled hydrogels. *Nature communications* **2013,** *4*, 2275.
155. Du, Y.; Lo, E.; Ali, S.; Khademhosseini, A., Directed assembly of cell-laden microgels for fabrication of 3D tissue constructs. *Proceedings of the National Academy of Sciences of the United States of America* **2008,** *105* (28), 9522-7.
156. Fedorovich, N. E.; Alblas, J.; Hennink, W. E.; Oner, F. C.; Dhert, W. J., Organ printing: the future of bone regeneration? *Trends in biotechnology* **2011,** *29* (12), 601-6.
157. Fedorovich, N. E.; De Wijn, J. R.; Verbout, A. J.; Alblas, J.; Dhert, W. J., Three-dimensional fiber deposition of cell-laden, viable, patterned constructs for bone tissue printing. *Tissue engineering. Part A* **2008,** *14* (1), 127-33.
158. Fedorovich, N. E.; Wijnberg, H. M.; Dhert, W. J.; Alblas, J., Distinct tissue formation by heterogeneous printing of osteo- and endothelial progenitor cells. *Tissue engineering. Part A* **2011,** *17* (15-16), 2113-21.
159. Sant, S.; Hancock, M. J.; Donnelly, J. P.; Iyer, D.; Khademhosseini, A., Biomimetic Gradient Hydrogels for Tissue Engineering. *The Canadian journal of chemical engineering* **2010,** *88* (6), 899-911.
160. Galperin, A.; Oldinski, R. A.; Florczyk, S. J.; Bryers, J. D.; Zhang, M.; Ratner, B. D., Integrated bi-layered scaffold for osteochondral tissue engineering. *Advanced healthcare materials* **2013,** *2* (6), 872-83.
161. Kim , K.; Lam, J.; Lu, S.; Spicer, P. P.; Lueckgen, A.; Tabata, Y.; Wong, M. E.; Jansen, J. A.; Mikos, A. G.; Kasper, F. K., Osteochondral tissue regeneration using a bilayered composite hydrogel with modulating dual growth factor release kinetics in a rabbit model. *Journal of controlled release : official journal of the Controlled Release Society* **2013,** *168* (2), 166-178.
162. Wang, X.; Wenk, E.; Zhang, X.; Meinel, L.; Vunjak-Novakovic, G.; Kaplan, D. L., Growth factor gradients via microsphere delivery in biopolymer scaffolds for osteochondral tissue engineering. *Journal of controlled release : official journal of the Controlled Release Society* **2009,** *134* (2), 81-90.
163. Chatterjee, K.; Lin-Gibson, S.; Wallace, W. E.; Parekh, S. H.; Lee, Y. J.; Cicerone, M. T.; Young, M. F.; Simon, C. G., Jr., The effect of 3D hydrogel scaffold modulus on osteoblast differentiation and mineralization revealed by combinatorial screening. *Biomaterials* **2010,** *31* (19), 5051-62.
164. Luginbuehl, V.; Meinel, L.; Merkle, H. P.; Gander, B., Localized delivery of growth factors for bone repair. *European journal of pharmaceutics and biopharmaceutics : official journal of Arbeitsgemeinschaft fur Pharmazeutische Verfahrenstechnik e.V* **2004,** *58* (2), 197-208.
165. Carmeliet, P., Mechanisms of angiogenesis and arteriogenesis. *Nature medicine* **2000,** *6* (4), 389-95.

166. Silva, A. K.; Richard, C.; Bessodes, M.; Scherman, D.; Merten, O. W., Growth factor delivery approaches in hydrogels. *Biomacromolecules* **2009,** *10* (1), 9-18.
167. Santo, V. E.; Frias, A. M.; Carida, M.; Cancedda, R.; Gomes, M. E.; Mano, J. F.; Reis, R. L., Carrageenan-based hydrogels for the controlled delivery of PDGF-BB in bone tissue engineering applications. *Biomacromolecules* **2009,** *10* (6), 1392-401.
168. Richardson, T. P.; Peters, M. C.; Ennett, A. B.; Mooney, D. J., Polymeric system for dual growth factor delivery. *Nature biotechnology* **2001,** *19* (11), 1029-34.
169. Oliviero, O.; Ventre, M.; Netti, P. A., Functional porous hydrogels to study angiogenesis under the effect of controlled release of vascular endothelial growth factor. *Acta biomaterialia* **2012,** *8* (9), 3294-301.
170. Kaigler, D.; Silva, E. A.; Mooney, D. J., Guided bone regeneration using injectable vascular endothelial growth factor delivery gel. *Journal of Periodontology* **2013,** *84* (3), 230-238.
171. Patel, Z. S.; Young, S.; Tabata, Y.; Jansen, J. A.; Wong, M. E.; Mikos, A. G., Dual delivery of an angiogenic and an osteogenic growth factor for bone regeneration in a critical size defect model. *Bone* **2008,** *43* (5), 931-40.
172. Cho, T. J.; Gerstenfeld, L. C.; Einhorn, T. A., Differential temporal expression of members of the transforming growth factor beta superfamily during murine fracture healing. *Journal of bone and mineral research : the official journal of the American Society for Bone and Mineral Research* **2002,** *17* (3), 513-20.
173. Kempen, D. H.; Lu, L.; Heijink, A.; Hefferan, T. E.; Creemers, L. B.; Maran, A.; Yaszemski, M. J.; Dhert, W. J., Effect of local sequential VEGF and BMP-2 delivery on ectopic and orthotopic bone regeneration. *Biomaterials* **2009,** *30* (14), 2816-25.
174. Moon, J. J.; Hahn, M. S.; Kim, I.; Nsiah, B. A.; West, J. L., Micropatterning of poly(ethylene glycol) diacrylate hydrogels with biomolecules to regulate and guide endothelial morphogenesis. *Tissue engineering. Part A* **2009,** *15* (3), 579-85.
175. Leslie-Barbick, J. E.; Shen, C.; Chen, C.; West, J. L., Micron-scale spatially patterned, covalently immobilized vascular endothelial growth factor on hydrogels accelerates endothelial tubulogenesis and increases cellular angiogenic responses. *Tissue engineering. Part A* **2011,** *17* (1-2), 221-9.
176. Lee, K. H.; Shin, S. J.; Park, Y.; Lee, S. H., Synthesis of cell-laden alginate hollow fibers using microfluidic chips and microvascularized tissue-engineering applications. *Small* **2009,** *5* (11), 1264-8.
177. Takei, T.; Sakai, S.; Yokonuma, T.; Ijima, H.; Kawakami, K., Fabrication of artificial endothelialized tubes with predetermined three-dimensional configuration from flexible cell-enclosing alginate fibers. *Biotechnology progress* **2007,** *23* (1), 182-6.
178. Trkov, S.; Eng, G.; Di Liddo, R.; Parnigotto, P. P.; Vunjak-Novakovic, G., Micropatterned three-dimensional hydrogel system to study human endothelial-mesenchymal stem cell interactions. *Journal of tissue engineering and regenerative medicine* **2010,** *4* (3), 205-15.

SECTION II

EXPERIMENTAL PROCEDURE

Chapter II

Materials and Methods

ABSTRACT

The main aim of this chapter is to describe, in a more detailed manner, the setups and protocols related to experiments performed in this PhD thesis. Although each chapter of the current thesis contains a “materials and methods” sections, herein it is intended to provide a more descriptive and comprehensive view over the procedures and the rationale for the selection of materials and characterization techniques.

II.1. MATERIALS

Hydrogels are tri-dimensional (3D) crosslinked insoluble networks of hydrophilic polymers. Due to their hydrated state, they exhibit a great versatility for incorporating bioactive molecules (drugs, growth factors) or cells, without threatening their activity and/or functionality. Even more, they enable the oxygen diffusion and fluid transport, such as nutrients and metabolic by-products, in and out of the network[1,2]. Altogether, these dynamic features resemble those of natural extracellular matrix (ECM)[3], hence hydrogels are recognized as cell instructive matrices with widespread applications in tissue engineering (TE) and regenerative medicine. The hydrogels developed under the context of this thesis were based on natural origin polymers. They possess functional groups (sulfates $–OSO_3^-$, amides $–NH_2$, carboxyl –COOH, etc.) that are encountered in the chemical backbone of biological relevant biomacromolecules, such as glycosaminoglycans (GAGs), which play an important role in developmental and structural cellular processes[4]. Specifically, *kappa*-carrageenan (κ-CA), a sulfated polysaccharide, was the material selected to develop hydrogels that could enable the encapsulation and controlled distribution of cells within the frame of bone TE (chapters VII and VIII). Chitosan (CHT), a cationic natural-origin material, was used in combination with κ-CA for the development of fiber-like hydrogel templates (chapter VII).

Inspired by the natural bone healing process, when inorganic elements act as nucleation sites for hydroxyapatite formation, enabling and reinforcing the integration with host surrounding bone tissue[5], silicate nanoplatelets (sNPs) were proposed as osteo-enhancers during osteogenic differentiation of stem cells (chapters V and VI).

II.1.1. Carrageenans

Carrageenans (CAs) are a class of marine-origin polysaccharides with a 15 to 40% of ester-sulfate content and a highly flexible structure that enables the formation of gels at room temperature[6]. They are widely used as gelling, emulsifier, thickening, or stabilizing agents in pharmaceutical, cosmetic and food industry[7]. CAs are high molecular-weight structures that consist of repeating β-D-galactose (G) and 3,6-anhydro-D-galactose (AG) units jointed by alternating α-(1→3) and β-(1→4) glycosidic linkages[8]. They are classified according to the number of $–OSO_3^-$ present on the repeating unit, which confers to the chemical backbone an anionic character. Briefly, while *kappa* (κ-) has one $–OSO_3^-$ group, *lambda* (λ-) and *iota* (ι-) have two and three $–OSO_3^-$ groups, respectively, per disaccharide unit[9,8] (**Figure II.1**). The galactose-based structure and the $–OSO_3^-$ content of CA resembles the chemistry of GAGs that compose the ECM of tissues (chondroitin sulfate, dermatan sulfate and keratin sulfate[8]). The presence of these functional groups allows CAs to be easily modified, rendering improved functions.

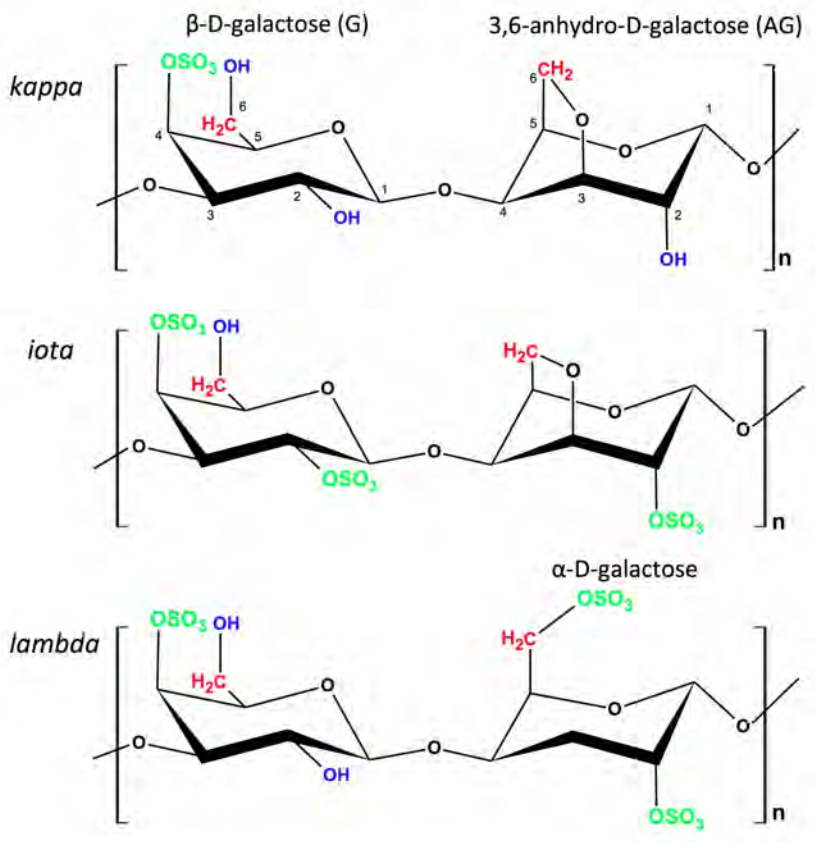

Figure II.1. Chemical structure of carrageenans (4-sulphate-β-D-galactose and 3,6-anhydro-D-galactose units jointed by alternating α-(1→3) and β-(1→4) glycosidic bonds.

Due to the half-ester sulfate moieties, CAs are strongly anionic, being comparable with inorganic sulfate in this respect[10]. In the case of κ- and ι- formulations, the structural architecture permits the formation of double-helical bundles that, under mild conditions, such as temperature and presence of cationic ions, can further organize into a gel conformation[8] (**Figure II.2**). At higher temperature, thermal agitation overcomes the tendency to form helices and the polymer exists in solution as a random coil. Upon cooling, it undergoes a sol-gel transition from random coil to coaxial double helices, forming small soluble clusters or "domains". This conformational organization renders the formation of 3D hydrogel network that is maintained by the interaction of the polymeric chains through hydrogen bridges. Further crosslinking of these domains into a cohesive gel structure involves the formation of junction zone through the side-by-side association of double helices from different domains. Helix-helix aggregation occurs *via* ionic interactions in the presence of cations (K^+ for κ- and Ca^{2+} for ι-CA), which can suppress the electrostatic repulsion between highly charged participating chains. For the λ-formulation, the removal of the anhydrous bridge locks the formation of double helix configurations, thus it does not undergo conformation rearrangement and consequently does not form gels.

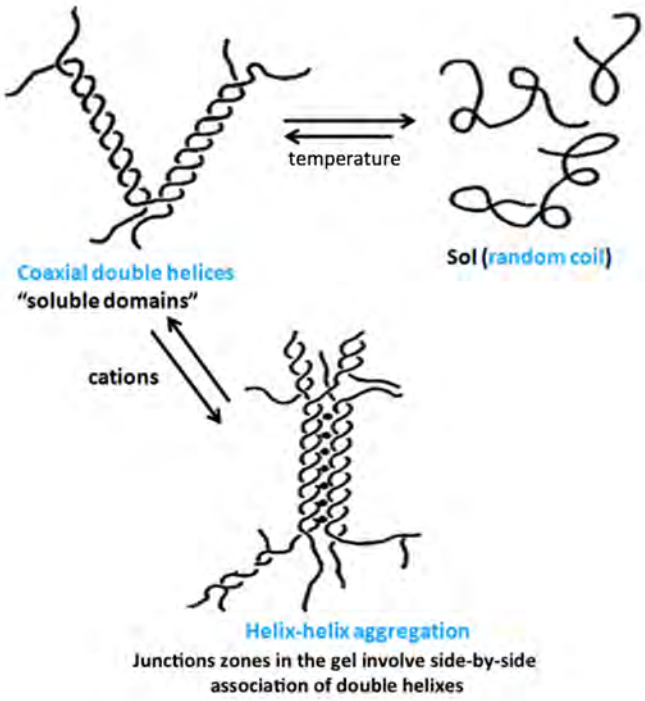

Figure II.2. Domain model gelation of carrageenans (adapted from[11]). The structural architecture permits the formation of double-helical bundles that, under mild conditions, such as temperature and presence of cationic ions, can further organize into a gel conformation. At higher temperature, thermal agitation overcomes the tendency to form helices and the polymer exists in solution as a random coil. Upon cooling, it undergoes a sol-gel transition from random coil to coaxial double helices, forming small soluble clusters or "domains".

Some of the advantages that distinguish CAs hydrogels from others described in the literature include the thermo-reversible and ionic characteristics that provide mild conditions for cell encapsulation purposes and versatility of processing into various shapes/formats.

II.1.1.1. Kappa-carrageenan

The primary differences that influence the properties of κ, ι- and λ-CA are the number and position of the ester $–OSO_3^-$ groups on the repeating galactose units. Higher levels of ester $–OSO_3^-$ lower the solubility temperature of the CAs and produce lower strength gels, or contribute to gel formation inhibition (λ-CA). For instance, κ-CA produces strong, rigid gels, while the ι-CA, which has intermediate $–OSO_3^-$ content, produces soft gels that provide excellent freeze/thaw stability. λ-CA, which is highly sulphated, is less likely to form a gel structure[9]. K-CA has been proposed as a potential candidate in TE and regenerative medicine applications[12,13] due to its gelation properties, mechanical strength and its higher resemblance to GAGs. These features together with the extensive knowledge in the development of κ-CA-based hydrogels[14,15,16] available at the 3B's Research Group

supported the selection of κ-CA under the scope of this thesis (chapters VII and VIII).

The κ-CA solutions possess a mild thixotropic behavior, which means that by applying mechanical stress (pumping, shear, agitation) the conformational arrangement of the double helices is destroyed, but it recovered once the deformation is removed. This thixotropic property is particularly useful for the development of injectable carrier devices for the delivery of cell and biomacromolecules at a specific implantation site, under minimally invasive procedures[17]. In the presence of K^+ ions, κ-CA forms firm, but brittle hydrogels that are unstable when temperature increases. However, due to the uncontrollable exchange of monovalent ions with other cations present in the physiological environment, the 3D structure collapses. To increase their stability, several methods are currently employed, among which complexation with cationic polymers, such as chitosan (CHT) and chemical modification, with photocrosslinkable moieties, which were used within the experimental setting of the present thesis. Thus, due to its versatility in processing, crosslinking mechanism and modification, κ-CA was considered as suitable to produce hydrogel microfibers for endothelial cells encapsulation along with their arrangement within a hydrogel disc containing osteoblast-like cells (chapter VII), as well as to obtain stable covalently-crosslinked micro-patternable hydrogels (chapter VIII).

For the work developed in this thesis, κ-CA (CAS 11114-20-8) was purchased from Sigma (Germany, Cat. N^o 22048) in chapter VII and from TCI (USA, Cat. N^o C1804) in chapter VIII, and used without further purification. The molecular weight (MV) of the commercial κ-CA ranges from 400 to 700kDa, however, the commercial forms of κ-CA usually contain traces of other CAs forms, whose exact concentration can vary from batch to batch[8,10].

II.1.1.2. Methacrylated κ-CA

The major drawback of ionically crosslinked κ-CA hydrogels is that they are highly dependent on the properties of the surrounding environment. Thus, once implanted *in vivo,* these ionotropic hydrogels might lose their stability, due to the permanent exchange of monovalent ions that are present in the physiological environment. To overcome this disadvantage, the chemical modification of κ-CA to introduce photocrosslinkable moieties, was expected to allow the formation of stable covalently crosslinked κ-CA hydrogels, while retaining the anionic character of κ-CA.

For the work described in this thesis (chapter VIII), ester bonds were introduced in the κ-CA backbone, enabling the formation of chemically crosslinked hydrogels upon exposure to ultraviolet (UV) light. Methacrylated κ-CA (MA-κ-CA), with various degrees of methacrylation (DM), was synthesized by substituting the hydroxyl (–OH) groups of κ-CA with methacrylic groups (**Figure II.3**). Briefly, κ-CA was dissolved in distilled water (diH_2O) at a final concentration of 1% (wt/v) at 50^{o}C until the polymer was fully dissolved. Methacrylic

anhydride (MA, Sigma, Germany, Cat N^{o} 276685) was added, at once, to the κ-CA at concentrations of 4, 8 and 12% (v/v) and allowed to react for 6h, under continuous stirring, at 50^{o}C. The pH of the mixture was kept constant (pH=8) by adding, when necessary, small volumes of 5M NaOH drop wise. After the completion of the reaction, the mixture was dialyzed against diH_2O using 12-14 kDa cut-off dialysis-tubing systems (Fischer Scientific, USA), at 4^{o}C, for 3 days, to remove unreacted MA. The dialysis bath was changed twice a day. Purified MA-κ-CA solutions were frozen at -80^{o}C and lyophilized for 3 days, protected from light. The obtained powder was stored at -20^{o}C until further use.

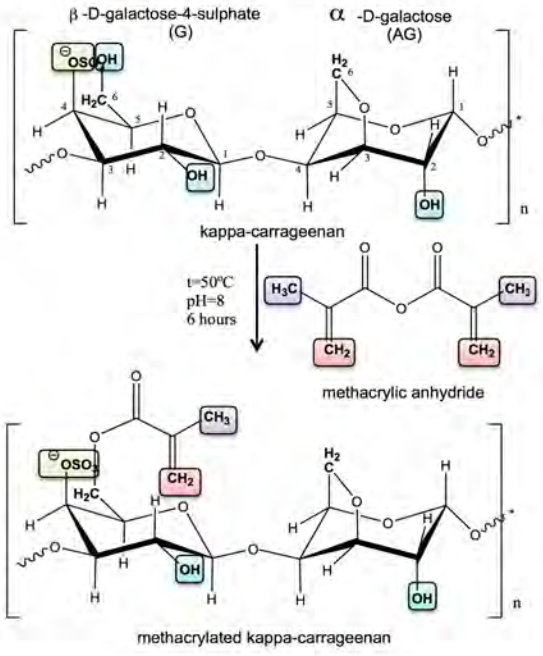

Figure II.3. Methacrylation of κ-CA in the presence of methacrylic anhydride. Methacrylated κ-CA (MA-κ-CA), with various degrees of methacrylation (DM), were synthesized by substituting the hydroxyl (–OH) groups of κ-CA with methacrylic groups.

II.1.1.2.1. Proton nuclear magnetic resonance

The principle of proton nuclear magnetic resonance (^{1}H NMR) is related to the magnetic properties of the isotope hydrogen-1 (^{1}H) nuclei. The technique is based on the fact that, at a specific radio frequency, each ^{1}H isotope found on the chemical backbone of the material to be analyzed requires a slightly different magnetic field to bring it to the resonance condition. This is dependent on the type of bonds the ^{1}H isotope is engaged in the molecule. Thus, ^{1}H NMR spectrum provides information regarding the ^{1}H isotope environment in the molecule. Since ^{1}H NMR spectra are recorded in solution, protons from the solvent should not interfere in the analysis, thus, samples must be dissolved in a proton-free solute. Deuterated solvents (e.g. deuterium oxide D_2O) are based on the used of deuterium (^{2}H), a stable isotope of hydrogen, and usually preferred for the analysis.

The chemical modification of κ-CA (chapter VIII) was quantified by ^{1}H NMR spectroscopy. Briefly, κ-CA and MA-κ-CA were dissolved in D_2O at a concentration of 10mg/mL and their ^{1}H NMR spectra were collected at 50^{o}C, at a frequency of 500 MHz using a Varian INOVA NMR spectrometer with a single axis gradient inverse probe. All spectra were analyzed using 1D NMR Processor software (ACD/Labs 12.0). Phase correction was applied to obtain accurate absorptive peaks, followed by a baseline correction to obtain the integrals of the peaks of interest. The obtained chemical shifts were normalized against the protons of the methylene group of the D-galactose units as an internal standard, which is present at δ= 3.89 ppm[18]. The DM was calculated referring to the peaks at δ= 1.9–2 ppm (methyl) and δ= 5.5–6 ppm (double bond region) as percentage (%) of the free –OH substituted with methacrylate groups.

II.1.1.2.2. Fourier transform infrared spectroscopy

Fourier transform infrared spectroscopy (FTIR) is an analytical method used to obtain information about the sample's chemical structure and chemical bonding. It is based on the adsorption of infrared (IR) light by the material that triggers discrete energy transitions of the vibrational states of atomic and molecular units within a molecule. Thus, one can identify the presence of chemical groups on the sample through the FTIR spectrum. The attenuated total reflection (ATR) sampling mode can be used to increase the intensity of the surface signal, because it analysis the region near the surface. However, FTIR-ATR is not truly surface sensitive, due to the high penetration depth of the IR beam (1-5μm)[19], thus care should be taken while preparing the sample. Nevertheless, the rich structural information that the IR spectra provide makes the FITR-ATR, a valuable technique to evaluate chemical changes, such as the grafting of polymers with functional groups.

The chemistry of the MA-κ-CA reported in chapter VIII was analyzed by FTIR-ATR. The infrared spectra were recorded on a Bruker Alpha FTIR spectrophotometer (Bruker Optics, USA). The spectra were recorded at a resolution of 4 cm^{-1} and the results were reported as an average of 24 scans. The peaks appearing around 1550cm^{-1} and 1680-1750 cm^{-1} correspond, respectively, to the C=C and C=O of the ester groups and are found in the MA-κ-CA, but not in κ-CA.

II.1.1.2.3. Rheological analysis

At room temperature, κ-CA solutions are highly viscous and are difficult to manipulate resulting in poor processability[20]. By increasing the temperature, the viscosity of κ-CA solutions dramatically decreased mainly due to the thermodynamic instability of the polymer chains. However, the range of temperature that must be employed (50–70°C) is higher than the physiological temperature (37^{o}C), which can compromise the viability of the cells or the

activity of other bioactive components at the time of incorporation. Even more, the information about the viscosity give indication over the injectability potential and the conditions that are required to extrude a solution through needles.

Within this context, the viscosity of the MA-κ-CA and κ-CA solutions was evaluated (chapter VIII). Furthermore, the effect of DM on the rheological properties of MA-κ-CA was also taken into consideration. Thus, 1mL of solution was injected between the plates of AR2000 stress controlled rheometer (TA instruments, New Castle, DE, USA) equipped with a 20mm flat geometry and a gap of 500µm. Flow experiments were performed to evaluate the viscosity of polymer solution at 37°C by varying the shear rate/frequency from 0.1 to 100 radians/s.

II.1.2. Chitosan

Chitosan (CHT) is a deacetylated variant of chitin, the second most abundant biopolymer found in nature, present in the exoskeleton of crustaceans, insects, spiders or the cell walls of many algae or fungi[21]. CHT has been reported to be biocompatible, biodegradable and to present antibacterial and wound-healing properties[22]. These features might result from the structural similarities of CHT with GAGs.

Structurally, CHT is a linear polysaccharide composed of randomly distributed β-(1→4)-linked D-glucosamine (deacetylated unit) and N-acetyl-D-glucosamine (acetylated unit) (**Figure II.4**). The free amino ($–NH_2$), and N-acetyl groups play a major role in determining CHT's solubility, particularly, below its pK_a (pH=6.5-6.8). At these range, the amino groups are protonated which triggers the solubilization of the polymeric chains. This strong and unique cationic behavior allows the formation of polyelectrolyte complexes (PECs) with anionic compounds[21] with improved properties, both in the terms of stability, as well as cellular behavior[23]. Likewise, the electrostatic interactions between κ-CA and CHT already lead to the development of nanoparticles[16], beads[24] and layer-by-layer systems[25]. Thus, in chapter VII, we took advantage of the cationic behavior of CHT to develop CHT-coated κ-CA fibers improving the stability of κ-CA fiber-shaped hydrogels.

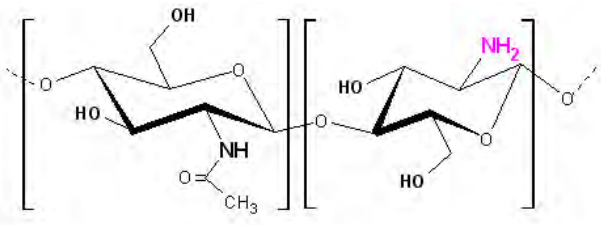

Figure II.4. Chemical structure of CHT consisting of N-acetyl-D-glucosamine (acetylated unit) and D-glucosamine (deacetylated unit) linked by β-D-(1→4) glycosidic bonds.

II.1.2.1. Purification of Chitosan

The term chitosan (CHT) refers to a series of deacetylated chitins with different molecular

weights (50-2000 kDa), viscosity and deacetylation degree (DD=40-98%). Prior use, a purification step was set up and the products from 3 independent purifications were mixed to obtain a final homogeneous batch of purified CHT. This batch was used for all the experiments described in chapter VII, in order to avoid concerns about the influence of the N-deacetylation (DD)/ N-acetylation (DA) degree or molecular weight (MW) on the material modification, formation of polyelectrolyte complexes and *in vitro* cellular behavior.

For the purification step, medium grade CHT obtained from crab shells and purchased from Sigma (Germany, Cat. N^{o} 448877**,** CAS 9012-76-4), was dissolved in an aqueous 1% (v/v) acetic acid solution at a final concentration of 1% (wt/v). The obtained solution was filtered (Whatman® ashless filter paper, 20-25µm) and then precipitated by adding a NaOH solution (final pH~8). The precipitated gel was sieved to remove the exuded liquid and thoroughly rinsed with distilled water until stable pH was reached. The CHT gel was further washed with ethanol, freeze-dried, grounded to powder and dried overnight at 50^{o}C. The DD of purified CHT was determined by ^{1}H NMR[26] at 83.8% (section II.1.1.2.1).

II.1.2.2. Optimization of the pH of CHT working solutions

Since CHT dissolves only at very low pH (<2), its use in combination with biological compounds (cells, bioactive agents, etc.) is limited. Previous studies[27,28] have demonstrated that the strong acid pH of CHT solutions can be increased up to physiological pH (=7.4) with the addition of beta-glycerophosphate (βGP), without jeopardizing its solubility (i.e. no precipitation). Thus, a curve of the variation of the pH of CHT solution as function of βGP/CHT ratio was performed, in order to establish those conditions upon which CHT solution exhibit a pH suitable for cell encapsulation, while maintaining its solubility and cationic character (**Figure II.5**). For this purpose, a CHT solution was prepared by dissolving the purified polymer into a 1% (v/v) acetic acid solution to a final concentration of 0.5% (wt/v). Slowly, anhydrous βGP (Sigma, Germany, Cat. N^{o} G9422) was added to the CHT solution and the pH of the solution was measured (**Figure II.5A**).

II.1.2.3. Optimization of zeta potential of CHT working solutions

Zeta (*ζ*–) potential was chosen as a parameter to evaluate the stability of polymeric dispersion. From a theoretical viewpoint, *ζ*–potential is the potential difference between the dispersion medium and the stationary layer of fluid attached to the dispersed particle. Thus, *ζ*–potential is an (relative) indicator for the surface potential of particles, as well as a fundamental parameter known to affect the stability of colloid dispersions. For molecules and particles that are small enough, a high *ζ*–potential will confer stability*, i.e.* the solution or dispersion will resist aggregation. When the potential is low, attraction exceeds repulsion and the dispersion will break and flocculate. So, colloids with high *ζ*–potential (negative or

positive) are electrically stable, while colloids with low ζ–potentials tend to coagulate or flocculate.

Within this thesis, ζ–potential was used as a parameter to predict the susceptibility of CHT solution to coagulate with the addition of βGP to the CHT solution. Additionally, a positive ζ–potential confirmed the strong cationic behavior of CHT, and thus its potential successful combination with anionic entities (e.g. κ-CA). Although the electrical charge is not measured directly, it can be calculated using established theoretical models. The most widely used theory is the one developed by Marian Smoluchowski, which was also applied for the measurements performed within the scope of this thesis. This model can be applied to dispersed particles of any shape and any concentration. Briefly, ζ–potential measurements were performed on CHT solutions with different pHs (upon addition βGP), by using a Malvern Zeta Sizer Nano ZS (Malvern Instruments, UK) and applying the Smoluchowski model. Each sample was diluted in de-ionized water at a final CHT concentration of 0.1% (wt/v). Each measurement was performed for 120sec, at 25^{o}C (**Figure II.5B**). The experiments were performed in triplicates.

Additionally, the ζ–potential of a κ-CA solution was determined to confirm its anionic character that can enable the interaction with a positively charged system, such as CHT.

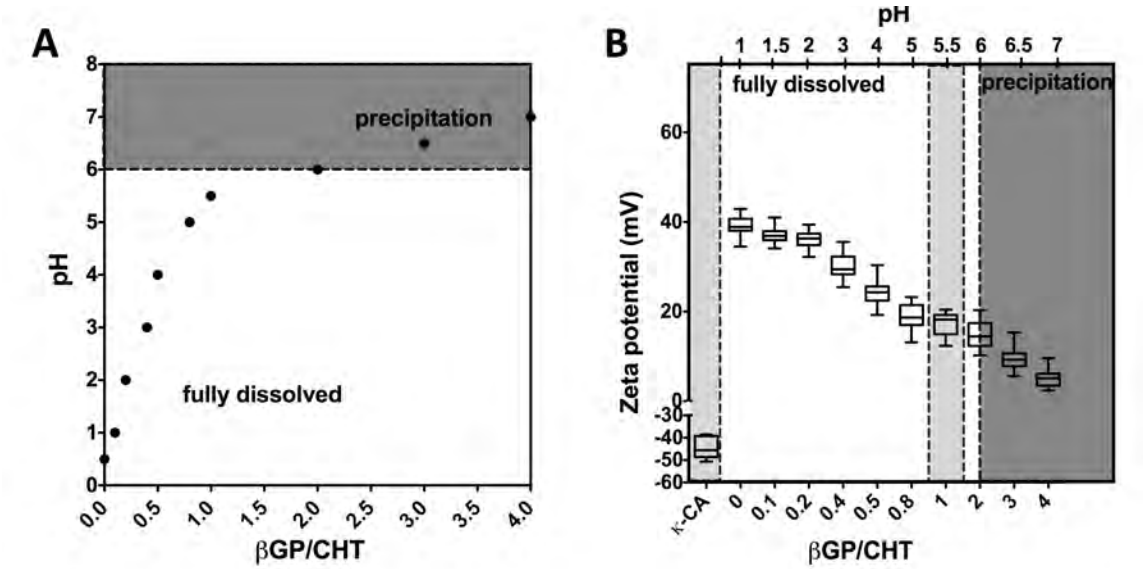

Figure II.5. Tuning the pH of CHT solutions with βGP. (**A**) A curve of pH variation of CHT solution with the addition of βGP was determined. At pH=5.5-6, CHT is fully dissolved and no sign of precipitation was noticed. However, above these values, the precipitation of CHT occurred. (**B**) With the addition of βGP, the overall charge of CHT solution dramatically decreased. Choosing pH=5.5 for the working solution, the full solubility and an overall positive charge of CHT was assured.

II.1.3. Silicate nanoplatelets

With a demand for therapies that are able to boost the regeneration and restoration of bone tissue function[29], new research routes have been exploring the potential of new bioactive materials that are able to direct stem cell differentiation and facilitate functional bone formation in a reproducible and highly controllable fashion[30]. Inorganic bioactive nanomaterials, including bioactive glasses ($Na_2O–CaO–SiO_2–P_2O_5$), hydroxyapatite (HA) ($Ca_{10}(PO_4)_6(OH)_2$), β-tricalcium phosphate (β-TCP) ($Ca_3(PO_4)_2$), β-wollastonite (CaO-SiO) and A-W (Apatite-Wollastonite) glass ceramics[31], due to their enhanced surface interactions with cells, are attractive for hard TE as bone replacement composites and nanovehicles for delivering therapeutics. However, difficulties persist, including lack of osteoinductive properties, poor processing abilities and insufficient degradation, with many of these materials.

Synthetic silicate nanoplatelets (sNPs) have drawn our attention mainly due to their intricate chemistry comprising a collection of elements and ions that are known to be involved in bone formation mechanisms. Even more, there are only few studies that highlight sNPs potential in TE application[32,33] and up to our knowledge and the conclusion of this thesis, there are no studies that have explored the interactions of sNPs with stem cells. Thus, under the scope of this thesis, Laponite XLG sNPs ($Na_{0.7}[Mg_{5.5}Li_{0.3}Si_8O_{20}(OH)_4]$) were evaluated as potential osteoinducers and osteoconductors during osteogenic differentiation of hMSCs (chapter V) and further, as tools to improve the osteogenic differentiation of SSEA-4$^+$hASCs (chapter VI).

Generally, Laponite sNPs consist of layers of [SiO_4] tetrahedra sandwiching sheets of Mg^{2+}, which complement their octahedral coordination by bridging –OH groups (**Figure II.6**). This unitary cell is repeated around 1500 times in two dimensions to form each disc shaped called Laponite platelet. The nanostructure of Laponite is best described as strongly anisotropic, characterized by a primary particle diameter of approximately 25nm, a thickness of less than 1 nm and a large surface area (applying Brunauer–Emmett–Teller theory) of 370m^2/g and bulk density of 1mg/cm^3. The partial substitution of Mg^{2+} in the octahedral sheets by Li^+ charges the faces of the sNPs with a -0.7eV charge. These elementary charges are uniformly distributed over the Laponite sNPs and therefore, depending on the pH of the solution, some positive charges appear on the edge originated by some broken bonds[34]. Thus, Na^+ is accommodated on or between the faces of the sNPs (interlayers) for charge compensation in the solid powders[35]. This charge distribution enables strong interactions with a range of compounds (ions, dyes, proteins, polymers). Laponite sNPs are soluble in water and at concentrations higher than 40mg/mL form a physical nanoclay gel due to electrostatic and van der Waals interactions, that result in the formation of a “house of cards” structure[36].

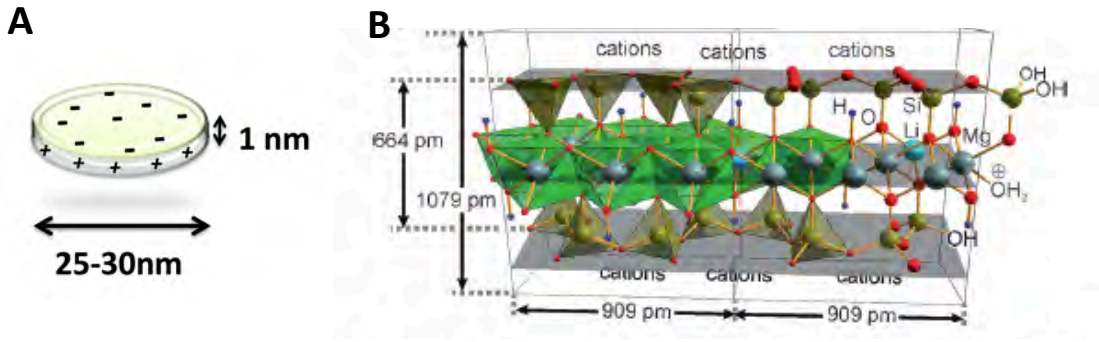

Figure II.6. Laponite sNPs. (**A**) An idealized single Laponite disc (1nm thick and 25-30nm in diameter) with specific charge distribution (negatively charged facets and positively charged sides). (**B**) A side view of two unit cells (the dimensions refer to a single crystal structure analysis, taken from Lezhnina *et al.*[35]): the chemical structure of the unitary cell of Laponite sNPs is constituted by six octahedral Mg^{2+} ions sandwiched between two layers of four tetrahedral Si atoms groups.

II.1.3.1. Transmission electron microscopy

Transmission electron microscopy (TEM) has been found to be an excellent tool for characterizing the size of nanoparticles, namely to determine the mean nanoparticle size (in projection). The projected area diameter estimated by TEM is theoretically defined as the area of a sphere equal to the projected area of a particle in a stable position[37].

TEM is a microscopy technique in which a beam of electrons is interacting with the specimen as it passes through. An image is then formed from the interaction of the electrons transmitted through the specimen, magnified and focused onto an imaging device. Generally, TEM analysis of a biomaterial requires it's sectioning, since a nano-sized sample is needed for the analysis. However, since sNPs are of nano-scale size, the embedding and sectioning steps were not necessary. Thus, samples were prepared by dispersing sNPs in diH_2O/ethanol solution. A drop of the mixture was placed on a copper grid coated with a thin layer of carbon (for contrast purposes) and allowed to dry in vacuum. The TEM images of sNPs were obtained using JEOL JEM-1400 TEM (JEM1400) installed with cool beam illumination system (resolution: 0.2nm line, 0.38nm point) and 11Mpix AMT cooled CCD camera at 80kV. The nano-size feature and the disc shape morphology of sNPs was confirmed (**Figure II.7**).

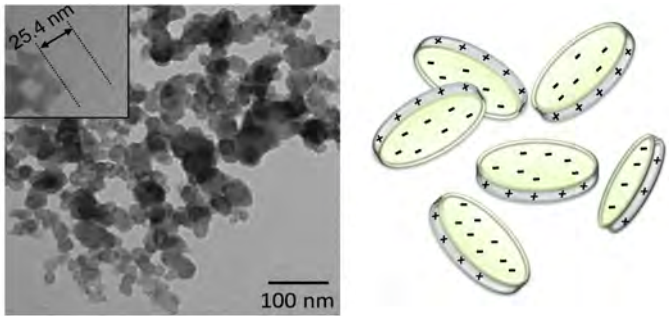

Figure II.7. TEM analysis confirmed the nano-size and disc-shaped morphology of Laponite sNPs.

II.1.3.2. Hydrodynamic size and zeta–potential of sNPs

When sNPs were added to water, they formed a clear and colorless solution with a viscosity similar to the water. In a diluted suspension, sNPs were well dispersed, negatively charged and kept their disc-like features. Laponite sNPs interact with each other through a short-range van der Waals attractive forces and long-range repulsive forces, due to the electrostatic screened interactions. Nevertheless, even at very low concentration of sNPs, the solution evolves spontaneously on time towards a more viscous state, until reaching an arrested phase (**Figure II.8**). The most likely explanation is that with the increase in the concentration, the attractive forces overtake the repulsive ones in such way that the sNPs will adhere to each other irreversibly, leading to the formation of agglomerates, and consecutively, to gelation[36,38].

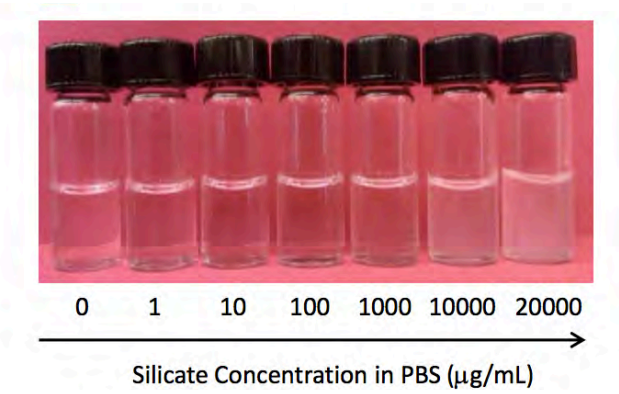

Figure II.8. Increased turbidity of sNPs solutions for increased concentrations (0-20mg/mL), associated with higher aggregate size.

Nowadays, the microstructure of the arrested state is widely studied by different methods such as neutron, x-ray and light scattering. Dynamic light scattering (DLS) technique provides an important contribution in these studies, because it provides information about the dynamics of the system. As far as DLS is concerned, the theory states that when a dispersed particle moves through a liquid medium, a thin electric dipole layer of the solvent adheres to its surface. This layer influences the movement of the particle in the medium[39]. Although, an estimation of the projected area diameter can be performed through TEM, the measurement is related solely to the inorganic core, as the hydration layer is not present. For aqueous solutions, the hydrodynamic diameter was suggested as an important parameter for understanding and optimizing the nanoparticles' performance in biological assays, as well as comprehending the *in vitro* mobility of the sNPs. Concretely, the hydrodynamic diameter provides information on the inorganic core along with any coating material and solvent layer attached to the particle, as it moves under the influence of the Brownian motion. Thus, the hydrodynamic diameter is always greater than the size estimated by TEM.

Together with hydrodynamic diameter, DLS enables the determination of the electrical charge of particles by ζ–potential measurements (see section II.1.2.3). Hydrodynamic size and ζ–potential of sNPs solutions (0-20mg/mL) were determined in de-ionized water and PBS using a 633nm laser in a Malvern ZEN3600 (Malvern Instruments, UK). SNPs were dissolved using vortex (10min) and ultrasonication (10min). The refractive index of sNPs was selected as 1.5 (obtained from MSDS of Laponite XLG), applying the Smoluchowski model. Each measurement was performed for 120sec, at 25^{o}C. The experiments were performed in triplicates.

II.2. DEVELOPMENT AND CHARACTERIZATION OF 3D HDYROGELS SYSTEMS

In order to recapitulate more closely the *in vivo* architectural features of tissues, a number of techniques have been employed *in vitro*[40]. As discussed in the first chapter of the present thesis, hydrogels are 3D cross-linked insoluble, hydrophilic networks of polymers that partially resemble the physical characteristics of native ECM[41]. They exhibit high permeability towards oxygen, nutrients and other soluble factors, essential for sustaining cellular metabolism[42]. The hydrogel network can be fabricated *via* physical or chemical crosslinking methods. While physical crosslinking is achieved by the formation of physical bonds, the chemical crosslinking consists in the formation of stable covalent bonds, mediated by crosslinking agents, between the polymer chains[43].

Within this thesis, κ-CA was the material selected to develop hydrogels for bone TE applications, due to its processing versatility and mild crosslinking conditions. The gelation of κ-CA occurs through ionic interactions, which foster the condensation of the double helices into strong 3D networks that can be processed different sizes and shapes. However, there is still inadequate control over the swelling properties, stability and mechanical performance of κ-CA hydrogels. In order to improve the stability and processability of κ-CA hydrogels, two strategies were taken into consideration: (**1**) reinforcement of the ionically crosslinked κ-CA hydrogels with a CHT coating (chapter VII) and (**2**) chemical modification of κ-CA to obtain covalently crosslinked κ-CA-based hydrogels (chapter VIII).

II.2.1. Development of CHT coated κ-CA fibers

Development of vessel-like structures *in vitro* has attracted attention to be used for applications in TE, as the lack of a vasculature system that can sustain the nutrient and oxygen demands within the tissue-engineered construct is a major limiting factor in creating thick artificial tissues[44]. Thus, developing vessel-like networks as integrated templates within bio-inspired TE constructs, will be essential for creating real-size replicas of the primary tissues or organs[45,46].

Several hydrogels-based processing methods (such as prototyping/printing[47], microfluidics[48]

and photolitography[49]) are available to encapsulate ECs and develop vessel-like architectures using fiber structures with microsize features (~50µm[49] to 1mm[47]) as building units. However, they usually involve extensive manipulation procedures, elaborated experimental settings and complex optimizations, thus limiting their applicability. As alternative to these methods, wet spinning of hydrogels was chosen as a simple and straightforward method to produce microfibers able to accommodate endothelial cells (chapter VII).

II.2.1.1. Development of κ-CA fibers through wet spinning and ionotropic gelation

The κ-CA hydrogel fibers were obtained by the wet spinning technique, which consists of the extrusion of a polymer solution through a needle immersed in a coagulation bath[50], and ionotropic gelation (IG) (**Figure II.9A**). Briefly, a 1.5% (wt/v) κ-CA solution was prepared by dissolving the polymer into diH_2O and heated up to 50°C, under constant stirring, until complete dissolution was achieved. Subsequently, the κ-CA solution was loaded into 5mL syringes headed with needles of different gauge (G). The needles were immersed into a 5% (wt/v) KCl solution prepared in diH_2O, which acted as a coagulation bath. κ-CA fibers with different diameters were obtained by extruding the polymeric solution through the needles directly into the coagulation bath. The presence of K^+ ions initiated the IG, by counterbalancing the negative charges of κ-CA. The fibers were allowed to harden in the coagulation bath for 10min, enough for the κ-CA hydrogels to assemble into a fiber shape[51]. Noteworthy, the gelation time was relatively short (10min), compared to standard gelation times (15 to 30min)[50-52].

The obtained fibers were then washed with phosphate buffered saline (PBS), in order to remove the excess of salts. Using a needle range from18 to 27G (0.838 - 0.210mm internal diameter), it was possible to obtain fibers with different diameters, directly proportional to the internal diameter of the needles. The fibers produced within these settings have a diameter ranging from 0.55 to 1.2mm (**Figure II.9B**). Fibers obtained with needles of 25 and 27G, with a diameter below 1mm more appealing for other applications[53,54,55], were selected for all the subsequent assays, such as carriers for SSEA-4^+hASCs-derived ECs (chapter VII).

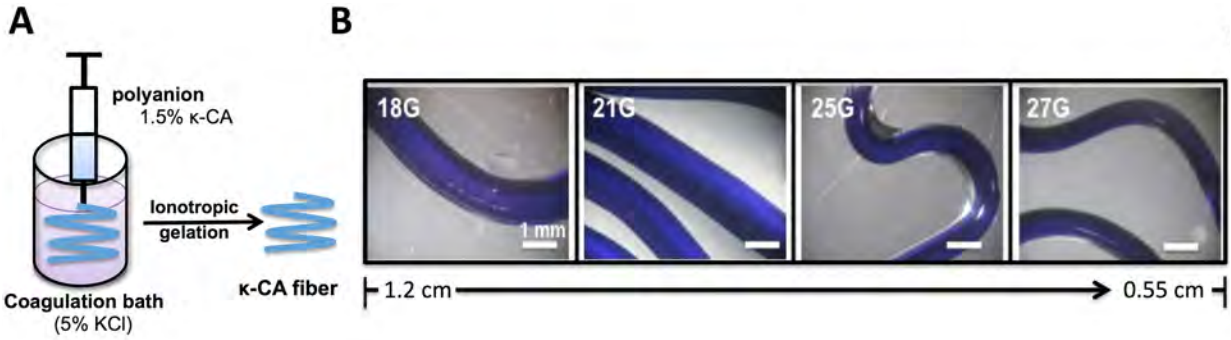

Figure II.9. Development of κ-CA fibers by IG. (**A**) A 1.5% (wt/v) κ-CA was extruded into a coagulation bath (5% KCl) through small needles. (**B**) By varying the needle size (18 to 27G), it was possible to control the diameter of the κ-CA fibers (from 1.2 cm to 0.55cm).

II.2.1.2. Development of CHT coated κ-CA fibers through polyelectrolyte complexation

Although, encouraging results have shown the potential of using κ-CA hydrogels in the TE field[50,56], the ionically crosslinked κ-CA hydrogels exhibits high swelling ratios and are mechanically unstable in physiological conditions[57]. To increase the stability of hydrogels, several approaches have been exploited, such as chemical modifications with photocrosslinkable moieties[58], blending with other biopolymers[50, 59], addition of nanocomposites to the polymer solution[60], formation of interpenetrating networks[61] or PECs with polycations, such as CHT[62].

The method of choice for the reinforcement of κ-CA fibers obtained through IG was the formation of a PEC with CHT, as it is a fast, straightforward and cell-friendly method (**Figure II.10**). The short gelation time during IG enabled the partial crosslinking of κ-CA so that negative $–OSO_3^-$ groups are still available to interact with protonated amino ($–NH_3^+$) groups of CHT. Thus, the immersion of the κ-CA fibers within the 0.5% (wt/v) CHT solution (pH=5.5, optimal pH, section II.1.2.2) for 20min, allowed the formation of PECs between CHT and the non-crosslinked chains of κ-CA at the surface of the fibers and to the formation of a localized CHT nano-sized layer, as also shown in other studies[23,25]. CHT coated κ-CA microfibers were washed with PBS in order to remove the excess of CHT.

Therefore, the formation of CHT-coated κ-CA fibers was achieved through a two-steps procedure that combines the IG of κ-CA into microfibers and the reinforcement of these fibers by PEC between κ-CA and CHT. The presence of the CHT coating was evaluated by staining the fibers with Eosin Y (Sigma, Germany) (**Figure II.10insert**).

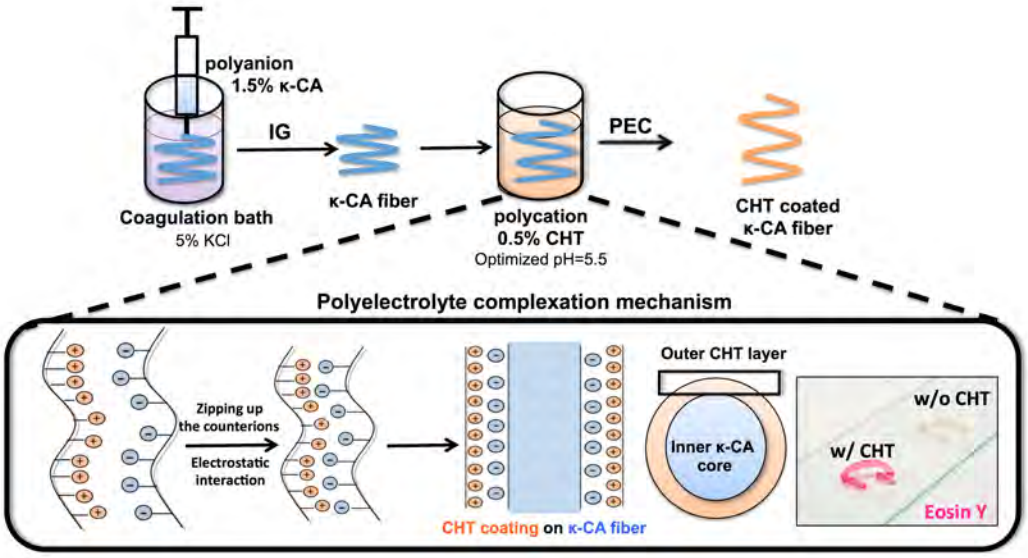

Figure II.10. Schematics of the development of CHT coated κ-CA hydrogel fibers. The process involved the formation of fibers by IG in a KCl coagulation bath, followed by their immersion in a CHT solution (at optimized parameters). The PEC occured between negatively the charged κ-CA chains and the positively charged CHT, by electrostatic interactions. (**insert**) By staining the fibers (without (w/o) or with (w/) CHT coating) with Eosin Y, it was possible to detect the CHT coating (pink).

II.2.2. Photocrosslinkable MA-κ-CA-based hydrogels

The chemical functionalization of κ-CA with methacrylate pendant groups enabled the crosslinking of the κ-CA hydrogel through covalent bonds, thus confering high stability to the polymer network[63]. Moreover, the chemical modification did not affect the inherent ionic character of κ-CA, thus, by combining chemical and physical crosslinking methods, it was possible to obtain physically, chemically and dual crosslinked hydrogels.

II.2.2.1. Preparation of TMSPMA treated glass slides

The surface modification of glass slides with 3-(trimethoxysilyl)propyl methacrylate (TMSPMA) allowed the production of hydrophobic glass surfaces. This surface treatment introduced terminal acrylate functional groups on the glass. During UV exposure-driven polymerization, these acryl groups established bonds with the (metha)acrylate groups of the MA-κ-CA, thus covalently anchoring the polymer on the surface of the treated glass. This procedure enabled the attachment of crosslinked hydrogel units on slides with different shapes and sizes, thus, reducing the direct manipulation of the hydrogel.

Briefly, glass slides (Fisherbrand plain microscope slides, 25x75x1mm) were cleaned overnight with a NaCl solution (10% w/v). After that period, glass slides were washed 3 times with deionized water. Afterwards, each slide was rinsed 3 times with 100% ethanol and left to dry. Cleaned glass slides were stacked in a clean beaker and 4mL of TMSPMA

(Sigma, Germany, Cat. N^{o} 440159, CAS 2530-85-0) were poured over the longitudinal side of the slides, using a syringe. After 30min, the stack was flipped upside down to get even coating due to capillary forces. The TMSPMA coated glass slides were incubated overnight at 80ºC. The final step of the surface modification consisted on cleaning with 100% ethanol (3 times) the TMSPMA treated surfaces and left to air dry. Treated glass slides were wrapped with aluminum foil and baked again for 1-2h at 80^{o}C, after which they were stored wrapped in aluminum foil at room temperature.

II.2.2.2. Photocrosslinked MA-κ-CA hydrogels

Freeze dried MA-κ-CA macromer with different DM, as well as non-modified κ-CA were added to a photoinitator (PI) solution consisting of 0.25% (wt/v) 2-hydroxy-1-(4-(hydroxyethoxy)phenyl)-2-methyl-1-propanone (Irgacure 2959, CIBA Specialy Chemicals) in diH_2O and left at 80°C until complete dissolution. Chemically crosslinked hydrogels were obtained by pipetting 100µL of polymer solution between a Teflon substrate and a glass coverslip separated by a 1mm spacer, followed by UV light exposure at 6.9mW/cm^2 (320–480nm, EXFO OmniCure S2000, Ontario, Canada) for 40sec (**Figure II.11**).

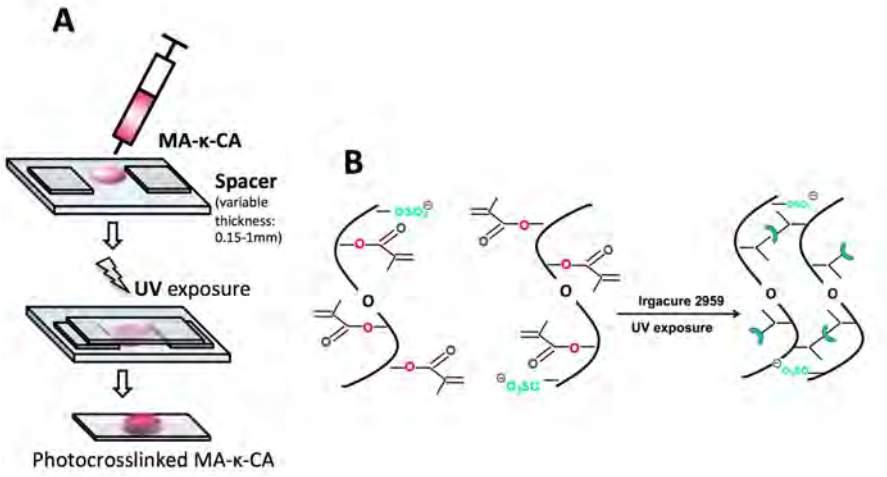

Figure II.11. Production of chemically crosslinked crosslinked MA-κ-CA. (**A**) Hydrogels discs with variable thickness were produced by varying the thickness of the spacers. (**B**) To create a hydrogel network, MA-κ-CA was crosslinked using UV irradiation in the presence of Irgacure 2959 as PI, leading to the formation of covalent bonds between the (metha)acrylate groups.

II.2.2.3. Dual crosslinked hydrogels

The introduction of methacrylate groups into the κ-CA backbone enabled the formation of chemically crosslinked gels *via* UV exposure. Furthermore, as the anionic character of MA-κ-CA was not affected, it was still possible to form gels in the presence of K^+ salts. Thus, the presence of two functional groups (–OSO_3^- and methacrylate) was independently used to tune physical properties.

Dual crosslinked hydrogels were prepared by combining UV exposure with immersion in 5% (wt/v) KCl coagulation bath for 10min (**Figure II.12**). As a consequence, hydrogels with different shape and sizes (discs and fibers) were produced, demonstrating the versatility of the system and the range of potential applications within the TE field.

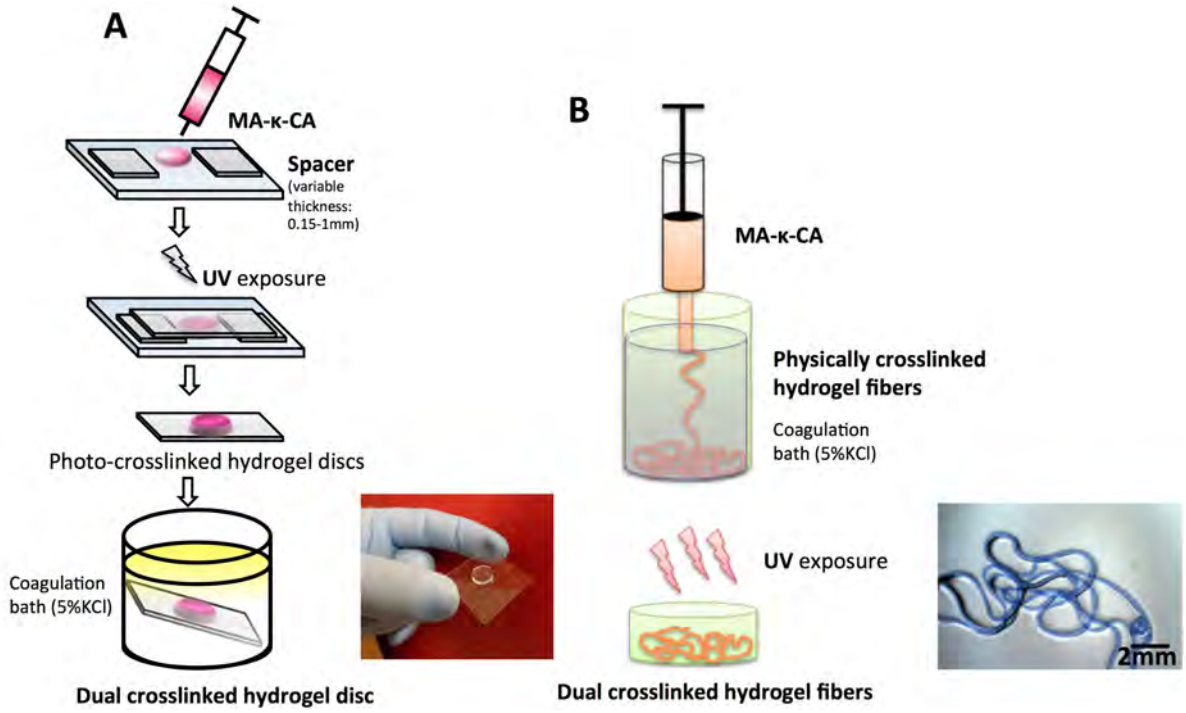

Figure II.12. Dual crosslinked MA-κ-CA hydrogels were produced either as (**A**) discs or (**B**) fibers by chemical and physical crosslinking methods.

II.2.3. Techniques used for characterizing the developed 3D hydrogel systems

II.2.3.1. Scanning electron microscopy

Scanning electron microscopy (SEM) is a method that has been widely used to study the morphology of polymeric materials and structures, at a smaller scale than optical microscopy[64]. SEM micrographs can be obtained from secondary electrons emitted from the surface of the sample, as a result of the impact of a focused electron beam, revealing the 3D topography of the specimen and providing details on its structure, down to the sub-micron level with a penetration depth of 5Å[65].

As wet samples (i.e., hydrogels) cannot be directly visualized under SEM, they need to undergo a process of dehydration. Thus, the hydrogels samples tested in chapters VII and VIII were subjected to a rapid snapshot cooling using liquid nitrogen, to maintain their microstructure features, and then to a freeze-drying process to remove the solvent (water) by sublimation.

Furthermore, high magnifications are generally not possible in SEM, because of the intensity

of the electron beams that damages the thin polymeric surface, leading to deformation, and even melting of the specimen. To overcome this limitation, polymeric samples are usually spur coated with conductive materials, such as gold or palladium.

Within this thesis, SEM technique was applied to visualize the outer surface of κ-CA fibers with and without CHT coating (chapter VII) and to analyse the effect of DM over the microstructure and pore size distribution of MA-κ-CA hydrogels. Briefly, the κ-CA fibers, with and without CHT coating (chapter VII) and the dual crosslinked MA-κ-CA (chapter VIII) were snap frozen in liquid nitrogen, transferred to micro-centrifuge tubes and freeze-dried overnight. The dried samples were carefully mounted on samples holders using double-sided carbon tape. Prior mounting, dried MA-κ-CA samples were fractured to expose the core of the sample. The coating of κ-CA fibers was performed with gold (Fisons Instruments, sputter coater SC502, UK), while MA-κ-CA samples were coated with gold and palladium using a Hummer 6.2 sputter (Ladd Research, Williston, VT, USA). The coating procedures were performed at 15mA for 2min. While κ-CA fibers were analyzed under a Nano-SEM FEI Nova 200 (FEI, Netherlands), MA-κ-CA samples were analyzed under a JSM 5600LV (JEOL, USA). The pore size distribution of MA-κ-CA samples was determined using NIH ImageJ software, based on the SEM pictures.

II.2.3.2. Energy-dispersive X-ray spectroscopy

SEM, which is closely related to the electron probe, is primarily designed for producing high-resolution images of a sample surface. Backscattered electron images in the SEM display compositional contrast that results from different atomic number elements and their distribution. Energy dispersive spectroscopy (EDS) allows identifying, mapping and localizing if needed, those particular elements, if an X-ray spectrometer is added (EDS/EDX). Thus, upon the interaction between X-ray and a sample, each unique atomic structure (i.e. atomic element) generates a unique set of peaks on a X-ray spectrum, thus providing information about the elemental composition of the sample.

EDS/EDX technique was applied in chapter VII, to confirm the presence of the CHT coating on κ-CA fibers, by tracing nitrogen (present in CHT, but not in κ-CA) on the surface of coated κ-CA. The presence of the coating was evaluated up to 21 days and at different time points on κ-CA and on CHT-coated κ-CA immersed in PBS. Elemental analysis was carried out with an energy dispersive spectrometer (EDS/EDX; EDAX-Pegasus X4M), attached to the SEM equipment used in section II.2.3.1. Therefore, the samples were analyzed as prepared for SEM. All observations/image acquisitions and measurements were made at an acceleration voltage of 15 kV.

II.2.3.3. Physical characterization

II.2.3.3.1. Swelling

In the context of TE, it is important to expose the polymeric networks to conditions that mimic as much as possible the *in vivo* environment. A proper evaluation of their behavior within this setup will help predicting their *in vivo* performance. Swelling is a trademark of hydrogels, as they are able to retain water in various percentages dependent on their chemistry[1]. Moreover, the swelling of polymeric networks is significantly influenced by water-material interactions. These affect the mass transport characteristics, determinant for nutrient and oxygen diffusion to encapsulated cells and their metabolic waste disposal, and consequently, the mechanical properties as well as overall features, such as shape and size of a given hydrogel geometry or pattern.

The swelling behavior of κ-CA-based hydrogels was evaluated as function of the CHT coating (chapter VII) and DM, as well as crosslinking mechanism for the MA-κ-CA hydrogels (chapter VIII) at physiological temperature (37°C) and under humidified atmosphere with 5% of CO_2.

The influence of the CHT coating on the swelling of κ-CA fibers was determined by evaluating the water absorption kinetics upon immersion of the coated and uncoated fibers in standard culture medium for up to 21 days. Standard medium, Dulbecco's Modified Eagle Medium (DMEM, Gibco, USA) supplemented with 10%(v/v) heat-inactivated fetal bovine serum (HiFBS, Gibco, USA) and 1%(v/v) penicillin/streptomycin (Pen/Strep, 100U/100µg/mL, Gibco, USA) was used envisioning the subsequent use of the fibers for cells encapsulation/culturing. Medium was replenished every 3-4 days. Fibers were allowed to reach equilibrium in DMEM and at days 7, 14, and 21, samples (n=3) were retrieved and blotted with KimWipe paper to remove the excess of liquid. Samples were weighted (wet weigth – M_w) and then freeze-dried to obtain the final dry weight (M_{DF}). The swelling kinetics was defined as the ratio between the liquid uptake (M_W-M_{DF}) and the final dry mass (M_{DF}), according to **equation I.1.**

$$\textbf{Mass swelling ratio} = (M_w - M_{DF}) / M_{DF} * 100 \quad (\textbf{equation I.1})$$

Complementarily, the diameter of the hydrogel fibers was measured in at least three micrographs of each sample using NIH ImageJ software (http://rsbweb.nih.gov/ij/).

Similarly, the effect of the DM of MA-κ-CA and of the crosslinking mechanisms on the hydrogel swelling ratio at equilibrium was evaluated in Dulbecco's Phosphate Buffered Saline (DPBS) and DMEM. For this purpose, MA-κ-CA hydrogels with different DM (Low, Medium or High) and obtained with different crosslinking procedures (physical, chemical and dual) were lyophilized and weighted (initial dry weight, M_{DI}) before being transferred to 1.5

mL micro-centrifuge tubes. MA-κ-CA hydrogels were allowed to reach equilibrium over 24h in PBS or DMEM under dynamic conditions (shaking plate 40 rpm). Then, samples were retrieved from the swelling solution and weighted to determine the M_W, after being blotted off with a KimWipe paper to remove the excess liquid. Then the samples were lyophilized to determine their W_{DF}. The mass swelling ratio of MA-κ-CA was obtained according to **equation II.1**.

Concomitantly, the dissolution degree for dual crosslinked MA-κ-CA hydrogels (with different DM) was defined as the percentage of dry mass loss after swelling (e**quation II.2**).

$$\textbf{Dissolution degree} = M_{DF} / M_{DI} * 100 \quad (\textbf{equation II.2})$$

The purpose of the dissolution studies was to evaluate the integrity and stability of the MA-κ-CA hydrogels in physiological conditions. The dissolution degree of dual crosslinked MA-κ-CA hydrogels in DPBS and DMEM was evaluated over a period of 21 days.

II.2.3.3.2. Viscoelastic properties

Most hydrogels in their swollen state can be considered as rubbers that are lightly crosslinked networks with a rather large free volume that allows them to respond to external stress with a rapid rearrangement of the polymer segments. The response of the polymer network to such external forces provides information on network susceptibility to collapse, and thus on its stability. The viscoelastic behavior reflects the combined elastic and viscous responses, under shear stress. Generally, the parameters that describe this behavior are the storage modulus *G'* (storage modulus), associated with the elastic properties, and *G''* (loss modulus), related to the viscous properties. The ratio between the *G''* and *G'* moduli is defined as the tangent of the phase angle (Tan Delta, $tan\delta = G''/G'$), is a useful quantifier of the presence and extent of elasticity in a fluid and a measure of the internal friction of the material in that condition. When $G''<G'$ then $tan\delta < 1$, which means the sample is solid-like (more elastic than viscous), and *vice versa,* when $G''>G'$ then $tan\delta > 1$ and one can say that the sample is more liquid-like (more viscous than elastic). The crossover point, when $tan\delta$ is 1 ($G''=G'$), corresponds to the change of the viscoelastic behavior from solid-like ($G''<G'$) to liquid-like ($G''>G'$) comportment. This transition is correlated to the collapse of polymeric network and consequently the disruption of the crosslinking bridges that hold the 3D network.

Within the present thesis, oscillatory shear experiments were performed to analyze the effect of DM on the viscoelastic properties of the dual crosslinked MA-κ-CA hydrogels (chapter VIII). An oscillatory stress sweep was applied between 0.1 to 1000Pa at 37^{o}C and at a constant frequency of 0.1Hz, in a AR2000 stress controlled rheometer (TA instruments,

USA). The *G' and G"* of the swollen samples, were measured using a gap of 500µm and a 20mm parallel plate geometry. A solvent (PBS) trap was used in order to minimize the drying of the swollen hydrogels undergoing analysis.

II.2.3.3.3. Mechanical properties

Considering hydrogels as cell carriers, modulators and delivery systems, it is important to address the stability of the polymeric network under stress-relaxation cycles, reproducing the repetitive force loads that native tissues are exposed to. The ionic crosslinking of κ-CA enables the formation of strong, but brittle network, not compatible with sustained loadings. In gels with ionic crosslinks, stress relaxes mainly through breakage and consecutive readjustment of the crosslinked bonds. In contrast, in gels with covalent crosslinks, like the methacrylate moieties, stress relaxes through the migration of water within the network[66] rendering a higher degree of stability to the network.

Thus, the mechanical performance of 1.5%(wt/v) κ-CA hydrogels prepared by physical (ionic) crosslinking and MA-κ-CA with different DM (Low, Medium, High) and concentrations (2.5, 5, 7.5 and 10%wt/v), prepared by physical (ionic), chemical (UV exposure) or both crosslinking mechanisms was evaluated (chapter VIII) using an Instron 5542 mechanical machine (Instron, USA). Samples obtained immediately after crosslinking (as prepared samples) and samples that were allowed to swell in PBS for 24h before testing (hydrated samples), were analyzed. κ-CA and MA-κ-CA hydrogel discs (1mm thick, 8mm in diameter, n=6) were tested at a rate of 10%strain/min (0.1mm/min) until fracture. The compressive modulus (or Young's modulus) was defined as the slope of the linear region of the strain-stress curve, corresponding to 5–15% strain.

Besides determining the strength of the hydrogel, that indicates how much force the hydrogels can withstand, toughness was also taken into consideration as an indication of how much energy the hydrogels can absorb before fracturing. In order to be tough, a material must be both strong and ductile, withstand both high stresses and high strains. For example, brittle materials (like ceramics) that are strong but with limited ductility, are not tough; conversely, very ductile materials with low strengths are also not tough. Toughness was determined by measuring the area under the strain-stress curves as energy of mechanical deformation per unit of volume prior to fracture (kJ/m^3).

For the dual-crosslinked 5%(wt/v) MA-κ-CA hydrogels with different DM (Low, Medium and High) and 1.5%(wt/v) κ-CA prepared by physical crosslinking, 5 complete loading-unloading cycles were applied (strain range=0-50%). These cycles involve the representation of two curves: one for applying increased force (loading curve) and another one for decreasing the applied force at the same rates it was applied (0.1mm/min). On unloading, the sample gives up less energy (area under the unloading curve) than the energy it takes up to deform (area

under the loading curve). The difference between these two energies (area enclosed by the loop) is the energy lost during deformation. This energy loss is absorbed by the polymeric chain and is eventually dissipated as heat. Measuring the energy loss provides information over the material response after applying external forces. The higher the energy loss, the less the sample is able to recover to its initial shape after deformation. Thus, energy loss during deformation was determined as the area under loading-unloading strain-stress curves (hysteresis) for cycle 1 and 2.

The energy loss during deformation (within a loading-unloading cycle or consecutive loading curves) is strongly related to the recovery percentage after removing the external force and the fatigue of the sample. The recovery of the samples measures the differences in loadings between cycles. The recovery of the samples between cycle 1 and 2 was determined by calculating the percentage of area under loading curve of cycle 2 from the area of the loading curve of cycle 1. The higher the percentage, the higher the recovery of the samples to their initial mechanical performance, which is an aspect to pursue for development of materials that can withstand repetitive loading cycles without losing their mechanical behavior.

II.3. CELL SOURCES AND CULTURING PROTOCOLS

Stem cells have raised increased interested due to their ability to self-renew and to differentiate into multiple lineages. Thus, the scientific and medical community recognizes the potential of stem cells in TE and regenerative medicine.

Adult stem cells can be isolated from different tissues, including bone marrow, adipose tissue, umbilical cord, blood, and skin, among others[67]. In the present thesis, two sources of stem cells were used: adipose tissue and bone marrow, respectively to isolate human adipose derived stem cells (hASCs, chapters III, IV, VI and VII) and human bone marrow stem cells (hMSCs, chapter V).

The concept of using hASCs for regenerative medicine applications is highly appealing, mainly due to their resemblances to hMSCs[68,69], the “gold standard” cells for bone TE, demonstrated by their similar morphology, common surface markers and gene expression profiles[70,71,67], as well as their differentiation potential towards multiple lineages, namely the osteogenic[72], chondrogenic[72], adipogenic[72], myogenic[72] and neurogenic[73].

The major advantage of hASCs over hMSCs is their accessibility for harvesting under minimally invasive procedures, and their abundance (upon isolation more than 2% of cells feature potential for multi-lineage differentiation compared to the 0.002% of the bone marrow[74,70,75]).

Primary endothelial cells isolated from human umbilical cord of newborn babies (HUVECs) (chapter III) and were used as positive control for the endothelial differentiation of hASCs.

For the work described in chapter V, hMSCs were used as a cell pool equivalent to ASCs.
In chapter VIII mouse fibroblast cell line NIH-3T3 was used to obtain a preliminary evaluation of the potential of MA-κ-CA with different DM for cell encapsulation purposes, as these cells were robust and easy to culture and expand.
HASCs were obtained from human adipose samples obtained under protocols previously established between the 3B's Research Group and Hospital da Prelada (Porto, Portugal) and (Hospital Sao Marcos, Braga, Portugal). These protocols were approved by the hospitals ethics committee to assure that the requirements concerning donors' informed consent and anonymity (declaration of Helsinki guidelines http://www.wma.net/en/30publications/10policies/b3/) were fulfilled. Donors were healthy females, with an average age of 42 years, undergoing lipoaspiration procedures under cosmetic/esthetic purposes.
Bone marrow hMSCs were purchased from Lonza, Switzerland (Cat. N^{o} PT-2501, passage 1).

II.3.1. Adipose derived stem cells

II.3.1.1. Isolation of stromal vascular fraction

Tissue samples were transported to the laboratory facilities in transportation buffer (PBS supplemented with 10%(v/v) Pen/Strep (Gibco, UK) at a final concentration of 1000U/1000µg/mL) and processed within 24h post-surgery, according to an adapted isolation protocol[72]. The lipoaspirates were washed in PBS to remove blood, anesthetic and transportation buffer residues, and digested with 0.075% (chapter III) or 0.05% (wt/v) (chapters IV, VI and VII) collagenase II A (Sigma, Germany, Cat. N^{o} C6885, CAS 9001-12-1) in PBS, for 30 min, at 37^{o}C in a shaking water bath. Following digestion, the crude was filtered using a 200-µm pore size strainer. Mature adipocytes and connective tissue cells were separated by centrifugation at 1000*xg*, for 10min at 4^{o}C. The cell pellet was resuspended and incubated for 10min at room temperature in an in-house prepared erythrocyte lysis buffer (155mM NH_4Cl (Merck, Germany), 5.7mM anhydrous K_2HPO_4 (Riedel-de-Haen, Germany), 0.1mM EDTA (Sigma, Germany) in diH_2O, final pH=7.4). The cell suspension was centrifuged at 800*xg* for 10min at 4^{o}C. The pellet was resuspended in PBS and filtered with a 100µm cell strainer to obtain the stromal vascular fraction (SVF) of the AT (**Figure II.13**).

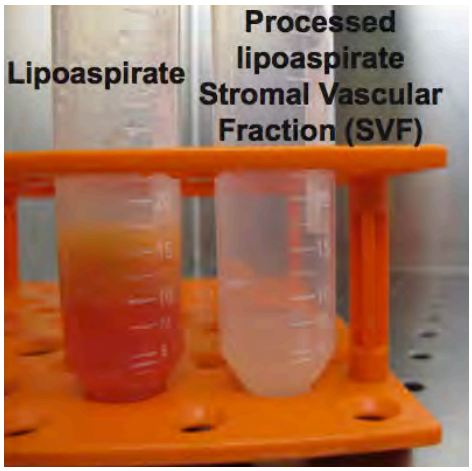

Figure II.13. The typical aspect of human lipoaspirates before (left) and after (right) processing. The lipoaspiration procedure consists in the disruption of fat depots and their collection in a container with transportation buffer. Since the fat tissue is light, tissue clumps float in a solution containing blood, anesthetic and buffers (left). After digestion of the tissue with collagenase and lysis of the red blood cells, the cellular suspension is homogeneous and deprived from tissue clumps.

II.3.1.2. Immunomagnetic beads coating and selection of SSEA-4^{+}hASCs

In the context of bone TE, the development of strategies that could effectively induce the microcirculation within the engineered constructs, while addressing the regeneration of the bone tissue, has become a major pursuit[76]. Previous *in vivo* studies showed that vascularization within engineered constructs using mature endothelial cells (ECs) improved blood perfusion, cell viability and their survival after implantation[77,78,79]. However, the limited availability and proliferation capability of mature ECs hinders their use in TE approaches[80]. Therefore, it became priority to find a suitable source of ECs that does not present such constrains and that will be ready-to-use for therapeutic applications.

The SVF of the AT is a heterogeneous cellular suspension that comprises several cellular sub-sets characterized by a specific surface marker signature. These cellular subpopulations are characterized by increased differentiation potential towards a certain lineage when compared with the heterogeneous population. For instance, STRO-1^{+}hASCs[81], CD49d^{+}hASCs[81], p75^{+}hASCs[81], CD90^{+}hASCs[81,82], and CD105^{-}hASCs[83] were shown to exhibit a higher osteogenic differentiation than the hASCs, while the CD29^{+}hASCs and CD105^{+}hASCs[81] exhibit a higher chondrogenic differentiation potential. These studies highlighted the potential of different cellular sub-sets that reside within SVF and, thus, the relevance of enriching SVF-derived cell population based on the expression of a surface marker. However, the greatest challenge for bone TE is to find the population that possesses a high differentiation potential towards both endothelial and osteogenic differentiation lineages that could act a single-cell source. Within the context of the current thesis, one of the aims was to establish a one-step cell selection protocol to deliver both

endothelial and osteoblast-like cells (chapter III) and to determine the culturing conditions in which both cell types retain their phenotype and functionality, envisioning the translation of these findings in a 3D cell-scaffold construct.

Stage specific embryonic antigen (SSEA-4) has been widely used as a marker to evaluate and monitor the undifferentiated state of human embryonic stem cells[84,85]. Based on the hypothesis that the SSEA-4$^+$hASCs are at an earlier maturation stage, thus exhibiting a higher potential towards endothelial and osteogenic lineages, relevant for bone TE, the selection of this subpopulation using immunomagnetic selection protocols was employed. This method is based on the attachment of small magnetic particles to cells *via* antibodies or lectins. When the mixed population of cells is placed in a magnetic field, those cells that have beads attached will be attracted to the magnet and may thus be separated from the unlabeled cells.

Within this thesis, immunomagnetic selection was employed to obtain the SSEA-4$^+$ subpopulation residing within the SVF (SSEA-4$^+$hASCs). For this purpose, immunomagnetic beads (4.5µm diameter, Dynabeads® M-450 Epoxy, Invitrogen, USA, Cat. N^o 14011) were coated with SSEA-4 antibody (clone MC813, 200µg/mL, SantaCruz Biotech, Cat. N^o sc-59368) as it follows: 50µL of immunomagnetic beads suspension were washed with 0.1M sodium phosphate buffer, resuspended with 10µL of the SSEA-4 antibody at a final concentration of 2µg/total volume, and then incubated, overnight, at room temperature, under gentle stirring. Following the coating, the SSEA-4 coupled beads were separated with Dynal MPC® magnet and washed with 0.2%(wt/v) bovine serum albumin (BSA) in PBS (BSA/PBS) and again separated using the magnet. This procedure was repeated three times. The SSEA-4 coupled beads were resuspended in 0.2%BSA/PBS at a concentration of 4x10^8 beads/mL. Coated beads were mixed with freshly isolated SVF in order to select the SSEA-4$^+$hASCs residing within the cell crude. The cells-bead coupling procedure was performed at 4°C, for 30 min, under gentle stirring. Subsequently, the mixture was washed with 0.2% BSA/PBS, and the cells bonded to the beads were separated from the rest of the cell suspension using the magnet (**Figure II.14**).

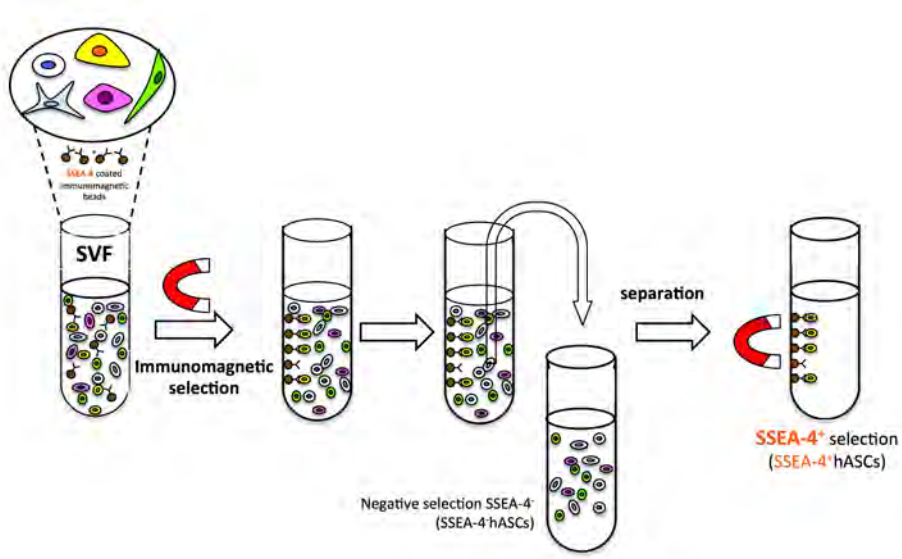

Figure II.14. Schematics of the immunomagnetic selection of SSEA-4^{+}hASCs from freshly isolated SVF.

II.3.2. Cell culturing protocols

All cells used under the experimental procedures of this thesis were cultured on tissue culture polystyrene surfaces (TCPS) such as flasks, well plates, coverslips, at 37^{o}C, in a humidified atmosphere with 5% $CO_{2.}$ The cell culture medium was chosen based on the pursued application (proliferation or differentiation, **Figure II.15**). All media formulations are described in **Table II.1**. During cell culture, medium was replenished every 3-4 days, if not otherwise specified, and cells were cultured until 70-80% confluency and trypsinized with trypsin (0.25% trypsin-EDTA solution, Sigma, Germany, chapters III, V and VIII) or 1xTrypLE^{TM} Express (Invitrogen, USA, Cat. N^{o} 12605-028, chapters IV, VI, VII). All cells, except the NIH 3T3 cell line, were used until passage 4.

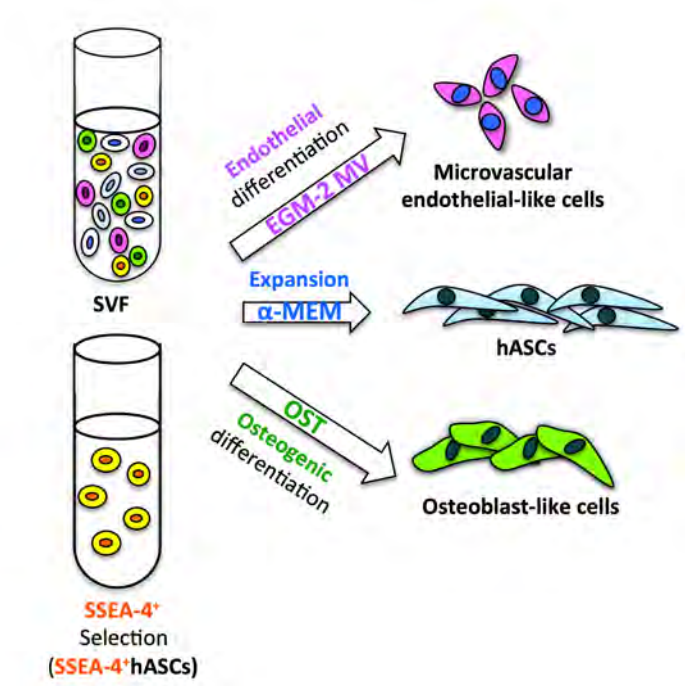

Figure II.15. Cell culturing schematics: hASCs and SSEA-4^{+}hASCs cells were expanded in expansion medium (α-MEM) and their differentiation potential towards endothelial and osteogenic lineages was assessed upon their culturing in specific media formulations.

The freshly isolated SVF was cultured in α-MEM medium. After 24h, non-adherent cells were removed by washing the tissue flasks with PBS. Adhered cells (i.e. hASCs) were cultured in α-MEM medium until confluence, trypsinized and then re-plated at a 1:5 ratio. The correspondent SSEA-4^{+}hASCs subsets were cultured following the same procedure, with the exception of the washing step. HMSCs were expanded in MSCs medium, while mouse fibroblast NIH3T3 cells were cultured in DMEM and HUVECs in M199 (**Table II.1.**)

Table II.1. Composition of the cell culture media

Cells	Medium	Composition	Chapter
SVF, hASCs and **SSEA-4$^+$hASCs**	**Expansion** medium **α-MEM**	1% (wt/v) α-MEM (Gibco, USA, Cat N^o 12000-063), supplemented with 1.1% (wt/v) $NaHCO_3$ (Sigma, Germany), 10% (v/v) FBS (Gibco, USA, Cat N^o 10270-106) and 1% (v/v) Pen/Strep (100U/100µg/mL, Gibco, USA, Cat N^o 15240-062)	III, IV
	Endothelial medium **ENDO**	**EGM-2 MV** (Lonza, Switzerland, Cat N^o CC-3162): 500 mL of EBM-2 (Cat N^o CC-3156) supplemented with EGM-2 SingleQuot Kit supplements and growth factors (Cat. N^o CC-4176)*: 25mL of FBS, 0.2mL hydrocortisone, 2mL hFGF-B, 0.5mL ascorbic acid, 0.5mL VEGF, 0.5 mL Long hR3-IGF-1, 0.5 mL hEGF, 0.5 mL heparin and 0.5mL gentamicin/amphotericin **concentrations of supplements are not disclosed by the manufacturer*	III, IV, VII
	Osteogenic medium **OC** and **OI**	**Osteoconductive (OC)** Osteogenic differentiation medium consisting in α-MEM medium with osteogenic supplements: 10mM (Sigma, Germany, Cat. N^o G9422) and 50µg/mL AA (Sigma, Germany, Cat. N^o A8960)	V
		Osteoinductive (OI or **OST)** OC medium supplemented with 10^{-8}M Dex (Sigma, Germany, Cat. N^{o}D4902)	III, IV V, VI
SSEA-4$^+$hASCs	**MIX** medium	EGM-2 MV with osteogenic supplements (βGP, AA and Dex at the same concentration as in OST medium)	IV
hMSCs	**MSCs** medium	Mesenchymal stem cell growth medium (Poietics^{TM} MSCGM^{TM} BulletKit^{TM}, Lonza, Switzerland, Cat. N^o PT-3001)* containing 440mL of MSCBM^{TM} supplemented with SingleQuots^{TM} of growth supplements **concentrations of supplements are not disclosed by the manufacturer*	V
HUVECs	**M199**	1.47% (wt/v) M199 medium (Sigma, Germany, Cat N^o M2520) supplemented with 20%(v/v) HiFBS (Gibco, USA, Cat N^o 10270-106, 1%(v/v) Pen/Strep (100U/100µg/mL, Gibco, USA, Cat. N^o 15240-062), 50µg/mL ECGS (BD Biosciences, USA, Cat. N^o 356006), 1.7mL Glutamax I (Gibco, USA, Cat N^o 35050-038) and 50µg/mL sodium heparin (Sigma, Germany, Cat N^o H3149)	III

NIH-373	**DMEM**	1% (wt/v) DMEM (Low glucose, L-glutamine and sodium pyruvate, phenol red, Gibco, USA, Cat. N^{o} 31885-023) supplemented with 1.1% (wt/v) $NaHCO_3$, 10% (v/v) HiFBS (Gibco, USA, Cat. N^{o} 10270-106) and 1% (v/v) Pen/Strep (100U/100µg/mL, Gibco, USA, Cat. N^{o} 15240-062)	VIII

Abbreviations:
α-MEM = Minimum Essential Medium Eagle-alpha Modification; **AA** = L-ascorbic acid 2-phosphate sesquimagnesium salt hydrate; **βGP** = beta-glycerophosphate disodium salt hydrate dehydrate; **Dex** = dexamethasone; **DMEM** = Dulbecco's Modified Eagle Medium; **EBM** = Endothelial basal medium; **ECGS** = endothelial cell growth supplement; **EGM-2 MV** = Endothelial growth medium; **FBS =** fetal bovine serum; **hEGF** = human epidermal growth factor; **HiFBS** = heat inactivated fetal bovine serum; **hFGF-B** = human fibroblat growth factor-basic with heparin; **MSCBM** = mesenchymal stem cell basal medium; **MSCGM** = mesenchymal stem cell growth medium; **$NaHCO_3$** = sodium bicarbonate; **Pen/Strep** = penicillin/streptomycin; h**R3-IGF-1** = human recombinant insulin-like growth factor (substitution of arginine for glutamine at position 3); **VEGF** = vascular endothelial growth factor.

II.3.2.1. Endothelial differentiation

Standard endothelial differentiation protocols involve the use of VEGF[86] in concentration that range from 10[87,88] to 50ng/mL[89]. However, concentration of 50ng/mL of VEGF might impair the therapeutic application of the differentiated cells, while lower VEGF concentrations are usually associated with other procedures such as applying shear stress[90] and/or co-culturing with other cells types (e.g. vascular smooth muscle cells[88]).

EGM-2 MV medium is a medium formulation that contains a cocktail of growth factors (see **Table II.1**) that was designed for the maintenance and growth of microvascular ECs cultures (e.g. umbilical vein, pulmonary artery, aortic artery, umbilical artery microvascular endothelial cells). Although the manufacturer does not provide the concentrations of the growth factors, the concentration of VEGF in the kit was determined to be < 5ng/mL[91].

Within the current thesis, freshly isolated SVF, adhered hASCs and corresponding SSEA-4^{+} hASCs were cultured in complete EGM-2 MV, without additional supplementation with VEGF. Cells were cultured until passage 5. At each passage, cells were retrieved to be characterized in terms of endothelial phenotype. Cells cultured in α-MEM were used as negative controls.

II.3.2.2. Osteogenic differentiation

The differentiation of MSCs towards the osteogenic lineage is very well documented in literature and it requires the supplementation of culture medium with ascorbic acid, beta-glycerophosphate (βGP) and dexamethasone (Dex), that trigger and support the commitment into the osteogenic pathway[92,93]. Ascorbic acid (or vitamin C) has been demonstrated to be involved in the hydroxylation of proline and lysine residues of collagen, thus enabling the organization of the polypeptide chains into the conformation necessary to

form the collagen triple helix. In fact, the prolonged exposure of cultures of human connective-tissue cells to ascorbic acid induced an eight-fold increase in the synthesis of collagen with no increase in the rate of synthesis of other proteins[94]. Ascorbic acid has also been demonstrated to increase alkaline phosphatase (ALP) activity, a prerequisite for the subsequent bone-like matrix deposition and mineralization[95]. As ascorbic acid has a very short half-life in cell culture conditions, a long active derivative, L-ascorbic acid 2-phosphate (AA), was used to supplement the culture medium.

Together with AA, βGP was found to be a prerequisite for the formation and mineralization of the extracellular matrix. βGP is the organic phosphate source, playing an important role in the modulation of osteoblasts activities, namely on the ALP activity and osteocalcin (OCN) production.

While AA and βGP favor the commitment into the osteogenic lineage by inducing the deposition of a collagen-enriched matrix and its further mineralization, Dex, a synthetic gluco-corticosteroid, triggers and sustains the cascade of events, including chemokine and calcium signaling[96] that lead to the full commitment and maturation of osteoblast-like cells.

Therefore, in order to address the osteogenic potential of hASCs and SSEA-4$^+$ (chapter VI) in the presence of sNPs, cells were seeded at a density of 2,000 cells/cm^2, allowed to adhere to TCPS and further in either growth or osteogenic media (**Table II.1**) after addition of sNPs suspensions (1, 10 and 100µg/mL. At pre-selected time points (3, 7, 14, 21 and 28 days), samples were retrieved to characterize the cells in terms of osteogenic phenotype. Furthermore, in chapter V, hMSCs were cultured with α-MEM medium with AA and βGP without Dex (osteoconductive medium, OC) and with Dex (OI medium), in order to address the effect of sNPs as a Dex substitute during the osteogenic differentiation. In all experiments, cultures in α-MEM were used as negative controls.

II.3.2.3. Establishment of the co-cultures

In the context of bone development and regeneration, the intimate association of the microvascular endothelium with osteogenic cells suggests that ECs may directly regulate the differentiation of osteoprogenitor cells and the mineralization ability of osteoblasts (OBs). The current co-culturing protocols involve the use of cells obtained from tissues containing fully committed cells (OBs from bone; ECs or EPCs from peripheral blood or new born umbilical cord) or undifferentiated hMSCs from bone marrow. However, the difficulty in retrieving these cells and their low availability might hamper their use in a prospective clinical application. Thus, after confirming that SSEA-4$^+$hASCs can be successfully differentiated into the endothelial and osteogenic lineages, this sub-population was considered as a suitable cell source for establishing a co-culture of osteoblast- and endothelial-like cells. In literature, the combination of mature OBs with ECs[97], hMSCs with

ECs[98,99,100], hMSCs with EPCs[101] or pre-differentiated osteoblast cells with ECs[102] have been proposed. Amongst these, the combination of less differentiated osteoblastic cells with mature and fully differentiated ECs proved to be the most effective[102,103]. Additionally, together with the cell sourcing, other questions regarding the optimal medium for the co-culture, which cell combination is the most effective and in which ratio, still exist.

The co-culture experiments performed under the scope of this thesis were designed considering the use of endothelial differentiated SSEA-4$^+$hASCs (*i.e.* ECs) and pre-conditioned osteoblast-like SSEA-4$^+$hASCs (pre-OBs) (**Figure II.16**). The latter were derived from SSEA-4$^+$hASCs cultured in α-MEM at passage 1, followed by a 7-day culture in osteogenic medium (OST). Cells were then trypsinized and mixed with SSEA-4$^+$hASCs-derived ECs at different cell ratios (ECs:pre-OBs; 100:0, 75:25, 50:50, 25:75 and 0:100). Cells suspensions, at appropriate ratios, were seeded in 24 well plates at a density of 2,000 cells/cm^2 with 500µL of EGM-2 MV, OST and MIX media. The MIX medium was defined to sustain the growth of ECs using the standard culture medium (EGM-2 MV) while accompanying the full differentiation of pre-OBs, due to the presence osteogenic factors (AA, βGP and Dex) (**Table II.1**). Monocultures of ECs (100:0) and pre-OBs (0:100) in the three media formulations served as controls.

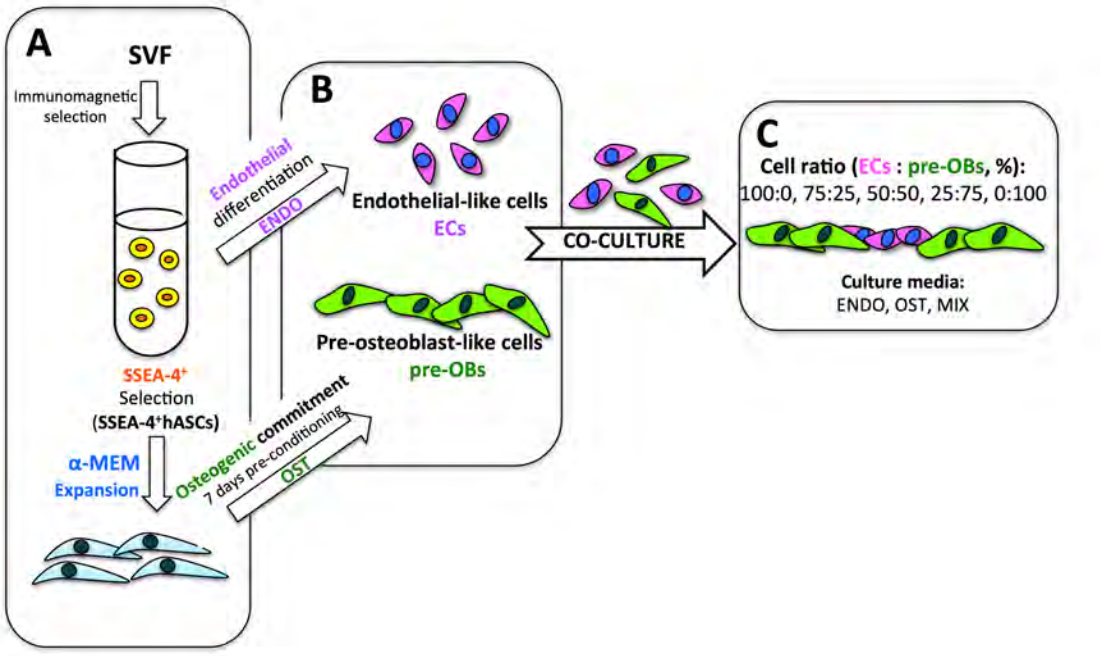

Figure II.16. Schematics of the experimental co-culture setup describing the (**A**) selection of SSEA-4$^+$hASCs, (**B**) endothelial differentiation of SSEA-4$^+$hASCs and osteogenic conditioning prior initiation of co-culture experiments, and (**C**) the co-culture conditions.

II.4. IN VITRO STUDIES

II.4.1. Culturing cells in the presence of *sNPs*

II.4.1.1. Fluorescent labeling of sNPs

In chapters V and VI, a fluorescent labeling of the sNPs was performed, in order to be able to visualize/track them. Briefly, sNPs were added to a 0.1%(wt/v) rhodamine B isothicyanate (Sigma, Germany, excitation: 550nm and emission: 570nm) or 0.05% Cy3 tagged lysozyme (Nanocs, USA, excitation: 550nm and emission: 570nm) solution prepared in dimethylsulphoxide (DMSO, Sigma, Germany), protected from light. The mixture was kept under continuous stirring, for 24h at 4^{o}C. Several washing steps with absolute ethanol were performed to promote the separation of the sNPs from the organic phase and to remove the excess of dye. The sNPs were air dried, and kept at room temperature in dark sealed vials until further use.

II.4.1.2. Addition of sNPs to cells

Intrinsic and extrinsic properties of nanoparticles such as specific surface area and charge, functionality, and size and shape play direct roles in determining specific cellular responses[104]. Thus, under the context of this thesis the effect of sNPs over the cell behavior was investigated by assessing the cytotoxicity, internalization mechanism and influence on cellular morphology and differentiation potential (**Figure II.17**). In chapter V, sNPs were added to hMSCs, while in chapter VI, SSEA-4^{+}hASCs were cultured in the presence of sNPs, at concentrations ranging from 0 to 2mg/mL, according to culturing protocols described in section II.3.2.2.

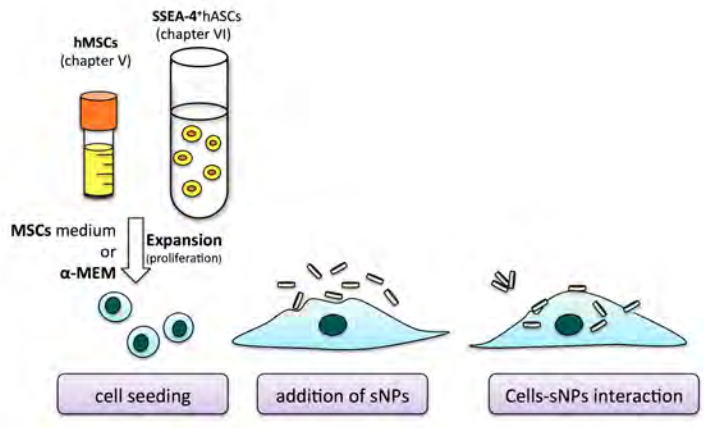

Figure II.17. Representation of the addition of sNPs to cells and the subsequent interaction.

II.4.2. Cell encapsulation

Encapsulating cells in hydrogels offers numerous attractive features for TE, including highly hydrated tissue-like environments for cell and tissue growth that potentiate the ability to form *in vivo* functional systems. Many of the properties that are important to the design of

hydrogels, such as swelling, mechanical properties, degradation, and diffusion patterns, are closely linked to the crosslinking degree of the hydrogel, which is controlled through a variety of different processing conditions. Within the present thesis, cells were encapsulated in hydrogels obtained by physical (IG and PEC, chapters VII and VIII) and chemical (UV exposure, chapter VIII) crosslinking (**Figure II.18)**. Because cells are present during the gelation process, it is important to use mild experimental methods (preparation, handling, culturing), so that the viability and functionality of the cells is not jeopardized.

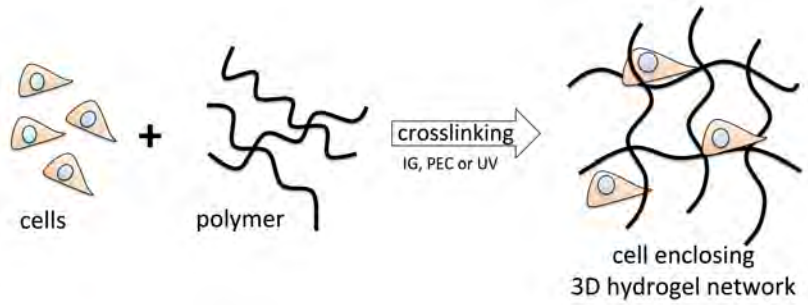

Figure II.18. Cell encapsulation in 3D hydrogel network obtained through physical (IG and PEC) and chemical (UV exposure) crosslinking methods.

II.4.2.1. Cell encapsulation within κ-CA fibers (with and without CHT coating)

In chapter VII, SSEA-4$^+$hASCs-derived ECs in passage 3 (obtained as described in section II.3.2.1), were resuspended in a 1.5%(wt/v) κ-CA solution, at a final cell density of 2x10^6 cells/mL, that was then extruded through 25 and 27G needles to produce the fibers with or without CHT coating, according to the procedure described in sections II.2.1.1 and II.2.1.2. The cell-loaded fibers were then transferred to adherent 24-well plate and maintained in culture for 21 days in EGM-2 MV medium at 37°C in a humidified atmosphere with 5% of CO_2, with the replenishment of cell culture medium every 3-4 days (**Figure II.19**). Prior encapsulation, the κ-CA, CHT and KCl solutions were sterilized at 120°C for 30min. Fiber formation and cell encapsulation procedures were carried out at room temperature and under asseptic conditions.

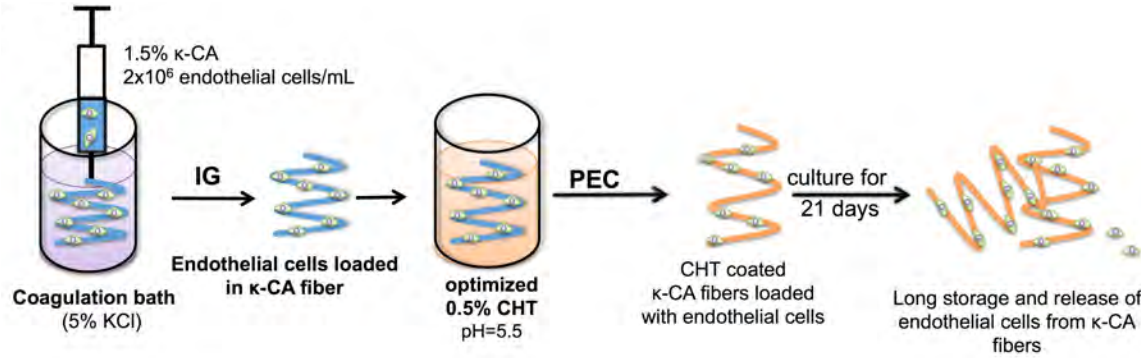

Figure II.19. Schematics of the encapsulation of endothelial cells derived from SSEA-4$^+$hASCs into κ-CA hydrogels fibers, with and without CHT coating.

The shape of the developed cell laden fibers (with or without CHT coating), as well as the presence/absence of cells on the bottom of the well, were examined using a stereomicroscope (Stemi 1000 PG-HITEC, Zeiss, Germany) and the images were obtained using a digital PowerShot G6 camera (Canon, Japan).

II.4.2.2. Assembling of κ-CA fibers into 3D hydrogel discs

Cell-laden κ-CA fibers containing SSEA-4^{+}hASCs-derived ECs were labeled with a green fluorescent (Calcein-AM) tag, transferred to a petri dish and allowed to settle randomly. A freshly prepared solution of 1.5% (wt/v) κ-CA containing SSEA-4^{+}hASCs-derived OBs (section II.3.2.2) labeled with a red fluorescent (rhodamine B) tag, was poured on top of the fibers until full coverage. The crosslinking of the κ-CA solution was achieved by the addition of a 5%(wt/v) KCl solution, for 10min. After crosslinking, the cells nuclei were stained with DAPI (Sigma, Germany). The hydrogels discs containing the fibers were then washed with PBS and observed under a confocal laser scanning microscope (CLSM, Fluoview 1000, Olympus, USA). YZ and XY projections were performed in order to evaluate the cellular distribution throughout the structures (chapter VII).

II.4.2.3. Retrieval of cells from κ-CA fibers

In order to assess the maintenance of the phenotype of the SSEA-4^{+}hASCs-derived ECs after 21 days of culture (chapter VII), κ-CA fibers containing cells were transferred to sterile micro-centrifuge tubes and treated with 0.1% (wt/v) proteinase K (vWR, Portugal) in 1mM EDTA (Sigma, Germany), 50mM TrisHCl (Sigma, Germany) and 1mM iodoacetamide buffer (Sigma, Germany), for 1h at 37^{o}C, under constant agitation, to release the cells from the fibers. The cellular pellet recovered after centrifugation (10min, 400x*g*) was resuspended in EGM-2 MV medium and plated into tissue culture flasks. Cells were cultured until reaching confluence, after which they were characterized as described in sections II.5.5-6 and II.5.9.3.

II.4.2.4. Cell encapsulation within MA-κ-CA hydrogels

The formation of MA-κ-CA hydrogels relies on the presence of a photoinitiator (PI), that under UV exposure generates free radicals that then initiate and propagate the crosslinking of the polymeric chains. It is important that PIs exhibit low toxicity, thus making it possible to polymerize a cell suspension and thus encapsulate viable cells within hydrogels. Amongst the PIs usually used during the photopolymerization process and implicitly during hydrogels formation, Irgacure 2959 (2-hydroxy-1-[4-(hydroxyethoxy)phenyl]-2-methyl-1-propanone) was proven to cause minimal cell death over a broad range of mammalian cell types[105]. Additionally, long exposures to UV light can affect cellular integrity and viability, thus short

exposures are desirable. Thus, in chapter VIII, a low concentration of Irgacure 2959 (0.25% wt/v) and a short exposure to UV (40sec) were the chosen parameters to obtain cell enclosing MA-κ-CA hydrogels.

NIH-3T3 fibroblasts were encapsulated within MA-κ-CA hydrogels with different DM (Low, Medium and High) prepared by applying both physical and chemical crosslinking. Briefly, cells were resuspended in 5% (wt/v) MA-κ-CA polymer containing 0.25% (wt/v) PI at a density of $2x10^6$ cells/mL polymer solution. The cells suspension was poured onto a Teflon sheet and using coverslip spacers, cell-laden hydrogels of 450μm and 1cm diameter were formed after UV light exposure. After attaching the crosslinked hydrogels on TMSPMA coated glass, the hydrogels containing cells were further crosslinked in a coagulation bath, as previously described (section II.2.2.3). Afterwards, hydrogels were rinsed with PBS, placed into 6-well culture plates and cultured in DMEM medium.

II.4.2.5. Cell encapsulation within patterned MA-κ-CA hydrogels

PDMS is an elastomeric silicon-based material widely used in microfabrication approaches owing to its biocompatibility, optical transparency, gas permeability, mechanical elasticity, and electrical insulation, as well as due to its capability to consistently replicate micro- and nano-features[106,107]. Since PDMS pre-polymer is liquid at room temperature, it can flow over nearly any micro- and nano-feature. At Increased temperatures PDMS cures forming an elastic material.

To obtain a PDMS mold, a mixture of PDMS pre-polymer and curing agent (10:1) was poured on a silicon wafer (master pattern) that was first silanized with (tridecafluoro-1,1,2,2,-tetrahydrooctyl)-1-trichlorosilane to facilitate subsequent release/detach of patterned PDMS stamp. The PDMS mold, replicating the feature of the master, was cured at 70^{o}C for 1h..

In chapter VIII, PDMS molds (100μm diameter x 300μm depth) were used to obtain circular patterns in cell loaded MA-κ-CA hydrogels (Medium DM), based on the fact that PDMS allows the UV light to pass through, so that the MA-κ-CA solution could be crosslinked. A MA-κ-CA cellular suspension (obtained as described in section II.4.2.4) was pipetted on a TMSPMA coated glass slide. The solution was stamped with the PDMS mold and the micro-patterns of the PDMS were transferred to the hydrogel upon UV exposure (6.9mW/cm^2, 40 sec, as described in section II.2.2.2). The non-crosslinked polymer was gently removed by immersing the TMSPMA slide containing the pattern in PBS (**Figure II.20**).

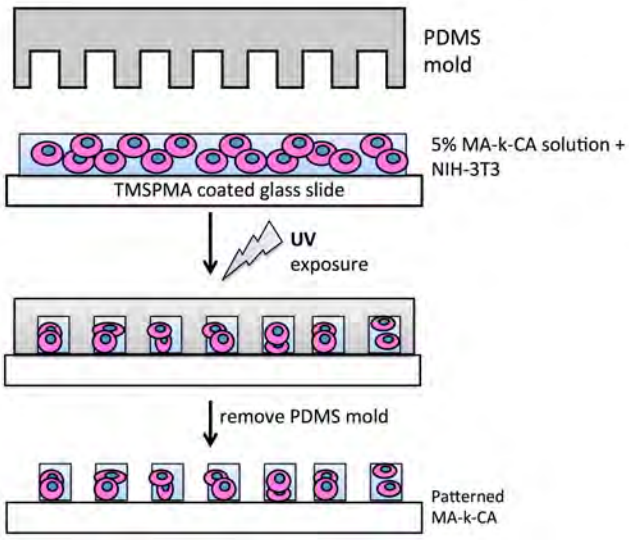

Figure II.20. Schematics for the fabrication of patterned MA-κ-CA hydrogels with controlled distribution of cells.

II.5. BIOLOGICAL EVALUATION OF THE DEVELOPED SYSTEMS

II.5.1. Morphological evaluation

II.5.1.1. Monitoring of the cultures

An initial indication of the cellular phenotype is the evaluation of the morphology of the cells. While undifferentiated hASCs, SSEA-4$^+$hASCs and hMSCs were characterized by an elongated, fibroblast-like morphology, SSEA-4$^+$hASCs-derived ECs and HUVECs displayed a cobblestone-like morphology. Based on these characteristics, the morphology of cells cultured in the absence (chapter III) and presence of sNPs (chapter V and VI), in co-culture (chapter IV) and released from the κ-CA fibers (chapter VII) was monitored along the time using a stereo microscope Stemi 1000 (Zeiss, Germany).

II.5.1.2. Evaluation of cytoskeleton organization upon addition of sNPs

The effect of sNPs concentrations over the morphology of cells was addressed in chapters V and VI. Briefly, hMSCs and SSEA-4$^+$hASCs, both at passage 2, were seeded on tissue culture polystyrene (TCPS) coverslips (Sarstedt, USA) in 24-well plates, at a cell density of $2x10^3$ cells/cm^2 and allowed to adhere. After 24h, rhodamine or lysozyme-cy3-labeled sNPs (at concentrations below IC_{80}: 0, 1, 10 and 100μg/mL) were added to the culture wells. After additional 24h of standard culture, samples were washed with PBS and fixed with 10% formalin. Cell cytoskeleton was stained either with phalloidin-rhodamine (Invitrogen, USA) or with CytoPainter F-actin (abcam, USA, Cat. N^o ab112124). Cell nuclei were counterstained with DAPI, at a 1:10,000 dilution in PBS, for 10min, and then washed three times. Samples were visualized under a fluorescence microscope and photographed by suitable acquisition software.

II.5.2. Cytotoxicity screening

II.5.2.1. Reactive species

Reactive oxygen species (ROS) and reactive nitrogen species (RNS) are generated as natural products of the cell respiratory metabolism and are overproduced as an immediate response to stress, upon which other cellular events are favored or not. For instance, elevated levels of ROS and RNS are implicated in cell injury and death by inducing oxidative and nitrosative stress[108]. It has been also reported that cancer cells could be locally damaged using specifically targeted gold nanoparticles and laser pulse irradiation, due to the high concentrations of ROS formed within the irradiated cells[109], with minimum damage to the nearby particle-free tissue.

The formation of photocrosslinked hydrogels relies on the presence of a PI that under UV exposure generates free radicals that initiate and propagate the crosslinking of the polymeric chains. Amongst the PIs usually used during the photopolymerization process and implicitly during hydrogels formation, Irgacure 2959 was proven to cause minimal toxicity (cell death) over a broad range of mammalian cell types[105].

Thus, envisioning TE applications and the therapeutic usage of nanoparticles or photocrosslinkable hydrogels, the levels of reactive species must be as low as possible. Therefore, it is important to determine the “safe dosage window” where cells are not significantly affected by the addition of nanoparticles[110,111] or UV light exposure and presence of PI. .

II.5.2.1.1. Reactive oxygen species production by hMSCs in the presence of sNPs

In chapter V, the production of reactive species by hMSCs upon exposure to a concentration range (0-10mg/mL) of sNPs was taken into consideration as the initial response of cells when encountering the sNPs. Superoxide (SOx) and nitric oxide (NOx) production was assessed as representative units for ROS and RNS, respectively.

Intracellular production of SOx and NOx was evaluated respectively using the dihydroethidium (DHE, Molecular Probes, USA, Cat. N^{o} D1168) and the 4,5-diaminofluorescein diacetate (DAF-2DA, Calbiochem, USA, Cat. N^{o} 251505) oxidation assays. HMSCs (2x10^{4} cells) in passage 4 were seeded on 24-well plate and allowed to adhere. After reaching 70% confluence, cells were pre-incubated with DHE (25µM) for 10 min and DAF-2DA (10µM) for 30min at 37^{o}C. Cells were then washed with PBS and sNPs suspensions (0, 1, 10, 100, 1.000, 10,000, 20,000µg/mL) in phenol red-free DMEM (Gibco, USA, Cat. N^{o} 11880-036) without FBS were added to the cells. After 2h of incubation, cells were washed with PBS and then fixed with 4% paraformaldehyde for 40min. Samples were examined using a Eclipse TE2000-U fluorescence microscope (Nikon,Japan) equipped with FITC filter (ex: 450–505nm; polychromatic mirror: 510–555nm; barrier filter: 515–545nm)

and FITC-Texas Red filter (ex: 560–580nm; polychromatic mirror: 585–665nm; barrier filter: 600–650nm).

The quantification of the fluorescent signal was performed using NIH ImageJ software and considering the intensity of fluorescence per single cell for each of the evaluated conditions.

II.5.2.1.2. Reactive species production in NIH-3T3 upon encapsulation in MA-κ-CA hydrogels

In chapter VIII, the production of SOx and NOx, as indicators of oxidative and nitrosative stress in cells, was evaluated to determine to which extent the chemistry (DM) and crosslinking mechanism (chemical, physical or both) of hydrogels affected the encapsulated cells. Intracellular production of SOx and NOx was evaluated as previously described (section II.5.2.1.1). NIH-3T3 fibroblasts ($2x10^5$ cells) pre-incubated with 25μM DHE and DAF-2DA were washed with PBS, centrifuged at 1200rpm, for 5min, and resuspended in 1.5% κ-CA (wt/v) and 5% (wt/v) MA-κ-CA solution with different DM (Medium, Low, High) and 0.25% PI (wt/v). The cells-containing MA-κ-CA solutions were UV crosslinked for 40sec and the obtained hydrogels were immersed in a bath of 5% KCl for 10min for further crosslinking. Control κ-CA hydrogels containing cells were obtained by crosslinking in the same coagulation bath for 10min, with and without the UV exposure. All cell-loaded hydrogels were washed with PBS and incubated at 37^{o}C in phenol-red free DMEM for 2h for SOx and 1h for NOx quantification. Pre-incubated cells (in suspension), mounted on glass slides using Fluoromount mounting media (Sigma, Germany), were used as threshold for SOx and NOx levels, respectively. Visualization and quantification were performed as described above. Initial SOx and NOx levels were attributed to stress exercised on cells by trypsinization, centrifugation, resuspension and incubation period with the reagents.

II.5.2.2. Released lactate dehydrogenase quantification

Lactate dehydrogenase (LDH) is a stable cytoplasmic enzyme that is found in all cells in small amounts. LDH is rapidly released into the cell culture supernatant when the plasma membrane is damaged, thus LDH is commonly used as an indicator of cell damage[110,111]. LDH has been also extensively used as a marker of lethal cell injury in both *in vitro* and *in vivo* screenings to assess the cytotoxicity of nanoparticles[112]. Thus, within this thesis, LDH was used to evaluate the cytotoxicity of sNPs (chapter V) by using the CytoTox96® Non-Radioactive Cytotoxicity Assay (Promega, WI, USA, Cat. N^o G1780). Cells (hMSCs) were seeded in a 96-well plate, in MSCs medium (**Table II.1**), and allowed to adhere for 24h , treated with different amounts of sNPs (0, 1, 10, 100, 1,000μg/mL) and incubated for 24h at 37^{o}C. Following the manufacturers protocol, the culture medium of untreated cells was used as negative control (0% cytotoxicity) and a suspension of the lysed cells was used as

positive control (100% cytotoxicity). At the end of the incubation time, the well plate was centrifuged at 600*xg* for 10min, 10µL of supernatant from each sample well and controls were transferred into 96 well plates, 100µL of the LDH reaction mix was added to each well and the plate was incubated for 30min at room temperature. Absorbance measurements were performed at 490nm in a SpectraMax M5 microplate reader (Molecular Devices, USA).

II.5.2.3. Metabolic activity quantification

After addressing the production of reactive species and LDH release as cells immediate response to the addition of sNPs, the assessment of the metabolic activity was carried on (chapters V and VI).

In chapter V, the metabolic activity of hMSCs upon addition of sNPs was evaluated using an MMT (3-[4,5-dimethylthiazol-2-yl]-2,5 diphenyl tetrazolium bromide)-based assay (MTT Cell Proliferation Assay, ATCC, USA, Cat. N^{o} 30-1010K). This assay is based on the conversion of MTT into formazan crystals by living cells, which determines mitochondrial activity. Since for most cell populations the mitochondrial activity is related to the number of viable cells, this assay is broadly used to measure *in vitro* cytotoxic effects on cell lines or primary cells[113]. HMSCs (passage 3) were seeded in 96-well plates at a density of 2x10^{3}/cm^{2} in MSCs medium (**Table II.1**) and allowed to adhere for 24h. SNPs (concentration 0, 1, 10, 100, 1,000, 10,000, 20,000µg/mL) were added to the cells and allowed to interact for 24h. After this period, the medium was replaced with 100µL of fresh culture medium and 10µL of MTT solution. Samples were incubated at 37^{o}C for 4h. After the incubation time, 100µL of lysis buffer were added to each well and plates were further incubated at 37^{o}C for 2h. The absorbance was measured at 540nm in 100µL of the lysed samples in a SpectraMax M5 microplate reader (Molecular Devices, USA). The metabolic activity was normalized with the control (without any sNPs). The concentration at which the metabolic activity of hMSCs was reduced to 50% was defined as the half maximal inhibitory concentration (IC_{50}) and determined to be 4mg/mL of silicate concentration.

In chapter VI, the effect of sNPs over the metabolism of adhered SSEA-4^{+}hASCs was investigated using the MTS ((3-(4,5-dimethylthiazol-2-yl)-5-(3-carboxymethoxyphenyl)-2-(4-sulfophenyl)-2H-tetrazolium) – based assay. The MTS assay is often described as a 'one-step' MTT assay, which offers the convenience of adding the reagent straight to the cell culture without the intermittent steps required in the MTT assay. However, this convenience makes the MTS assay susceptible to colorimetric interference, as the intermittent steps in the MTT assay remove traces of any colored compounds (e.g. phenol red, serum, etc.), whilst these remain in the microtitre plate in the one-step MTS assay. Thus the addition of MTS reagent is performed in phenol-free medium without FBS.

SSEA-4^{+}hASCs (passage 2) were seeded in 48-well plates, at a density of 2x10^{3} cells/cm^{2}

and cultured in complete α-MEM. After 3 days, sNPs were added to the cells in different concentrations (0, 0.5, 1, 5, 10, 25, 50, 100, 250, 500, 1,000, 2,000, 10,000µg/mL). At pre-selected time points (days 1, 3 and 7), cells were washed thoroughly with PBS, and 250µL MTS working solution consisting in serum- and phenol-red free DMEM medium and MTS reagent in a 5:1 ratio, was added to the cells. Samples were incubated for 3h, after which 100µL of each sample were transferred to 96-well plates and absorbance was measured at 490nm on a microplate reader (Synergy HT microplate reader, Biotek, USA). The metabolic activity was normalized with the cells-control group (without any sNPs) to determine the dose response. The concentration at which the metabolic activity of hMSCs was reduced to 80% was regarded as the inhibitory concentration-80 (IC_{80}) and was considered as an exclusion parameter.

MTS assay was also chosen to evaluate the metabolic activity of co-cultured SSEA-4^+hASCs-derived ECs and pre-OBs as a function of ratio, culture media and time (chapter IV). At pre-selected time points (days 4, 7, 14 and 21) cells were washed thoroughly with PBS and the assay performed as described above.

II.5.2.4. Cell proliferation assessment

II.5.2.4.1 AlamarBlue® assay

The AlamarBlue® assay incorporates a fluorometric/colorimetric oxidation-reduction (REDOX) that both fluoresces and changes color in response to chemical reduction of growth medium resulting from cell growth. The active ingredient of alamarBlue®, resazurin is a non-toxic, cell permeable dye that is blue and weakly fluorescent. It is used as an oxidation-reduction indicator that undergoes colorimetric change in response to chemical reduction of growth medium resulting from cell growth[114]. The reduced form resorufin is pink and highly fluorescent. The amount of fluorescence is proportional to the number of living cells; therefore it is an ideal indicator to generate a quantitative measure for cell growth and indirectly for cytotocixity

In chapter V, AlamarBlue® was used to evaluate the effect of sNPs (0, 1, 10 and 100µg/mL) over the growth of hMSCs. At determined time points, the culture media was removed and the cells were washed twice with PBS. Then the PBS was replaced with 10% (v/v) of AlamarBlue® reagent (AbD Serotec, UK, Cat. N^o BUF012B) and incubated at 37^{o}C, 5% CO_2 humidified atmosphere for 3h. At the end of the incubation period, the supernatant of the cultures was transferred into 96-well plate in triplicates and a colorimetric reading was performed using a microplate reader (Epoch, Biotek, USA) at 570 and 600nm, respectively excitation and emission wavelengths. Culture medium was used as negative control. After supernatant removal, cells were washed in PBS and fresh medium was added to maintain the culture. The proliferative potential of cells was reported as percentage (%) of reduced

AlamarBlue®

II.5.2.4.2 DNA Quantification

The total amount of double-stranded DNA (dsDNA) is constant for individual cell types and therefore its quantification directly correlates to the cell number. PicoGreen® is a fluorochrome that selectively binds to dsDNA, circumventing the interference from single stranded DNA (ssDNA) and other contaminants, such as proteins, RNA and extraction buffers in the quantification of the number of cells. When bound to dsDNA, fluorescence enhancement of PicoGreen® is exceptionally high and little background occurs since the unbound dye has virtually no fluorescence. In the present work, cell counts and proliferation rate were quantified by Quant-iT^{TM}PicoGreen®dsDNA assay (Invitrogen, USA, Cat. N^{o} P7589).

A protocol was defined according to manufacturer instructions and applied in chapters IV-VI after obtaining a cell lysate by subjecting the samples to consecutive osmotic and thermal shocks. The samples and standards were mixed with the PicoGreen® reagent, previously diluted 200-fold in Tris-EDTA buffer, on a 1:1 ratio in a 96-well opaque plate (Corning, USA) and incubated for 5min protected from light. The fluorescence of the dye was measured at an excitation wavelength of 485/20nm and at an emission wavelength of 528/20nm, in a microplate reader (Synergie HT, Bio-Tek, USA or SpectraMax M5, Molecular Devices, USA). Triplicates were made for each sample and per culturing time. The dsDNA concentration for each sample was calculated using a standard curve (dsDNA concentration ranging from 0.0 to 1.5µg/mL) relating the quantity of dsDNA and fluorescence intensity.

II.5.2.4.3. Calcein- Etidium/Propidium Iodide staining

The viability of the cells is an essential parameter that must be taken into consideration when designing hydrogel for TE application. Immediately after encapsulation, an evaluation of cellular viability will determine whether the tested system and its processing (crosslinking times, UV exposure, photoinitiator etc.) is suitable to retain the viability of the cells and whether it should be continued with longer culture periods. Also, one must take into consideration the chemistry of the material and the stiffness of the polymeric network that is formed upon crosslinking. A stiff and tight network with small pores, usually associated with low swelling rates, can “squize” the cells and thus, compromise their viability, growth and functionality.

The viability of the SSEA-4^{+}hASCs-derived ECs and NIH-3T3 (chapter VII and VIII) was assessed immediately after encapsulation and for culture times longer than 3 days, considering that the viability can be affected by the lack of diffusion of oxygen and nutrients (for thick samples) or presence of toxic photoinitiators, such as Irgacure 2959, was assessed. The standard method to qualitatively assess cellular viability relies on a Live/Dead

assay (Invitrogen, Carlsbad, CA, USA) that provides a two-color fluorescence simultaneous visualization of live and dead cells. It is based on the use of acetomethoxy derivate of calcein (Calcein-AM) that is a non-fluorescent dye that easily permeates live cells and is then hydrolytically converted to calcein, a strong green fluorescent dye (excitation/emission: 494/517nm). On the other hand, dead cells are identified with ethidium homodimer (EthD-1, excitation/emission: 571/617nm) or propidium iodide (excitation/emission: 536/617nm). These dyes pass the membrane of damaged cells and bind to the nucleic acids. Cells with intact plasma membrane exclude EthD-1 and propidium iodide.

In chapter VII, the viability of SSEA-4$^+$hASC-derived ECs (section II.3.2.1) loaded in κ-CA fibers without CHT (section II.2.1.1) and with CHT coating (section II.2.1.2), was evaluated at selected time culturing points (1, 7, 14 and 21 days). Cell-loaded fibers were washed with PBS and incubated with 4μM Calcein-AM (live) for 40min followed by 10min incubation with 1μM propidium iodide (dead). Samples were then washed and fixed for 40 min in 10% formalin. After fixation, samples were washed with PBS and cell nuclei were counterstained with DAPI. Representative fluorescent micrographs were acquired using the Axioplan Imager Z1 fluorescence microscope (Zeiss, Germany) and the AxioVision 4.8 software (Zeiss, Germany).

In chapter VIII, the effect of DM, as well as the photocrosslinking conditions, on the cells viability was evaluated by encapsulating NIH-3T3 fibroblasts within gels prepared by applying both physical and chemical crosslinking, as described in section II.2.2.3. The viability of the encapsulated cells was evaluated at 3 and 72h of culture. Briefly, cells were incubated with calcein AM/EthD-1 solution prepared by mixing 20 μL of EthD-1 (2 mM) and 5 μL of Calcein-AM (4mM) in 10 mL of phenol red-free DMEM (Gibco, USA, Cat. N^o 11880-036), without FBS for 40min. Samples were then washed and fixed for 40min in 10% formalin. Fluorescence images were taken with an inverted fluorescence microscope (Nikon, Eclipse TE 2000U, Japan).

II.5.3. Evaluation of SNPs contact with cells and internalization mechanism

In order to further investigate the interaction between cells and sNPs (cell-membrane interaction and intracellular uptake, chapter VI) and obtain an insight over the internalization mechanism, a cell suspension of SSEA-4$^+$hASCs (passage 2) cultured in complete α-MEM was transferred to 25cm^2 culture flasks (2x10^3 cells/cm^2). Upon cells adhesion, the culture medium was replaced by α-MEM-containing rhodamine-labeled sNPs (obtained in section II.4.1.1) at a final concentration of 0, 1, 10, 20, 50, 100 and 200μg/mL. In order to separate the two modes of interaction the internalization *via* endocytosis from the external contact of the cells with the sNPs, cells were cultured in the presence of rhodamine-labeled sNPs and 10^{-6}M colchicine, an endocytotic restrictive drug. Cells were cultured for 24h, after which

they were washed thoroughly with PBS, trypsinized and fixed with PBS containing 10% formalin and 0.1% sodium azide (acquisition buffer). SSEA-4$^+$hASCs cultured in α-MEM in the presence of colchicine, but without sNPs, were used as negative control. Samples were analyzed in a BD FACS Calibur flow cytometer (BD Biosciences, USA). Cells of interest were gated in a forward versus side scatter dot plot with a linear scale. Acquired data were displayed as histogram plots created using the CellQuest software (BD Biosciences, USA). All experiments were carried out in triplicate.

In parallel, SSEA-4$^+$hASCs (passage 2) were seeded on TCPS coverslips (Sarstedt, USA) in 24-well plates, at a cell density of 2x10^3 cells/cm^2 and allowed to adhere. After 24h, rhodamine-labeled sNPs were added to the culture wells. After additional 24h of culture, samples were washed with PBS and fixed with 10% formalin. Cell nuclei were counterstained with DAPI. Samples were visualized as previously described.

II.5.4. Flow cytometry

Flow cytometry technology provides multi-parametric single-cell measurements of a population of cells. Within this thesis, flow cytometry measurements were performed in order to determine the phenotype of isolated hASCs, SSEA-4$^+$hASCs and hMSCs (chapters III-VI). To address the undifferentiated, multipotent stage of mesenchymal stem cells, the choice of markers was based on the minimal criteria for defining multipotent mesenchymal stem/stromal cells established by the International Society for Cellular Therapy[115]. The cells to be analyzed were resuspended in cold PBS with 2% (w/v) bovine serum albumin (BSA, Sigma, USA) solution in PBS (BSA/PBS). Each cell suspension (100µL) containing 5x10^5 cells, was incubated with the antibodies at the concentration advised by the manufacturer (**Table II.2**).

After incubation for 20min at room temperature, in the dark, hASCs, SSEA-4$^+$hASCs and hMSCs were washed with PBS/BSA and resuspended in acquisition buffer until analysis. Cells were analyzed in a BD FACScalibur flow cytometer (BD Biosciences, USA). Cells of interest were gated in a forward versus side scatter dot plot with a linear scale. A minimum of 20,000 gated events were acquired and displayed as histograms or dot plots as previously described

Table II.2. Panels of antibodies used to characterize cells by means of flow cytometry

Cell type	Antibodies	Chapter
hMSCs	mouse anti-human CD31-APC (R&D Systems, USA) mouse anti-human CD34-PE (BD Biosciences, USA) mouse anti-human CD45-FITC (BD Biosciences, USA) mouse anti-human CD73-PE (BD Biosciences, USA) mouse anti-human CD90-APC (eBioscience, USA) mouse anti-human CD105-FITC (AbD Serotec, UK)	V
SVF	mouse anti-human SSEA-4-Alexa Fluor 488 (eBioscience, USA) mouse anti-human CD34-PE (BD Biosciences, USA) mouse anti-human CD45-FITC (BD Biosciences, USA) mouse anti-human CD73-PE (BD Biosciences, USA) mouse anti-human CD90-APC (eBioscience, USA) mouse anti-human CD105-FITC (AbD Serotec, UK)	III
hASCs	mouse anti-human SSEA-4-Alexa Fluor 488 (eBioscience, USA) mouse anti-human CD31-APC (R&D Systems, USA) mouse anti-human CD34-PE (BD Biosciences, USA) mouse anti-human CD45-FITC (BD Biosciences, USA) mouse anti-human CD73-PE (BD Biosciences, USA) mouse anti-human CD90-APC (eBioscience, USA) mouse anti-human CD105-FITC (AbD Serotec, UK)	III
SSEA-4$^+$hASCs	mouse anti-human CD31-APC (R&D Systems, USA) mouse anti-human CD34-PE (BD Biosciences, USA) mouse anti-human CD73-PE (BD Biosciences, USA) mouse anti-human CD90-APC (eBioscience, USA) mouse anti-human CD105-FITC (BD Bioscience, USA)	III, IV, VI, VII

II.5.5. Immunocytochemistry

Immunocytochemistry was used as a tool to detect specific cellular markers in order to assess the identity and localize a specific cell sub-set. Thus, in chapters III-VII, endothelial-specific markers, such as platelet endothelial cell adhesion molecule-1 or CD31, von Willebrand factor (vWF) and CD34, as well as osteogenic-specific markers: Runt-related transcription factor-2 (RUNX-2), osteopontin (OPN), osteocalcin (OCN), collagen type I and II were targeted. At selected time points, samples were washed with PBS, fixed with 10% formalin for 20min and washed again. Non-specific binding was blocked by incubating the fixed cells with a 1.5-3% (wt/v) BSA/PBS or 10% (v/v) goat serum for 30min. For the CD31, vWF and RUNX-2 detection, an additional permeabilization step was performed, by incubating the fixed samples with 0.1% (v/v) Triton^{TM} 100x (Sigma, Germany, Cat N^o T8787, CAS 9002-93-1) solution for 5min, followed by several washings with PBS. Further on, cells were incubated for 1h at room temperature or overnight at 4^{o}C with the primary antibodies, at optimized dilutions (**Table II.3**).

Table II.3. Antibodies used to perform immunocytochemistry to characterize different cultured cells

Cellular lineage	Antibody	Company Info	Dilution	Chapter
	PRIMARY ANTIBODIES			
	mouse anti-human **SSEA-4** (clone MC813)	Abcam, UK Cat. N^{o} ab16287	1:50	III
ENDOTHELIAL	polyclonal rabbit anti-human **von Willebrand factor**	Dako, Denmark Cat. N^{o} A0082	1:200	III
	mouse anti-human **CD31** (clone JC70A)	Dako, Denmark Cat. N^{o} JR610	1:50	III
	mouse anti-human **CD34-PE** (clone 8G12)	BD Biosciences, USA Cat. N^{o} 340667	1:50	III
	mouse anti-human **CD105-APC**	eBioscience, USA Cat. N^{o} 17-1057	1:50	III
OSTEOGENIC	monoclonal mouse anti-human **collagen I**	abcam, UK Cat. N^{o} ab90395	1:50	VI
	polyclonal rabbit anti-human **collagen II**	abcam, UK Cat. N^{o} ab34712	1:50	VI
	mouse anti-human **RUNX-2** (clone AS110)	Milipore Cat. N^{o} 05-1478	1:100	V
	polyclonal rabbit anti-human **osteocalcin**	abcam, UK Cat. N^{o} ab14173	1:100	V
	monoclonal mouse anti-human **osteocalcin** (clone 2H9F11F8)	AbD Serotec, UK Cat. N^{o} 0400-0041	1:50	III
	mouse anti-human **osteopontin**	Abcam, UK Cat. N^{o} ab69498	1:100	V
	rabbit anti-human **osteopontin**	Abcam, UK Cat. N^{o} ab8448	1:50	III
	SECONDARY ANTIBODIES			
	donkey anti-mouse **Alexa Fluor 488**	Invitrogen, USA Cat. N^{o} A21202	1:500	III
	rabbit anti-mouse **Alexa Fluor 488**	Invitrogen, USA Cat. N^{o} A11059	1:100	V
	donkey anti-mouse **Alexa Fluor 594**	Invitrogen, USA Cat. N^{o} A21203	1:500	III
	goat anti-mouse **Alexa Fluor 594**	Invitrogen, USA Cat. N^{o} A11055	1:100	V
Cell nuclei	4,6-Diamidino-2-phenylindole dilactate **DAPI**	Invitrogen, USA Cat. N^{o} D3571	1:10,000	III-VIII

All antibody dilutions were performed in 1.5% BSA/PBS. Upon this incubation, cells were washed three times with PBS and incubated with the appropriate secondary antibody for 1h (**Table II.3**). Cell nuclei were counterstained with DAPI for 10min, and then washed three times. Negative control samples were prepared by replacing the primary antibody with PBS. Immunolabeling was qualitatively analyzed under a Eclipse TE2000-U fluorescence microscope (Nikon, Japan) or Axioplan Imager Z1 fluorescence microscope (Zeiss, Germany).

II.5.6. Real Time Reverse Transcriptase-Polymerase Chain Reaction

Quantitative Real Time Reverse Transcriptase-Polymerase Chain Reaction (RT-PCR) was used to evaluate the expression of several endothelial (*CD31* and *vWF* in chapters III and IV) and osteogenic (*RUNX2, OPN, OCN*, chapters III, IV, and VI) related genes. The whole procedure consists of 3 steps: (**1**) extraction of mRNA, (**2**) single-strand complementary DNA (cDNA) production from the extracted messenger RNA (mRNA) and (**3**) amplification and real-time quantification of the expression of the defined genes.

II.5.6.1. RNA extraction and cDNA production

The mRNA of the samples (chapters III, IV and VI) was extracted using TRI Reagent® (Sigma, Germany, Cat. N^{o} T3809), following the manufacturer instructions. Proteins were extracted using 160µL chloroform (Sigma, Germany) and the RNA pellets were washed with an equal volume of isopropanol (Sigma, Germany) and 70% ethanol. The total mRNA was reconstituted in 12µL RNAse/DNAse-free water (Gibco, USA) and its quantity and purity were assessed with a NanoDrop ND-1000 Spectrophotometer (NanoDrop Technologies, USA). Samples with a 260/280 ratio between 1.6 and 2.0 were used for the synthesis of cDNA. The synthesis of cDNA was performed using qScript™ cDNA synthesis Kit (Quanta BIosciences, USA) and the thermoblock of the Mastercycler ep realplex thermal cycler (Eppendorf, USA). An initial amount of 1µg of mRNA was used in a total volume of 20µL.

II.5.6.2. Quantitative real time PCR

The quantification of the transcripts of the genes of interest was carried out by RT-PCR using 50ng of cDNA and PerfeCTA™ SYBR® Green FastMix kit (Quanta Biosciences, USA) following the procedure suggested by the manufacturer. The primers were previously designed using the Primer 3 online software (v0.4.0, Whitehead Institute, USA) and synthesized by MGW Biotech (Germany). For each sample, the transcripts expression data were normalized to *glyceraldehyde-3-phosphate-dehydrogenase* (*GAPDH*) as housekeeping gene. The primers sequences and annealing temperatures, specific for endothelial-specific genes: *CD31* and *vWF,* bone-specific genes: *RUNX-2*, *OPN*, *OCN,* and that of *GAPDH,* are

described in **Table II.4.** A concentration of 100nM of primer was used in a final volume of 20µl of sample. Each real time RT-PCR reaction as carried out with an initial incubation at 95^{o}C for 2min, followed by forty fives cycles of denaturation (95^{o}C, 10sec), annealing (specific for each gene, 30sec) and extension (72^{o}C, 30sec) in a real-time Mastercycler ep realplex thermal cycler (Eppendorf, USA). The relative quantification of targeted genes expression was performed using the $2^{-\Delta\Delta CT}$ method[116]. The transcripts expression data were first normalized against endogeneous *GAPDH* values and then against the values of corresponding controls in each experiment.

Table II. 4. Primer pair sequences for the studied genes

GENE		SEQUENCE	NCBI REFERENCE
GAPDH	Forward (5'→3')	ACAGTCAGCCGCATC	NM_002046.4
	Reverse (3'→5')	GACAAGCTTCCCGTTCTCAG	
CD31	Forward	AAGGCCAGATGCACATCC	NM_000442
	Reverse	TTCTACCCAACATTAACTTAGCGG	
vWF	Forward	CCCTGGGTTACAAGGAAGAAAT	NM_000552
	Reverse	AGTGTCATGTGTCCTCCTCTAG	
OPN	Forward	GGGGACAACTGGAGTGAAAA	NM_001040058
	Reverse	CCCACAGACCCTTCCAAGTA	
OCN	Forward	CTGGAGAGGAGCAGAACTGG	NM_099173
	Reverse	GGCAGCGAGGTAGTGAAGAG	

II.5.7. Quantification of ECM protein content

In chapter V, the amount of protein produced by hMSCs as a function of the sNPs concentrations was determined. hMSCs were allowed to grow in the presence of sNPs (0-100µg/mL) for 21 days. After 21 days, cells were washed thrice with PBS. The ECM proteins were extracted using sodium dodecyl sulphate (SDS), an ionic detergent used in biological buffers to dissolve and denature proteins. 2% (wt/v) SDS (Sigma, Germany, Cat. N^{o} L3771, CAS 151-21-3) solution in PBS was added to samples for 6h. The amount of total protein was determined by the Micro BCA^{TM} Protein Assay Kit (Thermo Fisher Scientific, USA, Cat N^{o} 23235), according to the manufacturer's indications.

II.5.8. Quantification of VEGF release

In chapter IV, the secretion of VEGF was determined by enzyme-linked immunosorbent assay (ELISA) in the supernatants of the co-cultures of days 14 and 21 stored at -80^{0}C. The amount of human VEGF was quantified following instructions provided in the ELISA

development kit (PeproTech, USA, Cat N^{o} 900-K10). Thawed samples were added to in-house coated ELISA plates (Nunc MaxiSorp, eBioscience, USA). Absorbance was measured in a multi-well microplate reader at 405/650nm. Standard samples in a range of concentrations of 0 to 1ng/mL of recombinant human VEGF were used to obtain a calibration curve.

II.5.9. Assessment of the endothelial phenotype

II.5.9.1. DIL-ac-LDL uptake

ECs possess scavenger receptors at their surface specific for acetylated low density lipoprotein (ac-LDL)[117]. When taken up by cells, ac-LDL accumulates intracellularly, which allows to target and to identify ECs. This technique was used to confirm the endothelial phenotype of the differentiated SSEA-4^{+}hASCs (section II.3.2.1).

In chapter III, ac-LDL uptake was assessed by incubating cells with 0.2µg/mL or 2 µg/mL of ac-LDL labeled with 1,1'-dioctadecyl-3,3,3',3'-tetramethylindocarbocyanine (DIL-ac-LDL, Invitrogen, USA, Cat. N^{o} L3484) for 4h or overnight, respectively. Cells were then washed with warm medium and fixed for 20min with 10% formalin solution, protected from light. Cell nuclei were counterstained with DAPI. Cells were visualized using Axioplan Imager Z1 fluorescence microscope (Zeiss, Germany). The same labeling was performed during co-culture as a discriminative marker for SSEA-4^{+}hASCs-derived ECs allowing identifying and analysing their distribution amongst SSEA-4^{+}hASCs-derived OBs (chapter IV).

II.5.9.2. Lectin binding

Human ECs possess the ability to selectively bind the lectin Ulex europaeus agglutinin I (UEA I)[118]. Thus this marker has been also used to confirm cells endothelial phenotype as was the case of the SSEA-4^{+}hASCs-derived ECs cultured in EGM-2 MV (chapter III). Cells were incubated with 100µg/mL FITC-conjugated lectin *UEA-1* (Sigma, Germany, Cat. N^{o} L9006) for 1 h at 37°C and protected from light. Cells were then washed twice with PBS, fixed for 20min in 10% formalin solution and analyzed by fluorescence microscopy as described for the immunocytochemistry.

II.5.9.3. Tubular-like structures formation on Matrigel

The capacity of cells to form tubular-like structures on Matrigel *in vitro* is associated to endothelial cells due to their ability to sprout, migrate, and form vascular networks *in vivo*. Matrigel contains a pro-angiogenic mixture of basement membrane components from Engelbreth-Holm-Swarm murine sarcoma. When seeded on Matrigel coated surfaces, ECs form intricate capillary-like hexagonal structures that cannot be observed when cells are cultured on plastic surfaces. Such networks are highly suggestive of the microvascular-like

potential of ECs, thus, it is extensively used to confirm the endothelial phenotype of ECs[119]. Thus, in this thesis, Matrigel assay was used to analyze the capacity of SSEA-4$^+$hASCs-derived ECs to form tubular-like structures in vitro thus confirming their phenotype (chapter. III, IV and VII). A 96-well cell culture plate, chilled at 4°C, was loaded with 32µL of Matrigel (BD Biosciences, USA) and incubated at 37°C. Cells were suspended in the EGM-2 MV medium at a concentration of 2.1x10^5 cells/mL and 64µL of this cell suspension was seeded onto the surface of the solidified Matrigel. Cells were incubated (37°C, 5% CO_2) for 4h. After incubation, samples were fixed with 10%(v/v) buffered formalin (Sigma, Germany) for 20min at room temperature. Images were recorded using an inverted microscope, Axiovert 40 (Zeiss, Germany), equipped with digital image capture software.

Once the cells were proven to have the ability to form capillary-like networks on Matrigel, they were used for the experiment described in sections II.3.2.3 and II.4.2.1-2 and as a confirmation of the maintenance of endothelial phenotype of the SSEA-4$^+$hASCs-derived ECs retrieved from the κ-CA fibers (chapter VII).

II.5.10. Osteogenic differentiation evaluation

The osteogenic differentiation of hMSCs (chapter V), hASCs and SSEA-4$^+$hASCs in the absence (chapters III) and presence of sNPs (chapter VI), as well as of SSEA-4$^+$hASCs-derived ECs (chapter IV) was evaluated by following specific markers at different temporal checkpoints. Within the present work, alkaline phosphatase activity (early marker), matrix deposition (intermediate marker) and matrix mineralization (end marker) were monitored along the culture period.

II.5.10.1. Alkaline phosphatase activity: quantification and qualitative analysis

Alkaline phosphatase (ALP), a membrane bound enzyme, is among the first functional genes expressed in the process of calcification. It is therefore likely that at least one of its roles in the mineralization process occurs at an early stage[121]. The mechanism with which this enzyme carries out its function is not completely understood, but it appears to act both to increase the local concentration of inorganic phosphate, a mineralization promoter, and to decrease the concentration of extracellular pyrophosphate, an inhibitor of mineral formation[122]. The enzyme is localized in the outerside of the cellular plasma membrane and of the membrane of matrix vesicles.

Within this thesis, the quantification of ALP activity was performed in the same cell lysates used for the dsDNA quantification, obtained by osmotic and thermal shocks, and using an end-point colorimetric procedure that quantified the conversion of colorless *p*-nitrophenol phosphate (pNPP) into yellow *p*-nitrophenol (pNP) by the ALP enzyme present in the sample.

In chapters IV and VI, 20µL of lysate were incubated with 80µL of pNPP, 0.2% wt/v in 1M diethanolamine (Fluka BioChemika, Austria), in a transparent 96-well microplate, at 37°C, for 45min. The reaction was stopped using 80µL of a 2M NaOH (Sigma, USA) and 0.4mM EDTA (Sigma, USA) solution. A calibration curve was previously prepared using the pNP (Sigma, USA) standards of 0, 0.05, 0.10, 0.15, 0.20 and 0.5µmol/mL and used to extrapolate the ALP activity values. Triplicates of each sample and standards were made, and the ALP activity read off from the standard curve. The optical density (OD) of the samples and standards was read at 405nm, using a microplate reader. Results were normalized against dsDNA results obtained for the same samples.

In chapter V, the ALP activity was measured using a commercially available colorimetric endpoint kit (Abcam, USA, N° ab83369). Briefly, samples and the assay buffer solution (5mM *pNPP)* were added to a 96-well plate. After 1h of incubation, the absorbance was read at 405nm in a microplate reader (Epoch microplate reader, Biotek, USA). A standard curve was made from standards (0–20µM) prepared with the provided *pNPP* and ALP enzyme solutions. Sample and standards triplicates were analyzed and sample concentrations read off from the standard curve, as described above.

Furthermore, to qualitatively analyse the ALP activity within the 2D cell cultures, the staining of ALP-enriched areas was performed based on the combination between nitro blue tetrazolium (NBT) and alkaline phosphatase substrate 5-bromo-4-chloro-3-indolyl phosphate (BCIP) (chapters V and VI). NBT/BCIP in the presence of ALP produces an insoluble NBT diformazan end-product that is blue to purple in color enabling the localization of ALP-containing areas. A ready-to-use, single component, 1-step NBT/BCIP (Thermo Scientific, USA, Cat. N° 34042) solution was added to fixed cells for 30min, after which the samples were washed with PBS and visualized under a transmitted light microscope.

II.5.10.2. Qualitative and quantitative analysis of collagenous and non-collagenous protein deposition

The presence and distribution of collagen and non-collagenous proteins within the extracellular matrix deposited by hASCs and SSEA-4^{+}hASCs in the presence and absence of sNPs (chapter VI) were determined by differential staining with two dyes, Sirius Red and Fast Green. Sirius Red binds specifically to collagen, whereas Fast Green stains the non-collagenous proteins. As a general remark, collagen stained by Sirius Red displays a fibrillar pattern, whereas non-collagen proteins stained with Fast Green show a more diffused pattern. Since many types of collagen can be detected with Sirius Red (type I, II, III, IV and V)[123] at a variety of ratios and the color equivalence for each type of collagen has not been determined, one color equivalent value is used for all types of collagen.

The effect of sNPs over the collagen-like matrix production was assessed by using the Sirius

Red/Fast Green collagen staining micro-assay kit (Chondrex, USA, Cat N° 9046). The dye (mixture of 0.1% Sirius Red and 0.1% Fast Green dissolved in water saturated with picric acid) was added to the fixed samples (21 days of culture). After 30min the dye was removed and samples rinsed with diH_2O water. Stained samples were imaged with a transmitted light microscope.

The quantification of the proteins was carried out after extraction of the dyes from the stained samples using 0.05M NaOH in methanol, and the absorbance measured at 540nm (Sirius Red) and 605nm (Fast Green). To calculate the amount of collagen, several corrections were performed. First, the OD540 was corrected by subtracting the contribution of Fast Green at 540nm, which is 29.1% of the OD605 value. The color equivalence (OD values/µg protein) is 0.0378 for collagen and 0.00204 for non-collagenous protein at OD540 and 605, respectively (**equations II.3** and **II.4**).

Collagen (µg/section) = [OD540 value - (OD605 value x 0.291)] / 0.0378 (**equation II.3**)

Non-collagenous proteins (µg/section) = OD605 value / 0.00204 (**equation II.4**)

The assay was performed independently three times for each experimental sample. Values were normalized against corresponding dsDNA values.

II.5.10.3. Mineralization

II.5.10.3.1. Direct calcium quantification

In chapter IV, the detection of inorganic calcium was performed at the end of 21 days of culture, using the o-cresolphtalein-complexon method with colorimetric detection (Roche Cobas kit, Roche Diagnostics, Germany), according to the manufacturer instructions. In a 96-well plate, 175µL of reagent 1 (ethanolamine, 1M, pH10.6) were mixed with 10µL of each sample, dissolved with a 6M HCl solution, and incubated for 5min at room temperature. 70µL of reagent 2 (o-cresolphtalein-complexon 0.3mM, hydroxy-8-quinoleine 13.8mM, HCl 122mM) were added and further incubated at 37°C for 2min. The absorbance of the samples was read at 570nm in a microplate reader. The calcium concentration was extrapolated from the calibration curve obtained using serial dilutions of a 200mg/L $CaCl_2$ solution and then normalized against the corresponding dsDNA content.

II.5.10.3.2. Indirect calcium quantification: Alizarin Red S

Alizarin Red S (ARS), an anthraquinone derivative, is one of the most used qualitative methods to detect the mineralization process in osteoblasts culture[124]. ARS forms a stable complex with calcium by chelation generating bi-refringent end product [124]. The identification of mineralized tissue with ARS was carried out to evaluate the osteogenic differentiation of

hMSCs in the presence of sNPs (chapter V), and of hASCs and SSEA-4^{+}hASCs in the presence and absence of sNPs (chapters III, V and VI), at the end point. Cells cultured on TCPS and at determined time points (days 7, 14, 21 and 28) were fixed in 10% (v/v) formalin solution (Sigma, Germany), at room temperature, for 20 min. After that, cells were washed in PBS to remove the formalin and then with diH_2O, in order to remove any salt residues. A solution of 2% (wt/v) of ARS (Sigma, Germany, Cat. N^{o} A5533, CAS 130-22-3) with a pH adjusted to 4.2, was then added and incubated for 10min at room temperature. The excess of ARS was washed with diH_2O and the staining was imaged using a reflected light microscope.

ARS is particularly versatile because the qualitative analysis can be coupled with its quantification after being extracted from the stained samples by acid solution. Samples were incubated in 10% acetic acid overnight (chapters V and VI), then centrifuged for 15min at 2,000*xg* and the supernatants neutralized with ammonium hydroxide, 10% (Sigma Aldrich, Germany). Finally, 100µL of each sample was added to 96-well plates and the absorbance was read at 405nm using an Epoch or Synergy HT microplate reader. A calibration curve obtained from different concentrations of ARS in diH_2O at pH=4.2, adjusted with 10% (v/v) ammonium hydroxide was drawn. The assay was performed three times independently for each experimental sample.

II.6. STATISTICAL ANALYSIS

Data was obtained from at least 3 separate experiments with 3 replicates for each condition and averaged. Standard deviation (SD) is reported as a measure of sample deviation. Statistical analysis was performed using GraphPad Prism 5.00 software (San Diego, USA). Firstly, a Shapiro-Wilk test was used to ascertain about the data normality[125]. Then either a student *t-test* for n>4 or one way ANOVA test was applied. The student *t-test* was applied to test the difference between the means of two independent groups subjected to different treatments (chapter VII). When more than two groups were compared at the same time (chapters III-VIII), one-way ANOVA was applied followed by a Tukey-Kramer method as a *post-hoc* pairwise comparison test. Values were considered statistically significant for $p<0.05$.

REFERENCES

1. Slaughter, B. V.; Khurshid, S. S.; Fisher, O. Z.; Khademhosseini, A.; Peppas, N. A., Hydrogels in regenerative medicine. *Advanced materials* **2009,** *21* (32-33), 3307-29.
2. Peppas, N. A.; Hilt, J. Z.; Khademhosseini, A.; Langer, R., Hydrogels in biology and medicine: from molecular principles to bionanotechnology. *Advanced materials* **2006,** *18* (11), 1345–1360.
3. Geckil, H.; Xu, F.; Zhang, X.; Moon, S.; Demirci, U., Engineering hydrogels as extracellular matrix mimics. *Nanomedicine* **2010,** *5* (3), 469-84.

4. Sasisekharan, R.; Raman, R.; Prabhakar, V., Glycomics approach to structure-function relationships of glycosaminoglycans. *Annual review of biomedical engineering* **2006,** *8*, 181-231.
5. Boccaccini, A. R.; Blaker, J. J., Bioactive composite materials for tissue engineering scaffolds. *Expert review of medical devices* **2005,** *2* (3), 303-17.
6. Necas, J.; Bartosikova, L., Carrageenan: a review. *Veterinarni Medicina* **2013,** *58* (4), 187–205.
7. Kirsch, P. P., Carrageenan: a safe additive. *Environmental health perspectives* **2002,** *110* (6), A288; author reply A288.
8. Imeson, A. P., Carrageenans. In *Handbook of hydrocolloids*, Phillips, G. O.; Williams, P. A., Eds. CRC Press: 2000.
9. Coviello, T.; Matricardi, P.; Marianecci, C.; Alhaique, F., Polysaccharide hydrogels for modified release formulations. *Journal of controlled release : official journal of the Controlled Release Society* **2007,** *119* (1), 5-24.
10. Necas, J.; Bartosikova, L., Carrageenan: a review. *Veterinarni Medicina* **2013,** *58* (4), 187-205.
11. Morris, E. R., Molecular interactions in polysaccharide gelation. *British Polymer Journal* **1986,** *18* (1), 14-21.
12. Mano, J. F.; Silva, G. A.; Azevedo, H. S.; Malafaya, P. B.; Sousa, R. A.; Silva, S. S.; Boesel, L. F.; Oliveira, J. M.; Santos, T. C.; Marques, A. P.; Neves, N. M.; Reis, R. L., Natural origin biodegradable systems in tissue engineering and regenerative medicine: present status and some moving trends. *Journal of the Royal Society, Interface / the Royal Society* **2007,** *4* (17), 999-1030.
13. (a) Li, L.; Ni, R.; Shao, Y.; Mao, S., Carrageenan and its applications in drug delivery. *Carbohydrate polymers* **2014,** *103*, 1-11; (b) Sharma, A.; Bhat, S.; Vishnoi, T.; Nayak, V.; Kumar, A., Three-dimensional supermacroporous carrageenan-gelatin cryogel matrix for tissue engineering applications. *Biomed Res Int* **2013,** *2013*, 478279.
14. Popa, E. G.; Carvalho, P. P.; Dias, A. F.; Santos, T. C.; Santo, V. E.; Marques, A. P.; Viegas, C. A.; Dias, I. R.; Gomes, M. E.; Reis, R. L., Evaluation of the in vitro and in vivo biocompatibility of carrageenan-based hydrogels. *Journal of biomedical materials research. Part A* **2014**.
15. Santo, V. E.; Frias, A. M.; Carida, M.; Cancedda, R.; Gomes, M. E.; Mano, J. F.; Reis, R. L., Carrageenan-based hydrogels for the controlled delivery of PDGF-BB in bone tissue engineering applications. *Biomacromolecules* **2009,** *10* (6), 1392-401.
16. Grenha, A.; Gomes, M. E.; Rodrigues, M.; Santo, V. E.; Mano, J. F.; Neves, N. M.; Reis, R. L., Development of new chitosan/carrageenan nanoparticles for drug delivery applications. *Journal of biomedical materials research. Part A* **2010,** *92* (4), 1265-72.
17. Bartkowiak, A.; Hunkeler, D., Carrageenan-oligochitosan microcapsules: optimization of the formation process(1). *Colloids and surfaces. B, Biointerfaces* **2001,** *21* (4), 285-298.
18. Tojo, E.; Prado, J., Chemical composition of carrageenan blends determined by IR spectroscopy combined with a PLS multivariate calibration method. *Carbohydrate research* **2003,** *338* (12), 1309-12.
19. Ratner, B. D., Surface properties of materials. In *Biomaterials Science: An Introduction to Materials in Medicine*, Ratner, B. D.; Hoffman, A. S.; Schoen, F. J.; Lemons, J. E., Eds. Academic Press: 1996; pp 21-35.
20. Raymond, M. C.; Neufeld, R. J.; Poncelet, D., Encapsulation of brewers yeast in chitosan coated carrageenan microspheres by emulsification/thermal gelation. *Artificial cells, blood substitutes, and immobilization biotechnology* **2004,** *32* (2), 275-91.
21. Yilmaz, E., Chitosan: a versatile biomaterial. *Advances in experimental medicine and biology* **2004,** *553*, 59-68.
22. Stephen, A. M.; Phillips, G. O.; Williams, P. A., Food Polysaccharides and their Applications. Press, C., Ed. Taylor & Francis Group: New York,, 2006; Vol. 2nd ed.
23. Colinet, I.; Dulong, V.; Mocanu, G.; Picton, L.; Le Cerf, D., Effect of chitosan coating on the swelling and controlled release of a poorly water-soluble drug from an amphiphilic and pH-sensitive hydrogel. *International journal of biological macromolecules* **2010,** *47* (2), 120-5.
24. Piyakulawat, P.; Praphairaksit, N.; Chantarasiri, N.; Muangsin, N., Preparation and evaluation of chitosan/carrageenan beads for controlled release of sodium diclofenac. *AAPS PharmSciTech* **2007,** *8* (4), E97.
25. Pinheiro, A. C.; Bourbon, A. I.; Medeiros, B. G. d. S.; Silva, L. s. H. M. d.; Silva, M. C. H. d.; Carneiro-da-Cunha, M. G.; Coimbra, M. A.; Vicente, A. n. A., Interactions between k-carrageenan and chitosan in nanolayered coatings—Structural and transport properties. *Carbohydrate Polymers* **2012,** *87*, 1081-1090.

26. Hirai, A.; Odani, H.; Nakajima, A., Determination of degree of deacetylation of chitosan by 1H-NMR spectroscopy. *Polymer Bulletin* **1991,** *26* (1), 87-94.
27. Chenite, A.; Buschmann, M.; Wang, D.; Chaput, C.; Kandani, N., Rheological characterisation of thermogelling chitosan/glycerol-phosphate solutions. *Carbohydrate Polymers* **2001,** *46* (1), 39-47.
28. Cho, J.; Heuzey, M. C.; Begin, A.; Carreau, P. J., Physical gelation of chitosan in the presence of beta-glycerophosphate: the effect of temperature. *Biomacromolecules* **2005,** *6* (6), 3267-75.
29. (a) Langer, R.; Tirrell, D. A., Designing materials for biology and medicine. *Nature* **2004,** *428* (6982), 487-92; (b) Khademhosseini, A.; Vacanti, J. P.; Langer, R., Progress in tissue engineering. *Scientific American* **2009,** *300* (5), 64-71; (c) Peppas, N. A.; Langer, R., New challenges in biomaterials. *Science* **1994,** *263* (5154), 1715-20; (d) Khademhosseini, A.; Langer, R.; Borenstein, J.; Vacanti, J. P., Microscale technologies for tissue engineering and biology. *Proceedings of the National Academy of Sciences of the United States of America* **2006,** *103* (8), 2480-7.
30. (a) Lutolf, M. P.; Gilbert, P. M.; Blau, H. M., Designing materials to direct stem-cell fate. *Nature* **2009,** *462* (7272), 433-41; (b) Kraehenbuehl, T. P.; Langer, R.; Ferreira, L. S., Three-dimensional biomaterials for the study of human pluripotent stem cells. *Nature methods* **2011,** *8* (9), 731-6; (c) Dvir, T.; Timko, B. P.; Kohane, D. S.; Langer, R., Nanotechnological strategies for engineering complex tissues. *Nature nanotechnology* **2011,** *6* (1), 13-22.
31. Hench, L. L., Bioceramics: from concept to clinic. *Journal of the American Ceramic Society* **1991,** *74* (7), 1487-1510.
32. Gaharwar, A. K.; Kishore, V.; Rivera, C.; Bullock, W.; Wu, C. J.; Akkus, O.; Schmidt, G., Physically crosslinked nanocomposites from silicate-crosslinked PEO: mechanical properties and osteogenic differentiation of human mesenchymal stem cells. *Macromolecular bioscience* **2012,** *12* (6), 779-93.
33. Goncalves, M.; Figueira, P.; Maciel, D.; Rodrigues, J.; Shi, X.; Tomas, H.; Li, Y., Antitumor Efficacy of Doxorubicin-Loaded Laponite/Alginate Hybrid Hydrogels. *Macromolecular bioscience* **2013**.
34. Bonn, D.; Kellay, H.; Tanaka, H.; Wegdam, G.; Meunier, J., Laponite: What is difference between gel and a glass? *Langmuir* **1999,** *15* (22), 7534–7536.
35. Lezhnina, M. M.; Grewe, T.; Stoehr, H.; Kynast, U., Laponite blue: dissolving the insoluble. *Angewandte Chemie* **2012,** *51* (42), 10652-5.
36. de Melo Marques, F. A., Aging phenomena in a clay polymer system. *PhD thesis, Universita di Roma "La Sapienza"* **2007**.
37. Williams, D. B.; Carter, C. B., *Transmission Electron Microscopy: A Textbook for Materials Science*. Springer: 2009; Vol. 1.
38. Nicolai, T.; Cocard, S., Dynamic light-scattering study of aggregating and gelling colloidal disks. *Journal of Colloid and Interface Science* **2001,** *244* (1), 51-57.
39. Lim, J.; Yeap, S. P.; Che, H. X.; Low, S. C., Characterization of magnetic nanoparticle by dynamic light scattering. *Nanoscale research letters* **2013,** *8* (1), 381.
40. Nichol, J. W.; Khademhosseini, A., Modular Tissue Engineering: Engineering Biological Tissues from the Bottom Up. *Soft matter* **2009,** *5* (7), 1312-1319.
41. Peppas, N. A.; Hilt, J. Z.; Khademhosseini, A.; Langer, R., Hydrogels in biology and medicine: from molecular principles to bionanotechnology. *Advanced Maeterials* **2006,** *18* (11), 1345–1360.
42. Drury, J. L.; Mooney, D. J., Hydrogels for tissue engineering: scaffold design variables and applications. *Biomaterials* **2003,** *24* (24), 4337-51.
43. Hennink, W. E.; van Nostrum, C. F., Novel crosslinking methods to design hydrogels. *Advanced drug delivery reviews* **2002,** *54* (1), 13-36.
44. Kannan, R. Y.; Salacinski, H. J.; Sales, K.; Butler, P.; Seifalian, A. M., The roles of tissue engineering and vascularisation in the development of micro-vascular networks: a review. *Biomaterials* **2005,** *26* (14), 1857-75.
45. Lovett, M.; Lee, K.; Edwards, A.; Kaplan, D. L., Vascularization strategies for tissue engineering. *Tissue engineering. Part B, Reviews* **2009,** *15* (3), 353-70.
46. Phelps, E. A.; Garcia, A. J., Engineering more than a cell: vascularization strategies in tissue engineering. *Current opinion in biotechnology* **2010,** *21* (5), 704-9.
47. Fedorovich, N. E.; Wijnberg, H. M.; Dhert, W. J.; Alblas, J., Distinct tissue formation by heterogeneous printing of osteo- and endothelial progenitor cells. *Tissue engineering. Part A* **2011,** *17* (15-16), 2113-21.
48. Kang, E.; Jeong, G. S.; Choi, Y. Y.; Lee, K. H.; Khademhosseini, A.; Lee, S. H., Digitally tunable physicochemical coding of material composition and topography in continuous microfibres. *Nature materials* **2011,** *10* (11), 877-83.

49. Aubin, H.; Nichol, J. W.; Hutson, C. B.; Bae, H.; Sieminski, A. L.; Cropek, D. M.; Akhyari, P.; Khademhosseini, A., Directed 3D cell alignment and elongation in microengineered hydrogels. *Biomaterials* **2010,** *31* (27), 6941-6951.
50. Popa, E. G.; Gomes, M. E.; Reis, R. L., Cell delivery systems using alginate--carrageenan hydrogel beads and fibers for regenerative medicine applications. *Biomacromolecules* **2011,** *12* (11), 3952-61.
51. Malafaya, P. B.; Silva, G. A.; Reis, R. L., Natural-origin polymers as carriers and scaffolds for biomolecules and cell delivery in tissue engineering applications. *Advanced drug delivery reviews* **2007,** *59* (4-5), 207-33.
52. Popa, E.; Reis, R.; Gomes, M., Chondrogenic phenotype of different cells encapsulated in kappa-carrageenan hydrogels for cartilage regeneration strategies. *Biotechnology and applied biochemistry* **2012,** *59* (2), 132-41.
53. Sakai, S.; Yamaguchi, S.; Takei, T.; Kawakami, K., Oxidized alginate-cross-linked alginate/gelatin hydrogel fibers for fabricating tubular constructs with layered smooth muscle cells and endothelial cells in collagen gels. *Biomacromolecules* **2008,** *9* (7), 2036-41.
54. Takei, T.; Sakai, S.; Ijima, H.; Kawakami, K., Development of mammalian cell-enclosing calcium-alginate hydrogel fibers in a co-flowing stream. *Biotechnology journal* **2006,** *1* (9), 1014-7.
55. Fedorovich, N. E.; De Wijn, J. R.; Verbout, A. J.; Alblas, J.; Dhert, W. J., Three-dimensional fiber deposition of cell-laden, viable, patterned constructs for bone tissue printing. *Tissue engineering. Part A* **2008,** *14* (1), 127-33.
56. Popa, E. G.; Caridade, S. G.; Mano, J. F.; Reis, R. L.; Gomes, M. E., Chondrogenic potential of injectable kappa-carrageenan hydrogel with encapsulated adipose stem cells for cartilage tissue-engineering applications. *Journal of tissue engineering and regenerative medicine* **2013**.
57. Kuo, C. K.; Ma, P. X., Maintaining dimensions and mechanical properties of ionically crosslinked alginate hydrogel scaffolds in vitro. *Journal of biomedical materials research. Part A* **2008,** *84* (4), 899-907.
58. Mihaila, S. M.; Gaharwar, A. K.; Reis, R. L.; Marques, A. P.; Gomes, M. E.; Khademhosseini, A., Photocrosslinkable Kappa-Carrageenan Hydrogels for Tissue Engineering Applications. *Advanced healthcare materials* **2013,** *2* (6), 895-907.
59. Hezaveh, H.; Muhamad, II; Noshadi, I.; Shu Fen, L.; Ngadi, N., Swelling behaviour and controlled drug release from cross-linked kappa-carrageenan/NaCMC hydrogel by diffusion mechanism. *Journal of microencapsulation* **2012,** *29* (4), 368-79.
60. Salgueiro, A. M.; Daniel-da-Silva, A. L.; Fateixa, S.; Trindade, T., kappa-Carrageenan hydrogel nanocomposites with release behavior mediated by morphological distinct Au nanofillers. *Carbohydr Polym* **2013,** *91* (1), 100-9.
61. Amici, E.; Clark, A. H.; Normand, V.; Johnson, N. B., Interpenetrating network formation in agarose--kappa-carrageenan gel composites. *Biomacromolecules* **2002,** *3* (3), 466-74.
62. Granero, A. J.; Razal, J. M.; Wallace, G. G.; Panhuis, M. i. h., Conducting gel-fibres based on carrageenan, chitosan and carbon nanotubes. *Journal of Material Chemistry* **2010,** *20*, 7953-7956.
63. Coutinho, D. F.; Sant, S. V.; Shin, H.; Oliveira, J. T.; Gomes, M. E.; Neves, N. M.; Khademhosseini, A.; Reis, R. L., Modified Gellan Gum hydrogels with tunable physical and mechanical properties. *Biomaterials* **2010,** *31* (29), 7494-502.
64. Hasirci, V.; Hasirci, N., Control of polymeric biomaterial surfaces. In *Surface and interfaces for biomaterials*, Vadgama, P., Ed. Cambridge and Boca Raton: Woodhead Publishing Limited and CRC Press LLC: 2005.
65. White, J. R.; Thomas, E. L., Advances in SEM of polymers. *Rubber Chemistry and Technology* **1984,** *57* (3), 457-506.
66. Zhao, X.; Huebsch, N.; Mooney, D. J.; Suo, Z., Stress-relaxation behavior in gels with ionic and covalent crosslinks. *Journal of applied physics* **2010,** *107* (6), 63509.
67. Wagner, W.; Wein, F.; Seckinger, A.; Frankhauser, M.; Wirkner, U.; Krause, U.; Blake, J.; Schwager, C.; Eckstein, V.; Ansorge, W.; Ho, A. D., Comparative characteristics of mesenchymal stem cells from human bone marrow, adipose tissue, and umbilical cord blood. *Experimental hematology* **2005,** *33* (11), 1402-16.
68. De Ugarte, D. A.; Morizono, K.; Elbarbary, A.; Alfonso, Z.; Zuk, P. A.; Zhu, M.; Dragoo, J. L.; Ashjian, P.; Thomas, B.; Benhaim, P.; Chen, I.; Fraser, J.; Hedrick, M. H., Comparison of multi-lineage cells from human adipose tissue and bone marrow. *Cells, tissues, organs* **2003,** *174* (3), 101-9.
69. Liu, T. M.; Martina, M.; Hutmacher, D. W.; Hui, J. H.; Lee, E. H.; Lim, B., Identification of common pathways mediating differentiation of bone marrow- and adipose tissue-derived human mesenchymal stem cells into three mesenchymal lineages. *Stem Cells* **2007,** *25* (3), 750-60.

70. Gimble, J. M.; Katz, A. J.; Bunnell, B. A., Adipose-derived stem cells for regenerative medicine. *Circulation research* **2007,** *100* (9), 1249-60.
71. Helder, M. N.; Knippenberg, M.; Klein-Nulend, J.; Wuisman, P. I., Stem cells from adipose tissue allow challenging new concepts for regenerative medicine. *Tissue Eng* **2007,** *13* (8), 1799-808.
72. Zuk, P. A.; Zhu, M.; Mizuno, H.; Huang, J.; Futrell, J. W.; Katz, A. J.; Benhaim, P.; Lorenz, H. P.; Hedrick, M. H., Multilineage cells from human adipose tissue: implications for cell-based therapies. *Tissue engineering* **2001,** *7* (2), 211-28.
73. Anghileri, E.; Marconi, S.; Pignatelli, A.; Cifelli, P.; Galie, M.; Sbarbati, A.; Krampera, M.; Belluzzi, O.; Bonetti, B., Neuronal differentiation potential of human adipose-derived mesenchymal stem cells. *Stem Cells Dev* **2008,** *17* (5), 909-16.
74. Vallee, M.; Cote, J. F.; Fradette, J., Adipose-tissue engineering: taking advantage of the properties of human adipose-derived stem/stromal cells. *Pathol Biol (Paris)* **2009,** *57* (4), 309-17.
75. Strem, B. M.; Hedrick, M. H., The growing importance of fat in regenerative medicine. *Trends Biotechnol* **2005,** *23* (2), 64-6.
76. Jain, R. K.; Au, P.; Tam, J.; Duda, D. G.; Fukumura, D., Engineering vascularized tissue. *Nat Biotechnol* **2005,** *23* (7), 821-3.
77. Kaigler, D.; Krebsbach, P. H.; Wang, Z.; West, E. R.; Horger, K.; Mooney, D. J., Transplanted endothelial cells enhance orthotopic bone regeneration. *Journal of dental research* **2006,** *85* (7), 633-7.
78. Levenberg, S.; Rouwkema, J.; Macdonald, M.; Garfein, E. S.; Kohane, D. S.; Darland, D. C.; Marini, R.; van Blitterswijk, C. A.; Mulligan, R. C.; D'Amore, P. A.; Langer, R., Engineering vascularized skeletal muscle tissue. *Nat Biotechnol* **2005,** *23* (7), 879-84.
79. Hegen, A.; Blois, A.; Tiron, C. E.; Hellesoy, M.; Micklem, D. R.; Nor, J. E.; Akslen, L. A.; Lorens, J. B., Efficient in vivo vascularization of tissue-engineering scaffolds. *J Tissue Eng Regen Med*.
80. Kim, S.; von Recum, H., Endothelial stem cells and precursors for tissue engineering: cell source, differentiation, selection, and application. *Tissue Eng Part B Rev* **2008,** *14* (1), 133-47.
81. Rada, T.; Reis, R. L.; Gomes, M. E., Distinct stem cells subpopulations isolated from human adipose tissue exhibit different chondrogenic and osteogenic differentiation potential. *Stem cell reviews* **2011,** *7* (1), 64-76.
82. Chung, M. T.; Liu, C.; Hyun, J. S.; Lo, D. D.; Montoro, D. T.; Hasegawa, M.; Li, S.; Sorkin, M.; Rennert, R.; Keeney, M.; Yang, F.; Quarto, N.; Longaker, M. T.; Wan, D. C., CD90 (Thy-1)-positive selection enhances osteogenic capacity of human adipose-derived stromal cells. *Tissue engineering. Part A* **2013,** *19* (7-8), 989-97.
83. Levi, B.; Wan, D. C.; Glotzbach, J. P.; Hyun, J.; Januszyk, M.; Montoro, D.; Sorkin, M.; James, A. W.; Nelson, E. R.; Li, S.; Quarto, N.; Lee, M.; Gurtner, G. C.; Longaker, M. T., CD105 protein depletion enhances human adipose-derived stromal cell osteogenesis through reduction of transforming growth factor beta1 (TGF-beta1) signaling. *The Journal of biological chemistry* **2011,** *286* (45), 39497-509.
84. Riekstina, U.; Cakstina, I.; Parfejevs, V.; Hoogduijn, M.; Jankovskis, G.; Muiznieks, I.; Muceniece, R.; Ancans, J., Embryonic stem cell marker expression pattern in human mesenchymal stem cells derived from bone marrow, adipose tissue, heart and dermis. *Stem Cell Rev* **2009,** *5* (4), 378-86.
85. Henderson, J. K.; Draper, J. S.; Baillie, H. S.; Fishel, S.; Thomson, J. A.; Moore, H.; Andrews, P. W., Preimplantation human embryos and embryonic stem cells show comparable expression of stage-specific embryonic antigens. *Stem Cells* **2002,** *20* (4), 329-37.
86. Wang, N.; Zhang, R.; Wang, S. J.; Zhang, C. L.; Mao, L. B.; Zhuang, C. Y.; Tang, Y. Y.; Luo, X. G.; Zhou, H.; Zhang, T. C., Vascular endothelial growth factor stimulates endothelial differentiation from mesenchymal stem cells via Rho/myocardin-related transcription factor--a signaling pathway. *The international journal of biochemistry & cell biology* **2013,** *45* (7), 1447-56.
87. Galas, R. J., Jr.; Liu, J. C., Surface density of vascular endothelial growth factor modulates endothelial proliferation and differentiation. *Journal of cellular biochemistry* **2014,** *115* (1), 111-20.
88. Wang, Y. H.; Yan, Z. Q.; Qi, Y. X.; Cheng, B. B.; Wang, X. D.; Zhao, D.; Shen, B. R.; Jiang, Z. L., Normal shear stress and vascular smooth muscle cells modulate migration of endothelial cells through histone deacetylase 6 activation and tubulin acetylation. *Annals of biomedical engineering* **2010,** *38* (3), 729-37.
89. Oswald J; Boxberger S; Jørgensen B; Feldmann S; Ehninger G; Bornhäuser M; C., W., Mesenchymal stem cells can be differentiated into endothelial cells in vitro. *Stem cells* **2004,** *22* (3), 377-384.

90. Fischer, L. J.; McIlhenny, S.; Tulenko, T.; Golesorkhi, N.; Zhang, P.; Larson, R.; Lombardi, J.; Shapiro, I.; DiMuzio, P. J., Endothelial differentiation of adipose-derived stem cells: effects of endothelial cell growth supplement and shear force. *The Journal of surgical research* **2009,** *152* (1), 157-66.
91. Ferreira, L. S.; Gerecht, S.; Shieh, H. F.; Watson, N.; Rupnick, M. A.; Dallabrida, S. M.; Vunjak-Novakovic, G.; Langer, R., Vascular progenitor cells isolated from human embryonic stem cells give rise to endothelial and smooth muscle like cells and form vascular networks in vivo. *Circulation research* **2007,** *101* (3), 286-94.
92. Hofmann, S.; Kaplan, D.; Vunjak-Novakovic, G.; Meinel, L., *Tissue Engineering of Bone*. John Wiley & Sons, Inc.: New Jersey, 2006.
93. Langenbach, F.; Handschel, J. R., Effects of dexamethasone, ascorbic acid and ?-glycerophosphate on the osteogenic differentiation of stem cells in vitro. *Stem cell research & therapy* **2013,** *4* (5), 117.
94. Murad, S.; Grove, D.; Lindberg, K. A.; Reynolds, G.; Sivarajah, A.; Pinnell, S. R., Regulation of collagen synthesis by ascorbic acid. *Proceedings of the National Academy of Sciences of the United States of America* **1981,** *78* (5), 2879-82.
95. Sugimoto, T.; Nakada, M.; Fukase, M.; Imai, Y.; Kinoshita, Y.; Fujita, T., Effects of ascorbic acid on alkaline phosphatase activity and hormone responsiveness in the osteoblastic osteosarcoma cell line UMR-106. *Calcified tissue international* **1986,** *39* (3), 171-4.
96. Porter, R. M.; Huckle, W. R.; Goldstein, A. S., Effect of dexamethasone withdrawal on osteoblastic differentiation of bone marrow stromal cells. *Journal of cellular biochemistry* **2003,** *90* (1), 13-22.
97. Hofmann, A.; Ritz, U.; Verrier, S.; Eglin, D.; Alini, M.; Fuchs, S.; Kirkpatrick, C. J.; Rommens, P. M., The effect of human osteoblasts on proliferation and neo-vessel formation of human umbilical vein endothelial cells in a long-term 3D co-culture on polyurethane scaffolds. *Biomaterials* **2008,** *29* (31), 4217-26.
98. Koob, S.; Torio-Padron, N.; Stark, G. B.; Hannig, C.; Stankovic, Z.; Finkenzeller, G., Bone formation and neovascularization mediated by mesenchymal stem cells and endothelial cells in critical-sized calvarial defects. *Tissue engineering. Part A* **2011,** *17* (3-4), 311-21.
99. Duffy, G. P.; Ahsan, T.; O'Brien, T.; Barry, F.; Nerem, R. M., Bone marrow-derived mesenchymal stem cells promote angiogenic processes in a time- and dose-dependent manner in vitro. *Tissue engineering. Part A* **2009,** *15* (9), 2459-70.
100. Ma, J.; van den Beucken, J. J.; Yang, F.; Both, S. K.; Cui, F. Z.; Pan, J.; Jansen, J. A., Coculture of osteoblasts and endothelial cells: optimization of culture medium and cell ratio. *Tissue engineering. Part C, Methods* **2011,** *17* (3), 349-57.
101. Rouwkema, J.; Westerweel, P. E.; de Boer, J.; Verhaar, M. C.; van Blitterswijk, C. A., The use of endothelial progenitor cells for prevascularized bone tissue engineering. *Tissue engineering. Part A* **2009,** *15* (8), 2015-27.
102. Guillotin, B.; Bareille, R.; Bourget, C.; Bordenave, L.; Amedee, J., Interaction between human umbilical vein endothelial cells and human osteoprogenitors triggers pleiotropic effect that may support osteoblastic function. *Bone* **2008,** *42* (6), 1080-91.
103. Valenzuela, C. D.; Allori, A. C.; Reformat, D. D.; Sailon, A. M.; Allen, R. J., Jr.; Davidson, E. H.; Alikhani, M.; Bromage, T. G.; Ricci, J. L.; Warren, S. M., Characterization of adipose-derived mesenchymal stem cell combinations for vascularized bone engineering. *Tissue engineering. Part A* **2013,** *19* (11-12), 1373-85.
104. Auffan, M.; Rose, J.; Bottero, J. Y.; Lowry, G. V.; Jolivet, J. P.; Wiesner, M. R., Towards a definition of inorganic nanoparticles from an environmental, health and safety perspective. *Nature nanotechnology* **2009,** *4* (10), 634-41.
105. Williams, C. G.; Malik, A. N.; Kim, T. K.; Manson, P. N.; Elisseeff, J. H., Variable cytocompatibility of six cell lines with photoinitiators used for polymerizing hydrogels and cell encapsulation. *Biomaterials* **2005,** *26* (11), 1211-1218.
106. Qin, D.; Xia, Y.; Whitesides, G. M., Soft lithography for micro- and nanoscale patterning. *Nature protocols* **2010,** *5* (3), 491-502.
107. Wolfe, D. B.; Qin, D.; Whitesides, G. M., Rapid prototyping of microstructures by soft lithography for biotechnology. *Methods in molecular biology* **2010,** *583*, 81-107.
108. Bergamini, C. M.; Gambetti, S.; Dondi, A.; Cervellati, C., Oxygen, reactive oxygen species and tissue damage. *Current pharmaceutical design* **2004,** *10* (14), 1611-26.
109. Minai, L.; Yeheskely-Hayon, D.; Yelin, D., High levels of reactive oxygen species in gold nanoparticle-targeted cancer cells following femtosecond pulse irradiation. *Scientific reports* **2013,** *3*, 2146.

110. Webster, T. J., *Safety of nanoparticles: from manufacturing to medical applications*. 2008.
111. Ramachandran, G., *Assessing nanoparticle risks to human health*. 2011.
112. Zaqout, M. S.; Sumizawa, T.; Igisu, H.; Wilson, D.; Myojo, T.; Ueno, S., Binding of titanium dioxide nanoparticles to lactate dehydrogenase. *Environmental health and preventive medicine* **2012,** *17* (4), 341-5.
113. van Meerloo, J.; Kaspers, G. J.; Cloos, J., Cell sensitivity assays: the MTT assay. *Methods in molecular biology* **2011,** *731*, 237-45.
114. Lancaster, M. V.; Fields, R. D. Antibiotic and cytotoxic drug susceptibility assays using resazurin and poising Agents. 1996.
115. (a) Dominici, M.; Le Blanc, K.; Mueller, I.; Slaper-Cortenbach, I.; Marini, F.; Krause, D.; Deans, R.; Keating, A.; Prockop, D.; Horwitz, E., Minimal criteria for defining multipotent mesenchymal stromal cells. The International Society for Cellular Therapy position statement. *Cytotherapy* **2006,** *8* (4), 315-7; (b) Phinney, D. G.; Prockop, D. J., Concise review: mesenchymal stem/multipotent stromal cells: the state of transdifferentiation and modes of tissue repair--current views. *Stem cells* **2007,** *25* (11), 2896-902.
116. Pfaffl, M. W., A new mathematical model for relative quantification in real-time RT-PCR. *Nucleic acids research* **2001,** *29* (9), e45.
117. Stein, O.; Stein, Y., Bovine aortic endothelial cells display macrophage-like properties towards acetylated 125I-labelled low density lipoprotein. *Biochimica et biophysica acta* **1980,** *620* (3), 631-5.
118. Holthofer, H.; Virtane, I.; Kariniemi, A. L.; Hormia, M.; Linder, E.; Miettinen, A., Ulex Europaeus I Lectin as a marker for vascular endothelium in human tissues. *Laboratory Investigation* **1982,** *47* (1), 60-66.
119. Crabtree, B.; Subramanian, V., Behavior of endothelial cells on Matrigel and development of a method for a rapid and reproducible in vitro angiogenesis assay. *In vitro cellular & developmental biology. Animal* **2007,** *43* (2), 87-94.
120. Khoo, C. P.; Micklem, K.; Watt, S. M., A comparison of methods for quantifying angiogenesis in the Matrigel assay in vitro. *Tissue engineering. Part C, Methods* **2011,** *17* (9), 895-906.
121. Golub, E. E.; Boesze-Battaglia, K., The role of alkaline phosphatase in mineralization. *Current Opinion in Orthopaedics* **2007,** *18* (5), 444-448.
122. Holtz, K. M.; Kantrowitz, E. R., The mechanism of the alkaline phosphatase reaction: insights from NMR, crystallography and site-specific mutagenesis. *FEBS letters* **1999,** *462* (1-2), 7-11.
123. Armendariz-Borunda, J.; Rojkind, M., A simple quantitative method for collagen typing in tissue samples: its application to human liver with schistosomiasis. *Collagen and related research* **1984,** *4* (1), 35-47.
124. Gregory, C. A.; Gunn, W. G.; Peister, A.; Prockop, D. J., An Alizarin red-based assay of mineralization by adherent cells in culture: comparison with cetylpyridinium chloride extraction. *Analytical biochemistry* **2004,** *329* (1), 77-84.
125. Shapiro, S. S.; Wilk, M. B., An analysis of variance test for normality (complete samples). *Biometrika* **1965,** *52* (3-4), 591-611.

SECTION III

THE SSEA-4^{+} SUB-POPULATION RESIDING WITHIN THE STROMAL VASCULAR FRACTION OF THE ADIPOSE TISSUE ACTS AS A SINGLE CELL SOURCE TO OBTAIN BOTH ENDOTHELIAL AND OSTEOBLAST-LIKE CELLS

Chapter III

Human Adipose Tissue-Derived SSEA-4 Sub-Population Multi-Differentiation Potential Towards the Endothelial and Osteogenic Lineages

ABSTRACT

Human adipose tissue has been recently recognized as a potential source of stem cells for regenerative medicine applications, including bone TE. Despite the gathered knowledge regarding the differentiation potential of hASCs, in what concerns the endothelial lineage many uncertainties are still present. The existence of a cell subpopulation within the human adipose tissue that expresses a SSEA-4 marker, usually associated to pluripotency, raises expectations on the differentiation capacity of these cells (SSEA-4$^+$hASCs). In the present study, the endothelial and osteogenic differentiation potential of the SSEA-4$^+$hASCs was analyzed, aiming at proposing a single-cell source/subpopulation for the development of vascularized bone TE constructs. SSEA-4$^+$hASCs were isolated using immunomagnetic sorting and cultured either in α-MEM, in EGM-2 MV (endothelial growth medium), or in osteogenic medium. SSEA-4$^+$hASCs cultured in EGM-2 MV formed endothelial cell-like colonies characterized by a cobblestone morphology and expression of CD31, CD34, CD105, and vWF as determined by quantitative reverse transcriptase-polymerase chain reaction, immunofluorescence and flow cytometry. The endothelial phenotype was also confirmed by their ability to incorporate ac-LDL and form capillary-like structures when seeded on Matrigel. SSEA-4$^+$hASCs cultured in α-MEM displayed a fibroblastic-like morphology and exhibited mesenchymal surface marker profile (>90% CD73$^+$/CD90$^+$/CD105$^+$). After culture in osteogenic conditions, an overexpression of osteogenic-related markers (OPN and OCN) was observed both at molecular and protein levels. Matrix mineralization confirmed SSEA-4$^+$hASCs osteogenic differentiation. Herein, we demonstrate that from a single-cell source, and by selecting the appropriate subpopulation it is possible to obtain microvascular-like endothelial cells and osteoblasts, the most relevant cell types for the creation of vascularized bone tissue-engineered constructs.

This chapter is based on the following publication:

Mihaila SM, Frias AM, Pirraco RP, Rada T, Reis RL, Gomes ME and Marques AP, "Human adipose tissue-derived SSEA-4 sub-population multi-differentiation potential towards the endothelial and osteogenic lineages", Tissue Engineering part A, 19(1-2): 235-46. doi: 10.1089/ten.TEA.2012.0092

III.1. INTRODUCTION

The concept of using adipose tissue (AT) as a source of adult stem cells for regenerative medicine applications is highly appealing mainly due to its abundance and accessibility for harvesting following minimally invasive procedures[1]. Human adipose-derived stem cells (hASCs) isolated from the stromal vascular fraction (SVF) of the adipose tissue bear resemblances to bone marrow-derived mesenchymal cells (BMSCs)[2,3] demonstrated by their similar morphology, and common surface markers and gene expression profiles[4,5,6]. However, the SVF of the AT harbors more than 2% of cells featuring potential for multi-lineage differentiation compared to the 0.002% of the bone marrow[1,4,7]. Additionally, a large number of studies have proven the hASCs differentiation potential towards multiple lineages, namely the osteogenic[8], chondrogenic[8], adipogenic[8], myogenic[8] and neurogenic[9]. Also, the developmental plasticity of hASCs was demonstrated both *in vitro*[10] and *in vivo*[11]. Therefore, hASCs clearly hold a great promise in tissue regeneration therapies, including the creation of a wide range of autologous tissue-engineered substitutes[1].

Although there has been extensive research effort to create functional engineered tissues, the success of such approaches still relies on the construction of vascular networks capable of delivering oxygen and nutrients within the engineered constructs[12]. Thus, in the context of bone tissue engineering (TE), the development of strategies that could effectively induce the microcirculation within the engineered constructs has become a major pursuit[13].

Previous *in vivo* studies showed that vascularization within engineered constructs using mature endothelial cells (ECs) improved blood perfusion, cell viability and their survival after implantation[14,15,16]. However, the limited availability and proliferation capability of mature ECs hinders their use in TE approaches[17]. Therefore, it became priority to find a suitable source of ECs that do not present such constrains and that will be ready-to-use for therapeutic applications. A significant number of studies has been reported regarding the isolation of endothelial progenitor cells (EPCs)[18,19,20] and the endothelial differentiation of both embryonic[21,22] and adult stem cells from different origins[23,24,25]. The distinction between adult mesenchymal stem cells and endothelial precursors based on cell surface markers is far from ideal as these cells share many common markers. However, the selection of specific sub-populations has gained increasing interest and has revealed significance for cell-based therapies as a way to overcome difficulties imposed by the heterogeneity of each tissue populations.

Considering AT as a pool of cells containing multipotent stem cells, Rada *et al.* demonstrated the osteogenic and chondrogenic differentiation potential of distinct sub-populations residing in the SVF[26,27]. These results together with other studies[28,29] underline the complexity of the SVF of AT composed by several sub-populations exhibiting distinct

differentiation potentials. Other sub-populations, within SVF and hASCs fractions have been identified as possessing endothelial differentiation[30,31,32,33]. Martínez-Estrada *et al*.[34] expanded the sub-population expressing Flk-1, a receptor for vascular endothelial growth factor and one of the earliest markers of EPCs[31], residing within the adipose stroma, and were able to lead their maturation into endothelial-like cells. Miranville *et al.*[32] and Sengenes *et al.*[30,33] have demonstrated that the $CD34^+/CD31^-$ sub-population when cultured under appropriate conditions give rise to functional endothelial cells as demonstrated after intravenous injection in a mouse ischemic hind limb model. The hASCs-derived $CD31^-/CD45^-$ sub-population under shear stress and treatment with endothelial cell growth supplement (ECGS) also acquired some endothelial characteristics but not others such as nitric oxide synthase (eNOS), von Willebrand factor (vWF) expression, which suggests the need to further knowledge regarding this sub-population prior to its use in cell-based therapies[35]. So far, the definition of the appropriate surface marker(s) to isolate a specific sub-population from human adipose tissue, relevant for vascularization purposes was restricted to endothelial or hematopoietic progenitor markers.

Stage-specific embryonic antigen (SSEA-4) has been widely used as one of the markers for monitoring the maintenance of an undifferentiated state of human embryonic stem cells[36,37]. Moreover, $SSEA\text{-}4^+$ cells retain features of pluripotency, characterized by nearly unlimited self-renewal and differentiation capacity into any of the three germ layers[37,38,39]. Riekstina *et al*.[36] examined the expression of embryonic stem cell markers within adult mesenchymal stem cell populations derived from different cell sources and showed the presence of approximately 8% of $SSEA\text{-}4^+$ cells within the AT[36]. Based on these findings, we hypothesized that the $SSEA\text{-}4^+$hASCs sub-population might exhibit multipotent features relevant for bone TE applications. By triggering its differentiation towards the endothelial and osteogenic lineages, we were able to demonstrate the usefulness of the proposed strategy to obtain these two cell types from the same cell source, in opposition to using the entire SVF. Furthermore, this work comprises the first step to assemble a TE construct using a sub-population whose differentiation level might be modulated towards the two most relevant lineages to achieve a successful in bone regeneration approach.

III.2. MATERIALS AND METHODS

III.2.1. HASCs and HUVECs cells harvest

All the human samples were obtained after written protocols were established between the 3B's Research Group and the provider-involved institutions. The protocols were approved y the respective ethical committees to assure that the requirements defined by the Helsinki

declaration guidelines regarding human rights, thus assuring the patient's informed consent as well as patient's anonymity were followed.

The lipoaspirate samples were kindly provided by Hospital de Prelada, Porto, Portugal and HUVECs were obtained from umbilical cord of healthy babies provided by Hospital de Sao Marcos (Braga, Portugal). In more detail, human abdominal subcutaneous fat tissue samples were obtained from healthy females (n=6), with an average age of 42 years old, undergoing lipoaspiration procedure, after informed consent. The tissue samples were transported to the laboratory in phosphate buffered saline (PBS) supplemented with 10% penicillin-streptomycin (Pen/Strep, Gibco, UK) at a final concentration of 1000U/1000µg/mL and processed within 24h after surgery, according to a standard isolation protocol[40]. Briefly, the lipoaspirates were digested with 0.075% collagenase II A (Sigma-Aldrich, Germany) in PBS, at pH 7.4 for 45min and at 37ºC in a shaking water bath and finally filtered using a strain with 200µm pore size. Mature adipocytes and connective tissue cells were separated by centrifugation at 1000*xg*, for 10 min at 4ºC. Cell pellet was resuspended and incubated for 10 min at room temperature in a pH 7.4 erythrocyte lysis buffer of 155mM NH_4Cl (Merck, Germany), 5.7mM K_2HPO_4 (Riedel-de-Häen, Germany) and 0.1mM EDTA (Sigma-Aldrich, Germany) in distillated water. The cell suspension was centrifuged at 800*xg* for 10min at 4ºC. The pellet was resuspended in PBS and filtered with a 100µm cell strainer to obtain the SVF.

Primary cultures of macrovascular human umbilical vein endothelial cells (HUVECs) were used as a positive control for endothelial phenotype. Cells were obtained according to a previously published method[41].

II.2.2. Immunomagnetic beads cell separation

The immunomagnetic beads (Dynal M-450 Epoxy beads from Dynal Biotech, Carlsbad, CA, USA) were first coated with SSEA-4 antibody (Abcam, Cambridge, UK) following the manufacturer instruction. For this purpose 50µL of the immunomagnetic beads solution containing $2x10^7$ beads, were washed in the coupling buffer (0.1M sodium phosphate buffer: pH 7.4-8.0), resuspended with 10µL of the SSEA-4 antibody at a concentration of 200 µg/mL and then incubated, overnight, at room temperature, under gentle stirring. After this period, the SSEA-4 coupled beads were separated with Dynal MPC® magnet (Dynal Biotech, Carlsbad, CA, USA) and the supernatant discarded. The coupled beads were mixed and incubated for 5min with gentle rotation in 1mL of a 0.2% (w/v) bovine serum albumin (BSA, Sigma-Aldrich, Germany) solution in PBS (0.2%BSA/PBS), at pH 7.4 and again separated using the magnet. This procedure was repeated three times. The antibody coupled beads

were resuspended in 0.2%BSA/PBS at a concentration of $4x10^8$ Dynabeads/mL until further use.

In order to select the SVF sub-population of interest for the study, (SSEA-4^+hASCs), the SSEA-4 antibody coated beads were mixed with the SVF and incubated for 30min at 4°C under gentle stirring. Subsequently, the mixture was washed with 0.2% BSA/PBS and the cells bonded to the beads were separated from the rest of the cell suspension using the magnet as previously described.

III.2.3. Cell culture

The SVF and the SSEA-4^+hASCs, were both cultured in α-MEM medium (Sigma Aldrich, Germany) with 10% fetal bovine serum (FBS, Gibco, UK) and 1% Pen/Strep (100U/100 µg/mL), and in microvascular endothelial cell growth medium (EGM-2 MV bullet kit (Lonza, Basel, Switzerland) containing 5% FBS and the supplemental growth factors (provided in the culture medium kit) and maintained until confluence. Cells were detached from the culture flasks using trypsin (0.25% trypsin–EDTA solution; Sigma, Germany) and kept under the same conditions along the passages. All the subsequent experimental procedures/ study groups are summarized in the **Supplemental Figure III.1**. HUVECs were cultured in M199 medium (Sigma, Germany) supplemented with 20% FBS (Sigma, Germany), 1% Pen/Strep (100U/100µg/mL), 2mM glutamax I (Life Technologies, Germany), 50 µg/mL sodium heparin (Sigma-Aldrich, Germany) and 50 µg/mL endothelial cell growth supplement (ECGS, BD Biosciences, Franklin Lakes, NJ, USA).

III.2.4. Osteogenic differentiation

Confluent hASCs and SSEA-4^+hASCs (passage 3), were removed from the culture flasks using trypsin and seeded at a density of 2,000 cells/cm^2 in α-MEM medium supplemented with 10% fetal bovine serum, 1% antibiotic/ antimycotic, 10mM β-glycerophosphate (Sigma Aldrich, Germany), 10^{-8}M dexamethasone (Sigma Aldrich, Germany) and 50µg/mL L-ascorbic acid 2-phosphate sesquimagnesium salt hydrate (Sigma Aldrich, Germany). Cells were incubated in a humidified environment at 37°C with 5% CO_2 for 7, 14, 21 and 28 days with culture media replenishment every 3-4 days. Cells cultured in the same medium, but without the osteogenic factors were used as controls.

III.2.5. Alizarin Red staining

Cells cultured under osteogenic differentiation conditions were fixed at the different time points with 10% formalin solution and washed, firstly with PBS and then with distilled water (diH_2O). The cells were then incubated for 10min with a 2% (wt/v) Alizarin Red S solution

(Merck, Germany) in diH_2O, at a pH of 4.1-4.3. After incubation, cells were washed again with diH_2O and the staining observed under a stereo microscope Stemi 1000 (Zeiss, Germany).

III.2.6. Flow cytometry

The freshly isolated SVF, the hASCs and SSEA-4$^+$hASCs cultured in α-MEM medium and EGM-2 MV were harvested with trypsin upon reaching 80% confluence, along 4 passages. About 5x10^5 cells from each one of the experimental conditions were incubated for 30min on ice with the following primary antibodies: mouse anti-human CD31-APC (R&D Systems, Germany), mouse anti-human CD90-APC (eBioscience, San Diego, CA, USA), CD73-PE (BD Biosciences, Franklin Lakes, NJ, USA), mouse anti-human CD105-FITC (AbD Serotec, UK), mouse anti-human SSEA-4-Alexa Fluor 488 (eBioscience, San Diego, CA, USA), mouse anti-human CD34-PE (BD Biosciences, Franklin Lakes, NJ, USA), mouse anti-human CD45-FITC (BD Biosciences, Franklin Lakes, NJ, USA). After washing with PBS, the cells were resuspended in acquisition buffer (PBS containing 1% formaldehyde and 0.1% sodium azide) until analysis. In each run, at least 20,000 events were acquired with FACS-Calibur flow cytometer (BD Biosciences, Franklin Lakes, NJ, USA) and the results analyzed with the CellQuest software (BD Biosciences, Franklin Lakes, NJ, USA). The number of positive events for each cell-specific marker was expressed as a percentage of the total cell number within each condition.

III.2.7. Immunocytochemistry

SSEA-4$^+$hASCs and hASCs cultured onto tissue culture polystyrene (TCPS) slides (Sarstedt, Newton, NC, USA) in α-MEM and EGM-2 MV, passage 0 to 4, and in osteogenic conditions at the selected time points, were washed twice with PBS, fixed with 10% formalin for 30min, washed again with PBS and stored at 4ºC until use. Fixed cells were washed with PBS, permeabilized with 0.2% Triton 100x solution for 2min and non-specific binding was blocked with a 3% BSA/PBS solution. Cells were incubated for one hour at room temperature with the primary antibodies mouse anti-human CD31 (1:50, Dako, Denmark), rabbit anti-human von Willebrand factor (1:200, vWF, Dako, Denmark), mouse anti-human SSEA-4 (1:50, Abcam, Cambridge, UK), CD34-PE (1:50, BD Biosciences, Franklin Lakes, NJ, USA), mouse anti-human CD105 (1:50, eBioscience, San Diego, CA, USA), mouse anti-human osteocalcin (OCN, 1:50, AbD Serotec, UK) and rabbit anti-human osteopontin (OPN, 1:50, Abcam, Cambridge, UK). All antibody dilutions were performed in 1.5% BSA/PBS. After incubation, cells were washed 3 times with PBS for 5min and incubated 1h with the appropriate secondary antibody, either donkey anti-rabbit Alexa Fluor 488 (Invitrogen,

Carlsbad, CA, USA), or donkey anti-mouse Alexa Fluor 594 (Invitrogen, Carlsbad, CA, USA) diluted 1:500 in 1.5% BSA/PBS. Cell nuclei were counterstained with 4,6-Diamidino-2-phenyindole dilactate (DAPI), at a 1:10,000 dilution in PBS, for 10min and then washed 3 times. Negative control samples were prepared by replacing the primary antibody incubation with PBS. Immunolabelling was qualitatively analyzed under the Axioplan Imager Z1 fluorescence microscope (Zeiss, Germany) and photographed using the Axio Cam MRm camera (Zeiss, Germany) and the AxioVision 4.8 software (Zeiss, Germany).

III.2.8. Real Time RT-PCR

III.2.8.1. mRNA extraction and cDNA synthesis

Total mRNA of hASCs and SSEA-4$^+$hASCs cultures in α-MEM and EGM-2 MV from passage 1 to 3 were extracted using TRIzol Reagent (Invitrogen, Carlsbad, CA, USA) according to the manufacturer instructions. Briefly, 800µL of TRIzol Reagent were added to each sample and stored at −80ºC until further analysis. Upon thawing, 160µL of chloroform (Sigma Aldrich, Germany) were added to each sample, incubated for 15min at 4ºC and centrifuged at the same temperature at 13,000×*g* for 15min. After the centrifugation, the aqueous part was collected and an equal part of isopropanol (Sigma Aldrich, Germany) was added. After a 2h incubation at −80ºC, the samples were washed in ethanol, centrifuged at 4ºC and 9,000×*g* for 5min and resuspended in 12µL of water RNase/DNase free (Gibco, UK). mRNA quantity and purity were determined using the NanoDrop ND-1000 Spectrophotometer (Thermo Fischer Scientific, MA, USA). For the complementary DNA (cDNA) synthesis only the samples with a 260/280 ratio between 1.7 and 2.0 were used. The cDNA synthesis was performed with the qScript cDNA Synthesis kit (Quanta Biosciences, Gaithersburg, MD, USA), and the Mastercycler ep realplex thermal cycler (Eppendorf, Hamburg, Germany), using an initial amount of total RNA of 2µg in a total volume of 20µL.

III.2.8.2. Real time RT-PCR

The quantification of the transcripts of the genes of interest was carried out by real time reverse transcriptase polymerase chain reactions (RT-PCR) method using 5ng of cDNA and the PerfeCTA SYBR Green FastMix kit (Quanta Biosciences, Gaithersburg, MD, USA) following the procedure suggested by the manufacturer, in a Real-Time Mastercycler ep realplex thermal cycler (Eppendorf, Hamburg, Germany). The primers were previously designed using the Primer 3 online software (v0.4.0) (**Supplemental Table III.1**) and synthesized by MGW Biotech, Germany. For each sample, *glyceraldehyde 3-phosphate dehydrogenase (GAPDH*) was used as housekeeping gene. A concentration of 300nM was

used for all the primers, in a final volume of 20µL. Samples with RNAse free water (Gibco, UK), SYBR Green (Quanta Biosciences, Gaithersburg, MD, USA) and without cDNAwere used as blanks. The relative quantification of the gene expression was performed using Pfaffl method to obtain the ΔΔCt[42]. All values were first normalized against GAPDH values and then to the SSEA-4$^+$cells separated from the freshly isolated SVF (for the expression of the endothelial markers: CD31 and vWF) or to the two cell types cultured in α-MEM: hASCs and SSEA-4$^+$hASCs, respectively (for the expression of osteogenic related markers: *OPN* and *OCN*).

III.2.9. Acetylated low density lipoprotein (ac-LDL) uptake and lectin binding

Low Density Lipoprotein (LDL) uptake was assessed by incubating the hASCs and SSEA-4$^+$hASCs cultured in EGM-2 MV and α-MEM (passage 4) for 4h at 37ºC with 2µg/mL of acetylated LDL labeled with 1,1´-dioctadecyl-3,3,3´,3´-tetramethylindocarbocyanine (Dil-ac-LDL, Invitrogen, Carlsbad, CA, USA). Cells were incubated with FITC-conjugated lectin *Ulex Europaeus-1* (UEA-1, Sigma Aldrich, Germany) 100µg/mL for 1h at 37ºC along with the Dil-ac-LDL and protected from light. Cells were then washed twice with PBS, fixed for 15min in 10% formalin solution and analyzed by fluorescence microscopy as described for the immunocytochemistry.

III.2.10. Matrigel assay

To analyze the capacity of the SSEA-4$^+$hASCs and hASCs cultured in EGM-2 MV and α-MEM to form tubular structures at different passages (1 to 4), a 96-well cell culture plate, chilled at 4ºC, was loaded with 32µL of Matrigel (BD Biosciences, Franklin Lakes, NJ, USA) and incubated at 37ºC. Cells were suspended in EGM-2 MV medium at a concentration of $2.1x10^5$ cells /mL and 64µL of this cell suspension was seeded in each well onto the surface of the solidified Matrigel. Cells were incubated at 37ºC in a 5% CO_2 humidified atmosphere for 4h. HUVECs cells were used as a control and were seeded following the procedure mentioned above. Three representative images of each condition were recorded using an inverted microscope Axiovert 40 (Zeiss, Germany) equipped with digital image capture software.

III.2.11. Statistical analysis

The flow cytometry data collected from 6 independent experiments, and the RT-PCR data, obtained from 3 independent experiments, with 3 replicates for each experiment are expressed as arithmetic means ± standard deviation (SD). The RT-PCR results were analyzed with the ANOVA single factor method (post-testing for pair wise comparisons were

performed using Tukey´s range test). The values were considered statistically significant for $p \leq 0.05$.

III.3. RESULTS

III.3.1. SVF and hASCs characterization

The percentage of cells expressing mesenchymal stem cell markers: CD105, CD90 and CD73, the pluripotency marker: SSEA-4, the endothelial marker: CD31 and the hematopoietic markers: CD34 and CD45, were examined by flow cytometry. Within the SVF, 2.86% of the total isolated cell expressed the pluripotency marker SSEA-4, while only about 1.86% were positive for the endothelial cell surface marker CD31 and 8.12% of the total population expressed CD34 (**Figure III.1A**). After selection by plastic adherence and culture in α-MEM, the obtained hASCs displayed a homogeneous fibroblast-like morphology characteristic of mesenchymal cells that was maintained up to passage 4 (**Figure III.1B-C**).

A

Surface marker	Percentage of positive cells within the SVF (%, mean±SD)
CD105	7.75 ± 2.17
CD90/CD73	12.6 ± 3.09
CD31	1.86 ± 0.19
SSEA-4	2.86 ± 1.06
CD34	8.12 ± 2.31
CD45	0.49 ± 0.08

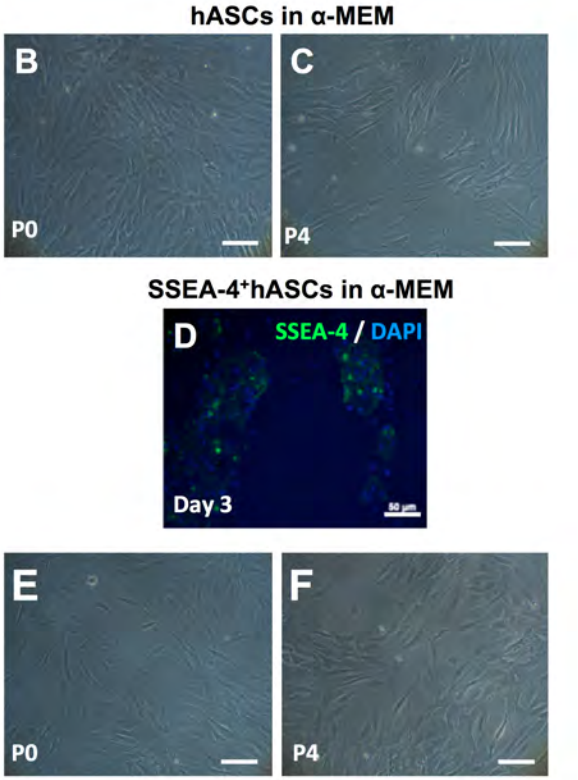

Figure III.1. Morphology and surface marker profile characterization of human adipose derived stem cells (hASCs) and SSEA-4$^+$hASCs. (**A**) Cell surface marker profile of stromal vascular fraction (SVF), obtained by flow cytometry. Optical micrographs showing the morphology of hASCs (**B, C**) and SSEA-4$^+$hASCs (**E, F**) cultured in α-MEM at passage 0 (P0) and 4 (P4). Immunocytochemistry of selected SSEA-4$^+$ cells cultured for 3 days in α-MEM confirming the majority of the cells expressing SSEA-4 (**D**). Cell nuclei were counterstained with DAPI. Scale bar represents 100µm.

The surface marker profile confirmed the hASCs mesenchymal phenotype by the co-expression of CD90, CD105 and CD73 in more than 90% of the cells, while lacking expression of CD45 and CD34 (**Table III.1**). The absence of cells expressing CD31 after the selection by adherence was also verified. These characteristics were conserved along the passages, contrarily to the percentage of cells expressing SSEA-4 that diminished from 9.18% to 1.86%, respectively from passages 1 to 4 (**Table III.1**).

Table III.1. Cell surface marker profile of hASCs cultured in α-MEM at different passages, obtained by flow cytometry

Percentage of positive cells within the considered population (%, mean ± SD)						
Passage	**CD105**	**CD90/CD73**	**CD31**	**SSEA-4**	**CD34**	**CD45**
1	87.9 ± 9.05	89.7 ± 8.98	0.17 ± 0.04	9.18 ± 3.21	5.52 ± 0.09	0.25 ± 0.02
2	88.3 ± 11.2	91.2 ± 11.1	0.11 ± 0.03	7.40 ± 3.23	0.23 ± 0.07	0.01 ± 0.01
3	89.5 ± 9.10	93.7 ± 8.45	0.01 ± 0.00	4.60 ± 2.45	0.13 ± 0.03	0.01 ± 0.00
4	94.2 ± 3.56	96.3 ± 7.67	0.02 ± 0.00	1.86 ± 0.23	0.34 ± 0.01	0.05 ± 0.01

III.3.2. SSEA-4$^+$hASCs sub-population characterization

SSEA-4$^+$hASCs were obtained by immunomagnetic selection of the SSEA-4$^+$ fraction (about 3%) of the SVF. The success of the method was confirmed by the immunocytochemistry results after 2 days of culture in α-MEM showing the majority of the adhered cells expressing SSEA-4 (**Figure III.1D**). SSEA-4$^+$hASCs cultured in α-MEM displayed the same fibroblast-like morphology as the hASCs cultured under the same conditions, independently of the passage, and up to passage 4 (**Figure III.1E-F**). However, from passages 1 to 4, the flow cytometry analysis revealed that CD105$^+$, CD90$^+$ and CD73$^+$ cells, comprised more than 90% of the total population, whereas SSEA-4$^+$ cells dramatically decreased (1.98 ± 0.59%) by passage 4. The selected SSEA-4$^+$hASCs sub-populations were also negative for CD31 and a low percentage of cells, from 3.34% at P1 to 1.40% at P4, were positive for CD45. The percentage of CD34$^+$ cells (13.2% at P1) did not significantly vary with the passage (**Table III.2**).

Table III.2. Cell surface marker profile of SSEA-4$^+$hASCs cultured in α-MEM at different passages, obtained by flow cytometry

Percentage of positive cells within the considered population (%, mean ± SD)						
Passage	**CD105**	**CD90/CD73**	**CD31**	**SSEA-4**	**CD34**	**CD45**
1	88.5 ± 12.2	94.8 ± 8.94	0.20± 0.02	4.35 ± 1.29	13.2 ± 4.69	3.34 ± 0.95
2	90.2 ± 6.34	93.5 ± 4.23	0.01 ± 0.00	5.23 ± 1.21	16.9 ±3.45	2.98 ± 1.03
3	89.2 ± 0.60	93.4 ± 5.14	0.00 ± 0.00	2.73 ± 1.57	15.8 ± 4.69	2.52 ± 0.70
4	94.5 ± 5.31	95.5 ± 4.82	0.00 ± 0.00	1.98 ± 0.59	13.6 ± 2.36	1.40 ± 0.62

III.3.3. hASCs and SSEA-4$^+$hASCs osteogenic differentiation

Induction of hASCs and SSEA-4$^+$hASCs into the osteogenic lineage was maintained up to 28 days of culture. Real Time RT-PCR analysis was performed in order to study the expression of the osteogenic related markers osteopontin (OPN) and osteocalcin (OCN). This analysis demonstrated that the osteogenic differentiation of both hASCs and SSEA-4$^+$hASCs was triggered within the first 7 days of culture in osteogenic medium and that by day 14 the expression of OPN reached a 600-fold increase (**Figure III.2A**). From day 21 to day 28 a significant down-regulation of OPN transcripts occurred in both cell populations. In contrast, a significant up regulation was observed for OCN from day 7 up to day 28 at which reached a maximum 2750-fold. Immunocytochemistry confirmed, at the protein level, the molecular analysis; both hASCs and SSEA-4$^+$hASCs cells cultured under osteogenic conditions started to deposit OPN and OCN (**Figure III.2B-C**). Furthermore, the Alizarin Red staining confirmed an intense matrix mineralization from day 14 onwards, again for both hASCs and SSEA-4$^+$hASCs cultured under osteogenic conditions, although it seems that mineralization occurred faster and in a more homogeneous mode by the SSEA-4$^+$hASCs (**Figure III.2D**).

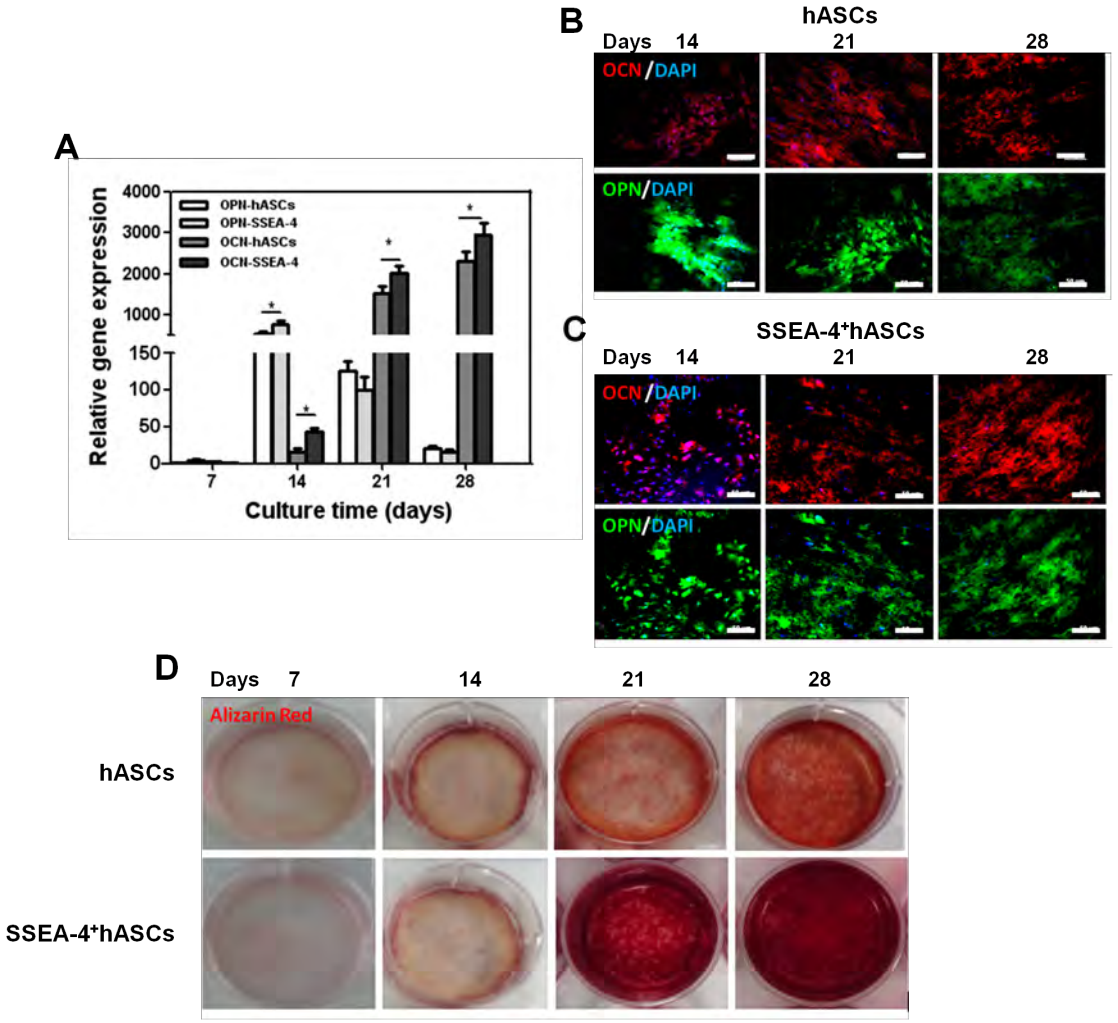

Figure III.2. *In vitro* osteogenic differentiation of hASCs and SSEA-4^{+}hASCs. (**A**) qRT-PCR results showing the over-expression of osteogenic related genes, osteocalcin (OCN) and osteopontin (OPN) in both cell populations along the culture in osteogenic conditions (**B-C**) Immunostaining of OPN (green) and OCN (red) deposition by hASCs (**B**) and SSEA-4^{+}hASCs (**C**) at days 14, 21 and 28 of culture under osteogenic conditions confirming the osteogenic differentiation. Cell nuclei were counterstained with DAPI (blue). (**D**) Optical micrographs showing the gradual mineralization of the deposited matrix after Alizarin Red S staining from day 7, 14, 21 and 28. Scale bar represent 50µm.

III.3.4. Endothelial differentiation

Cells differentiation into the endothelial lineage was pursued by culturing the SVF and the SSEA-4^{+}hASCs sub-population in EGM-2 MV. Despite the small endothelial-like colonies present in the SVF derived culture at early time points, these were surrounded by fibroblast-like cells (**Figure III.3A**), which took over the culture along the passages (**Figure III.3B**). In contrast, when the SSEA-4^{+}hASCs were cultured in the same conditions, small cobblestone-like colonies could be first observed between days 3 and 7. These colonies were able to

grow until confluence (**Figure III.3C**) maintaining the endothelial-like cobblestone morphology up to passage 4 (**Figure III.3D**).

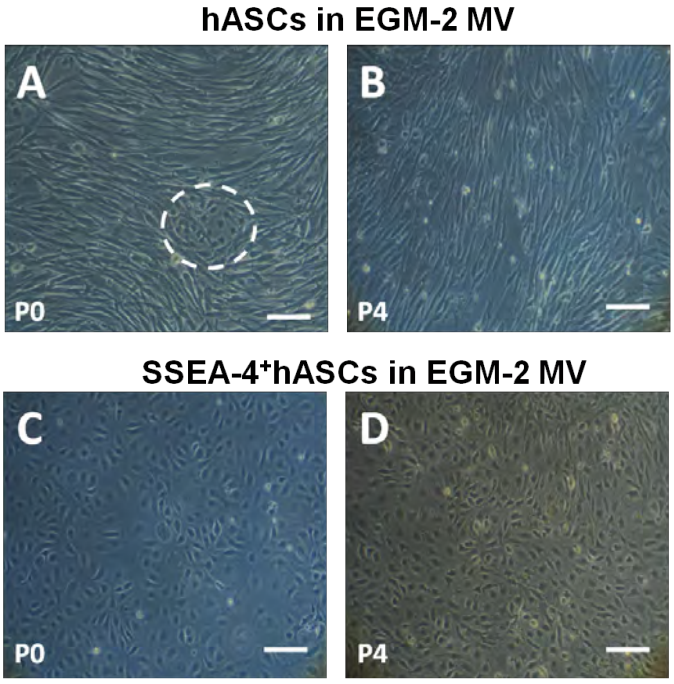

Figure III.3. Optical micrographs showing the morphology of hASCs (**A-B**) and SSEA-4$^+$hASCs (**C-D**) cultured in EGM-2 MV at passages 0 (**A,C**) and 4 (**B,D**). hASCs at passage 0 exhibit endothelial like colonies (limited by white dash line) surrounded by fibroblast-like cells (**A**) but depict a homogeneous fibroblast-like morphology at passage 4 (**B**). SSEA-4+hASCs at passage 0 are characterized by presenting a cobblestone morphology consistent with the endothelial phenotype (**C**), which was kept up to passage 4 (**D**). Scale bar represents 100µm.

The shifting of phenotype of the SSEA-4$^+$hASCs sub-population along the passages was followed by the analysis of the relative expression of *CD31* and *vWF* genes, in order to confirm the endothelial phenotype. As it can be seen in **Figure III.4A**, SSEA-4$^+$hASCs-derived cells cultured in EGM-2 MV exhibited significantly increased levels of expression of the endothelial markers at different passages when compared with freshly selected SSEA-4$^+$hASCs. The expression levels of *CD31* and *vWF* reached respectively around 1000- and 7000- fold increase in comparison to the initial selected sub-population. The gene expression study was complemented by flow cytometry analysis (**Figure III.4B**). The percentage of cells expressing CD31 and CD34 increased respectively from 79.2% and 79.0% (P1) to 97.3% and 94.3% (P4), respectively. Moreover, in comparison to the SSEA-4$^+$hASCs cultured in α-MEM, this sub-population grown in EGM-2 MV revealed a significant down regulation of CD90, maintaining similar percentages of the CD105$^+$ and CD73$^+$ fractions, around 90% of the total population.

Concerning hASCs cultured in EGM-2 MV, only 22% of the cells were positive for CD31 at passage 1. The expression of this marker rapidly decreased along passages and at passage 4, only around 2% of the total population was expressing it. Moreover, while the percentage of cells expressing CD34, CD45 and SSEA4 can be considered neglectable, $CD90^+$ and the $CD73^+$ cells comprise around 90% of the total population. These levels were maintained along passages. Contrarily, the percentage of $CD105^+$cells decreased from 26.3% at passage 1 to 15.3% at passage 4 (**Figure III.4C**). By passage 4, the percentage of $CD31^+/CD34^+$ cells within the hASCs cultured in EGM-2 MV was neglectable, whereas in the SSEA-4^+hASCs cultured under the same conditions reached 90.9% of the total population (**Figure III.4D**).

A

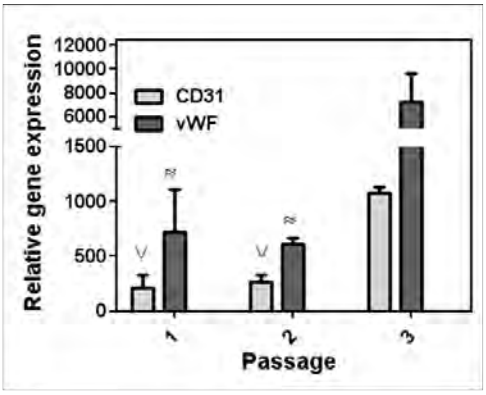

D

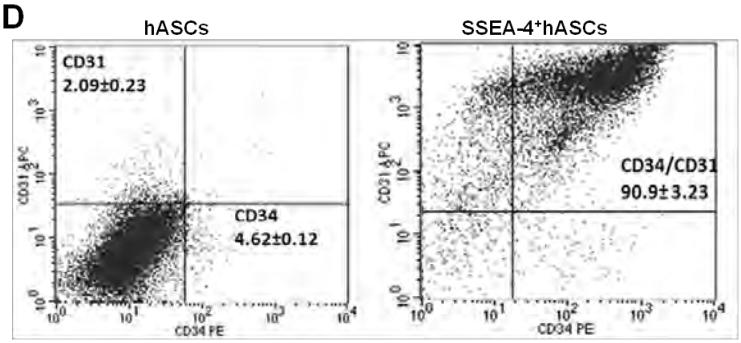

B

Percentage of positive cells within the SSEA-4⁺hASCs population cultured in EGM-2 MV (%, mean ± SD)

Passage	CD105	CD90	CD73	CD31	SSEA-4	CD34	CD45
1	80.0 ± 4.83	4.34 ± 1.27	88.7 ± 2.97	79.2 ± 3.78	3.09 ± 0.45	79.0 ± 2.09	1.04 ± 0.02
2	90.4 ± 4.12	3.29 ± 1.23	89.3 ± 6.82	84.3 ± 5.93	1.23 ± 0.45	83.5 ± 6.05	0.78 ± 0.01
3	94.2 ± 5.10	0.27 ± 0.03	91.3 ± 7.80	91.2 ± 5.10	1.54 ± 0.20	89.7 ± 2.98	0.10 ± 0.03
4	98.3 ± 3.20	0.21 ± 0.04	94.3 ± 5.67	97.3 ± 4.84	0.20 ± 0.01	94.3 ± 4.85	0.17 ± 0.01
				HUVECs			
3	96.06 ± 5.07	2.69 ± 0.50	87.6 ± 2.34	94.8 ± 5.23	1.54 ± 0.27	13.04 ± 2.89	0.02 ± 0.00

C

Percentage of positive cells within the hASCs population cultured in EGM-2 MV (%, mean ± SD)

Passage	CD105	CD90	CD73	CD31	SSEA-4	CD34	CD45
1	26.3 ± 1.13	84.3 ± 5.79	90.4 ± 6.53	22.4 ± 3.43	1.81 ± 0.31	2.34 ± 0.34	1.34 ± 012
2	25.2 ± 2.31	93.2 ± 4.34	91.7 ± 2.34	5.44 ± 0.94	1.59 ± 0.12	3.13 ± 0.14	3.49 ± 0.13
3	19.3 ± 1.23	91.3 ± 4.98	95.3 ± 3.21	2.90 ± 0.12	1.41 ± 0.34	3.01 ± 0.89	4.13 ± 0.48
4	15.3± 3.10	89.7 ± 3.24	96.3 ± 3.86	2.09 ± 0.23	1.59 ± 0.67	4.62 ± 0.12	2.09 ± 0.10

Figure III.4. Characterization of hASCs and SSEA-4^+hASCs cultured in EGM-2 MV. (**A**) RT-PCR results showing the over-expression of endothelial related genes, *CD31* and *vWF* at different passages in hASCs and SSEA-4^+hASCs in relation to freshly selected SSEA-4^+hASCs (P0). ^ and ≈ indicate statistical significance (*p<0.05) when compared with P3. (**B-C**) Cell surface marker profile of SSEA-4^+hASCs (**B**) and hASCs (**C**) at different passages, obtained by flow cytometry. (**D**) Representative dot plots of hASCs and SSEA-4^+hASCs expressing CD34 and CD31 markers at P4 demonstrating the endothelial differentiation of SSEA-4^+hASCs. Values in histogram plots indicate averages ± SD from 6 independent experiments.

The flow cytometry results regarding the endothelial phenotype were confirmed by immunocytochemistry to monitor the expression of vWF and CD31. A low number of hASCs cultured in EGM-2 MV showed expression of vWF at P0 (**Figure III.5A**). This feature was lost at passage 1. Contrarily, for the SSEA-4$^+$hASCs in EGM-2 MV, vWF was present in the cell cytoplasm as small dotted pattern surrounding the nuclei representing the Weibel-Palade bodies and in the majority of the cells starting with P0 (**Figure III.5B**). In addition, the CD31 pattern of SSEA-4$^+$hASCs-derived cells, corresponding to cell-cell contact, was found predominant for all the cells in passage 4 (**Figure III.5C**). Moreover, the CD34 marker was absent in hASCs cultured in EGM-2 MV (**Figure III.5D**), while the majority of SSEA-4$^+$hASCs in EGM-2 MV were found positive for the same marker (**Figure III.5E**).

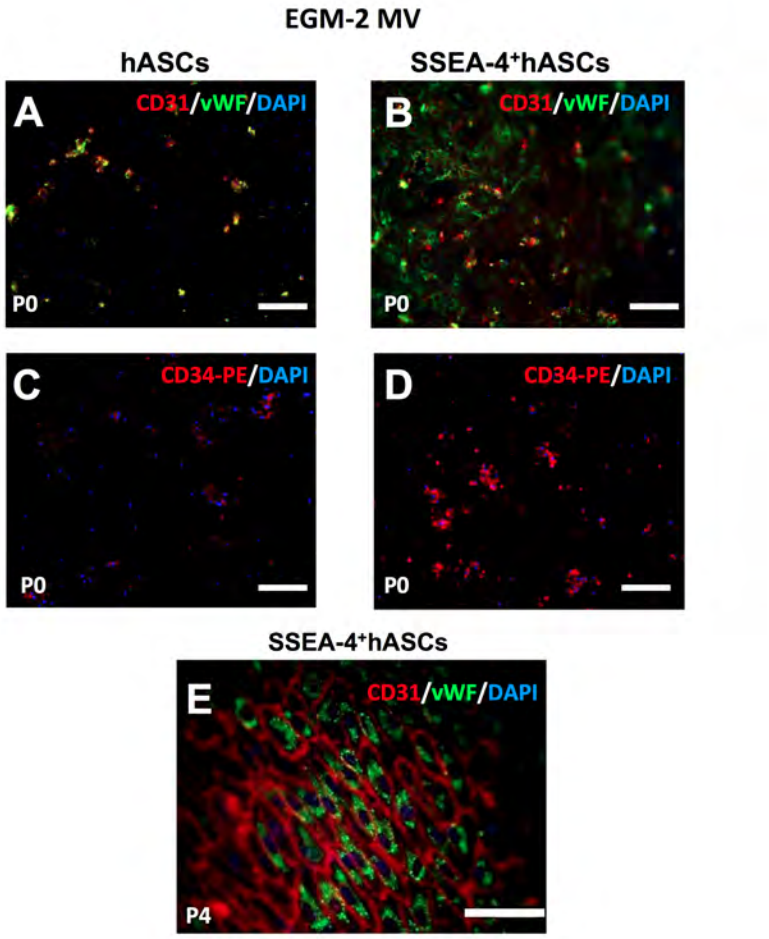

Figure III.5. Immunostaining of hASCs and SSEA-4$^+$hASCs cultured in EGM-2 MV. Immunostaining of (**A, B, E**) vWF (green) / CD31 (red) and (**C, D**) CD34 expressed by hASCs and SSEA-4$^+$hASCs. At P0, only some hASCs expressed (**A**) CD31 (red) and vWF (green) and (**C**) CD34 (red), while (**B, D**) the majority of the SSEA-4$^+$hASCs expressed these markers. (**E**) The stability of the expression of CD31/vWF by differentiated SSEA-4$^+$hASCs was confirmed at P4. Cell nuclei were counterstained with DAPI (blue).

The endothelial phenotype of the SSEA-4$^+$hASCs-derived cells was also assessed by their ability to uptake DIL-ac-LDL complex and to bind lectin *UEA-1*, as well as to form capillary-like network when seeded on Matrigel. In contrast to SSEA-4$^+$hASCs cultured in α-MEM, SSEA-4$^+$hASCs growing in EGM-2 MV were able to uptake the labeled acetylated lipoprotein into secondary lysosomes (**Figure III.6A**) and to bind the *UEA-1* (**Figure III.6B**). Furthermore, SSEA-4$^+$hASCs cultured in EGM-2 MV were capable of forming, similarly to HUVECs, tubular structures when seeded on Matrigel (**Figure III.6C**). When SSEA-4$^+$hASCs-derived cells and hASCs cultured in α-MEM medium were seeded on Matrigel, they remained spherical and formed cell aggregates without forming tubular structure (**Figure III.6D**). Nevertheless, hASCs cultured in EGM-2 MV exhibited a slow but evident formation of tubes on Matrigel substrate (**Figure III.6E**). Still, this ability was lost after passage 2.

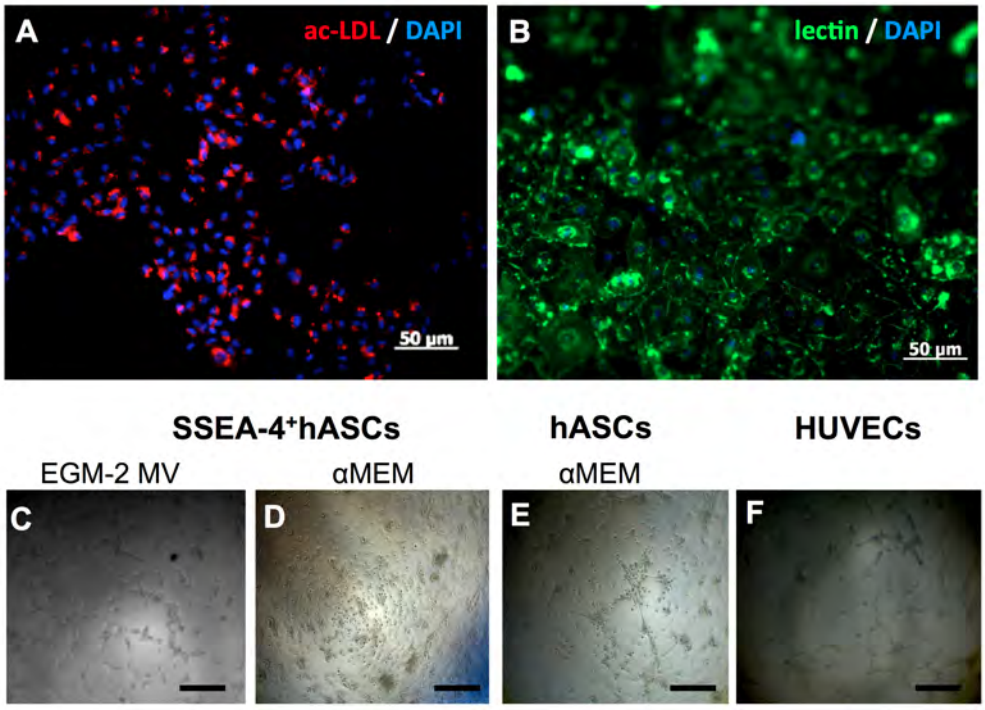

Figure III.6. Endothelial-like cells obtained by culturing SSEA-4$^+$hASCs in EGM-2 MV. Cells were able to (**A**) uptake acetylated low-density lipoprotein (ac-LDL) (red) and (**B**) bind lectin from *UEA-1* (green). Cell nuclei were counterstained with DAPI (blue). (**C**) When seeded on Matrigel at different passages, cells had the capacity to form capillary-like structures similarly to (**F**) HUVECS, used as control. (**D**) Contrarily, SSEA-4$^+$hASCs cultured in α-MEM, independently of the passage, aggregated in small clumps without any tubular-like structure appearance. (**E**) hASCs cultured in EGM-2 MV were only able to form these structures on Matrigel at passage 1. These are likely to result from the organization of the microvascular endothelial cells present in the stromal vascular fraction of the adipose tissue and proved to be present at this stage of culture as CD31$^+$ cells.

III.4. DISCUSSION

The use of human microvascular endothelial cells is limited by the low availability of the source, the reduced proliferation rates and the small number of the isolated cells that are often contaminated by fibroblasts and other stromal cells [43]. In addition, the benefits of mature endothelial cells, as well as of other endothelial progenitors, as part of tissue engineered constructs, over the anostomosis, perfusion and survival of those constructs are still not clear. The present study emphasizes the possibility of obtaining endothelial-like and osteogenic cells from a single cell source by selecting a sub-population residing within the adipose tissue that expresses a marker associated with pluripotency, the SSEA-4. This approach, in addition to provide new insights regarding the differentiation potential of the SSEA-4$^+$ sub-population present in the SVF of adipose tissue, might be of high value for defining innovative bone tissue engineering strategies. The co-existence of different cell sub-populations expressing CD105, CD90, CD73, CD31, CD34 and SSEA-4 within SVF confirmed previous works[26, 29]. Interestingly, a sub-population comprising almost 3% of the SVF was found to express the SSEA-4 marker, associated to the pluripotent character of other stem cells[36]. This marker was used to successfully select the sub-population of interest at the time of the SVF isolation. In fact, the percentage of hASCs, expressing SSEA-4, cultured both in α-MEM and EGM-2 MV medium, was reduced along the passages. Likewise, the selected sub-population also lost the SSEA-4 expression along the passages and under the same culture conditions. While in the culture with EGM-2 MV medium this feature could be associated to the differentiation of the SSEA-4$^+$hASCs into the endothelial lineage, in the culture in α-MEM was connected with the acquirement of a mesenchymal phenotype characterized by fibroblast-like morphology of the cells and the expression of mesenchymal cell surface markers. This phenotypic pattern was kept stable along passages and allowed the osteogenic differentiation when cells were cultured in osteo-inductive conditions.

Our data suggests that the composition of the culture medium exerted major effects on the differentiation of SSEA-4$^+$hASCs. The EGM-2 MV medium in particular, has been often presented as a suitable cell culture environment to trigger the endothelial differentiation of embryonic stem cells[21] and MSCs[44] or the maturation of endothelial progenitor cells[45]. We were also able to confirm that the selected SSEA-4$^+$hASCs were differentiating into endothelial-like cells as demonstrated by their morphology, markers profile and *in vitro* capacity to form tubular-like structures, when cultured in EGM-2 MV. In opposition, this sub-population cultured in α-MEM did not demonstrate this capacity of differentiation into the endothelial lineage. Therefore, these results confirm that factors present in EGM-2 MV, but not in α-MEM, such as angiogenic factors, fibroblast growth factors (FGFs) and vascular

endothelial growth factors (VEGFs), might be involved in the endothelial differentiation of the SSEA-4$^+$hASCs sub-population. Others have used VEGF in concentrations that range from 10[46] to 50ng/mL[23,45,47] to induce and lead endothelial differentiation. However, concentrations in the order of 50ng/ml of VEGF might significantly impair the therapeutic application of those cells. EGM-2 MV, with a concentration of VEGF lower than 5ng/ml [48], allowed deriving, from the SSEA-4$^+$hASCs sub-population, a population of cells in which around 80% expressed the CD31 and CD34 markers at passage 1 and more than 95% at passage 4. Moreover, cells were concomitantly expressing CD105 while lacking the expression of CD45, altogether a characteristic markers profile of endothelial cells [49].

Recent investigations have clearly confined the expression of CD34 in association with the expression of CD105, CD73 and CD31 to microvascular-like endothelial cells [50]. The fact that 95% of the differentiated SSEA-4$^+$hASCs were CD34$^+$ and within the control macrovascular HUVECs population (95% CD31$^+$) only 13% expressed CD34 reinforces that the cells generated by the differentiation of SSEA-4$^+$hASCs possess a microvascular endothelial-like phenotype. Interestingly, during the endothelial differentiation of SSEA-4$^+$hASCs, the levels of expression of CD90 rapidly decreased. Being counter-receptor for the leukocyte integrin Mac-1 (CD11b/CD18) present in polymorphonuclear neutrophils and in monocytes, the expression of CD90 by endothelial cells is only expected upon activation [51], which might indicate a resting state of the obtained cells. Future studies should be performed in order to analyze the molecular mechanism that governs the endothelial differentiation and the influence of other growth factors or other stimuli to trigger this process. An evaluation of the endothelial-specific markers and adhesion molecules upon stimulation with inflammatory cytokines would better assess the behavior of the endothelial-like SSEA-4$^+$hASCs.

SSEA-4$^+$hASCs can also give rise to fibroblastic-like cells, phenotypically resembling MSCs when cultured in α-MEM. Besides the expression (>90%) of CD90, CD73 and CD105 and absence of CD34 and CD45 positive cells, these cells were able to differentiate, in addition to the endothelial lineage, into osteoblasts and chondrocytes (data not shown). The osteogenic differentiation of hASCs and SSEA-4$^+$hASCs was followed at molecular and protein levels by the expression of the osteogenic related markers (OCN and OPN)[52] and by subsequent deposition and mineralization of the extracellular matrix. For each cell population, the inverse expression profile of OPN and OCN, respectively with higher levels at earlier and later time points, confirmed the expected progress of the osteogenic differentiation. Moreover, all together these results confirm the advanced stage of osteogenesis[53] in the later culturing time points.

Overall, the discussed results underline the high potential of SSEA-4$^+$hASCs sub-population. EGM-2 MV was sufficient to trigger the differentiation of SSEA-4$^+$hASCs into the endothelial lineage giving rise to microvascular-like endothelial cells while the same culture conditions were not sufficient to trigger the endothelial differentiation of hASCs. Moreover, the capacity of the SSEA-4$^+$hASCs to differentiate towards the osteogenic lineage is similar to the hASCs. Numerous advantages derive from the use of SSEA-4$^+$hASCs amongst which is the relatively ease retrieval of the SSEA-4$^+$cells, while preserving their differentiation potential. Furthermore, the acceptance of adipose tissue as an abundant source of cells allows overcoming the potential issue of the low percentage (<2%) of cells that SSEA-4$^+$cells sub-population represents within the SVF. Under this context, we consider that obtaining relevant number of SSEA-4$^+$cells to be applied in the future in a bone TE strategy to improve tissue vascularization constitute a realistic scenario.

III.5. CONCLUSIONS

This study reports that human adipose tissue contains a sub-population defined by the expression of the pluripotent marker, SSEA-4, that can be obtained using an immunomagnetic selection. Cells with mature microvascular-like endothelial profile could be generated by culturing the SSEA-4$^+$hASCs in EGM-2 MV. In addition, the same sub-population could undergo osteogenic differentiation, as observed by an intense extracellular matrix deposition and mineralization. Therefore, this sub-population contains cells that under specific culture condition can give rise to both osteoblastic and microvascular endothelial-like cells. We demonstrated that from a single cell source and by selecting the appropriate sub-population, it is possible to obtain the relevant types of cells when envisioning engineering vascularized bone tissue.

REFERENCES

1. Vallee, M.; Cote, J. F.; Fradette, J., Adipose-tissue engineering: taking advantage of the properties of human adipose-derived stem/stromal cells. *Pathol Biol (Paris)* **2009,** *57* (4), 309-17.
2. De Ugarte, D. A.; Morizono, K.; Elbarbary, A.; Alfonso, Z.; Zuk, P. A.; Zhu, M.; Dragoo, J. L.; Ashjian, P.; Thomas, B.; Benhaim, P.; Chen, I.; Fraser, J.; Hedrick, M. H., Comparison of multi-lineage cells from human adipose tissue and bone marrow. *Cells, tissues, organs* **2003,** *174* (3), 101-9.
3. Liu, T. M.; Martina, M.; Hutmacher, D. W.; Hui, J. H.; Lee, E. H.; Lim, B., Identification of common pathways mediating differentiation of bone marrow- and adipose tissue-derived human mesenchymal stem cells into three mesenchymal lineages. *Stem Cells* **2007,** *25* (3), 750-60.
4. Gimble, J. M.; Katz, A. J.; Bunnell, B. A., Adipose-derived stem cells for regenerative medicine. *Circulation research* **2007,** *100* (9), 1249-60.
5. Helder, M. N.; Knippenberg, M.; Klein-Nulend, J.; Wuisman, P. I., Stem cells from adipose tissue allow challenging new concepts for regenerative medicine. *Tissue Eng* **2007,** *13* (8), 1799-808.
6. Wagner, W.; Wein, F.; Seckinger, A.; Frankhauser, M.; Wirkner, U.; Krause, U.; Blake, J.; Schwager, C.; Eckstein, V.; Ansorge, W.; Ho, A. D., Comparative characteristics of mesenchymal stem cells from human bone marrow, adipose tissue, and umbilical cord blood. *Experimental hematology* **2005,** *33* (11), 1402-16.

7. Strem, B. M.; Hedrick, M. H., The growing importance of fat in regenerative medicine. *Trends Biotechnol* **2005,** *23* (2), 64-6.
8. Zuk, P. A.; Zhu, M.; Mizuno, H.; Huang, J.; Futrell, J. W.; Katz, A. J.; Benhaim, P.; Lorenz, H. P.; Hedrick, M. H., Multilineage cells from human adipose tissue: implications for cell-based therapies. *Tissue engineering* **2001,** *7* (2), 211-28.
9. Anghileri, E.; Marconi, S.; Pignatelli, A.; Cifelli, P.; Galie, M.; Sbarbati, A.; Krampera, M.; Belluzzi, O.; Bonetti, B., Neuronal differentiation potential of human adipose-derived mesenchymal stem cells. *Stem Cells Dev* **2008,** *17* (5), 909-16.
10. Prunet-Marcassus, B.; Cousin, B.; Caton, D.; Andre, M.; Penicaud, L.; Casteilla, L., From heterogeneity to plasticity in adipose tissues: site-specific differences. *Exp Cell Res* **2006,** *312* (6), 727-36.
11. Planat-Benard, V.; Menard, C.; Andre, M.; Puceat, M.; Perez, A.; Garcia-Verdugo, J. M.; Penicaud, L.; Casteilla, L., Spontaneous cardiomyocyte differentiation from adipose tissue stroma cells. *Circulation research* **2004,** *94* (2), 223-9.
12. Moon, J. J.; West, J. L., Vascularization of engineered tissues: approaches to promote angiogenesis in biomaterials. *Curr Top Med Chem* **2008,** *8* (4), 300-10.
13. Jain, R. K.; Au, P.; Tam, J.; Duda, D. G.; Fukumura, D., Engineering vascularized tissue. *Nat Biotechnol* **2005,** *23* (7), 821-3.
14. Kaigler, D.; Krebsbach, P. H.; Wang, Z.; West, E. R.; Horger, K.; Mooney, D. J., Transplanted endothelial cells enhance orthotopic bone regeneration. *J Dent Res* **2006,** *85* (7), 633-7.
15. Levenberg, S.; Rouwkema, J.; Macdonald, M.; Garfein, E. S.; Kohane, D. S.; Darland, D. C.; Marini, R.; van Blitterswijk, C. A.; Mulligan, R. C.; D'Amore, P. A.; Langer, R., Engineering vascularized skeletal muscle tissue. *Nat Biotechnol* **2005,** *23* (7), 879-84.
16. Hegen, A.; Blois, A.; Tiron, C. E.; Hellesoy, M.; Micklem, D. R.; Nor, J. E.; Akslen, L. A.; Lorens, J. B., Efficient in vivo vascularization of tissue-engineering scaffolds. *J Tissue Eng Regen Med*.
17. Kim, S.; von Recum, H., Endothelial stem cells and precursors for tissue engineering: cell source, differentiation, selection, and application. *Tissue Eng Part B Rev* **2008,** *14* (1), 133-47.
18. Asahara, T.; Murohara, T.; Sullivan, A.; Silver, M.; van der Zee, R.; Li, T.; Witzenbichler, B.; Schatteman, G.; Isner, J. M., Isolation of putative progenitor endothelial cells for angiogenesis. *Science* **1997,** *275* (5302), 964-7.
19. Mead, L. E.; Prater, D.; Yoder, M. C.; Ingram, D. A., Isolation and characterization of endothelial progenitor cells from human blood. *Curr Protoc Stem Cell Biol* **2008,** *Chapter 2*, Unit 2C 1.
20. Hristov, M.; Erl, W.; Weber, P. C., Endothelial progenitor cells: isolation and characterization. *Trends Cardiovasc Med* **2003,** *13* (5), 201-6.
21. Blancas, A. A.; Lauer, N. E.; McCloskey, K. E., Endothelial differentiation of embryonic stem cells. *Curr Protoc Stem Cell Biol* **2008,** *Chapter 1*, Unit 1F 5.
22. Rufaihah, A. J.; Haider, H. K.; Heng, B. C.; Ye, L.; Toh, W. S.; Tian, X. F.; Lu, K.; Sim, E. K.; Cao, T., Directing endothelial differentiation of human embryonic stem cells via transduction with an adenoviral vector expressing the VEGF(165) gene. *J Gene Med* **2007,** *9* (6), 452-61.
23. Oswald, J.; Boxberger, S.; Jorgensen, B.; Feldmann, S.; Ehninger, G.; Bornhauser, M.; Werner, C., Mesenchymal stem cells can be differentiated into endothelial cells in vitro. *Stem Cells* **2004,** *22* (3), 377-384.
24. Chen, M. Y.; Lie, P. C.; Li, Z. L.; Wei, X., Endothelial differentiation of Wharton's jelly-derived mesenchymal stem cells in comparison with bone marrow-derived mesenchymal stem cells. *Experimental hematology* **2009,** *37* (5), 629-40.
25. Zhang, P.; Baxter, J.; Vinod, K.; Tulenko, T. N.; Di Muzio, P. J., Endothelial differentiation of amniotic fluid-derived stem cells: synergism of biochemical and shear force stimuli. *Stem Cells Dev* **2009,** *18* (9), 1299-308.
26. Rada, T.; Reis, R. L.; Gomes, M. E., Distinct stem cells subpopulations isolated from human adipose tissue exhibit different chondrogenic and osteogenic differentiation potential. *Stem Cell Rev 7* (1), 64-76.
27. Rada, T.; Reis, R. L.; Gomes, M. E., Novel method for the isolation of adipose stem cells (ASCs). *J Tissue Eng Regen Med* **2009,** *3* (2), 158-9.
28. Zimmerlin, L.; Donnenberg, V. S.; Pfeifer, M. E.; Meyer, E. M.; Peault, B.; Rubin, J. P.; Donnenberg, A. D., Stromal vascular progenitors in adult human adipose tissue. *Cytometry A 77* (1), 22-30.
29. Astori, G.; Vignati, F.; Bardelli, S.; Tubio, M.; Gola, M.; Albertini, V.; Bambi, F.; Scali, G.; Castelli, D.; Rasini, V.; Soldati, G.; Moccetti, T., "In vitro" and multicolor phenotypic characterization of

cell subpopulations identified in fresh human adipose tissue stromal vascular fraction and in the derived mesenchymal stem cells. *Journal of Translational Medicine* **2007,** *5*, -.
30. Sengenes, C.; Miranville, A.; Maumus, M.; de Barros, S.; Busse, R.; Bouloumie, A., Chemotaxis and differentiation of human adipose tissue CD34+/CD31- progenitor cells: role of stromal derived factor-1 released by adipose tissue capillary endothelial cells. *Stem Cells* **2007,** *25* (9), 2269-76.
31. Yamashita, J.; Itoh, H.; Hirashima, M.; Ogawa, M.; Nishikawa, S.; Yurugi, T.; Naito, M.; Nakao, K., Flk1-positive cells derived from embryonic stem cells serve as vascular progenitors. *Nature* **2000,** *408* (6808), 92-6.
32. Miranville, A.; Heeschen, C.; Sengenes, C.; Curat, C. A.; Busse, R.; Bouloumie, A., Improvement of postnatal neovascularization by human adipose tissue-derived stem cells. *Circulation* **2004,** *110* (3), 349-55.
33. Sengenes, C.; Lolmede, K.; Zakaroff-Girard, A.; Busse, R.; Bouloumie, A., Preadipocytes in the human subcutaneous adipose tissue display distinct features from the adult mesenchymal and hematopoietic stem cells. *J Cell Physiol* **2005,** *205* (1), 114-22.
34. Martinez-Estrada, O. M.; Munoz-Santos, Y.; Julve, J.; Reina, M.; Vilaro, S., Human adipose tissue as a source of Flk-1+ cells: new method of differentiation and expansion. *Cardiovasc Res* **2005,** *65* (2), 328-33.
35. Fischer, L. J.; McIlhenny, S.; Tulenko, T.; Golesorkhi, N.; Zhang, P.; Larson, R.; Lombardi, J.; Shapiro, I.; DiMuzio, P. J., Endothelial differentiation of adipose-derived stem cells: effects of endothelial cell growth supplement and shear force. *The Journal of surgical research* **2009,** *152* (1), 157-66.
36. Riekstina, U.; Cakstina, I.; Parfejevs, V.; Hoogduijn, M.; Jankovskis, G.; Muiznieks, I.; Muceniece, R.; Ancans, J., Embryonic stem cell marker expression pattern in human mesenchymal stem cells derived from bone marrow, adipose tissue, heart and dermis. *Stem Cell Rev* **2009,** *5* (4), 378-86.
37. Henderson, J. K.; Draper, J. S.; Baillie, H. S.; Fishel, S.; Thomson, J. A.; Moore, H.; Andrews, P. W., Preimplantation human embryos and embryonic stem cells show comparable expression of stage-specific embryonic antigens. *Stem Cells* **2002,** *20* (4), 329-37.
38. Shamblott, M. J.; Axelman, J.; Wang, S.; Bugg, E. M.; Littlefield, J. W.; Donovan, P. J.; Blumenthal, P. D.; Huggins, G. R.; Gearhart, J. D., Derivation of pluripotent stem cells from cultured human primordial germ cells. *Proc Natl Acad Sci U S A* **1998,** *95* (23), 13726-31.
39. Heins, N.; Englund, M. C.; Sjoblom, C.; Dahl, U.; Tonning, A.; Bergh, C.; Lindahl, A.; Hanson, C.; Semb, H., Derivation, characterization, and differentiation of human embryonic stem cells. *Stem Cells* **2004,** *22* (3), 367-76.
40. Zuk, P. A.; Zhu, M.; Ashjian, P.; De Ugarte, D. A.; Huang, J. I.; Mizuno, H.; Alfonso, Z. C.; Fraser, J. K.; Benhaim, P.; Hedrick, M. H., Human adipose tissue is a source of multipotent stem cells. *Mol Biol Cell* **2002,** *13* (12), 4279-95.
41. Jaffe, E. A.; Nachman, R. L.; Becker, C. G.; Minick, C. R., Culture of human endothelial cells derived from umbilical veins. Identification by morphologic and immunologic criteria. *J Clin Invest* **1973,** *52* (11), 2745-56.
42. Pfaffl, M. W., A new mathematical model for relative quantification in real-time RT-PCR. *Nucleic Acids Res* **2001,** *29* (9), e45.
43. Arts, C. H.; Blankensteijn, J. D.; Heijnen-Snyder, G. J.; Verhagen, H. J.; Hedeman Joosten, P. P.; Sixma, J. J.; Eikelboom, B. C.; de Groot, P. G., Reduction of non-endothelial cell contamination of microvascular endothelial cell seeded grafts decreases thrombogenicity and intimal hyperplasia. *Eur J Vasc Endovasc Surg* **2002,** *23* (5), 404-12.
44. Zhou, J.; Lin, H.; Fang, T.; Li, X.; Dai, W.; Uemura, T.; Dong, J., The repair of large segmental bone defects in the rabbit with vascularized tissue engineered bone. *Biomaterials 31* (6), 1171-9.
45. Eggermann, J.; Kliche, S.; Jarmy, G.; Hoffmann, K.; Mayr-Beyrle, U.; Debatin, K. M.; Waltenberger, J.; Beltinger, C., Endothelial progenitor cell culture and differentiation in vitro: a methodological comparison using human umbilical cord blood. *Cardiovascular Research* **2003,** *58* (2), 478-486.
46. Ye, C.; Bai, L.; Yan, Z. Q.; Wang, Y. H.; Jiang, Z. L., Shear stress and vascular smooth muscle cells promote endothelial differentiation of endothelial progenitor cells via activation of Akt. *Clin Biomech (Bristol, Avon)* **2008,** *23 Suppl 1*, S118-24.
47. Quirici, N.; Soligo, D.; Caneva, L.; Servida, F.; Bossolasco, P.; Deliliers, G. L., Differentiation and expansion of endothelial cells from human bone marrow CD133(+) cells. *British Journal of Haematology* **2001,** *115* (1), 186-194.

48. Ferreira, L. S.; Gerecht, S.; Shieh, H. F.; Watson, N.; Rupnick, M. A.; Dallabrida, S. M.; Vunjak-Novakovic, G.; Langer, R., Vascular progenitor cells isolated from human embryonic stem cells give rise to endothelial and smooth muscle-like cells and form vascular networks in vivo. *Circulation research* **2007,** *101* (3), 286-294.
49. (a) Tanaka, F.; Otake, Y.; Yanagihara, K.; Kawano, Y.; Miyahara, R.; Li, M.; Ishikawa, S.; Wada, H., Correlation between apoptotic index and angiogenesis in non-small cell lung cancer: comparison between CD105 and CD34 as a marker of angiogenesis. *Lung Cancer* **2003,** *39* (3), 289-296; (b) Theuerkauf, I.; Zhou, H.; Fischer, H. P., Immunohistochemical patterns of human liver sinusoids under different conditions of pathologic perfusion. *Virchows Archiv-an International Journal of Pathology* **2001,** *438* (5), 498-504; (c) Nagatsuka, H.; Hibi, K.; Gunduz, M.; Tsujigiwa, H.; Tamamura, R.; Sugahara, T.; Sasaki, A.; Nagai, N., Various immunostaining patterns of CD31, CD34 and endoglin and their relationship with lymph node metastasis in oral squamous cell carcinomas. *J Oral Pathol Med* **2005,** *34* (2), 70-6.
50. (a) Zakrzewicz, A.; Grafe, M.; Terbeek, D.; Bongrazio, M.; Auch-Schwelk, W.; Walzog, B.; Graf, K.; Fleck, E.; Ley, K.; Gaehtgens, P., L-selectin-dependent leukocyte adhesion to microvascular but not to macrovascular endothelial cells of the human coronary system. *Blood* **1997,** *89* (9), 3228-35; (b) Muller, A. M.; Hermanns, M. I.; Skrzynski, C.; Nesslinger, M.; Muller, K. M.; Kirkpatrick, C. J., Expression of the endothelial markers PECAM-1, vWf, and CD34 in vivo and in vitro. *Exp Mol Pathol* **2002,** *72* (3), 221-9; (c) Fina, L.; Molgaard, H. V.; Robertson, D.; Bradley, N. J.; Monaghan, P.; Delia, D.; Sutherland, D. R.; Baker, M. A.; Greaves, M. F., Expression of the CD34 gene in vascular endothelial cells. *Blood* **1990,** *75* (12), 2417-26.
51. (a) Wetzel, A.; Chavakis, T.; Preissner, K. T.; Sticherling, M.; Haustein, U. F.; Anderegg, U.; Saalbach, A., Human Thy-1 (CD90) on activated endothelial cells is a counterreceptor for the leukocyte integrin Mac-1 (CD11b/CD18). *J Immunol* **2004,** *172* (6), 3850-9; (b) Saalbach, A.; Haustein, U. F.; Anderegg, U., A ligand of human thy-1 is localized on polymorphonuclear leukocytes and monocytes and mediates the binding to activated thy-1-positive microvascular endothelial cells and fibroblasts. *J Invest Dermatol* **2000,** *115* (5), 882-8; (c) Lee, W. S.; Jain, M. K.; Arkonac, B. M.; Zhang, D.; Shaw, S. Y.; Kashiki, S.; Maemura, K.; Lee, S. L.; Hollenberg, N. K.; Lee, M. E.; Haber, E., Thy-1, a novel marker for angiogenesis upregulated by inflammatory cytokines. *Circulation research* **1998,** *82* (8), 845-51.
52. Marom, R.; Shur, I.; Solomon, R.; Benayahu, D., Characterization of adhesion and differentiation markers of osteogenic marrow stromal cells. *Journal of Cellular Physiology* **2005,** *202* (1), 41-48.
53. Stains, J. P.; Civitelli, R., Cell-to-cell interactions in bone. *Biochem Biophys Res Commun* **2005,** *328* (3), 721-7.

SUPPLEMENTAL INFORMATION

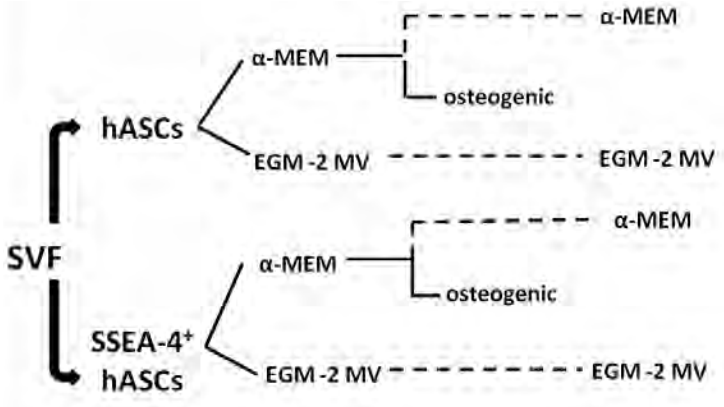

Supplemental Figure III.1. Scheme of the experimental setup. The SVF culture in α-MEM medium aimed at selecting by adherence the human adipose tissue-derived stem cells (hASCs) (P0) and at maintaining their MSCs phenotype along the passages. A sub-population expressing SSEA-4 marker was isolated from the SVF with magnetic beads (SSEA-4$^+$hASCs) and maintained in α-MEM as the hASCs. Both hASCs and SSEA-4$^+$hASCs were also cultured in EGM-2 MV intending to trigger their differentiation towards the endothelial lineage. The phenotypical evaluation of cultures was assessed from passage 0 up to passage 4. As the culture in α-MEM was regarded as the standard medium capable of maintaining the hASCs and SSEA-4$^+$hASCs subpopulation without significant phenotypic variations along passages, their differentiation into the osteogenic lineage was also carried out.

Gene	Product size (bp)	Annealing temperature (ºC)	Primer pair sequence	NCBI reference
vWF[1]	100	60	**Fwd:** CCCTGGGTTACAAGGAAGAAA AT **Rev:** AGTGTCATGTGTCCTCCTCTTAG	NM_000552
CD31[1]	179	60	**Fwd:** AAGGCCAGATGCACATCC **Rev:**TTCTACCCAACATTAACTTAGCAGG	NM_000442
OCN[2]	230	61.6	**Fwd:** CTGGAGAGGAGCAGAACTGG **Rev:** GGCAGCGAGGTAGTGAAGAG	NM_099173
OPN[2]	244	57.9	**Fwd:** GGGGACAACTGGAGTGAAAA **Rev:** CCCACAGACCCTTCCAAGTA	NM_001040058
GAPDH[1,2]	87	60.6	**Fwd:** TGCACCACCAACTGCTTAGC **Rev:** GGCATGGACTGTGGTCATGAG	NM_002046

Supplemental Table III.1. Product size, annealing temperature, primer (Fwd-forward and Rev-reverse) sequences and reaction conditions[1,2] used for the RT-PCR analyses of endothelial (*CD31*, *vWF*)- and osteogenic (*OCN* and *OPN*)-related markers and the housekeeping gene (GAPDH).

[1] PCR conditions: 2min at 95ºC (hot start) followed by 45 cycles of 95ºC for 15sec and annealing temperature (noted in the table) for 1min. A 20min melting curve at 55ºC was performed at the end.

[2]PCR conditions: 2min at 95ºC (hot start) followed by 45 cycles of 95ºC for 15sec, annealing temperature (noted in the table) for 1min and an extension step at 68ºC for 20sec. A 20min melting curve at 55 ºC was performed at the end.

Chapter IV

Co-culture of Single Source Derived Endothelial and Pre-Osteoblast Cells: Optimization of Culture Medium and Cell Ratio

ABSTRACT

New bone formation relies on several complex processes that require well-orchestrated interactions between several cell types, among which bone-forming cells (osteoblasts, OBs) and micro-vessel forming endothelial cells (ECs) play a crucial role. The co-culture of these cells has been proved relevant to investigate the mechanisms underlying their mutual interaction, as well as to mimic specific features of the bone niche.

Herein, we propose the co-culture of microvascular-like ECs and pre-OBs derived from a single cell source, the SSEA-4$^+$ cell sub-population from the stromal vascular fraction of human adipose tissue (SSEA-4$^+$hASCs), to define the conditions in which cells synergistically communicate to support the full differentiation of pre-OBs and the maintenance of ECs phenotype. Co-cultures of different ratios of both cell types were established and maintained up to 21 days in standard endothelial maintenance (ENDO) and osteogenic differentiation media (OST), as well as in a mixture of these two (MIX). The osteogenic maturation of pre-OBs (ALP activity, OPN and OCN expression, calcium deposition), as well as the evolution of ECs number (quantification of CD31$^+$ cells), maintenance of endothelial phenotype (CD31 and vWF expression, up-take of low density lipoprotein) were assessed as a function of cell ratio and culture media along the time. The obtained results demonstrate that the ECs number has a significant effect over the osteogenic differentiation of pre-OBs, depending on the medium used. While in the ENDO medium the osteogenic differentiation was not observed, in the OST and MIX medium it was attained at similar levels, except for the co-culture in MIX medium in which a higher number of ECs was initially used. These findings demonstrate that the use of SSEA-4$^+$hASCs as a single cell source, is a promising endeavor to attain 3D tissue-like models that require intricate settings and design to promote the regeneration of vascularized bone tissue.

This chapter is based on the following publication:

Mihaila SM, Resende MF, Reis RL, Gomes ME and Marques AP, "Co-culture of Single Source Derived Endothelial and Pre-Osteoblast Cells: Optimization of Culture Medium and Cell Ratio", submitted 2014

IV.1. INTRODUCTION

Bone is a complex and highly specialized tissue that undergoes continuous regeneration and remodeling throughout life[1]. This intrinsic feature enables bone development and growth under normal physiological conditions, as well as in case of injury or trauma. The pre-requisite to maintain this remarkable capability is an appropriate blood supply and the coupling of the vasculature with the bone remodeling cells. In fact, the intimate crosstalk between bone forming (osteoblasts, OBs) and bone resorbing (osteoclasts) cells, and the microvascular endothelium, orchestrates the spatial and temporal cellular activities that lead to bone regeneration[2,3,4]. Several *in vitro* studies have been investigating the mechanisms underlying this mutual interaction during bone formation using various co-culture models of OBs and endothelial cells (ECs) as tools, to replicate the bone niche[5,6]. Two dialogues were identified as essential for bone remodeling: a paracrine effect through growth factors, like vascular endothelial growth factor (VEGF)[7], insulin-like growth factor I and II[8] and bone morphogenetic proteins (BMPs)[9], and a juxtacrine mechanism through gap junctional communication[5].

Several research groups have been co-culturing osteogenic and vasculogenic cells to enable the occurrence of such dialogues, as well as the translation into complex 3D structures that recreate the native tissue. In the attempt to further mimic and eventually control the regenerative niche, the selection of the cellular combinations has been significantly varied; ECs were co-cultured with mature OBs[10], pre-committed osteoblast cells (pre-OBs)[6] or mesenchymal stem cells (MSCs)[11,12,13,14]. Similarly, the cell source ranges from bone samples to obtain fully committed OBs, peripheral and umbilical cord blood to retrieve ECs or endothelial progenitor cells (EPCs), and bone marrow to isolate undifferentiated MSCs. However, in addition to some limitations associated to the cell sources availability/accessibility, the ideal combination of cells and the respective conditions necessary to maximize their potential in a therapeutic approach are yet to be defined.

Adipose tissue has been widely exploited as a source of a myriad of cell types relevant in the context of tissue engineering (TE) and regenerative medicine. The relatively easiness of the adipose tissue harvesting (enabling low site morbidity and patient discomfort), and high cellular yield are among the factors that have been increasingly favoring the use of adipose-derived stem cells (hASCs) over bone marrow MSCs. Previous studies[15,16] have also showed that the stromal vascular fraction (SVF) of the adipose tissue comprises of several cellular subsets that, in comparison to the heterogeneous population, hASCs, are characterized by increased differentiation potential towards specific lineages. For instance, in the context of bone TE, STRO-1^{+}hASCs[15], CD105^{-}hASCs[17], CD90^{+}hASCs[15,18] and p75^{+}hASCs[15] were shown to possess higher osteogenic differentiation potential than hASCs.

Interestingly, few works and with limited outcomes have reported the isolation of microvascular ECs from SVF[19] or the differentiation of hASCs into the endothelial lineage[20]. In a previous work, we showed that within the SVF of the adipose tissue resides a sub-population that exhibits both osteogenic and endothelial differentiation capacity[21]. This sub-population, characterized by the expression of the pluripotent marker SSEA-4 (SSEA-4$^+$hASCs), can be selected from SVF and gives rise to osteoblastic and endothelial-like cells that can be further expanded into phenotypically stable populations. Thus, the use of SSEA-4$^+$hASCs as a single cell source to recreate a microenvironment that potentiates bone regeneration is considered of major relevance. Under which conditions can the potential of this sub-population be maximized is the question yet to be answered.

Previous studies have proved that the combination of less-differentiated osteoblastic cells (pre-OBs) with mature and fully differentiated ECs is the most effective in terms of osteogenic differentiation and endothelial tubule formation capacities[6,22]. Moreover, a major concern regarding the preservation of the ECs phenotype has been dictating the tested conditions[23]. Thus, this work was designed under the hypothesis that SSEA-4$^+$hASCs-derived pre-OBs and ECs synergistically communicate to support the concomitant full differentiation of pre-OBs into an osteogenic phenotype and the maintenance of ECs phenotype. Co-cultures of different ratios of both cell types were established and maintained up to 21 days. Moreover, in order to confirm the cellular crosstalk and assess its overall effect over the osteogenic and endothelial phenotypes along the culture, several culture media were tested and the involvement of VEGF evaluated.

IV.2. MATERIALS AND METHODS

IV.2.1. Isolation of SVF

Human abdominal subcutaneous adipose tissue samples were obtained from healthy females (42.3±15.9 years), undergoing lipoaspiration procedure, after informed consent. Samples were transported in phosphate buffer saline (PBS, Sigma, Germany) supplemented with 10% (v/v) penicillin/streptomycin (Pen/Strep, 1000U/1000µg/mL, Gibco, USA), under a protocol previously established between the Department of Plastic Surgery of Hospital da Prelada (Porto, Portugal) and the 3B's Research Group (Guimarães, Portugal) and approved by the local Ethical Committee. All tissue samples were processed within 24h after the surgical procedure, as described elsewhere[21]. Briefly, the lipoaspirates were digested with 0.05% (wt/v) collagenase type IIA from *Clostridium histolyticum* (Sigma, Germany) in PBS, for 45min and under agitation in a shaking bath set at 37°C. The digested tissue was filtered through a 200µm strainer, followed by centrifugation (800*xg*, 10min) to remove the floating mature adipocytes and connective tissue. Lysis was performed with an in-house

prepared lysis buffer consisting of 155mM NH_4Cl (Merck, Germany), 5.7mM anhydrous K_2HPO_4 (Riedel-de-Haën, Germany) and 0.1M EDTA (Sigma, Germany), in order to disrupt the red blood cells and further purify the cellular crude. After several centrifugation and washing steps, the crude was resuspended in PBS and filtered through a 100µm cell strainer to ensure a single cell suspension consisting of the SVF of adipose tissue.

IV.2.2. SSEA-4$^+$hASCs sub-population selection and culture

IV.2.2.1. Immunomagnetic selection of SSEA-4$^+$hASCs

The SVF sub-population expressing SSEA-4 (SSEA-4$^+$hASCs) was isolated by immunomagnetic selection with SSEA-4 (clone MC813) antibody (Santa Cruz Biotechnology, USA) coated Dynabeads® M-450 Epoxy beads (Invitrogen, USA) adapting the manufacturer's instructions, as previously described elsewhere[21].

IV.2.2.2. Endothelial differentiation

The freshly selected SSEA-4$^+$hASCs were filtered through a 100µm cell strainer to separate the single cells from the aggregates formed during coupling that might contain contaminating cells (fibroblasts, *etc.*). SSEA-4$^-$hASCs cells were immediately cultured in Endothelial Cell Basal Medium (EGM-2MV, Lonza, Switzerland) containing growth factors and 5% fetal bovine serum (FBS). Cells were incubated in a humidified environment at 37°C with 5% CO_2, with culture medium replenishments every 3-4 days. For all experiments, endothelial differentiated SSEA-4$^+$hASCs (microvascular-like endothelial cells, ECs) were used in passage 2, after 80% confluence and passaging with TrypLE^{TM} Express (Invitrogen, USA).

IV.2.2.3. Osteogenic pre-conditioning

Freshly selected SSEA-4$^+$hASCs were cultured in basal medium comprising of Minimum Essential Medium Eagle-Alpha modification (αMEM, Gibco, USA) supplemented with sodium bicarbonate ($NaHCO_3$, Sigma, Germany), 10% FBS (Gibco, USA) and 1% Pen/Strep (100U/100µg/mL) for expansion. Osteogenic pre-conditioning was achieved by culturing SSEA-4$^+$hASCs, at passage 1, for 7 days in osteogenic medium (basal medium supplemented with 10mM beta-glycerophosphate (βGP, Sigma, Germany), 10^{-8}M dexamethasone (Dex, Sigma, Germany), 50mg/mL L-ascorbic acid 2-phosphate sesquimagnesium salt hydrate (AA, Sigma, Germany)), prior the initiation of the co-culture experiments.

IV.2.3. Co-culture setup

The ECs derived from the SSEA-4$^+$hASCs sub-population were cultured together with osteogenic pre-conditioned SSEA-4$^+$hASCs (pre-OBs) at different cell ratios:

75%ECs:25%pre-OBs (75:25), 50%ECs:50%pre-OBs (50:50) and 25%ECs:75%pre-OBs (25:75) and in three different media: EGM-2 MV (ENDO), osteogenic (OST) and a combination of both (MIX), as detailed in **Table IV.1**. Monocultures of 100%ECs (100:0) and 100%pre-OBs (0:100) were used as controls. All cells were used in passage 2.

Table IV.1. Composition of the cell culture media used in the co-cultures

Medium	Composition
BASAL	αMEM supplemented with $NaHCO_3$, 10% FBS and 1% Pen/Strep (100U/100µg/mL)
ENDO	EGM-2 MV= each 500mL of EBM-2 are supplemented with 25mL of FBS, 0.2mL hydrocortisone, 2mL hFGF-B, 0.5mL ascorbic acid, 0.5mL Gentamicin/Amphotericin, 0.5mL VEGF, 0.5mL Long R3-IGF-1, 0.5mL hEGF, 0.5mL heparin
OST	Basal medium supplemented with 10mM βGP, 10^{-8}M Dex and 50µg/mL AA
MIX	EGM-2 MV supplemented with 10mM βGP, 10^{-8}M Dex and 50µg/mL AA

EBM-2 *= Endothelial basal medium;* ***hEGF*** *= human epidermal growth factor;* ***hFGF-B*** *= human fibroblast growth factor-basic with heparin;* ***hR3-IGF-1*** *= human recombinant insulin-like growth factor;* ***VEGF*** *= vascular endothelial growth factor.*

Cell suspensions at the defined ratios were seeded in 24-well plates at a density of $2x10^3$cells/cm^2 and in 500µL of the defined medium. Media were changed twice a week.

The morphology of cells was evaluated along the culture and at pre-selected time points (days 4, 7, 14 and 21) all groups were photographed using a stereo microscope Stemi 1000 (Zeiss, Germany).

In each experiment, each condition was always set in triplicate. Each experiment was carried out 3 independent times, each time with SSEA-4^+hASCs derived from a different donor.

IV.2.4. Flow cytometry

The phenotype of the cells used to set the co-cultures, after the endothelial differentiation and osteogenic pre-conditioning, was screened by flow cytometry using the following antibodies: CD73-PE, CD34-PE and CD31-APC (all from BD Bioscience, USA) and CD105-FITC and CD90-APC (eBiosciences, USA). Cells were harvested with TrypLE™ Express (Invitrogen, USA) and $2x10^5$ cells in 2% (wt/v) BSA/PBS in 0.1% (wt/v) sodium azide were incubated with the antibodies at the concentration recommended by the manufacturer, for 30min at room temperature, in the dark. After incubation, cells were washed with 2% (wt/v) BSA/PBS and resuspended in acquisition buffer (1% (v/v) formaldehyde, 0.1% (wt/v) sodium azide in PBS). During the co-culture time frame, at pre-selected time points, samples from

all experimental groups were retrieved and incubated with CD31-APC, as described above, to quantify the percentage of ECs present in culture.

Samples were analyzed in a BD FACScalibur flow cytometer (BD Biosciences, USA). A minimum of $2x10^4$ gated events were acquired and the cells of interest were gated in a forward versus side scatter dot plot with a linear scale using the FlowJo 10.0.6 software (Tree Star, USA). Histogram plots were used to determine the percentage of $CD31^+$ (ECs) and $CD31^-$ (pre-OBs).

IV.2.5. Endothelial phenotype analysis

In addition to the flow cytometry, the phenotype of the ECs used to set the co-cultures was further analyzed based on their capacity to form tubular-like structures and to uptake the acetylated low density lipoprotein (ac-LDL) complex. This distinctive capacity of ECs was also used to label the ECs at pre-selected time points (days 4, 7, 14 and 21) of the co-culture, to obtain information over the ECs distribution amongst the pre-OBs.

IV.2.5.1. Matrigel assay

A 96-well cell culture plate, chilled at 4°C, was loaded with 32µL of Matrigel (BD Biosciences, USA) and incubated at 37°C. Cells were suspended in the ENDO medium at a concentration of $2.1x10^5$ cells/mL and 64µL of this cell suspension was seeded in each well onto the surface of the solidified Matrigel. Cells were incubated (37°C, 5% CO_2) for 4h. After incubation, samples were fixed with 10% (v/v) buffered formalin (Sigma, Germany) for 20min at room temperature and further incubated with rhodamine-phalloidin (Sigma, Germany) to observe the organization of the cell cytoskeleton. Cells nuclei were counterstained with 4,6-diamidino-2-phenyindole dilactate (DAPI, Invitrogen, USA), for 10min, and then washed with PBS three times. Samples were visualized using an Axioplan Imager Z1 fluorescence microscope (Zeiss, Germany) and photographed using an Axio Cam MRm camera (Zeiss, Germany) running on AxioVision 4.8 software (Zeiss, Germany).

IV.2.5.2. DIL-ac-LDL uptake

ECs were incubated overnight with 0.2µg/mL of ac-LDL labeled with 1,1'-dioctadecyl-3,3,3',3'-tetramethylindocarbocyanine (DIL-ac-LDL, Invitrogen, USA). Pre-OBs were also submitted to the same procedure, to confirm the lack of DIL-ac-LDL complex uptake ability. Cells were then fixed with 10% (v/v) buffered formalin for 20min at room temperature, protected from light. Cell nuclei were counterstained with DAPI. Samples were further visualized as previously mentioned.

IV.2.6. Cell number: dsDNA quantification

The total amount of double stranded DNA (dsDNA) in each of the mono- and co-culture groups was determined using a fluorimetric dsDNA quantification kit (PicoGreen, Molecular Probes, Invitrogen, USA), according to the manufacturer's instructions. At pre-selected time points (days 4, 7, 14 and 21 of culture), cells were lysed by osmotic and thermal shocks. Fluorescence was measured using an excitation wavelength of 480nm and emission wavelength of 538nm in a microplate reader (Synergy HT, Biotek Instruments, USA). Standards were prepared with concentrations ranging between 0 and 2mg/mL.

IV.2.7. Metabolic activity assay

Cellular metabolic activity during co-culture was measured using the CellTiter® Proliferation assay (MTS, Promega, USA), according to the instructions of the manufacturer. Briefly, a MTS working solution was prepared in a 1:5 (v/v) ratio with phenol red- and serum-free Dulbecco's modified Eagle medium (DMEM, Gibco, USA). At pre-selected time points (days 4, 7, 14 and 21), cells were washed thoroughly with PBS and 50µL of MTS working solution were added to each well. Plates were incubated for 2h (37°C, 5% CO_2), protected from light, after which optical density (OD) at 490nm was measured. The metabolic activity was normalized against the total amount of dsDNA determined for the respective test condition.

IV.2.8. Alkaline phosphatase activity qualitative and quantitative analysis

The alkaline phosphatase (ALP) activity was measured using an end-point colorimetric procedure, following an adapted *p*-nitrophenol (*p*NP) assay, on the same cell lysates used for dsDNA quantification. Briefly, 20µL of sample were incubated with 80µL of 0.2% wt/v *p*-nitrophenyl phosphate solution (*p*NPP) in 1M diethanolamine (Fluka BioChemika, Austria). The OD of the samples and of the calibration curve samples, prepared using *p*-nitrophenol standards (Sigma, Germany) with values ranging from 0 to 1µM/mL, was read at 405nm. For the monocultures, ALP activity was normalized against the total dsDNA. In the co-cultures, values were normalized against the amount of dsDNA of the $CD31^-$cells (µmol *p*NP/h/µg dsDNA of $CD31^-$ cells), in the corresponding sample, with the assumption that ALP activity detected for the ECs monocultures is neglectable. ALP activity was represented as the amount of (*p*NP) obtained in 1h in each cell.

The ALP activity was also qualitatively assessed by staining the samples fixed with 10% (v/v) buffered formalin (Sigma, Germany) with nitro-blue tetrazolium/5-bromo-4-chloro-3-indolyl-phosphate (NBT/BCIP, Thermo Scientific, USA). Images were acquired as mentioned above.

IV.2.9. Real time reverse transcriptase-polymerase chain reaction (RT-PCR)

IV.2.9.1. RNA extraction and cDNA production

The mRNA of the mono- and co-culture samples was extracted using TRI Reagent® (Sigma, Germany), following the manufacturer's instructions. Proteins were extracted using 160µL chloroform (Sigma, Germany) and the RNA pellets were washed with an equal volume of isopropanol (Sigma, Germany) and 70% ethanol. The total mRNA was reconstituted in 12µL RNAse/DNAse-free water (Gibco, USA) and its quantity and purity were assessed with a NanoDrop ND-1000 Spectrophotometer (NanoDrop Technologies, USA). Samples with a 260/280 ratio between 1.6 and 2.0 were used for the synthesis of single-strand complementary DNA (cDNA). The synthesis of cDNA was performed using qScript™ cDNA synthesis Kit (Quanta BIosciences, USA) and the thermoblock of the Mastercycler ep realplex thermal cycler (Eppendorf, USA). An initial amount of 1µg of mRNA was used in a total volume of 20µL.

IV.2.9.2. Quantitative Real Time RT-PCR

The quantification of the transcripts of the genes of interest was carried out by reverse transcriptase polymerase chain reaction (RT-PCR) using 50ng of cDNA and PerfeCTA™ SYBR® Green FastMix kit (Quanta Biosciences, USA), following the procedure suggested by the manufacturer. The primers for the genes of interest (**Table IV.2**) were previously designed using the v0.4.0 Primer 3 online software (Whitehead Institute, USA) and synthesized by MGW Biotech, Germany. For each sample, the transcripts expression data were normalized against the *glyceraldehyde-3-phosphate-dehygrogenase* (*GAPDH*) housekeeping gene. A concentration of 100nM of each primer was used in a final volume of 20µL of sample.

Table IV.2. Primer pair sequences for the studied genes

Gene	Sequences		NCBI reference
	Forward (5'→3')	Reverse (3'→5')	
GAPDH	ACAGTCAGCCGCATC	GACAAGCTTCCCGTTCTCAG	NM_002046.4
CD31	AAGGCCAGATGCACATCC	TTCTACCCAACATTAACTTAGCGG	NM_000442
vWF	CCCTGGGTTACAAGGAAGAAAT	AGTGTCATGTGTCCTCCTCTAG	NM_000552
OPN	GGGGACAACTGGAGTGAAAA	CCC ACAGACCCTTCCAAGTA	NM_001040058
OCN	CTGGAGAGGAGCAGAACTGG	GGCAGCGAGGTAGTGAAGAG	NM_099173

Each real time RT-PCR reaction was carried out with an initial incubation at 95°C for 2min, followed by forty fives cycles of denaturation (95°C, 10sec), annealing (specific for each gene, 30sec) and extension (72°C, 30sec) in a Mastercycler ep realplex thermal cycler

(Eppendorf, USA). The absolute transcripts expression data was normalized against endogenous GAPDH values. The relative quantification of targeted genes expression, CD31, vWF, OCN and OPN, was performed using the $2^{-\Delta\Delta CT}$ method[24,25]. The CD31 and vWF expression values were normalized against the ECs monoculture (100:0) in ENDO and against the number of $CD31^+$cells obtained from the flow cytometry data for each condition. The OCN and OPN expression values were normalized against the pre-OBs monoculture in OST (0:100) and the number of $CD31^-$cells for each condition. The normalization was performed for each time point with the corresponding control samples.

IV.2.10. Immunocytochemistry

At day 21, the cells were fixed with 10% formalin for 30min, washed with PBS and incubated with a 3%(wt/v) BSA/PBS solution to block non-specific binding. Cells were incubated for 1h at room temperature with mouse anti-human osteocalcin (OCN, 1:50, AbD Serotec, UK) or rabbit anti-human osteopontin (OPN, 1:50, Abcam, Cambridge, UK) primary antibodies diluted in 1.5%(wt/v) BSA/PBS. Samples were then washed with PBS and incubated 1h with the appropriate secondary antibody, either donkey anti-mouse Alexa Fluor 488 (Invitrogen, Carlsbad, CA, USA), or donkey anti-rabbit Alexa Fluor 488 (Invitrogen, Carlsbad, CA, USA) diluted 1:500 in 1.5%(wt/v) BSA/PBS. Cell nuclei were counterstained with DAPI. Negative control samples were prepared by replacing the primary antibody incubation with PBS. Prior fixation, cells were incubated with DIL-ac-LDL, as described above, to allow ECs localization, by microscopic analysis, within the produced extracellular matrix.

IV.2.11. ELISA

The secretion of vascular endothelial growth factor (VEGF) was determined by enzyme-linked immunosorbent assay (ELISA) in the supernatants of the co-cultures between days 14 and 21. The supernatant was centrifuged and filtered before storing at -80°C. The amount of human VEGF was quantified following the instructions provided in the ELISA development kit (PeproTech, USA). Absorbance was read in a multi-well microplate reader at 405 and 650nm. Standard samples in a range of concentrations of 0 to 1ng/mL of recombinant human VEGF were used to obtain a calibration curve.

IV.2.12. Calcium content quantification

The detection of inorganic calcium was performed at the end time point of the co-cultures (21 days) using a colorimetric detection kit (Roche, Switzerland), according to the manufacturer's instructions. Briefly, samples were dissolved in a 6M HCl solution and transferred to microcentrifuge tubes. In a 96-well plate, 175µL of reagent 1 (ethanolamine,

1M, pH10.6) was mixed with 10µL of each sample and incubated for 5min at room temperature. 70µL of reagent 2 (0.3mM o-cresolphtalein-complexon, 13.8mM hydroxy-8-quinoleine and 122mM HCl) was added in each well and incubated at 37°C for 2min. The OD of the samples was read at 570nm and the calcium concentrations were extrapolated from the calibration curve obtained using serial dilutions of a 200µg/mL $CaCl_2$ solution.

IV.2.13. Statistical analysis

Statistical analysis was performed using GraphPad Prism 5.00 software (San Diego, USA). Shapiro-Wilk test was used to ascertain data normality. The results indicated that non-parametric test should be employed for all comparisons. Statistical analysis of the data was carried using one-way analysis of variance (ANOVA) test, followed by post hoc Tukey test for all pair-wise mean comparisons. Significance levels were set for *p* values lower than 0.05.

IV.3. RESULTS

IV.3.1.The endothelial phenotype and an osteogenic pre-commitment of the cells prior co-cultures setting confirmation

The phenotype of SSEA-4^+hASCs sub-population after endothelial differentiation and osteogenic pre-conditioning was analyzed prior setting the co-culture (**Figure IV.1**). Endothelial differentiated SSEA-4^+hASCs (ECs) were characterized by the co-expression of CD31 (94.6%), CD34 (98.6%), CD73 (97.8%) and CD105 (99.7%), while lacking CD90 (3%) (**Figure IV.1A)**. The osteogenic pre-conditioned SSEA-4^+hASCs (pre-OBs) exhibited a surface marker signature (>98% $CD31^-$/$CD34^-$/$CD73^+$/$CD90^+$/$CD105^+$) compatible with a mesenchymal phenotype[26] (**Figure IV.1B)**. Morphologically, ECs were characterized by a cobblestone-like appearance (**Figure IV.1C1)**, while pre-OBs displayed an elongated, spindle-like morphology, again characteristic of mesenchymal stem cells and similar to hASCs morphology (**Figure IV.1C2)**.

The ECs phenotype was also confirmed by their discriminative ability to uptake the LDL complex (**Figure IV.1D1**), as well as to form capillary-like network when seeded on Matrigel (**Figure IV.1E1**). In contrast, pre-OBs were not able to uptake DIL-ac-LDL (**Figure IV.1D2**), and on Matrigel formed aggregates (**Figure IV.1E2**). Moreover, the levels of endothelial-specific transcripts CD31 and vWF, also showed a 1500- and, 5000-fold increase in comparison with the levels displayed by undifferentiated SSEA-4^+hASCs (**Figure IV.1F**).

The commitment of the pre-OBs towards the osteogenic lineage was evaluated considering the activity of ALP, an early maker of differentiation, and the variation of the molecular expression of OPN and OCN, respectively intermediate and late osteogenic-specific

markers. The pre-OBs, SSEA-4$^+$hASCs cultured for 7 days in osteogenic medium, depicted significantly higher ALP activity (p<0.001) than un-committed cells (SSEA-4$^+$hASCs cultured in basal medium) and ECs (**Figure IV.1G**). Moreover, a 2.5-fold up-regulation was detected in the expression of OPN, while the levels of OCN transcripts did not vary in relation to the un-committed cells (**Figure IV.1H**).

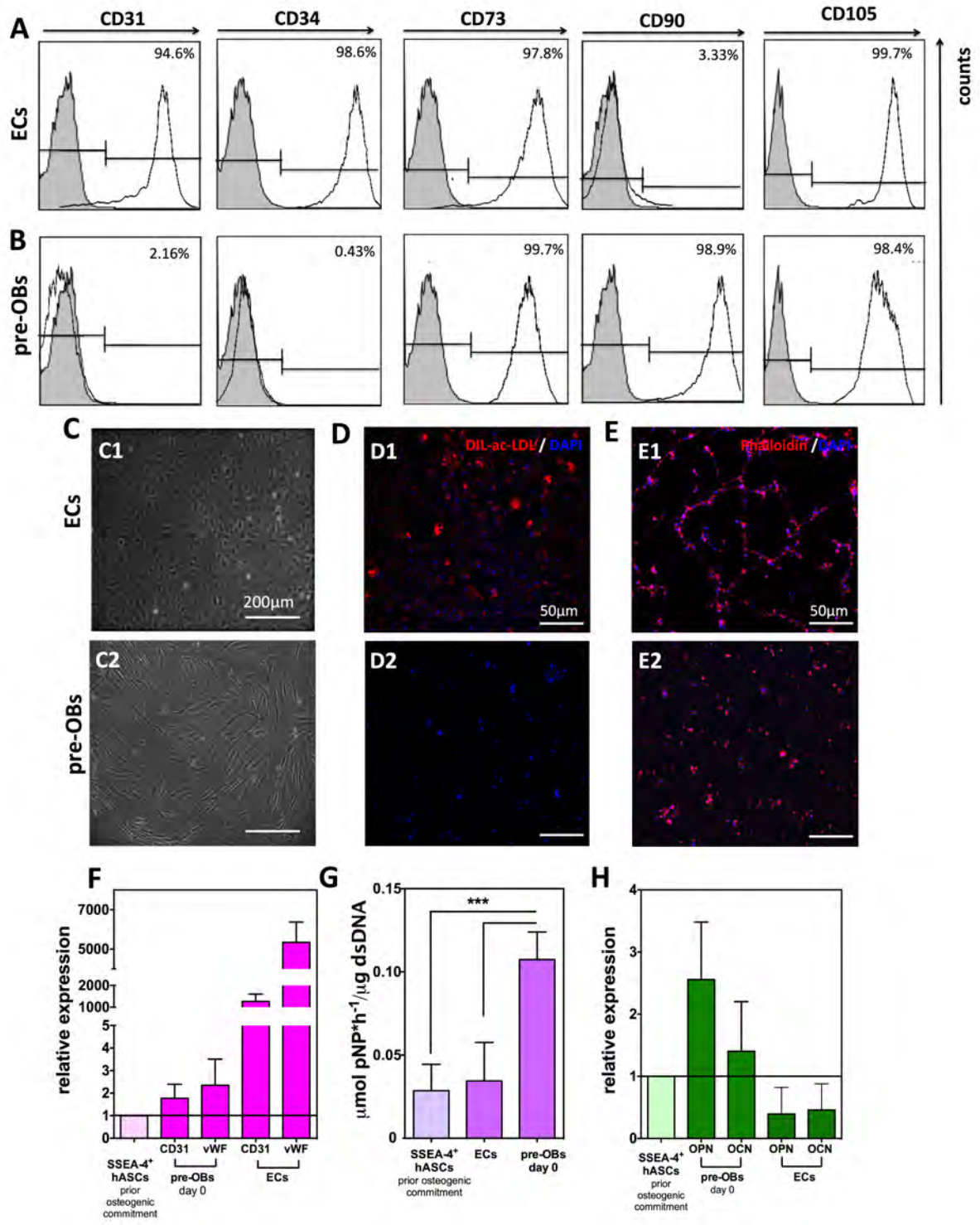

Figure IV.1. Characterization of the endothelial derived-(ECs) and osteogenic pre-conditioned (pre-OBs) SSEA-4$^+$hASCs. (**A**) ECs exhibit a >94% CD31$^+$/CD34$^+$/CD73$^+$/CD90$^-$/CD105$^+$ phenotype, (**B**)

while pre-OBs possess a typical mesenchymal surface markers pattern, >97% $CD31^-/CD34^-/CD105^+/CD73^+/CD90^+$. Both cells can be discriminated based on their characteristic morphology: (**C1**) ECs possess a cobblestone-like shape, (**C2**) whereas pre-OBs are characterized by an elongated, fibroblast-like morphology. (**D1**) ECs can also be discerned by their ability to uptake the LDL complex, (**D2**) while pre-OBs lack this behavior. (**E1**) ECs have the ability to form tubular-like networks when seeded on Matrigel. (**E2**) On the contrary, pre-OBs remain spherical and form aggregates without any evidence of a network formation. (**F**) Levels of endothelial-specific transcripts CD31 and vWF in ECs in comparison to undifferentiated $SSEA\text{-}4^+$hASCs. The commitment of the pre-OBs towards the osteogenic lineage was confirmed by (**G**) an increased activity of alkaline phosphatase and (**H**) an up-regulation of OPN and OCN transcripts in relation to undifferentiated $SSEA\text{-}4^+$hASCs. Data are expressed as mean±standard deviation (SD, n=3, ***p<0.001).

IV.3.2. Co-culture growth and cellular metabolism dependence with cell ratio and culture media

The behavior of ECs and pre-OBs along the (co-)culture was dependent on the cell ratio, as well as on the culture medium. At initial time points, it was possible to discern the spindle-like morphology of pre-OBs and the cobblestone-like aspect of the ECs, independently of the initial cell ratio. For longer time points, fibroblast-like cells took over the culture forming a dense cellular layer (**Supplemental Figure IV.1A).** The discriminative ability of ECs to uptake ac-LDL was used to visualize the presence and arrangement of ECs along the culture (**Figure IV.2A-B**). Stable ECs monocultures were maintained in both ENDO and MIX media until the end of culture. However, OST medium was not able to support ECs monocultures, although small DIL-ac-LDL^+ colonies were identified at day 21 in the 75:25 and 50:50 co-cultures (**Figure IV.2B**). Thus, although ECs colonies surrounded by DIL-ac-LDL^- cells (pre-OBs derived cells) were observed in all the co-cultures, fewer and smaller DIL-ac-LDL^+ colonies were identified with the decrease of ECs ratio.

The cell proliferation results confirmed the dependence of cellular growth with the cell ratio and culture medium (**Figure IV.2C**). In general, all the co-cultures exhibited significant proliferation up to day 14 (p<0.05). Pre-OBs monocultures in ENDO and MIX medium exhibited the highest growth rates and a significantly lower growth (p<0.05) than in OST. This trend was also observed for the co-cultures in the respective media. The dsDNA quantification also corroborated the morphological analysis of the cultures, showing that ECs have a significantly lower (p<0.05) proliferation rate than the pre-OBs mono- and co-cultures, in both ENDO and MIX media, and that OST medium does not support ECs culture.

The metabolic activity results showed that, for the earliest time point and independently of the ratio, cells were significantly more active (p<0.001) in the MIX than in the ENDO medium. However, differences were detected at day 14, for the 75:25 ratio in MIX in

comparison to the same ratio in ENDO and OST. Moreover, the metabolic activity of ECs monocultures in OST medium was significantly lower than in the other two media, and in the other cell ratios in the same medium (**Figure IV.2D**). Thus, cellular metabolism was mainly influenced by the culture medium and predominantly at early time points.

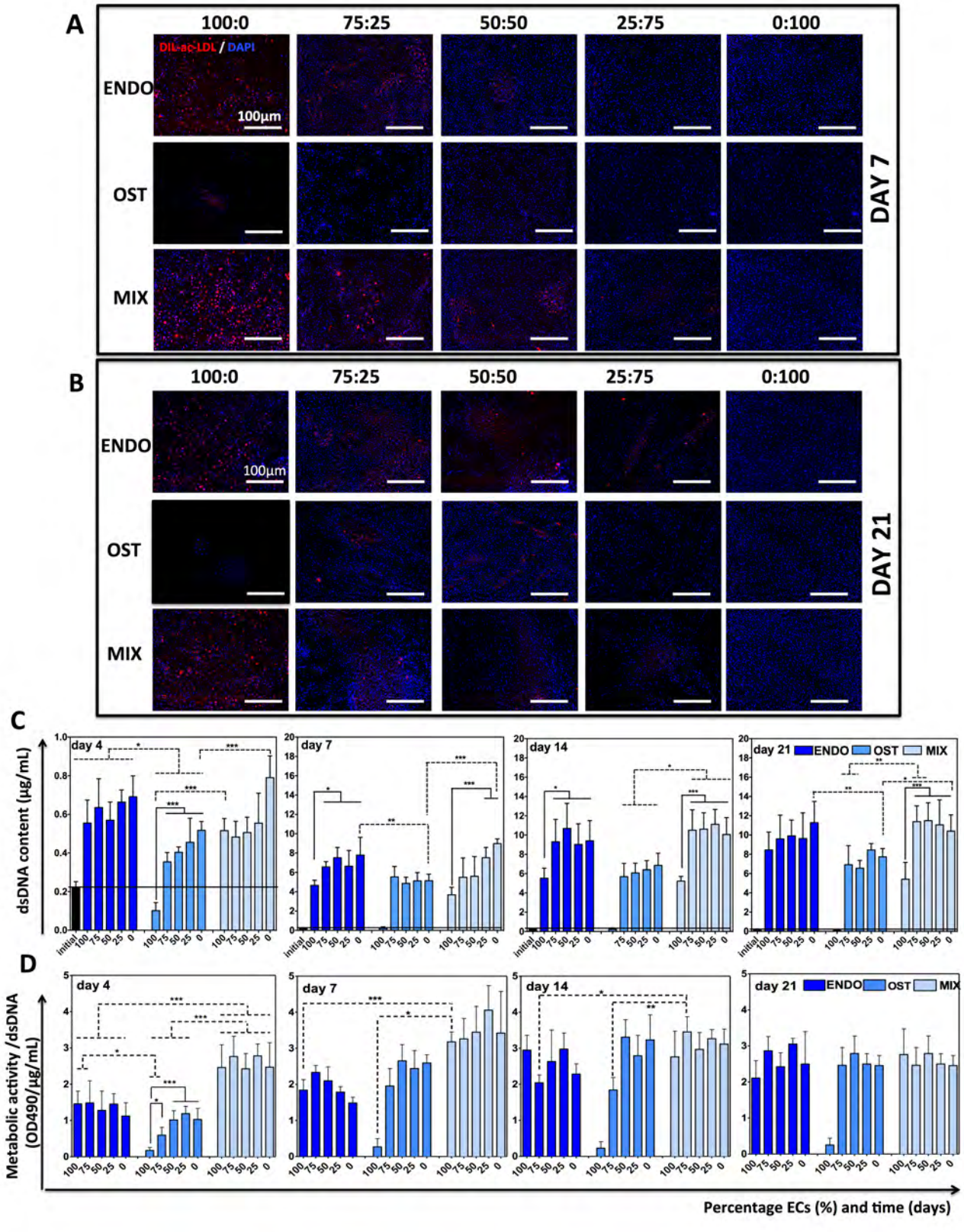

Figure IV.2. Evaluation of cells' organization and proliferation along the culture. (**A-B**) ECs were distinguished from the pre-OBs by their specific ability to uptake the LDL complex (red), and were found arranged in small colonies amongst DIL-ac-LDL$^-$cells in all the co-cultures, although fewer and smaller colonies were identified with the decrease of ECs ratio. Stable ECs monocultures were maintained in both ENDO and MIX, but not in OST media. Cells' nuclei were counterstained with DAPI (blue). (**C**) Cell proliferation, traduced by the dsDNA content along time shows a strong dependency on the cell ratio and culture medium. (**D**) The cellular metabolism was influenced by the culture media, but only at early time points. Along time, only the metabolic activity of ECs in monoculture and the 75:25 condition in OST medium was significantly lower than in the other two media. Data is expressed as mean±SD (n=3, *p<0.05, **p<0.01, ***p<0.001).

IV.3.3. Evolution of endothelial phenotype along the culture

To clearly follow the behavior of ECs along the culture, the percentage of CD31$^+$ in the co-cultures was determined by flow cytometry. The CD31$^-$ profile of pre-OBs monocultures was confirmed by the lack of CD31 expression during the 21 days of culture, regardless of the culture media. On the contrary, more than >95% of the ECs in monocultures in ENDO and MIX media expressed CD31, which was maintained until the end of culture (**Figure IV.3A)**. The percentage of CD31$^+$ cells in each one of the cell ratios did not vary between the ENDO and the MIX media for the entire duration of the culture, except for the 75:25 cell ratio at day 21 in MIX, in which the percentage of ECs cells was significantly higher (p<0.001) than in the ENDO medium. Nonetheless, neither ENDO, nor MIX media were capable to preserve the initial cell ratio. Even more, the percentage of CD31$^+$ cells in the OST medium was always significantly lower than in those two media up to 7 days for all the defined cell ratios. However, at day 14, for the 25:75 cell ratio, and at day 21, for the 50:50 and 25:75 cell ratios, the percentage of CD31$^+$ cells in the three media was similar.

In addition to the evolution in terms of growth, the stability of the endothelial phenotype of ECs in co-culture was evaluated by the analysis of the expression of CD31 and vWF genes (**Figure IV.3B-C**) in relation to the ECs monocultures in ENDO medium, that showed a stable expression of both CD31 and vWF during 21 days of culture (**Supplemental Figure IV.2A**). We also confirmed that the pre-OBs monocultures did not express CD31 or vWF in any of the three culture media, maintaining this neglectable expression profile along the culture (**Supplemental Figure IV.2B**). While the expression levels of CD31 and vWF were not affected by the culture in MIX and ENDO media, the ECs phenotype was altered by the culture in OST medium. A down-regulation of both genes was observed in the ECs monocultures up to 21 days of culture, and of CD31 in the 75:25 co-cultures at day 4. However, in all the other co-culture conditions, the expression of CD31 and vWF was stable regardless of the culture media (**Figure IV.3B-C**).

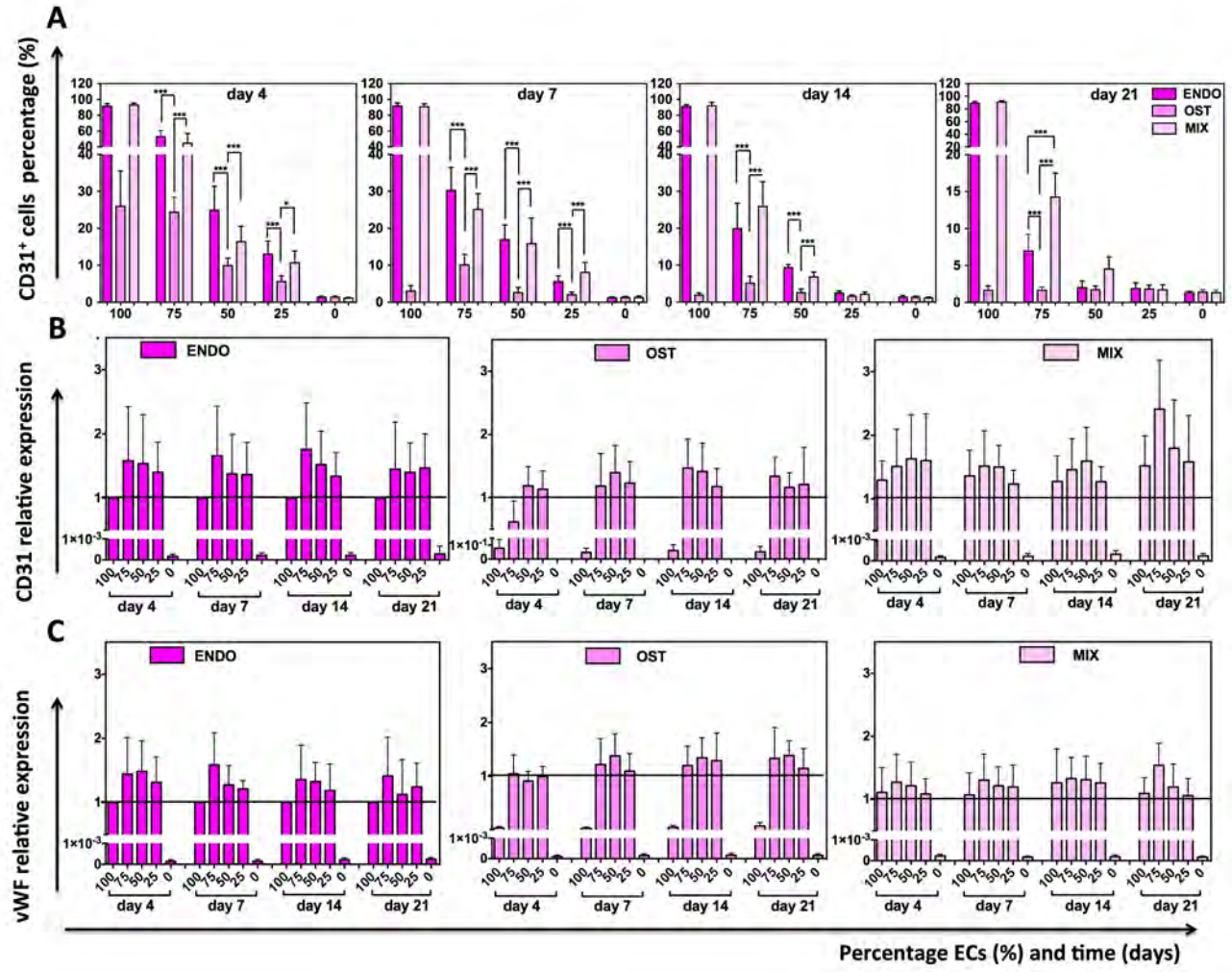

Figure IV.3. Evolution of endothelial phenotype along the culture. (**A**) Percentage of $CD31^+$cells determined by flow cytometry. The $CD31^-$ profile of pre-OBs monocultures was confirmed by their lack of CD31 expression during the 21 days of culture, regardless of the culture media. On the contrary, more than >95% of the ECs monocultures in ENDO and MIX media expressed CD31, which was maintained until the end of culture. Neither ENDO nor MIX media were capable to preserve the initial cell ratio. The stability of the endothelial phenotype of ECs in co-culture was evaluated by the analysis of the expression of (**B**) CD31 and (**C**) vWF genes in relation to the ECs monocultures in ENDO medium. While the expression levels of CD31 and vWF were not influenced by the MIX medium, the ECs phenotype in the monocultures up to 21 days of culture, and in the 75:25 co-cultures at day 4, was affected by the OST medium. The relative expression of each gene was normalized against ECs monocultures in ENDO medium and against the number of $CD31^+$cells obtained from the flow cytometry data for each condition with the assumption that only the $CD31^+$ cells contribute to CD31 and vWF transcripts. Data is expressed as mean±SD (n=3, *p<0.05, **p<0.01, ***p<0.001).

IV.3.4. Evolution of osteogenic differentiation along the culture

To analyze the progress of the pre-OBs along the culture time and under the various study conditions, a panel of markers associated to the different stages of osteogenic differentiation

was assessed. The quantification of the ALP activity of the cultures in ENDO medium did not reveal variations along time in relation to the initial pre-OBs value for any of the cell ratios, including the pre-OBs monocultures **(Figure IV.4A)**. In opposition, the typical profile of ALP activity associated to osteogenic differentiation was observed for all the co-cultures and the pre-OBs monocultures both in OST and MIX media. An activity peak was reached at day 7, with significantly higher (p<0.001) values than the constitutive activity and the corresponding group in ENDO medium. Interestingly, the ALP activity detected for the 75:25 cell ratio in MIX medium was significantly higher (p<0.05) than for the pre-OBs monocultures in MIX and OST media.

The quantitative analysis of the ALP activity was corroborated by the qualitative results. The constitutive ALP activity of both ECs and pre-OBs was represented by the staining of the randomly dispersed cells in the different conditions in ENDO medium at day 4 (**Figure IV.4B**). At the endpoint of the experiment, a slight variation of the staining intensity due to the higher number of cells was detected in ENDO medium, but significantly less intense than for the co-cultures and pre-OBs monocultures in OST and MIX media (**Figure IV.4B**).

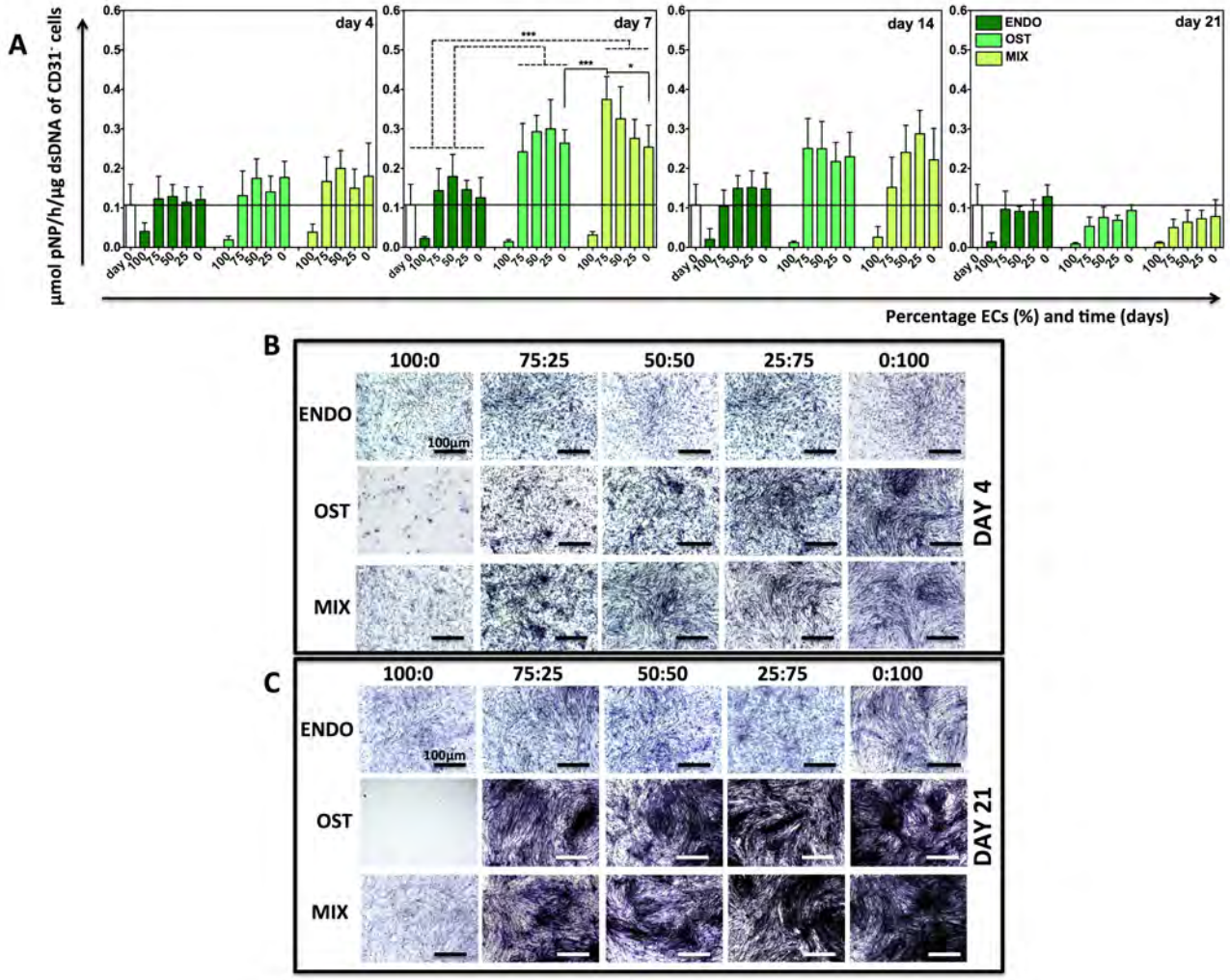

Figure IV.4. Alkaline phosphatase (ALP) activity along the culture. (**A**) The quantification of the ALP

activity of the cultures in ENDO medium did not reveal variations along the time in relation to the initial pre-OBs value for any of the cell ratios, including the pre-OBs monocultures. In opposition, the typical profile of ALP activity associated to osteogenic differentiation was observed for all the co-cultures and the pre-OBs monocultures both in OST and MIX media. The quantitative analysis of the ALP activity was corroborated by the qualitative results showing (**B)** the constitutive ALP activity of both ECs and pre-OBs (purple) in the different conditions in ENDO medium at day 4, with a significantly lower intensity than in the co-cultures and pre-OBs monocultures in OST and MIX media and (**C**) the confirmation of osteogenic differentiation only in OST and MIX, at day 21. For the monocultures, ALP activity was normalized against the total dsDNA. In the co-cultures, values were normalized against the amount of dsDNA of the $CD31^-$cells (µmol pNP/h/µg dsDNA of $CD31^-$cells), in the corresponding sample, with the assumption that ALP activity detected for the ECs monocultures is neglectable. ALP activity is represented as the amount of (pNP) obtained in 1h in each cell. Data is expressed as mean±SD (n=3, *p<0.05, **p<0.01, ***p<0.001).

The osteogenic differentiation of the pre-OBs in the co-cultures was confirmed at the molecular levels by quantifying the expression of the osteogenic-specific genes osteopontin (OPN) and osteocalcin (OCN) in relation to the pre-OBs monoculture in OST (**Figure IV.5A-B**), at each corresponding time point. In order to make this comparison, the complete differentiation of the pre-OBs monoculture in OST was confirmed (**Supplemental Figure IV.3A1-A2).** The expression of OPN, an intermediate marker of differentiation, significantly (p<0.001) increased until reaching a maximum of 90-fold at day 7. Consistently, the expression of OCN, known as a late marker of differentiation, significantly increased (p<0.001) along time reaching at day 21 a 2500-fold gain**.** Thus, the analysis of the expression of OPN and OCN in the co-cultures in OST and MIX media did not show significant differences in relation to the pre-OBs monocultures. An exception was noticed for the 75:25 cell ratio in MIX medium, in which the expression of OPN and OCN, respectively at days 7 and 14, was significantly higher (p<0.01) than in the pre-OBs monocultures in both in OST and MIX media (**Figure IV.5A-B**). Additionally, pre-OBs mono- and co-cultures in ENDO medium displayed significantly (p<0.001) lower expression of OPN and OCN than the respective reference conditions, pre-OBs monoculture in OST (**Figure IV.5A-B**). The gene expression results were confirmed at the protein level. The deposition of an OPN- and OCN-enriched matrix surrounding small ac-LDL^+ colonies was confirmed by immunocytochemistry **(Figure IV.5C).**

The ultimate marker of osteogenic differentiation, matrix mineralization, was indirectly assessed by quantification of the amount of inorganic calcium present in culture[27] (**Figure IV.5D**). While in the ECs monocultures the residual amount of calcium (approx. 0.5 µg/µgdsDNA) did not vary with the medium, in the pre-OBs monocultures and co-cultures a

medium- and ratio-dependent calcium content was detected. Moreover, the level of calcium found in the ECs monocultures and in the pre-OBs monocultures and co-cultures in ENDO medium, was comparable. In opposition, in OST and MIX media the levels of calcium significantly increased (p<0.001). Interestingly, in MIX medium, the amount of calcium detected in the 75:25 co-culture was significantly higher than in all the other conditions in the same medium (p<0.001), and in co-cultures in OST (p<0.001) and pre-OBs monoculture (p<0.001) in OST medium, observation that is valid for the 50:50 ratio in MIX as well. No differences between the 25:75 and pre-OBs monocultures in MIX and OST were observed.

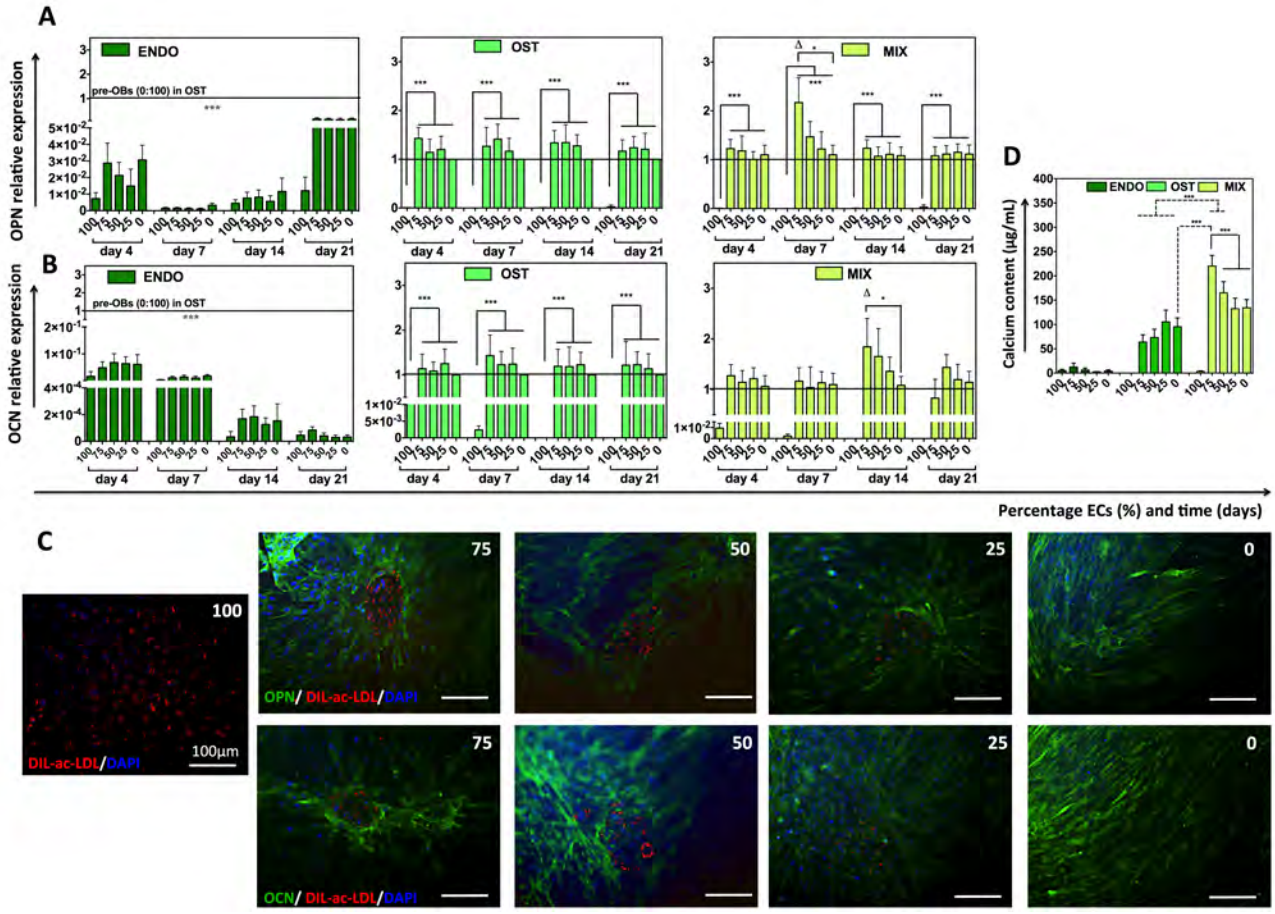

Figure IV.5. Characterization of the osteogenic differentiation along the culture. The osteogenic differentiation of the pre-OBs in the co-cultures was confirmed by the expression of the osteogenic-specific genes (**A**) osteopontin (OPN) and (**B**) osteocalcin (OCN) at the molecular and (**C**) protein levels as indicated by the deposition of an OPN- and OCN-enriched matrix surrounding small DIL-ac-LDL^{+} colonies. The OPN and OCN expression values were normalized against the pre-OBs monoculture in OST (0:100) and the number of CD31^{-}cells for each condition. (**D**) The amount of inorganic calcium deposited in the extracellular matrix, an indirect indicator of mineralization, was evaluated after 21 days of culture for all conditions. The highest levels of calcium were found in the 75:25 ratio. Data is expressed as mean±SD (n=3, *p<0.05, **p<0.01, ***p<0.001). Δ represents a significant difference (p<0.05) from 0:100 in OST condition at the same time point.

IV.3.5 Osteogenic differentiation synergizes with culture medium to support endothelial phenotype through VEGF

The amount of VEGF secreted in the different cultures at the end time point was determined in order to confirm a possible VEGF-mediated crosstalk between the endothelial and osteogenic cells in different conditions (**Figure IV.7A**). In OST medium, the amount of VEGF did not vary with the cell ratios. In opposition, both the cells ratios and the ENDO and MIX media affected the secretion of VEGF. The 75:25 cellular ratio in ENDO medium showed a significantly higher (p<0.001) VEGF release than the ECs and pre-OBs monocultures, and the 25:75 ratio. Nonetheless, that amount of VEGF was significantly lower (p<0.001) than the one detected for the same cell ratio (75:25) in MIX medium (9.1±1.8ng/mL), in turn significantly higher (p<0.01) than in the other conditions in MIX medium. Notably, the VEGF level for the 75:25 and 50:50 in MIX were significantly higher than in all cultures in OST. Furthermore, the VEGF secretion in the ECs monocultures in ENDO (0.61±0.34ng/mL) and MIX (0.60±0.36ng/mL) media and in the pre-OBs monoculture in ENDO was comparable and significantly lower (p<0.001) than in all the other conditions.

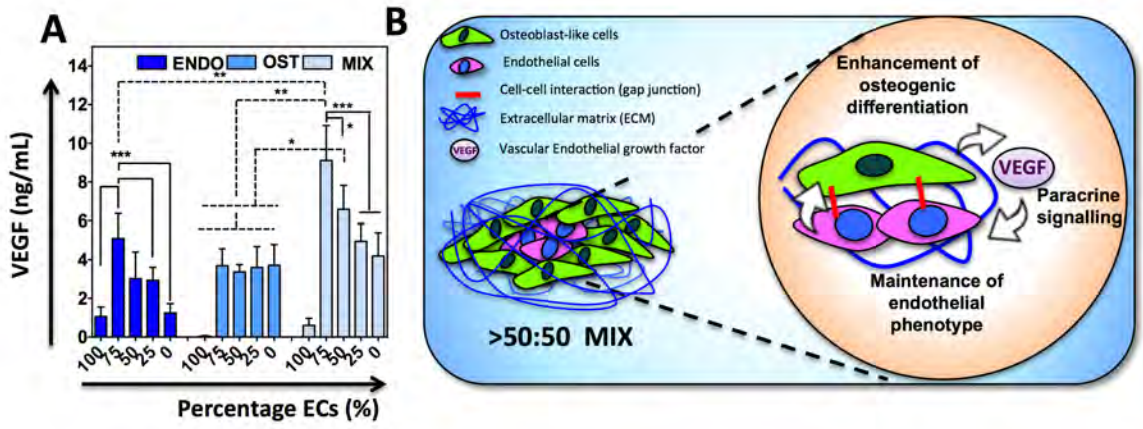

Figure IV.6. VEGF-mediated crosstalk between the endothelial and osteogenic cells. (**A**) VEGF secretion quantified in the supernatant of the cultures at the end time point. Data is expressed as mean±SD (n=3, *p<0.05, **p<0.01, ***p<0.001). (**B**) Schematic representation of the paracrine signaling between differentiated pre-OBs and ECs involved in the increased matrix mineralization and maintenance of the endothelial phenotype in the 75:25 MIX condition. It is proposed that the presence of ECs, maintained by the VEGF of the medium, synergizes with the osteogenic factors present in the medium enhancing osteogenic differentiation of the pre-OBs. This leads to increased VEGF release by the pre-OBs/differentiated cells sustaining the ECs phenotype and growth and promoting a VEGF-associated signaling loop.

IV.4. DISCUSSION

During bone tissue regeneration, the metabolic requirements of the local environment lead

to the up-regulation of multiple downstream events that aim at promoting vessel ingrowth and support osteogenic functionality. These phenomena rely on the intimate cooperation between bone forming cells precursors and microvascular endothelial cells. There are several studies[4,22,28] on the reciprocal regulation and functional relationship between pre-osteoblasts and endothelial cells which, in turn, may be greatly influenced by the degree of osteogenic maturation of pre-OBs and culturing conditions. Though the beneficial effects seem to be conserved, there is still lack of consensus regarding the ideal combination of cells and the respective conditions necessary to maximize their potential. This work intends to tackle this issue by determining in which cell ratio and culture conditions SSEA-4$^+$-derived pre-OBs and ECs synergistically communicate to support the full differentiation of pre-OBs and the maintenance of the ECs phenotype.

Culture medium has been the most useful tool in *in vitro* cell culture to guarantee the minimal requirements for cell survival, growth and eventually differentiation. We defined the ENDO medium composed by a cocktail of growth factors, amongst which VEGF (<5ng/mL[29]) that significantly contributes to the maintenance of the endothelial phenotype, and the standard osteogenic medium[30] (OST), as the ideal conditions respectively for SSEA-4$^+$-derived ECs and pre-OBs. Considering our goal, we assumed that by combining the ingredients of the two media (MIX), both cell types would be provided with the required factors at the standard optimum concentrations. Similar approaches have been followed in previous works[13,22], though, the ENDO and OST media were mixed at a 1:1 ratio reducing to half the concentrations of the provided factors.

While the selection of the media is somehow consensual, the EC:pre-OBs ratios that have been tested represent a wide range of variations from 95:5[13], 80:20[13,31,32], 75:25[23], 66:33[5-6,33], 50:50[10,34], 25:75[23] down to 2:98[13]. A common outcome refers to the need for a higher percentage of ECs in long-term cultures, as pre-OBs, OBs or even hMSCs have a higher proliferation rate, and thus overtake ECs and hinder their modulatory behaviour[5,31], and consequently, the osteogenic commitment. Based on this, and considering our previous knowledge regarding the SSEA-4$^+$hASCs-derived ECs proliferation ability, we selected the 75:25 (ECs:pre-OBs) and the 50:50 ratios, as well as the 25:75 ratio to corroborate the literature findings with other cells.

Both cell ratio and culture medium impacted cell growth and the metabolic activity of the co-cultures. Although ECs did not survive in OST medium as expected, ECs colonies were found in the 75:25 and 50:50 conditions. Thus, our results showed that not only the presence of the pre-OBs supports the ECs survival, but also that an equivalent or higher starting number of SSEA-4$^+$hASCs-derived ECs allows the maintenance of the co-cultures up to 21 days. This is in agreement with previous studies[13,23,35] that showed the lowest

reduction of ECs coupled with the highest proliferation of differentiating cells, in the conditions with the highest ratios of ECs in the starting culture. We were also able to prove that both cell types were metabolically active and highly proliferating in both ENDO and MIX, although with significantly different growth rates as expected. Interestingly MIX and ENDO media showed similar results in terms of cell proliferation, but cells were significantly metabolically more active in the MIX medium, particularly at early time points. Interestingly, each monoculture displayed a higher initial metabolic activity in the MIX, than in its own standard culture medium. We believe that the enriched formulation of the MIX medium potentiates the immediate adjustment of both ECs and pre-OBs, alone or in co-culture, to its components, as they were previously cultured in ENDO and OST.

In agreement with the conditions that support the survival of ECs along the culture, in the ENDO and MIX media, ECs monocultures retain their endothelial signature. In the OST medium, a down-regulation of OPN and OCN expression was observed only in the ECs monocultures. Moreover, the percentage of $CD31^+$ cells in the 75:25 cell ratio and MIX medium was significantly higher than in ENDO. These results suggest that the supplements present the ENDO medium are essential for the survival, growth and maintenance of the endothelial phenotype, as already reported elsewhere[13, 23], but not sufficient to enhance their growth when cultured together with pre-OBs. Moreover, the presence of pre-OBs is mandatory to maintain the endothelial phenotype most likely due to the crosstalk with the ECs. In fact, pre-OBs at different stages of differentiation are known to influence ECs activity by the release of angiogenic factors, among which VEGF[7,36,37], present in both the MIX and ENDO media, but not in the OST.

Interestingly, both ENDO and MIX media, containing the elements that were shown to trigger the endothelial differentiation of freshly isolated SSEA-4^+hASCs[21], failed to induce the acquisition of endothelial-like features by pre-OBs. This, in addition to the increased values of ALP activity, an early hallmark of osteogenic differentiation and a pre-requisite for the upfront events involving osteogenic matrix deposition and consequent mineralization[38], confirmed the SSEA-4^+hASCs osteogenic pre-conditioning after 7 days of culture in OST medium. The absence of expression of intermediate (OPN) and late (OCN) markers of differentiation also proved the early stage of the process. Osteogenic differentiation was completed in all the co-cultures and pre-OBs monocultures both in OST and MIX media, but not in ENDO, as demonstrated by the ALP activity profile, the expression and deposition of OPN and OCN, and the amount of calcium. Our results with ENDO medium are in agreement with several works that showed higher ALP activity in co-cultures of hMSCs and ECs than in hMSCs monocultures, but the completion of the osteogenic differentiation, characterized by an extensive matrix mineralization, had not been achieved[5,10]. Thus, though

the activation of ALP occurs upon co-culturing, in the absence of osteo-inductive factors (Dex, AA and βGP), the osteogenic differentiation is not completed.

Additionally, the concentration of the osteogenic factors is also of relevance, as it was confirmed in another work[13]. A 1:1 mixture of ENDO and OST media did not support the osteogenic differentiation of hMSCs in co-culture with ECs and in monoculture, in opposition to the increased mineralization observed in OST medium. These findings reinforce the need for defining a suitable composition of the medium that besides sustaining the maintenance of the endothelial phenotype would foster the crosstalk between ECs and osteogenic cells. This was attained with our MIX medium that contains the required factors at the standard optimum concentrations.

Moreover, the differences observed for the varied cell ratios suggest an additional modulatory effect of the ECs over pre-OBs differentiation. A significantly higher ALP activity (at day 7) and expression of OPN and OCN, respectively at day 7 and 14, as well as calcium content was detected in the 75:25 cell ratio in relation to pre-OBs monocultures (in both MIX and OST media) and the other cell ratios (in MIX medium). The same trend was observed for the levels of VEGF, known to be secreted by osteoblasts[7] in response to the presence of ECs[7]. Interestingly, significantly higher levels of VEGF were also detected for the 50:50 group in MIX medium in comparison to 25:75 and pre-OBs monocultures in MIX and OST media. However, no differences were observed regarding the osteogenic markers suggesting that the minimal number of SSEA-4$^+$hASCs-derived ECs at which cells in co-culture synergistically communicate to support the full differentiation of the pre-OBs and the maintenance of the ECs phenotype was reached.

Based on our observations and on previous knowledge on deciphering the intimate dialogue between bone forming cells and microvascular-like ECs, we propose a model of the cellular interactions responsible for superior osteogenic maturation that occurs in the presence of a specific ECs:pre-OBs cell ratio in MIX medium (**Figure IV.7B**). We believe that the presence of ECs in a high percentage is maintained by the VEGF in the medium and synergizes with the osteogenic factors present in the medium enhancing the osteogenic differentiation of the pre-OBs. This leads to increased VEGF release by the pre-OBs/differentiated cells sustaining the ECs phenotype and growth and promoting a VEGF-associated signaling loop.

IV.5. CONCLUSIONS

The herein presented findings allow defining the ideal combination of SSEA-4$^+$hASCs-derived pre-OBs and ECs, as well the conditions necessary to maximize their potential under the context of engineering vascularized bone tissue. By co-culturing SSEA-4$^+$hASCs-$^+$-derived ECs and pre-OBs at an initial rate above 50:50 in a mixture of standard endothelial

maintenance and osteogenic differentiation media, cells synergistically communicate to support the full differentiation of the pre-OBs and the maintenance of the ECs phenotype, through the activation of a VEGF-mediated signaling loop. Therefore, SSEA-4^{+}hASCs can act as an optimal cellular source to build a bone tissue engineering construct combining pre-committed cells into the osteogenic lineage and fully differentiated ECs with potential to promote the regeneration of vascularized bone tissue.

REFERENCES

1. Rodan, G. A., Introduction to bone biology. *Bone* **1992,** *13 Suppl 1*, S3-6.
2. Kaigler, D.; Krebsbach, P. H.; Wang, Z.; West, E. R.; Horger, K.; Mooney, D. J., Transplanted endothelial cells enhance orthotopic bone regeneration. *Journal of dental research* **2006,** *85* (7), 633-7.
3. Grellier, M.; Bordenave, L.; Amedee, J., Cell-to-cell communication between osteogenic and endothelial lineages: implications for tissue engineering. *Trends in biotechnology* **2009,** *27* (10), 562-71.
4. Pirraco, R. P.; Marques, A. P.; Reis, R. L., Cell interactions in bone tissue engineering. *Journal of cellular and molecular medicine* **2010,** *14* (1-2), 93-102.
5. Villars, F.; Guillotin, B.; Amedee, T.; Dutoya, S.; Bordenave, L.; Bareille, R.; Amedee, J., Effect of HUVEC on human osteoprogenitor cell differentiation needs heterotypic gap junction communication. *American journal of physiology. Cell physiology* **2002,** *282* (4), C775-85.
6. Guillotin, B.; Bareille, R.; Bourget, C.; Bordenave, L.; Amedee, J., Interaction between human umbilical vein endothelial cells and human osteoprogenitors triggers pleiotropic effect that may support osteoblastic function. *Bone* **2008,** *42* (6), 1080-91.
7. Street, J.; Lenehan, B., Vascular endothelial growth factor regulates osteoblast survival - evidence for an autocrine feedback mechanism. *Journal of orthopaedic surgery and research* **2009,** *4*, 19.
8. Huang, Z.; Ren, P. G.; Ma, T.; Smith, R. L.; Goodman, S. B., Modulating osteogenesis of mesenchymal stem cells by modifying growth factor availability. *Cytokine* **2010,** *51* (3), 305-10.
9. Groeneveld, E. H.; Burger, E. H., Bone morphogenetic proteins in human bone regeneration. *European journal of endocrinology / European Federation of Endocrine Societies* **2000,** *142* (1), 9-21.
10. Hofmann, A.; Ritz, U.; Verrier, S.; Eglin, D.; Alini, M.; Fuchs, S.; Kirkpatrick, C. J.; Rommens, P. M., The effect of human osteoblasts on proliferation and neo-vessel formation of human umbilical vein endothelial cells in a long-term 3D co-culture on polyurethane scaffolds. *Biomaterials* **2008,** *29* (31), 4217-26.
11. Koob, S.; Torio-Padron, N.; Stark, G. B.; Hannig, C.; Stankovic, Z.; Finkenzeller, G., Bone formation and neovascularization mediated by mesenchymal stem cells and endothelial cells in critical-sized calvarial defects. *Tissue engineering. Part A* **2011,** *17* (3-4), 311-21.
12. Duffy, G. P.; Ahsan, T.; O'Brien, T.; Barry, F.; Nerem, R. M., Bone marrow-derived mesenchymal stem cells promote angiogenic processes in a time- and dose-dependent manner in vitro. *Tissue engineering. Part A* **2009,** *15* (9), 2459-70.
13. Ma, J.; van den Beucken, J. J.; Yang, F.; Both, S. K.; Cui, F. Z.; Pan, J.; Jansen, J. A., Coculture of osteoblasts and endothelial cells: optimization of culture medium and cell ratio. *Tissue engineering. Part C, Methods* **2011,** *17* (3), 349-57.
14. Rouwkema, J.; Westerweel, P. E.; de Boer, J.; Verhaar, M. C.; van Blitterswijk, C. A., The use of endothelial progenitor cells for prevascularized bone tissue engineering. *Tissue engineering. Part A* **2009,** *15* (8), 2015-27.

15. Rada, T.; Reis, R. L.; Gomes, M. E., Distinct stem cells subpopulations isolated from human adipose tissue exhibit different chondrogenic and osteogenic differentiation potential. *Stem cell reviews* **2011,** *7* (1), 64-76.
16. Astori, G.; Vignati, F.; Bardelli, S.; Tubio, M.; Gola, M.; Albertini, V.; Bambi, F.; Scali, G.; Castelli, D.; Rasini, V.; Soldati, G.; Moccetti, T., "In vitro" and multicolor phenotypic characterization of cell subpopulations identified in fresh human adipose tissue stromal vascular fraction and in the derived mesenchymal stem cells. *Journal of translational medicine* **2007,** *5*, 55.
17. Levi, B.; Wan, D. C.; Glotzbach, J. P.; Hyun, J.; Januszyk, M.; Montoro, D.; Sorkin, M.; James, A. W.; Nelson, E. R.; Li, S.; Quarto, N.; Lee, M.; Gurtner, G. C.; Longaker, M. T., CD105 protein depletion enhances human adipose-derived stromal cell osteogenesis through reduction of transforming growth factor beta1 (TGF-beta1) signaling. *The Journal of biological chemistry* **2011,** *286* (45), 39497-509.
18. Chung, M. T.; Liu, C.; Hyun, J. S.; Lo, D. D.; Montoro, D. T.; Hasegawa, M.; Li, S.; Sorkin, M.; Rennert, R.; Keeney, M.; Yang, F.; Quarto, N.; Longaker, M. T.; Wan, D. C., CD90 (Thy-1)-Positive Selection Enhances Osteogenic Capacity of Human Adipose-Derived Stromal Cells. *Tissue engineering. Part A* **2013,** *19* (7-8), 989-97.
19. Hutley, L. J.; Herington, A. C.; Shurety, W.; Cheung, C.; Vesey, D. A.; Cameron, D. P.; Prins, J. B., Human adipose tissue endothelial cells promote preadipocyte proliferation. *American journal of physiology. Endocrinology and metabolism* **2001,** *281* (5), E1037-44.
20. Fischer, L. J.; McIlhenny, S.; Tulenko, T.; Golesorkhi, N.; Zhang, P.; Larson, R.; Lombardi, J.; Shapiro, I.; DiMuzio, P. J., Endothelial differentiation of adipose-derived stem cells: effects of endothelial cell growth supplement and shear force. *The Journal of surgical research* **2009,** *152* (1), 157-66.
21. Mihaila, S. M.; Frias, A. M.; Pirraco, R. P.; Rada, T.; Reis, R. L.; Gomes, M. E.; Marques, A. P., Human adipose tissue-derived SSEA-4 subpopulation multi-differentiation potential towards the endothelial and osteogenic lineages. *Tissue engineering. Part A* **2013,** *19* (1-2), 235-46.
22. Valenzuela, C. D.; Allori, A. C.; Reformat, D. D.; Sailon, A. M.; Allen, R. J., Jr.; Davidson, E. H.; Alikhani, M.; Bromage, T. G.; Ricci, J. L.; Warren, S. M., Characterization of adipose-derived mesenchymal stem cell combinations for vascularized bone engineering. *Tissue engineering. Part A* **2013,** *19* (11-12), 1373-85.
23. Bidarra, S. J.; Barrias, C. C.; Barbosa, M. A.; Soares, R.; Amedee, J.; Granja, P. L., Phenotypic and proliferative modulation of human mesenchymal stem cells via crosstalk with endothelial cells. *Stem cell research* **2011,** *7* (3), 186-97.
24. Pfaffl, M. W., A new mathematical model for relative quantification in real-time RT-PCR. *Nucleic acids research* **2001,** *29* (9), e45.
25. Livak, K. J.; Schmittgen, T. D., Analysis of relative gene expression data using real-time quantitative PCR and the 2(-Delta Delta C(T)) Method. *Methods* **2001,** *25* (4), 402-8.
26. Zimmerlin, L.; Donnenberg, V. S.; Rubin, J. P.; Donnenberg, A. D., Mesenchymal markers on human adipose stem/progenitor cells. *Cytometry. Part A : the journal of the International Society for Analytical Cytology* **2013,** *83* (1), 134-40.
27. Amosi, N.; Zarzhitsky, S.; Gilsohn, E.; Salnikov, O.; Monsonego-Ornan, E.; Shahar, R.; Rapaport, H., Acidic peptide hydrogel scaffolds enhance calcium phosphate mineral turnover into bone tissue. *Acta biomaterialia* **2012,** *8* (7), 2466-75.
28. Grellier, M.; Bordenave, L.; Amédée, J., Cell-to-cell communication between osteogenic and endothelial lineages: implications for tissue engineering. *Trends in biotechnology* **2009,** *27*, 562–571.
29. Ferreira, L. S.; Gerecht, S.; Shieh, H. F.; Watson, N.; Rupnick, M. A.; Dallabrida, S. M.; Vunjak-Novakovic, G.; Langer, R., Vascular progenitor cells isolated from human embryonic stem cells give rise to endothelial and smooth muscle like cells and form vascular networks in vivo. *Circulation research* **2007,** *101* (3), 286-94.

30. Porter, R. M.; Huckle, W. R.; Goldstein, A. S., Effect of dexamethasone withdrawal on osteoblastic differentiation of bone marrow stromal cells. *Journal of cellular biochemistry* **2003,** *90* (1), 13-22.
31. Unger, R. E.; Sartoris, A.; Peters, K.; Motta, A.; Migliaresi, C.; Kunkel, M.; Bulnheim, U.; Rychly, J.; Kirkpatrick, C. J., Tissue-like self-assembly in cocultures of endothelial cells and osteoblasts and the formation of microcapillary-like structures on three-dimensional porous biomaterials. *Biomaterials* **2007,** *28* (27), 3965-76.
32. Santos, M. I.; Unger, R. E.; Sousa, R. A.; Reis, R. L.; Kirkpatrick, C. J., Crosstalk between osteoblasts and endothelial cells co-cultured on a polycaprolactone-starch scaffold and the in vitro development of vascularization. *Biomaterials* **2009,** *30* (26), 4407-15.
33. Grellier, M.; Ferreira-Tojais, N.; Bourget, C.; Bareille, R.; Guillemot, F.; Amedee, J., Role of vascular endothelial growth factor in the communication between human osteoprogenitors and endothelial cells. *Journal of cellular biochemistry* **2009,** *106* (3), 390-8.
34. Kaigler, D.; Krebsbach, P. H.; West, E. R.; Horger, K.; Huang, Y. C.; Mooney, D. J., Endothelial cell modulation of bone marrow stromal cell osteogenic potential. *FASEB journal : official publication of the Federation of American Societies for Experimental Biology* **2005,** *19* (6), 665-7.
35. Xue, Y.; Xing, Z.; Hellem, S.; Arvidson, K.; Mustafa, K., Endothelial cells influence the osteogenic potential of bone marrow stromal cells. *Biomedical engineering online* **2009,** *8*, 34.
36. Ding, Y.; Gao, Z. G.; Jacobson, K. A.; Suffredini, A. F., Dexamethasone enhances ATP-induced inflammatory responses in endothelial cells. *The Journal of pharmacology and experimental therapeutics* **2010,** *335* (3), 693-702.
37. Scutt, A.; Bertram, P., Basic fibroblast growth factor in the presence of dexamethasone stimulates colony formation, expansion, and osteoblastic differentiation by rat bone marrow stromal cells. *Calcified tissue international* **1999,** *64* (1), 69-77.
38. Zhou, L.; Ogata, Y., Transcriptional regulation of the human bone sialoprotein gene by fibroblast growth factor 2. *Journal of oral science* **2013,** *55* (1), 63-70.
39. Boilly, B.; Vercoutter-Edouart, A. S.; Hondermarck, H.; Nurcombe, V.; Le Bourhis, X., FGF signals for cell proliferation and migration through different pathways. *Cytokine & growth factor reviews* **2000,** *11* (4), 295-302.
40. Reyes, J. M.; Fermanian, S.; Yang, F.; Zhou, S. Y.; Herretes, S.; Murphy, D. B.; Elisseeff, J. H.; Chuck, R. S., Metabolic changes in mesenchymal stem cells in osteogenic medium measured by autofluorescence spectroscopy. *Stem cells* **2006,** *24* (5), 1213-7.
41. Ito, K.; Suda, T., Metabolic requirements for the maintenance of self-renewing stem cells. *Nature reviews. Molecular cell biology* **2014,** *15* (4), 243-56.
42. Dohle, E.; Fuchs, S.; Kolbe, M.; Hofmann, A.; Schmidt, H.; Kirkpatrick, C. J., Sonic hedgehog promotes angiogenesis and osteogenesis in a coculture system consisting of primary osteoblasts and outgrowth endothelial cells. *Tissue engineering. Part A* **2010,** *16* (4), 1235-7.
43. Deckers, M. M.; Karperien, M.; van der Bent, C.; Yamashita, T.; Papapoulos, S. E.; Lowik, C. W., Expression of vascular endothelial growth factors and their receptors during osteoblast differentiation. *Endocrinology* **2000,** *141* (5), 1667-74.
44. Marom, R.; Shur, I.; Solomon, R.; Benayahu, D., Characterization of adhesion and differentiation markers of osteogenic marrow stromal cells. *Journal of cellular physiology* **2005,** *202* (1), 41-8.
45. Tokuda, H.; Kozawa, O.; Uematsu, T., Basic fibroblast growth factor stimulates vascular endothelial growth factor release in osteoblasts: divergent regulation by p42/p44 mitogen-activated protein kinase and p38 mitogen-activated protein kinase. *Journal of bone and mineral research : the official journal of the American Society for Bone and Mineral Research* **2000,** *15* (12), 2371-9.

SUPPLEMENTAL INFORMATION

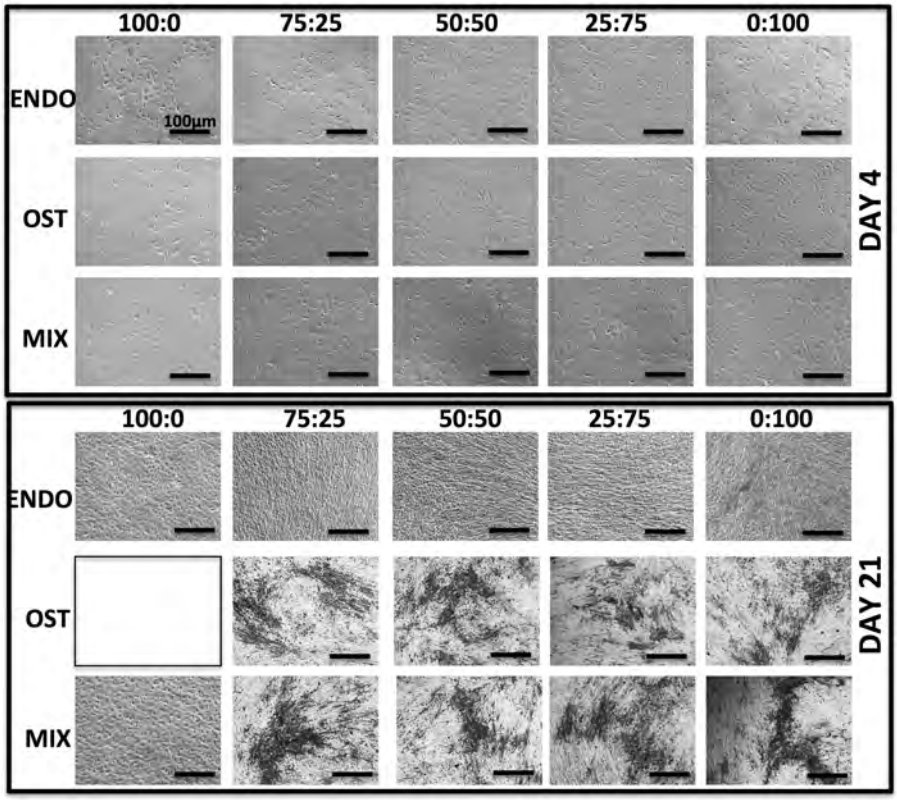

Supplemental Figure IV.1. Effect of culture conditions over cell morphology. ECs maintain their cobblestone-like morphology in ENDO and MIX, whereas in OST, they are sparse not being able to recover along the culture.

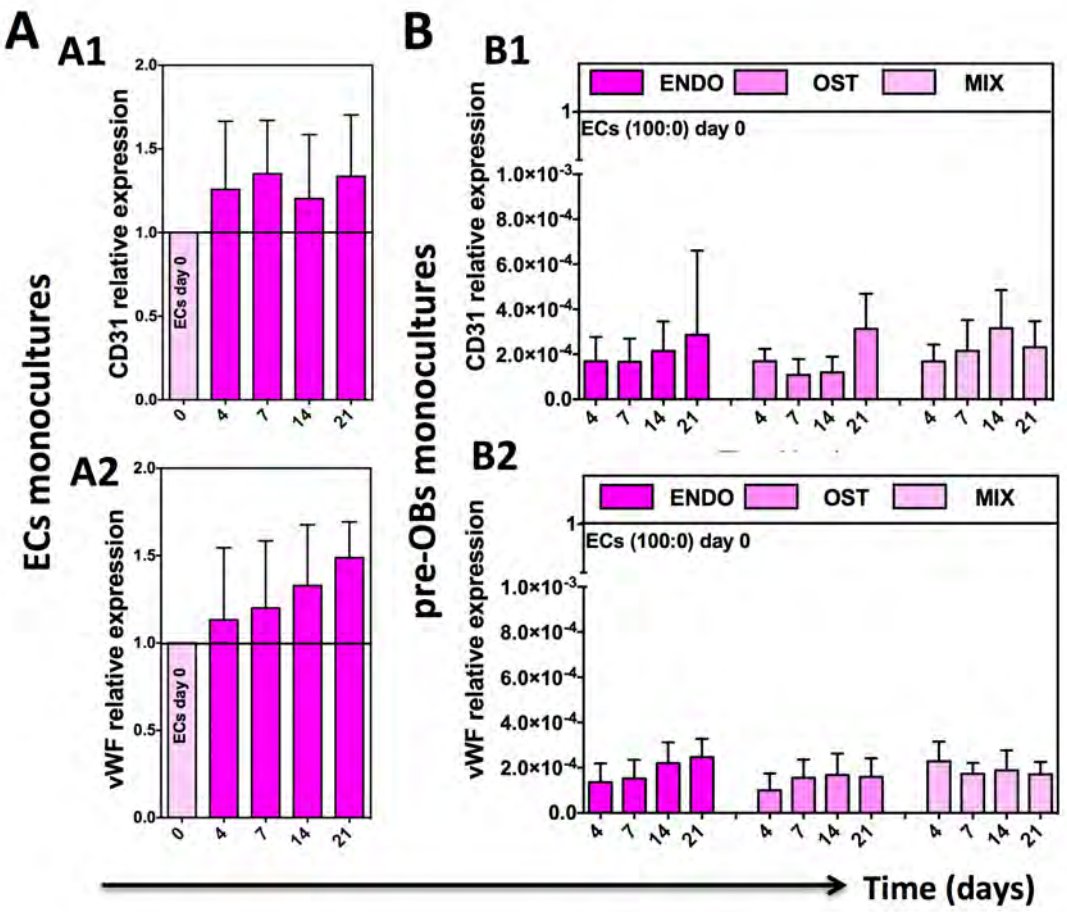

Supplemental Figure IV.2. Relative expression levels of endothelial-specific markers *CD31* and *vWF* for ECs monocultures in ENDO medium (**A1-2**) and pre-OBs monocultures in all three culture media (**B1-2**) in comparison to ECs monocultures at the beginning of the experiment. While ECs were characterized by a stable expression, pre-OBs in ENDO medium lack the expression of these markers as in the beginning of the experiment. Data is expressed as mean±SD (n=3).

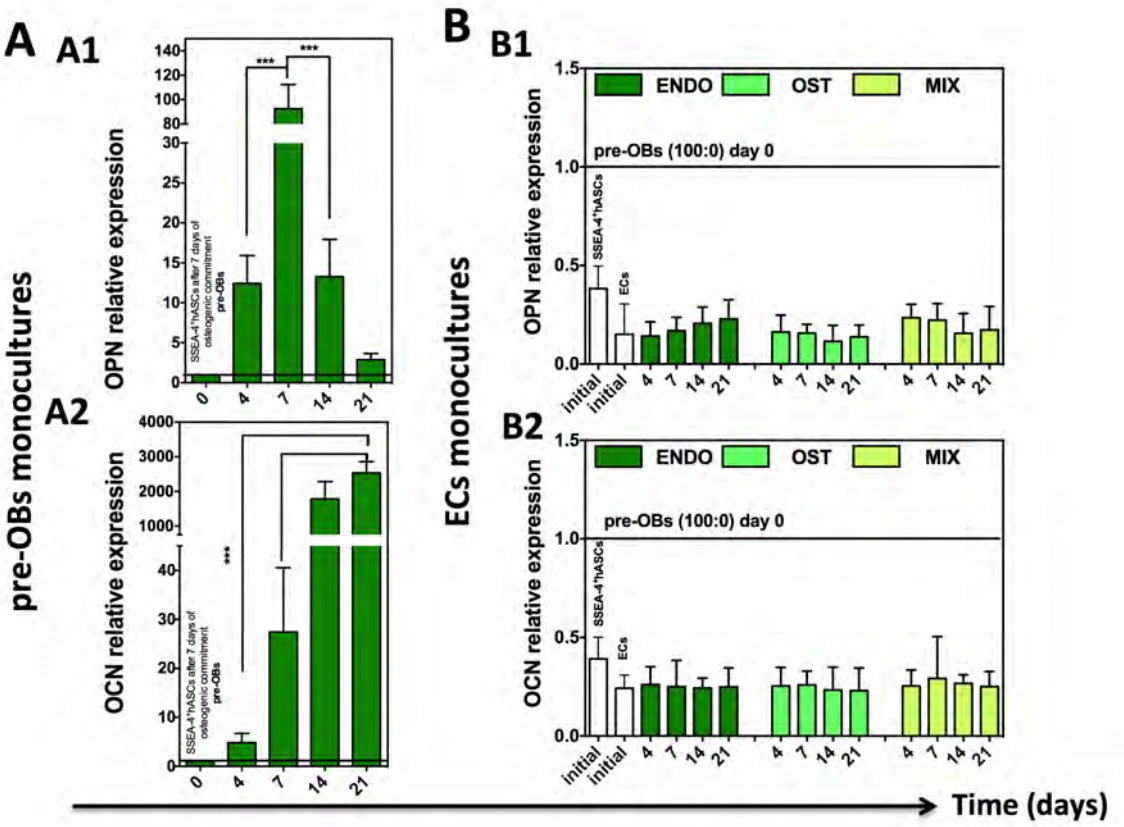

Supplemental Figure IV.3. Relative expression levels of osteogenic-specific markers *OPN* and *OCN* for pre-OBs monocultures in OST medium (**A1-2**) and ECs monocultures in all three media (**B1-2**) in comparison to pre-OBs monocultures at day 0. While pre-OBs gained an osteoblastic-like phenotype as shown by the significant up-regulation of *OPN* and *OCN*, ECs were characterized by stable gene expression levels. Data is expressed as mean±SD (n=3, ****p<0.001*).

SECTION V

THE OSTEOINDUCTIVE POTENTIAL OF SILICATE NANOPLATELETS

Chapter V

Bioactive Silicate Nanoplatelets for Osteogenic Differentiation of Human Mesenchymal Stem Cells

ABSTRACT

Novel silicate nanoplatelets (sNPs) that induce osteogenic differentiation of human mesenchymal stem cells (hMSCs) in the absence of any osteoinductive factor are reported. The presence of the sNPs triggers a set of events that follows the temporal pattern of osteogenic differentiation. These findings underscore the potential applications of these sNPs in designing bioactive scaffolds for musculoskeletal tissue engineering (TE).

This chapter is based on the following publication:

Gaharwar AK*, **Mihaila SM***, Swami A, Patel A, Sant S, Reis RL, Marques AP, Gomes ME, Khademhosseini A, "Bioactive Silicate Nanoplatelets for Osteogenic Differentiation of Human Mesenchymal Stem Cells", Advanced Materials 2013, 25(24): 3329–3336, doi: 10.1002/adma.20130058

V.1. INTRODUCTION

With an aging U.S. population, the occurrence of injuries and degenerative conditions are subsequently on the rise. As a direct result, there is an increase in demand for therapies that are able to repair damaged tissues and produce replacement organs[1]. In particular, there is a great need for new bioactive materials that can direct stem cell differentiation and facilitate the formation of functional tissues[2]. Several types of bioactive materials have been reported for musculoskeletal tissue engineering (TE) in the last few years that have clinical relevance including bioactive glasses ($Na_2O–CaO–SiO_2–P_2O_5$), hydroxyapatite (HA) ($Ca_{10}(PO_4)_6(OH)_2$), β-tricalcium phosphate (β-TCP) ($Ca_3(PO_4)_2$), β-wollastonite (CaO-SiO) and A-W (Apatite-Wollastonite) glass ceramics[3]. Difficulties persisting with many of these known materials include lack of osteoinductive properties, poor processing abilities and insufficient degradation. Although, demineralized bone matrix (DBM) have been identified as an alternative to autografts (gold standard), its clinical application has been limited by its batch to batch variability due to its biological nature, immunogenicity and high production costs[4].

Recently, bioactive nanomaterials have emerged as the next generation of advanced materials for biotechnological and biomedical applications due to their enhanced surface interactions. Synthetic silicate nanoplatelets (sNPs) have shown promise in developing strong matrix[5], high-performance elastomers[6], super hydrophobic surfaces[7], super barrier thin films[8], flame retardant materials[9], moldable hydrogels[10], hierarchical structures[11], and drug delivery devices[12]. Although the above-mentioned reports have investigated synthetic sNPs for a range of applications, their interaction with biological tissue at cellular levels has not yet been taken into consideration. Here, we present bioactive sNPs based on synthetic silicate (Laponite ($Na^+_{0.7}[(Mg_{5.5}Li_{0.3})Si_8O_{20}(OH)_4]^-_{0.7}$)) that are cytocompatible and promote *in vitro* osteogenic differentiation of human mesenchymal stem cells (hMSCs) in the absence of any osteoinductive factor, such as BMP-2 or dexamethasone. To our knowledge, this is the first study that shows sNPs can induce osteogenic differentiation of hMSCs. The impetus for introducing this material for biological applications is due to the urgent unmet needs for bioactive materials for therapeutic applications in the field of regenerative medicine.

Synthetic sNPs are plate-like poly-ions composed of simple or complex salts of silicic acids with a heterogeneous charge distribution and patchy interactions[13]. Synthetic sNPs forms physical gel at higher concentration (40 mg/mL) due to electrostatic and van der Waals interactions that result in the formation of a “house of card” structure[14]. This is attributed to the discotic charged nature and patchy interactions of the silicate sNPs[15]. Due to strong physical interaction between sNPs, they have been extensively used for various commercial and industrial applications such as food additives, filler materials (glass, ceramics,

refractories), catalysts, adsorbents and anticaking agents, but have not been previously considered for biological and medical applications[16].

We are highly interested to introduce these sNPs to the field of regenerative medicine, as their dissolution products have properties that are useful for TE applications[17]. Synthetic sNPs (such as Laponite) dissociate into non-toxic products (Na^+, Mg^{2+}, $Si(OH)_4$, Li^+) in aqueous solution[14]. It is reported that magnesium ions play a significant role in cellular adhesion to biomaterial surfaces mediated by the adhesion proteins of the integrin family[18]. Orthosilicic acid ($Si(OH)_4$), another dissolution product of silicate, promote collagen type I synthesis[19] and has been shown to be absorbed by the human body[20]. Additionally, lithium activates Wnt-responsive genes by inhibiting the glycogen synthase kinase-3-[beta] activity that controls osteogenesis via regulating Runt-related transcription factor-2 (RUNX2) activity[21]. Thus, we believe that sNPs may have potential in triggering specific cellular responses towards bone-related TE approaches.

V.2. MATERIALS AND METHODS

V.2.1. Materials

Synthetic sNPs (Laponite XLG) containing SiO_2 (59.5%), MgO (27.5%), Na_2O (2.8%) and Li_2O (0.8%) with low heavy metals content was kindly gifted by Southern Clay Products, Inc. (Louisville, USA). The specific surface area (Brunauer–Emmett–Teller, BET) of sNPs was 370 m^2/g and bulk density of 1 mg/cm^3. Hydrodynamic size and zeta potential of the sNPs were determined in deionized water (DI) and PBS using a 633 nm laser in a Malvern ZEN3600 (Malvern Instruments, UK). sNPs were dissolved in the solution using vortexes (10 minutes) and ultrasonication (10 minutes). The refractive index of sNPs was selected as 1.5 (obtained from MSDS of Laponite XLG). The transmission electron microscopy (TEM) images of sNPs was obtained using JEOL JEM-1400 TEM (JEM1400) installed with cool beam illumination system (resolution: 0.2 nm line, 0.38 nm point) and 11 Mpix AMT cooled CCD camera at 80 KV. The sample was prepared by dispersing silicate nanoplatelets in DI/ethanol solution and then putting a drop on the TEM grid and allowed it to dry in vacuum.

V.2.2. Human mesenchymal stem cell culture

Bone marrow-derived hMSCs (Lonza, Switzerland) were grown in normal growth (N) medium (Poietics™ MSCGM™ BulletKit™ (Lonza, Switzerland). The cells were cultured until 70-75% confluence and were used before passage 5 for all the experiments. The cells were trypsinized (trypsin/EDTA, Lonza, Switzerland) and seeded in 24-well plates at the density of 4,000 cells/well (2,000 cells/cm^2) in normal growth medium. After 24 hours, the media was replaced with the N, osteoconductive (OC) and osteoinductive (OI) media. OC

medium was supplemented with 10mM β-glycerophosphate (Sigma, Germany) and 50µg/mL L-ascorbic acid 2-phosphate sesquimagnesium salt hydrate (Sigma, Germany) and OI medium consisted in supplemented with 10^{-8}M dexamethasone (Sigma, Germany) to induce osteogenic differentiation of hMSCs. We used N and OC media without sNPs as negative controls.

V.2.3. Cytotoxicity assays: LDH and reactive species (SOx/NOx)

Cytotoxicity of sNPs was determined using (3-(4,5-dimethylthiazol-2-yl)-2,5-diphenyltetrazolium bromide (MTT) and lactate dehydrogenase (LDH) assay. Pre-seeded hMSCs were treated with different amount of sNPs solution for 24 hours. MTT assay was performed as described by the manufacturer's protocol (ATCC, USA). In brief, media was removed and replaced with 100µL of fresh culture medium and 10µL of MTT solution to each well. Samples were incubated at 37°C for 4 hours. After the incubation, 100µL of lysis buffer was added to each well and incubated at 37°C for 2 hours. Samples were nicely mixed and absorbance was measured at 540 nm. For LDH assay (Promega, USA), following the manufacturers protocol, the culture medium of untreated ells were used as negative control (0%) and a suspension of lysed cells was used as positive control (100%). It was made sure that the cell seeding in all the wells was uniform. Cells were incubated with the samples at 37°C for 24 hours. At the end of the incubation time, cells were centrifuged at 600*xg* for 10 min. 10µl supernatant from each sample well and the controls were transferred into 96 well plates and 100µl LDH reaction mix was added to each well and incubated for 30 min at room temperature. Absorbance measurement was done at 450 nm.

Intracellular production of (a) superoxide was evaluated using dihydroethidium (DHE, Molecular Probes, Eugene, USA) oxidation assay and (b) nitric oxide was assessed using 4,5-diaminofluorescein diacetate (DAF-2DA, Calbiochem, San Diego, USA) oxidation assay. hMSCs ($2x10^4$ cells), passage 4, were seeded on 24-well plate and allowed to adhere. After reaching 70% confluency, cells were pre-incubated with 25µM DHE for 10 min and 10µM DAF-2DA for 30 min at 37°C. Cells were then washed with PBS and sNPs suspension (0, 1, 10, 100, 1000, 10000, 20000 µg/mL) in phenol-red-free DMEM without FBS was added to the cells. After 2 hours of incubation, cells were washed with PBS and then fixed with 4% paraformaldehyde (pFA) in PBS for 40 min. Samples were examined using Nikon Eclipse TE2000-U fluorescence microscope (Japan) equipped with FITC filter (ex: 450–505 nm; polychromatic mirror: 510–555 nm; barrier filter: 515–545 nm) and FITC-Texas Red filter (ex: 560–580 nm; polychromatic mirror: 585–665 nm; barrier filter: 600–650 nm).

V.2.4. Alkaline phosphatase activity

Alkaline phosphatase (ALP) activity was measured using a colorimetric endpoint assay (abcam, USA), which quantified the conversion of *p*-nitrophenol phosphate (pNPP) to yellow *p*-nitrophenol (pNP) by ALP enzyme. Briefly, samples and the assay buffer solution of 5mM *pNPP* were added to a 96-well plate. After 1 hour of incubation, the absorbance was read at 405 nm in a microplate reader (Epoch microplate reader, Biotek, USA). A standard curve was made from standards (0–20µM) prepared with a *pNPP* solution. Sample and standard triplicates were analyzed and sample concentrations read off from the standard curve. The amount of double-stranded DNA (dsDNA) was measured using a PicoGreen dsDNA Quantification Kit (Invitrogen, USA). For this purpose, cells were washed with PBS after each end point. 1ml filtered DI water was added to each well and then the cell lysate was transferred to eppendorfs and stored at −80°C. Prior to DNA quantification, samples were thawed and sonicated for 15 min. Experimental samples and standards (0–2µg/ml) were added to a 96-well plate and analysed according to the manufacturer instructions. Fluorescence was quantified using a microplate reader (SpectraMax M5) at an excitation at 480 nm and emission at 520 nm.

V.2.5. Quantification of extracellular matrix protein content

HMSCs were allowed to grow in presence of different concentration of sNPs for 21 days. After 21 days, cells were washed thrice to remove any intracellular component or dissolved protein. Then 2% sodium dodecyl sulphate (SDS) solution was added to samples for 6 hours. This step aimed to dissociate and dissolve the proteins constituting the extracellular matrix. The amount of protein was determined by Micro BCA Protein Assay Kit (Thermo Fisher Scientific, USA) according to manufacturer's protocol.

V.2.6. Immunocytochemistry

Cells were cultured in N, OC and OI media in the presence of sNPs as described above. At different time points (0, 7, 14, 21 and 28 days) after the addition of sNPs, cells were fixed with 4% pFA for 20 min, washed again with PBS and stored at 4ºC until cytochemistry labeling. Cells were permeabilized with 0.1% Triton-100x solution for 5 minutes and nonspecific binding blocked with a 10% goat serum solution (Invitrogen). Cells were incubated overnight at 4ºC with the primary antibodies: mouse monoclonal anti-human RUNX2 (1:100 dilution, Millipore, USA), mouse monoclonal anti-human osteocalcin (1:100 dilution, Abcam, USA) and mouse monoclonal anti-human osteopontin (1:100 dilution, Abcam, USA). After incubation, cells were washed 3 times with PBS for 5 minutes and incubated for one hour with the appropriate secondary antibody, either Alexa Fluor 488

rabbit anti-mouse (IgG) (Invitrogen, USA), or Alexa Fluor 594 goat anti-mouse (IgG) (Invitrogen, USA), at a 1:100 dilution. Cell nuclei were counterstained with 4,6-diamidino-2-phenyindole dilactate (DAPI), at a 1:1000 dilution in PBS, for 10 minutes and then washed 3 times. Negative control samples were not subjected to primary antibody incubation. Immunolabeling was qualitatively analyzed under a Nikon Eclipse TE2000-U fluorescence microscope (Japan) equipped with FITC filter (ex: 450–505 nm; polychromatic mirror: 510–555 nm; barrier filter: 515–545 nm) and FITC-Texas Red filter (ex: 560–580 nm; polychromatic mirror: 585–665 nm; barrier filter: 600–650 nm).

V.2.7. Alizarin Red S staining

At different time points (1, 7, 14, 21 and 21 days), cells were fixed with 4% pFA (20 minutes) and then washed three times with PBS. The fixed cell were further washed with DI in order to remove any salt residues and then a solution of 2% (wt/v) Alizarin Red S (ARS, Sigma Aldrich, Germany) with a pH adjusted to 4.2, was added so that it covered the entire surface of the wells containing cells. After an incubation of 10 minutes at room temperature, the excess of ARS was washed with DI. The ARS staining was imaged using a Zeiss Discovery V8 Stereo Microscope (DISV8). To quantify the orange-red coloration of ARS, 10% acetic acid (Sigma Aldrich, Germany) was added to the cells. After an overnight incubation, the cells with the acetic acid were transferred to tubes and centrifuged for 15 minutes at 20,000*xg*. The supernatant was removed to other tubes and neutralized with ammonium hydroxide, 10% (Sigma Aldrich, Germany). 100µL of each sample was added to 96-well plates and the absorbance was read at 405nm was read using an Epoch microplate reader (Biotek, USA).

V.2.8. Flow cytometry

Before differentiation, hMSCs cultured in normal media were harvested with trypsin and analyzed for the presence of mesenchymal panel surface markers. About 10^6 cells were incubated for 1 hour in ice with the primary antibodies at an optimized dilution as follows: mouse anti-human CD31-APC (R&D Systems, Germany), mouse anti-human CD34-PE (BD Bioscience, USA), mouse anti-human CD45-FITC (BD Bioscience, USA), CD73-PE (BD Bioscience, USA), mouse anti-human CD90-APC (eBioscience, USA) and mouse anti-human CD105-FITC (AbD Serotec, UK). After washing with PBS, the cells were resuspended in acquisition buffer until further analysis. At least 20,000 events were acquired using a BD LSRFortessa Cell Analyzer High Throughput Sampler (BD Bioscience, USA). The results were analyzed with the CellQuest software (BD Bioscience, USA). The number

of positive cells was expressed as a percentage of the total cell number when compared with non-labeled cells.

V.2.9. Cytoskeleton organization

Cell morphology and cytoskeleton organization were evaluated by treating the pre-seeded hMSCs (5,000 cells/well in 24-well plate) on circular glass coverslips (number 1.5) in 1 mL of media, with different concentration of silicate nanoplatelets. After 24 hours, the media was removed and the cells were washed with PBS twice and were fixed with 4% pFA (in PBS), followed by PBS washing three times. Subsequently the cells were treated with 0.1% Triton X100 in PBS. The actin filaments (F-actin) were stained with Alexa Fluor 488 Phalloidin (Invitrogen, USA, 25µL/ml of 1% BSA in PBS) for 20 minutes.). After the incubation, cells were washed thrice with PBS. The coverslips were loaded in mounting media on glass slides and sealed. The slides were stored in dark, at 4°C until imaged. Imaging was performed using a confocal microscopy (Olympus FV1000).

V.2.10. Metabolic activity assay (Alamar Blue)

The metabolic activity of hMSCs was determined using alamarBlue® assay (Invitrogen, USA). Alamar blue is an indicator dye, which incorporates an oxidation-reduction reaction. Active ingredient of Alamar Blue is resazurin, which is a non-toxic, cell permeable compound and virtually non-fluorescent. Upon entering cells, viable cells reduce resazurin to resorufin, which produces very bright red fluorescence. This assay was performed on the day 0, 1, 3, 7, 10, 14, 21 and 28 according the manufacture's protocol. After predetermined duration, the media was removed and the cells were washed twice with PBS. Then the PBS was replaced with 10% (v/v) of Alamar blue reagent and incubated at 37°C, 5% CO_2 humidified atmosphere for 3 hours. At the end of the incubation period the supernatant of the cultures was aliquoted into 96-well plate in triplicates and a colorimetric reading was performed using a microplate reader (Epoch, Biotek, USA) at 570 nm and 600 nm, respectively excitation and emission wavelengths. Culture medium was used as negative control. After supernatant removal, cells were washed in PBS and fresh medium was added.

V.2.11. Statistical analysis

Data are presented as mean ± standard deviation (SD) of the mean values. Statistical analysis was performed using GraphPad Prism 5.00 software (San Diego, USA) to determine the statistical differences. Statistical differences ($p<0.05$) were determined using one-way analysis of variance (ANOVA) for an average of three to six replicates followed by post hoc Tukey's method to test all pair-wise mean comparisons.

V.3. RESULTS AND DISCUSSION

Intrinsic and extrinsic properties of sNPs such as specific surface areas, surface charge, functionality, size and shape, play direct roles in determining specific cellular responses[22]. Synthetic sNPs show a disc-shaped morphology, 20–30 nm in diameter (**Figure V.1A** and **Supplemental Figure V.1**). The effect of sNPs on cellular metabolism was investigated by monitoring the metabolic activity of adhered hMSCs. The metabolic activity was normalized to the hMSCs control (without any sNPs) to determine the dose response. The addition of sNPs did not significantly affect the metabolic activity of hMSCs until the concentration of sNPs reached 1 mg/mL (**Figure V.1B**). However, at higher sNPs concentrations (5 mg/mL) the metabolic activity dropped drastically. The concentration at which the metabolic activity of hMSCs was reduced to 50% was regarded as the half maximal inhibitory concentration (IC_{50}). The IC_{50} for sNPs was determined by fitting the dose response curve and was obtained as 4 mg/mL of sNPs concentration. A possible explanation to the decrease in the metabolic activity of hMSCs could be that, at a high sNPs concentration, a significant amount of sNPs adhere to the cell surface and are internalized, which restricts the cellular functionality. The confocal imaging confirmed the attachment of the sNPs to the cells and also showed the internalization of the sNPs within the cell body as seen by the middle section of the z -stacked images of the cells (**Figure V.1C**). Additionally, the charged sNPs also interact with the media proteins and results in the formation of aggregates that cannot be engulfed by the cells. This might also contribute to decrease in metabolic activity at higher sNPs concentrations. Contrary to other bioactive materials such as hydroxyapatite nanoparticles (size = 50 nm, $IC_{50} \approx 250$ µ g/mL)[23] and silica nanoparticles (size = 30 nm, $IC_{50} \approx$ 400–500 µg/mL)[24], synthetic sNPs show cytotoxicity at 10-fold higher concentration ($IC_{50} \approx$ 4 mg/mL).

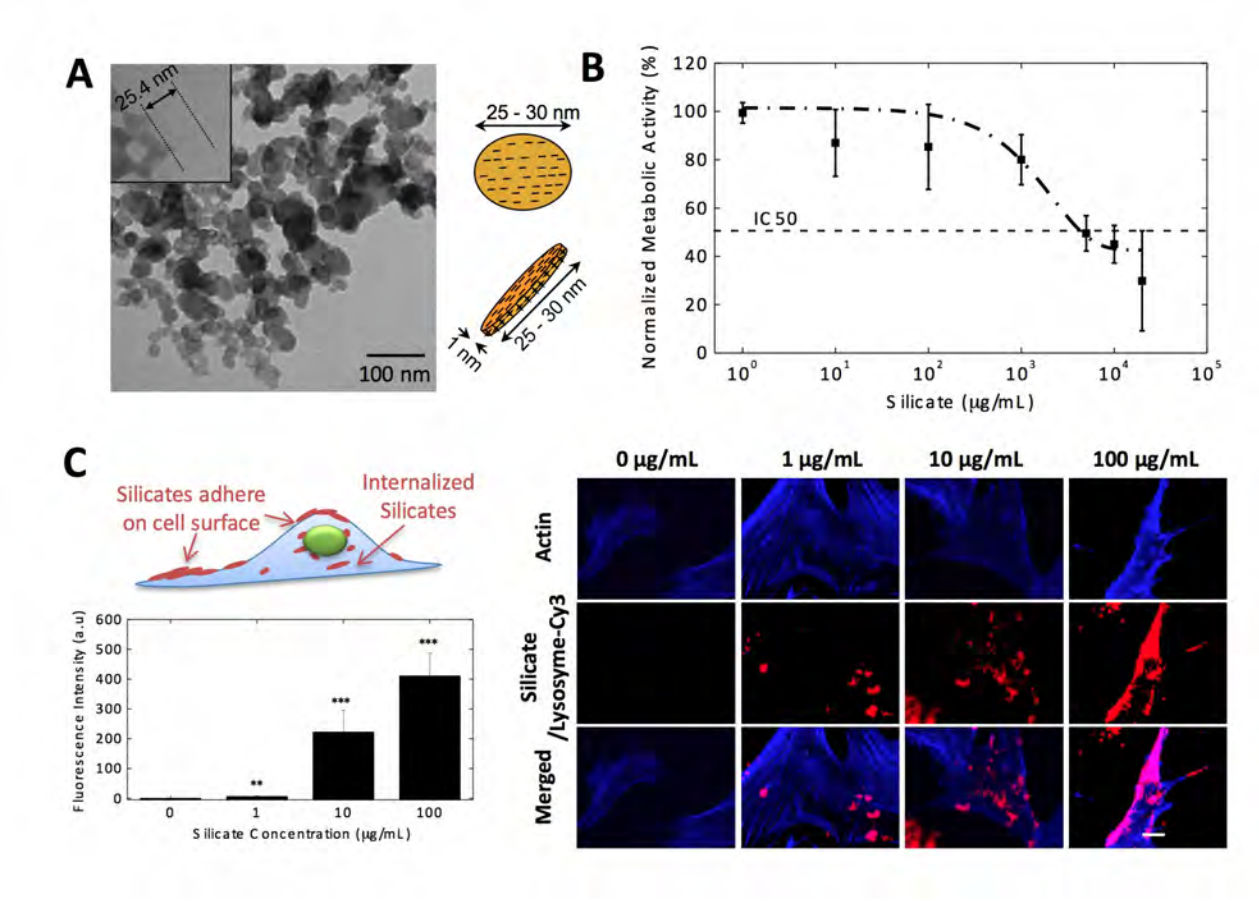

Figure V.1. Cytotoxicity and cellular evaluation of sNPs. (**A**) TEM image showing the size and morphology of sNPs. The inset shows the image of a single sNP platelet with 25.4 nm in diameter. (**B**) IC_{50} of the sNPs was assessed by evaluating the metabolic activity of hMSCs in the presence of sNPs in the media using MTT assay at 48 hours of post seeding. The metabolic activity was normalized with the control (without any sNPs). The dotted line shows fitted dose response curve, and the IC_{50} was found at sNPs concentration of 4 mg/mL. (**C**) Internalization of sNPs was determined by incubating hMSCs with different concentrations of sNPs (0, 1, 10 and 100µg/mL). Cells cytoskeleton was stained for F-actin (blue) and the sNPs were tagged with Cy3-labeled Lysozyme (red). Fluorescence images depicting cells fibroblast-like morphology, specific for hMSCs, as noticed by the stretch of F-actin (blue), which also indicates that the addition of sNPs does not interfere with the adhesion properties of the cells. The overlapping of F-actin with sNPs suggests the high interaction between cells and sNPs, both at membrane and cytoplasmatic levels (scale bar = 20 µm). The quantification of the fluorescence intensity indicates significant uptake of sNPs by hMSCs was observed due to the increase in sNPs concentrations, confirming the strong affinity of the sNPs towards hMSCs (one-way ANOVA, followed by Tukey post-hoc, *$p < 0.05$, ***$p < 0.001$).

The high surface area of sNPs, due to their disc shaped morphology, provides them with a high chemical reactivity as well as high biological activity. The chemical reactivity and cytotoxicity of sNPs can also be determined by monitoring the generation of intracellular reactive oxygen species (ROS), such as super oxide (SOx) and reactive nitrogen species

(RNS), such as nitric oxide (NOx), as an evaluation of the immediate responses of cells when put in contact with the sNPs. An appropriate amount of ROS and RNS plays a vital role in the functionality of stem cells, which directly affects their self-renewal capacity, and differentiation potential[25]. However, an excessive amount of ROS and RNS results in increased oxidative stress, inflammation and consequent damage to proteins, membranes and DNA, triggering a series of events that can lead to senescence, apoptosis and/or stem cell transformation[25].

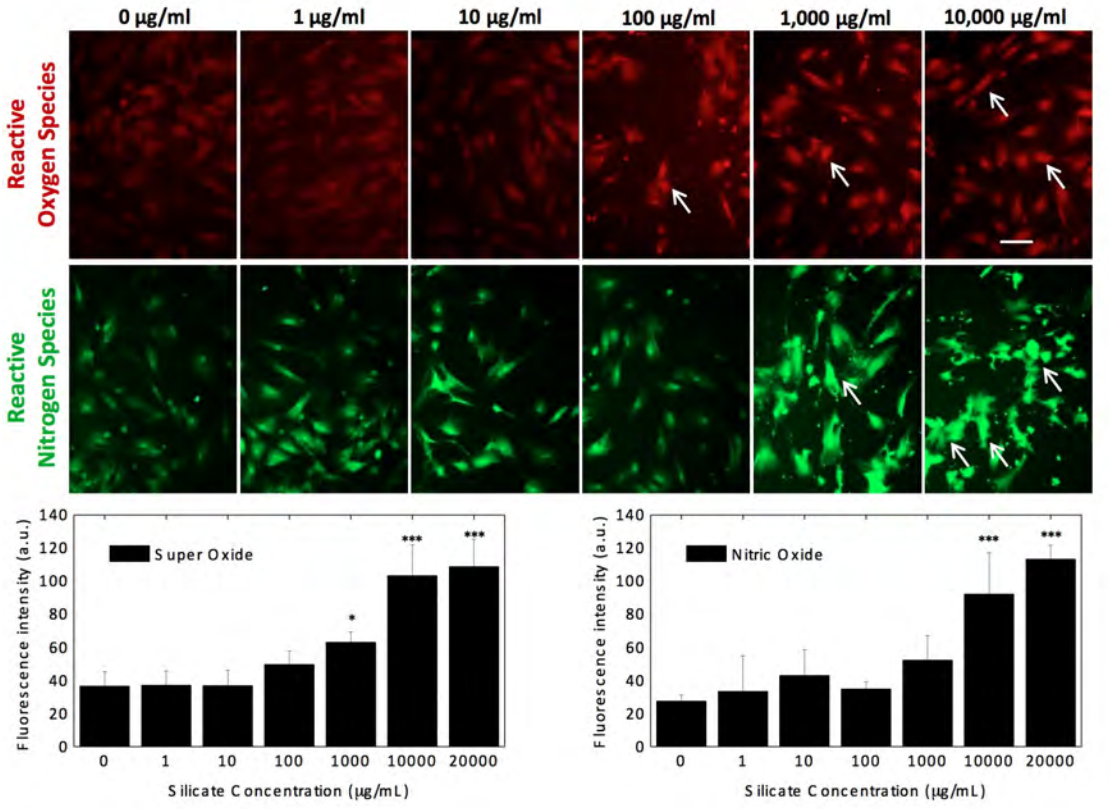

Figure V.2. The formation of radicals as a measure of intracellular stress that usually generates a cytotoxic response was determined. The intracellular production of two reactive species, ROS and RNS, was evaluated after hMSCs incubation in the presence of different sNPs concentrations. As the sNPs concentration increased, no intracellular ROS was noticed until 100µg/mL. However, at higher sNPs concentrations (>1 mg/mL), a significant increase in ROS was observed as quantified using ImageJ. Similarly, at higher sNPs concentrations (>10 mg/mL), a significantly higher amount of RNS was observed. These results are in agreement with the IC_{50} results (determined by MTT assay) that indicated that particle concentration >1 mg/mL affects cellular function. Therefore, further studies were carried out with the sNPs concentration below 1 mg/mL (scale bar = 100 µm) (one-way ANOVA followed by Tukey post-hoc, *$p < 0.05$, ***$p < 0.001$).

To investigate the interaction of sNPs with hMSCs, pre-seeded hMSCs were exposed to several sNPs concentrations (0–20 mg/mL). The addition of sNPs to hMSCs resulted in the enhanced production of ROS and RNS. At a low sNPs concentration (<1 mg/mL), hMSCs

were able to effectively manage oxidative stress, but at higher sNPs concentrations (>1 mg/mL), a significant increase in ROS and RNS production was observed (**Figure V.2**). These results are in agreement with the cytotoxicity findings that highlight that the cellular metabolic activity was affected at high concentrations of sNPs (>1 mg/mL). The high concentration of sNPs enables the formation of large aggregates that can jeopardize the internalization efficiency of the sNPs, while at the same time, generating external stress to the cell cytoskeleton.

We further investigated the cytotoxicity of sNPs by quantifying plasma membrane damage using LDH assay. It was also observed that the addition of sNPs below the IC_{50} values did not change the LDH levels in media, compared with the control (without sNPs), providing additional evidence of cytocompatibility of sNPs in the given concentration range (**Supplemental Figure V.2**). Furthermore, attachment and internalization of sNPs did not alter cellular morphology and the function of the hMSCs, as we did not observe any alterations in cell-proliferation profiles over the period of 28 days (**Supplemental Figure V.3**). Based on the cell-nanoplatelets interactions, cytotoxicity, and proliferation studies, we selected sNPs concentrations of 0, 1, 10 and 100 µg/mL for further long-term studies. Overall, it can be concluded that sNPs show nearly no cytotoxicity at concentrations lower than 1 mg/mL and can potentially be used for biomedical applications.

We hypothesize that these sNPs possess a bioactive feature that promotes and further enhances the osteogenic phenotype of hMSCs. Furthermore, we believe that these sNPs could act as an osteoinductive agent when cells are cultured in N medium, by triggering the formation of mineralized matrix. The bioactivity of sNPs was investigated by monitoring the ALP activity of hMSCs and the production of mineralized matrix in N, OC and OI media. We had chosen different culture media to investigate the effect of sNPs on the osteogenic differentiation of hMSCs in the absence or presence of osteoinducting factors (such as dexamethasone). The N medium is a maintenance medium that does not trigger the osteogenic differentiation of hMSCs[26]. On the other hand, OC medium (N medium supplemented with β-glycerophosphate and ascorbic acid salts) supports the osteogenic differentiation of hMSCs and also promotes the formation of mineralized matrix in presence of bioactive materials[26]. In contrast, the OI (N medium supplemented with β-glycerophosphate, ascorbic acid and dexamethasone) induces and supports the osteogenic differentiation of hMSCs[26].

Amongst the major osteogenic hallmarks, the up-regulation of ALP activity is a key event occurring during the early time points of osteogenesis[27]. In N medium, residual ALP activity was observed that was stable during the culture period (**Supplemental Figure V.4**), which was considered as a residual activity of non-differentiated hMSCs, we did not observe any

significant increase in ALP activity due to the addition of sNPs in N medium. On the other hand, an increase in ALP activity was observed in OC medium with a peak at day 21 (**Figure V.3A**). The addition of sNPs significantly enhances the upregulation of ALP activity, indicating that the presence of sNPs within the intra- and extra-cellular environment can trigger an up-regulation of ALP, correlated with the first check-point for osteogenic differentiation. More than a 3-fold increase in peak ALP activity was observed due to the addition of a small amount of sNPs (1 and 10 µg/mL) in OC media compared to the control (without sNPs in OC media). As expected, in OI media, ALP peak was shifted towards day 14, due to the addition of dexamethasone, known for triggering the osteogenic differentiation. An almost 2-fold increase in peak ALP activity was observed due to the addition of sNPs (1 µg/mL). Moreover, it is important to note that the addition of silicates (1 µg/mL) has a similar effect in ALP peak activity and cellular organization (**Supplemental Figure V.5**) when compared to the positive control (hMSCs in OI media). Overall, the results indicate that sNPs can support and sustain the upregulation of ALP activity without the addition of dexamethasone.

At the same time, it is equally important for the cells to produce extracellular matrix (ECM), followed by a subsequent mineralization. The effect of sNPs on the production of ECM was investigated by determining the amount of insoluble proteins after 21 days. We show that the addition of sNPs significantly enhanced the ECM production (**Figure V.3A**). Further evaluation of ECM indicates that cells subjected to sNPs are characterized by an increase in the RUNX2 and an enhanced production of osteo-related proteins, like osteocalcin (OCN) and osteopontin (OPN) (**Figure V.3B-C**). RUNX2 belongs to the RUNX family of transcription factors and is exclusively expressed in mineralized tissues[28]. It is considered as a focal point for integration of a variety of signals affecting osteogenesis as it stimulates osteo-related genes that encode type I collagen, OCN, and OPN[28]. We observed that the addition of sNPs significantly promotes RUNX2 expression. In the OC medium condition, the addition of sNPs significantly promotes an increase of RUNX2 when compared with the OC medium without sNPs. On the other hand, in the OI condition the effect is similar.

Concomitantly, we also evaluated the presence of osteo-related proteins (OCN, OPN) that constitute the ECM produced by osteoblast-like cells. OCN is the most abundant bone-specific non-collagenous protein synthesized by osteoblasts and serves as a marker to evaluate osteogenic maturation and bone formation[29]. On the other hand, OPN is a structural protein synthesized by pre-osteoblasts, osteoblasts, and osteocytes, and is considered an important factor in bone remodeling[30]. The presence of these two proteins sets the basis for the upcoming mineralization as they sustain the formation of bone-like nodules that can further develop into complex 3D mineralized structures. Due to the addition

of sNPs, an enhancement in the deposition of these bone-related proteins was observed (**Figure V.3B-C**). The presence of the sNPs results in two-fold increase in bone-related matrix proteins deposition (OCN and OPN) when compared to hMSCs subjected to dexamethasone. Taken together, we believe that the sNPs act as a trigger from both the exterior (by acting as growth nuclei for matrix deposition), as well as from the interior of the cells (by proving the chemical cues to the cells organelle to shift their metabolism towards the osteogenic differentiation). Even more, the concentration of sNPs directly affects the intensity of this outcome and the further mineralization process.

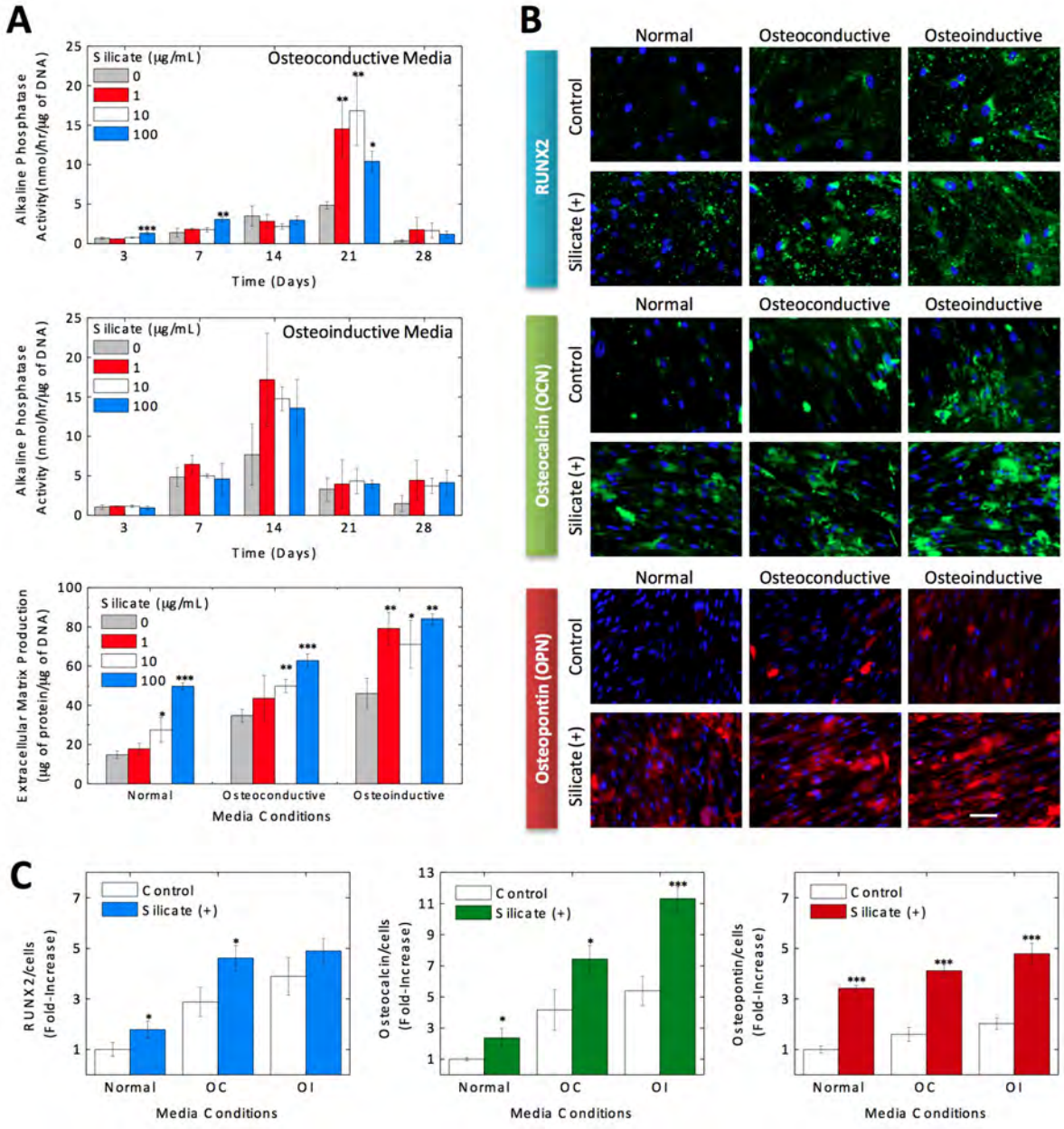

Figure V.3. Effect of sNPs on hMSCs differentiation. (A) The addition of sNPs up-regulates alkaline ALP activity of hMSCs. Cells grown in N medium show a residual ALP activity, which is stable during the considered cell culture period (**Supplemental Figure V.3**). In OC medium, an up-regulation of

ALP activity was observed and a ALP peak was observed at day 21. The addition of small amounts of sNPs (1 and 10 µg/mL) resulted in an almost 3-fold increase in ALP activity. On the other side, for the cells grown in OI medium, the ALP activity peaks shifts to an earlier time point (day 14). These data suggest that sNPs enhance the ALP activity that results in osteogenesis. Addition of sNPs significantly enhances production of ECM after 21 days. A similar trend was observed in OC and OI media. (**B**) The increase in the RUNX2 (green) and production of bone-related proteins, such as OCN (green) and OPN (red) was observed due to the addition of sNPs (scale bar = 200 µm). Cells in N medium, without sNPs, acted as negative control, whereas cells in OI served as a positive control. Cell nuclei were counterstained with DAPI (blue). (**C**) The protein production was quantified using image analysis from the fluorescence images. The intensity of protein per cell was quantified and later normalized by the control (hMSCs in N media with no sNPs) to obtain the fold increase in the production of protein. The addition of sNPs (100 µg/mL) results in the production of RUNX2, OCN, and OPN in N medium, which indicates a strong bioactive character of sNPs. The addition of OC and OI media further enhances the production of bone-related proteins. The results indicate that the sNPs promote an increase in the production of essential proteins for the osteogenesis of hMSCs (one-way ANOVA followed by Tukey post-hoc, *$p < 0.05$, **$p < 0.01$, ***$p < 0.001$).

We analyzed the efficiency of the mineralization stage by using the Alizarin Red S staining as a marker for the inorganic calcium, a common characteristic to bone-like structures. **Figure V.4** and **Supplemental Figures V.6** and **V.7** show the effect of sNPs concentration on the formation of mineralized matrix in N, OC and OI media on days 14 and 21. The effect of sNPs on nodule formation was evident at higher sNPs concentrations (100 µg/mL) in N medium. These findings reinforce the statement that the sNPs can act as a promoter of osteogenic differentiation, by enhancing the protein production and its subsequent mineralization. On the other hand, in OC media, a significant increase in the number of nodules and the amount of mineralized matrix was observed due to addition of sNPs. The negative controls (N and OC media, without sNPs) did not show any nodules formation. These results indicate that sNPs are bioactive and promote osteogenic differentiation of hMSCs in the absence of other osteoinductive factors. Similar results were obtained in OI medium, where samples containing small amounts of sNPs had much higher amount of mineralized matrix compared to the positive control (OI medium without sNPs), underlining the role of sNPs in the enhancement of osteogenic differentiation efficiency.

Taken together, the data presented here clearly showcases that synthetic sNPs can induce osteogenic differentiation of stem cells in the absence of any external osteoinductive factors (e.g., dexamethasone). Our results indicate that these synthetic sNPs are cytocompatible and strongly interact with the cells. Even more, the presence of the sNPs triggers a set of events that follow the temporal pattern of osteogenic differentiation (ALP/ RUNX2 transcripts up-regulation, bone-related matrix protein deposition (OCN and OPN), followed by matrix

mineralization).

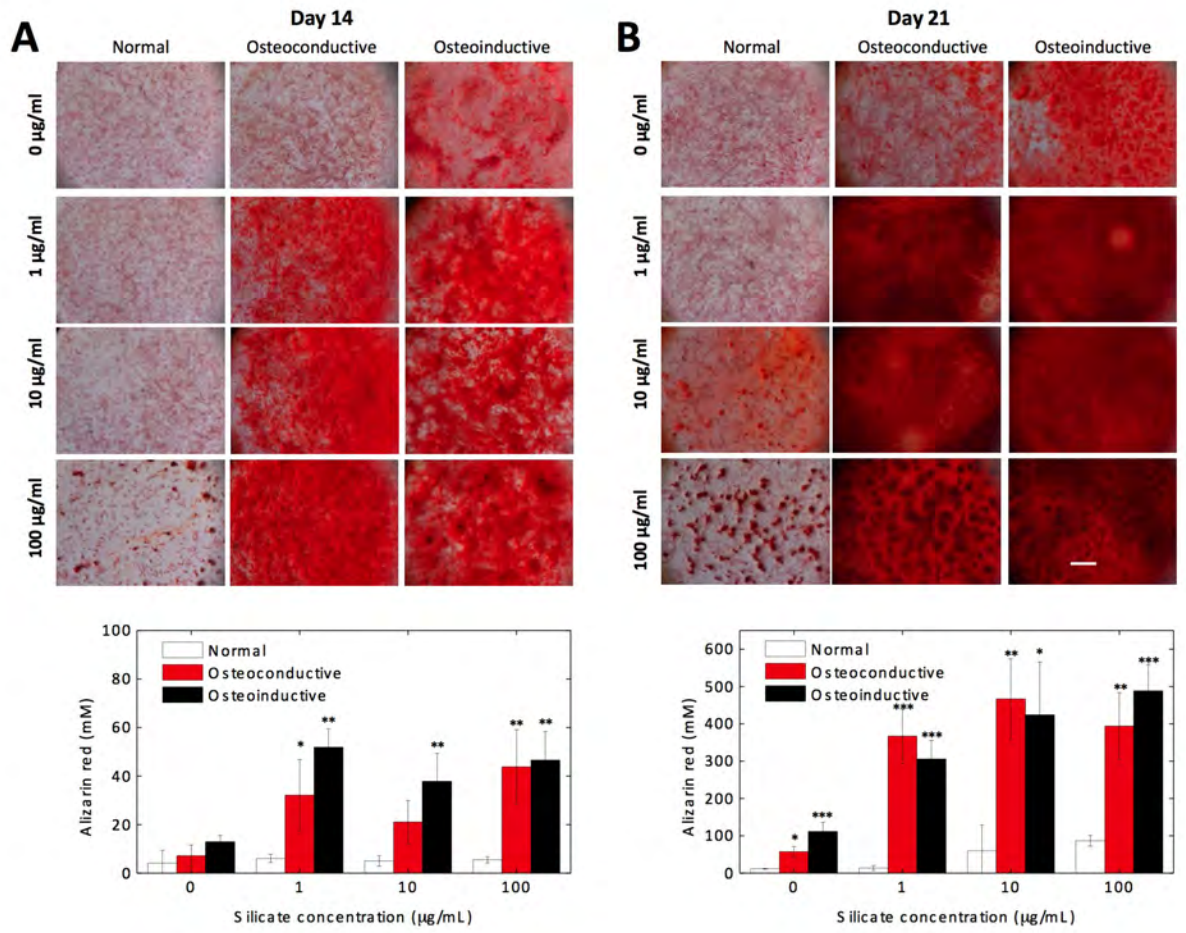

Figure V.4. Effect of sNPs on production of mineralized ECM. The mineralized matrix was stained with ARS on days 14 and 21. (**A**) At day 14, hMSCs were not able to produce any mineralized matrix in N medium (negative control). Similarly, in OC medium, no obvious mineralization was observed, however the presence of sNPs triggered the formation of large mineralized depots. In OI medium (positive control), formation of mineralized nodules was observed. Addition of sNPs significantly enhanced the production of mineralized matrix as determined by the quantification of ARS staining. (**B**) Similar behavior was observed on day 21. In N medium, mineralized matrix was not observed, but the addition of sNPs significantly enhanced the ability of hMSCs to promote the matrix mineralization. This indicates that the sNPs induce the reorganization and remodeling of the ECM towards osteogenesis. On the other hand, in OC and OI media, with the increase in sNPs composition, an enhanced calcification response was observed (scale bar = 1 mm) (one-way ANOVA followed by Tukey post-hoc, *p < 0.05, **p < 0.01, ***p < 0.001).

IV.4. CONCLUSIONS

The advantage of using silicate nanoplatelets as osteoinductive agents is that they are applied in a single dose, while other agents (dexamethasone and BMP-2) have to be added when changing the culture media (every 3–5 days). To our knowledge, this is the first study

showing that synthetic silicate nanoplatelets alone can induce osteogenic differentiation of hMSCs. This unique bioactive property of silicate nanoplatelets may be processed to construct devices such as injectable tissue repair matrixes, bio-active fillers, or therapeutic agent for triggering specific cellular responses towards bone-related tissue engineering approaches.

REFERENCES

1. (a) Langer, R.; Tirrell, D. A., Designing materials for biology and medicine. *Nature* **2004,** *428* (6982), 487-92; (b) Khademhosseini, A.; Vacanti, J. P.; Langer, R., Progress in tissue engineering. *Scientific American* **2009,** *300* (5), 64-71; (c) Peppas, N. A.; Langer, R., New challenges in biomaterials. *Science* **1994,** *263* (5154), 1715-20; (d) Khademhosseini, A.; Langer, R.; Borenstein, J.; Vacanti, J. P., Microscale technologies for tissue engineering and biology. *Proceedings of the National Academy of Sciences of the United States of America* **2006,** *103* (8), 2480-7.
2. (a) Lutolf, M. P.; Gilbert, P. M.; Blau, H. M., Designing materials to direct stem-cell fate. *Nature* **2009,** *462* (7272), 433-41; (b) Kraehenbuehl, T. P.; Langer, R.; Ferreira, L. S., Three-dimensional biomaterials for the study of human pluripotent stem cells. *Nature methods* **2011,** *8* (9), 731-6; (c) Dvir, T.; Timko, B. P.; Kohane, D. S.; Langer, R., Nanotechnological strategies for engineering complex tissues. *Nature nanotechnology* **2011,** *6* (1), 13-22.
3. Hench, L. L., Bioceramics: from concept to clinic. *Journal of the American Ceramic Society* **1991,** *74* (7), 1487-1510.
4. Urist, M. R., Bone: formation by autoinduction. *Science* **1965,** *150* (3698), 893-9.
5. (a) Podsiadlo, P.; Kaushik, A. K.; Arruda, E. M.; Waas, A. M.; Shim, B. S.; Xu, J.; Nandivada, H.; Pumplin, B. G.; Lahann, J.; Ramamoorthy, A.; Kotov, N. A., Ultrastrong and stiff layered polymer nanocomposites. *Science* **2007,** *318* (5847), 80-3; (b) Bonderer, L. J.; Studart, A. R.; Gauckler, L. J., Bioinspired design and assembly of platelet reinforced polymer films. *Science* **2008,** *319* (5866), 1069-73; (c) Gaharwar, A. K.; Schexnailder, P.; Kaul, V.; Akkus, O.; Zakharov, D.; Seifert, S.; Schmidt, G., Highly extensible bio-nanocomposite films with direction-dependent properties. *Advanced Functional Materials* **2010,** *20* (3), 429-436; (d) Gaharwar, A. K.; Schexnailder, P. J.; Kline, B. P.; Schmidt, G., Assessment of using laponite cross-linked poly(ethylene oxide) for controlled cell adhesion and mineralization. *Acta biomaterialia* **2011,** *7* (2), 568-77.
6. (a) Liff, S. M.; Kumar, N.; McKinley, G. H., High-performance elastomeric nanocomposites via solvent-exchange processing. *Nature materials* **2007,** *6* (1), 76-83; (b) Gaharwar, A. K.; Rivera, C. P.; Wu, C. J.; Schmidt, G., Transparent, elastomeric and tough hydrogels from poly(ethylene glycol) and silicate nanoparticles. *Acta biomaterialia* **2011,** *7* (12), 4139-48.
7. Lin, L.; Liu, M.; Chen, L.; Chen, P.; Ma, J.; Han, D.; Jiang, L., Bio-inspired hierarchical macromolecule-nanoclay hydrogels for robust underwater superoleophobicity. *Advanced materials* **2010,** *22* (43), 4826-30.
8. Priolo, M. A.; Gamboa, D.; Holder, K. M.; Grunlan, J. C., Super Gas Barrier of Transparent Polymer-Clay Multilayer Ultrathin Films. *Nano letters* **2010**.
9. Li, Y. C.; Schulz, J.; Mannen, S.; Delhom, C.; Condon, B.; Chang, S.; Zammarano, M.; Grunlan, J. C., Flame retardant behavior of polyelectrolyte-clay thin film assemblies on cotton fabric. *ACS nano* **2010,** *4* (6), 3325-37.
10. (a) Wang, Q.; Mynar, J. L.; Yoshida, M.; Lee, E.; Lee, M.; Okuro, K.; Kinbara, K.; Aida, T., High-water-content mouldable hydrogels by mixing clay and a dendritic molecular binder. *Nature* **2010,** *463* (7279), 339-43; (b) Haraguchi, K., Synthesis and properties of soft nanocomposite materials with novel organic/inorganic network structures. *Polymer Journal* **2011,** *43*, 223–241.
11. (a) Gaharwar, A. K.; Schexnailder, P. J.; Dundigalla, A.; White, J. D.; Matos-Perez, C. R.; Cloud, J. L.; Seifert, S.; Wilker, J. J.; Schmidt, G., Highly extensible bio-nanocomposite fibers. *Macromolecular rapid communications* **2011,** *32* (1), 50-7; (b) Dundigalla, A.; Lin Gibson, S.; Ferreiro, V.; Malwitz, M. M.; Schmidt, G., Unusual Multilayered structures in PEO/Laponite nanocomposite films. *Macromolecular rapid communications* **2005,** *26*, 143-149; (c) Gaharwar, A. K.; Kishore, V.; Rivera, C.; Bullock, W.; Wu, C. J.; Akkus, O.; Schmidt, G., Physically crosslinked nanocomposites from silicate-crosslinked PEO: mechanical properties and osteogenic differentiation of human mesenchymal stem cells. *Macromolecular bioscience* **2012,** *12* (6), 779-93.

12. Dawson, J. I.; Kanczler, J. M.; Yang, X. B.; Attard, G. S.; Oreffo, R. O., Clay gels for the delivery of regenerative microenvironments. *Advanced materials* **2011,** *23* (29), 3304-8.
13. (a) Pignon, F.; Piau, J. M.; Magnin, A., Structure and pertinent length scale of a discotic clay gel. *Physical review letters* **1996,** *76* (25), 4857-4860; (b) Ruzicka, B.; Zaccarelli, E.; Zulian, L.; Angelini, R.; Sztucki, M.; Moussaid, A.; Narayanan, T.; Sciortino, F., Observation of empty liquids and equilibrium gels in a colloidal clay. *Nature materials* **2011,** *10* (1), 56-60.
14. Thompson, D. W.; Butterworth, J. T., The nature of laponite and its aqueous dispersions. *Journal of Colloid and Interface Science* **1992,** *151*, 236–243.
15. Kegel, W. K.; Lekkerkerker, H. N., Colloidal gels: Clay goes patchy. *Nature materials* **2011,** *10* (1), 5-6.
16. Okada, A.; Usuki, A., Twenty years of polymer- clay nanocomposites. *Macromol Mater Eng* **2006,** *291*, 1449-76.
17. Hoppe, A.; Guldal, N. S.; Boccaccini, A. R., A review of the biological response to ionic dissolution products from bioactive glasses and glass-ceramics. *Biomaterials* **2011,** *32* (11), 2757-74.
18. (a) Zreiqat, H.; Howlett, C. R.; Zannettino, A.; Evans, P.; Schulze-Tanzil, G.; Knabe, C.; Shakibaei, M., Mechanisms of magnesium-stimulated adhesion of osteoblastic cells to commonly used orthopaedic implants. *Journal of biomedical materials research* **2002,** *62* (2), 175-84; (b) Anast, C. S.; Mohs, J. M.; Kaplan, S. L.; Burns, T. W., Evidence for parathyroid failure in magnesium deficiency. *Science* **1972,** *177* (4049), 606-8.
19. Reffitt, D. M.; Ogston, N.; Jugdaohsingh, R.; Cheung, H. F. J.; Evans, B. A. J.; R.P.H, T.; Powell, J. J.; Hampson, G. N., Orthosilicic acid stimulates collagen type 1 synthesis and osteoblastic differentiation in human osteoblast-like cells in vitro. *Bone* **2003,** *32*, 127–135
20. (a) Martin, K. R., The chemistry of silica and its potential health benefits. *J Nutr Health Aging* **2007,** *11* (2), 94-7; (b) Carlisle, E. M., Silicon: a possible factor in bone calcification. *Science* **1970,** *167* (3916), 279-80.
21. (a) De Sarno, P.; Li, X.; Jope, R. S., Regulation of Akt and glycogen synthase kinase-3 beta phosphorylation by sodium valproate and lithium. *Neuropharmacology* **2002,** *43* (7), 1158-64; (b) Kubota, T.; Michigami, T.; Ozono, K., Wnt signaling in bone metabolism. *Journal of bone and mineral metabolism* **2009,** *27* (3), 265-71; (c) Kugimiya, F.; Kawaguchi, H.; Ohba, S.; Kawamura, N.; Hirata, M.; Chikuda, H.; Azuma, Y.; Woodgett, J. R.; Nakamura, K.; Chung, U. I., GSK-3beta controls osteogenesis through regulating Runx2 activity. *PloS one* **2007,** *2* (9), e837.
22. Auffan, M.; Rose, J.; Bottero, J. Y.; Lowry, G. V.; Jolivet, J. P.; Wiesner, M. R., Towards a definition of inorganic nanoparticles from an environmental, health and safety perspective. *Nature nanotechnology* **2009,** *4* (10), 634-41.
23. Motskin, M.; Wright, D. M.; Muller, K.; Kyle, N.; Gard, T. G.; Porter, A. E.; Skepper, J. N., Hydroxyapatite nano and microparticles: correlation of particle properties with cytotoxicity and biostability. *Biomaterials* **2009,** *30* (19), 3307-17.
24. (a) Napierska, D.; Thomassen, L. C.; Rabolli, V.; Lison, D.; Gonzalez, L.; Kirsch-Volders, M.; Martens, J. A.; Hoet, P. H., Size-dependent cytotoxicity of monodisperse silica nanoparticles in human endothelial cells. *Small* **2009,** *5* (7), 846-53; (b) Park, M. V.; Annema, W.; Salvati, A.; Lesniak, A.; Elsaesser, A.; Barnes, C.; McKerr, G.; Howard, C. V.; Lynch, I.; Dawson, K. A.; Piersma, A. H.; de Jong, W. H., In vitro developmental toxicity test detects inhibition of stem cell differentiation by silica nanoparticles. *Toxicology and applied pharmacology* **2009,** *240* (1), 108-16.
25. Barry, F. P.; Murphy, J. M.; English, K.; Mahon, B. P., Immunogenicity of adult mesenchymal stem cells: lessons from the fetal allograft. *Stem cells and development* **2005,** *14* (3), 252-65.
26. Coelho, M. J.; Fernandes, M. H., Human bone cell cultures in biocompatibility testing. Part II: effect of ascorbic acid, beta-glycerophosphate and dexamethasone on osteoblastic differentiation. *Biomaterials* **2000,** *21* (11), 1095-102.
27. Pittenger, M. F.; Mackay, A. M.; Beck, S. C.; Jaiswal, R. K.; Douglas, R.; Mosca, J. D.; Moorman, M. A.; Simonetti, D. W.; Craig, S.; Marshak, D. R., Multilineage potential of adult human mesenchymal stem cells. *Science* **1999,** *284* (5411), 143-7.
28. Ducy, P.; Schinke, T.; Karsenty, G., The osteoblast: a sophisticated fibroblast under central surveillance. *Science* **2000,** *289* (5484), 1501-4.
29. Ducy, P.; Desbois, C.; Boyce, B.; Pinero, G.; Story, B.; Dunstan, C.; Smith, E.; Bonadio, J.; Goldstein, S.; Gundberg, C.; Bradley, A.; Karsenty, G., Increased bone formation in osteocalcin-deficient mice. *Nature* **1996,** *382* (6590), 448-52.
30. Butler, W. T., The nature and significance of osteopontin. *Connect Tissue Res.* **1989,** *23* (2-3), 123-36.

SUPPLEMENTAL INFORMATION

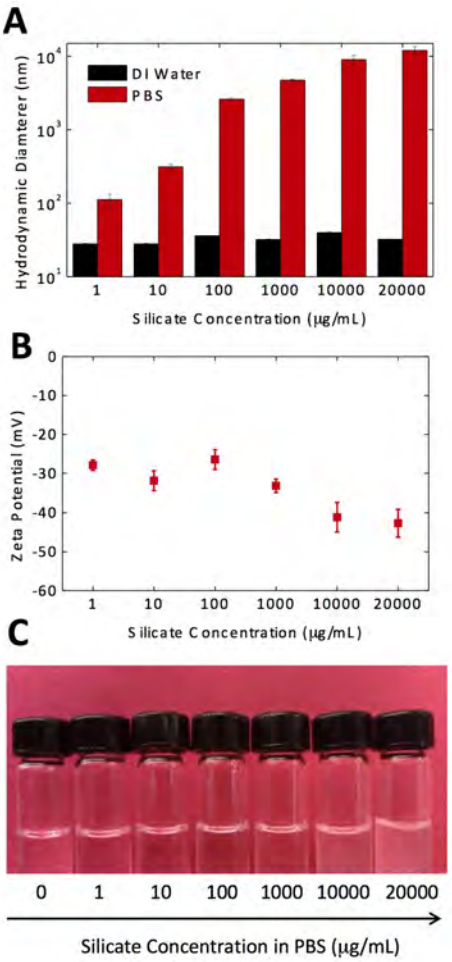

Supplemental Figure V.1. Physiochemical characterization of sNPs suspension at different concentrations in DI and PBS. These characteristics mainly govern nanoparticle interactions with other biomolecules present in *in vitro* and *in vivo* conditions. These interactions are determined by measuring aggregation, state of dispersion and effective surface charge (zeta potential) of sNPs in different biologically relevant solvents: DI, PBS and cell culture media. (**A**) The data for hydrodynamic diameter of the sNPs shows no aggregation at low concentrations in DI, whereas in PBS, a clustering effect is observed, probably due to the ionic interactions in the solution. The results indicated formation of aggregates (~200 nm) in solution containing 10µg/ml silicates (in PBS) and the size of aggregates increased to 4µm with an increase in sNPs concentration to 1 mg/mL. (**B**) Zeta potential measurements of sNPs suspensions in both DI and PBS show increase in the overall charge with increase in concentration, indicating a possible reorganization of the particles due to the interactions that occur at the nanoscale. (**C**) The increase of the hydrodynamic diameter when resuspended in PBS is evidenced by the turbidity of the solution as the sNPs concentration is increased. This is especially evident at higher concentration (10 and 20 mg/mL). Similar behavior was observed when sNPs were dissolved in different protein solutions (fibronectin, collagen, laminin and lysozyme) and cell culture media (containing FBS).

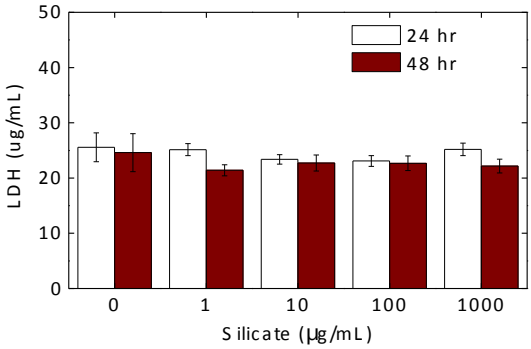

Supplemental Figure V.2. Effect of addition of sNPs on LDH release from hMSCs. We further investigated cytotoxicity of sNPs by quantifying plasma membrane damage using LDH assay. LDH is a stable enzyme present in all the cells and is released after the plasma membrane is damaged. Our results indicated that the addition of sNPs below the IC_{50} values did not significantly increase LDH levels after 24 and 48 hours compared to the control, providing evidence of cytocompatibility of sNPs in the given concentration range.

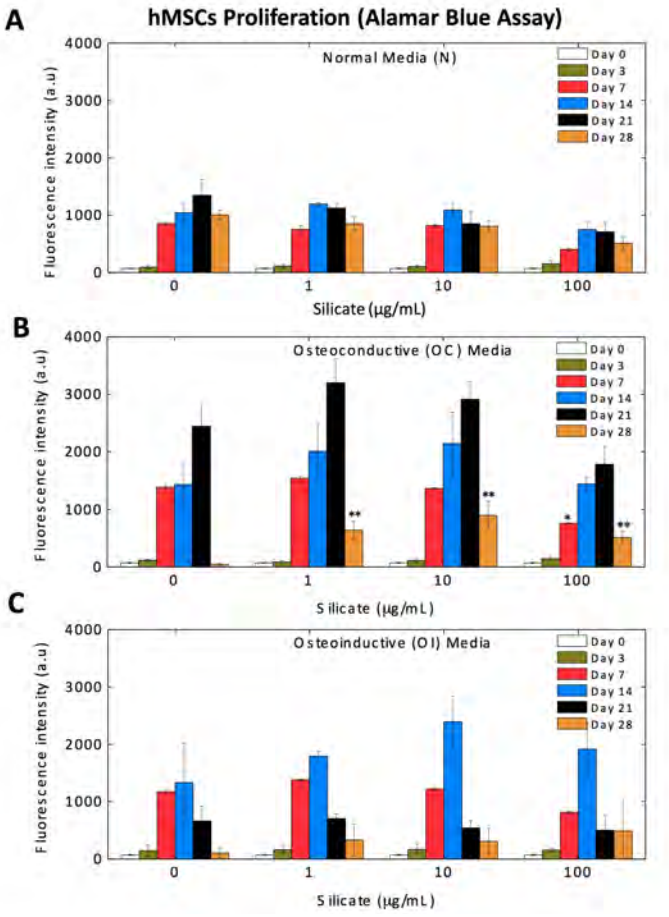

Supplemental Figure V.3. Effect of addition of sNPs on metabolic activity of hMSCs in N, OC and OI media as determined by alamarBlue® assay. Addition of sNPs does not significantly alter the metabolic activity of hMSCs that shows a typical profile for osteogenic differentiation. At early time

points, cells proliferate and organize on the culture surface. When reaching confluency, due to area restriction and already up-regulated ALP, the cells switch their metabolism towards the matrix deposition.

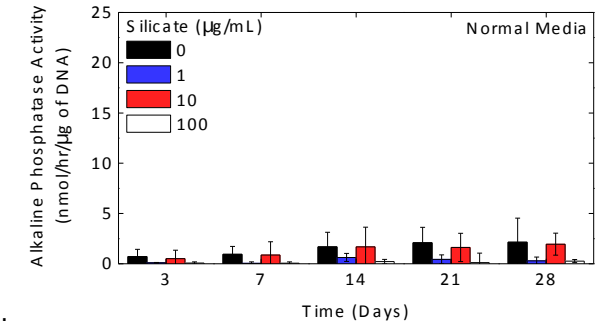

Supplemental Figure V.4. Residual ALP activity of hMSCs in N medium monitored for 28 days. We did not observe any significant change in ALP activity with the addition of sNPs in N medium.

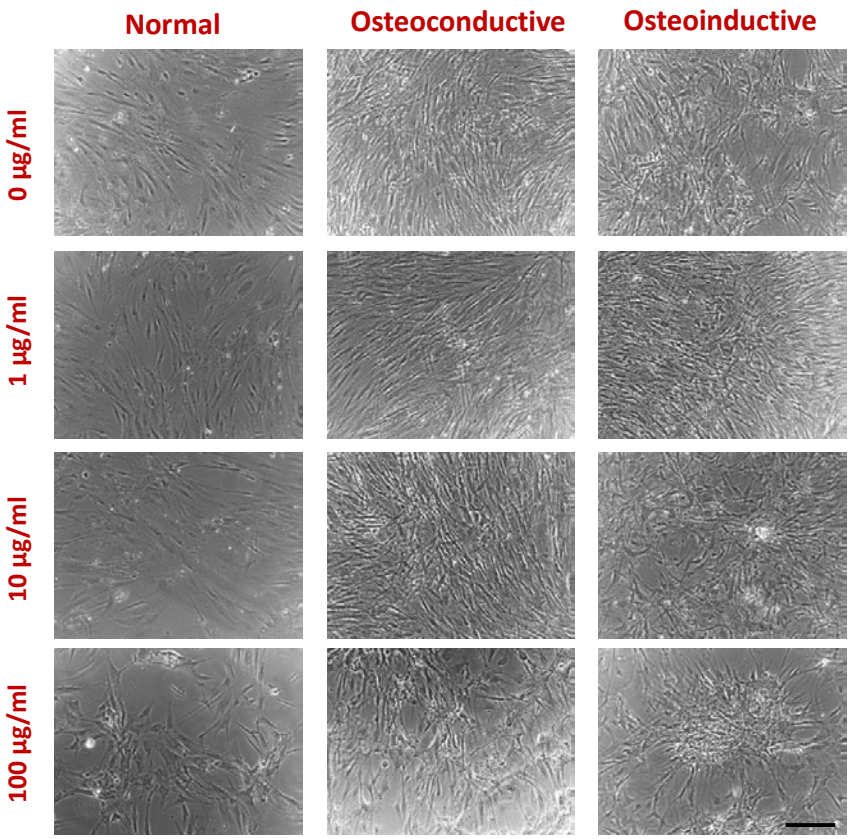

Supplemental Figure V.5. Effect of sNPs on cellular organization after 7 days in different media. In N and OC media, cells show random organization, whereas in OI medium, cells organize in colonies. This is typical behavior of hMSCs when they start differentiation. We also observed that there is significant decrease in cell number in OI medium compared to N and OC media. Addition of sNPs induces cellular organization in N, OC and OI media. (Scale bar = 200µm)

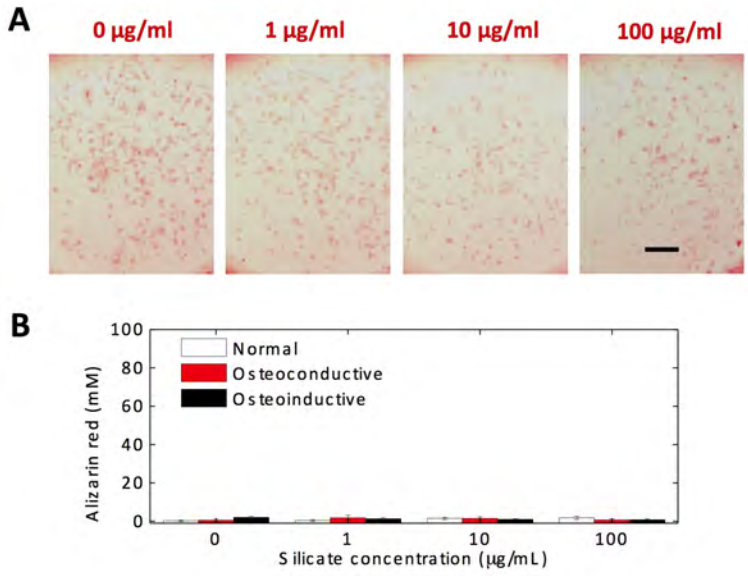

Supplemental Figure V.6. hMSCs incubated with sNPs does not stain for ARS staining. (**A**) Optical images showing cell adhered to well plate and stained for ARS. (**B**) Addition of sNPs does not have any effect on ARS staining as determined by image quantification. (Scale bar = 1 mm)

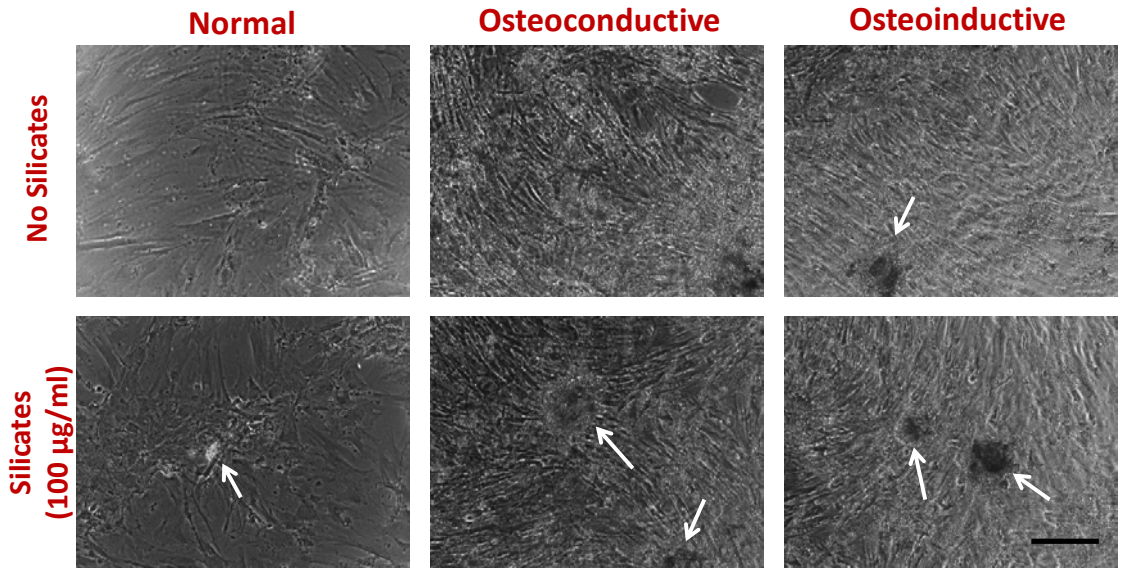

Supplemental Figure V.7. Effect of sNPs on cellular organization after 21 days in different media. In N mediim without sNPs, no change in cellular organization compared to day 7 is observed. In OC medium, we observed random cellular organization and cell reached confluences similar to day 7, whereas in OI medium, we observed very specific cellular organization that resulted in a deposition of ECM in concentrated circular regions. After ARS straining, we observed that these ECM deposits are rich in inorganic calcium. When cells were treated with sNPs, similar cellular organization was observed in N, OC and OI media. Although in N medium, dense cellular packing was not observed,

the circular regions were strained with ARS indicating deposition of mineralized ECM. (Scale bar = 200µm)

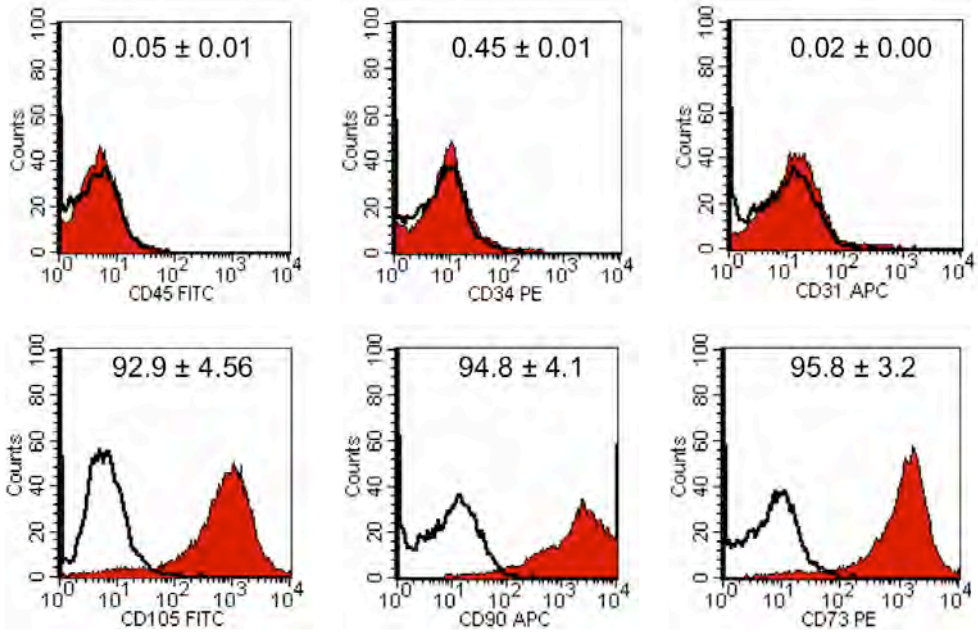

Supplemental Figure V.8. Evaluation of the mesenchymal stem cell marker profile by flow cytometry of hMSCs prior inducing the osteogenesis. Cells are mainly $CD45^-/CD34^-/CD31^-/CD105^+/CD90^+/CD73^+$.

Chapter VI

Silicate Nanoplatelets Enhance the Osteogenic Differentiation of SSEA-4 Positive Selection of Human Adipose Derived Stem Cells

ABSTRACT

How to surpass in vitro stem cell differentiation, reducing cell manipulation, and lead the *in situ* regeneration process after transplantation, remains to be unraveled in bone tissue engineering (bTE). Recently, we showed that the combination of human bone marrow stromal cells with bioactive silicate nanoplatelets (sNPs) promotes the osteogenic differentiation without the use of standard osteogenic inductors. Even more, using SSEA-4$^+$ cell-subpopulations (SSEA-4$^+$hASCs) residing within the adipose tissue, as a single-cellular source to obtain relevant cell types for bone regeneration, was also proposed. Herein, sNPs were used to promote the osteogenic differentiation of SSEA-4$^+$hASCs. The interactions between SSEA-4$^+$hASCs and sNPs, namely the internalization pathway and effect on cells osteogenic differentiation, were evaluated. SNPs below 100µg/mL showed high cytocompatibility and fast internalization via clathrin-mediated pathway. SNPs triggered an overexpression of osteogenic-related markers (RUNX2, osteopontin, osteocalcin) accompanied by increased alkaline phosphatase activity and deposition of a predominantly collagen-type I matrix. Consequently, a robust matrix mineralization was achieved, covering >90% of the culturing surface area. Overall, we demonstrated the high osteogenic differentiation potential of SSEA-4$^+$hASCs, further enhanced by the addition of sNPs in a dose dependent manner. This strategy endorses the combination of an adipose-derived cell-subpopulation with inorganic compounds to achieve bone matrix-analogs with clinical relevance.

This chapter is based on the following publication:

Mihaila SM, Gaharwar AK, Reis RL, Khademhosseini A, Marques AP, Gomes ME, "Silicate nanoplatelets enhance the osteogenic differentiation of SSEA-4 positive selection of human adipose derived stem cells", Biomaterials 2014, 35(33): 9087-99, doi: 10.1016/j.biomaterials.2014.07.052

VI.1. INTRODUCTION

Bone tissue engineering (TE) requires a readily available source of cells, combined with cell-templates (scaffolds) providing bio-instructive agents (inductive and/or growth factors, cytokines) to trigger and control the osteogenic phenotype and consequently an adequate biological functionality. Osteoinductivity is the key process to induce the differentiation of osteoprogenitor cells into osteoblast cells to eventually form new bone. Thus, extensive research has been focused on determining the appropriate conditions to trigger osteoinductive events. A range of inorganic bioactive materials such as bioactive glasses, calcium phosphates (CaPs)[1], hydroxyapatite (HA), beta tri-calcium phosphates (β-TCP)[2], and orthosilicic acid ($Si(OH)_4$)[3] are exploited as osteoinducers[4]. However, due to their limited processability and insufficient degradation, there is a need to develop a new generation of bioactive materials.

Recent studies have focused on developing new bioactive materials such as synthetic silicates[5,6] and graphene[7], suggesting unexploited routes for biomaterials design and regenerative medicine.In particular, bioactive silicate nanoplatelets (sNPs) based on synthetic silicate (Laponite, $Na^+_{0.7}[(Mg_{5.5}Li_{0.3})Si_8O_{20}(OH)_4]^-_{0.7}$) have shown to induce osteogenic differentiation of bone marrow human mesenchymal stem cells (hMSCs) in the absence of osteoinductive factors, such as BMP-2 or dexamethasone[6]. A single dose of these sNPs enhances the osteogenic differentiation of hMSCs, when compared to hMSCs cultured in standard osteogenic differentiation conditions (in the presence of dexamethasone). Moreover, these synthetic silicates have shown to physically interact with both synthetic and natural polymers and can be used as injectable matrices for cellular therapies[8-11]. Although these findings foster the development of new bioactive nanomaterials for bone TE[8,12-14], limited availability of bone marrow hMSCs, invasive retrieval procedures and high donor-site morbidity compromise the clinical applicability of the sNPs combined with these cells.

Recently, human adipose derived stem cells (hASCs) isolated from the stromal vascular fraction (SVF) of adipose tissue (AT) have emerged as one of the most promising stem cell populations identified thus far[15,16]. Moreover these cells have the ability to differentiate along multiple lineage pathways as reported in literature[15,16]. From a practical standpoint, human AT is abundant and easily obtained in large quantities with low donor-site morbidity or patient discomfort. The use of autologous hASCs as a research tool and as basis of cellular therapeutic strategies is feasible, making them preferential cells for TE, compared to bone marrow hMSCs. Furthermore, considering the limitations of hASCs in terms of differentiation potential (osteogenic[17], chondrogenic[17], adipogenic[17], myogenic[17] and neurogenic[18]), recent studies have shown that a selected and enriched cellular subset has significantly higher

differentiation potential. For instance, STRO-1$^+$hASCs[19], CD105$^-$hASCs[20], CD90$^+$hASCs[19,21] and p75$^+$hASCs[19] were found to exhibit higher osteogenic potential when compared to hASCs. Nonetheless, considering that the majority of biological systems rely on the different cellular interactions, it is important to classify a cell source that can act as starting point for several differentiation pathways. Thus, the isolation of cells from AT is relevant for bone TE and more appealing for clinical translation.

In our previous work[22], we have shown that SVF of the human AT, contains a subpopulation defined by the their positive expression of the pluripotency-associated marker, SSEA-4 that is capable of differentiating into mature microvascular-like endothelial cells. Interestingly, this cell subpopulation also showed a superior potential to differentiate towards the osteogenic lineage, compared to hASCs. Therefore, AT can be used as a single cell source to obtain a sub-population of cells, SSEA-4$^+$hASCs, that under specific conditions give rise to endothelial- and osteoblast-like cells, further reinforcing its relevance in designing bone-mimicking constructs.

Herein, we propose to use sNPs to promote and induce the osteogenic differentiation of SSEA-4$^+$hASCs by intracellular interplay, as well as through direct cellular interactions. We hypothesize that the addition of sNPs to SSEA-4$^+$hASCs induces osteogenic differentiation of SSEA-4$^+$hASCs. The combination of cells with high potential towards osteogenic differentiation with inorganic compounds that are able to sustain and improve the extent of mineralization can be a potential avenue towards formation of functional bone tissue. This approach up-holds the promise of developing feasible solutions for the induction of higher levels of new bone formation.

VI.2. MATERIALS AND METHODS

VI.2.1. Hydrodynamic diameter and surface charge of sNPs

Laponite silicate nanoplatelets (sNPs, $Na^+_{0.7}[(Mg_{5.5}Li_{0.3})Si_8O_{20}(OH)_4]^-_{0.7}$, Rockwood, USA) were dissolved in ultrapure water at different concentrations (<10mg/mL). The hydrodynamic diameter and zeta potential of the sNPs were measured by photon correlation spectroscopy and laser Doppler anemometry, respectively, using a Malvern Zetasizer Nano ZS (Malvern Instruments, UK). Each analysis was performed at 25^{o}C, with a detection angle of 90^o and a refractive index of 1.5 (for inorganic particles). Each formulation was analyzed in triplicate.

VI.2.2. SSEA-4$^+$hASCs selection and culture

Human abdominal subcutaneous AT samples were obtained from healthy female with an average age of 44 years, undergoing lipoaspiration procedure, after informed consent. The retrieval and transportation of the samples to the 3B's Research Group laboratorial facilities

were performed under a protocol previously established with the Department of Plastic Surgery of Hospital da Prelada, Porto, Portugal and approved by the local Ethical Committee. All the samples were processed within 24 hours after the surgical procedure, as previously described[22]. Briefly, the AT was digested with 0.05% (wt/v) collagenase II A (Sigma, Germany) in phosphate buffer saline (PBS), for 45min, under agitation in a shaking bath at 37^{o}C. The digested tissue was filtered through a 200µm mesh pore size strain, followed by centrifugation to remove the mature adipocytes and undigested connective tissue. After performing lysis to disrupt the red blood cells, the crude was centrifuged and resuspended in PBS to obtain the SVF.

The immunomagnetic selection of the SSEA-4^{+}hASCs was performed based on the coating of commercially available magnetic beads (Dynabeads® M-450 Epoxy beads, Invitrogen, USA) with SSEA-4 (clone MC813) antibody (Santa Cruz Biotechnology, USA) following the manufacturer's instruction and as previously reported[22]. Briefly, 2x10^{7} immunomagnetic beads resuspended with 10µL of the SSEA-4 antibody at a final concentration of 2µg/mL, and then incubated, overnight, at room temperature, under gentle stirring. Subsequently, the SSEA-4 coupled beads were separated with a magnet and mixed with freshly isolated SVF in order to select the SSEA-4^{+} cells residing within the cell crude (SSEA-4^{+}hASCs). The cells bonded to the beads were separated from the rest of the cell suspension using the magnet.

The SVF and the SSEA-4^{+}hASCs were both cultured with basal medium (Minimum Essential Medium Eagle-alpha Modification, α-MEM, Gibco, USA), supplemented with sodium bicarbonate (Sigma, Germany), 10% fetal bovine serum (FBS, Gibco, USA) and 1% penicillin/streptomycin (Pen/Strep, 100U/100µg/mL, Gibco, USA). When reaching 80% confluence, cells were detached from the culture flasks using TrypLE^{TM} Express (Invitrogen, USA) and kept under the same conditions along the passages. Both cell subgroups were used at passage 2 for further experiments.

VI.2.3. SNPs cytotoxicity screening

The effect of sNPs on cells metabolic activity was investigated by monitoring metabolic activity of adhered SSEA-4^{+}hASCs (passage 2), cultured in basal medium, for a period of 7 days. Cells were seeded in 48-well plates at a density of 2x10^{3} cells/cm^{2} and sNPs were added to a final concentration ranging from 0 to 2mg/mL. At pre-selected time points, cells were washed thoroughly with PBS, and a mixture of serum- and phenol-red free culture medium and MTS reagent (Promega, USA) in a 5:1 ratio, was added to the cells. Samples were incubated for 3 hours, after which 100µL of each sample were transferred to 96-well plates and optical density (OD) at 490nm was measured on a microplate reader (Synergy HT microplate reader, Biotek, USA). The metabolic activity of the test groups was

normalized with the control group (cells without sNPs) to determine the dose response. Aiming at further assessing the effect of the sNPs over cells cytoskeleton organization, cells were fixed with formalin and stained with Phalloidin-TRITC (Sigma, USA) for visualization of the F-actin filaments.

VI.2.4. Assessment of internalization efficiency of sNPs by SSEA-4$^+$hASCs

The sNPs were labeled with rhodamine B prior to assessing their internalization ability. For this purpose, 2g of sNPs were added to 100mL of 0.1% (wt/v) of rhodamine B isothiocyanate (Sigma, Germany) solution prepared in anhydrous DMSO, in dark conditions. The mixture was kept under continuous stirring, overnight, at 4^{o}C. Several washing steps with absolute ethanol were performed in order to separate the sNPs from the organic phase and excess rhodamine B. Finally, sNPs were air-dried and kept at room temperature, protected from light, until further used.

The SSEA-4$^+$hASCs (passage 2) were seeded at a cell density of 2x10^3 cells/cm^2 and allowed to adhere. After 24 hours, rhodamine-labeled sNPs (1, 10, 20, 50, 100 and 200µg/mL) were added to the culture wells and cultures were maintained in basal medium, in the presence/absence of 10^{-6}M colchicine, for additional 24 hours. SSEA-4$^+$hASCs cultured in basal medium in the presence of colchicine, but without the sNPs, were used as negative control. Cells were then washed thoroughly with PBS, trypsinized and fixed with acquisition buffer (PBS containing 10% formalin and 0.1% sodium azide) and 10% formalin respectively for analysis in a FACS Calibur flow cytometer (BD Biosciences, USA). In the flow cytometry analysis cells of interest were gated in a forward versus side scatter dot plot with a linear scale. Acquired data were displayed as histogram plots created using the CellQuest software (BD Biosciences, USA). Apart from that, for rhodamine samples fixed on coverslips, cell nuclei were counterstained with 4,6-diamidino-2-phenyindole dilactate (DAPI). Samples were visualized and images were acquired using the Axioplan Imager Z1 fluorescence microscope (Zeiss, Germany) and the AxioVision 4.8 software (Zeiss, Germany).

VI.2.5. Osteogenic differentiation

Confluent SSEA-4$^+$hASCs (passage 1) were removed from the culture flasks using TrypLE^{TM} Express (Invitrogen, USA) and seeded at a density of 2x10^3 cells/cm^2 in basal medium. Cells were allowed to adhere and after 24 hours, medium was replaced with either sNPs-containing (1, 10 and 100µg/mL) basal medium or osteogenic medium (osteo) consisting in basal medium supplemented with 10mM beta-glycerophosphate (Sigma, Germany), 10^{-8}M dexamethasone (Sigma, Germany), and 50mg/mL L-ascorbic acid 2-phosphate

sesquimagnesium salt hydrate (Sigma, Germany). Cells were incubated in a humidified environment at 37°C with 5% CO_2 for 7, 14, 21, and 28 days, with culture media replenishment every 3–4 days. SSEA-4$^+$hASCs and hASCs cultured in basal and osteo media in the absence of sNPs were used as controls. The experimental setup is depicted in **Figure VI.1**.

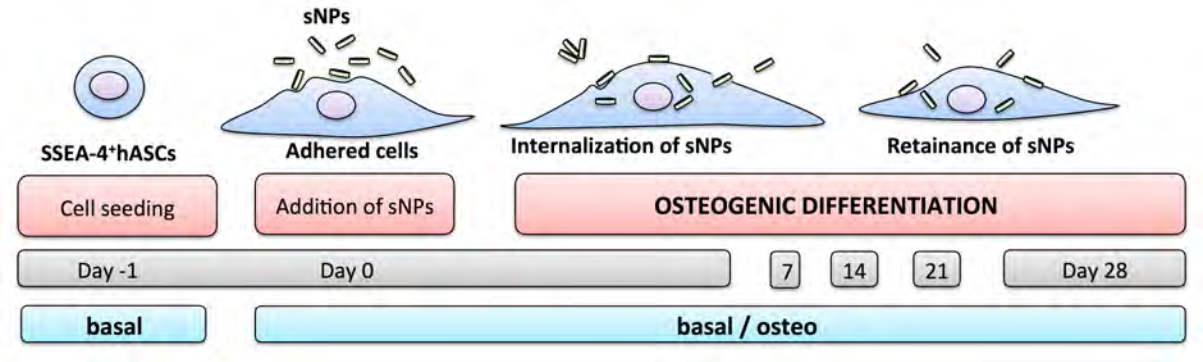

Figure VI.1. Experimental setup depicting the temporal approach followed to induce the osteogenic differentiation of SSEA-4$^+$hASCs. After selection from the freshly isolated SVF, SSEA-4$^+$hASCs were cultured in basal medium up to passage 2, then seeded at a density of 2000 cells/cm^2 and allowed to adhere for 24 hours until the sNPs were added. Cultures were maintained either in basal medium or under osteogenic differentiation conditions. At pre-selected time points (days 7, 14, 21 and 28) samples were retrieved to assess the extent of differentiation.

VI.2.6. Cell number quantification

The amount of double strained DNA (dsDNA), that is directly proportional with the cell number, was determined using a fluorometric dsDNA quantification kit (PicoGreen, Molecular Probes, Invitrogen, USA), according to the manufacturer's instructions. Samples collected at days 7, 14, 21 and 28 of culture were subjected to thermal and osmotic shocks to lyse the cells. Cell lysates were then used for the dsDNA quantification. Fluorescence was measured using an excitation wavelength of 480nm and emission wavelength of 538nm in a microplate reader (Synergy HT, Biotek, USA). Standards were prepared at a concentration ranging between 0 and 2mg/mL. Triplicates were made for each sample and per condition.

VI.2.7. Real-time reverse transcriptase-polymerase chain reaction (RT-PCR)

VI.2.7.1. RNA extraction and cDNA production

mRNA was extracted using TRI Reagent® (Sigma, Germany), following the manufacturer instructions. Proteins were extracted using chloroform and the RNA pellets were washed with isopropyl alcohol and 70% ethanol. The total mRNA was reconstituted in RNAse-free water (Gibco, USA). MRNA quantity and purity were assessed with a NanoDrop ND-1000 Spectrophotometer (NanoDrop Technologies, USA). First-stranded complementary DNA

(cDNA) synthesis was performed using qScript™ cDNA synthesis Kit (Quanta BIosciences, USA) on a Mastercycler ep realplex thermal cycler (Eppendorf, USA). An initial amount of 1µg of mRNA was used in a total volume of 20µL.

Table VI.1. Primer pair sequences for the studies genes

Gene	Sequences		NCBI reference
	Forward (5'→3')	Reverse (3'→5')	
GAPDH	ACAGTCAGCCGCATC	GACAAGCTTCCCGTTCTCAG	NM_002046.4
RUNX2	TTCCAGACCAGCAGCACTC	CAGCGTCAACACCATCATTC	NM_001145920.1
OPN	GGGGACAACTGGAGTGAAAA	CCC ACAGACCCTTCCAAGTA	NM_001040058
OCN	CTGGAGAGGAGCAGAACTGG	GGCAGCGAGGTAGTGAAGAG	NM_099173

VI.2.7.2. Quantitative real time RT-PCR

The quantification of the transcripts of the genes of interest was carried out by RT-PCR using 50ng of cDNA and PerfeCTA™ SYBR® Green FastMix kit (Quanta Biosciences, USA) following the procedure suggested by the manufacturer. The primers were previously designed using the Primer 3 online software (v0.4.0, Whitehead Institute, USA) and synthesized by MGW Biotech (Germany). For each sample, the transcripts expression data were normalized to *glyceraldehyde-3-phosphate-dehydrogenase (GAPDH)* as housekeeping gene. The primers sequences and annealing and annealing temperatures for bone-specific genes, *Runt-related transcription factor 2* (*RUNX2)*, *osteocalcin* (*OCN)* and *osteopontin* (*OPN),* and for *GAPDH* are described in **Table VI.1.** A concentration of 100nM of primer was used in a final volume of 20µl of sample. Reactions were performed in a real-time Mastercycler ep realplex thermal cycler (Eppendorf, USA). The relative quantification of the targeted genes was performed using the $2^{-\Delta\Delta CT}$ method[23]. The transcripts expression data were first normalized against endogeneous *GAPDH* values and then against the values of hASCs cultured in basal or osteo medium, respectively for basal and osteo conditions.

VI.2.8. Alkaline phosphatase activity quantification and staining

The alkaline phosphatase (ALP) activity was measured on the cell lysates obtained for dsDNA quantification, using an adapted end-point colorimetric procedure based on the p-nitrophenol (pNP) assay. Briefly, 20µL of lysate were incubated with 80µL p-nitrophenol phosphate solution (pNPP, 0.2% wt/v in 1M diethanolamine, Fluka BioChemika, Austria). A calibration curve was prepared using the pNP standards (Sigma, Germany) with values ranging from 0 to 0.5µmol/mL. The OD of the samples and standards was read at 405nm, using a microplate reader (Synergy HT, Biotek, USA). Triplicates of each sample and

standard were made, and the ALP activity was read off from the standard curve. Results were normalized against dsDNA results obtained for the same samples. The qualitative detection of ALP was performed by staining the fixed samples with nitro-blue tetrazolium/indolylphosphate (NBT/BCIP, Thermo Scientific, USA). Samples were visualized and images were acquired as described above.

VI.2.9. Collageneous and non-collageneous protein staining and quantification

The presence and distribution of collagen and non-collagenous proteins within the extracellular matrix (ECM) were determined by differential staining with two dyes, Sirius Red and Fast Green. Sirius Red binds specifically to collagen, whereas Fast Green stains the non-collagen proteins. As so, the effect of sNPs over the ECM deposition was assessed using the micro-assay kit (Chondrex, USA). Briefly, a mixture of 0.1% Sirius Red and 0.1% Fast Green solution saturated with picric acid was added to the fixed samples. After 30min, the dye was removed and samples rinsed with distilled water. Stained samples were visualized and images were acquired as described above.

For the quantification the dyes were extracted from the stained samples using 0.05M NaOH solution in methanol and the OD measured at 540nm (Sirius Red) and 605nm (Fast Green). The amount of collagenous and non-collageneous proteins was calculated according to the manufacturers indications and normalized against the dsDNA of the corresponding samples.

VI.2.10. Immunocytochemistry for collagen I and II

Samples were washed and fixed with 10% formalin for 20min, washed again with PBS and blocked with a 1.5% BSA/PBS solution. Cells were incubated for 1h at room temperature with the primary antibodies, mouse anti-human collagen I (abcam, ab90395, UK) and mouse anti-human collagen II (abcam, ab34712, UK). All antibody dilutions were performed in 1.5% BSA/PBS. Upon this incubation, cells were washed three times with PBS and incubated with the appropriate secondary antibody, either goat anti-mouse Alexa Fluor 488 (Invitrogen, USA), or donkey anti-mouse Alexa Fluor 594 (Invitrogen, USA) diluted 1:500 in 1.5% BSA/PBS. Cell nuclei were counterstained with DAPI, at a 1:10,000 dilution in PBS. Negative control samples were prepared by replacing the primary antibody incubation with PBS. Samples were visualized and images were acquired as described above.

VI.2.11. Alizarin Red staining and quantification

Staining with Alizarin Red was performed in order to assess calcium deposition. The cells were fixed with 10% formalin, for 20min, and washed prior staining with PBS and, again with distilled water to remove any contaminating salts. A 2% (wt/v) Alizarin Red solution (Sigma,

Germany) was added and 10min after, the cells were washed with distilled water and imaged as previously described. Subsequently, in order to obtain quantitative data, the extraction of the dye from the stained cell monolayer was performed by the addition of a 10% (v/v) acetic acid (vWR, Portugal). The dissolved samples were transferred to microcentrifuge tubes, centrifuged and neutralized with 10% (v/v) ammonium hydroxide (Sigma, Germany). Finally, 100µL of each sample was transferred in 96-well plate and the absorbance was read at 405 nm. A calibration curve was obtained from different concentrations of Alizarin Red in distilled water at pH=4.2, adjusted with 10% (v/v) ammonium hydroxide.

VI.2.12. Statistical analysis

Statistical analysis was performed using GraphPad Prism 5.00 software (San Diego, USA). Each experiment was carried out three times independently and performed with at least three replicates. First, a Shapiro-Wilk test was used to ascertain the data normality. The results indicated that non-parametric test should be employed for all comparisons. Statistical significances were determined using one-way analysis of variance (ANOVA), followed by post hoc Tukey test for all pair-wise mean comparisons, with the limit for statistical significance being defined as $p<0.05$.

VI.3.RESULTS

VI.3.1. SNPs characterization

Silicate nanoplateletes (sNPs) are synthetic disc-shaped crystals, characterized by a high aspect ratio (25-30nm in diameter and 1nm in width) and with an empirical formula given by $Na^{+}_{0.7}[(Si_8Mg_{5.4}Li_{0.3})O_{20}(OH)_4]^{-}_{0.7}$ (**Figure VI.2A**). The unit cell of the crystal is comprised of layers of $[SiO_4]$ tetrahedral sheets of Mg^{2+}, which complement their octahedral coordination by bridging with OH^- groups. The partial substitution of Mg^{2+} in the octahedral sheets by Li^+, charges the faces of the sNPs negatively, so that Na^+ ions are accommodated between the faces of the platelets for charge compensation, leading to a defined spatial distribution of charge on the sNPs[24]. When sNPs are dispersed in distilled water, the Na^+ ions are released into the solution leading to the formation of a double layer that causes the particles to electrostatically repeal each other, hence stabilizing them in overall negative charge of 10-15mV. However, with the increase of concentration (>100µg/mL), a significant increase in the overall size of the sNPs, accompanied by a slight decrease of the overall charge, was observed (**Figure VI.2B-C**).

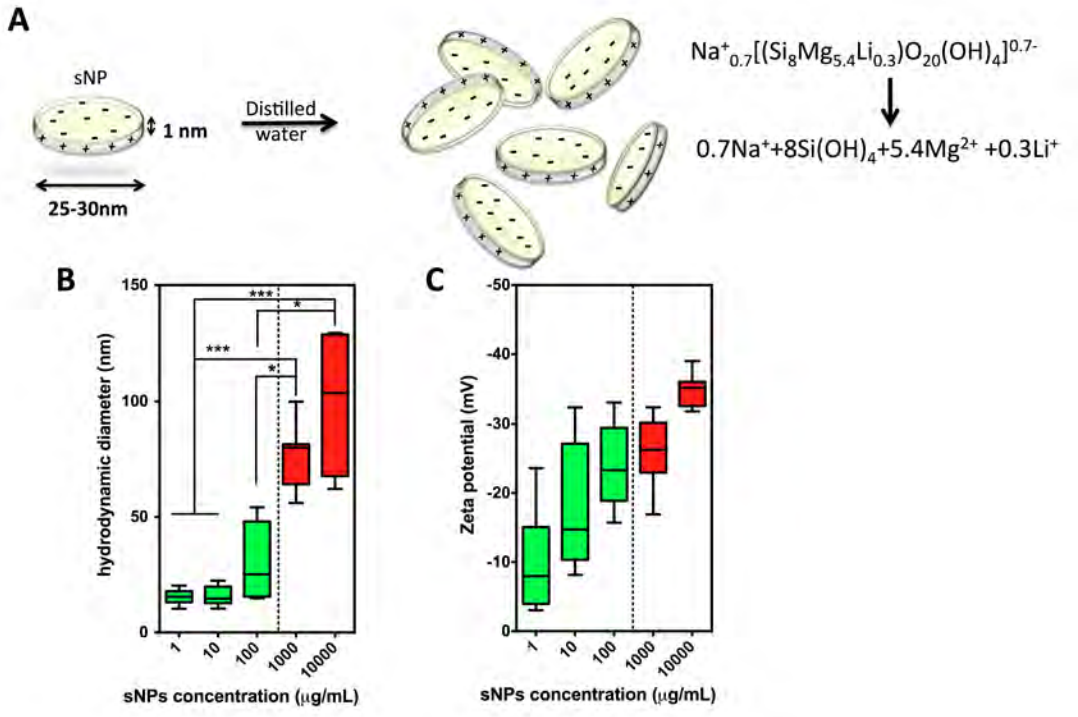

Figure VI.2. Physical properties of the sNPs. (**A**) The sNPs, with the $Na^+_{0.7}[(Si_8Mg_{5.4}Li_{0.3})O_{20}(OH)_4]^-_{0.7}$ empirical formula, are characterized by a high aspect ratio (25:1 to 30:1) and charge distribution (negatively charged facets and positively charged sides). Due to surface charge, upon dispersion in distilled water, sNPs electrostatically repel each other, avoiding aggregation. (**B-C**) Box plots depicting the sNPs hydrodynamic diameter and zeta potential. In dilute suspension, the sNPs are well dispersed and negatively charged. However, at increased concentrations, strong van der Waals forces make the sNPs to adhere to each other, such as in the mechanism of flocculation or aggregation (*p<0.05, **p<0.01, ***p<0.001).

VI.3.2. Cells and sNPs interactions and potential internalization mechanism

The potential cytotoxic effects of the sNPs were assessed after exposing the SSEA-4$^+$hASCs to different concentrations of sNPs over a period of 7 days. MTS test was performed to assess the metabolic activity of cells in the presence of sNPs. The addition of up to 100µg/mL sNPs to the cells did not cause changes in their metabolic activity, however at concentrations ranging from 250 to 10,000µg/mL) an abrupt decrease in the metabolic activity of cells was observed (**Figure VI.3A**). Moreover, SSEA-4$^+$hASCs cultured in the presence of sNPs at concentrations lower than 100µg/mL displayed a homogeneous fibroblast-like morphology characteristic of mesenchymal cells (**Figure VI.3B** and **Supplemental Figure VI.1**). However, at high concentrations (>100µg/mL), small sNPs clusters were observed on the surface of the cells. At those concentrations, cells were covered with a gel-like aggregate that lead to an apparent shrinkage of the cells cytoskeleton (**Supplemental Figure VI.1**). Previous report also indicates that sNPs

concentration of <100µg/mL does not result in significant production of reactive oxygen species (ROS) and reactive nitrogen species (RNS), indicating the cytocompatible nature of sNPs[13]. Thus, for further experiments, it was decided not to consider sNPs concentrations higher than 100µg/mL, as these lead to a reduction of cells metabolic activity greater than 20% and significant cellular morphological alterations.

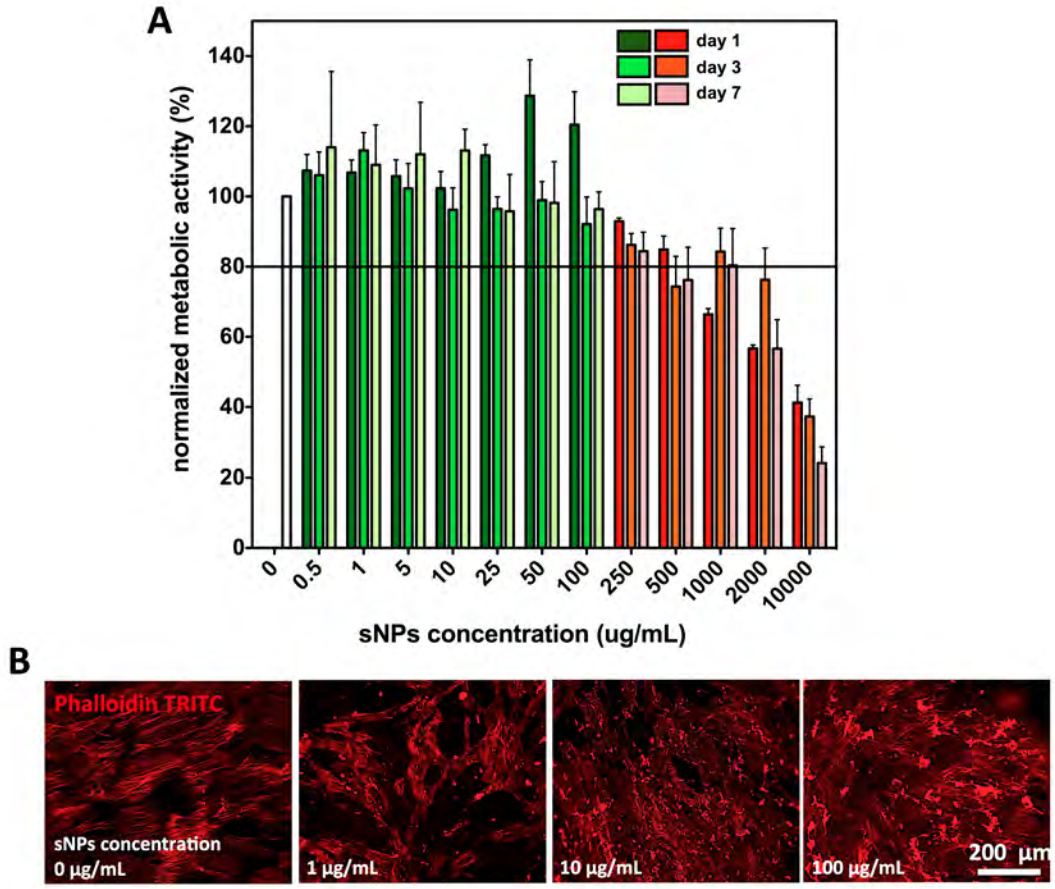

Figure VI.3. Dependence of cellular behavior with sNPs concentration. (**A**) Metabolic activity of cells in the presence of different concentrations of sNPs. Results are presented as percentage of metabolic activity of SSEA-4^{+}hASCs in the presence of sNPs in relation to the metabolic activity of SSEA-4^{+}hASCs cultured without sNPs (control) at the considered time point (average±SD, n=3). The metabolic activity threshold for choosing the appropriate sNPs concentrations was set to 80% in relation to the control. The half maximal inhibitory activity (IC_{50}) was found at a concentration of 1mg/mL. (**B**) Cytoskeleton (F-actin fibers) organization (red) upon addition of sNPs. The addition of sNPs (<100µg/mL) does not alter the morphology of the cells. Small sNPs aggregates can be observed on the surface of the cells, for higher concentrations of the sNPs.

Labeled sNPs were internalized and widely distributed in the cell cytoplasm, around the cells nuclei (**Figure VI.4A**), but also attached to the cell membranes (**Supplemental Figure VI.1**). In order to elucidate the internalization mechanism and deplete internalization from external contact of the cells with the sNPs, cells were cultured in the presence of rhodamine-labeled

sNPs and colchicine, an endocytotic restrictive drug, for a period of 24 hours. When cells were cultured in the absence of colchicine (green peak), a strong shift was observed, which is associated with cell-sNPs interaction derived from fluorescent sNPs externally attached to the cells, as well as internalized (**Figure VI.4B)**. At high concentration of sNPs (100-250µg/mL), more than 80% of cells interacted with the sNPs. However, in the presence of colchicine, there was a noticeable decrease (white peak). At high concentrations, only 30% of the cells were positive (interacting with the sNPs). Considering the difference between the results with and without colchicine as the internalization efficiency, with the premise that the internalization of the sNPs is solely endocytotic, the internalization efficiency ranges from 5% for 1µg/mL and can reach 40% for 100µg/mL of sNPs (**Figure VI.4C**).

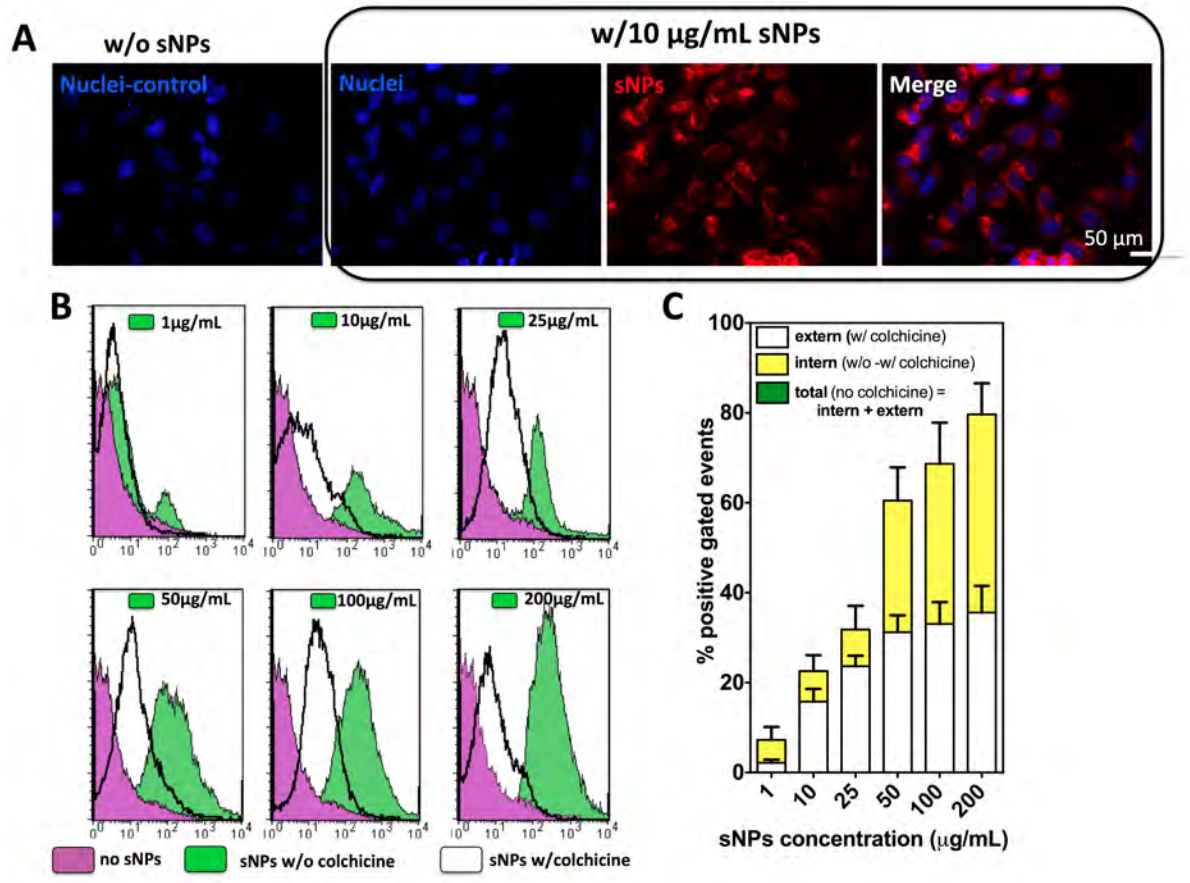

Figure VI.4. Internalization of sNPs by SSEA-4^{+}hASCs. (**A)** Fluorescence microscopy images of cells cultured in the presence of rhodamine-labeled sNPs (red) for 24 h. Rhodamine-labeled sNPs were found distributed in the cell cytoplasm, around the cells nuclei (blue). (**B**) Flow cytometry data of cells interacting with the in the presence (white) or absence (green) of colchicine. Cells without sNPs were used as negative control (purple). (**C**) Quantification of the internalization (yellow) by subtracting the sNPs-cell interaction in the presence of colchicine (white) from the total sNPs-cell interaction (without colchicine, green). The internalization efficiency ranges from 5% for 1µg/mL and can reach 40% for 100µg/mL of sNPs. *Abbreviation: w/ = with, w/o = without.*

VI.3.3. SNPs effect on the SSEA-4$^+$hASCs osteogenic differentiation

Prior differentiation SSEA-4$^+$hASCs were characterized as previously described[22] for the expression of surface markers such as CD105, CD90, CD73, CD45 and CD34. The cells showed mesenchymal-like phenotype, displaying the characteristic multiple-parametric pattern[25]: CD90$^+$/CD105$^+$/CD73$^+$/CD45$^-$/CD34$^-$ (**Supplemental Figure VI.2**).

VI.3.3.1. The effect the expression of RUNX2, OPN and OCN transcripts in SSEA-4$^+$hASCs cultures

The acquisition of an osteogenic phenotype by SSEA-4$^+$hASCs when the culturing with sNPs was evaluated by following the expression levels of *RUNX2*, *OCN* and *OPN* genes. In basal medium, no fold changes were observed concerning any of the studied genes for SSEA-4$^+$hASCs, when compared to hASCs cultured in the same medium. However, with the addition of sNPs, a 2-fold increase for *RUNX2* and *OPN*, and of 8- for *OCN* was noticed (***p<0.001, **Figure VI.5A**). For instance, a significant up-regulation of *RUNX2* occurred at day 7 for the higher sNPs concentration. This effect was successively delayed to days 14 and 21, when cells were cultured with 10 and 1µg/mL sNPs, respectively. Concomitantly, the *OPN* expression is significantly increased at day 14 for the 10 and 100µg/mL sNPs, followed by an immediate decrease to basal levels, while a significant up-regulation of *OCN* occurred at day 21 for all sNPs concentrations.

In osteogenic medium, there was a clear difference in the osteogenic performance between hASCs (control) and SSEA-4$^+$hASCs. A significant up-regulation of *RUNX2*, *OPN* and *OCN* gene transcripts was observed for SSEA-4$^+$hASCs (**p<0.01). After reaching a maximum (day 7 for *RUNX2*, day 14 for *OPN*, day 21 for *OCN*), a down-regulation reaching baseline levels of hASCs control cultures was observed (**Figure 5B**). The addition of sNPs further increased the up-regulation of the genes of interest in such a manner that the 100µg/mL sNPs induced a 70-fold increase (*p<0.05) in the expression of *RUNX2* at day 7, a 9-fold increase (*p<0.05) for *OPN* at day 14 and 45-fold increase (*p<0.05) for *OCN* at day 21 in relation to both the hASCs control cultures and SSEA-4$^+$hASCs in the absence of the sNPs.

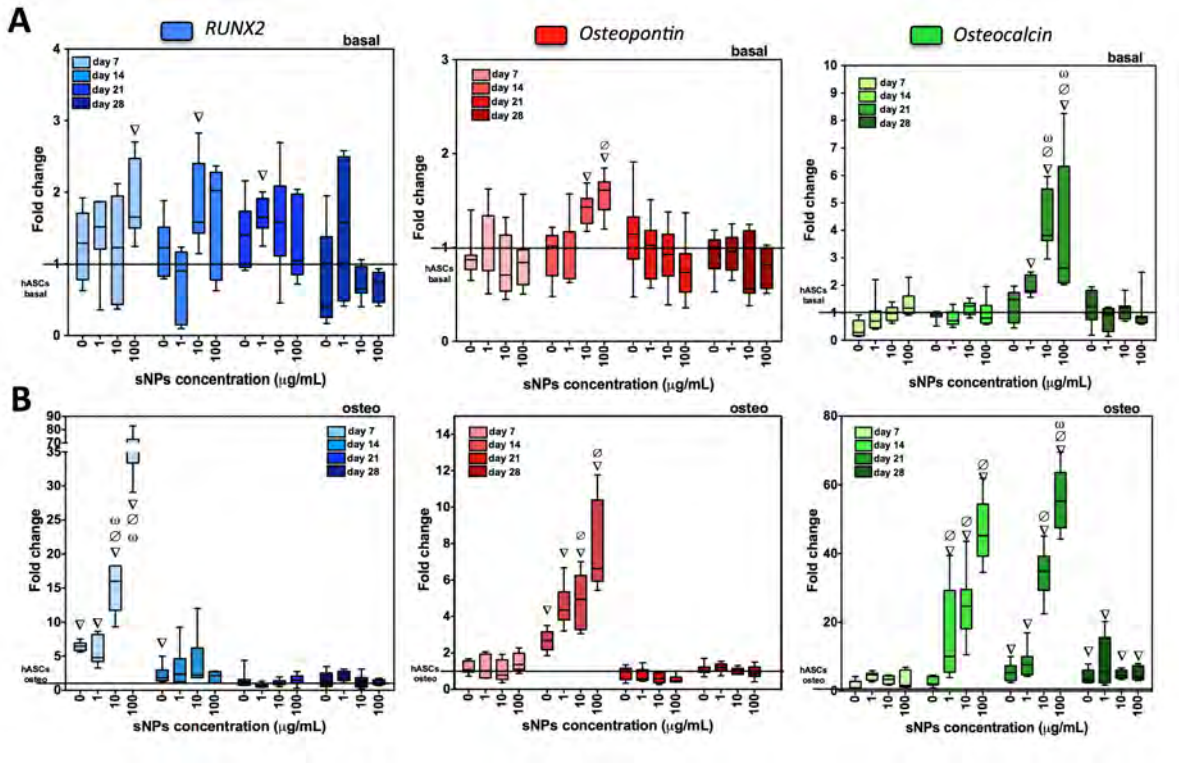

Figure VI.5. RT-PCR results for early (*RUNX2)*, intermediate (*OPN)* and late (*OCN*) osteo-related markers in SSEA-4^{+}hASCs cultures, in relation to hASCs cultures established in correspondent basal and osteogenic media. In basal medium (**A**) the expression of these transcripts is up-regulated in the presence of sNPs, in a dose-dependent manner, that also varies with the gene of interest. (**B**) Under osteogenic differentiation conditions, a significant increase in the expression of these markers was observed both in the absence and the presence of sNPs. A dependence with the sNPs concentration was observed for all the genes. ∇ depicts statistical difference (*p<0.05), when compared with hASCs group, ∅ corresponds to statistical differences when compared with SSEA-4^{+}hASCs without sNPs, while ω shows the statistical differences when compared with SSEA-4^{+}hASCs in the presence of 1μg/mL sNPs.

VI.3.3.2. The effect of sNPs over ALP activity

The osteogenic differentiation of the SSEA-4^{+}hASCs under the different culture conditions was confirmed, by qualitative and quantitative assessment of the levels of ALP activity, an early marker of differentiation, along the time of culture. ALP activity was confirmed in all groups, hASCs and SSEA-4^{+}hASCs, with and without sNPs, cultured in osteo medium. A clear increase of the ALP activity was evident up to 14 days of culture and for increased sNPs concentrations as demonstrated by the dark purple color (**Figure VI.6A**). The quantitative analysis of ALP activity, normalized to the total dsDNA, confirmed the trend of these observations, with a 10-fold increase at day 14 (**Figure VI.6C**). A slight increase of ALP activity occurred during initial time points, up to day 10, followed by a burst at day 14

(*p<0.05) and a successive rapid decrease at day 21. Additionally, the significantly higher ALP activity in SSEA-4$^+$hASCs (*p<0.05) when compared to hASCs cultured in the same conditions, and thus their enhanced predisposition to differentiate towards the osteogenic lineage, is noteworthy.

Concerning the cultures in basal medium, the constitutive ALP activity did not noticeably vary along the time of culture in both SSEA-4$^+$hASCs and hASCs. However, in the presence of sNPs the ALP activity in the SSEA-4$^+$hASCs cultures increased as demonstrated by more intense staining at day 14, for the 10 and 100µg/mL sNPs formulations (**Figure VI.6A**). The quantitative analysis confirmed the observed trend. At day 14, a significant increase in ALP activity (*p<0.05) was observed for SSEA-4$^+$hASCs cultured with increasing concentrations of sNPs (**Figure VI.6B**).

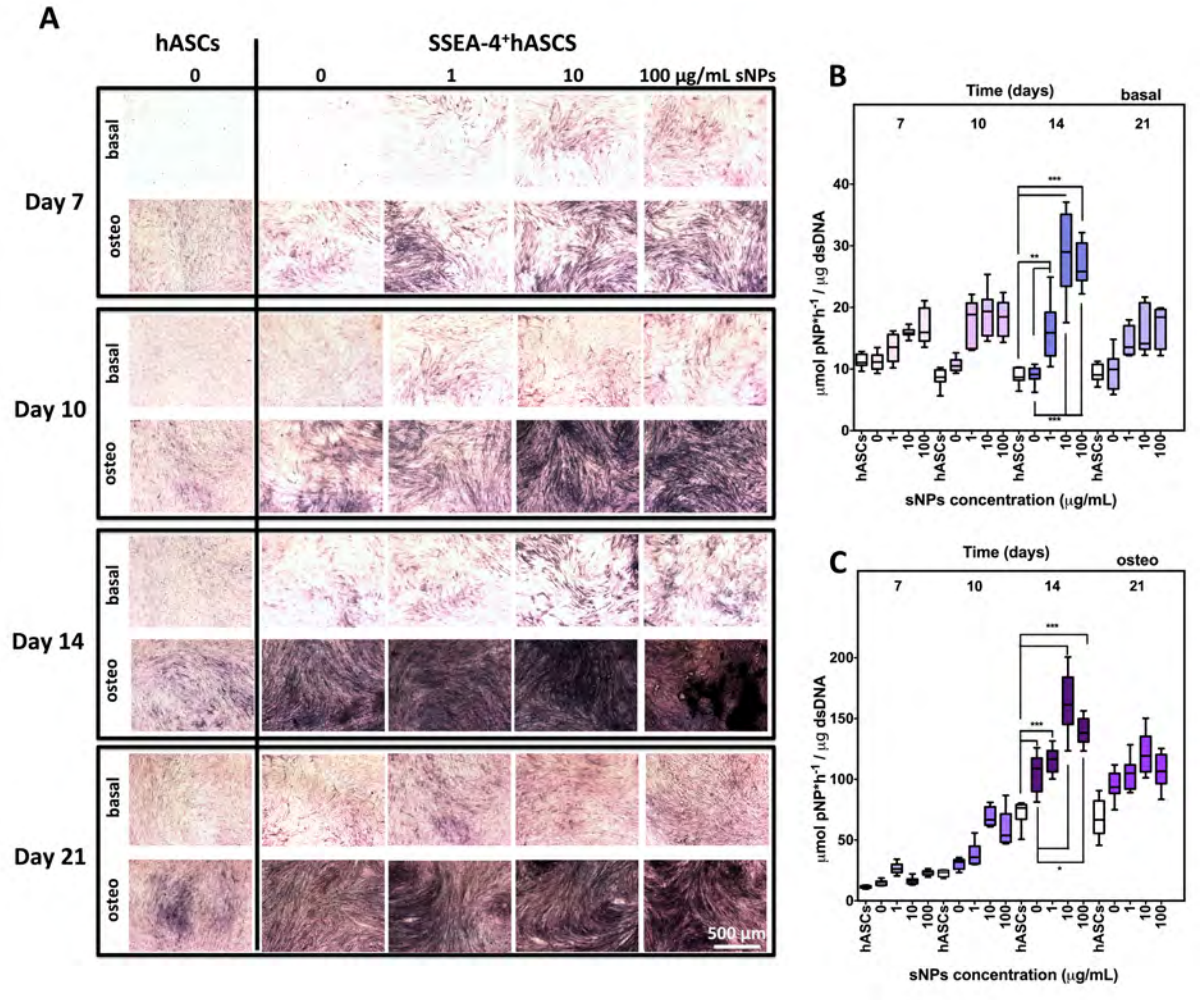

Figure VI.6. Qualitative and quantitative analysis of alkaline phosphatase (ALP) activity during 21 days of culture. (**A**) NBT/BCIP staining (dark purple) highlights an intense coloration with the addition of sNPs, suggesting that the sNPs enhance ALP activity. (**B-C**) The presence of sNPs lead to significantly enhanced ALP activity at day 14 of culture in SSEA-4$^+$hASCs in basal and osteogenic media, when compared to hASCs cultured in the same conditions (*p<0.05, **p<0.01, ***p<0.001).

VI.3.3.3. The effect of sNPs over the deposition of collagenous proteins and matrix mineralization

The deposition and distribution of the proteins that form the extracellular matrix was evaluated by Sirius Red/ Fast Green staining, aiming at discriminating the collagenous from the non-collagenous proteins. When cells (hASCs and SSEA-4$^+$hASCs) were cultured in basal medium for 21 days, an uniformly distributed cyan coloration, corresponding to non-collagenous proteins, was observed. However, in the presence of sNPs, small purple regions, corresponding to collagen deposition, were observed. In osteogenic medium cultures, both in the presence and absence of sNPs, the cyan/purple ratio switched, so that large fibrillar-like collagenous regions overtook the regions that correspond to non-collagenous proteins. (**Figure VI.7A**) The qualitative results were confirmed by the quantification of the total amount of collagen deposited in the different conditions. While no significant differences were observed in the amount of collagen deposited by hASCs and SSEA-4$^+$hASCs cultured in basal medium, the addition of sNPs led to significantly higher (*p<0.05) collagenous proteins deposition (**Figure VI.7B**). Successively higher amounts were detected with increasing sNPs concentration reaching a nearly 8-fold in the presence of 100µg/mL of sNPs. The SSEA-4$^+$hASCs cultured in osteogenic medium revealed a similar behavior, with cells being able to deposit a significantly higher amount of collagenous proteins (*p<0.05). The addition of 100µg/mL sNPs to hASCs and SSEA-4$^+$hASCs resulted in a 3.4-fold and 2.1-fold increase, respectively when compared to cells cultured without sNPs (**Figure VI.7C**). The quantification of non-collagenous proteins revealed constant levels of proteins both in basal and osteogenic media, except for the 100µg/mL sNPs formulation in osteogenic medium which showed significantly higher values than the hASCs and SSEA-4$^+$hASCs cultured without sNPs (**Supplemental Figure VI.3A-B**).

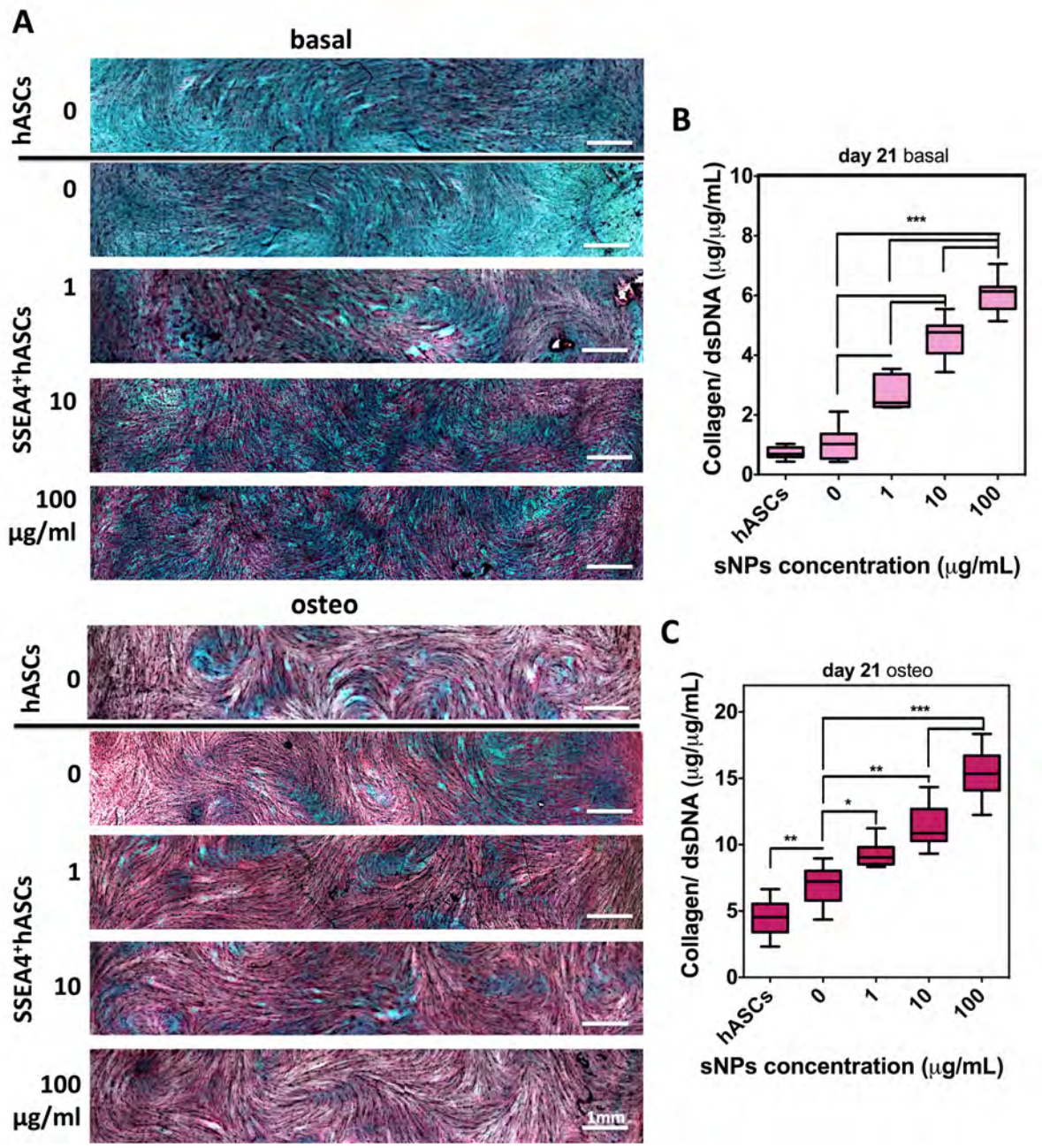

Figure VI.7. Detection of proteins produced by hASCs and SSEA-4^{+}hASCs when cultured in basal and osteogenic media for 21 days. (**A**) Fast Green and Sirius Red staining depicts the distribution of collagenous (purple) and non-collagenous (cyan) proteins within the matrix. **(B-C**) Quantification of collagenous proteins normalized against the amount of dsDNA. The osteogenic differentiation of SSEA-4^{+}hASCs is characterized by a significantly enhanced collagen production in comparison to the hASCs. The addition of sNPs lead also to an increased production of collagenous proteins in both basal and osteogenic conditions (*p<0.05, **p<0.01, ***p<0.001).

In order to determine the type of collagen composing the deposited collagenous matrix, the presence of collagen type I was evaluated at days 14, 21 and 28 by immunocytochemistry

(**Figure VI.8).** In basal media, only residual collagen type I was detected for both hASCs and SSEA-4$^+$hASCs,. However, when sNPs were added to the SSEA-4$^+$hASCs, increased evidence of collagen type I was noticed. By day 28, only small collagen type I depots were identified in all conditions, including sNPs in basal medium. On the other hand, in osteogenic medium, collagen type I was dominantly present in all conditions. Moreover, an increased and uniformly distributed deposition seemed to be detected for the SSEA-4$^+$hASCs with the addition of sNPs. A similar trend was observed for collagen type II (**Supplemental Figure VI.3C**). When the ratio between collagen type I and type II was analyzed, the highest percentage of collagen type I was found for the SSEA-4$^+$hASCs with 100µg/mL of sNPs in osteogenic medium. Interestingly the highest percentage of collagen type II was found for SSEA-4$^+$hASCs treated with 100µg/mL of sNPs in basal medium (**Supplemental Figure VI.3D**).

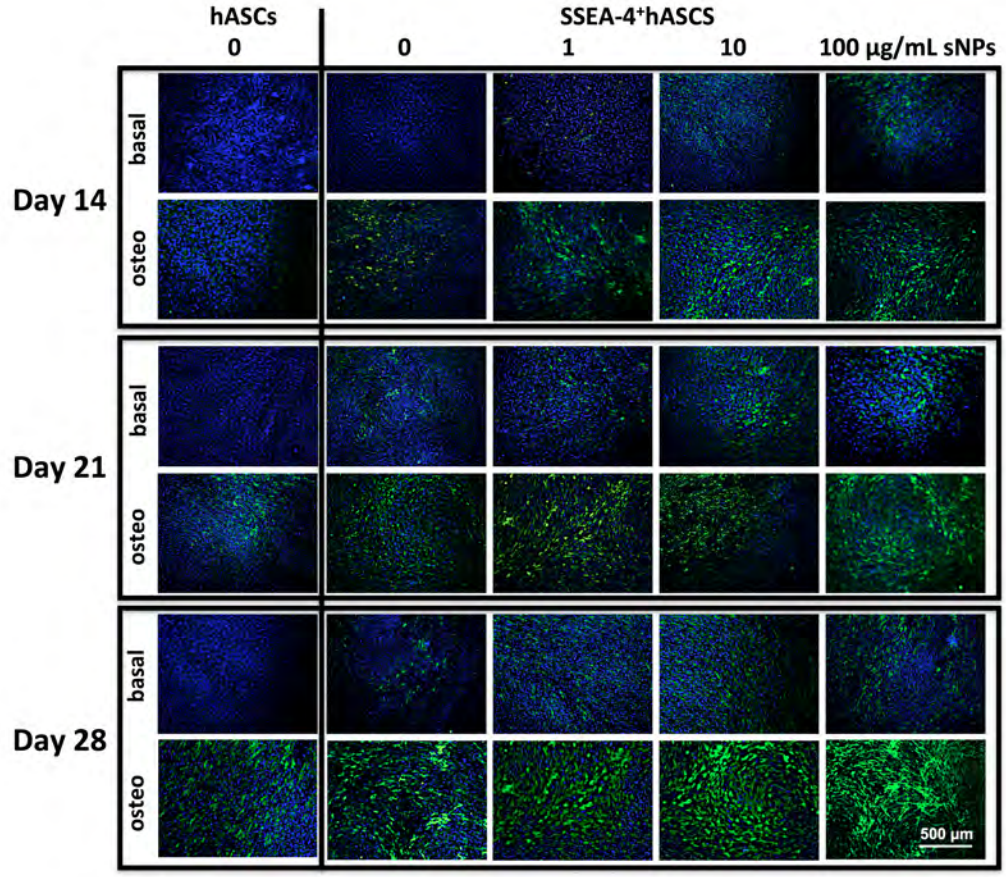

Figure VI.8. Representative immunofluorescence images of the detection of collagen type I (green) over time and for the different experimental conditions. The addition of sNPs triggers the deposition of collagen type I in both basal and osteogenic media. Cell nuclei were counterstained with DAPI (blue).

Alizarin Red staining confirmed that in basal medium, matrix mineralization depots were only detected in the presence of sNPs (**Figure VI.9A**). Moreover these significantly increased with increasing sNPs concentrations and longer timepoints (**Figure VI.9B).** At day 28, the amount of inorganic calcium in the SSEA-4^{+}hASCs culture with sNPs was significantly higher (*p<0.05) than in the hASCs or SSEA-4^{+}hASCs cultures without sNPs. In osteogenic medium, significant mineral deposition was observed in the hASCs cultures as evidenced by the intensity of the staining. Nonetheless, SSEA-4^{+}hASCs cultures showed enhanced mineralization levels, with a more intense overall staining and higher number of mineralized regions in the presence of the sNPs (**Figure VI.9A**). The extent of mineralization in osteogenic medium by day 28, 10-fold higher level than in basal medium, confirmed by significant differences (*p<0.05) between SSEA-4^{+}hASCs and hASCs cultures, both in the presence and absence of sNPs (**Figure VI.9C**).

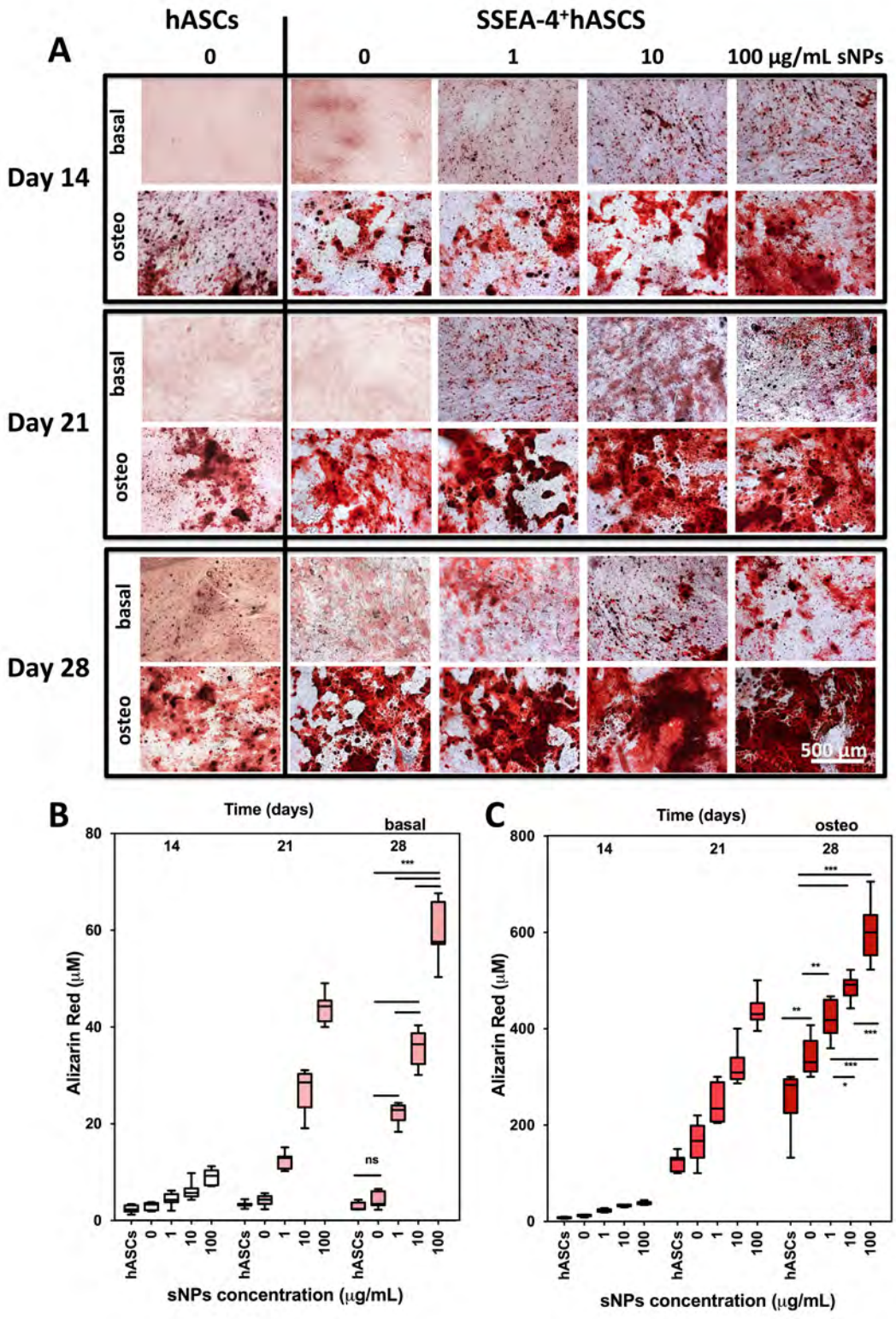

Figure VI.9. Alizarin Red staining and respective quantification of the gradual mineralization of the deposited matrix along the culture. **(A)** Alizarin Red staining showed an intense coloration for increased sNPs concentrations. (**B-C**) Quantification of Alizarin Red staining confirmed a significant higher matrix mineralization in the SSEA-4^{+}hASCs cultures in the presence of sNPs, both in basal and osteogenic media (*p<0.05, **p<0.01, ***p<0.001).

VI.4. DISCUSSION

One of the goals of bone TE is to design adequate supportive matrices for skeletal stem cells or progenitor cells to sustain the repair and regenerate damaged tissue. Focus has been given to AT as an alternative cell source to bone marrow MSCs[26]. At present, isolating homogenous stem cell subpopulations from the SVF of human AT that are more prone to differentiate into a certain lineage (osteogenic, chondrogenic, endothelial, etc) is being exploited as an approach to use this cell source more efficiently. So far $CD49d^{+}$hASCs[19], $CD90^{+}$hASCs[21] or $CD105^{-}$hASCs[20] were shown to possess an enhanced osteogenic differentiation potential when compared to unsorted cells (hASCs). However, as bone healing and regeneration relies on heterogeneous cellular interactions (eg. endothelial- and osteoblast-like cells), the use of a cell source/subpopulation with potential to differentiate towards these lineages relevant for bone tissue engineering might be advantageous. Our previous work[22] showed that besides being able to differentiate towards osteogenic lineage, the SSEA-4^{+}hASCs subpopulation residing within the SVF of the AT could differentiate into microvascular-like endothelial cells. This dual-differentiation potential features the possibility to obtain the relevant type of cells using a single-source and a single step-isolation procedure to engineer vascularized bone tissue.

Recently, the potential of sNPs (Laponite, $Na^{+}_{0.7}[(Si_8Mg_{5.4}Li_{0.3})O_{20}(OH)_4]^{-}_{0.7}$) to induce the osteogenic differentiation of bone marrow stromal cells in the absence of any external osteoinductive factors was demonstrated[13]. Thus, we herein propose the use of sNPs as instruments to promote and improve the osteogenic differentiation of SSEA-4^{+}hASCs.

Intrinsic and extrinsic properties of nanoparticles such as surface area, charge and functionalities, as well as size and shape, might impact cytotoxicity. Cytotoxicity tests were carried out considering the threshold of 20% reduction of SSEA-4^{+}hASCs metabolic activity. Our data is in agreement with previously published studies[13]: nanoparticles with negative zeta potential were shown to be significantly less internalized by cells than nanoparticles with positive zeta potential[27]. The cationic surface of sNPs is responsible for their interactions with the anionic glycoproteins and phospholipids of the cell membrane, which possibly facilitates their internalization[28]. This suggests that the cellular uptake occurs when sNPs are oriented with their positive side towards the cell membrane, ensuring a low area[29] and their engulfment and the disguise of the negative facet. However, the use of positively charged systems remains problematic *in vivo* as their interaction with negatively charged serum proteins and red blood cells may form large clusters and interfere with normal metabolic processes[30]. In fact, our *in vitro* data reproduced this observation, as for sNPs concentrations higher than 100µg/mL, the formation of clusters that could hinder the internalization mechanism was observed. As a consequence, these clusters attached to the

cell membrane, impairing cell cytoskeletal organization and metabolism. At the same time, it is known that the optimal nanoparticle diameter for cellular uptake is in the order of 25–30nm[31], which is in good agreement with the radius reported for the sNPs[13,32] at concentrations below 100µg/mL. In addition to being uptaken by cells, as suggested by the rhodamine-labeled sNPs homogeneously localized around the cellular nuclei, sNPs were also found attached to the cellular membrane, without affecting the cells fibroblastic-like morphology. Therefore, the cells-sNPs interaction comprise the sum of the external contact at the membrane level, and of the internal effect, due to the engulfed sNPs. In order to isolate these two types of interactions, complementary experiments were carried out by inhibiting the endocytotic internalization mechanism using colchicine, an endocytotic restrictive drug. Colchicine is known to bind tightly to microtubules causing microtubule depolymerization, further affecting the endocytosis mechanism[28]. Based on the narrow sNPs range size, our hypothesis was that the cellular uptake predominately occurred *via* clathrin-mediated endocytosis pathway, as already reported elsewhere[31,33] (**Supplemental Figure VI.4**). Our data suggests that the interactions that occur at the membrane level are equally important as the ones that occur internally. Particularly, it was possible to estimate that for the 100µg/mL sNPs, both the cytoplasmic effect and external interactions have an equal contribution (approx. 35% each).

Independent of being entrapped within the endosome, attached to the cell membrane, or in suspension in the culture medium, particularly at low pH[32,34], sNPs are subjected to constant acidic and/or enzymatic degradation, dissociating into silicic acid ($Si(OH)_4$), Na^+, Mg^{2+} and Li^+. All of these were shown to improve the osteogenic differentiation by different mechanisms[35-37]. *In vitro* osteogenic differentiation is characterized by several temporal milestones that demonstrate the commitment of the cells towards the osteoblastic phenotype. At early stages of differentiation, the activation of the *RUNX2* transcription factor occurs to facilitate the convergence of numerous osteogenic signaling pathways[38,39]. Our data features an intense up-regulation of *RUNX2* for the SSEA-4$^+$hASCs cultured in osteogenic medium, in comparison to hASCs. Moreover, in the presence of sNPs a significantly higher up-regulation, proportional to the sNPs concentration, was observed which indicates that the osteogenic differentiation was triggered due to a signal provided by the sNPs. Interestingly, *RUNX2* expression up-regulation was also noted in basal medium at different timepoints for the different concentrations of sNPs. Earlier up-regulation was detected for higher sNPs concentration, which is in accordance to our previously published data that showed the osteogenic differentiation of bone marrow stromal cells in the absence of any external osteoinductive factors[13].

Considered to be the central control gene within the acquisition of osteoblast phenotype,

RUNX2 directly stimulates ALP activity[40] and the up-regulation of osteogenic-related genes such as *OPN* or *OCN*[39,41] , and genes responsible for encoding collagenous-like matrix, mainly constituted of type I collagen[42], which is a prerequisite for mineralization[43,44]. The follow-up of the temporal cascade of events after confirming *RUNX2* up-regulation, showed that the nature of the deposited matrix was dependent on the cell type and/or culture media and/or addition of sNPs. A maximum of ALP activity was detected, independent of the culture media, although at different levels, at day 14, as expected as an indication of the osteogenic phenotype acquisition[40,45]. As for *RUNX2* expression, sNPs alone lead to increased ALP activity; however, a plateau was reached when 10µg/mL sNPs were used. In opposition to *RUNX2*, the dependence of the *OPN* and *OCN* expression with the sNPs concentration did not affect its temporal profile. As expected during osteogenic differentiation[46], the maximum up-regulation of *OPN* transcripts was observed at day 14 while for *OCN* a peak was detected between days 14 and 21.

Among the dissociation products of sNPs, soluble silicate ions have been found to stimulate the expression of collagen type I in osteoblast-like cell cultures[3], while magnesium[36] and lithium[37,47] were shown to facilitate mineralization[44,48]. Thus, upon triggering the cells differentiation towards the osteogenic lineage, it was expected that the sNPs would also affect the nature of the deposited extracellular matrix (ECM). The deposition of collagenous-proteins, in detriment of non-collagenous proteins, gradually took over when SSEA-4$^+$hASCs were cultured together with sNPs, in basal medium, although the levels observed in osteogenic medium were not reached. As a general remark, collagen stained by Sirius Red displayed a fibrillar pattern, whereas non-collagen proteins stained with Fast Green showed a more diffused pattern. In fact, the deposited matrix under osteogenic conditions was mainly composed of collagen type I, known to be produced by developing osteoblast-like cells and an early indicator of the osteogenic differentiation[44], a prevalence of collagen II was detected when cells were cultured in basal medium.

Different works have shown that the enzymatic activity of ALP has a direct role in initiating the calcification process[40,49,50]. Taken together, the ALP enriched cuboid-shaped clusters, the pattern of collagen deposition and the Alizarin Red staining, confirmed the conclusion of the differentiation process. This was achieved with greater efficiency for the SSEA-4$^+$hASCs cultures in the presence of sNPs under osteogenic conditions, as demonstrated by more than 90% of the culture area depicting the formation of new mineralized nodules. Nonetheless, the SSEA-4$^+$hASCs cultures in basal medium with presence of sNPs also generated calcium depots, indicating successful differentiation of SSEA-4$^+$hASCs into osteoblast-like cells, although at lower rates than in osteogenic conditions. Therefore, by applying a single dose of sNPs to cells with high osteogenic differentiation potential

promotes up-regulation of bone-related markers, which lead to production of enhanced mineralized matrix.

VI.5. CONCLUSIONS

By means of immunomagnetic selection targeting the SSEA-4 surface marker, it is possible to select a subpopulation with high differentiation potential (SSEA-4$^+$hASCs). Our data suggest that the SSEA-4$^+$hASCs bear higher osteogenic differentiation potential than hASCs, which can be further enhanced by the addition of sNPs in a dose dependent manner. Thus, envisioning bone tissue regeneration, the association of SSEA-4$^+$hASCs with sNPs harbors great potential in a TE approach towards the development of highly mineralized templates using an independent differentiation process. Even more, this unique combination can be further exploited in association with endothelial derived SSEA-4$^+$hASCs and 3D-templates to design improved bone analogs.

REFERENCES

1. Muller P, Bulnheim U, Diener A, Luthen F, Teller M, Klinkenberg ED, et al. Calcium phosphate surfaces promote osteogenic differentiation of mesenchymal stem cells. Journal of cellular and molecular medicine. 2008;12(1):281-91.
2. Barradas AM, Monticone V, Hulsman M, Danoux C, Fernandes H, Tahmasebi Birgani Z, et al. Molecular mechanisms of biomaterial-driven osteogenic differentiation in human mesenchymal stromal cells. Integrative biology : quantitative biosciences from nano to macro. 2013;5(7):920-31.
3. Reffitt DM, Ogston N, Jugdaohsingh R, Cheung HF, Evans BA, Thompson RP, et al. Orthosilicic acid stimulates collagen type 1 synthesis and osteoblastic differentiation in human osteoblast-like cells in vitro. Bone. 2003;32(2):127-35.
4. Gaharwar AK, Peppas NA, Khademhosseini A. Nanocomposite hydrogels for biomedical applications. Biotechnology and Bioengineering. 2014:DOI: 10.1002/bit.25160.
5. Dawson JI, Oreffo RO. Clay: new opportunities for tissue regeneration and biomaterial design. Advanced materials. 2013;25(30):4069-86.
6. Gaharwar AK, Mihaila SM, Swami A, Patel A, Sant S, Reis RL, et al. Bioactive silicate nanoplatelets for osteogenic differentiation of human mesenchymal stem cells. Advanced materials. 2013;25(24):3329-36.
7. Goncalves G, Cruz SM, Ramalho A, Gracio J, Marques PA. Graphene oxide versus functionalized carbon nanotubes as a reinforcing agent in a PMMA/HA bone cement. Nanoscale. 2012;4(9):2937-45.
8. Gaharwar AK, Kishore V, Rivera C, Bullock W, Wu CJ, Akkus O, et al. Physically Crosslinked Nanocomposites from Silicate-Crosslinked PEO: Mechanical Properties and Osteogenic Differentiation of Human Mesenchymal Stem Cells. Macromolecular bioscience. 2012.
9. Gaharwar AK, Schexnailder P, Kaul V, Akkus O, Zakharov D, Seifert S, et al. Highly Extensible Bio-Nanocomposite Films with Direction-Dependent Properties. Advanced Functional Materials. 2010;20(3):429-36.
10. Gaharwar AK, Schexnailder PJ, Dundigalla A, White JD, Matos-Pérez CR, Cloud JL, et al. Highly Extensible Bio-Nanocomposite Fibers. Macromolecular Rapid Communications. 2011;32(1):50-7.
11. Gaharwar AK, Schexnailder PJ, Jin Q, Wu C-J, Schmidt G. Addition of chitosan to silicate cross-linked PEO for tuning osteoblast cell adhesion and mineralization. ACS Applied Materials & Interfaces. 2010;2(11):3119.
12. Dawson JI, Oreffo RO. Clay: New Opportunities for Tissue Regeneration and Biomaterial Design. Advanced materials. 2013.

13. Gaharwar AK, Mihaila SM, Swami A, Patel A, Sant S, Reis RL, et al. Bioactive Silicate Nanoplatelets for Osteogenic Differentiation of Human Mesenchymal Stem Cells. Advanced materials. 2013.
14. Gaharwar AK, Schexnailder PJ, Kline BP, Schmidt G. Assessment of using Laponite cross-linked poly (ethylene oxide) for controlled cell adhesion and mineralization. Acta biomaterialia. 2011;7(2):568-77.
15. Zuk PA, Zhu M, Ashjian P, De Ugarte DA, Huang JI, Mizuno H, et al. Human adipose tissue is a source of multipotent stem cells. Mol Biol Cell. 2002;13(12):4279-95.
16. Schaffler A, Buchler C. Concise review: adipose tissue-derived stromal cells--basic and clinical implications for novel cell-based therapies. Stem cells. 2007;25(4):818-27.
17. Zuk PA, Zhu M, Mizuno H, Huang J, Futrell JW, Katz AJ, et al. Multilineage cells from human adipose tissue: implications for cell-based therapies. Tissue engineering. 2001;7(2):211-28.
18. Anghileri E, Marconi S, Pignatelli A, Cifelli P, Galie M, Sbarbati A, et al. Neuronal differentiation potential of human adipose-derived mesenchymal stem cells. Stem Cells Dev. 2008;17(5):909-16.
19. Rada T, Reis RL, Gomes ME. Distinct stem cells subpopulations isolated from human adipose tissue exhibit different chondrogenic and osteogenic differentiation potential. Stem cell reviews. 2011;7(1):64-76.
20. Levi B, Wan DC, Glotzbach JP, Hyun J, Januszyk M, Montoro D, et al. CD105 protein depletion enhances human adipose-derived stromal cell osteogenesis through reduction of transforming growth factor beta1 (TGF-beta1) signaling. The Journal of biological chemistry. 2011;286(45):39497-509.
21. Chung MT, Liu C, Hyun JS, Lo DD, Montoro DT, Hasegawa M, et al. CD90 (Thy-1)-Positive Selection Enhances Osteogenic Capacity of Human Adipose-Derived Stromal Cells. Tissue engineering Part A. 2013;19(7-8):989-97.
22. Mihaila SM, Frias AM, Pirraco RP, Rada T, Reis RL, Gomes ME, et al. Human adipose tissue-derived SSEA-4 subpopulation multi-differentiation potential towards the endothelial and osteogenic lineages. Tissue engineering Part A. 2013;19(1-2):235-46.
23. Pfaffl MW. A new mathematical model for relative quantification in real-time RT-PCR. Nucleic Acids Res. 2001;29(9):e45.
24. Lezhnina MM, Grewe T, Stoehr H, Kynast U. Laponite blue: dissolving the insoluble. Angewandte Chemie. 2012;51(42):10652-5.
25. Bourin P, Bunnell BA, Casteilla L, Dominici M, Katz AJ, March KL, et al. Stromal cells from the adipose tissue-derived stromal vascular fraction and culture expanded adipose tissue-derived stromal/stem cells: a joint statement of the International Federation for Adipose Therapeutics and Science (IFATS) and the International Society for Cellular Therapy (ISCT). Cytotherapy. 2013;15(6):641-8.
26. Izadpanah R, Trygg C, Patel B, Kriedt C, Dufour J, Gimble JM, et al. Biologic properties of mesenchymal stem cells derived from bone marrow and adipose tissue. Journal of cellular biochemistry. 2006;99(5):1285-97.
27. Gratton SE, Ropp PA, Pohlhaus PD, Luft JC, Madden VJ, Napier ME, et al. The effect of particle design on cellular internalization pathways. Proceedings of the National Academy of Sciences of the United States of America. 2008;105(33):11613-8.
28. Jevprasesphant R, Penny J, Jalal R, Attwood D, McKeown NB, D'Emanuele A. The influence of surface modification on the cytotoxicity of PAMAM dendrimers. International journal of pharmaceutics. 2003;252(1-2):263-6.
29. Herd H, Daum N, Jones AT, Huwer H, Ghandehari H, Lehr CM. Nanoparticle geometry and surface orientation influence mode of cellular uptake. ACS Nano. **2013**;7(3):1961-73.
30. Hillaireau H, Couvreur P. Nanocarriers' entry into the cell: relevance to drug delivery. Cellular and molecular life sciences : CMLS. **2009**;66(17):2873-96.
31. Zhang S, Li J, Lykotrafitis G, Bao G, Suresh S. Size-Dependent Endocytosis of Nanoparticles. Advanced materials. **2009**;21:419-24.
32. Ruzicka B, Zulian L, Ruocco G. More on the phase diagram of Laponite. Langmuir : the ACS journal of surfaces and colloids. **2006**;22(3):1106-11.
33. Rejman J, Oberle V, Zuhorn IS, Hoekstra D. Size-dependent internalization of particles via the pathways of clathrin- and caveolae-mediated endocytosis. The Biochemical journal. **2004**;377(Pt 1):159-69.
34. Shahin A, Joshi YM. Physicochemical effects in aging aqueous Laponite suspensions. Langmuir : the ACS journal of surfaces and colloids. **2012**;28(44):15674-86.

35. Zhai W, Lu H, Wu C, Chen L, Lin X, Naoki K, et al. Stimulatory effects of the ionic products from Ca-Mg-Si bioceramics on both osteogenesis and angiogenesis in vitro. Acta biomaterialia. 2013.
36. Gu H, Guo F, Zhou X, Gong L, Zhang Y, Zhai W, et al. The stimulation of osteogenic differentiation of human adipose-derived stem cells by ionic products from akermanite dissolution via activation of the ERK pathway. Biomaterials. 2011;32(29):7023-33.
37. Satija NK, Sharma D, Afrin F, Tripathi RP, Gangenahalli G. High throughput transcriptome profiling of lithium stimulated human mesenchymal stem cells reveals priming towards osteoblastic lineage. PloS one. 2013;8(1):e55769.
38. Gersbach CA, Le Doux JM, Guldberg RE, Garcia AJ. Inducible regulation of Runx2-stimulated osteogenesis. Gene therapy. 2006;13(11):873-82.
39. Ducy P, Zhang R, Geoffroy V, Ridall AL, Karsenty G. Osf2/Cbfa1: a transcriptional activator of osteoblast differentiation. Cell. 1997;89(5):747-54.
40. Takahashi T. Overexpression of Runx2 and MKP-1 stimulates transdifferentiation of 3T3-L1 preadipocytes into bone-forming osteoblasts in vitro. Calcified tissue international. 2011;88(4):336-47.
41. Harada H, Tagashira S, Fujiwara M, Ogawa S, Katsumata T, Yamaguchi A, et al. Cbfa1 isoforms exert functional differences in osteoblast differentiation. The Journal of biological chemistry. 1999;274(11):6972-8.
42. Kern B, Shen J, Starbuck M, Karsenty G. Cbfa1 contributes to the osteoblast-specific expression of type I collagen genes. The Journal of biological chemistry. 2001;276(10):7101-7.
43. Eijken M, Koedam M, van Driel M, Buurman CJ, Pols HA, van Leeuwen JP. The essential role of glucocorticoids for proper human osteoblast differentiation and matrix mineralization. Molecular and cellular endocrinology. 2006;248(1-2):87-93.
44. Lees S. Mineralization of type I collagen. Biophysical journal. 2003;85(1):204-7.
45. Jaiswal N, Haynesworth SE, Caplan AI, Bruder SP. Osteogenic differentiation of purified, culture-expanded human mesenchymal stem cells in vitro. Journal of cellular biochemistry. 1997;64(2):295-312.
46. Kirkham GR, Cartmell SH. Genes and proteins involved in the regulation of osteogenesis. In: Ashammakhi N, Reis RL, Chiellini E, editors. Topics in Tissue Engineering. 32007.
47. Zamani A, Omrani GR, Nasab MM. Lithium's effect on bone mineral density. Bone. 2009;44(2):331-4.
48. Buxton PG, Bitar M, Gellynck K, Parkar M, Brown RA, Young AM, et al. Dense collagen matrix accelerates osteogenic differentiation and rescues the apoptotic response to MMP inhibition. Bone. 2008;43(2):377-85.
49. Bellows CG, Aubin JE, Heersche JN. Initiation and progression of mineralization of bone nodules formed in vitro: the role of alkaline phosphatase and organic phosphate. Bone and mineral. 1991;14(1):27-40.
50. Orimo H, Shimada T. The role of tissue-nonspecific alkaline phosphatase in the phosphate-induced activation of alkaline phosphatase and mineralization in SaOS-2 human osteoblast-like cells. Molecular and cellular biochemistry. 2008;315(1-2):51-60.

SUPPLEMENTAL INFORMATION

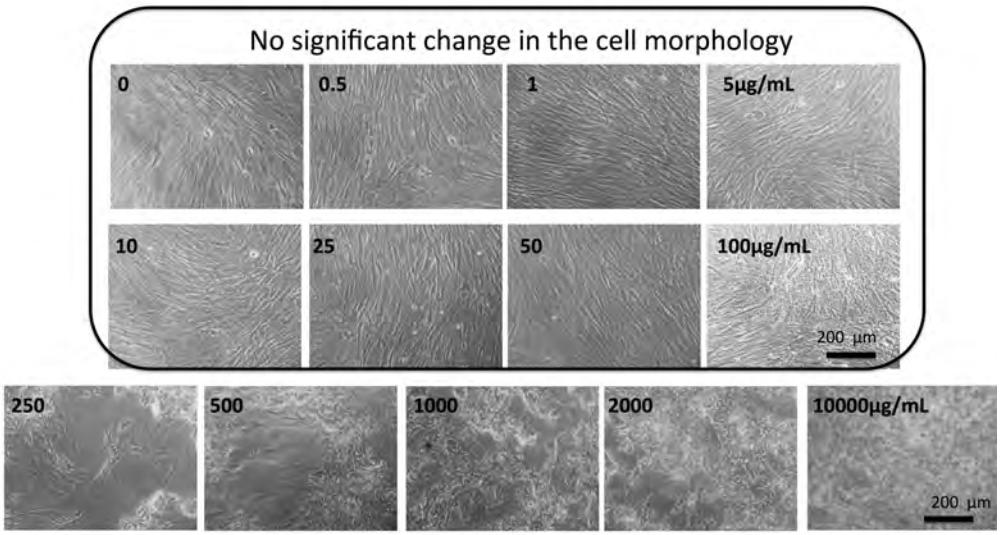

Supplemental Figure VI.1. Optical micrographs depicting the modification of cell morphology with the addition of sNPs. For concentrations <100µg/mL, cells maintain their fibroblast-like morphology. However, at concentrations >100µg/mL, cells begin to shrink and ultimately are covered by a dense sNPs "cloud".

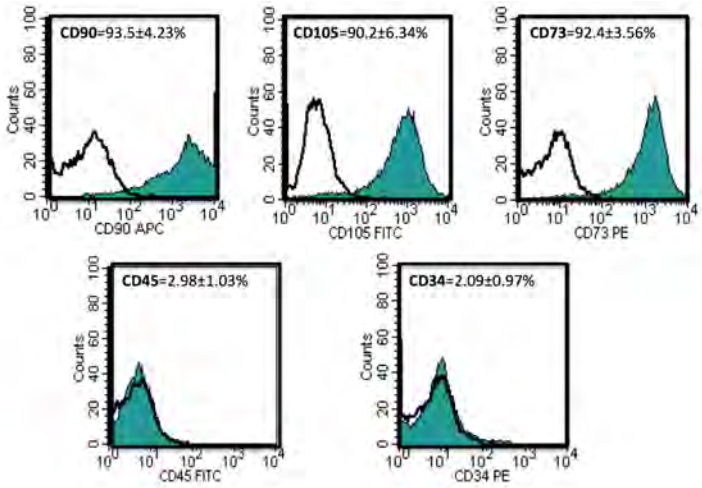

Supplemental Figure VI.2. SSEA-4^{+}hASCs characterization prior differentiation by flow cytometry. The cells were shown to possess a mesenchymal-like phenotype, exhibiting the characteristic panel of markers: CD90^{+}/CD105^{+}/CD73^{+}/CD45^{-}/CD34^{-}.

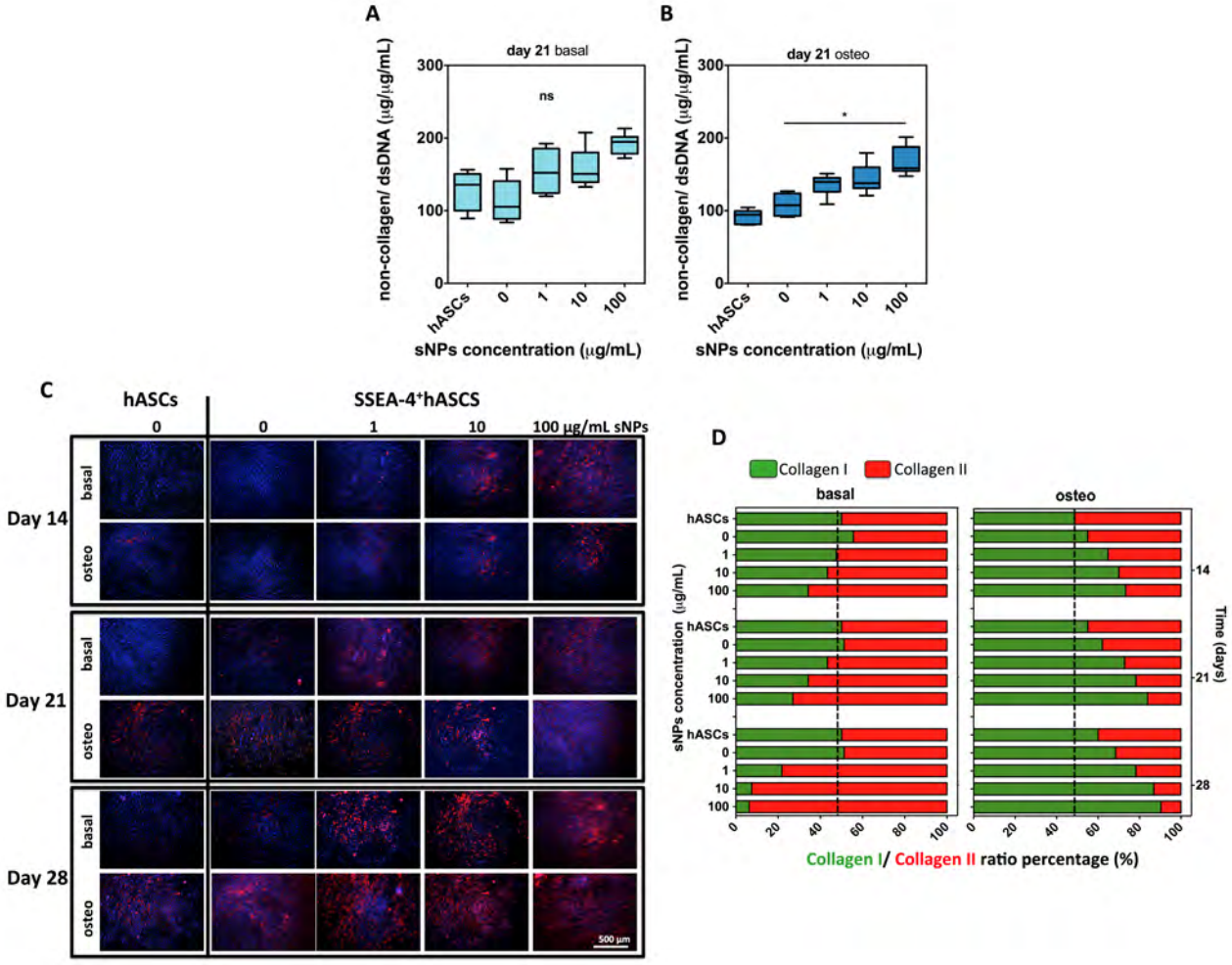

Supplemental Figure VI.3. Matrix characterization. Quantification of non-collagenous proteins normalized against the amount of dsDNA in basal (**A**) and osteogenic (**B**) media after 21 days of culture. In basal medium, the levels on non-collagenous proteins are kept at a constant level for all the conditions, while in osteogenic medium, only the SSEA-4^{+}hASCs with 100µg/mL sNPs exhibit a significant increase in the deposition of those proteins (*p<0.05). (**C**) Representative immunofluorescence images of the detection of collagen type II (red) over time for the different experimental conditions. Cell nuclei were counterstained with DAPI (blue). The addition of sNPs triggers the deposition of collagen type II in both basal and osteogenic media. (**D**) Collagen type I and Collagen type II ratio based on quantification of the staining area of immunocytochemistry images.

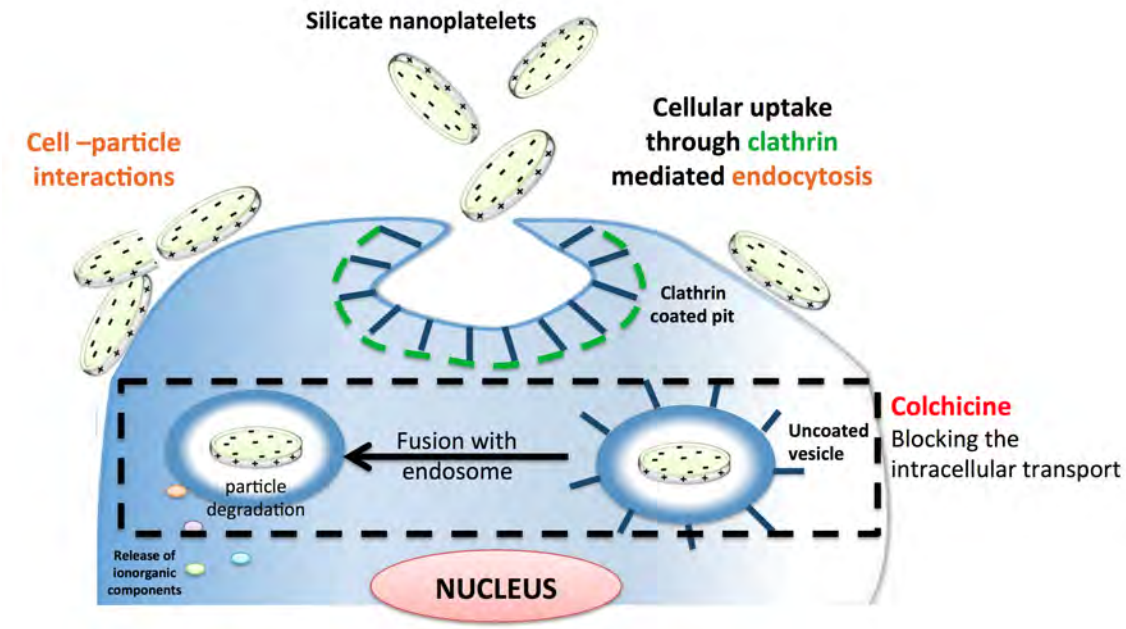

Supplemental Figure VI.4. Potential internalization mechanism of sNPs by SSEA-4^{+}hASCs. Based on the narrow sNPs range size, our hypothesis was that the cellular uptake predominately occured *via* clathrin-mediated endocytosis pathway. To confirm, an endocytotic restrictive drug (colchicine) was used to block the internalization of sNPs.

SECTION IV

KAPPA-CARREGEENAN-BASED HDYROGELS FOR THE CONTROLLED DISTRIBUTION OF CELLS

Chapter VII

Fabrication of Endothelial Cell-Laden Carrageenan Microfibers for Microvascularized Bone Tissue Engineering Applications

ABSTRACT

Angiogenesis, a critical process in bone tissue formation, remodeling and healing, is regulated by a number of biochemical factors produced by different cellular players. Among these, endothelial and osteoblastic cells sustain a finely orchestrated signaling network that determines the formation and organization of the new vasculature. This work proposes a system based on micro-sized hydrogel fibers that might be used as building blocks for the establishment of 3D hydrogel constructs for bone tissue engineering. For this purpose, chitosan (CHT) coated *kappa*-carrageenan (κ-CA) microfibers were developed using a two-step procedure involving ionotropic gelation (for the fiber formation) and polyelectrolyte complexation with CHT (for the enhancement of fiber stability). The performance of the obtained fibers was assessed regarding their swelling and stability profiles as well as their ability to carry and subsequently promote the outward release microvascular-like endothelial cells, without compromising their viability, phenotype and *in vitro* functionality. Finally the possibility of assembling and integrating these cell-laden fibers within a 3D hydrogel matrix containing osteoblast-like cells was evaluated.

Overall, the obtained results demonstrated the suitability of the proposed fibers for delivering microvascular-like endothelial cells and/or support the possibility of assembling these cell-laden micro-sized fibers into 3D hydrogels heterotypic constructs that may be used in bone tissue engineering approaches with improved vascularization.

This chapter is based on the following publication:

Mihaila SM, Popa EG, Reis RL, Marques AP, Gomes ME, "Fabrication of endothelial cell-laden carrageenan microfibers for microvascularized bone tissue engineering applications", Biomacromolecules 2014, 15(8): 2849-60, doi: 10.1021/bm500036a

VII.1. INTRODUCTION

In the last decade, tissue engineering (TE) has emerged as a multidisciplinary field at the interface of medicine, biology and engineering, aiming to fabricate tissue-like biological constructs[1]. However, the lack of a vasculature that can sustain the nutrient and oxygen demands within the tissue-engineered construct is a major limiting factor in creating thick artificial tissues[2]. Thus, developing vessel-like networks, as integrated templates within TE constructs[3], will be essential for creating real-size replicas of primary tissues or organs[4,5].

Hydrogels have been proven to be ideal cellular matrices, due to their hydrated state resembling native extracellular matrix (ECM)[6] and their high permeability to oxygen, nutrients and metabolites diffusion[7]. Additionally, natural-origin derived hydrogels showed high potential in the TE field, due to their macromolecular components and properties, similar to tissues ECM[8]. Several hydrogels-based processing methods (such as prototyping/printing[9], microfluidics[10] and photolitography[11]) are available to encapsulate endothelial cells (ECs) and develop vessel-like architectures using fiber structures with microsize features (~50μm[11] to 1mm[9]) as building units. However, they usually involve extent manipulation procedures, elaborated experimental settings and complex optimizations, thus limiting their applicability.

Alternatively to, wet spinning of hydrogels is a very simple and straightforward method, requiring minimal laboratorial utensils and short processing times. The wet spinning of hydrogels fibers involves the extrusion of polymer solution into a physiological solution that triggers the crosslinking of the polymer into a fiber-like shape. By applying this principle, hydrogel fibers of natural-origin biopolymers, such as alginate[12], collagen[13], gellan gum[14] and CHT[15], have been already developed.

Amongst natural-origin polymers, the carrageenans (CA) family stands out as potential candidate for TE applications, due to their mild gelation properties and resemblance with glycosaminoglycans (GAGs), highly present within the ECM of natural biological systems. Carrageenans occur as matrix material in several species of marine red algae (class of *Rhodophyceae*) acting structurally. Due to these half-ester sulphate moieties present on their backbone, carrageenans are strongly anionic polymers. As a consequence, their gelation occurs in the presence of appropriate counterions (K^+, Na^+ or Ca^{2+}), by ionic interactions. These hydrophilic polysaccharides are widely used as emulsifiers, gelling, thickening or stabilizing agents in food or pharmaceutical industry[16]. However, the noteworthy intrinsic thixotropic behavior of one type of carrageenans, kappa-carrageenan (κ-CA) has justified its exploitation as injectable matrix for the delivery of living cells[17,18,19] and

biomacromolecules[20,21]. Encouraging results have shown the potential of using κ-CA in the TE field[17-22], despite the high swelling ratios and mechanically instability in physiological conditions that have been attributed to the ionically crosslinked κ-CA hydrogels[23]. To increase the stability of hydrogels, several approaches such as chemical modifications with photocrosslinkable moieties[24], blending with other biopolymers[19, 25], addition of nanocomposites to the polymer solution[21], formation of interpenetrating networks[26] or polyelectrolyte complexation with polycations, such as CHT[27], have been exploited. Numerous studies have reported CHT polyelectrolyte complexation-based system with positive outcomes, both in the terms of stability, as well as cellular behavior[28]. Likewise, the electrostatic interactions between κ-CA and CHT lead to the development of nanoparticles[29], beads[30], layer-by-layer systems[31].

Herein, we report the production of CHT-coated κ-CA microfibers using a two-step-procedure aiming at being used as building blocks within 3D hydrogel constructs for bone tissue engineering. Firstly, κ-CA fibers of various diameters within the micron range were obtained by a wet spinning technique. Secondly, κ-CA fibers were coated with CHT, by means of electrostatic interaction between the polymers, in order to reinforce the fibers and enhance their stability under a physiological microenvironment. The produced fibers were then loaded with microvascular-like ECs obtained from the SSEA-4$^+$ sub-population of adipose tissue. Thus, we took advantage of our knowledge to obtain ECs in relevant cell numbers[32] to developed cell-laden κ-CA-based hydrogel fibers to be used as vascularization promoters with tri-dimensional (3D) TE constructs. The phenotype and functionality of the ECs were evaluated prior and after entrapment within the fibers. Ultimately, envisioning the vascularization of bone-like constructs, we proposed an innovative 3D build-up of fibers loaded with ECs, entrapped within a hydrogel disc containing osteoblast-like cells.

VII.2. MATERIALS AND METHODS

VII.2.1. Materials

κappa-carrageenan (κ-CA), potassium chloride (KCl) and beta-glycerophosphate disodium salt hydrate (βGP) were purchased from Sigma, Germany. Reagent grade medium molecular weight chitosan (CHT) (Sigma, Germany) with a 90% degree of acetylation was used. Prior use, CHT was purified using a precipitation method[33]. All other reagents were used as received.

VII.2.2. Development of CHT coated κ-CA fibers

VII.2.2.1. Production of κ-CA fibers through ionotropic gelation

The *κ*-CA hydrogel fibers were obtained by a wet spinning technique, which consists of the

extrusion of the polymer solution through a needle immersed in a coagulation bath, as previously described elsewhere[19]. Briefly, a 1.5% (wt/v) κ-CA solution was prepared by dissolving the polymer into distilled water under temperature (up to 50°C) and constant stirring until complete dissolution was achieved. Subsequently, the κ-CA solution was loaded into 5 mL syringes headed and κ-CA fibers with different diameters were obtained by extruding the polymeric solution through needles of different gauges directly into the coagulation bath, a 5% (wt/v) KCl solution prepared in distilled water. The presence of K^+ ions initiates the ionotropic gelation, by counterbalancing the negative charges of κ-CA. The fibers were allowed to harden in the coagulation bath for about 10 min, sufficient time for the fibers to retain their shape. Finally, the fibers were washed with phosphate buffered saline (PBS) in order to remove the excess of salt. Fibers obtained with needles of 25 and 27G with a diameter below 1mm, were selected for all the subsequent assays.

VII.2.2.2. Optimization of the pH of the CHT working solution

CHT, a natural-origin polycation, dissolves in acid solution, which limits its use in the presence of living cells. Based on previous studies[34], βGP, a weak base, was shown to increase the pH of the CHT solution, without jeopardizing its solubility. In this context, a curve of variation of pH with the addition of βGP to the CHT solution was determined in order to establish the conditions that may enable the incorporation of cells, while allowing the formation of polyelectrolyte complexes. The CHT solution was prepared by dissolving the polymer into a 1% (v/v) acetic acid solution to a final concentration of 0.5% (wt/v). In order to determine the degree to which the addition of βGP affects the overall charge of the CHT solution, zeta potential measurements were performed using a Malvern Zeta Sizer Nano ZS (Malvern Instruments, UK). Each sample was diluted in water at a concentration of 0.1% (wt/v) and analyzed at 25°C for 60 seconds.

VII.2.2.3. Coating of κ-CA fibers through polyelectrolyte complexation with CHT

The κ-CA fibers, previously obtained by ionotropic gelation, were immersed in the optimized CHT solution (0.5% (wt/v) and pH=5.5) for 20 min, followed by several washing steps with PBS in order to remove the excess of CHT. The presence of the CHT coating was evaluated by staining the fibers with Eosin Y (Sigma, Germany), an anionic dye. Fibers without coating were used as negative control.

VII.2.3. Physico-chemical characterization of the developed fibers

VII.2.3.1. Swelling kinetics

The influence of the CHT coating on the swelling and stability of the developed κ-CA fibers was determined by evaluating the water absorption kinetics and fibers diameter variation

upon immersion of the coated and uncoated fibers in standard culture medium for up to 21 days. Standard medium, Dulbecco's Modified Eagle Medium (DMEM, Gibco, USA) supplemented with 10% (v/v) HiFBS (Gibco, USA) and 1% (v/v) antibiotic/antimycotic (penicillin/streptomycin, 100U/100 µg/mL, Gibco, UK) was used, envisioning fibers use for cell encapsulation/culturing. For the same reason, the experimental parameters were set at physiological temperature (37°C) and under humidified atmosphere with 5% of CO_2. Medium was replenished every 3-4 days. Fibers were allowed to reach equilibrium in the culture medium and at days 7, 14 and 21, samples (n=3) were retrieved and blotted with KimWipe paper to remove the excess of liquid. The wet weight (M_W) was determined by weighting the samples, and their final dry weight (M_{DF}) was determined upon lyophilization. The swelling kinetics was defined as the ratio between the liquid uptake (M_W-M_{DF}) and the final dry mass of polymer (M_{DF}), according to **equation VII.1**.

$$\text{Mass swelling ratio} = (M_W - M_{DF}) / M_{DF} * 100 \qquad (\textbf{equation VII.1})$$

The final diameter of the hydrogel fibers was also measured applying software-measuring tools (ImageJ software, http://rsbweb.nih.gov/ij/) to at least three micrographs of each sample.

VII.2.3.2. Morphological and chemical characterization

Concomitant with the swelling behavior analysis at the pre-selected time points, samples were retrieved for surface morphological evaluation by scanning electron microscopy (SEM) and elemental analysis using energy-dispersive X-ray spectroscopy (EDX/EDS). Briefly, fibers were snap frozen in liquid nitrogen, transferred to eppendorfs and freeze dried overnight. The dried samples were carefully mounted on samples holders using double-side carbon tape. Before being analyzed by SEM (Nano-SEM FEI Nova 200), the samples were gold sputter coated (Fisons Instruments, sputter coater SC502, UK). Elemental analysis was carried out with an energy dispersive spectrometer (EDAX-Pegasus X4M). All observations/image acquisitions and measurements were made at an acceleration voltage of 15 kV.

VII.2.4. Isolation and endothelial differentiation of SSEA-4$^+$hASCs

Lipoaspirate samples from healthy donors were kindly provided by Hospital de Prelada (Porto, Portugal), under previously established protocols and with informed consent of the patients. The selection of SSEA-4 positive cells (SSEA-4$^+$hASCs) residing within the stromal vascular fraction of the adipose tissue and differentiation towards the endothelial lineage were performed according to our previously published[32]. Briefly, the SSEA-4$^+$hASCs were

selected using immunomagnetic beads (Dynal M-450 Epoxy beads from Dynal Biotech, Carlsbad, CA, USA) coated with SSEA-4 antibody (Abcam, Cambridge, UK). Then, the selected SSEA-4$^+$hASCs cells were differentiated towards endothelial lineage by culturing them for 2 weeks in endothelial cell growth medium, EGM-2 MV bullet kit (Lonza, Switzerland), containing 5% FBS and supplemental growth factors: hydrocortisone, hFGF-B, ascorbic acid, gentamicin/amphotericin, VEGF, Long R3-IGF-1, hEGF and 0.5 mL, at concentrations established by the manufacturer.

VII.2.5. SSEA-4$^+$hASCs-derived ECs encapsulation within κ-CA fibers

The *κ*-CA, CHT and KCl solutions for producing cell-loaded fibers were sterilized at 120°C for 30 mins. Endothelial differentiated SSEA-4$^+$hASCs at passage 3, were trypsinized and centrifuged, and further suspended in EGM-2 MV at a final cell density of 2x10^6 cells per mL of polymeric suspension. Fibers containing cells and with and without CHT coating were produced as described above. The cell-loaded fibers were then transferred to 24-well plates and maintained in culture for 21 days, at 37°C in a humidified atmosphere with 5% of CO_2. Cell culture medium was replenished every 3-4 days.

In order to assess the maintenance of the phenotype of the SSEA-4$^+$hASCs cells upon 21 days of culture, fibers containing cells were transferred to sterile eppendorfs and digested with 0.1% proteinase K (vWR, Portugal) in 1mM EDTA (Sigma, Germany), 50 mM TrisHCl (Sigma, Germany) and 1mM iodoacetamide buffer (Sigma, Germany), for one hour at 37°C, under constant agitation. The cellular pellet recovered after centrifugation (10 min, 400x*g*) was resuspended in EGM-2 MV medium and plated into tissue culture flasks until reaching confluence and for further analysis.

VII.2.6. Characterization of the constructs

VII.2.6.1. Microscopic analysis

Variations of the shape and diameter of the developed cell-loaded fibers, with or without CHT coating, as well as the potential migration of the cells from the fibers to the culture well, were examined using a stereomicroscope (Stemi 1000, Zeiss, Germany) along the time of culture.

VII.2.6.2. Calcein-AM assay

At selected time culturing points (1, 7, 14 and 21 days), cell-loaded fibers were washed with PBS and incubated with 4µM calcein-AM (Invitrogen, USA) for 40 minutes followed by 10 min incubation with 1µM propidium iodide (Invitrogen, USA). Samples were then washed and fixed for 40 mins in 10% formalin. After fixation, samples were washed with PBS and

cell nuclei were counterstained with DAPI. Representative fluorescent micrographs were acquired using the Axioplan Imager Z1 fluorescence microscope (Zeiss, Germany) and the AxioVision 4.8 software (Zeiss, Germany).

VII.2.6.3. Flow cytometry

Endothelial differentiated SSEA-4$^+$hASCs expanded to passage 4 and the ones recovered from the fibers and further expanded were retrieved from cell culture flasks using TrypLE Express (Invitrogen, USA)**.** 5x10^5 cells were incubated for 30 min, at 4°C with the following markers: CD45-FITC, CD34-PE, CD73-PE, CD31-APC (all from BD Pharmingen, USA) and CD105-FITC and CD90-APC (eBiosciences, USA) at a concentration of 6µg/mL, as recommended by the manufacturer. After washing with PBS, the cells were resuspended in the acquisition buffer (PBS containing 1% formaldehyde and 0.1% sodium azide) and analyzed in a BD FACS-Calibur flow cytometer (BD Biosciences, USA). A minimum of 20,000 events was acquired and gated in a forward versus side-scatter dot plot with a linear scale. Results were displayed in histogram plots created using the CellQuest software (BD Biosciences, USA). The number of positive events for each cell-specific marker was expressed as the percentage of the total cell number.

VII.2.6.4. Matrigel assay

Endothelial differentiated SSEA-4$^+$hASCsat passage 2 were trypsinized and plated at a density of 3x10^4 cells/well in triplicate in 48-well plates coated with 64µL of Matrigel (BD Biosciences, USA). Cells were incubated for 4h at 37°C before fixation with 10% formalin. One hour prior fixation, calcein-AM (Invitrogen, USA) was added to the wells at a final concentration of 4µM. Upon fixation, cell nuclei were counterstained with 4,6-diamidino-2-phenyindole dilactate (DAPI, Sigma, Germany), at a 1:10,000 dilution in PBS, for 10 min, and then washed three times with PBS. Three representative images were acquired under an Axioplan Imager Z1 fluorescence microscope (Zeiss, Germany) using the Axio Cam MRm camera (Zeiss, Germany) and the AxioVision 4.8 software (Zeiss, Germany).

VII.2.7. Assembling of κ-CA fibers into 3D hydrogel discs

Cell-laden fibers containing endothelial differentiated SSEA-4$^+$hASCs labeled with a green fluorescent protein (GFP) tag were transferred to a petri dish and allowed to settle randomly. A freshly prepared solution of κ-CA containing osteogenic differentiated SSEA-4$^+$hASCs obtained according to a method described elsewhere[32], and labeled with a rhodamine tag, was poured onto of the fibers until full coverage. The crosslinking of the κ-CA solution forming stable 3D hydrogel discs was achieved with a 5% (wt/v) KCl solution. After crosslinking, the cells nuclei were stained with DAPI. The hydrogels discs containing the

fibers were then washed with PBS and observed under a confocal laser scanning microscopy (CLSM, Olympus, Fluoview 1000). YZ and XY projections were performed in order to evaluate the cellular distribution throughout the structures.

VII.2.8. Statistical analysis

Statistical analysis was performed using GraphPad Prism 5.00 software (San Diego, USA). Statistical differences ($p<0.05$) were determined using one-way ANOVA, followed by a Tukey post test.

VII.3. RESULTS AND DISCUSSION

3D cell-culture models have recently received great attention because they often promote tissue organization which does not occur in conventional 2D culture systems[35]. Since the architecture and chemical composition of hydrogels can be easily engineered, hydrogels have been utilized as tools and platforms to design selective capture and release of cells in/from 3D cell culture systems[36]. For instance, microfabrication methods have been engineered to replicate the spatial complexity of vasculature within tissue by creating vessel-like hydrogel fibers with controlled spatial distribution of cells[9-11]. In the perspective of generating vascular templates within bone-mimicking matrices, co-culture systems that enclose both ECs and osteoblasts, in an organized manned[37], have been proposed as ideal to recreate the major heterotypic cellular interactions within bone. However, these methods require sophisticated equipment and elaborated experimental setups that are not available in all research laboratories.

Thus, we aimed to develop hydrogel microfibers that can accommodate ECs without jeopardizing their functionality, envisioning their use for microvascularization in bone TE. The method of choice was wet spinning as it implies simple experimental minimal laboratorial reagents and consumables.

VII.3.1. Different diameter κ-CA fibers formation through ionotropic gelation

Carrageenans are highly sulphated galactans and have the common feature of being linear polysaccharides with a repeating structure of alternating 3,6-anhydro-D-galactose and β-D-galactose-4-sulphate[38]. In the particular case of κ-CA, gels can be formed by ionotropic gelation. Due to the highly negative charged sulphate group present on its backbone, κ-CA is a strong anionic polymer. As a consequence, its gelation can occur in the presence of in the presence of cations (K^+ ions), κ-CA chains undergo a conformational transition from random coil to coaxial double helices, and consequently, to an organization of the helices into a strong and rigid 3D gel-like network[39,40].

Moreover, κ-CA has been exploited as injectable matrix, due to its intrinsic sheer thinning behavior, particularly thixotropic. This means that upon applied stress, the organization of the κ-CA chains is disrupted, but it will reset once the deformation is removed[24]. This property renders the use of κ-CA solutions as injectable matrixes, as they can be easily extruded through narrow needles without affecting the entrapped biomolecules or cells[22,41]. Taken together, the temperature-induced and ionotropic gelation enable the formation of gels into different shapes, including fibers, highlighting therefore the versatility of κ-CA processability[8].

In the present study, κ-CA hydrogel fibers were formed by extruding the κ-CA solution through needles of different gauges (**Figure VII.1A**), into a coagulation bath containing K^+ salts, as described elsewhere[19]. Using a needle gauge range from 18 to 27G (0.838 - 0.210 mm internal diameter), it was possible to obtain fibers with different diameters, directly proportional with the internal diameter of the needles. The fibers produced within these settings have a diameter ranging from 0.5 to 1.25 mm (**Figure VII.1B**), making them more appealing for further applications[12,42,43]

Taking into consideration that the microvasculature relies on the interconnectivity of micro-sized vessel, we decided to explore the potential to sustain ECs viability of κ-CA fibers with the smallest diameters, obtained by the extrusion of κ-CA solutions through the 25G and 27G.

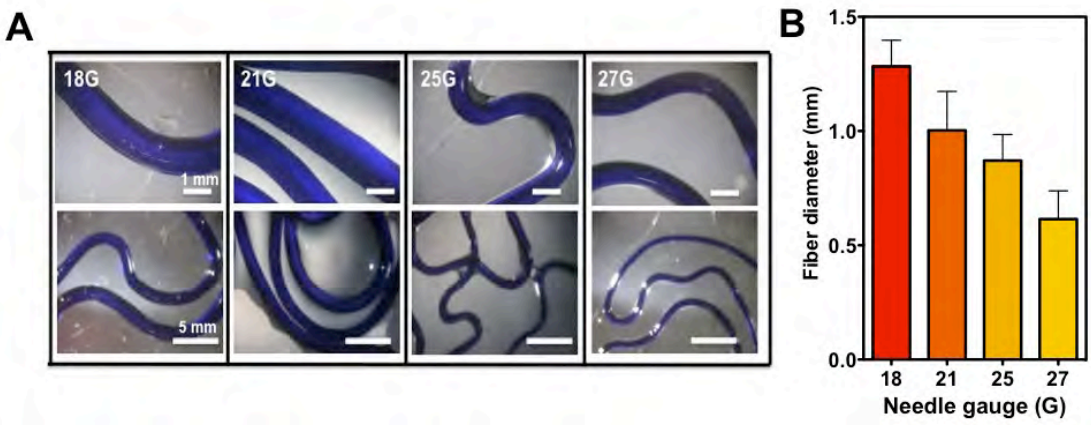

Figure VII.1. κ-CA fibers formed by ionotropic gelation and stained with methylene blue for contrast purposes. (**A**) Needles with different gauges, from 18G to 27G, were used to form the hydrogel fibers. (**B**) Depending on the needle gauge used to extrude the κ-CA solution, the fibers display various diameters ranging from 1.25 cm down to 0.5 cm.

VII.3.2. CHT coated κ-CA fibers through polyelectrolyte complexation depict improved stability

Although encouraging results have shown the potential of using κ-CA in tissue engineering applications, the ionically crosslinked κ-CA hydrogels exhibit high swelling ratios, as a result

of uncontrollable and permanent exchange of K^+ ions with other positive ions present in different physiological relevant settings[23]. Furthermore, this behavior leads to loosening of the inner chain network strength and weakening of the structures mechanical stability[24, 44].

In order to reinforce the structure of κ-CA hydrogels, several methodologies have been employed[19,24,26], including the formation of a polyelectrolyte complex (PEC). PECs are formed by the ionic interaction between oppositely charged polyelectrolytes. We hypothesized that by coating the κ-CA hydrogels fibers with CHT we would be able to stabilize the fibers structure. CHT, composed of β-1,4-linked glucosamine and N-acetyl-D-glucosamine and one of the few positively charged natural-origin polysaccharides, is one of the most used polycations for the formation of PECs. Furthermore, it has been extensively used within TE strategies due to its appealing properties such as biocompatibility, biodegradability, low toxicity and relatively low production costs from abundant sources[45]. Since CHT is positively charged at low pH values (below its pK_a value), the cationic amino groups of CHT can spontaneously associate with negatively charged groups (carboxylic acid, hydroxyl or sulphate groups) of other polymers, to form PECs. In an acidic solution, the negatively charged sulfate groups of κ-CA bind to the positively charged amino groups of CHT and form an acid-base type PECs.

As the formation and stability of these polyelectrolyte complexes depends on the degree of ionization of each one of polyelectrolytes, which is dictated by the pH at which the PECs are being formed and because CHT only dissolves at pH~1, extremely harsh conditions for cells, βGP, a weak base, was used[34]. By adding βGP, the pH slowly increased, until it reached the CHT pK_a, from 6.5 to 6.8[46], at which precipitation occurred (**Figure VII.2A**). Moreover, upon increasing pH, the amino groups of CHT are de-ionized and the binding affinity to a polyelectrolyte molecule (like κ-CA) becomes weaker, which would lead to less stable PECs. With the addition of βGP, and consecutively with the increase of pH, the electrical charge of the CHT solution also varied as evaluated by zeta potential measurements (**Figure VII.2B**). As expected, with the increase of the pH of CHT solution, the overall charge of the solution decreased, though still in the positive range (> +10eV). This finding indicates that albeit the pH modification, up to pH 5.5 the protonation of the amino groups occurs, and consequently CHT continues to act as a polycation, being suitable for association with polyanions, i.e. κ-CA, to form PECs. In the perspective of encapsulating cells in the presence of a CHT solution in combination with the negatively charged κ-CA, the pH 5.5 was considered both for allowing the complete CHT dissolution and the maintenance of mild conditions that do not compromise cell viability.

Therefore, the formation of CHT coated κ-CA fibers was achieved in a two-steps procedure that combined the ionotropic gelation of κ-CA into microfibers, followed by the reinforcement

of the fibers by polyelectrolyte complexation between κ-CA and CHT (**Figure VII.2C**). As the gelation time was relatively short (10 minutes), compared to standard gelation times (15 to 30 minutes)[19,22]. κ-CA was only partially crosslinked. This allowed maintaining some available negative sulphate groups, prone for binding to the protonated amino groups of CHT. Consequently, the immersion of the κ-CA fibers within the CHT solution at pH 5.5, allowed the formation of PECs between CHT and the un-crosslinked chains of κ-CA present at the surface of the fibers, leading to the formation of a localized CHT nano-sized layer, as already shown in previous studies[28-31]. The presence of the CHT coating was confirmed by the intense, specific pink coloration observed only on the coated fibers after staining with Eosin Y (**Figure VII.2C-C1insert**).

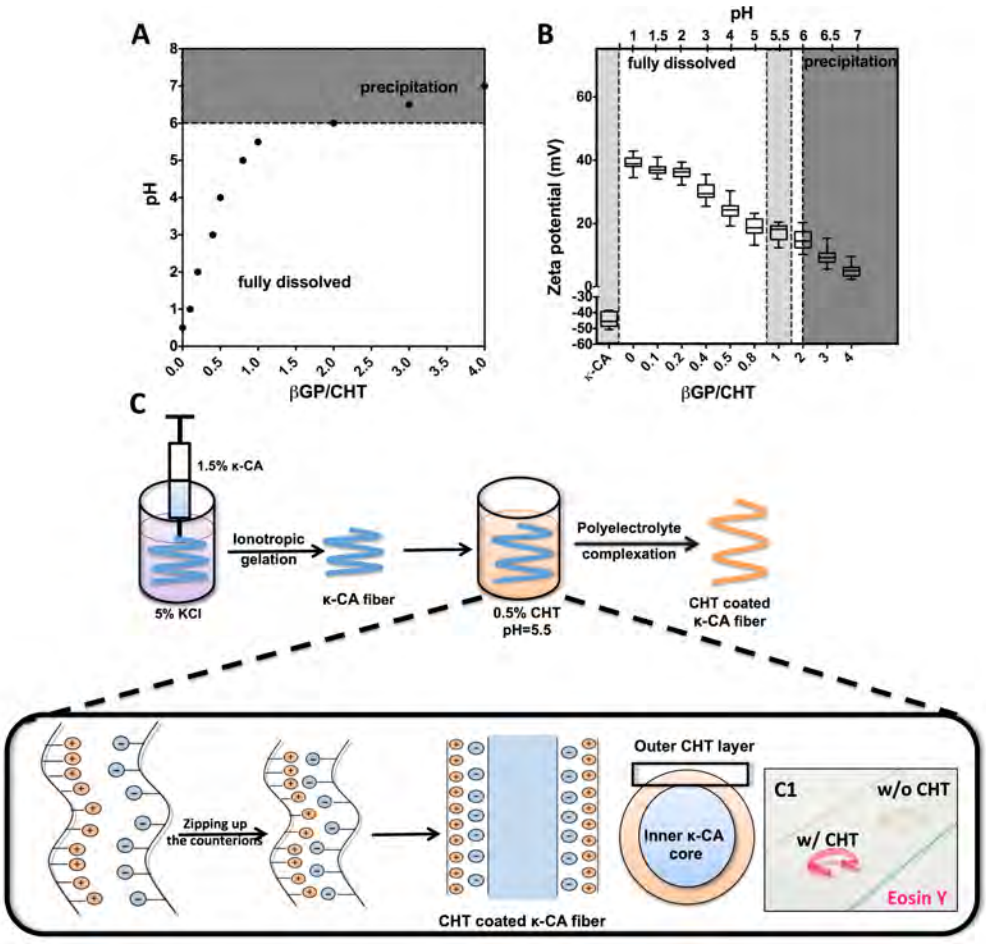

Figure VII.2. Production of CHT coated κ-CA hydrogel fibers. (**A**) Variation of the pH relative to the beta glycerophosphate (βGP)/Chitosan (CHT) ratio. With the addition of βGP, CHT solutions can be obtained at physiologically relevant conditions (pH 5.5-6). Above this point the precipitation of CHT occurs (dark grey areas). (**B**) With the addition of βGP the zeta potential of the CHT solution is dramatically affected. The zeta potential of k-CA solution was used as reference (~-40 mV). Values reported correspond to n=10 (**C**) Schematics of the production of CHT coated κ-CA hydrogel fibers. The process involves the formation of fibers by ionotropic gelation in a KCl coagulation bath, followed

by immersion in a CHT solution. (**C1**) Identification of the CHT (pink) after staining with Eosin Y only in the coated fibers.

Upon coating, our concern was to confirm that the stability of the developed fibers was improved. In fact, fibers were easy to separate and stable during manipulation, despite their small diameters. Swelling studies performed by immersion of the coated and uncoated κ-CA fibers in culture medium revealed that the swelling ratio of ionically crosslinked κ-CA fibers increased along time, which is in agreement with previous studies performed on κ-CA hydrogels discs[22], but the CHT coated fibers exhibits a stable swelling ratio over time (**Figure VII.3A**). In the uncoated fibers, the destabilization of the ionically crosslinked κ-CA network due to the continuous exchange of K^+ ions entrapped within the network with other ions present in the culture medium is likely to be occurring. Similar results have been reported for ionically crosslinked alginate[23] and gellan gum[44], where prolonged immersion in culture medium led to the destabilization and weakening of the hydrogels network. Along the time, the uncoated fibers became soft and easy to break, limiting their manipulation. However, with the CHT coating, the fibers remained stable over the 21 days of exposure to culture medium and maintained their initial swelling, being easy to handle and to manipulate. This behavior can be due to the strong electrostatic interactions between the amino groups of CHT and sulphate moieties of κ-CA that lead to the formation of a robust, protective PEC layer that coats the fibers and prevents them from collapsing. A similar behavior was described in other studies, concerning the use of CHT in combination with alginate to form a PEC layer wrapping alginate beads for the controlled release of drugs[28].

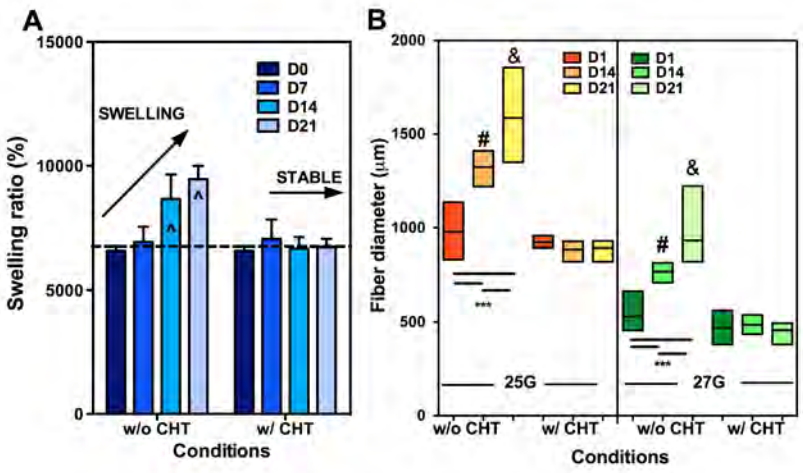

Figure VII.3. Swelling behavior of κ-CA fibers, without (w/o) and with (w/) CHT coating, in culture medium (DMEM). (**A**) Swelling ratio increases along time for the fibers without CHT coating. On the other side, the CHT coating stabilizes the hydrogels fibers, hampering their swelling. Values correspond to averages (n=3) ± standard deviation. "^" corresponds to statistical difference when compared with day 0 and day 7 values. (**B**) The diameter of the developed fibers is a direct

consequence of the swelling behavior. The behavior is independent of the needle gauge tested (25 and 27G). Values correspond to n=10. The symbols "#" and "&" represents a statistical difference between the w/o and w/ CHT within the same day (one-way ANOVA, Tukey post test).

Increased swelling ratios can affect some features of the hydrogels characteristics such as shape, size, mechanical properties and consequently, its stability. In accordance, the diameter of the κ-CA fibers increased over time, as a consequence of their increasing swelling ratio (**Figure VII.3B**), and independently of their size. On the other hand, as the CHT coating protects the fibers from swelling, it also leads to the maintenance of the initial diameter of the fibers up to 21 days. SEM analysis of the morphology of the fibers upon immersion in culture medium for different time periods revealed that the uncoated κ-CA fibers started to lose their integrity around day 14 (**Figure VII.4A1,3,5**), as predicted by the swelling ratio results (**Figure VII.3A**). Oppositely, the fibers with the CHT coating, exhibited a rougher surface that wrapped the open-pore-like structure of the κ-CA core. These fibers maintained their shape, size and integrity until day 21, when small cracks become visible on the surface of the fibers (**Figure VII.4A2,4,6**).

A

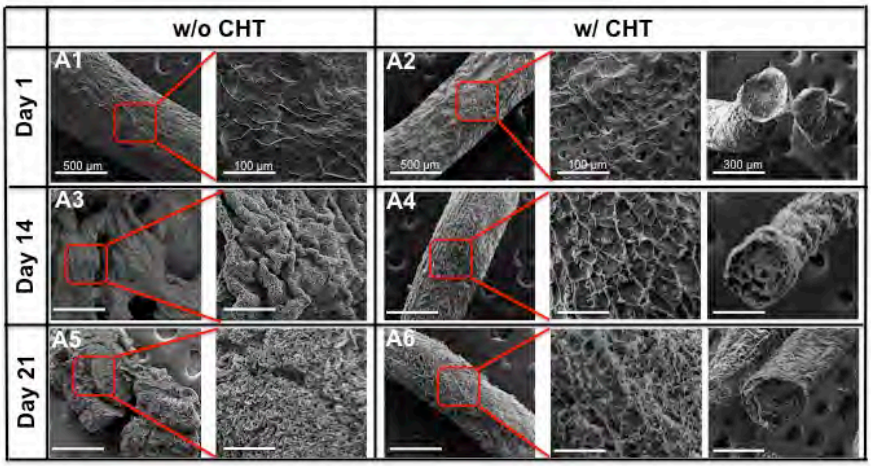

B

Time (days)	Conditions	EDX/EDS elemental analysis (%wt) C	O	S	K	Cl	N
1	w/o CHT	26.01	25.82	4.49	9.64	22.32	-
	w/ CHT	35.40	31.67	4.04	1.33	13.19	5.79
14	w/o CHT	31.27	18.8	3.85	7.90	25.15	-
	w/ CHT	41.62	22.38	5.15	1.81	12.04	7.01
21	w/o CHT	41.54	13.5	2.58	1.71	26.67	-
	w/ CHT	24.79	12.88	3.64	1.28	35.25	4.47

Figure VII.4. Physico-chemical characterization of the freeze-dried fibers. (**A**) SEM micrographs depicting the alterations of fibers morphology in culture media along time. The structure of the uncoated fibers is not stable and disintegrates after 21 days (A1-A3-A5), while the CHT coating exhibits a protective role that hinders the disintegration of the fibers and therefore, enhances their

stability when immersed in culture media (A2-A4-A6). (**B**) The integrity of the CHT coating along the time was followed by tracing by EDX/EDS the amount of nitrogen (from the $–NH_2$ groups present on the CHT backbone) present on the surface of the fibers. The element was detected until day 21, suggesting that the CHT is still present on the fibers. The defined squares in the SEM micrographs represent the area where the magnification and elemental analysis were performed.

The integrity of the CHT coating along the time was further demonstrated by tracing the N content on the surface of the CHT-coated κ-CA fibers by EDS/EDX (**Figures VII.4B**) along the time. Its detection up to day 21, suggests that the CHT-κ-CA electrostatic interactions are strong enough to withstand the presence of other ions and proteins that constitute the culture medium, leading to a robust and stable structure.

VII.3.3. CHT coating of the cell-loaded κ-CA fibers does not affect the endothelial differentiated SSEA-4$^+$hASCs phenotype in the long-term

The success of creating a functional engineered tissue relies on the development of a proper microvascular network that can provide the venue for nutrients and oxygen delivery within the constructs[47]. A major hurdle is encountered when engineering thick tissues and large organs, where the lack of such network leads to immediate failure[48,49]. Pre-vascularization of engineered constructs taking advantage of progenitor/ECs has been considered the most promising strategy to tackle this issue[50]. However, the use of human progenitor/ECs has been hampered by the limited sources and the reduced yields[51]. Our earlier work[32] has shown that the SSEA-4$^+$ sub-population, selected amongst the heterogeneous stromal vascular fraction, can be differentiated towards both the endothelial and the osteogenic lineages. Moreover, the endothelial differentiated SSEA-4$^+$hASCs hold features of microvascular ECs, worth to explore to trigger the formation of 3D vascular networks within engineered constructs. Therefore, we took advantage of our knowledge to obtain ECs from the SSEA-4$^+$ sub-population (**Supplemental Figure VII.1**) in relevant cell numbers to develop cell-laden κ-CA-based hydrogel fibers to be used as vascularization promoters within 3D TE constructs. Endothelial differentiated SSEA-4$^+$hASCs were encapsulated within the κ-CA and CHT coated κ-CA fibers with 2 different diameters and cultured for a period of 21 days (**Figure VII.5A**). As the encapsulation procedure requires several steps, many times associated to reduced cellular performance[52,53], the direct effect of the experimental conditions over the viability of the encapsulated cells was assessed 24 hours upon encapsulation. Independently of the size and coating of the fibers the majority (>80%) of the cells was viable and homogeneously distributed within the fibers (**Figure VII.5B**) confirming that the processing conditions were not harsh for cells. Additionally, viable cells were predominantly observed within the fibers along the time in culture and independently of the

conditions (**Figure VII.6**).

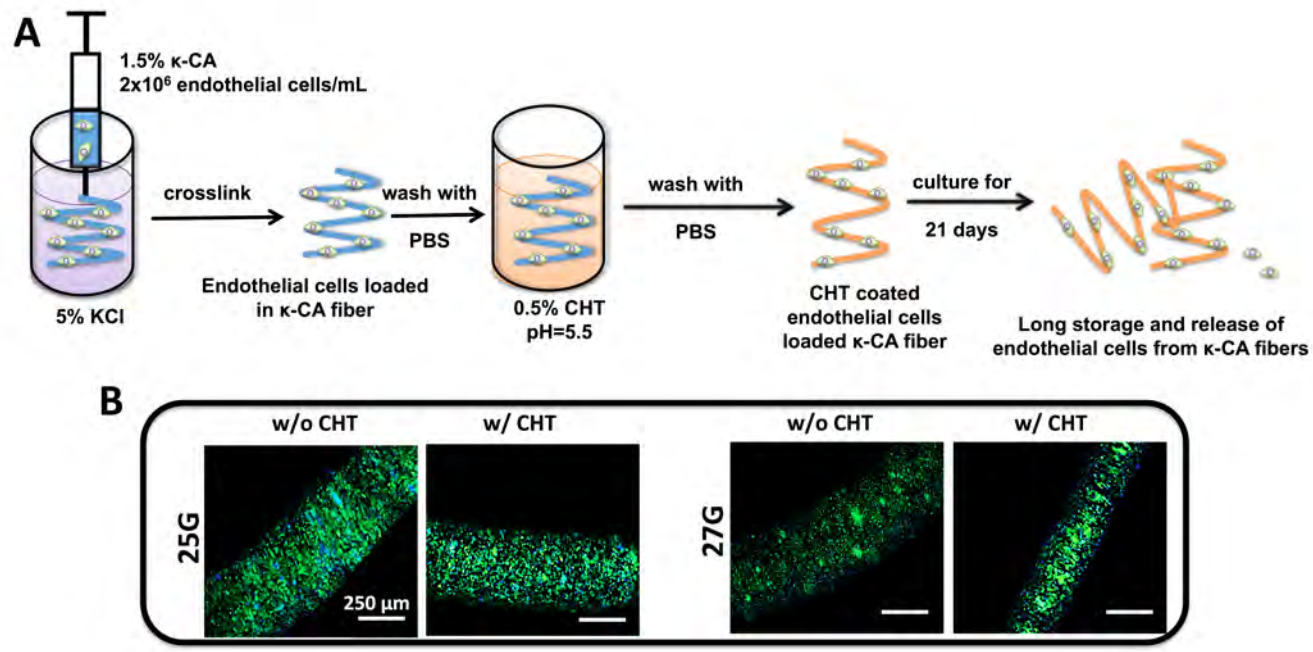

Figure VII.5. Encapsulation of endothelial differentiated SSEA-4^{+}hASCs into κ-CA fibers. (**A**) Schematics of the encapsulation procedure and experimental setup. (**B**) The assessment of cell viability (live/dead) 24 hours after encapsulation, shows that the cells were not affected by the processing method or by the size and CHT coating of the fibers. Cell nuclei were counterstained with DAPI (blue).

The optical microscopy analysis of the cell-loaded κ-CA fibers showed an increased diameter along the time in culture and subsequent disintegration of the fibers, in agreement with the results obtained with acellular fibers. Concisely, at day 7, fibers were intact, with a well-delimited smooth surface but at day 14, uncoated fibers presented signs of disintegration. This allowed the entrapped cells to “escape” from the fiber, and to adhere to and proliferate on the well (**Figure VII.6A1-C1**). In opposition, the CHT coating delayed the disintegration of fibers, as they maintained their initial diameter and their surface was smooth without disruptions up to day 14 (**Figure VII.6A2-B2**). Only at the last timepoint the CHT coated κ-CA fibers started to exhibit cracks along their surface, and consequently, ECs colonies were observed on the bottom of the well (**Figure VII.6C2**).

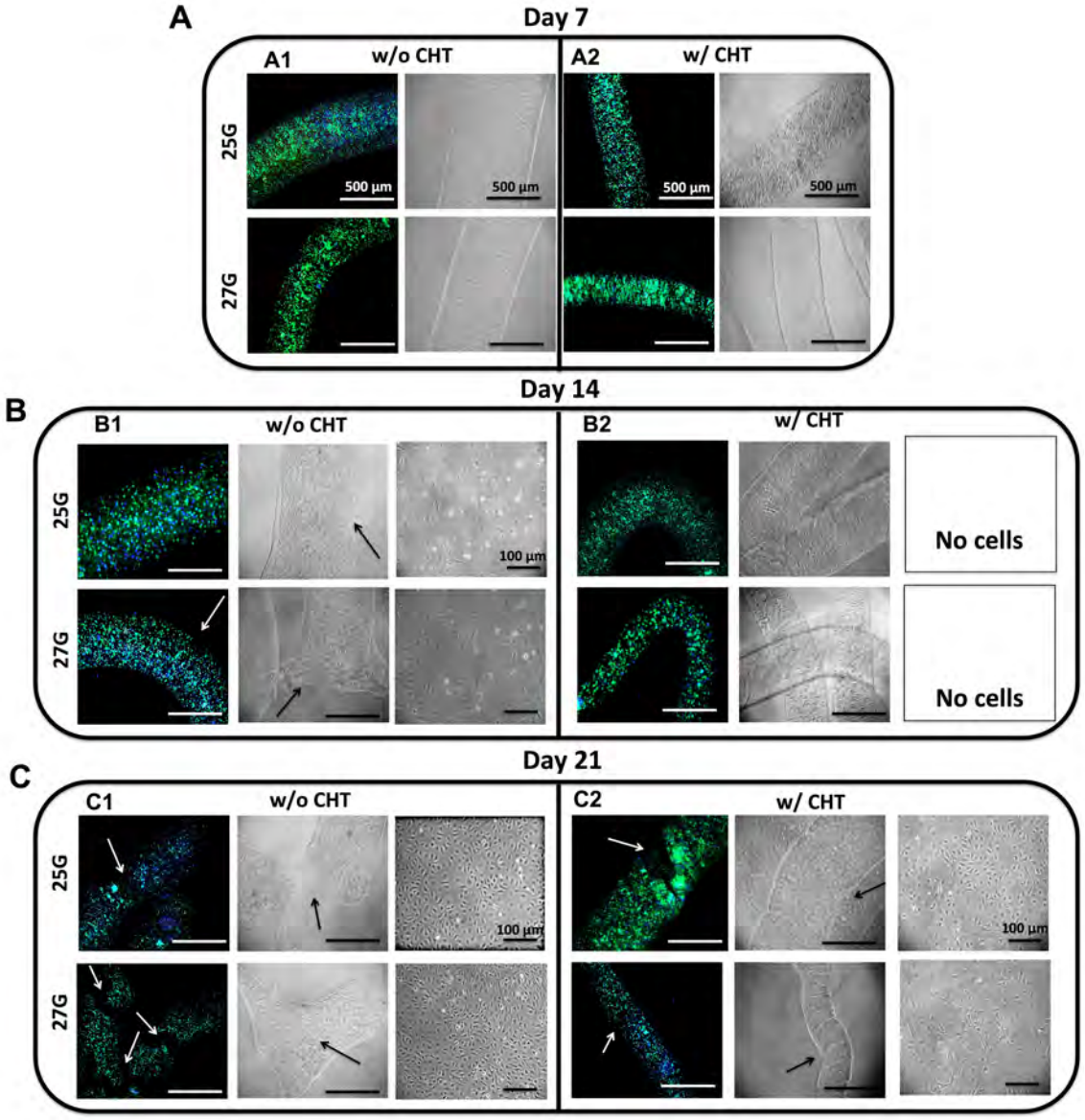

Figure VII.6. Evaluation of the cell-laden κ-CA hydrogel fibers, along 21 days of culture. The viability of encapsulated cells (live/dead) was maintained during the culture time frame in all conditions. (**A**) At day 7, independently of the conditions fibers were intact, without displaying signs of disintegration. (**B1**) At day 14, small endothelial-like colonies could be observed at bottom of the culture well for both fiber diameters (25 and 27G) and without coating (w/o CHT), due to disintegration so that by day 21 (**C1**) fibers lose their integrity (arrows), allowing further release of cells into the well plate. (**B2** and **C2**) The chitosan coating (w/ CHT) delays the disintegration of the fibers, hence the release of the cells. At day 21, the coated fibers diameter did not alter, however, small cracks (arrows) can be observed along the fibers allowing the release of cells. Cell nuclei were counterstained with DAPI (blue).

In addition to cell viability issues due to limited diffusion[7,48], cell encapsulation within hydrogels might also compromise cells functionality by affecting their phenotype[17,54]. In order to address this question, cells were retrieved from the cell-laden fibers upon culturing for 21

days and seeded into tissue culture flasks. Cells were able to adhere and organize into small endothelial-like colonies (**Figure VII.7A**) and more importantly, they maintained their ability to form tubular-like structures, when seeded on Matrigel (**Figure VII.7B**). Moreover, when screened for the initial cell surface marker panel, cells were shown to be $CD105^{+}/CD73^{+}/CD31^{+}/CD45^{-}/CD34^{-}/CD90^{-}$, a phenotype that matches the one registered prior encapsulation. Taken together, these results show that the encapsulation process, followed by a prolonged culture of cell-laden fibers and their enzymatic degradation, did not affect the phenotype and *in vitro* functionality of endothelial differentiated SSEA-4^{+}hASCs.

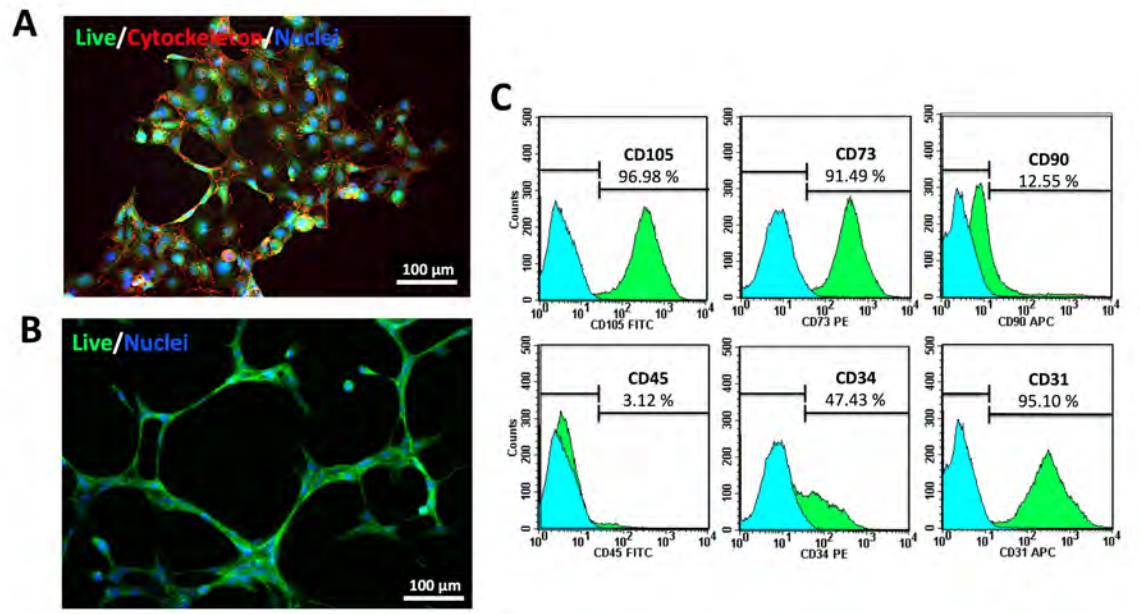

Figure VII.7. Endothelial phenotype of cells retrieved from the fibers after 21 days of culture. (**A**) After retrieval of cells through an enzymatic digestion of the fibers, and the subsequent seeding, cells adhere and form small colonies, characterized by a closed contact between cells (live/cytoskeleton/nuclei). (**B**) Cells maintained their ability to form tubular-like structures (green) when seeded on Matrigel and (**C**) the expression of the characteristic markers of the endothelial phenotype ($CD105^{+}/CD73^{+}/CD31^{+}/CD45^{-}/CD34^{-}/CD90^{-}$). Cell nuclei were counterstained with DAPI (blue).

Overall, as κ-CA fibers exhibit high swelling ratio, the weakening of the network occurs and, consequently cells are able to escape from the fibers. CHT coating maintained the fibers diameter, delaying their disintegration and the consequent release of cells into the surrounding environment. Nonetheless, the CHT layer is still permissive to culture medium, allowing the diffusion of its components, as suggested by the subsequent remarkable results concerning the viability and functionality of encapsulated cells. These findings further demonstrate the potential of using these fibers as ECs carriers within different TE constructs.

VII.3.4. Cell-loaded κ-CA-based fibers can act as building blocks within 3D κ-CA hydrogel constructs

The integration and assembly of cell-laden templates as building blocks within 3D constructs may allow the development of replicas of complex primary tissues. Herein, we propose a straightforward method to integrate the κ-CA-based fibers enclosing ECs, within a 3D hydrogel containing osteoblast-like cells. As κ-CA is a polymer that can be easily molded into different shapes by ionotropic gelation, the κ-CA fibers, used as building blocks, were randomly assembled within a κ-CA hydrogel disc (**Figure VII.8**), thus combining cells obtained from a common source, but which were independently organized. The proposed system is entirely formed by a κ-CA matrix, with a controlled spatial distribution of two cell types. Fibers loaded with endothelial differentiated SSEA-4^{+}hASCs can be singled out or stacked in a random or organized manner (**Figure VII.8A**). When the cell-laden fibers were integrated in a hydrogel disc containing other type of cells (e.g. osteoblast-like cells) the formation of a 3D co-culture platform with a defined cellular topography suitable for bone-vascularization strategies was achieved (**Figure VII.8B-C**). The fibers are expected to act as cell delivery-vehicles for the release of cells within the surrounding matrix. In addition, the 3D hydrogels structures containing the microfibers can be easily manipulated and cultured within well plates. Further experiments are aimed to deeply assess the nature and kinetics of the cellular interactions within the 3D structure and the consequent outcome both concerning ECs rearrangement and organization in 3D vessel-like structures, as well as osteogenic matrix deposition and mineralization.

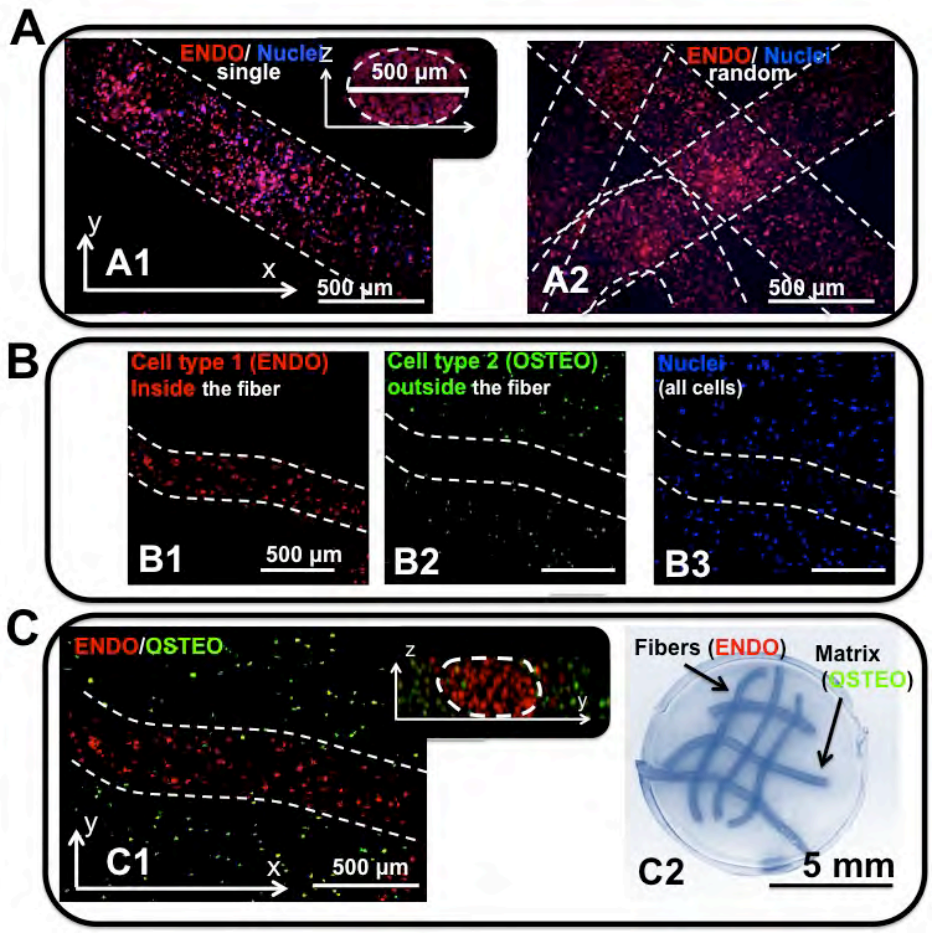

Figure VII.8. Proof of concept of the use of cell-loaded κ-CA-based fibers as building blocks within 3D κ-CA hydrogel constructs. Confocal laser scanning micrographs of (**A1-2**) encapsulated ECs (ENDO, rhodamine tag) within κ-CA fibers. Fibers can be (**A1**) singled out or (**A2**) randomly stacked. (**B-C**) Heterotypic 3D κ-CA-based structure. (**B**) The encapsulation of ECs (ENDO) precedes the integration of the fibers within the κ-CA containing the osteoblast-like cells (OSTEO, GFP tag) localization outside the fiber. All cells (blue) are evenly distributed within the hydrogel. (**C**) 3D build-up of fiber stacks within a hydrogel disc consists of a controlled spatial localization of two cell types within a single hydrogel matrix. (C1) The co-localization of ECs (ENDO) and osteoblast like-cells (OSTEO) is relevant for developing spatial controlled heterotypic systems aimed for bone vascularization approaches. Cell nuclei were counterstained with DAPI (blue). (**C2**) A macroscopic view of the 3D construct. The discs can be manually manipulated without damage. κ-CA fibers were stained with methylene blue (dark blue).

VII.4. CONCLUSIONS

Herein, we report the development of CHT reinforced κ-CA fibers using a two-step procedure, under cell-friendly experimental settings, aiming at homogeneous immobilization of microvascular-like ECs. The diameter of the fibers can be easily tuned by selecting the appropriate needle gauge during processing. The presence of the CHT coating enhanced

the stability and the diameter of κ-CA fibers, restraining their swelling. Moreover, these fibers support the maintenance of the viability and the phenotype of encapsulated cells during long-term culturing, enabling their use as cell-delivery systems within 3D TE constructs. Furthermore, using a bottom-up approach, these fibers can be used as building blocks for the development of suitable 3D platforms of independently organized heterotypic cell-containing hydrogels, relevant for bone vascularization approaches based on adipose-derived stem cells.

REFERENCES

1. Berthiaume, F.; Maguire, T. J.; Yarmush, M. L., Tissue engineering and regenerative medicine: history, progress, and challenges. *Annual review of chemical and biomolecular engineering* **2011,** *2*, 403-30.
2. Kannan, R. Y.; Salacinski, H. J.; Sales, K.; Butler, P.; Seifalian, A. M., The roles of tissue engineering and vascularisation in the development of micro-vascular networks: a review. *Biomaterials* **2005,** *26* (14), 1857-75.
3. Bae, H.; Puranik, A. S.; Gauvin, R.; Edalat, F.; Carrillo-Conde, B.; Peppas, N. A.; Khademhosseini, A., Building vascular networks. *Science translational medicine* **2012,** *4* (160), 160ps23.
4. Lovett, M.; Lee, K.; Edwards, A.; Kaplan, D. L., Vascularization strategies for tissue engineering. *Tissue engineering. Part B, Reviews* **2009,** *15* (3), 353-70.
5. Phelps, E. A.; Garcia, A. J., Engineering more than a cell: vascularization strategies in tissue engineering. *Current opinion in biotechnology* **2010,** *21* (5), 704-9.
6. Geckil, H.; Xu, F.; Zhang, X.; Moon, S.; Demirci, U., Engineering hydrogels as extracellular matrix mimics. *Nanomedicine* **2010,** *5* (3), 469-84.
7. Drury, J. L.; Mooney, D. J., Hydrogels for tissue engineering: scaffold design variables and applications. *Biomaterials* **2003,** *24* (24), 4337-51.
8. Malafaya, P. B.; Silva, G. A.; Reis, R. L., Natural-origin polymers as carriers and scaffolds for biomolecules and cell delivery in tissue engineering applications. *Advanced drug delivery reviews* **2007,** *59* (4-5), 207-33.
9. Fedorovich, N. E.; Wijnberg, H. M.; Dhert, W. J.; Alblas, J., Distinct tissue formation by heterogeneous printing of osteo- and endothelial progenitor cells. *Tissue engineering. Part A* **2011,** *17* (15-16), 2113-21.
10. Kang, E.; Jeong, G. S.; Choi, Y. Y.; Lee, K. H.; Khademhosseini, A.; Lee, S. H., Digitally tunable physicochemical coding of material composition and topography in continuous microfibres. *Nature materials* **2011,** *10* (11), 877-83.
11. Aubin, H.; Nichol, J. W.; Hutson, C. B.; Bae, H.; Sieminski, A. L.; Cropek, D. M.; Akhyari, P.; Khademhosseini, A., Directed 3D cell alignment and elongation in microengineered hydrogels. *Biomaterials* **2010,** *31* (27), 6941-6951.
12. Sakai, S.; Yamaguchi, S.; Takei, T.; Kawakami, K., Oxidized alginate-cross-linked alginate/gelatin hydrogel fibers for fabricating tubular constructs with layered smooth muscle cells and endothelial cells in collagen gels. *Biomacromolecules* **2008,** *9* (7), 2036-41.
13. Enea, D.; Henson, F.; Kew, S.; Wardale, J.; Getgood, A.; Brooks, R.; Rushton, N., Extruded collagen fibres for tissue engineering applications: effect of crosslinking method on mechanical and biological properties. *Journal of materials science. Materials in medicine* **2011,** *22* (6), 1569-78.
14. Oliveira, J. T.; Martins, L.; Picciochi, R.; Malafaya, P. B.; Sousa, R. A.; Neves, N. M.; Mano, J. F.; Reis, R. L., Gellan gum: a new biomaterial for cartilage tissue engineering applications. *Journal of biomedical materials research. Part A* **2010,** *93* (3), 852-63.
15. Berger, J.; Reist, M.; Mayer, J. M.; Felt, O.; Peppas, N. A.; Gurny, R., Structure and interactions in covalently and ionically crosslinked chitosan hydrogels for biomedical applications. *European journal of pharmaceutics and biopharmaceutics : official journal of Arbeitsgemeinschaft fur Pharmazeutische Verfahrenstechnik e.V* **2004,** *57* (1), 19-34.
16. Kirsch, P. P., Carrageenan: a safe additive. *Environmental health perspectives* **2002,** *110* (6), A288; author reply A288.

17. Popa, E. G.; Reis, R. L.; Gomes, M. E., Chondrogenic phenotype of different cells encapsulated in kappa-carrageenan hydrogels for cartilage regeneration strategies. *Biotechnology and applied biochemistry* **2012,** *59* (2), 132-41.
18. Popa, E. G.; Rodrigues, M. T.; Coutinho, D. F.; Oliveira, M. B.; Mano, J. F.; Reis, R. L.; Gomes, M. E., Cryopreservation of cell laden natural origin hydrogels for cartilage regeneration strategies. *Soft Matter* **2013,** *9* (3), 875-885.
19. Popa, E. G.; Gomes, M. E.; Reis, R. L., Cell delivery systems using alginate--carrageenan hydrogel beads and fibers for regenerative medicine applications. *Biomacromolecules* **2011,** *12* (11), 3952-61.
20. Santo, V. E.; Frias, A. M.; Carida, M.; Cancedda, R.; Gomes, M. E.; Mano, J. F.; Reis, R. L., Carrageenan-based hydrogels for the controlled delivery of PDGF-BB in bone tissue engineering applications. *Biomacromolecules* **2009,** *10* (6), 1392-401.
21. Salgueiro, A. M.; Daniel-da-Silva, A. L.; Fateixa, S.; Trindade, T., kappa-Carrageenan hydrogel nanocomposites with release behavior mediated by morphological distinct Au nanofillers. *Carbohydr Polym* **2013,** *91* (1), 100-9.
22. Popa, E. G.; Caridade, S. G.; Mano, J. F.; Reis, R. L.; Gomes, M. E., Chondrogenic potential of injectable kappa-carrageenan hydrogel with encapsulated adipose stem cells for cartilage tissue-engineering applications. *Journal of tissue engineering and regenerative medicine* **2013**.
23. Kuo, C. K.; Ma, P. X., Maintaining dimensions and mechanical properties of ionically crosslinked alginate hydrogel scaffolds in vitro. *Journal of biomedical materials research. Part A* **2008,** *84* (4), 899-907.
24. Mihaila, S. M.; Gaharwar, A. K.; Reis, R. L.; Marques, A. P.; Gomes, M. E.; Khademhosseini, A., Photocrosslinkable Kappa-Carrageenan Hydrogels for Tissue Engineering Applications. *Advanced healthcare materials* **2013,** *2* (6), 895-907.
25. Hezaveh, H.; Muhamad, II; Noshadi, I.; Shu Fen, L.; Ngadi, N., Swelling behaviour and controlled drug release from cross-linked kappa-carrageenan/NaCMC hydrogel by diffusion mechanism. *Journal of microencapsulation* **2012,** *29* (4), 368-79.
26. Amici, E.; Clark, A. H.; Normand, V.; Johnson, N. B., Interpenetrating network formation in agarose--kappa-carrageenan gel composites. *Biomacromolecules* **2002,** *3* (3), 466-74.
27. Granero, A. J.; Razal, J. M.; Wallace, G. G.; Panhuis, M. i. h., Conducting gel-fibres based on carrageenan, chitosan and carbon nanotubes. *Journal of Material Chemistry* **2010,** *20*, 7953-7956.
28. Colinet, I.; Dulong, V.; Mocanu, G.; Picton, L.; Le Cerf, D., Effect of chitosan coating on the swelling and controlled release of a poorly water-soluble drug from an amphiphilic and pH-sensitive hydrogel. *International journal of biological macromolecules* **2010,** *47* (2), 120-5.
29. Grenha, A.; Gomes, M. E.; Rodrigues, M.; Santo, V. E.; Mano, J. F.; Neves, N. M.; Reis, R. L., Development of new chitosan/carrageenan nanoparticles for drug delivery applications. *Journal of biomedical materials research. Part A* **2010,** *92* (4), 1265-72.
30. Piyakulawat, P.; Praphairaksit, N.; Chantarasiri, N.; Muangsin, N., Preparation and evaluation of chitosan/carrageenan beads for controlled release of sodium diclofenac. *AAPS PharmSciTech* **2007,** *8* (4), E97.
31. Pinheiro, A. C.; Bourbon, A. I.; Medeiros, B. G. d. S.; Silva, L. s. H. M. d.; Silva, M. C. H. d.; Carneiro-da-Cunha, M. G.; Coimbra, M. A.; Vicente, A. n. A., Interactions between k-carrageenan and chitosan in nanolayered coatings—Structural and transport properties. *Carbohydrate Polymers* **2012,** *87*, 1081-1090.
32. Mihaila, S. M.; Frias, A. M.; Pirraco, R. P.; Rada, T.; Reis, R. L.; Gomes, M. E.; Marques, A. P., Human adipose tissue-derived SSEA-4 subpopulation multi-differentiation potential towards the endothelial and osteogenic lineages. *Tissue engineering. Part A* **2013,** *19* (1-2), 235-46.
33. Signini, R.; Filho, S. P. C., Characteristics and properties of purified chitosan in the neutral, acetate and hydrochloride forms. *Polím. Ciênc Tecnol* **2001,** *11*, 58–64.
34. Cho, J.; Heuzey, M. C.; Begin, A.; Carreau, P. J., Physical gelation of chitosan in the presence of beta-glycerophosphate: the effect of temperature. *Biomacromolecules* **2005,** *6* (6), 3267-75.
35. Huh, D.; Hamilton, G. A.; Ingber, D. E., From 3D cell culture to organs-on-chips. *Trends in cell biology* **2011,** *21* (12), 745-54.
36. Hahn, M. S.; Miller, J. S.; West, J. L., Three-dimensional biochemical and biomechanical patterning of hydrogels for guiding cell behavior. *Advanced Materials* **2006,** *18* (20), 2679 - 2684.
37. Chueh, B. H.; Zheng, Y.; Torisawa, Y. S.; A.Y., H.; Ge, C.; Hsiong, S.; Huebsch, N.; Franceschi, R.; Mooney, D. J.; Takayama, S., Patterning alginate hydrogels using light-directed release of caged calcium in a microfluidic device. *Biomedical Microdevices* **2010,** *12* (1), 145-151.

38. Coviello, T.; Matricardi, P.; Marianecci, C.; Alhaique, F., Polysaccharide hydrogels for modified release formulations. *Journal of controlled release : official journal of the Controlled Release Society* **2007,** *119* (1), 5-24.
39. Mangione, M. R.; Giacomazza, D.; Bulone, D.; Martorana, V.; Cavallaro, G.; San Biagio, P. L., K(+) and Na(+) effects on the gelation properties of kappa-Carrageenan. *Biophysical chemistry* **2005,** *113* (2), 129-35.
40. Yuguchi, Y.; Urakawa, H.; Kajiwara, K., Structural characteristics of carrageenan gels: various types of counter ions. *Food Hydrocolloids* **2003,** *17* (4), 481–485.
41. Pereira, R. C.; Scaranari, M.; Castagnola, P.; Grandizio, M.; Azevedo, H. S.; Reis, R. L.; Cancedda, R.; Gentili, C., Novel injectable gel (system) as a vehicle for human articular chondrocytes in cartilage tissue regeneration. *Journal of tissue engineering and regenerative medicine* **2009,** *3* (2), 97-106.
42. Takei, T.; Sakai, S.; Ijima, H.; Kawakami, K., Development of mammalian cell-enclosing calcium-alginate hydrogel fibers in a co-flowing stream. *Biotechnology journal* **2006,** *1* (9), 1014-7.
43. Fedorovich, N. E.; De Wijn, J. R.; Verbout, A. J.; Alblas, J.; Dhert, W. J., Three-dimensional fiber deposition of cell-laden, viable, patterned constructs for bone tissue printing. *Tissue engineering. Part A* **2008,** *14* (1), 127-33.
44. Coutinho, D. F.; Sant, S. V.; Shin, H.; Oliveira, J. T.; Gomes, M. E.; Neves, N. M.; Khademhosseini, A.; Reis, R. L., Modified Gellan Gum hydrogels with tunable physical and mechanical properties. *Biomaterials* **2010,** *31* (29), 7494-502.
45. Stephen, A. M.; Phillips, G. O.; Williams, P. A., Food Polysaccharides and their Applications. Press, C., Ed. Taylor & Francis Group: New York,, 2006; Vol. 2nd ed.
46. Polk, A.; Amsden, B.; De Yao, K.; Peng, T.; Goosen, M. F., Controlled release of albumin from chitosan-alginate microcapsules. *Journal of pharmaceutical sciences* **1994,** *83* (2), 178-85.
47. Kaully, T.; Kaufman-Francis, K.; Lesman, A.; Levenberg, S., Vascularization--the conduit to viable engineered tissues. *Tissue engineering. Part B, Reviews* **2009,** *15* (2), 159-69.
48. Griffith, C. K.; Miller, C.; Sainson, R. C.; Calvert, J. W.; Jeon, N. L.; Hughes, C. C.; George, S. C., Diffusion limits of an in vitro thick prevascularized tissue. *Tissue engineering* **2005,** *11* (1-2), 257-66.
49. Santos, M. I.; Reis, R. L., Vascularization in bone tissue engineering: physiology, current strategies, major hurdles and future challenges. *Macromolecular bioscience* **2010,** *10* (1), 12-27.
50. Fedorovich, N. E.; Haverslag, R. T.; Dhert, W. J.; Alblas, J., The role of endothelial progenitor cells in prevascularized bone tissue engineering: development of heterogeneous constructs. *Tissue engineering. Part A* **2010,** *16* (7), 2355-67.
51. Urbich, C.; Dimmeler, S., Endothelial progenitor cells: characterization and role in vascular biology. *Circulation research* **2004,** *95* (4), 343-53.
52. Kong, H. J.; Smith, M. K.; Mooney, D. J., Designing alginate hydrogels to maintain viability of immobilized cells. *Biomaterials* **2003,** *24* (22), 4023-9.
53. Lutolf, M. P.; Gilbert, P. M.; Blau, H. M., Designing materials to direct stem-cell fate. *Nature* **2009,** *462* (7272), 433-41.
54. Murphy, C. L.; Sambanis, A., Effect of oxygen tension and alginate encapsulation on restoration of the differentiated phenotype of passaged chondrocytes. *Tissue engineering* **2001,** *7* (6), 791-803.

SUPPLEMENTAL INFORMATION

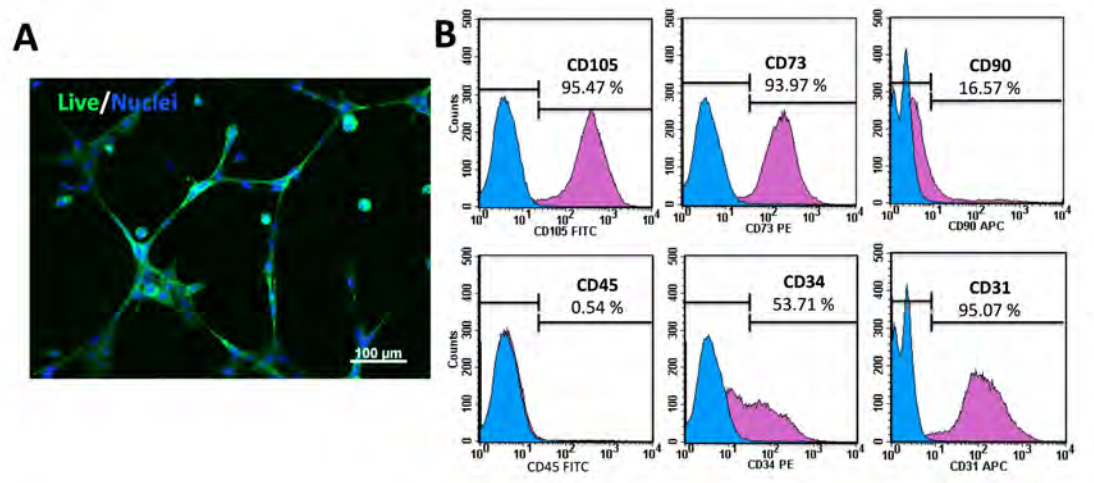

Supplemental Figure VII.1. SSEA-4^{+}hASCs endothelial-like cells phenotype prior encapsulation. (A) Matrigel assay confirmed the capacity of the endothelial differentiated SSEA-4^{+}hASCs to form tubular-like structures (green). (B) The endothelial phenotype was also demonstrated by flow cytometry analysis. Cell nuclei were counterstained with DAPI (blue).

Chapter VIII

Photocrosslinkable *Kappa*-Carrageenan Hydrogels for Tissue Engineering Applications

ABSTRACT

Kappa carrageenan (κ-CA) is a natural-origin polymer that closely mimics the glycosaminoglycan structure, one of the most important constituents of native tissues extracellular matrix. Previously, it has been shown that κ-CA can crosslink via ionic interactions rendering strong, but brittle hydrogels. In this study, we introduce photocrosslinkable methacrylate moieties on the κ-CA backbone to create physically and chemically crosslinked hydrogels highlighting their use in the context of tissue engineering. By varying the degree of methacrylation (DM), the effect on hydrogel crosslinking was investigated in terms of hydration degree, dissolution profiles, morphological, mechanical, and rheological properties. Furthermore, the viability of fibroblast cells cultured inside the photocrosslinked hydrogels was investigated. The combination of chemical and physical crosslinking procedures enables the formation of hydrogels with highly versatile physical and chemical properties, while maintaining the viability of encapsulated cells. To our best knowledge, this is the first study reporting the synthesis of photocrosslinkable κ-CA with controllable compressive moduli, swelling ratios and pore size distributions.

Moreover, by micromolding approaches, spatially controlled geometries and cell distribution patterns could be obtained, thus enabling the development of cell-material platforms that can be applied and tailored to a broad range of tissue engineering strategies.

This chapter is based on the following publication:

Mihaila SM, Gaharwar AG, Reis RL, Marques AP, Gomes ME and Khademhosseini A, "Photocrosslinkable *Kappa*-Carrageenan Hydrogels for Tissue Engineering Applications", Advanced Healthcare Materials, 2(6): 895-907, 2013. doi: 10.1002/adhm.201200317

VIII.1. INTRODUCTION

Hydrogels are insoluble three-dimensional (3D) crosslinked networks of hydrophilic polymers, widely used as platforms in bio- medical applications such as tissue engineered constructs[1], drug delivery systems[2], cell-based therapies[3], wound dressings[4] and anti-adhesion materials[5]. As the physical properties of hydrogels resemble the hydrated state of the native extracellular matrix (ECM)[6], they exhibit high permeability towards oxygen, nutrients and other soluble factors[7] essential for sustaining cellular metabolism[1a, 8]. The hydrogel networks can be fabricated by using physical or chemical crosslinking methods[9]. Physical crosslinking is achieved through the formation of physical bonds between the different polymer chains. For example, ionically crosslinked gels are formed by the interactions between charged polymer chains and counterions[9a]. However, the uncontrollable exchange of ions in physical conditions reduces their applicability in the tissue engineering (TE) field.

On the other hand, through chemical crosslinking, stable covalent bonds between polymer chains are created[1a, 1c]. Suitable crosslinking agents mediate the formation of these permanent bonds. Particularly, photocrosslinking, a type of chemical crosslinking, is performed in the presence of an ultraviolet (UV) light and a chemical photoinitiator (PI). Many photocrosslinkable materials are currently being investigated for TE applications, due to their processability and micromolding potential[10]. Furthermore, it is possible to achieve a homogeneous distribution of cells and bioactive factors (e.g. proteins, growth factors) throughout the hydrogel matrix that can be easily delivered in situ.

Recently, natural origin polymers have attracted much interest due to their resemblance to the ECM, high chemical versatility, controlled degradability and interaction with biological systems[11]. Amongst natural polymers gellan gum[12], alginate[13], gelatin[14], hyaluronic acid[15], chitosan[16], chondroitin sulphate[17] were modified in order to form hydrogels *via* photocrosslinking processes, while maintaining the viability of encapsulated cells. These natural polymers are also blended with other synthetic polymers to obtain unique property combinations for biomedical and biotechnological applications.

Carrageenans are a class of natural origin polymers, widely used as gelling, emulsifier, thickening, or stabilizing agents in pharmaceutical and food industry[18]. Carrageenans are extracted from red seaweeds of the class *Rhodophyceae* and classified according to the presence and number of the sulphated groups on the repeating disaccharide units. Briefly, *kappa* (κ-) possesses one sulphated group, while *iota* (γ-) and *lambda* (λ-) possess two and three sulphate groups, respectively, per disaccharide unit[18,19]. Their gelation occurs upon cooling under appropriate salt conditions by hydrogen bonds and ionic interactions, as both κ- and γ- undergo coil-helix conformational transitions, rendering ionotropic and thermotropic gels[20]. The gelation of κ-carrageenan (κ-CA) is enhanced mainly by potassium ions, forming

firm, but brittle gels that dissolve when heated[21], while λ-carrageenan gelation is dependent on the presence of calcium ions, forming soft and elastic gels[9a].

κ-CA has been proposed as a potential candidate for TE applications, due to its gelation properties, mechanical strength and its resemblance to natural glycosaminoglycans (GAGs)[22]. Furthermore, due to its inherent thixotropic behavior, κ-CA has been used as an injectable matrix to deliver macromolecules and cells for minimally invasive therapies[23]. Although previous studies have shown encouraging results[24] there is still inadequate control over the swelling properties, degradation characteristic and mechanical properties of ionically crosslinked κ-CA hydrogels. This is mainly attributed to the uncontrollable exchange of monovalent ions with other positive ions from the surrounding physiological environment[11]. Therefore, a modification of κ-CA that would enable the formation of stable crosslinked gels for cell encapsulation in which cell viability is preserved is a new challenge to be addressed. Previously, our work has shown successful chemical modification of natural polymers, leading towards the development of cell-laden platforms, based on photolithography and micromolding[12,14,25,26].

The primary aim of the current study is to design and develop a highly versatile micropatterned κ-CA hydrogel platform through dual-crosslinking mechanisms. We hypothesize that the crosslinking mechanism will influence the mechanical and viscoelastic performance of the developed system. Furthermore, cellular viability within modified κ-CA hydrogels, as well as the production of reactive oxygen species, will be evaluated as an assessment of their biocompatibility, potentiating their use in TE applications.

VIII.2. MATERIALS AND METHODS

VIII.2.1.Synthesis of methacrylated-κ-carrageenan (MA-κ-CA)

Methacrylated κ-CA (MA-κ-CA) was synthesized by reacting κ-CA with methacrylic anhydride (MA). Briefly, κ-CA was mixed at 1% (wt/v) into deionized water (diH_2O) at 50°C until the polymer was fully dissolved. To this solution, MA was added and allowed to react for 6 hours at 50°C. The pH (8.0) of the reaction was periodically adjusted with 5.0 M NaOH (Sigma, Germany) solution in diH_2O. The modified κ-CA was dialyzed against diH_2O using 12-14 kDa cutoff dialysis tubing (Fisher Scientific, Cambridge, MA, USA) for 3 days at 4°C to remove excess of unreacted MA. Purified MA-κ-CA solutions were frozen at −80°C and then lyophilized. The obtained powder was stored at −20°C, protected from light until further use. To modify the degree of methacrylation (DM), the volumes of MA added in the methacrylation reaction (i.e., 4% (v/v) - Low, 8% (v/v) - Medium and 12% (v/v) - High (v/v)) were varied.

VIII.2.2. Characterization of MA-κ-CA

The chemical modification of κ-CA was quantified by proton nuclear magnetic resonance (^{1}H NMR) spectroscopy. The ^{1}H NMR spectra of κ-CA and MA-κ-CA were collected in deuterated water (D_2O) at 50°C, at a frequency of 500 MHz on a Varian INOVA NMR spectrometer with a single axis gradient inverse probe. All spectra were analyzed using 1D NMR Processor software (ACD/Labs 12.0). Phase correction was applied to obtain accurate absorptive peaks, followed by a baseline correction to obtain the integrals of the peaks of interest. The obtained chemical shifts were normalized against the protons of the methylene group of the D-galactose units (G) as an internal standard, which is present at δ = 3.89 ppm[27]. The DM was calculated referring to the peaks at δ = 1.9–2 ppm (methyl) and δ = 5.5–6 ppm (double bond region) as percentage (%) of the free hydroxyl groups (-OH) substituted with methacrylate groups. Fourier transform infrared spectroscopy with attenuated total reflection (FTIR-ATR) analysis was performed on a Bruker Alpha FTIR spectrometer (Bruker Optics, MA, USA). The spectra were recorded at a resolution of 4 cm^{-1} and the results are shown as an average of 24 scans. The zeta potential of the modified κ-CA was measured by laser Doppler anemometry using a Malvern Zeta Sizer 300HS (Malvern Instruments, UK). Each sample was diluted in water at a concentration of 0.1% (wt/v). Each analysis was performed at 25°C, and lasted 60sec.

VIII.2.3. Preparation of dual crosslinked MA-κ-CA hydrogels

Freeze dried MA-κ-CA macromer with different DM, as well as non-modified κ-CA were added to a PI solution consisting of 0.25% (wt/v) 2-hydroxy-1-(4- (hydroxyethoxy)phenyl)-2-methyl-1-propanone (Irgacure 2959, CIBA Chemicals), in diH_2O, at 80°C until complete dissolution. Physically crosslinked MA-κ-CA hydrogels were obtained by pouring the polymer solution into polydimethylsiloxane (PDMS) circular molds (8cm diameter) followed by gently adding a solution of 5% (wt/v) of potassium chloride (KCl, Sigma, Germany) to initiate the crosslinking. After 10 min of gentle shacking, samples were removed from the molds and washed Dulbecco's phosphate buffered saline (DPBS, Gibco, USA) in order to remove the salt residues. The chemically crosslinked hydrogels were obtained by pipetting 100µL of polymer solution between a Teflon substrate and a glass coverslip separated by a 1mm spacer followed by UV light exposure at 6.9 mW/cm^2 (320–480 nm, EXFO OmniCure S2000, Ontario, Canada) for 40sec. To obtain dual crosslinked hydrogels, the chemically crosslinked samples were immersed in a 5% (wt/v) KCl coagulation bath for 10 min and rinsed with DPBS.

VIII.2.4. Swelling behavior and in vitro dissolution properties

The effect of the DM and crosslinking mechanisms on the swelling behavior and stability of

the hydrogels was determined by evaluation of the hydration kinetics and dissolution behavior. Briefly, MA-κ-CA hydrogels obtained with different crosslinking procedures were lyophilized and weighted (initial dry weight, W_{DI}) before being transferred to 1.5 mL microtubes and soaked in 1 mL of DPBS and Dulbecco´s Modified Eagle Medium (DMEM, Gibco, USA) at physiological temperature (37°C), under constant shaking (60 rpm).

To assess the swelling properties, hydrogels (n=3) were allowed to reach equilibrium in the swelling solution and weighted to determine the wet weight (M_W) after being blotted off with a KimWipe paper to remove the excess liquid from the samples surface. Then the samples were lyophilized to determine their final dry weight (W_{DF}). The mass swelling ratio was defined as the weight ratio of the liquid (DPBS or DMEM) uptake (M_W) to the weight of the dried hydrogel (M_{DF}), according to **equation VIII.1**.

$$\textbf{Mass swelling ratio} = (M_W - M_{DF})/M_{DF} * 100 \qquad (\textbf{equation VIII.1})$$

The dissolution degree was calculated by measuring the mass loss of the sample (**equation VIII.2**).

$$\textbf{Dissolution degree} = M_{DF}/M_{DI} * 100 \qquad (\textbf{equation VIII.2})$$

VIII.2.5. Scanning electron microscopy (SEM) of dried dual crosslinked MA-κ-CA hydrogels

The microstructure of hydrogels was evaluated using scanning electron microscopy (SEM, JSM 5600LV, JEOL USA Inc., Peabody, MA, USA) at an acceleration Voltage of 5 kV and a working distance of 5–10 mm. First, hydrogel samples were plunged in liquid nitrogen slush, transferred to 1.5 mL microtubes and freeze-dried for 24 hours. The dry samples were fractured and then mounted on samples holders using double-sided carbon tape. The coating of the samples was performed with gold and palladium using a Hummer 6.2 sputter coated (Ladd Research, Williston, VT, USA). The quantification of the pore size distribution was performed using NIH ImageJ software, based on the SEM pictures.

VIII.2.6. Viscoelastic properties of MA-κ-CA hydrogels

The effect of DM on the viscoelastic behavior of MA-κ-CA was determined using an AR2000 stress controlled rheometer (TA instruments, New Castle, DE, USA). Flow experiments were performed to evaluate the viscosity of polymer solution at 37°C (shear rate varying from 0.01 to 100 s^{-1}). For dual crosslinked hydrogels, oscillatory stress sweep was applied between 0.1 to 1000 Pa at 37°C and at a frequency of 0.1 Hz. The *G′,* as well as the *G″* of the swollen samples, was measured using a gap of 500µm and a 20 mm parallel plate geometry. A solvent (DPBS) trap was used in order to minimize the drying of the swollen hydrogels undergoing analysis.

VIII.2.7. Uniaxial compression testing

To assess the effect of the DM, crosslinking mechanism and polymer concentration over the mechanical behavior of the MA-κ-CA crosslinked hydrogels, cyclic compressive tests were performed using an Instron 5542 mechanical machine (Instron, Norwood, MA, USA). κ-CA and MA-κ-CA hydrogel discs (1 mm thick, 8 mm in diameter, n = 6) were tested at a rate of 10% strain/min (0.1 mm/min) until 50% of strain, for 5 complete compression-recovery cycles. Samples obtained immediately after crosslinking (as prepared samples) and samples that were allowed to swell in DPBS for 24 hours before testing (hydrated samples) were analyzed. The compressive modulus was defined as the slope of the linear region of the strain/stress curve, corresponding to 5–15% strain.

VIII.2.8. Reactive species production

Intracellular production of superoxide (SOx) and nitric oxide (NOx) species was evaluated respectively using dihydroethidium (DHE, Molecular Probes, Eugene, OR, USA) and 4,5-diaminofluorescein diacetate (DAF-2DA, Calbiochem, San Diego, CA, USA) oxidation assays. NIH-3T3 mouse fibroblasts were cultured in basal DMEM, containing with 10% of heat-inactivated fetal bovine serum (HiFBS, Gibco, USA) and 1% Pen/Strep (penicillin/streptomycin, 100U/100µg/mL, Gibco, USA), at 37°C, in a humidified atmosphere with 5% of CO_2. When reached 70% confluency, cells were trypsinized (0.05% Trypsin/EDTA, Gibco, USA) and further centrifuged at 1200 rpm for 5 min. Cells (2×10^5 cells) were preincubated with DHE (25µM) for 10 min and DAF-2DA (5µM) for 30 min, at 37°C, respectively for SOx and NOx detection. Cells were then washed with DPBS, centrifuged at 1200rpm for 5min, and resuspended in 5% (wt/v) MA-κ-CA solution with different DM (Medium, Low, High) in 0.25% PI (wt/v) and 1.5% κ-CA (wt/v). The methacrylated polymers containing cells were UV crosslinked for 40sec and the obtained hydrogels were immersed in a 5% KCl bath for 10min for further crosslinking. The obtained hydrogels were washed with DPBS and incubated at 37°C in phenol-red free DMEM (Gibco, USA) for 2 and 1h, respectively, for SOx and NOx detection. Preincubated cells, mounted on glass slides using Fluoromount mounting media (Sigma, Germany), were used as controls. All samples were examined under an inverted fluorescence microscope (Nikon, Eclipse TE 2000U, Japan). The quantification of the intensity of fluorescence was analyzed using NIH ImageJ software, considering the intensity of fluorescence per single cell for each of the evaluated conditions.

VIII.2.9. 3D Cell encapsulation in MA-κ-CA microfabricated patterns

The effect of DM, as well as the photocrosslinking conditions, on the cells viability was evaluated by encapsulating NIH-3T3 mouse fibroblasts within gels prepared by applying

both physical and chemical crosslinking. Cells were resuspended in 5% (wt/v) MA-κ-CA polymer containing 0.25% (wt/v) PI at a density of 2×10^6 cells/mL polymer solution. The cells suspension was poured onto Teflon sheet and using coverslip spacers, cell-laden hydrogels of 450μm were formed after UV light exposure and further crosslink in a coagulation bath, as described previously. Afterwards, hydrogels were rinsed with DPBS and placed into 6-well cell culture plates. To form circular patterns, PDMS molds were used while crosslinking (100μm diameter × 300μm depth × 450μm height). The viability of the encapsulated cells within the hydrogels was evaluated at 3 and 72h of culture with a Live/ Dead (Invitrogen, Carlsbad, CA, USA) assay. Briefly, cells were incubated with calcein AM/ethidium homodimer-1 in phenol-red free DMEM for 40min. Fluorescence images were taken as previously mentioned.

VIII.2.10. Statistical analysis

All data values are presented as mean ± standard deviation (SD). Statistical analysis was performed using GraphPad Prism 5.00 software (San Diego, USA). Statistical significances (p<0.05) were determined using one-way analysis of variance (ANOVA) for an average of three to six replicates, followed by post hoc Tukey's test for all pair-wise mean comparisons.

VIII.3. RESULTS AND DISCUSSION

VIII.3.1. Synthesis of MA-κ-CA

κ-CA is a linear, sulfated polysaccharide, composed of alternating 3,6 anhydro-D-galactose (AG) and β-D-galactose (G)-4-sulphate repetitive units. It has recently been proposed for drug delivery applications[27,28] and was shown to induce specific cellular responses, such as chondrogenesis of mesenchymal stem cells[24b], or regeneration of an articular defect[24a]. κ-CA hydrogels can be formed via ionic crosslinking methods[29], however, these hydrogels present low stability in physiological settings, mainly due to the exchange of monovalent ions with the ones present in the surrounding environment. To overcome this drawback, we proposed the chemical functionalization of κ-CA with methacrylate pendant groups, yielding photocrosslinkable hydrogels. The covalent bonds formed during crosslinking render high stability to the polymer network. Moreover, we hypothesized that the chemical modification along with the already present ionic character of κ-CA, will allow the formation of dual crosslinked hydrogels by combining chemical and physical crosslinking methods.

MA-κ-CA with various DM was synthesized by substituting the hydroxyl groups on κ-CA with methacrylate groups. The extent of substitution of hydroxyl groups was considered equivalent with the DM (**Figure VIII.1A**), and was dependent on the volumes of MA that were added to the reaction. ^{1}H NMR spectroscopy of the modified polymer, confirmed the methacrylation of κ-CA by the presence of double peaks (vinyl) in the double bond region (δ

= 5.5-6ppm) and one peak corresponding to the methyl (-CH_3) of the methacrylate group at δ = 1.9–2ppm (**Figure VIII.1B**). To quantify the DM, the degree of substitution of free hydroxyl groups present on the κ-CA backbone was evaluated by comparing the average integrated intensity of the methyl protons peak of the methacrylate group with the methylene groups present in the β-D-galactose (G6) of κ-CA. By adding 4%, 8% and 12% (v/v) MA to κ-CA during the synthesis, it was possible to create three different MA-κ-CA polymers with Low (14.72 ± 5.14%), Medium (28.91 ± 7.32%) and High (37.11 ± 7.41%) DM, respectively.
Furthermore, FTIR-ATR spectra revealed the appearance of the carbon-carbon double bond (C=C) at 1550 cm^{-1}, accompanied by the occurrence of the characteristic ester peak (C=O) at around 1680-1750 cm^{-1}, not present in κ-CA, thus confirming the methacrylation of κ-CA (**Figure VIII.1C**). Moreover, all spectra showed an absorbance band at 1250 cm^{-1}, corresponding to the sulphate content characteristic of κ-CA. This indicates that the intrinsic sulphate group of κ-CA is also present in the modified formulations, thus it was not affected by the methacrylation reaction conditions. Furthermore, the zeta potential measurements confirmed the anionic potential of modified κ-CA and no significant difference in the overall charge was observed between non methacrylated and the MA-κ-CA (zeta potential = −62.6 ± 1.3mV and electrophoretic mobility = −5.54 ± 1.1μm·cm/V·s).

VIII.3.2. Viscoelastic behavior of MA-κ-CA solutions

κ-CA exhibits a reversible, temperature-sensitive gelation in salt-free conditions, through physical crosslinking. As a consequence, κ-CA chains undergo a sol-gel transition from random coil to coaxial double helix (soluble domains) configuration[30], as the temperature decreases. The conformational organization into double helices renders the formation of a 3D network maintained by the interaction of the polymeric chains with water through hydrogen bridges[31]. The stability of this interaction allows the 3D network to undertake desired patterns, additionally conferring versatility to the κ-CA[32]. Nevertheless, at room temperature, the κ-CA solutions are highly viscous and are difficult to manipulate resulting in poor processability[33]. By increasing the temperature, the viscosity of κ-CA solutions dramatically decreased mainly due to the thermodynamic instability of the polymer chains. However, the range of temperature that must be employed (50–70°C) is higher than the physiological temperature, which can compromise the viability of encapsulated cells or the activity of other incorporated bioactive components. Within this context, the viscosity of the precursor solutions of MA-κ-CA was evaluated. At physiological temperature, the modified κ-CA solution showed lower viscosities when compared with the non-modified κ-CA (**Figure VIII.1D**). This change in viscosity can be attributed to the reduced interactions between side chains, ultimately leading to less double helix configurations.
Viscoelastic properties of κ-CA pre-polymer solutions show shear thinning behavior. At low

shear rate (0.1 s^{-1}) the viscosity of κ-CA was around 500Pa·s, while at higher shear rate (100s^{-1}) the viscosity decreased to 1Pa·s. After modifying κ-CA with methacrylation moieties, the shear thinning behavior was suppressed. It was observed that MA-κ-CA requires lower applied shear rates to achieve the same viscosity values of κ-CA. This can be mainly attributed to the disruption of the ordered arrangement of double helix conformations by the presence of the methacrylate side chains.

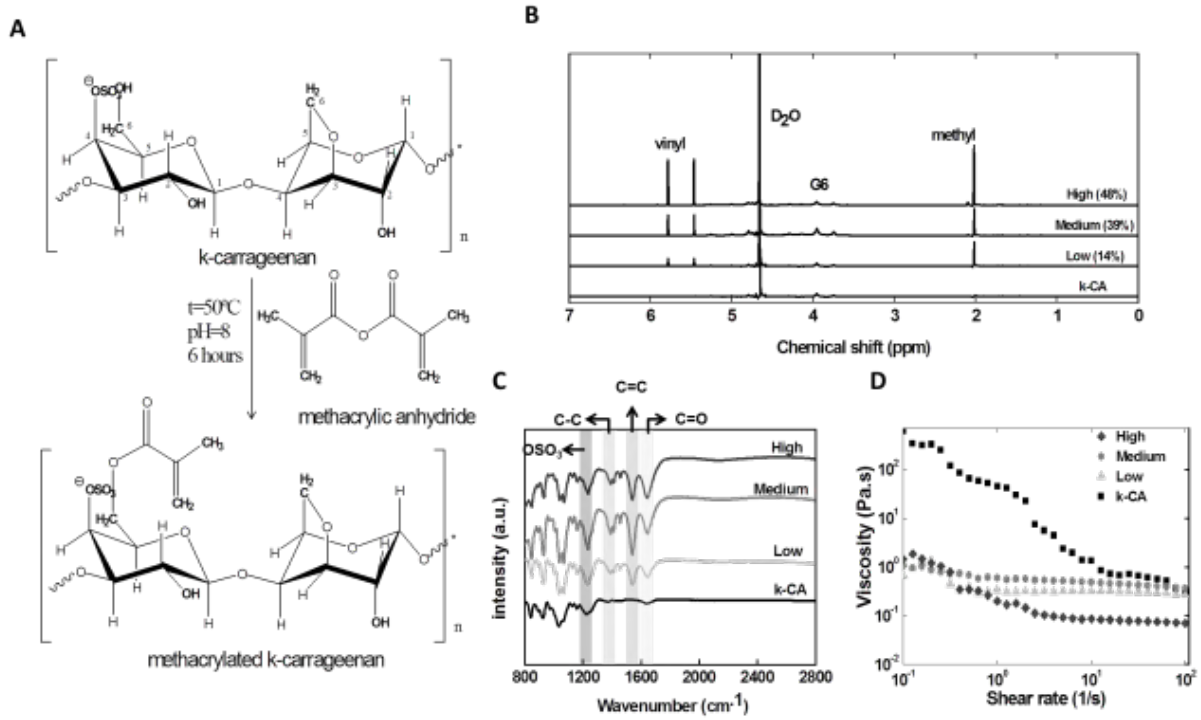

Figure VIII.1. Characterization of MA-κ-CA. (**A**) Schematic representation of the chemical modification of k-CA. (**B**) ^{1}H NMR spectra (T=50^{0}C) of k-CA, Low, Medium and High MA-κ-CA recorded in deuterated water (D_2O). The methylene protons of the β-galactose subunit of κ-CA (G6) were located at δ=3.89ppm and vinyl groups of the methacrylate (=CH_2) were found around δ=5.5-6 ppm, while the methyl group (-CH_3) was located at δ=1.9-2ppm. The D_2O peak at δ=4.7ppm was used as internal reference. The degree of methacrylation (DM) was calculated as percentage (%) of the hydroxyl groups substitution with the methacrylate groups per each repeating unit. (**C**) FTIR-ATR spectra of modified κ-CA confirmed the grafting of methacrylate groups onto the polymer backbone. The peak appearing around 1550cm^{-1} corresponds to the C=C bond of MA and is present in Low (L), Medium (M) and High (H) MA-k-CA, while is absent in the non-modified counterpart. The C=O absorption band of the ester present around 1680-1750cm^{-1} appears in all modified formulations. (**D**) The viscoelastic behavior of the polymer solutions shows that the methacrylation degree reduces the viscosity of the solutions highlighting the shear thinning behavior of the materials, suitable for injectable approaches. The data acquisition was performed at physiological temperature (37ºC).

VIII.3.3. MA-κ-CA hydrogel fabrication via different crosslinking mechanisms

κ-CA is capable of forming hydrogels through ionic interactions. Potassium salts are

essential for κ-CA hydrogel formation, due to the interactions with the sulphate groups present on the backbone of κ-CA. These ionic interactions promote the condensation of the double helices into strong 3D networks. Moreover, the gelation, as well as the density of the ionic bonds in hydrogels, is strongly dependent on the presence, type and concentration of electrolytes. The introduction of methacrylate groups into the κ-CA backbone enables the formation of chemically crosslinked gels via UV exposure. Furthermore, as the anionic character of MA-κ-CA was not affected, it was still possible to form gels in the presence of K^+ salts. The presence of two functional groups (sulphate and methacrylate) can be independently used to tune physical properties as well as to encapsulate cells. As a consequence, the combination of two distinct crosslinking mechanisms enhances the versatility of the system, hence the range of potential applications within the TE field. Also, it was noticed that the modified κ-CA showed a weaker response to temperature changes, which might be attributed to the additional methacrylate moieties that can hinder the complete packing of the double helix domains. The weak association between a polymer chains in double helix configuration due to functional groups grafted on the polymeric backbone was already reported for other natural origin polymers (e.g., gellan gum[12]).

The schematic of the crosslinking of MA-κ-CA is depicted in **Figure VIII.2**, and highlights the proposed crosslinking mechanisms employed in this study. Briefly, we developed physically (P) crosslinked hydrogels by crosslinking MA-κ-CA in the presence of K^+ ions; chemically (C) crosslinked hydrogels by photocrosslinking procedure, and a combination of the physical and chemical crosslinking mechanism, denominated as dual (D) crosslinked hydrogels.

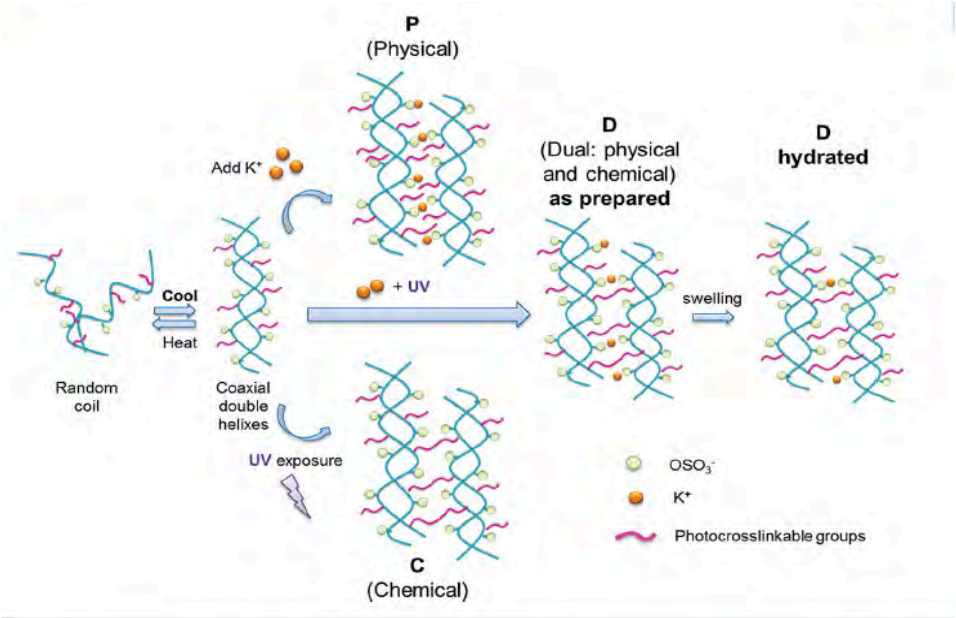

Figure VIII.2. Proposed crosslinking mechanisms of MA-κ-CA. The thermo-responsive character allows the gelation of MA-κ-CA under salt-free conditions through the formation of physical bonds between the chains at low temperature. Due to the ionic nature of MA-κ-CA, the physical crosslinking (P) can occur in the presence of monovalent ions (K^+) forming stable gels. The pendant methacrylate

groups can render the chemical crosslinking (C) by UV exposure. The association of the chemical and physical crosslinking approach allows the formation of dual crosslinked (D) hydrogels that are stable at physical conditions, as prepared or after reaching the swelling equilibrium.

VIII.3.4. Effect of DM on swelling properties of the hydrogels

In the context of TE, it is important to expose the polymeric networks to conditions that mimic *in vivo* environment. A proper evaluation of their behavior within this setup will allow predicting the *in vivo* performance of the developed hydrogels. The swelling properties are a trademark of hydrogels properties, as these polymeric networks are able to retain water in various percentages dependent on their chemistry[1d]. Moreover, the swelling properties of polymeric networks are significantly influenced by water-material interactions. These affect the mass transport characteristics (nutrient and oxygen diffusion, waste disposal) and, consequently, their mechanical properties[34,35].

κ-CA is a hydrophilic polysaccharide that has shown significant properties changes when dissolved in aqueous solutions with different concentrations in ions[36]. As mass swelling ratio can affect the overall features (shape and size) of a given patterned hydrogel the effect of DM and crosslinking mechanism on the mass swelling ratio of the polymers hydrogels was evaluated under physiological conditions in DPBS and DMEM, at 37°C. For this purpose, Low, Medium or High DM MA-κ-CA hydrogels were allowed to reach equilibrium over 24h in DPBS or DMEM at 37°C, under dynamic conditions, to measure the mass swelling ratio (**Figure VIII.3A-B**).

Holding the DM constant, a significant decrease in the mass swelling ratio (***p<0.001) was observed, dependent on the crosslinking mechanism (**Figure VIII.3A**). The chemical crosslinking mechanism allows the hydrogels to retain large volumes of solvent, due to the presence of covalent bonds/ interactions. The chemically crosslinked network is highly flexible and allows the extension of the polymeric network without disrupting it. On the other hand, the short exposure to the KCl treatment (physically crosslinking) of the MA-κ-CA hydrogels allows the diffusion of monovalent cations within the inner polymeric network and the formation of strong ionic bonds between the chains. These bonds are less flexible; hence the ability of the polymer to retain the solvent is reduced by the physically crosslinking. By combining both crosslinking mechanisms (P+C=D) it is possible to obtain hydrogels that significantly reduce their mass swelling ratio in DPBS.

Conversely, by maintaining the crosslinking mechanism constant, the mass swelling ratio is strongly dependent on the DM. The high MA-κ-CA exhibited significantly lower swelling ratios (*p<0.05 when compared with the Medium MA-κ-CA and ***p<0.001 when compared with Low MA-κ-CA), due to high crosslinking density. A similar behavior was observed for methacrylated alginate hydrogels where the decrease of dissociation degree occurred with

the increase of the DM[13], as entanglement of covalent bonds reduces the degree of freedom of the network, hence reducing the ability to retain the solvent and enlarge its volume.

When immersed in cell culture media (DMEM) containing monovalent ions, divalent ions and proteins, hydrogels exhibit a similar swelling to DPBS (**Figure VIII.3B**). However, the extent of the swelling is increased in DMEM when compared with DPBS. It is possible that the medium destabilizes the physically crosslinked network, by the substitution of the monovalent ions already present in the inner network of the hydrogel with the divalent ions or proteins present in the media. This allows the hydrogel to expand more and have higher swelling ratios.

Overall, these data suggest that efficient pattern fidelity can be achieved by increasing the DM and applying both chemically and physically crosslinking procedures. Within these conditions the swelling ratios of the hydrogels are the lowest. Concluding, it is possible to produce hydrogels with adjustable swelling ratios.

VIII.3.5. Degradation/dissolution characteristic of the MA-κ-CA hydrogels

The purpose of the dissolution studies was to evaluate the integrity and stability of the crosslinked MA-κ-CA hydrogels in physiological conditions. The dissolution of dual crosslinked hydrogels in DPBS (ions content) and DMEM (ions and protein content) was evaluated over a period of 21 days. During the dissolution period, κ-CA (physically crosslinked) showed to be less stable when compared with the dual crosslinked MA-κ-CA, in both dissolution media (**Figure VIII.3C,D**). At day 21, 15% of the initial weight of physical crosslinked κ-CA was lost in DPBS, while in DMEM more than 25% of the initial weight was dissolved in the media. Contrary, it was observed that in the first 7 days of the experiment, all methacrylated formulations present a high stability and no evidence of disintegration/dissolution. At specific incubation time, it was noticed that the High DM samples were less affected by the experimental conditions. This suggests that the increase in the DM renders hydrogels with strong bonding, upon chemical crosslinking, that cannot be disrupted by ionic exchange and interaction with proteins present in the culture media. Tuning the dissolution parameters is an interesting tool to use in order to address specific requirements of the TE objective. Therefore, MA-κ-CA presents a versatile behavior in physiological conditions dependent on the DM. Envisioning TE applications, matching the extent to which the hydrogel loses its integrity with the rate at which native ECM is produced is a requirement[24b,37]. MA-κ-CA-based hydrogels possess different degrees of degradation, dependent on their DM.

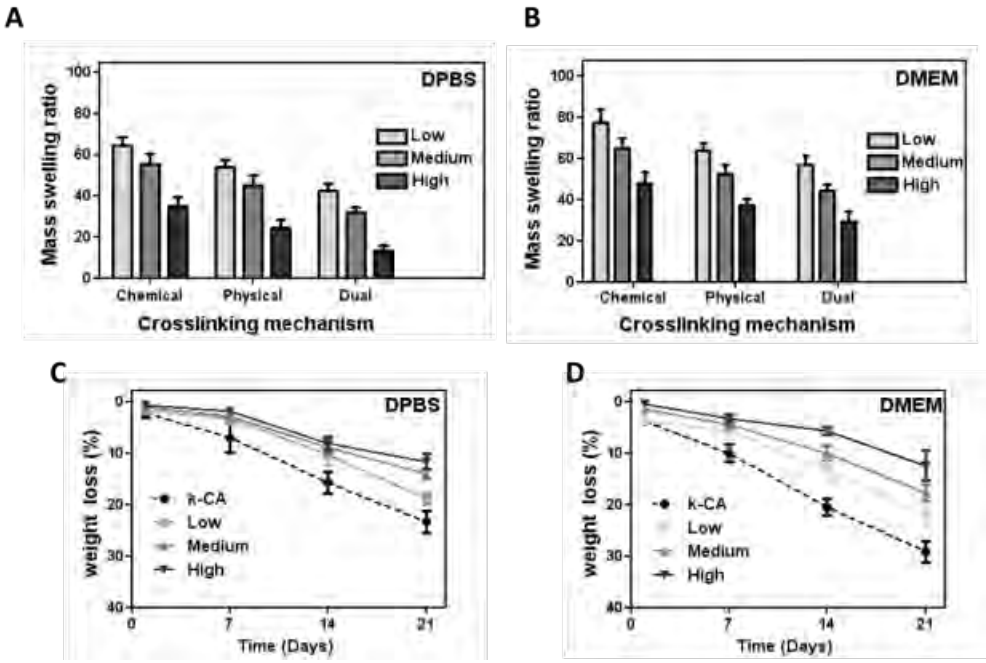

Figure VIII.3. Swelling and stability of MA-κ-CA hydrogels in DPBS and DMEM. (**A-B**) The mass swelling ratios of 5% (wt/v) MA-κ-CA hydrogels in DPBS and culture medium, DMEM, show statistically significant differences. The D crosslinking approach leads to the formation of hydrogels with low swelling properties. Representation of weight loss percentage *vs* time of dual crosslinked 5% MA-κ-CA hydrogels with different DM, immersed in DPBS (**C**) and (**D**) DMEM at 37°C. All values are reported as corresponding to averages (n=3) ± SD.

VIII.3.6. Effect of DM on hydrogels microstructure

The effect of DM on the dry microstructure of polymeric networks was evaluated using SEM. We used freeze-drying method to obtain dried polymeric structures. In this method, dual crosslinked hydrogels made from κ-CA with different DM were subjected to a rapid snapshop cooling using liquid nitrogen and then the solvent (water) was removed by sublimation. Although this method cannot be used to visualize the original wet-polymeric network, can be used as a predictive tool of the effect of DM on the dried microstructure of MA-κ-CA, by evaluation of the pore size formed upon drying. The results indicated that κ-CA with High MA-κ-CA possess a compact pore structure, with pore size of 18.5±5.3μm, while the Medium and Low methacrylated hydrogel showed interconnected structure with pore size of 33.2±8.2μm and 48.8±10.4μm, respectively (***p<0.001, **Figure VIII.4A-G**). The decrease in pore size with an increase in DM of dried structure can be attributed to high degree of crosslinking between polymeric chains. These observations in dried conditions are in agreement with the reported swelling behavior and rheological evaluation of the dual crosslinked hydrogels in fully hydrated conditions. In summary, hydrogels with low DM have larger pores compared with hydrogels with High DM.

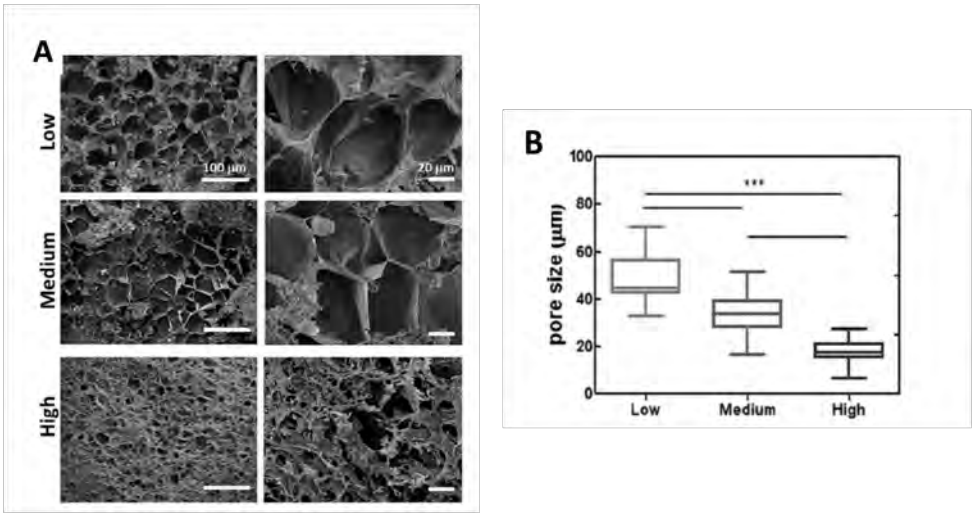

Figure VIII.4. Microstructure of MA-κ-CA dual crosslinked dried hydrogels. (**A**) Representative SEM images of MA-κ-CA Low, Medium and High. (**B**) A significant decrease in pore size diameter with the increase in the DM can be observed. All values are significantly different from each other (n=20, one-way ANOVA, ***p<0.001 Tukey post-hoc test).

VIII.3.7. Effect of the DM on 3D network stability and mechanical strength

VIII.3.7.1. Viscoelastic behavior

The oscillatory shear experiments were performed to analyze the viscoelastic properties of the dual crosslinked hydrogels networks. The effect of the DM on the viscoelastic properties was evaluated by monitoring the storage (*G'*) and loss (*G''*) moduli. These parameters provide valuable information about the viscoelastic properties of hydrogels and have been taken into consideration in order to predict the stability of polymeric networks under shear forces. The ratio between the loss and storage moduli is defined as the loss tangent (tanδ = *G''/G'),* where δ is the loss angle. A stress sweep from 0.1 to 1000 Pa was performed at a constant frequency in order to evaluate the viscoelastic behavior of the dual crosslinked hydrogels.

Figure VIII.5A shows the evolution of storage moduli with the increase of oscillatory stress. The non-modified κ-CA hydrogels formed only by physical crosslinking exhibits a shorter linear viscoelastic region, indicating a weak network that can be deformed at higher stress. However, the increase in the DM enlarges the viscoelastic region of the polymer network, suggesting that the chemical crosslinking via photocrosslinkable moieties renders highly stable networks. On the other hand, **Figure VIII.5B** indicates the evolution of the viscous moduli with the increase of oscillatory stress. The low values of *G''* show a trend similar to the *G',* mainly dependent on the DM. At low stresses the *G'* values were higher than the ones corresponding to *G'',* for all the samples. The loss angle (δ) of the crosslinked polymers also showed a dependence on the DM.

Figure VIII.5C presents the crossover point where the value of tan δ is 1 (*G''=G').* This

critical point corresponds to the change of viscoelastic behavior from solid-like (*G′>G″)* to liquid-like (*G′<G″)* behavior. This transition is correlated to the collapse of polymeric network and consequently of the crosslinking bridges that bear the 3D network. The shift of the crossover point towards higher stresses indicates that hydrogel networks are more stable for increased DM. This behavior was found to be similar to that showed by alginate containing both ionic and covalent links[38] and polyethylene glycol nanocomposite hydrogels[9b,39].

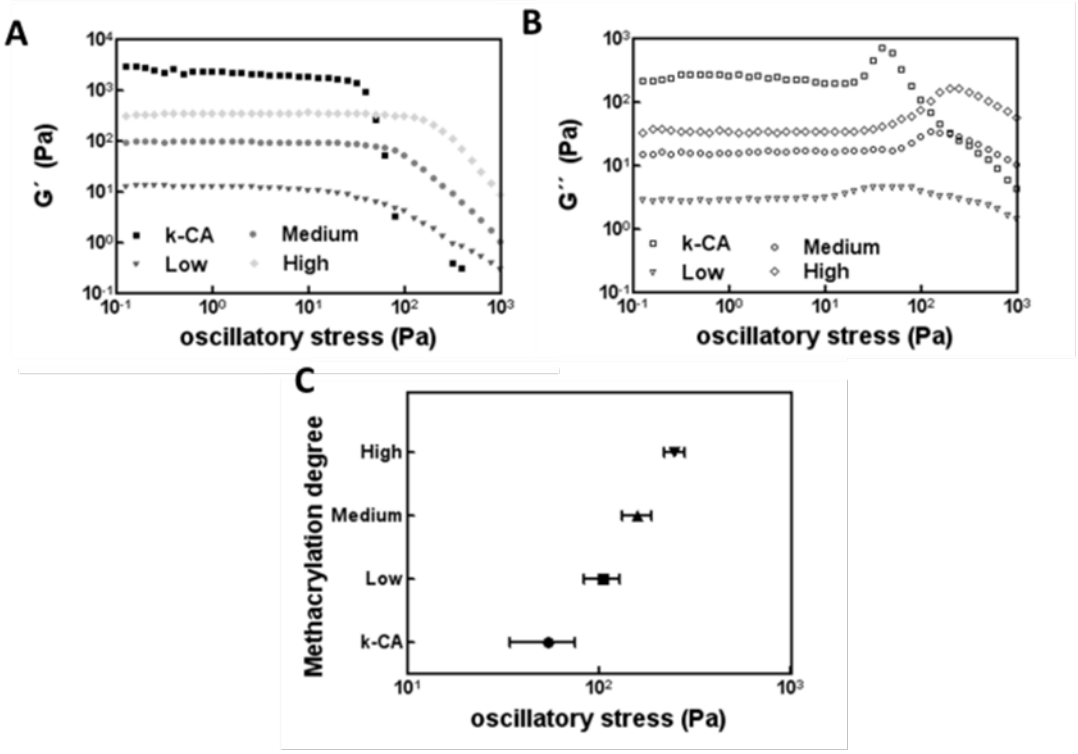

Figure VIII.5. Viscoelastic properties, storage modulus (G´) (**A**) and loss modulus (G´´) (**B**) of swollen dual crosslinked hydrogels are strongly affected by DM. (**C**) The increase of the DM increases the photocrosslinkable units and the yielding of the internal network upon deformation, confirmed by the shifting to the right of the crossover point (tan δ=1) between G' and G''.

VIII.3.7.2. Compressive properties

Considering hydrogels as cell carrier, modulator and delivery systems, it is important to address the stability of the polymeric network under stress-relaxation cycles, reproducing the repetitive force loads that native tissue are being exposed. The ionic crosslinking of κ-CA enables the formation of strong, but brittle network, not compatible with sustained loadings. In gels with ionic crosslinks, stress relaxes mainly through breakage and consecutive readjustment of the crosslinked bonds. In contrast, in gels with covalent crosslinks, like the methacrylate moieties, stress relaxes through the migration of water within the network[38], rendering a higher degree of stability within the network.

The mechanical properties of MA-κ-CA hydrogels were characterized by applying repetitive compression cycles on crosslinked hydrogels obtained from MA-κ-CA with different DM

(Low, Medium and High). The influence of the applied crosslinking mechanisms and MA-κ-CA concentration on the mechanical performance of the developed hydrogels were also considered. Hydrated *vs* as prepared samples highlight the influence of the hydrated state on the mechanical properties of the hydrogels (**Figure VIII.6A-D**). The increase in the density of photocrosslinkable units and thus, in the DM, lead to the formation of hydrogels with higher compressive moduli (**Figure VIII.6A-B**). We observed that due to swelling, compressive moduli of all formulations decreased dramatically, however maintaining a certain trend dependent on DM and crosslinking mechanism. Dual crosslinked hydrogels depicted significantly higher compressive moduli when compared with the chemical crosslinking (***p<0.001), and physical crosslinking (**p<0.01), respectively.

Keeping DM constant, chemical crosslinking enabled the formation of hydrogels with relatively lower compressive modulus (***p<0.01) values, comparative to those fabricated only with the physical method (**Figure VIII.6C**). However, the combination of both physical and chemical crosslinking mechanisms, led to the development of hydrogels with significantly increased mechanical properties for all modified formulations (**p<0.01). Even if the polymeric chain is occupied with methacrylate groups, the ionic interactions between chains are possible due to solvent transport throughout the network allowing the entrapment of monovalent ions between the chains and therefore an increase in elastic modulus values.

Even more, with increased concentrations of Medium MA-κ-CA (2.5, 5, 7.5, and 10% w/v), the compressive modulus significantly (*p<0.05) increased, due to the increased number of tight interaction formed upon crosslinking.

Nevertheless, when samples were hydrated, a significant decrease in the mechanical performance was observed, for all the formulations. (**Figure VIII.6D**). As mentioned above, it was also found a dramatic decrease of the compression modulus in hydrated samples, as compared to that registered for the samples tested as prepared. As explained previously, the affinity for water molecules allows the loss of monovalent ions and loosens the interactions between chains, thus, the increased mass swelling ratios play an important role in the mechanical performance of hydrogels, as the solvent molecules can easily penetrate the network loosening the chain-chain interactions. On the other hand, due to the presence of photocrosslinkable groups in MA-κ-CA polymer, the double helix conformation is compromised. However, the chemical crosslinking and the combination with physical procedure, lead to the formation of hydrogels with broad range of mechanical properties. On the contrary, κ-CA hydrogels presented higher compressive modulus, due to the formation of double helix configurations that allow the chains aggregation.

Furthermore, the toughness of chemical physical and dual crosslinked hydrogels with different DM was measured as an indication of network resistance to disruptive forces. As expected, the increase in DM rendered the formation of tougher hydrogels (**Figure VIII.6E**),

regardless of the crosslinking mechanism. This might be explained by the increase in the number of covalent bonds, due to the increase in the photocrosslinkable units. This is in agreement with studies that sustain that hydrogels resistance to network disruption is usually correlated with the density of the covalent bonds[40]. Even more, the photocrosslinkable units hinder the formation of tight ionic bonds between. Chains, when physical corsslinking mechanism is applied. Thus, even though, the network becomes loser than the one of non modified κ-CA, it allows a better dissipation of stress and arrangement of chains without breaking the bonds.

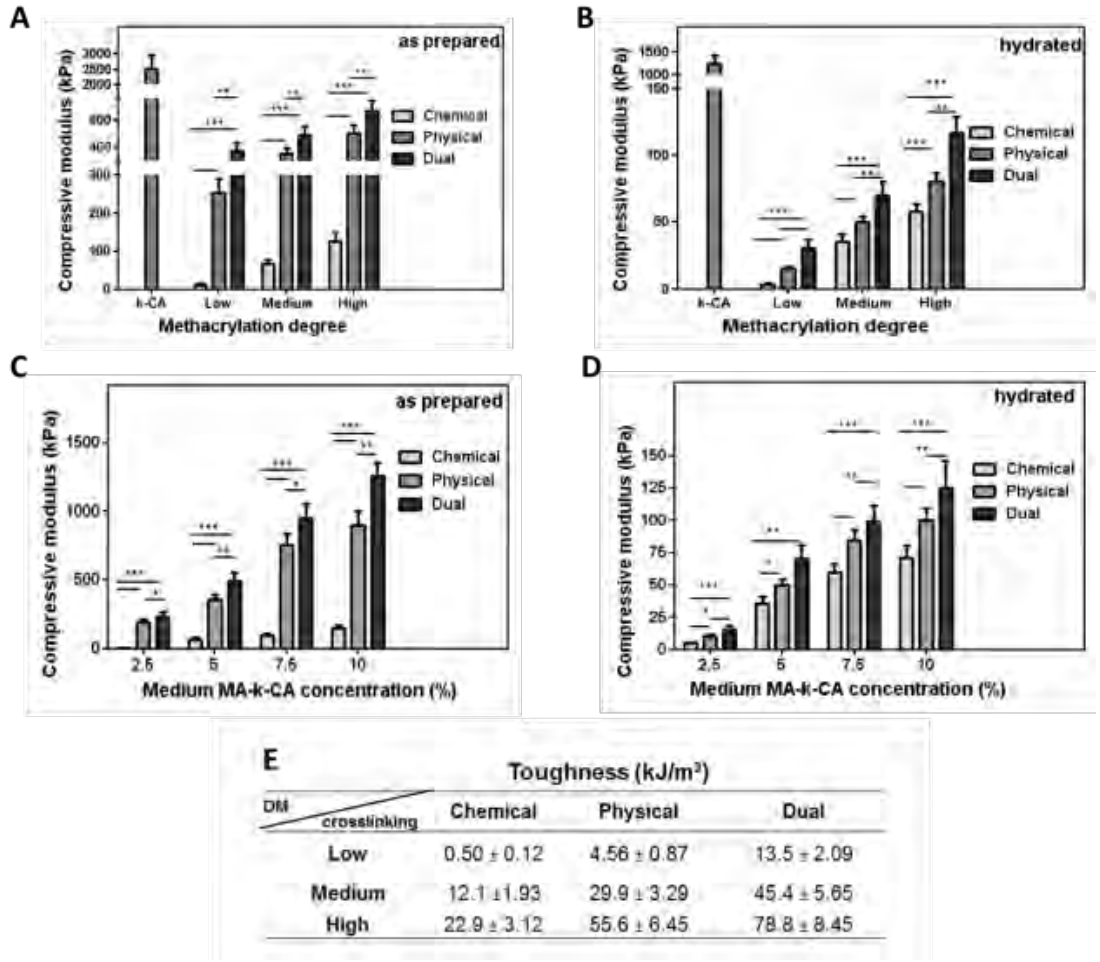

E

Toughness (kJ/m³)

DM / crosslinking	Chemical	Physical	Dual
Low	0.50 ± 0.12	4.56 ± 0.87	13.5 ± 2.09
Medium	12.1 ± 1.93	29.9 ± 3.29	45.4 ± 5.65
High	22.9 ± 3.12	55.6 ± 6.45	78.8 ± 8.45

Figure VIII.6. Mechanical properties of MA-κ-CA hydrogels obtained by different crosslinking mechanisms. The effect of DM, crosslinking mechanism and hydration state over the compressive moduli of crosslinked hydrogels (containing 5 wt/v % polymer) was evaluated in (**A**) as prepared and (**B**) hydrated states. The effect of polymer concentration (Medium DM) over the values of compressive moduli for hydrogels in (**C**) as prepared and (**D**) hydrated state. (**E**) The increase of DM, as well as the crosslinking mechanism applied, significantly increases the toughness of the hydrogels.

Interestingly, with the increase of DM the hydrogels acquired the ability to reversibly deform, without loss of energy. This behavior was not noticed for physical crosslinked κ-CA (**Figure VIII.7A**). The energy loss during deformation is proportional to the hysteresis of the loading

curves for the two first cycles (**Figure VIII.7B**). Using 50% strain level, the recovery of the gels after applying a loading cycle is ranging from 84.2±6.5% for Low DM to 96.5±4.1% for the High DM. Contrary, the κ-CA hydrogels, even possessing higher compressive moduli are not able to recover after the initial loading cycle. This behavior is supported by high-energy loss (166.7±17.23 kJ/m^3 for the first cycle and 87.23±10.34 kJ/m^3 for the second cycle) and significantly (***p<0.001) lower recovery percentage (47.5±5.4%) when compared with the modified formulations (**Figure VIII.7C**).

The elastic behavior of the dual crosslinked MA-κ-CA can represent an important asset if we consider the dynamic *in vivo* conditions. This data is in agreement with the rheology results that demonstrate the stability of the covalent network when applying increased stress rates. For a hydrogel with ionic crosslinks, the stress relaxes as the crosslinks dissociate and reform elsewhere, so that the network undergoes plastic deformation, hence, the hydrogel cannot recover to its initial shape. On the contrary, introducing covalent crosslinks into the hydrogels network, by the photopolymerization process, the stress relaxes as water migrates out of the gel. Therefore, the network undergoes elastic deformation and can recover to the shape prior deformation[38].

Overall, the combination of physical and chemical crosslinking mechanisms resulted in the development of MA-κ-CA hydrogels with tunable mechanical properties, ranging from 3.0±1.7kPa to 107.0±11.6kPa. Hydrogels with biologically relevant mechanics can be obtained by means of physiologically compatible procedures, addressing a broad range of applications within the TE framework. Other methacrylate based hydrogels, e.g. gellan gum, displayed similar tunable mechanical properties features, by changing the DM, concentration of polymer and/or crosslinking mechanism[12].

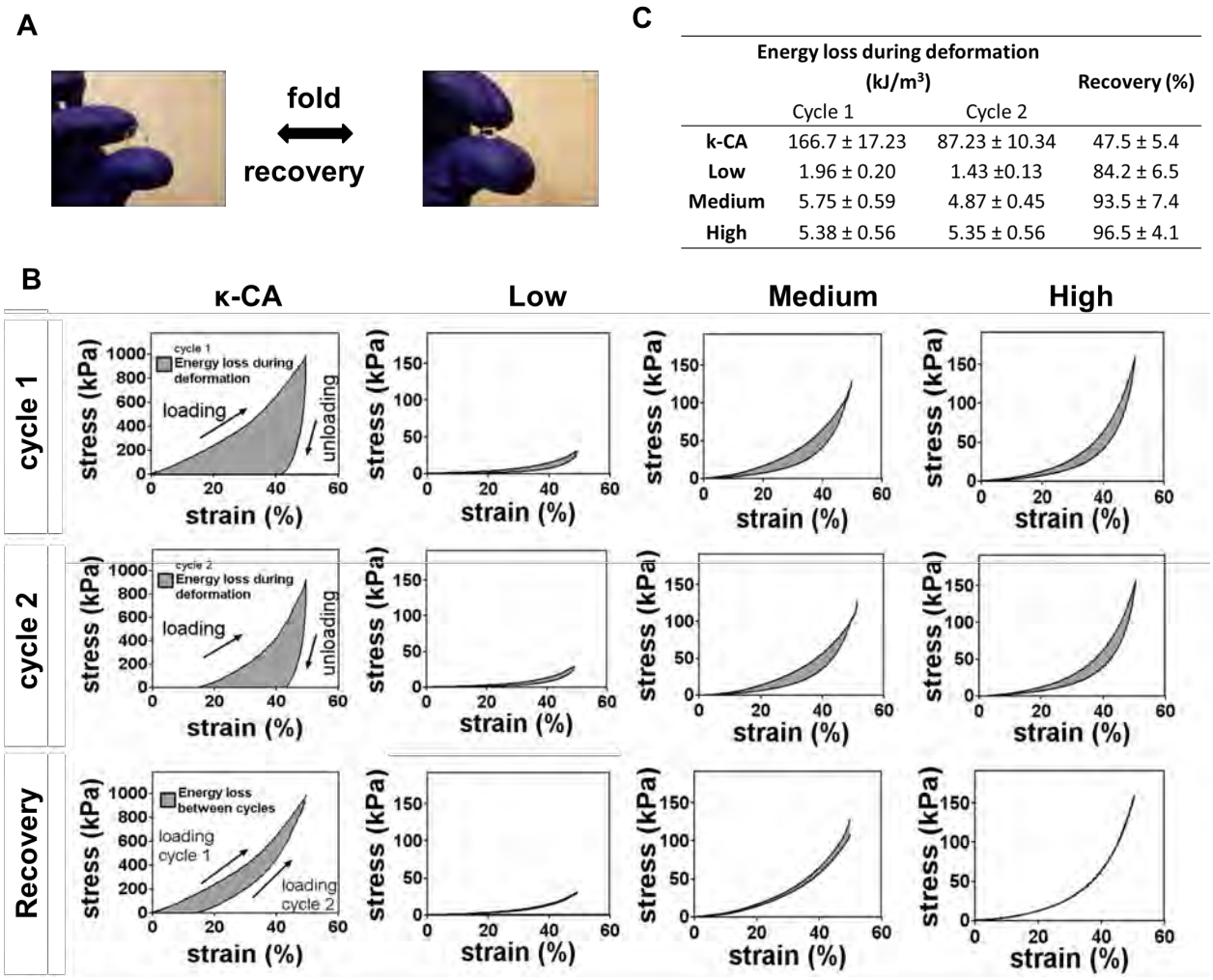

C

	Energy loss during deformation (kJ/m³)		Recovery (%)
	Cycle 1	Cycle 2	
k-CA	166.7 ± 17.23	87.23 ± 10.34	47.5 ± 5.4
Low	1.96 ± 0.20	1.43 ±0.13	84.2 ± 6.5
Medium	5.75 ± 0.59	4.87 ± 0.45	93.5 ± 7.4
High	5.38 ± 0.56	5.35 ± 0.56	96.5 ± 4.1

Figure VIII.7. Compressive properties of MA-κ-CA hydrogels determined using unconfined cyclic compression. (**A**) Qualitative image showing the recovery of hydrogels undergoing deformation. This elastic behavior is not present for the non-modified κ-CA. (**B**) The effect of DM on the loading and unloading cycle during the compression test is shown in hydrogels containing 5 wt. % polymer. The increase in the DM increases the density of covalent bonds. As the hydrogels undergoes deformation, these bonds are flexible enough to allow the reorganization of the inner network, and therefore the recovery after deformation. Contrarily the κ-CA exhibits an irreversible plastic deformation as the polymer chain collapse after deformation. (**C**) The energy lost during the cycle can be calculated by determining the area between the curves. Polymer hydrogels are highly elastic and have negligible hysteresis. Increase in the DM results in a decrease of energy lost during the cycle. For High DM the recovery was about 95% compared with the Low DM, which possessed a 72% potential for recovery.

VIII.3.8. 3D cell encapsulation in MA-κ-CA hydrogels

VIII.3.8.1. Reactive species production (SOx/NOx)

Reactive oxygen species (ROS), such as superoxide anion (SOx), and reactive nitrogen species (RNS), such as the nitric oxide (NOx), are generated as natural products of the cell respiratory metabolism and are produced in response to stress. It has been reported that

apoptotic events are associated with direct or indirect activation of ROS[40]. Therefore, the evaluation of the production of these species is of utmost importance to assess to which extent cells are exposed to stress conditions within the developed hydrogels.

The production of SOx and NOx, as indicators of oxidative and nitrosative stress in cells, was evaluated to determine to which extent the chemistry and formulation of hydrogels affected the encapsulated cells (**Figure VIII.8A**). The initial SOx and NOx levels were attributed to stress exercised on cells as these were removed from cell culture flasks by trypsinization and consecutive centrifugation and resuspension. However all of these procedures can perturb the levels of the oxides production, as cells react and adjust to the external stress. The encapsulation of cells in hydrogel networks increased the levels of SOx and NOx. As mentioned before, external stress generates a cascade of cellular events that can lead to increased levels of oxidative and nitrosative stress that can cause DNA damage, morphological transformations and cell membrane disruptions[41].

However, the encapsulation in physical crosslinked κ-CA hydrogels does not significantly change the levels of SOx/NOx, when compared with cells alone, except for the High DM MA-κ-CA hydrogels.

On the other hand, the use of PI, UV exposure and presence of methacrylate groups can seriously affect the cells integrity and viability, leading to poor functional response[42]. We evaluated the production of SOx/NOx production levels in NIH-3T3 fibroblast cells as a function of crosslinking mechanism and DM. The PI and UV light did not show any significant influence on both residual production of SOx and NOx. However, High DM caused a significant increase on the local levels of reactive species.

VIII.3.8.2. 3D cell-laden hydrogels

Previous studies have showed that κ-CA hydrogels sustain the viability and enable proliferation of different cell types[24b,37]. Herein, we evaluated the NIH-3T3 fibroblast cells viability encapsulated within photocrosslinked MA-κ-CA hydrogels by using a standard Live/Dead assay (**Figure VIII.8B**). Cell viability was evaluated 3h after encapsulation, in order to assess the immediate effect of the applied crosslinking mechanism. The UV exposure time, PI concentration and methacrylate groups density of the MA-κ-CA formulations, showed no significant effect over the encapsulated cells viability. A long-term effect of the mentioned factors was assessed after 3 days of culture. Again, the viability of the encapsulated cells was not significantly affected.

The feasibility of the modified κ-CA to be used as materials for micromolding approaches was evaluated by creating MA-κ-CA patterns using PDMS templates. Cell-laden hydrogels of different shapes and sizes and easily manipulated were obtained (**Figure VIII.8C**). It was noticed that the most reliable and consistent patterns were achieved using High MA-κ-CA,

mainly due to their low swelling behavior. Overall, the consecutive crosslinking procedures (UV and KCl) and the presence of PI showed no significant effect on the viability of the cells. These results strengthen the potential of MA-κ-CA hydrogels to be used as cell carriers within a spatially controlled distribution.

Apart from NIH-3T3 fibroblast cells, we also encapsulated MC3T3 E1-4 preosteoblast cell line, as well as human mesenchymal stem cells (hMSCs), within the MA-κ-CA hydrogels (data not shown). Preliminary results indicated that cells encapsulated for long time periods (up to 21 days), possess high viability (~75%) within hydrogels. This indicates that dual crosslinked MA-κ-CA systems can exhibit a high potential for a range of biomedical applications.

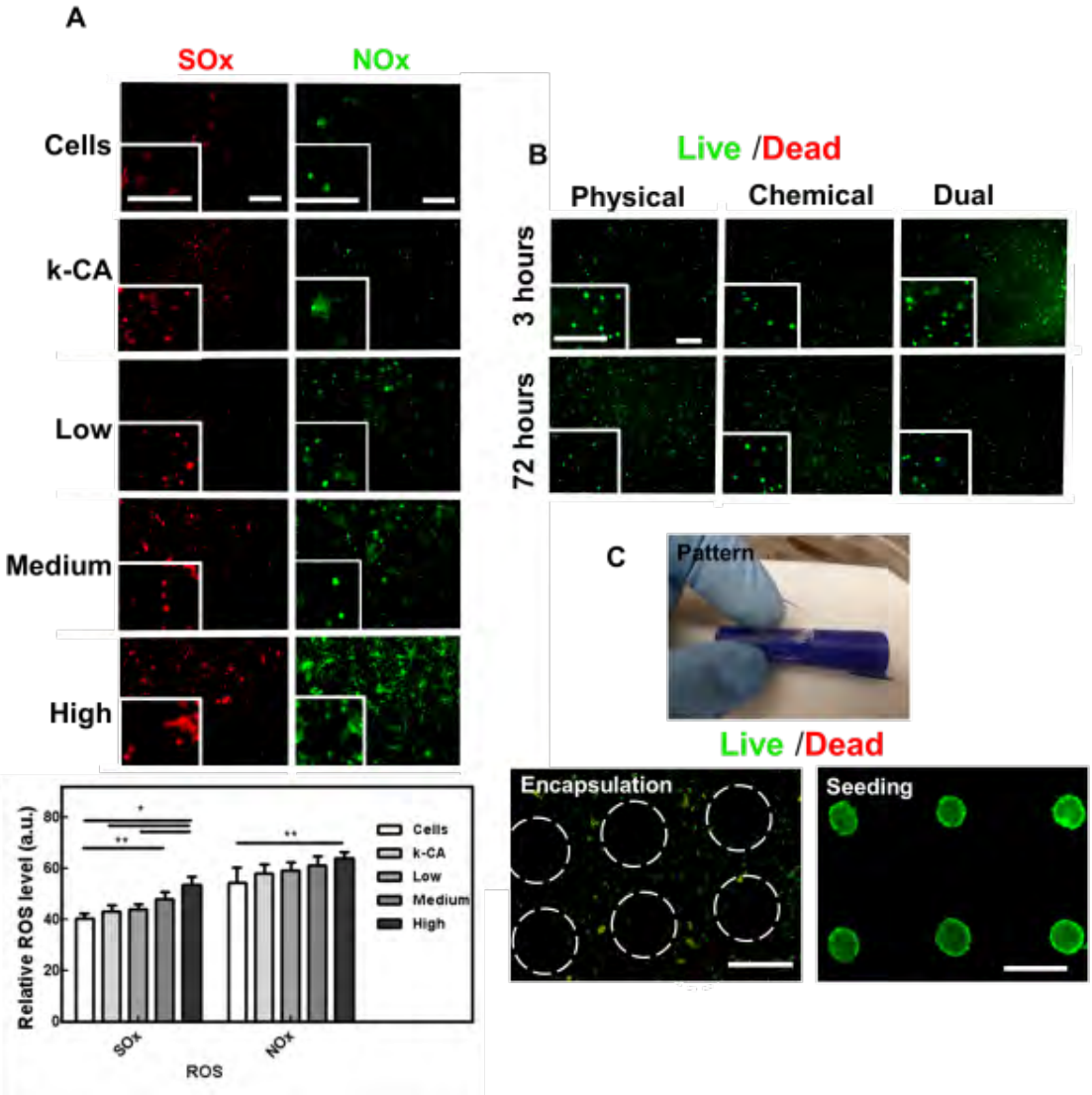

Figure VIII.8. Cell encapsulation in MA-κ-CA hydrogels. (**A**) Production of intracellular superoxide (SOx) and nitric oxide (NOx) by NIH-3T3 cells after encapsulation in MA-κ-CA (5%, wt/v), 0.25% PI (w/v), under UV exposure (40sec) and 10min KCl (5%, wt/v) treatment. Trypsinized and encapsulated cells in κ-CA with KCl treatment were used as controls. The assay was carried out using DHE and DAF-2DA oxidation assay, respectively for SOx and NOx identification. The quantification of the

fluorescence intensity was assessed using NIH ImageJ software. Values are represented as average ± SD, n=3. Statistical differences (*p<0.05, **p<0.01) using one way-ANOVA followed by a Tukey post-test). (**B**) Representative fluorescence images of live (green) and dead (red) encapsulated NIH-3T3 cells in Medium MA-κ-CA 5% obtained with different crosslinking mechanism, 3h and 72 hours after encapsulation. (**C**) Patterns of different shapes and sizes can be obtained with the developed materials by micromolding. Cells can be encapsulated or seeded on a predefined pattern. Scale bar represent 100μm.

VIII.4. CONCLUSIONS

MA-κ-CA was synthesized by reacting κ-CA with various amounts of MA, rendering the development of MA-κ-CA with different DM. To our best knowledge, this is the first study introducing a photocrosslinked κ-CA with controllable elastic moduli, swelling ratios and pore size distributions. These physical properties can be easily tailored by varying the DM. Moreover, the combination of physical and chemical crosslinking procedure led to the formation of hydrogels with versatile mechanical and physical performance, while permitting maintenance of viable encapsulated cells. By micromolding approaches, spatially controlled geometries and cell distribution patterns can be obtained thus enabling the development of cell-material platforms that can be applied and tailored to specific functionalities in tissue engineering applications.

REFERENCES

1. (a) Peppas, N. A.; J. Z. Hilt, J. Z.; Khademhosseini, A.; Langer, R., Hydrogels in biology and medicine: from olecular principles to bionanotechnology. *Advanced Materials* **2006,** *18* (11), 1345–1360; (b) Nikkhah, M.; Edalat, F.; Manoucheri, S.; Khademhosseini, A., Engineering microscale topographies to control the cell-substrate interface. *Biomaterials* **2012,** *33* (21), 5230-46; (c) Khademhosseini, A.; Vacanti, J. P.; Langer, R., Progress in tissue engineering. *Scientific American* **2009,** *300* (5), 64-71; (d) Slaughter, B. V.; Khurshid, S. S.; Fisher, O. Z.; Khademhosseini, A.; Peppas, N. A., Hydrogels in regenerative medicine. *Adv Mater* **2009,** *21* (32-33), 3307-29.
2. (a) Peppas, N. A., Hydrogels and drug delivery. *Current Opinion in Colloid & Interface Science* **1997,** *2* (5), 531–537; (b) Sant, S.; Tao, S. L.; Fisher, O. Z.; Xu, Q.; Peppas, N. A.; Khademhosseini, A., Microfabrication technologies for oral drug delivery. *Advanced drug delivery reviews* **2012,** *64* (6), 496-507; (c) Casadei, M. A.; Pitarresi, G.; Calabrese, R.; Paolicelli, P.; Giammona, G., Biodegradable and pH-sensitive hydrogels for potential colon-specific drug delivery: characterization and in vitro release studies. *Biomacromolecules* **2008,** *9* (1), 43-9.
3. (a) Lutolf, M. P.; Hubbell, J. A., Synthetic biomaterials as instructive extracellular microenvironments for morphogenesis in tissue engineering. *Nature biotechnology* **2005,** *23* (1), 47-55; (b) Ponce, S.; Orive, G.; Hernandez, R.; Gascon, A. R.; Pedraz, J. L.; de Haan, B. J.; Faas, M. M.; Mathieu, H. J.; de Vos, P., Chemistry and the biological response against immunoisolating alginate-polycation capsules of different composition. *Biomaterials* **2006,** *27* (28), 4831-9.
4. Balakrishnan, B.; Mohanty, M.; Fernandez, A. C.; Mohanan, P. V.; Jayakrishnan, A., Evaluation of the effect of incorporation of dibutyryl cyclic adenosine monophosphate in an in situ-forming hydrogel wound dressing based on oxidized alginate and gelatin. *Biomaterials* **2006,** *27* (8), 1355-61.
5. (a) Carrigan, S. D.; Tabrizian, M., Reducing nonspecific adhesion on cross-linked hydrogel platforms for real-time immunoassay in serum. *Langmuir : the ACS journal of surfaces and colloids* **2005,** *21* (26), 12320-6; (b) Kim, I. L.; Mauck, R. L.; Burdick, J. A., Hydrogel design for cartilage tissue engineering: a case study with hyaluronic acid. *Biomaterials* **2011,** *32* (34), 8771-82.

6. (a) Petrini, P.; Fare, S.; Piva, A.; Tanzi, M. C., Design, synthesis and properties of polyurethane hydrogels for tissue engineering. *Journal of materials science. Materials in medicine* **2003,** *14* (8), 683-6; (b) Fedorovich, N. E.; Alblas, J.; de Wijn, J. R.; Hennink, W. E.; Verbout, A. J.; Dhert, W. J., Hydrogels as extracellular matrices for skeletal tissue engineering: state-of-the-art and novel application in organ printing. *Tissue engineering* **2007,** *13* (8), 1905-25.
7. Drury, J. L.; Mooney, D. J., Hydrogels for tissue engineering: scaffold design variables and applications. *Biomaterials* **2003,** *24* (24), 4337-51.
8. (a) Hoffman, A. S., Hydrogels for Biomedical Applications. *Advanced drug delivery reviews* **2002,** *54*, 3-12; (b) Khademhosseini, A.; Langer, R., Microengineered hydrogels for tissue engineering. *Biomaterials* **2007,** *28* (34), 5087-92.
9. (a) Hennink, W. E.; van Nostrum, C. F., Novel crosslinking methods to design hydrogels. *Advanced drug delivery reviews* **2002,** *54* (1), 13-36; (b) Gaharwar, A. K.; Kishore, V.; Rivera, C.; Bullock, W.; Wu, C. J.; Akkus, O.; Schmidt, G., Physically crosslinked nanocomposites from silicate-crosslinked PEO: mechanical properties and osteogenic differentiation of human mesenchymal stem cells. *Macromolecular bioscience* **2012,** *12* (6), 779-93.
10. (a) Nguyen, K. T.; West, J. L., Photopolymerizable hydrogels for tissue engineering applications. *Biomaterials* **2002,** *23* (22), 4307-14; (b) Sant, S.; Hancock, M. J.; Donnelly, J. P.; Iyer, D.; Khademhosseini, A., Biomimetic Gradient Hydrogels for Tissue Engineering. *The Canadian journal of chemical engineering* **2010,** *88* (6), 899-911; (c) West, J. L.; Hubbell, J. A., Comparison of covalently and physically cross-linked polyethylene glycol-based hydrogels for the prevention of postoperative adhesions in a rat model. *Biomaterials* **1995,** *16* (15), 1153-6.
11. Malafaya, P. B.; Silva, G. A.; Reis, R. L., Natural-origin polymers as carriers and scaffolds for biomolecules and cell delivery in tissue engineering applications. *Advanced drug delivery reviews* **2007,** *59* (4-5), 207-33.
12. Coutinho, D. F.; Sant, S. V.; Shin, H.; Oliveira, J. T.; Gomes, M. E.; Neves, N. M.; Khademhosseini, A.; Reis, R. L., Modified Gellan Gum hydrogels with tunable physical and mechanical properties. *Biomaterials* **2010,** *31* (29), 7494-502.
13. Jeon, O.; Bouhadir, K. H.; Mansour, J. M.; Alsberg, E., Photocrosslinked alginate hydrogels with tunable biodegradation rates and mechanical properties. *Biomaterials* **2009,** *30* (14), 2724-34.
14. Nichol, J. W.; Koshy, S. T.; Bae, H.; Hwang, C. M.; Yamanlar, S.; Khademhosseini, A., Cell-laden microengineered gelatin methacrylate hydrogels. *Biomaterials* **2010,** *31* (21), 5536-44.
15. Baier Leach, J.; Bivens, K. A.; Patrick, C. W., Jr.; Schmidt, C. E., Photocrosslinked hyaluronic acid hydrogels: natural, biodegradable tissue engineering scaffolds. *Biotechnology and bioengineering* **2003,** *82* (5), 578-89.
16. Amsden, B. G.; Sukarto, A.; Knight, D. K.; Shapka, S. N., Methacrylated glycol chitosan as a photopolymerizable biomaterial. *Biomacromolecules* **2007,** *8* (12), 3758-66.
17. Wang, D. A.; Varghese, S.; Sharma, B.; Strehin, I.; Fermanian, S.; Gorham, J.; Fairbrother, D. H.; Cascio, B.; Elisseeff, J. H., Multifunctional chondroitin sulphate for cartilage tissue-biomaterial integration. *Nature materials* **2007,** *6* (5), 385-92.
18. Kirsch, P. P., Carrageenan: a safe additive. *Environmental health perspectives* **2002,** *110* (6), A288; author reply A288.
19. Coviello, T.; Matricardi, P.; Marianecci, C.; Alhaique, F., Polysaccharide hydrogels for modified release formulations. *Journal of controlled release : official journal of the Controlled Release Society* **2007,** *119* (1), 5-24.
20. Chronakis, I. S.; Doublier, J. L.; Piculell, L., Viscoelastic properties for kappa- and iota-carrageenan in aqueous NaI from the liquid-like to the solid-like behaviour. *International journal of biological macromolecules* **2000,** *28* (1), 1-14.
21. Mangione, M. R.; Giacomazza, D.; Bulone, D.; Martorana, V.; Cavallaro, G.; San Biagio, P. L., K(+) and Na(+) effects on the gelation properties of kappa-Carrageenan. *Biophysical chemistry* **2005,** *113* (2), 129-35.
22. Bhattacharyya, S. N.; Manna, B.; Ashbaugh, P.; Coutinho, R.; Kaufman, B., Differentiation of respiratory epithelium: the effects of retinoic acid and carcinogens on the expression of mucociliary vs. squamous phenotype. *Inflammation* **1997,** *21* (2), 133-43.
23. Bartkowiak, A.; Hunkeler, D., Carrageenan-oligochitosan microcapsules: optimization of the formation process(1). *Colloids and surfaces. B, Biointerfaces* **2001,** *21* (4), 285-298.
24. (a) Pereira, R. C.; Scaranari, M.; Castagnola, P.; Grandizio, M.; Azevedo, H. S.; Reis, R. L.; Cancedda, R.; Gentili, C., Novel injectable gel (system) as a vehicle for human articular chondrocytes in cartilage tissue regeneration. *Journal of tissue engineering and regenerative medicine* **2009,** *3* (2), 97-106; (b) Popa, E. G.; Gomes, M. E.; Reis, R. L., Cell delivery systems using alginate--carrageenan hydrogel beads and fibers for regenerative medicine applications. *Biomacromolecules* **2011,** *12* (11), 3952-61; (c) Santo, V. E.; Frias, A. M.; Carida, M.; Cancedda, R.; Gomes, M. E.; Mano, J. F.; Reis, R.

L., Carrageenan-based hydrogels for the controlled delivery of PDGF-BB in bone tissue engineering applications. *Biomacromolecules* **2009,** *10* (6), 1392-401.
25. Bae, H.; Ahari, A. F.; Shin, H.; Nichol, J. W.; Hutson, C. B.; Masaeli, M.; Kim, S. H.; Aubin, H.; Yamanlar, S.; Khademhosseini, A., Cell-laden microengineered pullulan methacrylate hydrogels promote cell proliferation and 3D cluster formation. *Soft matter* **2011,** *7* (5), 1903-1911.
26. Hutson, C. B.; Nichol, J. W.; Aubin, H.; Bae, H.; Yamanlar, S.; Al-Haque, S.; Koshy, S. T.; Khademhosseini, A., Synthesis and characterization of tunable poly(ethylene glycol): gelatin methacrylate composite hydrogels. *Tissue engineering. Part A* **2011,** *17* (13-14), 1713-23.
27. Tojo, E.; Prado, J., Chemical composition of carrageenan blends determined by IR spectroscopy combined with a PLS multivariate calibration method. *Carbohydrate research* **2003,** *338* (12), 1309-12.
28. (a) Tapia, C.; Corbalan, V.; Costa, E.; Gai, M. N.; Yazdani-Pedram, M., Study of the release mechanism of diltiazem hydrochloride from matrices based on chitosan-alginate and chitosan-carrageenan mixtures. *Biomacromolecules* **2005,** *6* (5), 2389-95; (b) Sjoberg, H.; Persson, S.; Caram-Lelham, N., How interactions between drugs and agarose-carrageenan hydrogels influence the simultaneous transport of drugs. *Journal of controlled release : official journal of the Controlled Release Society* **1999,** *59* (3), 391-400.
29. Draget, K. I.; Stokke, B. T.; Yuguchi, Y.; Urakawa, H.; Kajiwara, K., Small-angle X-ray scattering and rheological characterization of alginate gels. 3. Alginic acid gels. *Biomacromolecules* **2003,** *4* (6), 1661-8.
30. van de Velde, F.; Antipova, A. S.; Rollema, H. S.; Burova, T. V.; Grinberg, N. V.; Pereira, L.; Gilsenan, P. M.; Tromp, R. H.; Rudolph, B.; Grinberg, V. Y., The structure of kappa/iota-hybrid carrageenans II. Coil-helix transition as a function of chain composition. *Carbohydrate research* **2005,** *340* (6), 1113-29.
31. Kara, S.; Tamerler, C.; Bermek, H.; Pekcan, O., Cation effects on sol-gel and gel-sol phase transitions of kappa-carrageenan-water system. *International journal of biological macromolecules* **2003,** *31* (4-5), 177-85.
32. Daniel-da-Silva, A. L.; Ferreira, L.; Gil, A. M.; Trindade, T., Synthesis and swelling behavior of temperature responsive kappa-carrageenan nanogels. *Journal of colloid and interface science* **2011,** *355* (2), 512-7.
33. Raymond, M. C.; Neufeld, R. J.; Poncelet, D., Encapsulation of brewers yeast in chitosan coated carrageenan microspheres by emulsification/thermal gelation. *Artificial cells, blood substitutes, and immobilization biotechnology* **2004,** *32* (2), 275-91.
34. Brandl, F.; Sommer, F.; Goepferich, A., Rational design of hydrogels for tissue engineering: impact of physical factors on cell behavior. *Biomaterials* **2007,** *28* (2), 134-46.
35. Kara, S.; Tamerler, C.; Arda, E.; Pekcan, O., Photon transmission study on swelling of kappa-carrageenan gels prepared in various concentrations. *International journal of biological macromolecules* **2003,** *33* (4-5), 235-43.
36. Kara, S.; Tamerler, C.; Pekcan, O., Cation effects on swelling of kappa-carrageenan: a photon transmission study. *Biopolymers* **2003,** *70* (2), 240-51.
37. Popa, E.; Reis, R.; Gomes, M., Chondrogenic phenotype of different cells encapsulated in kappa-carrageenan hydrogels for cartilage regeneration strategies. *Biotechnology and applied biochemistry* **2012,** *59* (2), 132-41.
38. Zhao, X.; Huebsch, N.; Mooney, D. J.; Suo, Z., Stress-relaxation behavior in gels with ionic and covalent crosslinks. *Journal of applied physics* **2010,** *107* (6), 63509.
39. Kong, H. J.; Lee, K. Y.; Mooney, D. J., Nondestructively Probing the Cross-Linking Density of Polymeric Hydrogels. *Macromolecules* **2003,** *36*, 7887-7890.
40. Wen, J.; You, K.-R.; Lee, S.-Y.; Song, C.-H.; Kim, D.-G., Oxidative stress-mediated apoptosis. *Journal of Biological Chemistry* **2002,** *277* (41), 28954-64.
41. Dalle-Donne, I.; Rossi, R.; Colombo, R.; Giustarini, D.; Milzani, A., Biomarkers of oxidative damage in human disease. *Clinical Chemistry* **2006,** *52* (4), 601-23.
42. Fedorovich, N. E.; Oudshoorn, M. H.; van Geemen, D.; Hennink, W. E.; Alblas, J.; Dhert, W. J., The effect of photopolymerization on stem cells embedded in hydrogels. *Biomaterials* **2009,** *30* (3), 344-53.

SECTION VI

CONCLUSIONS AND FINAL REMARKS

CHAPTER IX

GENERAL CONCLUSIONS AND FINAL REMARKS

In the last decade, the implementation of tissue engineering (TE) concepts has emerged as a highly appealing strategy for addressing the regeneration of damaged tissues. The core essence of TE is the use of the native biological environment as a source of inspiration in designing its hypothesis and strategies. Thus, TE approaches aim at folding over the specific requirements of a tissue, while providing the adequate settings to achieve regeneration. Bearing this in mind, researchers borrowed concepts from a wide range of disciplines to provide a multi-faceted view of a strategy to be applied. Taking advantage of the arising of new and elaborated nano- and micro-materials, as well as the refinement of the understanding of the biological mechanisms and functions, new and sophisticated routes are nourished to provide further insight on complex biological systems. The simultaneous incorporation of cells, and biochemical, mechanical and topographical cues into a tri-dimensional (3D) scaffolding material has been the most explored and the most promising approach to promote the regeneration of functional tissues. However, the current TE strategies lack the ability to merge the various technological and know-how advances, typically obtained independently, into a single construct in order to generate more powerful platforms. Moreover, from a practical standpoint, there is a need to achieve the equilibrium between functionality and complexity, as a highly complex system might be too difficult to translate into clinical practice. Thus, generating simple, but yet highly efficient strategies seems to be the necessary mind-set for addressing the hurdles of TE.

With this in mind, the major objective of this thesis was to tackle this hurdles by generating a cohesive approach for directing stromal/stem cell differentiation, fabricating bone-relevant setups and providing the cues for the establishment of vascular-like structures. To do so, we explored the use of adipose derived stem cells (hASCs) as a single cell source to obtain bone forming (OBs) and endothelial cells (ECs), relevant in the context of bone vascularization TE, towards establishing hydrogel-3D based systems that would be able to host and maintain the cells' intrinsic features, while controlling their arrangement. The use of silicate nanoplatelets (sNPs) as intracellular osteoinductive triggers brought into spotlight the possibility to sustain an *in situ osteogenic* differentiation upon implantation by a pre-treatment with sNPs.

Hence, the major outcomes of this thesis pave the way towards more clinical relevant experimental designs *in vitro* as well as *in vivo*, as it is described under the topics presented bellow:

1) SSEA-4$^+$hASCs from a single cell source generate both endothelial and osteoblast-like cells (chapter III)

The stromal vascular fraction (SVF) of the human adipose tissue (AT) was proven to contain a cellular sub-set defined by the expression of a marker associated with pluripotency, SSEA-4. SSEA-4$^+$ human adipose derived stem cells (SSEA-4$^+$hASCs) were successfully isolated from the SVF by means of immunomagnetic selection. By culturing SSEA-4$^+$hASCs in endothelial growth medium (EGM-2 MV), cells with a mature endothelial signature were generated, in opposition to what was attained with non-selected hASCs cultured under the same conditions. Additionally, the culture of SSEA-4$^+$hASCs in osteogenic standard conditions triggered their differentiation into osteoblast-like cells (OBs), at superior levels than those achieved with hASCs. Thus, we demonstrated that from a single cell source, human AT, and by selecting the appropriate sub-population and culturing conditions, it is possible to obtain cells with relevance for bone TE. Other attempts of obtaining ECs-like cells from bone marrow MSCs and hASCs involve the use of high concentrations of VEGF which was proven to considerable impair the therapeutic applications of these cells. On the contrary, our approach involves the use of significantly lower concentrations of VEGF to successfully generate microvascular-like ECs, known to be directly involved in the establishment of capillary-like structures and, consequently, of an enriched vascular network within tissues. The use of SSEA-4$^+$hASCs-derived microvascular-like ECs could overcome the shortfalls of primary ECs usage, mainly related to the harvesting site, isolation procedure and cellular yield. Nonetheless, the differentiation potential of SSEA-4$^+$hASCs is not limited to the endothelial lineage, thus broadening the opportunity window to tackle not only the vascularization aspect of tissue-engineered constructs, but also other differentiation pathways.

2) SSEA-4$^+$hASCs-derived pre-osteoblasts and ECs potential maximized under optimal co-culture conditions (chapter IV)

Beside a reliable and high versatile cell source, bone TE requires a thorough understanding of the mechanism of cellular interaction between the most important cell-players within the context of vascularization: OBs and ECs. This type of studies aims at reproducing within *in vitro* settings and thus, in a more accurate manner, part of the highly complex signaling cascade found within bone natural biological environment. Thus, the outcome of these works allows a faster acquisition of knowledge and provides a framework to design more complex

scenarios that resemble even more the *in vivo* natural environment. By culturing SSEA-4^{+}hASCs-derived ECs and pre-OBs, at several ratios and in several media compositions, it was found that an above 50:50 in a mixture of standard endothelial maintenance and osteogenic differentiation media, cells synergistically communicate to support the full differentiation of the pre-OBs and the maintenance of the ECs phenotype, through the activation of a VEGF-mediated signaling loop.. These findings demonstrate that the use of SSEA-4^{+}hASCs as a single cell source is a promising endeavor to attain 3D tissue-like models that require intricate settings and design to promote the regeneration of vascularized bone tissue.

The combination of pre-committed cells into the osteogenic lineage and fully differentiated ECs, derived from the SSEA-4^{+}hASCs, endorses the development of 3D bone-like constructs, defined by a controlled/designed spatial distribution of ECs within a pre-OBs-loaded 3D matrix to maximize the continuous crosstalk between ECs and pre-OBs. Besides improving the osteogenic outcome of pre-OBs, the pre-organization of ECs within hydrogel microfibers is expected to favor the sprout and the formation of an ECs-driven capillary-like network. The anastomosis of these capillary structures with the host vasculature upon implantation will be determinant to guarantee the survival of the bone-like tissue but will certainly contribute to an improved regeneration process.

3) Silicate nanoparticles as intracellular osteoinductive agents (chapter V and VI)

Osteoinductivity is the key process that masters the differentiation of osteoprogenitor cells (i.e. pre-OBs) into osteoblasts, eventually leading to the formation of new bone. Several inorganic materials were found to be osteoinductive however, several limitations such as poor processability and insufficient degradation, are associated, harboring the need for a new generation of bioactive materials.

In this thesis, Laponite silicate nanoparticles (sNPs) were brought into the spotlight of bone TE, intrigued by their chemistry ($Na^{+}_{0.7}[(Mg_{5.5}Li_{0.3})Si_8O_{20}(OH)_4]^{-}_{0.7}$), shape (25-30nm disc with a 1nm thickness) and charge distribution (positive charged facets, negative charged sides). To our best knowledge, sNPs are introduced for the first time for bone TE applications. SNPs alone induced the osteogenic differentiation of human mesenchymal stem cells (hMSCs) without the addition of other osteoinductive factors, such as dexamethasone. Even more, when hMSCs were cultured in standard osteogenic conditions, but in the presence of sNPs, a significant increase in matrix deposition and mineralization was noticed. This observation was further expanded to the SSEA-4^{+}hASCs sub-population cultured in the same conditions. A strong up-regulation of osteo-related transcripts (*RUNX-2, OPN, OCN*), high levels of collagen type I deposition and increased mineralization was observed. The mechanism of cell-sNPs interaction was found to be correlated with their uptake and

interaction with the cytoplasmatic membrane. In fact, this mechanism of action represents a major advantage of using sNPS as osteoinductive agents. The osteogenic differentiation progresses due to the intracellular signaling which avoids a repeated *in vitro* administration of other agents such as dexamethasone and BMP-2, and endorse an *in situ* osteogenic differentiation *in vivo*. Considering that SSEA-4^{+}hASCs *per se* bear a higher differentiation potential towards the osteogenic lineage, their association with sNPs harbors great potential in TE approaches towards the development of highly mineralized templates using an independent differentiation process. Taking advantage of the outcomes achieved under this thesis described above, namely on the optimization of SSEA-4^{+}hASCs-based co-culture conditions (chapter IV), the association of the SSEA-4^{+}hASCs-sNPs system with SSEA-4^{+}hASCs-derived ECs might be proven worthwhile. The driven-sNPs osteogenic differentiation is expected to produce a boost in the intercellular crosstalk based on an enhancement of VEGF secretion by SSEA-4^{+}hASCs-sNPs, which would be translated in a better integration of ECs within the culture and, consequently, into a highly improved osteogenic outcome, compatible with that of bone tissue.

4) Bottom-up approaches for designing 3D micro geometries for cells encapsulation (chapter VII and VIIII)

In addition to cell phenotype, the delivery of cells in controlled spatial distribution within a 3D setup seems to be a concern of the field of TE. For that, micro and nanofabrication technologies coupled with advances in materials chemistry have allowed for progresses in the development of biomaterials with spatially controlled microenvironments.

In this thesis, several techniques were developed to engineer this aspect of tissue microenvironments. *Kappa*-carrageenan (κ-CA), a natural origin polymer, was used to develop robust 3D hydrogel structures that could accommodate cells in well-defined geometries. Using a two-step procedure, chitosan (CHT) coated κ-CA micro fibers were obtained, with diameters ranging from 0.5 to 1.25µm. The presence of the CHT coating enhanced the stability and the diameter of κ-CA fibers, restraining their swelling. Moreover, these fibers supported the viability and phenotype of encapsulated ECs, enabling their use as cell-delivery systems within 3D TE constructs. Furthermore, using a bottom-up approach, these fibers were used as building blocks for the development of suitable 3D platforms of independently organized heterotypic cell-containing hydrogels, relevant for bone vascularization approaches.

However, in the majority of existing strategies in TE, once implanted, hydrogels can have an inconsistent behavior. This observation is valid for κ-CA hydrogels, which due to ionotropic character are not stable in physiological-like environments. Thus, when implanted, the strong bonds previously established for their formation are disrupted leading to the hydrogel

disintegration. To overtake this obstacle, κ-CA was chemically modified to incorporate C=C bonds to allow its crosslinking by ultraviolet light (UV) and thus its microfabrication into pre-established patterns. The modification was accomplished by using methacrylic anhydride (MA), yielding a methacrylated κ-CA (MA-κ-CA) hydrogel crosslinkable not only through physical, but also through chemical mechanisms. As a result, by selecting the appropriate crosslinking mechanisms, hydrogels with versatile mechanical, swelling and degradability properties were produced. Moreover, the obtained hydrogels possessed high recovery rates, a property that is highly attractive for those TE applications where repetitive mechanical loads are involved.

In conclusion, this thesis proposes the use of SSEA-4$^+$hASCs as a single cell sub-set to obtain both ECs and OBs, of sNPs as osteoinductive agents and of κ-CA-based hydrogels as 3D matrices, towards the development of 3D architectures that would resemble that of native bone. Envisioning engineering vascularized bone tissue, the κ-CA hydrogels (fibers and discs) act as highly structured 3D template matrix where ECs are distributed in a microfibers-like structures surrounded by SSEA-4$^+$hASCs-sNPs.

FINAL REMARKS AND FUTURE WORK

Despite the overwhelming number of studies that deal with the development of new biomaterials in TE, and in particular in bone-related applications, few of them take into consideration the anatomical and functional complexity of bone, by addressing the synergistic relation that exists between the three components of bone anatomy, cells, inorganic and organic extracellular matrix, and a functional vasculature. The current thesis recognizes the importance of concomitantly addressing these viewpoints by establishing a know-how platform that will enable the development of advanced bone tissue engineered constructs aimed at recreating the native tissue.

Thus, we were able to successfully identify a cell sub-set, SSEA-4$^+$hASCs, that allows overcoming the current shortage in cell types relevant for vascularization purposes in bone TE. Herein, we proposed a straightforward endothelial differentiation of SSEA-4$^+$hASCs, which prevails over the complex protocols applied for the differentiation of other stem/stromal cells, and by-passes the reduced availability of primary microvascular endothelial cells. Moreover, by questioning about the interactions between SSEA-4$^+$hASCs-derived ECs and pre-OBs, we established a one-source co-culture system, which would provide the clues to reproduce, in a more accurate manner, the complex situations found *in vivo* and ultimately would enable the creation of an improved vascularized bone tissue-like construct. This strategy provides a significant leverage over the traditional co-culture settings that, for example, rely on cells harvested from separate sources, or are set with primary macrovascular endothelial cells.

Having proven the dual-differentiation potential of SSEA-4$^+$hASCs, two parallel strategies were exploited, each covering either the SSEA-4$^+$hASCs-derived OBs or SSEA-4$^+$hASCs-derived ECs, to inquire over their use in combination with inorganic agents and ECM-like matrices, respectively. The original combination of SSEA-4$^+$hASCs with inorganic sNPs resulted in a boost of their privileged osteogenic differentiation capacity. The intracellular signaling of sNPs brings into discussion the possibility to pre-trigger SSEA-4$^+$hASCs into osteogenic lineage by exposing the cells to a short treatment with sNPs. By doing so, a series of options in achieving the full differentiation commitment are foreseen. Probably the most appealing is the pursual of complete osteogenic differentiation upon implantation, which would enable *in situ* deposition of ECM and its subsequent mineralization, but also the embedding of ECs within the newly formed matrix. This strategy would minimize the *in vitro* culturing steps, while replicating the in vivo bone regeneration context.

Though the scientific and technological knowledge obtained in this thesis is very promising, future research has to be focused on merging the proposed strategies into a single 3D construct, to foster the synergistic contribution of its parts.

Even more, the properties of the MA-κ-CA hydrogel matrices must be properly designed to foster the sprouting of SSEA-4$^+$hASCs-derived ECs and the formation of a vascular-like network. In this direction, we have performed several preliminary experiments to improve the adhesion of cells on the surface of MA-κ-CA hydrogels. First, a standard RGD modification was applied, however, the chemistry of MA-κ-CA was proved not to be suitable for the covalent grafting of RGD on its backbone. Since it was proven that besides being efficient osteoinductive agents, sNPs improve cellular adhesion, we mixed them with MA-κ-CA solutions to form nanocomposite hydrogels. When SSEA-4$^+$hASCs were seeded on the surface of these hydrogels, cells were able to adhere and spread.

However, taking in consideration the combination of ECs with pre-OBs, it is still unknown whether the OBs-derived ECM could be both mechanically and biochemically sufficient to sustain the sprout of ECs and their organization of a 3D microvasculature-like network within the matrix. If this is the case, the mutual regulation of pre-OBs and ECs becomes evident.

Therefore, we expect that the pre-triggering of SSEA-4$^+$hASCs with sNPs and the consequent encapsulation in ECs-containing hydrogel matrices, would trigger a highly enriched ECM-hydrogel that would allow the deposition of a highly enriched ECM within the hydrogels, that would sustain the ECs sprouting .

This is a step forward towards developing 3D functional structures, such as injectable matrixes, bioactive fillers or hierarchical platforms aimed at triggering specific cellular responses towards bone TE-related approaches, while enabling cell adhesion, proliferation and organization. Thus, this unique combination could be further exploited in association with SSEA-4$^+$hASCs-derived ECs and pre-OBs to address the most appropriate 3D template

that could accommodate both cells types, either in a random or spatially organized design, and concomitantly meet the mechanical and functional demands of bone.

Complementarily, a thorough study to unravel the specific mechanisms that govern the osteoinductive behavior of sNPs, namely addressing the aging phenomenon of sNPs and the evaluation of effect of the dissolution products on the osteogenic differentiation of SSEA-4^+hASCs, should be carried out. Moreover, since sNPs triggered the deposition of a collagen type II-enriched matrix, experiments focused on addressing the chondrogenic differentiation of SSEA-4^+hASCs in the presence of sNPs could also be a route to pursuit.

In an ultimate instance, the translation of the know-how acquired within this thesis into *in vivo* experiments would provide further insight over the possibility of developing fully autologous and vascularized bone-like 3D constructs. The challenge lies on combining the focus of engineering, biology and tissue functionality within the same approach to encounter the most suitable template to generate the vascularization of a bone tissue engineered construct.